Национальный исследовательский университет ИТМО

(Университет ИТМО)

На правах рукописи

Корнован Данил Феодосьевич

Временная динамика и спектральные свойства одиночных квантовых излучателей и их ансамблей, находящихся вблизи нанофотонных интерфейсов, с учетом хиральности взаимодействия

Диссертация на соискание учёной степени

кандидата физико-математических наук

Санкт-Петербург 2020

Национальный исследовательский университет ИТМО

(Университет ИТМО)

На правах рукописи

Корнован Данил Феодосьевич

Временная динамика и спектральные свойства одиночных квантовых излучателей и их ансамблей, находящихся вблизи нанофотонных интерфейсов, с учетом хиральности взаимодействия

Специальность 01.04.05

«Оптика (физико-математические науки)»

Диссертация на соискание учёной степени

кандидата физико-математических наук

Научный руководитель:
кандидат физико-математических наук
Петров Михаил Игоревич

Санкт-Петербург 2020

Диссертация подготовлена в: федеральное государственное автономное образовательное учреждение высшего образования «Национальный исследовательский университет ИТМО».

Научный руководитель: кандидат физико-математических наук
Петров Михаил Игоревич

Официальные оппоненты: Юдсон Владимир Исаакович, Доктор физико-математических наук, Национальный исследовательский университет «Высшая школа экономики», Главный научный сотрудник, Международная лаборатория физики конденсированного состояния

Ченг Дэррик Эдвард, доктор философии, Институт Фотонных Наук, Профессор, Руководитель Группы, Группа Теоретической Квантовой Нанофотоники

Защита состоится 17.12.2020 г. в 16:30 часов на заседании диссертационного совета 05.19.29 Университета ИТМО. Санкт-Петербург, Кронверкский пр., д. 49, лит. А, ауд. 422.

С диссертацией можно ознакомиться в библиотеке Университета ИТМО по адресу: 197101, Санкт-Петербург, Кронверкский пр., д.49 и на сайте fppo.ifmo.ru.

Ученый секретарь диссертационного совета 05.19.00 Университета ИТМО, кандидат физико-математических наук, Старовойтов Антон Андреевич.

ITMO University

As a manuscript

Kornovan Danil Feodosevich

Temporal dynamics and spectral properties of individual quantum emitters and their ensembles in the vicinity of nanophotonic interfaces with account for chiral interactions

Speciality 01.04.05
Optics (Physics and Mathematics)

Academic dissertation candidate of physics and mathematics

Supervisor:
PhD
Petrov Mihail Igorevich

Saint-Petersburg 2020

The research was carried out at: ITMO University.

Supervisor:	PhD Petrov Mihail Igorevich
Official opponents:	Yudson Vladimir Isaakovich, Doctor of science, Higher School of Economics — National Research University, Chief Research Fellow Laboratory for Condensed Matter Physics
	Chang Darrick Edward, PhD in physics, ICFO – The Institute of Photonic Sciences, Full Professor, Group Leader Theoretical Quantum-Nano Photonics Group

The defense will be held on 17.12.2020 at 16:30 at the meeting of the ITMO University Dissertation Council 05.19.29, 49 Kronversky pr., Saint-Petersburg, Russia.

The thesis is available in the Library of ITMO University, 49 Kronversky pr., Saint-Petersburg, Russia and on https://dissovet.itmo.ru website.

Science Secretary of the ITMO University Dissertation Council 05.19.00, Candidate of Physics and Mathematics, Starovoytov Anton A.

Contents

Synopsis

Relevance. The topic discussed in this thesis is of relevance for the modern and rapidly developing field of quantum nanophotonics. This field of research merges the areas of quantum optics [1] and nanophotonics [2] in the context of light-matter interaction. The former one historically was mainly covering the statistical properties of light [3], and its interaction with matter at the level of individual particles - photons and atoms [4]. However, for quite a while it was mostly about the light propagating in free-space and its interaction with atomic matter either in the vacuum or in high-quality cavities [5]. In turn nanophotonics, as a field of research, studies in details how one can control different properties of light at the nanoscale with the use of nanostructures, the creation of which became possible with the outstanding progress in fabrication technology methods.

Clearly, on the intersection of these two fields there are a lot of novel and exotic phenomena: both already discovered, and yet unknown ones. In this regard the collective effects in light-matter interactions are of relevance as the strength of atom-field coupling can be significantly increased due to the lightfield localization at the interfaces of nanophotonic structures. Within this perspective, the appearance of sub-, and superradiance [6; 7] are the appealing phenomena to consider with potential applications in quantum technologies. Being well-studied for atomic ensembles in free-space [8; 9], their features in the presence of nanophotonic structures are still not fully explained and understood. The atom-field coupling, besides the aforementioned enhancement, can be drastically modified with the use of photonic structures, for instance, by taking control over the polarization degree of freedom. This can lead to the appearance of chiral coupling [10] between the quantum emitters and propagating electromagnetic fields: the strength of coupling in this case strongly depends on whether the light wave propagates in forward or backward direction. In the extreme limit it leads to a one-way emitter-mode coupling with absent back reflection, and, therefore, with a unidirectional emitter-emitter interaction mediated by this mode. Such a propagation direction-dependent atom-field coupling strongly modifies optical properties of light-matter interfaces [11–14], and allows to observe novel quantum mechanical phenomena.

The goal. The main goal of this thesis is to discover the manifestation of the interference phenomenon in the radiative properties of individual quantum emitters and their ensembles, which interact with electromagnetic modes of different nanophotonic structures, with account for chiral interactions.

Scientific tasks. With regard to the goal above, we can formulate the following scientific tasks (problems to consider):

- Analyzing collective states with low radiation losses in a periodic subdiffractional chain of two-level atoms in free-space, and in proximity of dielectric nanofiber.
- Quantifying, and explaining chiral sub- and superradiance in a system that is a chain of two-level atoms unidirectionally coupled to a guided mode.
- Studying the temporal dynamics and spectral properties of a quantum emitter with multiple excited states in the vicinity of an anisotropic metasurface.
- Explore the possibility to asymmetrically couple circular dipole transitions of a V-type atom put in the vicinity of a plasmonic dimer formed by two asymmetric scatterers - prolate ellipsoids.

Scientific statements:

- In periodic subdiffractional chains consisting of N dipoles there exist modes with low radiation losses at a particular separation distance much smaller than the resonant wavelength of an individual dipole. This optimal period for large N can be found from the flat-band condition right at the band-edge. The radiation losses of such modes decrease as N^{α} with $\alpha < -6$, contrary to a well known N^{-3} behavior observed for non-optimal period. These extremely low radiation losses are a result of simultaneous minimization of multipolar contributions to the radiated field up to high multipolar order.
- For a perfectly asymmetric interaction of N two-level quantum emitters through a single guided mode, the collective spontaneous emission rate in case of superradiance is $N\Gamma_g$, while for subradiance it becomes 0 for even N, and Γ_g/N for odd N. The latter happens as a result of imperfect destructive interference between the decay channels.
- When coupling the transitions in a multilevel quantum emitter through the modes of an anisotropic metasurface, it is possible to achieve asymmetry in the excitation transfer dynamics. This asymmetry appears only if the quantization axis is tilted with respect to high-symmetry planes, and if the dressed states of the emitter are not degenerate. The effect arises from the phaseshift in the interference part of the temporal dynamics, and it is prominent in both detected temporal intensity or the total emitted light spectrum, making them dependent on the spin orientation of the initially excited state.
- By using a plasmonic dimer structure consisting of two anisotropic dipole scatterers (prolate ellipsoidal particles), one can achieve an

asymmetric coupling of circularly polarized transitions in a single V-type quantum emitter. This coupling asymmetry results in an uneven steady-state populations of the excited states even when pumping strengths for both transitions are equal, and it also makes the optical response of the system being strongly dependent on the local helicity of the total field at the atomic position.

Scientific novelty. The novelty and practical importance of the research results can be formulated as follows:

- The emergence of long-lived states in a system consisting of a periodic chain of atoms polarized perpendicular to the chain axis has been studied theoretically. It is shown that with the right choice of the system period, it is possible to achieve a significant increase in the lifetime of such states, as well as the fact that their lifetimes can grow much faster with the increasing system size than was shown previously. The mechanism of the appearance of such states is revealed, which is associated with the interaction of the eigenmodes of the system and destructive interference of their constituents. The mode interaction becomes possible due to the flattening of the dispersion curve, and the appearance of the inflection point. Moreover, the multipole analysis was performed, and it showed that such states allow for the simultaneous reduction of multipolar contributions up to a high multipolar order.
- The rates of sub- and superradiance for a system of atoms strongly asymmetrically interacting through the guided mode have been obtained theoretically, the mechanism of the phenomenon and the reasons for the deviations from the symmetric interaction case are explained.
- The effect of symmetry breaking of direct and reverse electron transitions between the excited states of a quantum emitter interacting with the modes of the photonic structure is theoretically predicted. In a simple model, criteria for the observation of such an asymmetry are derived and explicitly formulated. The effect of this phenomenon on the physically measurable quantities was studied (intensity dynamics and spectrum of the emitted light). A numerical calculation of the temporal intensity dynamics, and also the detected spectra for an emitter located near an anisotropic metasurface is carried out.
- It is also shown that for an atom with two circularly polarized transition dipole moments (V-type level structure) one can realize a strongly asymmetric coupling of these transitions by placing such an atom in the vicinity of a plasmonic dimer consisting of two geometrically asymmetric dipole scatterers, which were taken to be prolate ellipsoids

made of silver. We demonstrated that such an asymmetric coupling leads to a unidirectional excitation transfer between the excited states. We have demonstrated that if one illuminates the system with a plane wave, which induces equal pumping rates (the respective Rabi frequencies) on both transitions, then the populations of the excited states will be unequal due to the asymmetric coupling. Moreover, we demonstrated that the response of the system strongly depends on the local helicity of the total field at the atomic position.

Practical significance. The research carried out within the framework of the dissertation are valuable from the point of view of fundamental science, since in it we studied different physical effects and clarified the mechanisms of their occurrence, and we also derived the conditions for their observation. Of a special interest some of the presented results are for the modern rapidly developing field of waveguide quantum electrodynamics in particular, and quantum nanophotonics in general. From a practical point of view, the phenomena studied can serve for the development of new quantum nanophotonic devices. In particular, the dependence of the response of the system on the orientation of the initially excited electron spin in a quantum emitter can potentially be used as the basis for the creation of nonreciprocal optical devices. This can be done if the spin (or polarization) of the field incident on the system will be also coupled to the direction of propagation - a situation which is called spin-momentum locking. In addition, the knowledge about the occurrence mechanism of long-lived optical states in one-dimensional chains of dipole scatterers can be extremely useful in the development of optical resonators, hybrid waveguide structures, and in the applications related to quantum technologies like communication, computing, and metrology.

Reliability and the validity:

The reliability degree of the results of studies conducted by the applicant is based on the use of generally accepted theoretical approaches, and a clear indication of the approximations used in order to obtain analytical results. In addition, these results are consistent with those previously obtained by other researchers when considering the relevant limits. Some of the observed effects were also demonstrated during the numerical simulations for realistic structures by the author's colleagues, however, these results are not presented in this thesis. Moreover, the reliability of the results is due to their approbation at international scientific conferences, scientific seminars, publication of articles in international peer-reviewed journals.

Approbation. Approbation of the scientific research results was confirmed by 9 public reports at Russian and international conferences

over the past 3 years. The applicant's research was also acknowledged and supported from funds in the form of grants and scholarships: The Ostrogradski Scholarship of the Embassy of France in Russia for a scientific internship in the Kastler-Brossel Laboratory, University of the Sorbonne, Russian Foundation for Basic Research, a grant from the Foundation for the Advancement of Theoretical Physics and Mathematics "BASIS", a grant from the Committee for Science and Higher Education in St. Petersburg.

Author contribution. The author's contribution to this work consists in constructing theoretical models, obtaining analytical results, analyzing the obtained results, explaining the studied physical effects, finding out the mechanisms of their occurrence, and also in performing the numerical calculations. The author not only contributed significantly to the solution of the problems under consideration, but also to their formulation.

The scientific statements submitted for defense fully reflect the personal contribution of the author to the work.

Publications. The main content of the research work (dissertation) is published in 7 articles, of which 7 publications were published in peer-reviewed journals indexed by Web of Science or Scopus, 7 publications were published in journals from the list of Higher Attestation Commission. Out of these 7 publications, 4 were published in American Physical Society regular journals, while other 3 as peer-reviewed conference proceedings.

This thesis consists of 3 chapters, and 4 appendices. The thesis is 247 pages long, has 34 figures, and 192 references.

Main contents of the work:

Increasing interest in the subject of quantum emitters coupled with or through the modes of different nanophotonic structures has been stimulated by a huge success in experimental relizations of such systems. For instance, it became possible to arrange atoms in 1D [15], 2D [16], and 3D [17] ordered arrays in a controllable way. Simultaneously, quasi-1D systems gained a special attention as a possible platform for quantum light-matter interfaces in the context of waveguide-QED [18;19] - a modern and rapidly developing field of research in which many remarkable results have been already demonstrated experimentally such as Bragg reflection from just $\sim$ 1000 atoms [20], generation of single photons [21], and observation of sub-, and superradiance [22], to mention a few.

In this regard, a new field of research has emerged called chiral quantum optics [10], where the asymmetric interaction of quantum emitters with the photonic modes propagating in opposite directions arises as a result, for example, of non-zero tranversal component of the optical spin momentum density [23]. This area of research is especially important for the development of nanophotonic devices operating at few-photon level: optical circulators [12], optical diodes for a single-photon [13], a single-atom optical switches [14], deterministic single-photon emitters based on a quantum dot coupled to a waveguide [24], and others.

As an alternative to atoms and quantum dots, semiconducting two-dimensional materials is another promising platform for studying chiral interactions [25], where chirality is provided by the circularly polarized optical transitions associated with spin states of valley electrons. The important progress has been recently demonstrated in coupling excitons in such 2D materials with plasmonic waveguides [26], and metasurfaces [27–29], for instance. The latter are naturally considered as photonic counterparts to two-dimensional semiconductor materials, and have already demonstrated the unprecedented flexibility in optical properties.

All of the mentioned above confirms that quantum emitters coupled with the electromagnetic modes of different nanophotonic structures is a very versatile tool not only to investigate exotic effects in light-matter interaction from a point of view of a fundamental science, but also a quite promising platform for future optical devices working at a few-particle level.

Now, below we provide a quick overview of the presented work, highlighting the most important results.

In **the first chapter**, the author studied subradiant states (with very large radiative lifetimes) in a system consisting of two-level atoms arranged

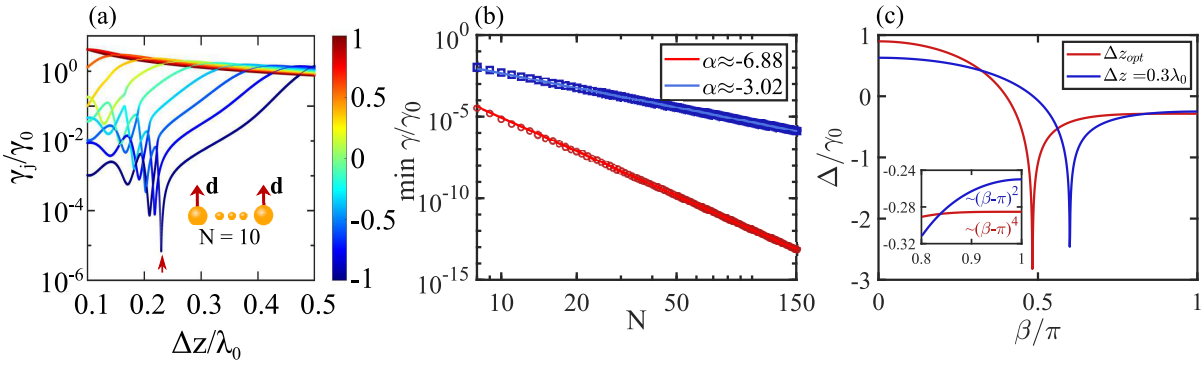

Figure 1 — (a) Emission rates versus system period for a chain of $N = 10$ atoms with transverse dipole moments, the color represents the average correlation between the dipole moments of the neighboring atoms. Red arrow specifies a state of interest. (b) Scaling of the emission rate with N for some fixed period (blue for $\Delta z = 0.3\lambda_0$), and for the subradiant state identified by the red arrow in (a) (red). (c) Dispersion of eigenwaves in an infinite chain of atoms. For the same periods as in (b). Note how flat the dispersion becomes for Δz_{opt}

in a periodic subdiffractional chain. It was found that there are specific periods of the system at which certain states close to the band-edge have a significantly smaller emission rate (see Fig. 1 (a)), and such states were found only for the case of dipole moments transversally oriented with respect to the chain axis. These states were found to have an unusual scaling of the emission rate with the number of atoms N, namely, it falls down much faster than it was known before for similar systems - $\gamma \sim N^{-6.88}$ instead of the usual $\gamma \sim N^{-3}$ scaling law [30–32] (see Fig. 1 (b)). By considering an infinite chain rather than a finite one, we managed to obtain the equation which defines an exact limiting value for the period at which the most long-lived state occurs. It turned out that it is related to a period at which the dispersion becomes flat at the band-edge: instead of $\sim (\beta - \pi)^2$ behavior that is typical for such systems, it starts to demonstrate $\sim (\beta - \pi)^4$ dependence on the dimensionless quasi-wavenumber $\beta = k_z \Delta z$ (see Fig. 1 (c)), a situation that is known as Degenerate Band Edge (DBE), first predicted theoretically for photonic crystals [33].

Moreover, it was found that the corresponding eigenstate (distribution of the excitation among the atoms, or, equivalently, distribution of dipole moments in a chain) for these strongly subradiant states is much more localized (see Fig. 2 (a)). We empirically found that this state can be well approximated by two dominant contributions of the basis states from the tight-binding problem solution (see Fig. 2 (b)), namely, that it can be approximately represented as $\sim C_N \sin\left(\frac{\pi N n}{N+1}\right) + C_{N-2} \sin\left(\frac{\pi(N-2)n}{N+1}\right)$. It is also of interest that these two contributions interfere destructively as

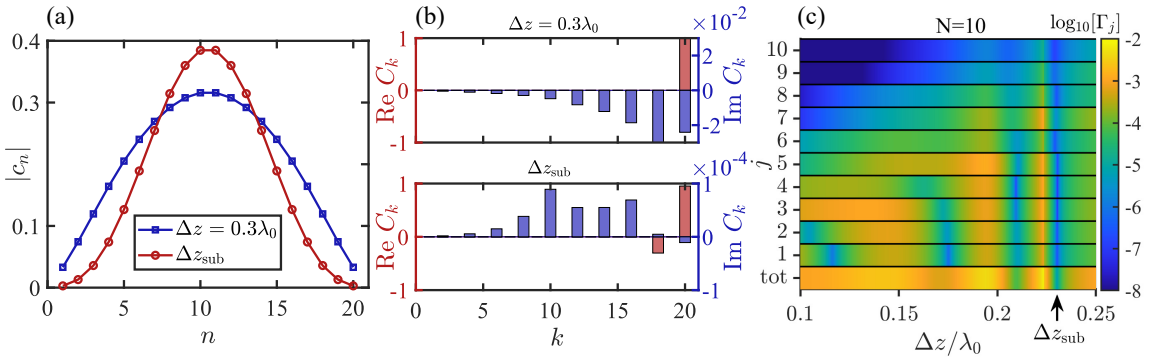

Figure 2 — (a) The absolute value of the probability amplitude of atom n to be excited for period $\Delta z = 0.3\lambda_0$ (blue), and optimal period $\Delta z_{\rm sub}$ (red). (b) Expansion of the eigenstates from (a) in a basis of the tight-binding solution in a form $C_k\psi^{(k)}$. (c) Expansion of the total emission rate Γ_j in terms of Vector Spherical Harmonics contributions with order j versus the system period Δz. Note a point specifying $\Delta z_{\rm sub}$, and how many contributions Γ_j experience a local minima close to this point.

$\mathrm{Re}\,[C_N C_{N-2}] < 0$, and the reduction of the emission rate for this eigenstate can be attributed to this destructive interference. This finding also shed light on the relation between the formation of the long-lived band-edge state, and band-edge degeneracy. As the dispersion at a certain value of the period becomes flat, than the corresponding eigenmodes have very close values of eigenfrequencies (real parts of the corresponding eigenvalues). However, the states N, and $N-2$, which have the same symmetry with respect to the reflection around the system's central point, are not allowed to have the same values of eigenfrequencies. Therefore, the avoided crossing takes place, which "mixes" these eigenstates (Fig. 2 (b), bottom plot). At a certain period these states are mixed in such a way that one of them becomes even more subradiant due to the aforementioned destructive interference of the constituent components.

There is also another peculiar property of such a subradiant state, which can be found if one performs the multipolar decomposition of the emission rate. By expanding the total value of it into contributions of Vector Spherical Harmonics (VSHs) of different orders j as $\Gamma = \sum_j \Gamma_j$, and plotting them versus the period Δz, it can be seen from Fig. 2 (c) that in a region around $\Delta z_{\rm sub}$ functions Γ_j experience a local minima simultaneously for all Γ_j up to large values of j: if there are $N = 10$ atoms this happens at least for Γ_j with j up to 10. This situation is somewhat rare as usually the reduction of the radiated power into the far-field is related to the decrease of the lowest order multipoles as they contribute the most to the total value of the spontaneous emission Γ. The reason why many Γ_j are simultaneously reduced for this state can be easily understood if we recall that

the corresponding eigenstate can be roughly approximated by the expression $\sim C_N \sin\left(\frac{\pi N n}{N+1}\right) + C_{N-2} \sin\left(\frac{\pi(N-2)n}{N+1}\right)$. For large enough $N \gg 1$, the functions $\sin\left(\frac{\pi N n}{N+1}\right)$, and $\sin\left(\frac{\pi(N-2)n}{N+1}\right)$ are very similar to each other. Therefore, the multipolar contents of the fields emitted by the system with dipole moments destributed according to these functions are also similar. Taking into account that $\mathrm{Re}\,[C_N C_{N-2}] < 0$, the destructive interference of the two allows for many Γ_j to be minimized simultaneously.

In the first chapter we mostly discuss the appearance of strongly subradiant states in periodic arrays of two-level atoms which interact through a vacuum dipole-dipole interaction. At first glance it might seem that such a phenomenon is an exclusive feature of this particular type of interaction, and that the presence of other interaction channels might lead to the disappearance of such non-radiative states. However, as we show in the main text, this is not true at least for a particular additional interaction channel, which was taken to be the coupling through a single guided mode of an optical nanofiber. We have shown that not only the aforementioned subradiant states are present, but also states of two other types: 1) the subradiant states at the first Bragg resonance for the guided mode, and 2) the subradiant states which arise as a result of the interference between the two interaction channels (vacuum dipole-dipole coupling, and interaction via the guided mode). We discuss the emission rate scaling with the system size for this case, and also show how do these states are prominent in the optical properties of the system like single photon transmission and reflection spectra.

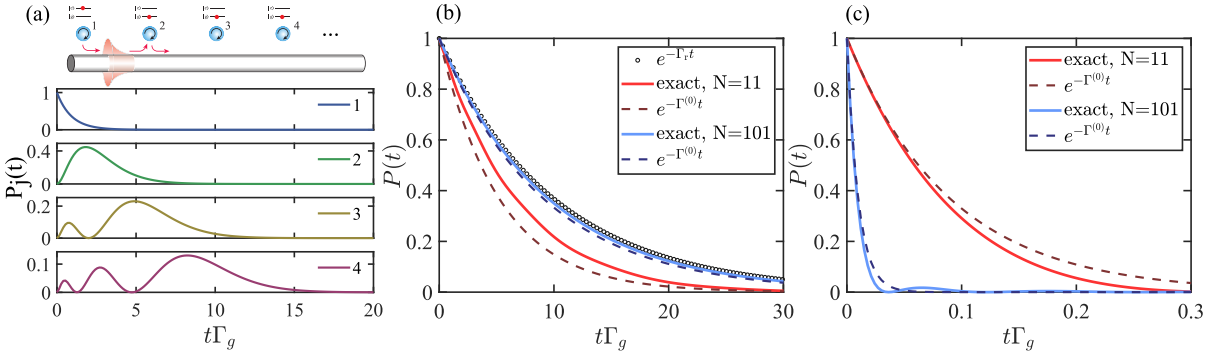

Figure 3 — (a) Transport of a single excitation for a system of atoms unidirectionally coupled through a guided mode. (b)-(c) Collective dynamics for subradiance (b), and superradiance (c). Solid lines are the exact solutions, while dashed lines - exponential functions with a decay rate $\Gamma^{(0)}$ substituted. Emission rate solely into non-guided (radiation) modes $e^{-\Gamma_r t}$ is in dotted black. For all figure we set $\Gamma_g = 10, \Gamma_r = 1$

In **the second chapter**, the author studies the collective emission of a system of N two-level atoms, which are unidirectionally coupled through a single guided mode. The unidirectionality of atom-mode interaction can

arise due to the spin-orbit interaction of light [23; 34] for a surface localized propagating mode, which leads to the dependence of the local helicity on the propagation direction: forward-, and backward propagating modes have different helicities in this case. As a result, the modes propagating in opposite directions can couple differently to an atom with circularly polarized active transition dipole moment if the latter is properly oriented in space [35].

As a first step, the single excitation transport problem has been solved, and the analytical solution was obtained in a form:

$$C_k(t) = e^{-\Gamma_{\text{tot}} t/2 + i\varphi_{k,1}} L_{k-1}^{(-1)}(\Gamma_g t), \tag{1}$$

where $C_k(t)$ is the probability amplitude for atom k to be excited at time t, $\Gamma_{\text{tot}} = \Gamma_g + \Gamma_r$ is the total emission rate into both guided Γ_g, and unguided (radiation) modes Γ_r, $\varphi_{k,1}$ is the phase acquired by a photon during the propagation from atom 1 to atom k, and $L_{k-1}^{(-1)}(x)$ is a generalized Laguerre polynomial of index -1, and degree $k-1$. The respective probabilities $P_k(t) = |C_k(t)|^2$ are shown in Fig. 3 (a) for first 4 atoms. One of the features of the transport problem being solved is that the dynamics is not described through hyperbolic, and trigonometric functions, as it happens for a symmetrically interacting emitters, but it is rather of a polynomial type as a result of the degeneracy of the problem. Moreover, we found that the number of excitation absorption-emission events is strictly related to the ordinal atom number in a chain k as $k-1$, which directly follows from the mathematical properties of the $L_{k-1}^{(-1)}(x)$ function.

Apart from solving a toy model with a perfectly unidirectional excitation transfer between the atoms, for which an exact analytical solution of a single excitation transport problem was obtained, we also considered a more realistic problem. In order to do that, we took a metallic nanowire made of silver that supports a propagating surface plasmon polariton that demonstrates a strong spin-momentum locking effect. Even though it does not allow for a perfectly asymmetric interaction of atoms, we showed that the asymmetry of interaction exceeds the value of 10 for spatially separated atoms. With the help of the resolvent formalism [4], we were able to find the probabilities for the excitation to be transferred between the atoms, and then compare the obtained results with the analytical expressions describing the solution for a toy model with equivalent parameters. The comparison took into account the averaging over the random deviations of atomic positions along the nanowire, and it is demonstrated that the dynamics provided by Eq. (6) is in a very good agreement with calculations obtained for a metallic nanowire despite the imperfect coupling asymmetry.

From the solution of the transport problem, it was possible to solve the dynamics for an arbitrary state in a single excitation domain. Some specific

collective states like sub- and superradiant states are of special interest in this regard as under certain conditions in the case of symmetric coupling they demonstrate either the supression or the enhancement of the emission rate, correspondingly. If we set the initial state to be of the form $|D\rangle = \sum_{k=1}^{N} \frac{1}{\sqrt{N}} |e_k\rangle |g\rangle^{N-1}$ (symmetric Dicke state), then one can find that:

$$C_{\text{sub}}(t) = \frac{e^{-\Gamma_{\text{tot}} t/2}}{N} \sum_{k=1}^{N} (N - (k-1))(-1)^{k-1} L_{k-1}^{(-1)}(\Gamma_g t),$$
$$C_{\text{sup}}(t) = \frac{e^{-\Gamma_{\text{tot}} t/2}}{N} L_{N-1}^{(1)}(\Gamma_g t), \tag{2}$$

where $C_{\text{sub/sup}}(t)$ are the probability amplitudes for the system to remain in a state $|D\rangle$, if any two neighboring atoms are emitting photons out-of-/in-phase. Even though the dynamics is polynomial, not exponential, we can still find the emission rate of the system at small time arguments given by: $P_{|D\rangle}(t) \approx 1 - \Gamma^{(0)} t + ...$

The author found that the approximate emission rate in the guided mode for the superradiant case is equal to $\Gamma_g^{(0)} = N\Gamma_g$ (similar to the symmetric case), while for the subradiance the emission rate becomes $\Gamma_g^{(0)} = \Gamma_g \frac{1-(-1)^N}{2N}$ (instead of 0 for the symmetric case). As one can see, the chiral subradiant emission rate depends on whether there are even or odd number of atoms N. The author reveals the reason for this to happen, namely, it is due to the imperfect destructive interference between the pathways for a system to emit a photon as a natural consequence of the interaction unidirectionality.

From Fig. 3 (b), one can see that for the collective subradiant emission, the bigger the system, the smaller discrepancy there is between the curve given by Eq. (2) (top), and the $e^{-\Gamma^{(0)} t}$ function. Therefore, one can conclude, that for a sufficiently large systems the collective subradiant emission rate adequately describes the temporal dynamics of the system. However, as one can see from Fig. 3 (c), this is not true for superradiance: for large N the $e^{-\Gamma^{(0)} t}$ function and the dynamics given by Eq. (2) (bottom) are in a good agreement only for very small values of $\Gamma_g t$, while at later times there is some small probability for the system to re-absorb the emitted photon. This behavior has been straightforwardly linked to the mathematical properties of the function $L_{N-1}^{(1)}(x)$ as it has $N-1$ real positive roots, therefore, the are $N-1$ acts of the photon re-absorption, but only the first one is observed, while the rest are supressed by an overall $e^{-\Gamma_{\text{tot}} t}$ factor.

In **the third chapter**, the author considers the problem of excitation transfer between the excited states of a quantum emitter having an active $s \leftrightarrow p$ transition, and put in the proximity of some nanophotonic environment (see Fig. 4 (a)), which was an anisotropic metasurface in our case. It was

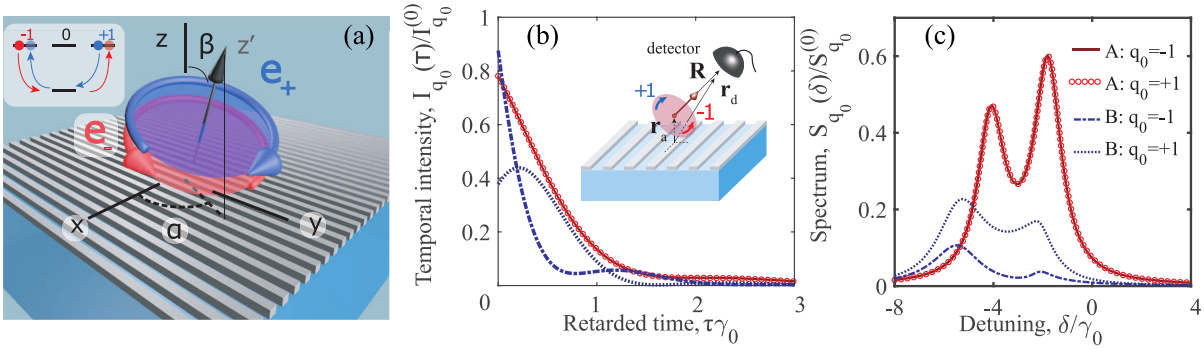

Figure 4 — (a) Pictorial representation of the system studied: an atom with a triply degenerate excited state is put in the vicinity of a nanophotonic structure (anisotropic metasurface). Note that the transition dipole moments are arbitrarily oriented here. Temporal intensity (b), and the total emitted light spectra (c) for an atom initially excited in state $|e_{q_0}\rangle$. Red lines/markers correspond to the isotropic metasurface, while blue - for the anisotropic one. Note that in the latter case both intensity and spectra differ for different initial excited states

shown that under certain conditions, the excitation transfer probability differs in forward and backward directions: $P_{q,q'}(t) \neq P_{q',q}(t)$. As an example we took q,$q' \in \{-1, +1\}$, and obtained:

$$P_{-,+}(t) - P_{+,-}(t) = f(\alpha,\beta) \sum_{(k,l)}^{(x,y),(y,z),(z,x)} e^{(g_k''+g_l'')t} \sin\left((g_k' - g_l')\, t\right),$$
$$f(\alpha,\beta) = \tfrac{1}{8}\sin(2\alpha)\sin(2\beta)\sin(\beta), \qquad (3)$$

where g_k',g_k'' are related to the frequencies of the eigenstates, and the modified emission rates, respectively, while α, β are the angles defining the orientation of emitters quantization axis (and, therefore, the orientation of transition dipole moments). From the equation above it follows that the transfer asymmetry $P_{-,+}(t) \neq P_{+,-1}(t)$ happens if the transition dipole moments of the emitter are arbitrarily oriented with respect to high symmetry directions of the problem, and, when the nanostructure is locally fully anisotropic. The former means that the local quantization z' axis of the emitter (the dipole moment of the π-polarized transition) should not lie in the planes formed by principal axes of the metasurface. Mathematically speaking, it provides the restrictions on the values of rotation angles: $\alpha \neq \frac{\pi}{2}m$, and $\beta \neq \frac{\pi}{2}m'$, where m, m' are integer numbers. In the latter "locally fully anisotropic" means that from a point of view of an emitter all 3 principal exes of the structure are physically unequivalent, or, one can say that $g_k' \neq g_l'$ for any k,l. One can also state that the condition $g_k' \neq g_l'$ means that the eigenstates formed due to the interaction of the emitter with the modes of the nanostructure should not be degenerate.

The author also analyzed the transition probabilities in the basis of eigenstates, and a special interest here is in the interference part of the dynamics, which reads as:

$$P_{q',q}^{(k,l)}(t) = 2\left|C_{k,l}^{(q',q)}\right| \cos\left[(g_k' - g_l')t - \varphi_{k,l}^{(q',q)}\right] e^{(g_k''+g_l'')t}, \tag{4}$$

where $C_{k,l}^{(q',q)}$ is a complex-valued constant, while $\varphi_{k,l}^{(q',q)} = \arg\left(C_{k,l}^{(q',q)}\right)$ is it's phase, both of these constants depend solely on the rotation angles α, β. From the mathematical definition of the latter we found that $\varphi_{k,l}^{(q',q)} = -\varphi_{k,l}^{(q,q')}$, from which one can conclude that the studied effect has a nature of a phase-shift in the dynamics of the transition probabilities. It occurs as a result of interference between the eigenstates of the emitter appearing due to the interaction with the eletromagnetic modes of the environment.

As the transision of an electron between the excited states of the emitter can not be measured directly, we also studied how the internal dynamics of the system with such a broken symmetry affects the measurable quantities: temporal detected intensity, and the total emitted light spectrum. By exploiting the eigenstate picture once again, we obtained the following expressions:

$$I_{q_0}(t) = \langle\psi(t)|\hat{\mathbf{E}}^{(-)}(\mathbf{r_d})\hat{\mathbf{E}}^{(+)}(\mathbf{r_d})|\psi(t)\rangle \approx 16\pi^2 k_0^4 |\mathbf{d}|^2 \left|\sum_j \mathbf{f_j} e^{-ig_j\tau}\right|^2,$$

$$S_{q_0}(\omega) = \int_0^\infty dt_2 \int_0^\infty dt_1 \left[e^{-i\omega(t_2-t_1)}\langle\hat{\mathbf{E}}^{(-)}(\mathbf{r},t_2)\hat{\mathbf{E}}^{(+)}(\mathbf{r},t_1)\rangle\right] \approx \left|\sum_j \frac{\boldsymbol{f}_j^{q_0}(\mathbf{r_d},\mathbf{r_a})}{(\delta - g_j)}\right|^2, \tag{5}$$

where $q_0 \in \{-1,0,+1\}$ is the label for the initially excited state, $\mathbf{r_d}$ is the detector position, $\delta = \omega - \omega_0$ is the detuning from the bare atomic transition frequency, $\tau = t - |\mathbf{R}|/c$ is the retarded time, and the vectorial quantities $\mathbf{f_j}, \boldsymbol{f}_j^{q_0}(\mathbf{r_d},\mathbf{r_a})$ are related to the far-fields produced by each eigenstate j (please, see the main text for more details). These functions obey the property $\mathbf{A}(q_0 = +1) = -\mathbf{A}^*(q_0 = -1)$, which leads to both intensity, and spectrum being dependent upon the sign of q_0. Indeed, as one can see from Fig. 4 (b), and (c), it results in the optical properties of an overall system becoming dependent upon the orientation of the spin of the initially excited state, provided that the conditions discussed previously are satisfied.

More than that, it was shown that if one puts an atom with two excited states (also called a V-type atom) close to a structure made of two plasmonic anisotropic scatterers (the author proposed prolate ellipsoids, see Fig. 5 (a), (c)), it is possible to obtain a strong asymmetry in the coupling constants of transitions $|g_{+,-}|/|g_{-.+}| \gg 1 (\ll 1)$. The first proposed scheme is based

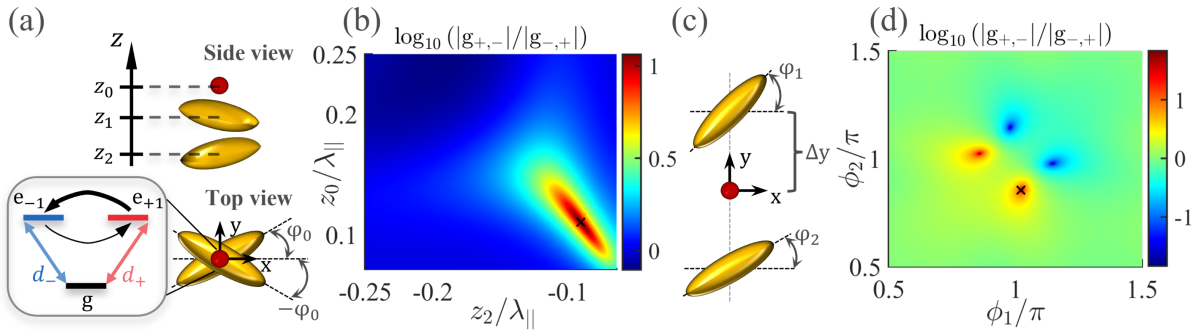

Figure 5 — (a) A scheme of the system under consideration: a dimer consisting of two ellipsoidal particles with their long axes being in the parallel planes, and rotated with respect to each other on angle $2\varphi_0$. V-type atom with rotating transition dipole moments is placed nearby, and centers of both scatterers and the atom are on the z-axis. (b) Dependence of the coupling constant asymmetry on the coordinate of the atom z_0, and one of the scatterers z_2, here $z_1 = 0$, $\varphi_0 = \pi/8$. $\lambda_{||}$ is the wavelength at which $\mathrm{Im}\,[\tilde{\alpha}_{xx}(\omega)]$ (polarizability along the long principal axis of the ellipsoid) is maximal. (c) Another scheme in which both particles and the atom are in the xy-plane with two long axes of the scatterers being rotated independently, while the atom is positioned right in between them at a distance Δy. (d) Coupling asymmetry versus orientation angles φ_1, φ_2. The atom-scatterers distance is $\Delta y = a_x + \lambda_{||}/20$, where a_x is the long semiaxis of each ellipsoid. The black crosses in (b), (d) indicate points of maximal coupling asymmetry

on a known plasmonic Born-Kuhn model (see Fig. 5 (a)), where the long axes of the ellipsoids are assumed to be in parralel planes (defined by two constant values z_1, z_2, for instance). For the sake if simplicity, the centers of both scatterers, and the atom were taken to be on the z-axis. The second scheme (see Fig. 5 (c)) is quasi-2D, so that both ellipsoids and the atom are in the xy-plane, and the centers of all three are on the y-axis. The geometry in this case is controlled by the distance Δy from the atom to the center of each scatterer, and the rotation angles φ_1, φ_2. As one can see from Fig. 5 (b), (d) both schemes allow for a strong coupling asymmetry, but the latter is preferrable as it grants the possibility to easily switch from $|g_{-,+}|/|g_{+-}| \gg 1$ to $|g_{-,+}|/|g_{+-}| \ll 1$ with a slight change of φ_1, φ_2. Needless to say that geometrically the second scheme is simpler, which might be an advantage if one considers a realistic structure made of a 2D array of such scatterers.

We proceed with the second scheme, and show that it, indeed, allows for an almost unidirectional excitation transport from state $|e_{-1}\rangle$ to state $|e_{+1}\rangle$ as seen from the excitation transfer dynamics in Fig. 6 (b). Interestingly, the dynamics for $P_{+,-}(t)$ can be simply described by the equation we derived in the second chapter $P_{+,-}(t) = e^{-\gamma_{\mathrm{tot}}t}|L_N^{(-1)}(|g_{+,-}|t)|^2$ (for $N = 2$) obtained

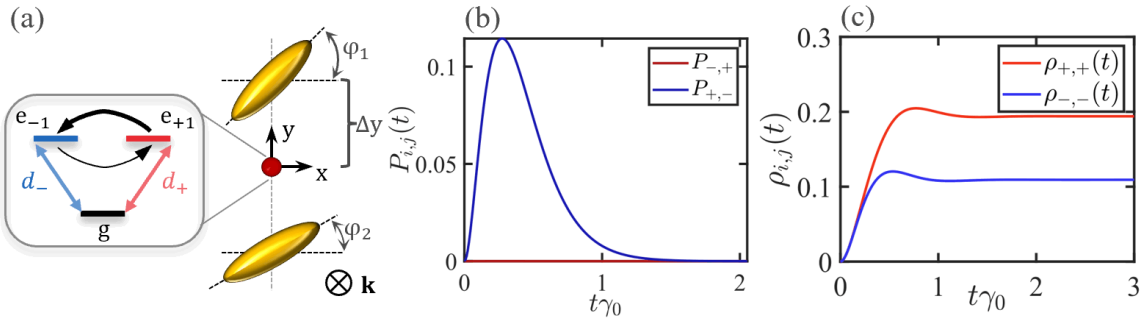

Figure 6 — (a) Scheme of the considered system. Vector **k** defines the propagation direction of the external driving laser field. (b) Asymmetry in the population transfer probabilities $P_{-,+}(t)$, and $P_{+,-}(t)$. Parameters were chosen such that they maximize the coupling asymmetry (indicated by a black cross in Fig. 5 (d)). (c) Populations of the excited states as a function of time under the external pumping. Parameters of the pumping plane wave are chosen such that they maximize the value of $|\rho_{+,+}(\infty) - \rho_{-,-}(\infty)|$, and also provide equal Rabi frequencies for both transitions $\Omega_- = \Omega_+$

for a single excitation transport in a chain of unidirectionally coupled atoms. This is natural as two transitions in a V-type emitter can be thought of as a pair of interacting two-level atoms, which are located at the same spatial point and have corresponding transition dipole moments.

Apart from studying vaccum-induced dynamics, we also study the behavior of the system under the action of an external continuous pumping laser field. In this situation we, first, demonstrated that the coupling asymmetry leads to the unequal stationary populations of the excited states even though the incident plane wave parameters were chosen such that the corresponding pumping rates are equal (the magnitudes of the respective Rabi frequencies obey $\Omega_- = \Omega_+$), which is illustrated in Fig. 6 (c).

Another pumping scheme that was considered is the one presented in Fig. 7 (a), where the parameters of the incident plane wave were tuned such that the total field at the emitter's position selectively interacts with either σ^- or σ^+ transition. Once the interaction is strongly asymmetric $|g_{-,+}|/|g_{+,-}| \gg 1$, for $\Omega_- \neq 0, \Omega_+ = 0$ case, the atom is pumped from the initial state $|g\rangle$ into the $|e_{-1}\rangle$ state, and then can undergo a transition to $|e_+\rangle$ due to the coupling $g_{+,-}$. After a sufficiently long time a stationary population level $\rho_{+,+}(t \to \infty)$ is achieved (see solid red curve in Fig. 7 (b)). However, if $\Omega_+ \neq 0, \Omega_- = 0$, a negligibly small value of the coupling constant $|g_{+,-}|$ compared to any other parameter does not allow for the population transfer, and the excited state on the orthogonal transition remains unpopulated $\rho_{-,-}(t) \approx 0$ (see dashed blue curve in Fig. 7 (b)). The latter essentially means that in this case the atom behaves as a perfect two-level atom, and that the optical response of

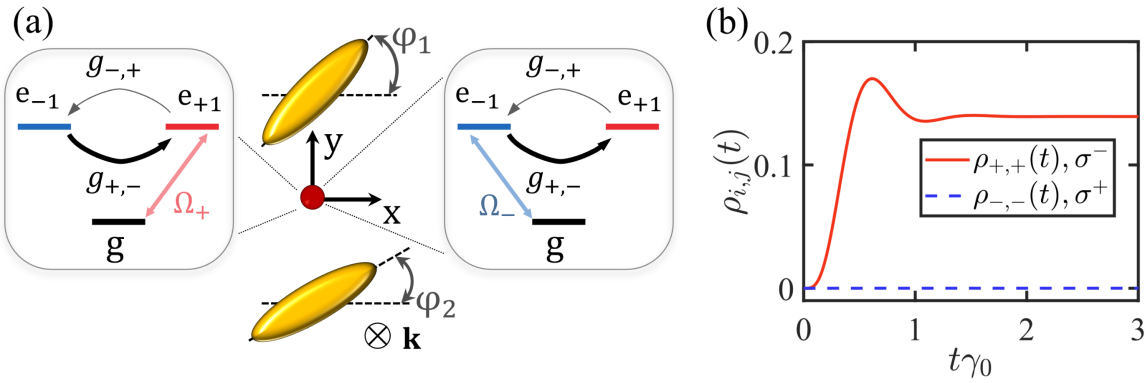

Figure 7 — (a) The sheme providing the selective pumping of each transition in a V-type emitter. (b) The evolution of excited states populations on the transition that is orthogonal to the one being under the action of the laser field. The solid red curve is the population $\rho_{+,+}(t)$ for the σ^- polarization of the total field at the atomic position (right situation in (a)), while blue dashed is the $\rho_{-,-}(t)$ population for σ^+-polarized pumping (left situation in (a))

the atom+nanostructure system strongly depends on the helicity of the total field at the atomic position.

In the **conclusion** the key results of this thesis are highlighted, as well as the future directions of work are discussed.

1. In the first chapter we have discussed the appearance of strongly subradiant states at the edge of a Brilluoin zone in subdiffractional periodic chains of two-level atoms, where the enhancement in lifetimes of such states was possible due to the mixing of eigenmodes, and the consequent destructive interference of their constituents. This led to several distinct features of such states as much faster decrease of the emission rate with the system size ($\sim N^{-6.8}$ instead of a regular $\sim N^{-3}$ dependency), as well as a better eigenstate localization due to the suppression of dipole moments at the edges of a chain. More than that, the aforementioned destructive interference is found to lead to a simultaneous reduction of many multipolar contributions into the far-field radiation for this kind of subradiant state. We also demonstrated that the presence of an additional interaction channel, apart from the vacuum dipole-dipole interaction, does not necessarily lead to the disappearance of this effect, and we have shown this for the case of atomic chain near a single-mode optical nanofiber.
2. In the second chapter we have revealed a peculiar polynomial temporal behavior of a single excitation transport in a one-dimensional chain of atoms, which are unidirectionally coupled through a guided mode. We have solved the problem analytically for arbitrary system sizes, and

based on this result, we have also estimated the approximate collective sub-, and superradiant emission rates. For subradiance it was found to be different from the case of symmetrically coupled atoms, which is given by the Dicke theory. In order to reveal the reason for this discrepancy to appear, we have analyzed the single-excitation dynamics in the lowest non-vanishing order of perturbation theory, and found that it happens due to the imperfect destructive interference.

3. In the third chapter we have demonstrated how, by using an anisotropic photonic structure (metasurface), and by controlling the orientation of transition dipole moments in an $s \rightarrow p$ atom, one can break the symmetry of forward, and backward quantum-mechanical processess related to the probabilities for an electron to make a transition from one excited states to another. We derived analytically the requirements for the observation of this phenomenon, and also attributed it to the interference of the eigenstates, which appear as a result of emitter's interaction with the electromagnetic modes of the environment. It is demonstrated that this interference gives rise to a phaseshift in the transition probability dynamics. We have also shown how these unequal transition probabilities in such a system affect the measurable quantities: detected light intensity dynamics, and total emitted light spectrum.
4. In the third chapter we have also proposed another way to break this symmetry in transitions by using a simple plasmonic structure - a dimer made of two asymmetric dipolar matallic scatterers. By properly tuning the geometry of the system, we have shown that it is possible to almost completely forbid transitions of an electron in one direction between the excited states with circularly polarized dipole moments in a V-type atom. We have also analyzed the dynamics of the system under the external continuous-wave pumping, and demonstrated that, for instance, the steady-state populations of excited states can be unequal due to their asymmetric coupling despite the Rabi frequencies for corresponding transitions being equal. More than that, it is shown that in this case the response of the system strongly depends on the local helicity of the total field at the position of the atom.

The results presented in this thesis were published in the following **publications**:

I. Extremely subradiant states in a periodic one-dimensional atomic array / **Kornovan D. F.**, Corzo N. V., Laurat J., Sheremet A. S. // Phys. Rev. A. — 2019. — Dec. — Vol. 100. — P. 063832. — URL: https://link.aps.org/doi/10.1103/PhysRevA.100.063832.

II. Noninverse dynamics of a quantum emitter coupled to a fully anisotropic environment / **Kornovan D. F.**, Petrov M. I., Iorsh I. V. // Phys. Rev. A. — 2019. — Sep. — Vol. 100. — P. 033840. — URL: https://link.aps.org/doi/10.1103/PhysRevA.100.033840.

III. Strong coupling and non-reciprocity in the dynamics of a V-atom placed near an anisotropic metasurface / **Kornovan D. F.**, Petrov M. I., Iorsh I. V. // 2018 12th International Congress on Artificial Materials for NovelWave Phenomena (Metamaterials). — 2018. — Aug. — Pp. 228–230. — URL: https://ieeexplore.ieee.org/document/8534098

IV. Temporal dynamics of a quantum emitter with multiple excited states in the vicinity of an anisotropic metasurface / **Kornovan D. F.** , Toftul I. D., Chebykin A. V., Petrov M. I., Iorsh I. V. — Vol. 1092. — IOP Publishing, 2018. — sep. — P. 012063. — URL: https://iopscience.iop.org/article/10.1088/1742-6596/1092/1/012063.

V. Transport and collective radiance in a basic quantum chiral optical model / **Kornovan D. F.**, Petrov M. I., Iorsh I. V. // Phys. Rev. B. — 2017. — Sep. — Vol. 96. — P. 115162. — URL: https://link.aps.org/doi/10.1103/PhysRevB.96.115162.

VI. Light interaction and quantum transport in atomic chain chirally coupled to a waveguide / **Kornovan D. F.**, Sheremet A. S., Iorsh I. V., Petrov M. I. // 2017 11th International Congress on Engineered Materials Platforms for Novel Wave Phenomena (Metamaterials). — 2017. — Aug. — Pp. 262–264. — URL: https://ieeexplore.ieee.org/document/8107912

VII. Collective polaritonic modes in an array of two-level quantum emitters coupled to an optical nanofiber / **Kornovan D. F.**, Sheremet A. S., Petrov M. I. // Phys. Rev. B. — 2016. — Dec. — Vol. 94. — P. 245416. — URL: https://link.aps.org/doi/10.1103/PhysRevB.94.245416.

Реферат

Актуальность. Тематика представленной диссертационной работы имеет значимость для современной и быстроразвивающейся области исследования под названием квантовая нанофотоника. Данная сфера исследования совмещает в себе две другие в контексте взаимодействия света и вещества, а именно: квантовую оптику [1] и нанофотонику [2]. Исторически, квантовая оптика изначально была посвящена изучению статистических свойств света [3], а также описанию взаимодействия излучения с веществом на уровне одиночных частиц - фотонов и атомов [4]. Значительное время ученые в этой области занимались исследованием излучения, которое распространяется в свободном пространстве и его взаимодействием с атомами, находящимися либо в вакууме, либо в высокодобротных резонаторах [5]. В свою очередь, в нанофотонике рассматривается то, каким образом возможно управлять различными степенями свободы света, и его распространением в различных структурах нанофотоники, что стало возможным благодаря существенному технологическому развитию методов фабрикации таких структур.

На пересечении этих двух областей исследования находятся много новых и экзотических физических феноменов: как уже открытых, так и еще неизвестных. В этой связи коллективные эффекты во взаимодействии света и вещества представляют особый интерес, поскольку взаимодействие атом-поле может быть значительно усилено за счет локализации излучения вблизи интерфейсов нанофотонных структур. С этой точки зрения феномены суб- и сверхизлучения [6;7] являются интересными для исследования с возможными приложениями в квантовых технологиях. Будучи хорошо изученными для случая атомных ансамблей в свободном пространстве [8; 9], их характерные особенности в случае наличия взаимодействия посредством мод структур нанофотоники всё ещё не объяснено полностью для многих случаев. Характер взаимодействия атома с полем, помимо упомянутого ранее усиления взаимодействия, также может быть модифицирован путём, например, контроля за поляризационной степенью свободы. Это может привести к возникновению хирального взаимодействия [10] между квантовыми излучателями и распространяющимися электромагнитными полями: случай, когда сила связи значительным образом зависит от того, распространяется ли волна в прямом или обратном направлении. В предельном случае это может привести к полностью однонаправленному взаимодействию излучателя с модой поля с отсутствием отражения назад, и, следовательно, однонаправленным взаимодействием между различными излучателями

через такую моду. Такая зависящая от направления распространения сила связи атом-поле радикально изменяет оптические свойства интерфейсов свет-вещество [11–14], а также позволяет наблюдать различные новые квантово-механические феномены.

Цель исследования. Основная цель данной работы заключается в исследовании различных проявлений явления интерференции в оптических свойствах как одиночных квантовых излучателей (атомов), так и их инсамблей, в случае их взаимодействия с электромагнитными модами различных структур нанофотоники. При этом особое внимание будет уделено возможности реализовать хиральность такого взаимодействия.

Научные задачи. В соответствие с упомянутой выше целью могут бысть сформулированы следующие научные задачи:

- Проанализировать коллективные состояния с низкими рациационными потерями в периодических субдифракционных цепочках двухуровневых атомов, находящихся в вакууме и вблизи диэлектрического нановолокна.
- Описать количественно и качественно хиральное суб- и сверхизлучение в системе, которая представляет из себя цепочку двухуровневых атомов, однонаправленно взаимодействующих посредством волноводной моды.
- Изучить временную динамику и спектральные свойства квантового излучателя с вырождением в возбужденном состоянии, который находится вблизи анизотропной метаповерхности.
- Рассмотреть возможность асимметричной связи циркулярно поляризованных дипольных переходов в излучателе с V-образной структурой уровней, который взаимодействует с модами плазмонного димера, состоящего из двух асимметричных рассеивателей - вытянутых эллипсоидальных частиц.

Основные положения, выносимые на защиту:

- В периодических субдифракционных цепочках, состоящих из N диполей, существуют собственные моды с низкими оптическими потерями для определенных значений периода системы, меньших длины волны, резонансной одиночному диполю. Такое оптимальное значение периода может быть найдено для большого числа диполей N из условия уплощения дисперсии собственных мод на краю зоны Бриллюэна. Темпы эмиссии таких мод спадают как N^{α} с $\alpha < -6$, в отличие от известного закона N^{-3}, наблюдаемого для не оптимального периода. Такие низкие значения радиационных потерь

являются результатом одновременной минимизации мультипольных вкладов в излучаемое системой поле вплоть до мультиполей высоких порядков.

– Для N двухуровневых излучателей, идеально асимметрично взаимодействующих через волноводную моду, коллективный темп спонтанной эмиссии в случае сверхизлучения равен $N\Gamma_g$, тогда как для субизлучения он равен 0 при четных N, и Γ_g/N при нечетных N. Последний факт является следствием неполной деструктивной интерференции между различными способами для системы излучить фотон.
– При взаимодействии переходов в многоуровневом квантовом излучателе через моды анизотропной метаповерхности возможно добиться асимметрии в динамике вероятностей перехода между возбужденными состояниями. Такая асимметрия проявляется только если локальная ось квантования излучателя наклонена по отношению к плоскостям высокой симметрии метаповерхности, а собственные состояния излучателя, обусловленные его взаимодействием с модами структуры, не являются вырожденными. Эффект проявляется в виде фазовой задержки в интерференционных вкладах во временную динамику вероятностей переходов, и проявляется также в зависимости детектируемой интенсивности излучения от времени и в полном излученном системой спектре, что делает обе эти величины зависящими от ориентации спина в начальном состоянии излучателя.
– С помощью плазмонного димера, состоящего из двух анизотропных дипольных рассеивателей (вытянутых эллипсоидальных частиц), возможно реализовать асимметричную связь циркулярно поляризованных переходов в излучателе с V-образной структурой уровней. Такая асимметричная связь приводит к неравной стационарной населенности возбужденных уровней даже при внешней накачке, обеспечивающей равные частоты Раби на обоих переходах. Также асимметрия взаимодействия переходов приводит к сильной зависимости отклика системы от локальной циркулярности полного поля в точке нахождения атома.

Научная новизна данного исследования заключается в следующем:

– Теоретически изучено образование состояний с большими временами жизни в системе, которая представляет из себя периодическую цепочку атомов, дипольные моменты переходов которых перпендикулярны оси цепочки. Показано, что при правильно подобранном периоде системы, возможно добиться существенного увеличения

времени жизни таких состояний, а также то, что время их жизни растет быстрее, чем было показано ранее другими исследователями для состояний близ края зоны Бриллюэна. Выяснен механизм образования этих состояний, который заключается во взаимодействии собственных мод системы и деструктивной интерференции составляющих эти моды вкладов. Взаимодействие собственных мод оказывается возможным благодаря уплощению дисперсии системы на краю зоны и возникновению точки её перегиба. Также проведен мультипольный анализ излучения таких состояний и с его помощью показано, что для таких долгоживущих состояний происходит одновременная минимизация многих мультипольных вкладов вплоть до высоких порядков.

– Рассмотрена задача транспорта одиночного возбуждения в системе атомов, которые однонаправленно взаимодействуют посредством волноводной моды, и показано, что временная динамика передачи возбуждения носит полиномиальный характер. На основе данного результата также исследованы излучательные свойства коллективных одночастичных возбуждений, а именно были впервые аналитически получены значения темпов спонтанной эмиссии для случая суб- и сверхизлучения в такой системе. С помощью теории возмущений на простой теоретической модели объяснена причина отличия полученных значений от уже хорошо известных для случая симметричной связи посредством волноводной моды. Также на примере структуры на основе плазмонного волновода продемонстрировано численным моделированием, что для использования полученных результатов не обязательна идеальная однонаправленность взаимодействия, достаточна его сильная асимметричность.
– Теоретически изучен эффект нарушения симметрии между прямыми и обратными переходами электрона между возбужденными уровнями квантового излучателя с дипольно разрешенным $s \leftrightarrow p$ переходом (трехкратное вырождение возбужденного состояния), который взаимодействует с электромагнитными модами фотонной структуры. Найдены аналитически и явно сформулированы критерии для наблюдения данного эффекта. Также изучено, каким образом он проявляется в экспериментально измеряемых величинах, таких как временная динамика детектируемой интенсивности и полный спектр излученного света. Проведено численное моделирование временной динамики переходов, детектируемой интенсивности и спектров для излучателя, который находится вблизи анизотропной метаповерхности.

– Также впервые теоретически предсказано, что для излучателя с двумя циркулярно-поляризованными дипольными моментами переходов (атом с V-образной структурой уровней) возможно реализовать сильно асимметричное взаимодействие переходов посредством электромагнитных мод структуры, представляющей из себя плазмонный димер, который состоит из двух асимметричных дипольных рассеивателей (вытянутых металлических эллипсоидов). Показано, что асимметричная связь переходов приводит к однонаправленному переносу возбуждения между верхними уровнями излучателя. Предсказано, что если на систему падает плоская электромагнитная волна с параметрами, обеспечивающими одинаковую по силе накачку обоих переходов (одинаковые соответствующие частоты Раби), то в таком случае асимметричное взаимодействие приводит к неравной стационарной населенности возбужденных уровней, а, значит, спиновой поляризации излучателя. Также в работе показано, что отклик такой системы сильно зависит от локальной спиральности полного электрического поля в точке нахождения излучателя.

Практическая значимость. Выполненные в рамках данного диссертационного исследования работы представляют ценность с точки зрения физики как фундаментальной науки, поскольку в работе рассматриваются различные физические эффекты, проясняются механизмы их возникновения, а также устанавливаются условия для их наблюдения. Особый интерес часть из представленных результатов имеют для таких быстроразвивающихся областей как квантовая электродинамика волноводов и квантовая нанофотоника. С практической точки зрения изученные феномены могут послужить фундаментом для разработки новых устройств квантовой нанофотоники. Например, зависимость отклика системы от ориентации начального спина электрона в излучателе может быть потенциально использована для создания невзаимных оптических устройств. Это может быть реализовано, если спин (поляризация) падающего поля будет также связан с направлением распространения волны - эффект под названием спиновая блокировка. Знание механизмов возникновения долгоживущих состояний в одномерных массивах дипольных рассеивателей также может быть крайне полезно при разработке и создании оптических резонаторов, гибридных волноводных структур, и в приложениях, имеющих отношение к квантовым технологиям, а именно в квантовых коммуникациях, вычислениях и метрологии.

Достоверность. Степень достоверности результатов проведенных соискателем исследований основана на использовании общепринятых теоретических подходов, явном указании использованных с целью

получения аналитических результатов приближений. Помимо этого, полученные результаты согласуются с аналогичными результатами, полученными ранее другими исследователями, при рассмотрении необходимых пределов. Некоторые из рассматриваемых на примере простых моделей эффектов были позднее подтверждены при численном моделировании для более реалистичных структур коллегами соискателя, но данные результаты не вошли представленную диссертацию. Также достоверность результатов основана на их аппробации путем представления докладов на международных научных конференциях, семинарах, публикации статей в международных рецензируемых изданиях.

Аппробация работы. Аппробация научных результатов исследования подтверждена 9 публичными выступлениями на всероссийских и международных конференциях за последние 3 года.

Исследования, проводимые соискателем, также были отмечены различными фондами и получали финансовую поддержку на их проведение в форме различных грантов и стипендий, например: стипендия им. Остроградского посольства Франции в России на стажировку в лаборатории Кастлера-Бросселя, (Университет Сорбонны, Париж, Франция), гранты Российского Фонда Фундаментальных Исследований (грант «мол_а»), грант PhD Student Фонда Развития Теоретической Физики и Математики «БАЗИС».

Личный вклад автора в данную работу состоит в создании теоретических моделей, получении аналитических рузельтатов, анализе этих результатов, в объяснении изучаемых физических эффектов, нахождении механизмов их возникновения, а также в выполнении сопутствующих численных вычислений. Автор не только внес основной вклад в решение рассматриваемых задач, но также принимал самое непосредственное участие в их постановке и формулировке.

Предлагаемые к защите положения полностью отражают персональный вклад автора в работу.

Публикации. Основные работы по данной диссертации опубликованы в 7 научных статьях, из которых 7 опубликованы в рецензируемых изданиях, индексируемых Web Of Science и Scopus, 7 в журналах из списка Высшей Аттестационной Комиссии. Из этих 7 публикаций 4 опубликованы в периодических изданиях American Physical Society, а остальные 3 в виде рецензируемых трудов конференций.

Объём и структура работы. Диссертация состоит из 3-х глав и 4-х приложений. Полный объём диссертационной работы составляет 247

страниц, включая 34 рисунка. Список литературы содержит 192 наименования.

Основное содержание работы:

Возрастающий интерес к тематике взаимодействия квантовых излучателей посредством или с модами различных нанофотонных структур был вызван значительными успехами в экспериментальной реализации подобных систем. Для примера, стало возможным организовывать атомы в одномерные [15], двумерные [16], и трехмерные [17] упорядоченные массивы контролируемым путем. В то же время квазиодномерные системы представляют особый интерес как одна из возможных платформ реализации интерфейса свет-вещество в контексте области исследований под названием волноводная квантовая электродинамика (ВКЭД) [18;19] - современной и быстроразвивающейся области знания, в которой уже были продемонстрированы экспериментально многие выдающиеся результаты, например, Брэгговское отражение света от порядка тысячи атомов [20], генерация одиночных фотонов [21], а также наблюдение коллективных эффектов вроде субизлучения и сверхизлучения [22], и многое другое.

Также появилось новое направление исследований под названием хиральная квантовая оптика [10], в которой интерес представляют квантовые излучатели, асимметрично взаимодействующие с фотонными модами, распространяющимися в различных направлениях. Такая асимметрия может появляться, например, как результат наличия ненулевой поперечной компоненты плотности оптического спина [23]. Данная сфера исследований особо важна для создания и развития устройств нанофотоники, которые функционируют на уровне нескольких фотонов, таких как: оптические циркуляторы [13] и диоды [12] для одиночных фотонов, оптические переключатели на основе одиночного атома [13], источники одиночных фотонов с контроллируемыми свойствами на основе квантовых точек и волноводов [24], и многих других.

Как альтернатива атомам и квантовым точкам, полупроводниковые двумерные материалы также являются многообещающей платформой для изучения хиральных взаимодействий [25], в них хиральность обеспечивается наличием циркулярно поляризованных переходов между спиновыми состояниями долинных электронов. Значительный прогресс был продемонстрирован в возможности взаимодействия экситонов в таких двумерных материалах с модами плазмонных волноводов [26], а также метаповерхностей [27–29]. Метаповерхности можно также назвать фотонными эквивалентами двумерных полупроводниковых материалов, и для них уже были продемонстрированы довольно гибкие возможности в управлении их оптическими свойствами.

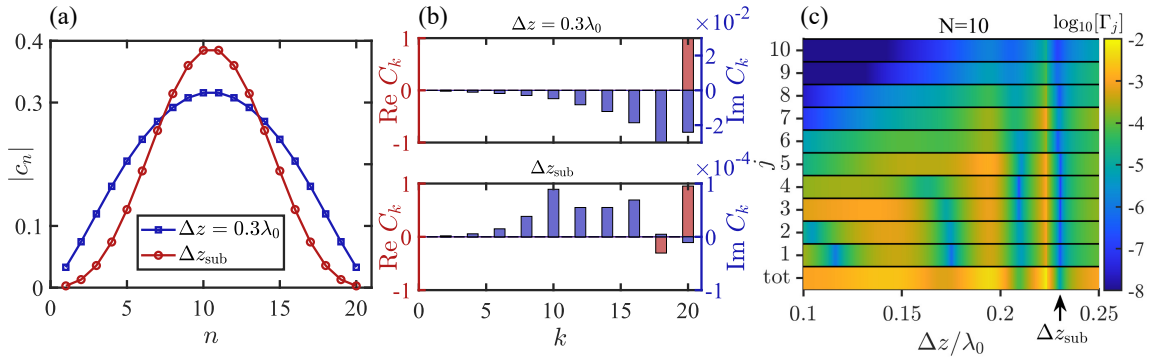

Рисунок 1 — (a) Абсолютные значения амплитуд вероятности для атома быть возбужденным в самом долгоживущем собственном состоянии в зависимости от номера атома n для периода системы $\Delta z = 0.3\lambda_0$ (синим), и оптимального периода Δz_{sub} (красным). (b) Разложение собственного состояния из (a) по базису функций решения задачи в приближении взаимодействия только ближайших соседей $C_k\psi^{(k)}$. (c) Разложение полного темпа излучения состояния Γ_j на вклады Векторных Сферических Гармоник разного порядка j в зависимости от периода Δz. Особое внимание на отмеченную точку Δz_{sub} и то, каким образом вблизи от этого значения одновременно много вкладов Γ_j имеют локальные минимумы

Все указанное выше подтверждает, что квантовые излучатели, которые взаимодействуют с электромагнитными модами структур нанофотоники, представляют из себя универсальный инструмент не только для изучения экзотических эффектов во взаимодействии света и вещества с точки зрения чисто фундаментальной науки, но также являются многообещающей платформой для разработки будущих оптических устройств, функционирующих на уровне нескольких частиц.

Ниже представлен короткий обзор результатов, представляющих основу диссертации.

В первой главе мы рассматриваем субрадиационные состояния (с большими временами жизни) в системе, представляющей из себя ансамбль двухуровневых атомов, упорядоченных в виде периодического субдиффракционного одномерного массива. Было установлено, что в такой системе существуют определенные значения периода, для которого некоторые собственные состояния, лежащие близко к краю зоны Бриллюэна, имеют сильно уменьшенный темп спонтанной эмиссии (см. Рис. 2 (a)), причем подобные состояния были найдены только для случая, когда дипольные моменты ориентированы перпендикулярно оси цепочки. Было показано, что эти состояния имеют необычный закон изменения темпа спонтанной эмиссии с числом атомов N, а именно, темп спадает значительно быстрее, чем было известно ранее для подобных систем - $\gamma \sim N^{-6.88}$ в отличие от известного закона $\gamma \sim N^{-3}$ (см. Рис. 2 (b)). Пу-

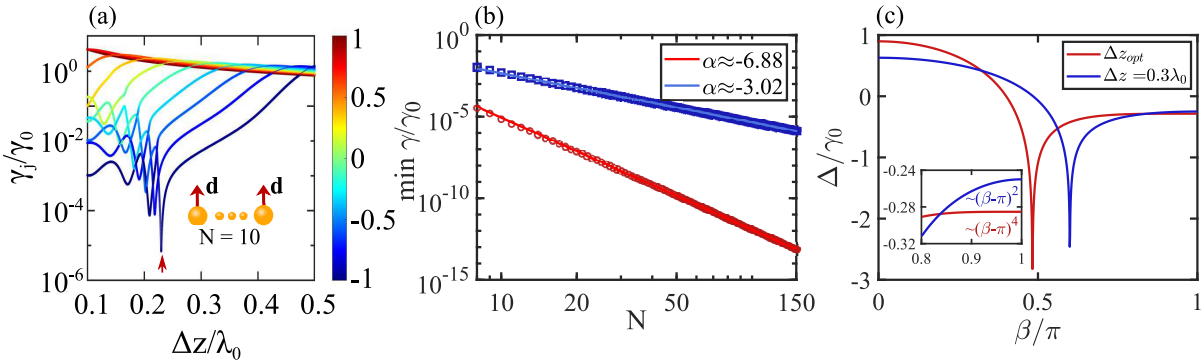

Рисунок 2 — (a) Темпы эмиссии собственных состояний системы в зависимости от периода для $N = 10$ двухуровневых атомов с поперечно ориентированными дипольными моментами, цвет обозначает среднюю величину корреляций между дипольными моментами ближайших соседей. (b) Зависимость темпа эмиссии от N для некоторого фиксированного периода (синим цветом, $\Delta z = 0.3\lambda_0$), и для оптимального периода, позволяющего получить самое долгоживущее состояние (красным). (c) Дисперсия собственных мод в бесконечной цепочке атомов для тех же значений периода, что в (b). Как видно, дисперсия становится более плоской для Δz_{opt}

тём рассмотрения бесконечной периодической цепочки вместо конечной, было получено трансцендентное уравнение, которое определяет точное предельное значение периода, для которого наблюдается самое долгоживущее состояние. Оказалось, что это значение связано с ситуацией, при которой дисперсия собственных мод становитя плоской вблизи края зоны Бриллюэна: вместо привычного для таких систем $\sim (\beta - \pi)^2$ поведения, дисперсия имеет зависимость $\sim (\beta - \pi)^4$ от обезразмеренного волнового числа $\beta = k_z \Delta z$ (см. Рис. 2 (c)). В литературе данный эффект известен как Вырожденный Край Зоны (ВКЗ), и он впервые был теоретически предсказан для фотонных кристаллов [33].

Кроме того, было установлено, что соответствующее собственное состояние (распределение возбуждения между атомами, или, что эквивалентно, распределение дипольного момента по цепочке) для таких сильно субрадиационных состояния значительно более локализовано (см Рис. 1 (a)) по сравнению с типичными состояниями на краю зоны для бóльших периодов. Было эмпирически установлено, что сильно субрадиационное состояние может быть хорошо приближено двумя доминирующими вкладами в виде состояний из базиса решения аналогичной одномерной задачи, но с учетом взаимодействия только ближайших соседей (см. Рис. 1 (b)), а именно, оно может быть приближено функцией вида $\sim C_N \sin\left(\frac{\pi N n}{N+1}\right) + C_{N-2} \sin\left(\frac{\pi(N-2)n}{N+1}\right)$. Интересно, что эти два доминирующих вклада интерферируют деструктивно, поскольку $\mathrm{Re}\,[C_N C_{N-2}] < 0$,

потому уменьшение темпа эмиссии может быть объяснено именно такой деструктивной интерференцией. Также была объяснена взаимосвязь между образованием долгоживущих состояний на краю зоны и вырождением. Поскольку дисперсия для некоторого периода становится более плоской, тогда соответствующие собственные состояния, лежащие близко к краю зоны, имеют очень близкие по значению собственные частоты (действительные части собственных чисел задачи). Однако, состояния с номерами N, $N-2$, которые имеют одинаковую симметрию по отношению к отражению относительно геометрического центра цепочки, не могут иметь одинаковые значения собственных частот. Соответствующие энергетические уровни этих состояний будут расталкиваться, а вблизи точки сильного расталкивания собственные вектора будут замешиваться (Рис. 1 (b), нижний график). Для определенного значения периода эти состояния замешаны в таком виде, что одно из них оказывается еще более безызлучательным вследствие уже упомянутой деструктивной интерференции.

Также было показано, что у данного субизлучательного состояния имеется еще одно интересное свойство, которое может быть выявлено, если осуществить для него мультипольную декомпозицию темпа спонтанной эмиссии. Путем разложения полного темпа излучения на вклады Векторных Сферических Гармоник (ВСГ) различных порядков j в виде $\Gamma = \sum_j \Gamma_j$, и построив их как функции периода системы Δz, можно увидеть из Рис. 1 (c), что в области близ Δz_{sub} функции Γ_j имеют локальные минимумы для многих j. В рассмотренном примере для цепочки из $N = 10$ атомов это происходит для всех Γ_j вплоть до $j = 10$. Такая ситуация не является типичной, поскольку обычно уменьшение мощности, излучаемой системой в дальнее поле, обычно связано с подавление низших мультиполей, которые и дают основной вклад в величину полного темпа эмиссии Γ. Причина по которой одновременно много вкладов Γ_j имеют минимум для такого состояния может быть легко объяснена, если вспомнить, что данное состояние может быть приближенно описано выражением $\sim C_N \sin\left(\frac{\pi N n}{N+1}\right) + C_{N-2} \sin\left(\frac{\pi (N-2) n}{N+1}\right)$. Для системы из достаточно большого числа атомов $N \gg 1$, функции $\sin\left(\frac{\pi N n}{N+1}\right)$ и $\sin\left(\frac{\pi (N-2) n}{N+1}\right)$ довольно похожи. Следовательно, мультипольные составы полей, излучаемых системой с такими распределениями дипольных моментов, также являются похожими. Если принять во внимание, что $\mathrm{Re}\left[C_N C_{N-2}\right] < 0$, то становится понятным, что одновременная минимизация Γ_j оказывается возможной именно благодаря деструктивной интерференции этих вкладов.

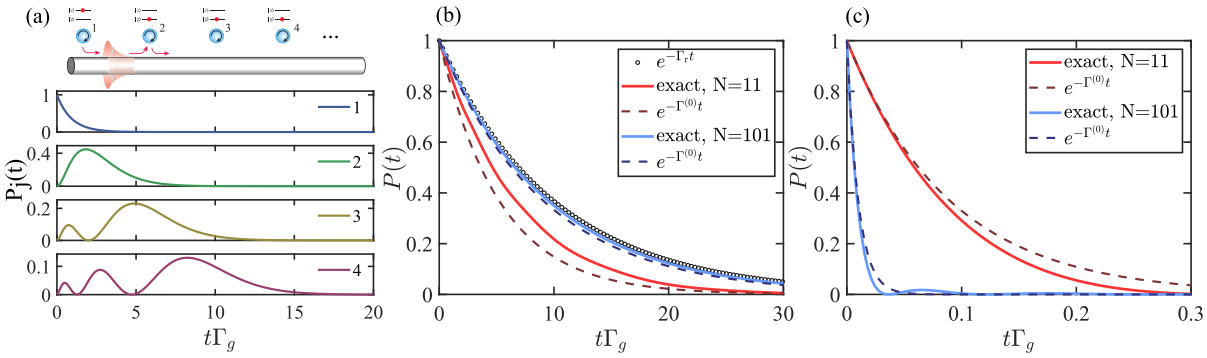

Рисунок 3 — (a) Транспорт одиночного возбуждения в системе атомов, однонаправленно (хирально) взаимодействующих посредством волноводной моды. (b)-(c) Динамика коллективного одночастичного состояния Дике для случая субизлучения (b), и сверхизлучения (c). Сплошные линии показывают точное решение, а штрихованные - экспоненты с найденным темпом эмиссии $\Gamma^{(0)}$ в показателе. Динамика темпа эмиссии только в неволноводные излучательные моды $e^{-\Gamma_r t}$ изображена точечной черной линией. Для всех графиков было положено, что $\Gamma_g = 10, \Gamma_r = 1$

В первой главе преимущественно рассматривается возникновение сильно субизлучательных состояний в периодических цепочках двухуровневых атомов, которые связаны через вакуумное диполь-дипольное взаимодействие. С первого взгляда может показаться, что рассмотренный эффект может быть исключительным свойством взаимодействия рассмотренного типа, и что наличие других каналов взаимодействия между атомами может привести к исчезновению этих состояний. Однако, как показано более подробно в основной части диссертационной работы, это не так по крайней мере для рассмотренного дополнительного канала - взаимодействия излучателей посредством одной фундаментальной волноводной моды оптического нановолокна. Дополнительно показано, что в такой системе присутствуют не только описанные выше субизлучательные состояния, но и состояния двух тругих типов: 1) субизлучательные состояния на первом Брэгговском резонансе для волноводной моды, а также 2) субизлучательные состояния, которые появляются в результате интерференции между двумя имеющимися каналами взаимодействия (через вакуумную диполь-дипольную связь и посредством волноводной моды). Рассмотрен характер изменения темпа эмиссии для состояний данных трёх типов, и то, как они проявляют себя в таких оптических свойствах системы, как однофотонные коэффициенты прохождения и отражения.

Во второй главе автор рассматривает коллективное излучение в системе, состоящей из N двухуровневых атомов, которые однонаправленно взаимодействуют с одной волноводной модой. Однонаправленность

взаимодействия атома с модой может быть обусловлена, например, спин-орбитальным взаимодействием для света [23; 34] в поверхностно-локализованной распространяющейся волне, что в свою очередь приводит к зависимости локальной спиральности (направления вращения) поля от направления распространения волны: распространяющиеся вперед и назад моды в случае одномерной системы будут иметь противоположные спиральности. В результате моды, которые распространяются в противоположных направлениях, будут по-разному взаимодействовать с излучателем, который обладает циркулярно-поляризованным дипольным моментом активного перехода, если дипольный момент ориентирован в пространстве должным образом по отношению к полю моды [35].

На первом шаге была решена задача транспорта одиночного возбуждения в такой системе, аналитическое решение которой было получено в следующем виде:

$$C_k(t) = e^{-\Gamma_{\text{tot}} t/2 + i\varphi_{k,1}} L_{k-1}^{(-1)}(\Gamma_g t), \tag{6}$$

где $C_k(t)$ - амплитуда вероятности того, что атом с номером k возбужден в момент времени t, $\Gamma_{\text{tot}} = \Gamma_g + \Gamma_r$ - это полный темп спонтанной эмиссии, состоящий из темпа излучения в волноводные Γ_g и неволноводные (излучательные) моды Γ_r, $\varphi_{k,1}$ отвечает за фазу распространения, которую получил фотон при движении от атома 1 к атому k, и $L_{k-1}^{(-1)}(x)$ - обобщенные полиномы Лагерра порядка $k-1$ с индексом -1. Соответствующие вероятности $P_k(t) = |C_k(t)|^2$ показаны на Рис. 3 (а) для первых 4 атомов. Как видно, одна из особенностей динамики возбуждения в такой системе заключается в том, что решение записывается не в виде комбинации гиперболических и тригонометрических функций, как было бы в случае симметричного взаимодействия атомов, а имеет полиномиальный характер в результате наличия вырождения в спектре задачи. Также можно сказать, что количество актов поглощения-излучения выражается через порядковый номер излучателя k в цепочке как $k-1$, что является прямым следствием математических свойств обобщенных полиномов Лагерра $L_{k-1}^{(-1)}(x)$.

Помимо рассмотрения модельной задачи с идеально асимметричным взаимодействием между атомами, для которого оказывается возможным точно аналитически решить задачу транспорта одиночного возбуждения, также была изучена и более реалистичная система. С этой целью в качестве волноводной структуры был рассмотрен плазмонный волновод из серебра, который поддерживает распространяющийся плазмон-поляритон, и для которого возможно реализовать сильный эффект спиновой блокировки (спин-орбитального взаимодействия света). Несмотря на

то, что для такой системы невозможно реализовать идеально однонаправленное распространение возбуждения среди атомов посредством плазмон-поляритона, в работе показано, что степень асимметрии взаимодействия может достигать величины порядка и больше 10 для атомов, находящихся достаточно далеко друг от друга. С помощью формализма резольвенты Гамильтониана системы [4] найдены вероятности передачи возбуждения от первого атома остальным, а также произведено сравнение этих результатов с аналитическими выражениями, полученными ранее для модельной задачи с использованием соответствующих параметров системы. При сравнении также было произведено усреднение по случайным отклонениям в положениях атомов вдоль плазмонного волновода, и показано, что динамика, которую описывает выражение (6), находится в хорошем соответствии с результатами, полученными для металлического волновода, даже не смотря на неидеальность асимметрии связи атомов.

Имея решения задачи транспорта одиночного возбуждения, можно найти также и динамику любого другого состояния с не более чем одним возбуждением в системе. В этом контексте особый интерес представляют состояния, которые демонстрируют эффекты суб- и сверхизлучения, поскольку при определенных условиях в случае симметричного возбуждения известно, что они демонстрируют уменьшение или увеличение темпа эмиссии, соответственно. Если система изначально находится в симметричном состоянии Дике вида $|D\rangle = \sum_{k=1}^{N} \frac{1}{\sqrt{N}} |e_k\rangle |g\rangle^{N-1}$, тогда можно показать, что:

$$C_{\text{sub}}(t) = \frac{e^{-\Gamma_{\text{tot}} t/2}}{N} \sum_{k=1}^{N} (N - (k-1))(-1)^{k-1} L_{k-1}^{(-1)}(\Gamma_g t),$$

$$C_{\text{sup}}(t) = \frac{e^{-\Gamma_{\text{tot}} t/2}}{N} L_{N-1}^{(1)}(\Gamma_g t), \tag{7}$$

где $C_{\text{sub/sup}}(t)$ - это амплитуды вероятности для системы остаться в состоянии $|D\rangle$, когда любые два ближайших атома излучают фотоны в противофазе или синфазно, соответственно. Даже не смотря на то, что динамика в этом случае полиномиальная, и не имеет вид экспоненты, мы по-прежнему можем найти темп эмиссии системы на малых временах: $P_{|D\rangle}(t) \approx 1 - \Gamma^{(0)} t + ...$

Было показано, что приближенный темп эмиссии в волноводную моду для случая сверхизлучения равен $\Gamma_g^{(0)} = N\Gamma_g$ (как и в случае симметричного взаимодействия), в то время как для случая субизлучения он равен $\Gamma_g^{(0)} = \Gamma_g \frac{1-(-1)^N}{2N}$ (вместо 0, как в случае симметричной связи атомов). Как видно, хиральный субизлучательный темп эмиссии зависит от того,

является ли полное число излучателей в системе N четным или нет. Была выяснена причина наличия такой зависимости, а именно, показано, что это происходит по причине неполной деструктивной интерференции между различными реализациями того, как система может излучить фотон, и является прямым следствием однонаправленности взаимодействия излучателей.

На Рис. 3 (b) можно увидеть, что для коллективного субрадиационного излучения различие между точным решением в виде полинонов из Ур. (7) (верхняя строчка) и экспонентой $e^{-\Gamma^{(0)}t}$ тем меньше, чем больше размер системы N. Это позволяет заключить, что для систем из достаточно большого числа атомов субрадиационный темп эмиссии адекватно описывает временную динамику системы. Однако, как видно из Рис. 3 (c), это не вполне так для сверхизлучения: для больших N экспонента $e^{-\Gamma^{(0)}t}$ и выражение из Ур. (2) (нижняя строчка) естественным образом близки для малых значений $\Gamma_g t$, тогда как для более поздних времен есть конечная вероятность того, что система поглотит излученный ранее фотон. Такое поведение напрямую связано с математическими свойствами функции $L^{(1)}_{N-1}(x)$, поскольку она имеет $N-1$ действительный положительный корень, а, значит, имеется $N-1$ актов излучения-поглощения фотона. Тем не менее, из этих $N-1$ актов только самый первый виден явно, тогда как все последующие имеют крайне малое значение вероятности в локальном максимуме по причине наличия экспоненты $e^{-\Gamma_{\rm tot}t}$, отвечающей за спонтанную эмиссию.

В третьей главе рассматривается задача переноса возбуждения между возбужденными состояниями квантового излучателя с дипольно разрешенным $s \to p$ переходом, когда излучатель находится в непосредственной близости от нанофотонной структуры (см. Рис. 4 (a)) - анизотропной метаповерхности. Было показано, что при определенных условиях, перенос возбуждения отличается в прямом и обратном направлении: $P_{q,q'}(t) \neq P_{q',q}(t)$. В качестве примера были взяты состояния $q,q' \in -1,+1$, для которых было получено:

$$P_{-,+}(t) - P_{+,-}(t) = f(\alpha,\beta) \sum_{(k,l)}^{(x,y),(y,z),(z,x)} e^{(g''_k+g''_l)t} \sin\left((g'_k - g'_l)\,t\right),$$
$$f(\alpha,\beta) = \tfrac{1}{8}\sin(2\alpha)\sin(2\beta)\sin(\beta), \qquad (8)$$

где g'_k,g''_k связаны с частотами собственных состояний и модифицированными темпами эмиссии, соответственно, а α,β - углы, задающие ориентацию локальной оси квантования излучателя (и, следовательно, ориентацию дипольных моментов). Из уравнения выше следует, что асимметрия в транспорте $P_{-,+}(t) \neq P_{+,-1}(t)$ появляется тогда, когда дипольные моменты переходов излучателя ориентированы произвольным

образом по отношению к направлениям высокой симметрии структуры, а также, когда наноструктура локально полностью анизотропна. Первое означает, что локальная ось квантования излучателя z' (эквивалентно, дипольный момент π-поляризованного перехода) не должна лежать ни в одной из плоскотей, образованных главными осями метаповерхности. Математически это означает следующее ограничение на значения углов: $\alpha \neq \frac{\pi}{2}m$, и $\beta \neq \frac{\pi}{2}m'$, где m, m' - целые числа. Фраза же "локально полностью анизотропна" значит, что с точки зрения излучателя все 3 главные направления структуры (метаповерхности) должны быть физически не эквивалентными, или, что $g'_k \neq g'_l$ для любых k и l. Последнее утверждение также можно сформулировать в такой форме: никакие два собственных состояния системы не должны иметь одинаковые частоты.

В работе также получены выражения для вероятности перехода системы между возбужденными уровнями в представлении собственных состояний. Особый интерес здесь представляют интерференционные вклады, которые имеют следующий вид:

$$P_{q',q}^{(k,l)}(t) = 2\left|C_{k,l}^{(q',q)}\right| \cos\left[(g'_k - g'_l)t - \varphi_{k,l}^{(q',q)}\right] e^{(g''_k+g''_l)t}, \tag{9}$$

где $C_{k,l}^{(q',q)}$ комплекснозначная величина, $\varphi_{k,l}^{(q',q)} = \arg\left(C_{k,l}^{(q',q)}\right)$ - её фаза, причем обе величины являются функциями только углов поворота локальной оси квантования излучателя α, β. Из явных выражений для этих функций можно выявить следующее свойство $\varphi_{k,l}^{(q',q)} = -\varphi_{k,l}^{(q,q')}$, из которого можно заключить, что рассматриваемый эффект является ничем иным как фазовым сдвигом в динамике вероятностей перехода, который появляется как результат интерференции собственных состояний излучателя, обусловленных его взаимодействием с электромагнитными модами окружения.

Поскольку переходы электрона между возбужденными уровнями излучателя не являются напрямую наблюдаемыми, также было изучено то, каким образом подобное нарушение симметрии во внутренней динамике излучателя влияет на измеряемые величины: временной профиль детектируемой интенсивности излучения, а также полный излученный системой спектр. С помощью использования представления собственных состояний были получены следующие выражения для данных величин:

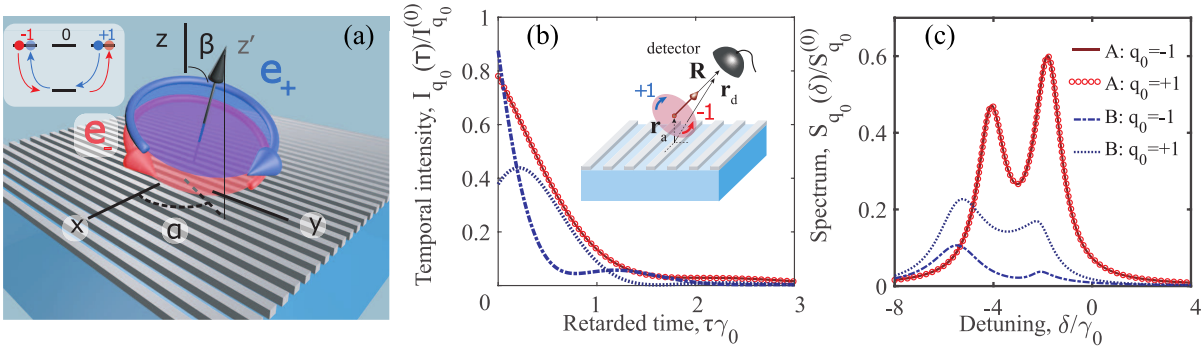

Рисунок 4 — (a) Схематическое изображение рассматриваемой системы: атом с трехкратно вырожденным возбужденным состоянием находится вблизи нанофотонной структуры (анизотропной метаповерхности). Дипольные моменты переходов здесь произвольно ориентированы в пространстве. Временная динамика интенсивности (b), и полный излученный спектр системы (c) для атома, который в начальный момент времени находился в состоянии $|e_{q_0}\rangle$. Красные линии и маркеры соответствуют случаю изотропной метаповерхности, а синие - анизотропной. В последнем случае как интенсивность, так и спектры отличаются для различных начальных состояний q_0

$$I_{q_0}(t) = \langle\psi(t)|\hat{\mathbf{E}}^{(-)}(\mathbf{r_d})\hat{\mathbf{E}}^{(+)}(\mathbf{r_d})|\psi(t)\rangle \approx 16\pi^2 k_0^4 |\mathbf{d}|^2 \left|\sum_j \mathbf{f_j} e^{-ig_j\tau}\right|^2,$$

$$S_{q_0}(\omega) = \int_0^\infty dt_2 \int_0^\infty dt_1 \left[e^{-i\omega(t_2-t_1)}\langle\hat{\mathbf{E}}^{(-)}(\mathbf{r},t_2)\hat{\mathbf{E}}^{(+)}(\mathbf{r},t_1)\rangle\right] \approx \left|\sum_j \frac{\boldsymbol{f}_j^{q_0}(\mathbf{r_d},\mathbf{r_a})}{(\delta - g_j)}\right|^2, \tag{10}$$

где $q_0 \in \{-1,0,+1\}$ - индекс состояния, в котором в начальный момент времени находился излучатель, $\mathbf{r_d}$ - положение детектора, $\delta = \omega - \omega_0$ - отстройка частоты детектора от невозмущенной частоты перехода излучателя, $\tau = t - |\mathbf{R}|/c$ время наблюдения интенсивности с учетом запаздывания, а векторные величины $\mathbf{f_j}$, и $\boldsymbol{f}_j^{q_0}(\mathbf{r_d},\mathbf{r_a})$ связаны с генерируемыми собственным состоянием с индексом j в дальней зоне полями (детали можно найти в основном тексте). Данные векторные функции имеют следующее свойство $\mathbf{A}(q_0 = +1) = -\mathbf{A}^*(q_0 = -1)$, что приводит к тому, что как интенсивность, так и спектр зависят от знака величины q_0. Действительно, как показывают расчеты, представленные на Рис. 4 (b), (c), интенсивность и спектр начинают зависеть от знака проекции спина начального состояния излучателя, если упомянутые ранее условия, вытекающие из выражения (8), выполнены.

Помимо рассмотренной ранее системы, в которой атом находится вблизи анизотропной метаповерхности, также было показано, что если

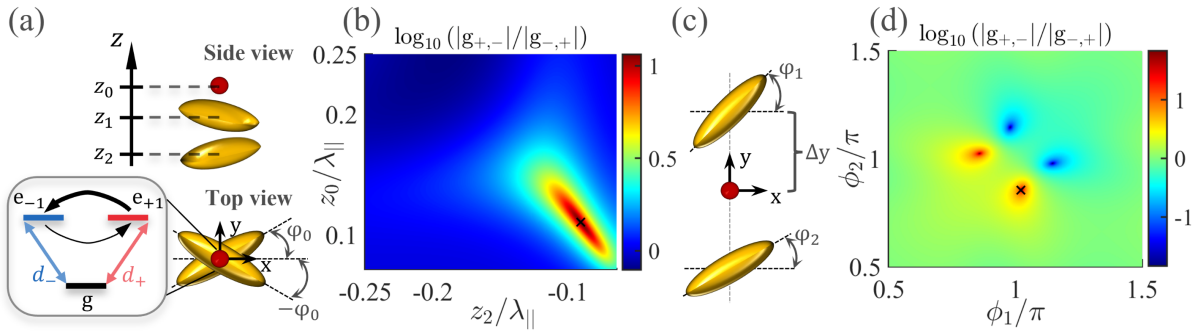

Рисунок 5 — (a) Рассматриваемая система: димер, состоящий из двух частиц-эллипсоидов, длинные полуоси которых лежат в параллельных плоскостях и повернуты друг относительно друга на угол $2\varphi_0$. Атом с V-образной структурой уровней и циркулярно поляризованными дипольными моментами находится вблизи димера, причем центры обоих частиц и атом лежат на оси z. (b) Зависимость асимметрии в константах связи от координаты атома z_0 и одной из частиц z_2 (координата другой предполагается равной нулю $z_1 = 0$), угол поворота длинных полуосей $\varphi_0 = \pi/8$. $\lambda_{||}$ - это длина волны, при которой максимально значение $\mathrm{Im}\,[\tilde{\alpha}_{xx}(\omega)]$, где $\tilde{\alpha}_{xx}$ - компонента поляризуемости эллипсоида вдоль длинной полуоси. (c) Другая схема, в которой обе частицы и атом лежат в плоскости xy, а длинные полуоси каждого эллипсоида ориентированы произвольно, в то время как атом находится посреди отрезка, соединяющего центры частиц на равном от каждой из них расстоянии Δy. (d) Зависимость асимметрии в константах связи от углов поворота длинных полуосей φ_1, φ_2. Расстояние $\Delta y = a_x + \lambda_{||}/20$, где a_x - величина длинной полуоси эллипсоида. Черными крестами на (b), (d) отмечены точки максимальной асимметрии в константах связи

атом со структурой уровней V-типа находится вблизи плазмонного димера, состоящего из анизотропных рассеивателей (в качестве последних были взяты вытянутые эллипсоиды), то оказывается возможным получить сильную асимметрию в константах взаимодействия циркулярно поляризованных переходов $|g_{+,-}|/|g_{-.+}| \gg 1 (\ll 1)$. Одна из рассмотренных геометрий такой системы основана на известной плазмонной модели Борна-Куна [36–38] (см. Рис. 5 (a)), когда длинные полуоси эллипсоидов предполагаются находящимися в различных параллельных плоскостях (например, заданных двумя постоянными координатами z_1, z_2). Для простоты центры обоих рассеивателей и атом предполагаются находящимися на одной оси (оси z). Вторая схема (Рис. 5 (c)) является квази-двумерной, так как для неё длинные полуоси обоих эллипсоидов и атом лежат в одной плоскости (xy), а центры частиц и атом на оси y. Геометрия в таком случае меняется расстоянием атом-рассеи-

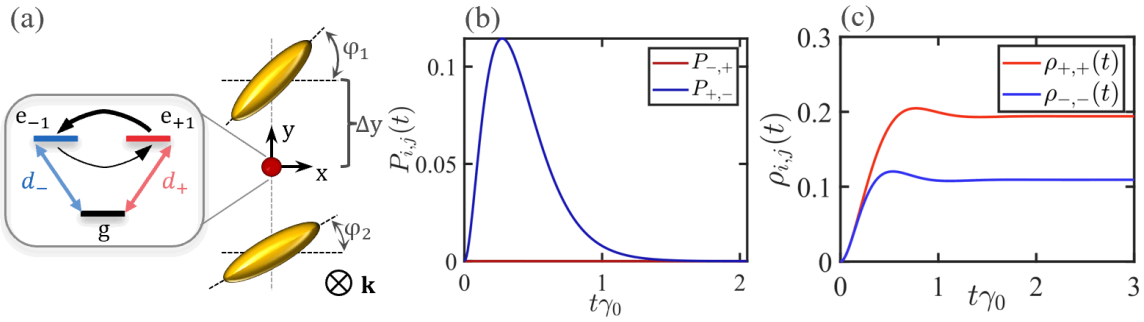

Рисунок 6 — (a) Схема рассматриваемой системы, вектор $\mathbf{k}$ здесь показывает направление падения внешнего накачивающего поля. (b) Асимметрия в вероятностях переноса возбуждения $P_{-,+}(t)$, и $P_{+,-}(t)$. Параметры выбраны таким образом, чтобы максимизировать асимметрию связи переходов (отмечено черным крестом на Рис. 5 (d)). (c) Населенности возбужденных состояний как функции времени при наличии внешней накачки. Параметры накачивающего поля подобраны таким образом, чтобы максимизировать разницу стационарных населенностей уровней $|\rho_{+,+}(\infty) - \rho_{-,-}(\infty)|$, и чтобы соответствующие частоты Раби на обоих переходах были равны $\Omega_- = \Omega_+$

вители Δy, и углами, задающими ориентации длинных полуосей φ_1, φ_2 эллипсоидов. Как можно видеть из Рис. 5 (b), (d) обе схемы позволяют получить сильную асимметрию в константах связи, но последняя является более интересной, так как в ней возможно осуществить переключение из режима $|g_{-,+}|/|g_{+-}| \gg 1$ в режим $|g_{-,+}|/|g_{+-}| \ll 1$ лишь небольшим изменением углов φ_1, φ_2. В то же время такая схема является более простой геометрически, что может быть её преимуществом при создании, например, реалистичной структуры типа метаповерхность на основе двумерного периодического массива анизотропных рассеивателей.

На примере структуры, представленной на Рис. 5 (c), показано, что с её помощью действительно возможно реализовать практически однонаправленный перенос возбуждения из состояния $|e_{-1}\rangle$ в состояние $|e_{+1}\rangle$ как видно из динамики передачи возбуждения на Рис. 6 (b). Стоит отметить, что вероятность $P_{+,-}(t)$ описывается выражением, которое было получено во второй главе $P_{+,-}(t) = e^{-\gamma_{\text{tot}}t}|L_N^{(-1)}(|g_{+,-}|t)|^2$ для задачи транспорта одиночного возбуждения в цепочке из двух ($N = 2$) однонаправленно взаимодействующих атомов. Это объясняется тем, что переходы в V-атоме можно представить как два взаимодействующих двухуровневых атома, находящихся в одной точке пространства и имеющих соответствующие дипольные моменты переходов.

Помимо изучения свободной динамики системы, индуцированной вакуумом, также был рассмотрен случай, когда присутствует внешнее накачивающее классическое поле. В этом случае было продемонстрирова-

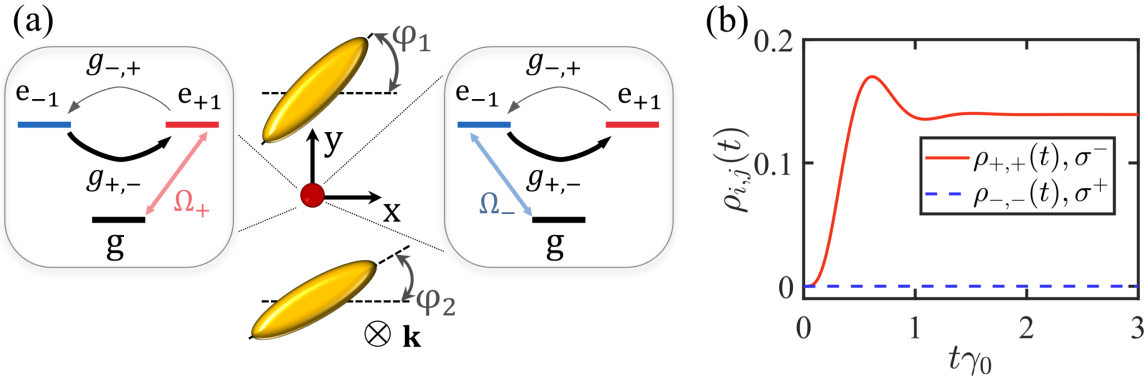

Рисунок 7 — (a) Схема по селективной накачке каждого из двух переходов в излучателе с V-образной структурой уровней. (b) Временная динамика населенностей возбужденных состояний на переходах, ортогональных тем, на которых действует внешнее накачивающее поле. Сплошная красная линия для населенности $\rho_{+,+}(t)$ при σ^- накачке (правая схема в (a)), синяя штрихованная линия для $\rho_{-,-}(t)$ населенности при σ^+ накачке (левая схема в (a))

но, что асимметрия во взаимодействии переходов приводит к неравным стационарным населённостям возбужденных уровней, не смотря на то, что параметры накачки подбирались таким образом, чтобы сила накачки на каждом переходе была одинаковой (равны соответствующие частоты Раби $\Omega_- = \Omega_+$), что продемонстрировано на Рис. 6 (c).

В работе также рассматривается еще одна схема накачки, показанная на Рис. 7 (a). В ней параметры падающей плоской волны таковы, что полное поле в точке нахождения излучателя селективно взаимодействует либо с σ^-, либо с σ^+ переходом. При сильной асимметрии взаимодействия $|g_{-,+}|/|g_{+,-}| \gg 1$ и накачке с параметрами $\Omega_- \neq 0, \Omega_+ = 0$, атом переходит из начального состояния $|g\rangle$ в состояние $|e_{-1}\rangle$, после чего есть ненулевая вероятность перехода системы в $|e_{+1}\rangle$ в силу конечности соответствующей константы связи $g_{+,-}$. Следовательно, по прошествии достаточного количества времени устанавливается стационарное значение населенности $\rho_{+,+}(t \to \infty)$ (сплошная красная кривая на Рис. 7 (b)). Однако, если накачка имеет параметры $\Omega_+ \neq 0, \Omega_- = 0$, по причине малости величины константы связи $|g_{+,-}|$ по сравнению со всеми другими параметрами в системе, отсутствует перенос населенности между возбужденными уровнями, и вероятность нахождения системы в возбужденном состоянии на ортогональном переходе пренебрежимо мала $\rho_{-,-}(t) \approx 0$ (штрихованная синяя линия на Рис. 7 (b)). Это означает, что в таком случае излучатель ведет себя как двухуровневая система, и что оптические свойства системы в целом сильно зависят от спиральности полного поля в точке нахождения атома.

В **заключении** перечислены основные результаты данной диссертационной работы, а также обсуждаются возможные будущие направления исследований.

1. В первой главе мы рассмотрели возникновение сильно субизлучательных состояний, возникающих на краю зоны Бриллюэна, в субдифракционных периодических цепочках двухуровневых атомов, где увеличение времени жизни этих состояний происходит по причине взаимодействия собственных мод и последующей деструктивной интерференции составляющих собственные моды вкладов. Это приводит к наличию у этих состояний некоторых специфических свойств, таких, например, как значительно более быстрое уменьшение темпа спонтанной эмиссии с увеличением размера системы ($\sim N^{-6.8}$ вместо известной $\sim N^{-3}$ зависимости), а также более сильная локализация собственной моды за счет уменьшения дипольных моментов на краях цепочки. Также, упомянутая ранее деструктивная интерференция приводит к одновременному уменьшению многих мультипольных вкладов в дальнопольное излучение изучаемых субизлучательных состояний. Показано, что наличие дополнительного канала взаимодействия между атомами, помимо вакуумного диполь-дипольного взаимодействия, не приводит к исчезновению рассматриваемого эффекта, что было продемонстрировано на примере цепочки атомов вблизи оптического одномодового нановолокна.
2. Во второй главе изучена полиномиальная динамика транспорта одиночного возбуждения в одномерной цепочке двухуровневых атомов, которые однонаправленно взаимодействуют посредством волноводной моды. Данная задача решена аналитически для произвольного числа атомов, и на основании этого результата также оценены величины темпа коллективного суб- и сверхизлучения в одночастичном приближении. Для субизлучения темп эмиссии в общем случае оказывается отличным от такового для случая симметричного взаимодействия между атомами, предсказываемого теорией Дике. Для того, чтобы объяснить возникающее отличие была проанализирована динамика системы в одночастичном приближении в низшем нетривиальном порядке теории возмущений, и показано, что это отличие связано с наличием неполной деструктивной интерференции между различными возможными реализациями процесса излучения фотона системой.
3. В третьей главе продемонстрировано, каким образом с помощью анизотропной фотонном структуры (метаповерхности), и осуществления контроля за ориентацией дипольных моментов переходов в $s \to p$ атоме, оказывается возможным нарушить симметрию меж-

ду прямыми и обратными квантово-механическими процессами, которые связанны с переходом электрона из одного возбужденного состояние в другое. Аналитически выведены критерии для наблюдения данного эффекта, а также показано, что он связан с интерференцией собственных состояний системы, которые возникают за счет взаимодействия излучателя с электромагнитными модами окружения. Продемонстрировано, что данная интерференция приводит к наличию фазового сдвига в динамике вероятностей перехода. Помимо этого показано, каким образом различные вероятности переходов в прямом и обратном направлении в такой системе отражаются в измеряемых величинах: динамике детектируемой интенсивности и полном излученном системой спектре.

4. В третьей главе также предложен альтернативный способ нарушить симметрию в вероятностях перехода системы между состояниями с помощью структуры на основе плазмонного димера, состоящего из двух асимметричных дипольных рассеивателей. Путем должного выбора геометрии системы, продемонстрирована возможность практически полностью запретить переходы между возбужденными уровнями излучателя V-типа в одном из направлений. Была также проанализирована динамика системы под действием внешнего накачивающего поля и показано, что стационарные населенности возбужденных уровней в такой системе могут быть различны, даже не смотря на равные частоты Раби для обоих переходов. Помимо этого показано, что отклик системы на внешнее накачивающее поле сильно зависит от локальной спиральности полного поля в точке нахождения излучателя.

Публикации:

Результаты, представленные в данной диссертационной работе, опубликованы в следующих статьях:

I. Extremely subradiant states in a periodic one-dimensional atomic array / **Kornovan D. F.**, Corzo N. V., Laurat J., Sheremet A. S. // Phys. Rev. A. — 2019. — Dec. — Vol. 100. — P. 063832. — URL: https://link.aps.org/doi/10.1103/PhysRevA.100.063832.

II. Noninverse dynamics of a quantum emitter coupled to a fully anisotropic environment / **Kornovan D. F.**, Petrov M. I., Iorsh I. V. //

Phys. Rev. A. — 2019. — Sep. — Vol. 100. — P. 033840. — URL: https://link.aps.org/doi/10.1103/PhysRevA.100.033840.

III. Strong coupling and non-reciprocity in the dynamics of a V-atom placed near an anisotropic metasurface / **Kornovan D. F.**, Petrov M. I., Iorsh I. V. // 2018 12th International Congress on Artificial Materials for NovelWave Phenomena (Metamaterials). — 2018. — Aug. — Pp. 228–230.

IV. Temporal dynamics of a quantum emitter with multiple excited states in the vicinity of an anisotropic metasurface / **Kornovan D. F.** , Toftul I. D., Chebykin A. V., Petrov M. I., Iorsh I. V. — Vol. 1092. — IOP Publishing, 2018. — sep. — P. 012063. — URL: https://iopscience.iop.org/article/10.1088/1742-6596/1092/1/012063.

V. Transport and collective radiance in a basic quantum chiral optical model / **Kornovan D. F.**, Petrov M. I., Iorsh I. V. // Phys. Rev. B. — 2017. — Sep. — Vol. 96. — P. 115162. — URL: https://link.aps.org/doi/10.1103/PhysRevB.96.115162.

VI. Light interaction and quantum transport in atomic chain chirally coupled to a waveguide / **Kornovan D. F.**, Sheremet A. S., Iorsh I. V., Petrov M. I. // 2017 11th International Congress on Engineered Materials Platforms for Novel Wave Phenomena (Metamaterials). — 2017. — Aug. — Pp. 262–264.

VII. Collective polaritonic modes in an array of two-level quantum emitters coupled to an optical nanofiber / **Kornovan D. F.**, Sheremet A. S., Petrov M. I. // Phys. Rev. B. — 2016. — Dec. — Vol. 94. — P. 245416. — URL: https://link.aps.org/doi/10.1103/PhysRevB.94.245416.

Introduction

Below we provide a literature overview along with discussions of topics covered in each chapter as well as the brief motivation to study each of them.

The first chapter of this thesis is devoted to the study of optical properties of periodic one-dimensional arrays of two-level atoms with dipole moments transverse to the array axis as shown in Fig. 0.1 (a). More specifically, we are going to focus on the states lying close to the edge of the first Brillouin zone (Fig. 0.1 (b)), which are known to be long-lived or subradiant [6], when the period of the system is less than a half of the resonant wavelength $a < 0.5\lambda_0$ ($\lambda_0 = 2\pi c/\omega_0$).

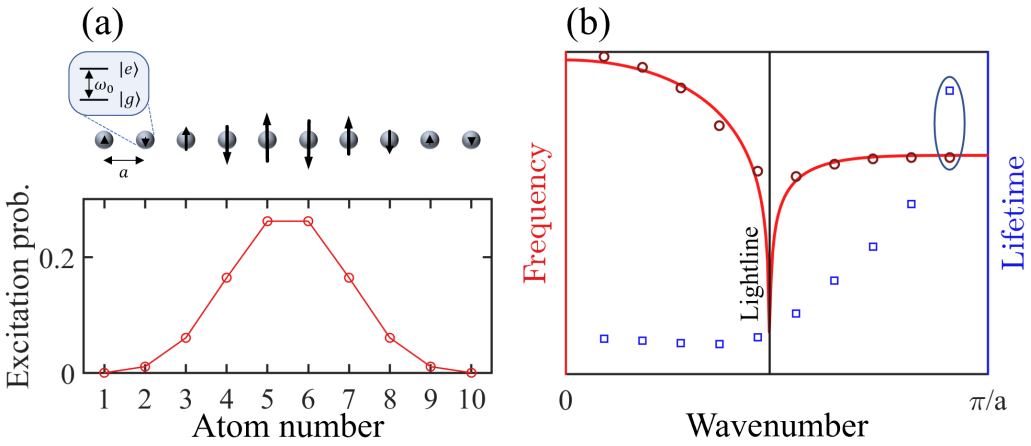

Figure 0.1 — (a) Top figure - a pictorial representation of a 1D array of $N = 10$ two-level atoms regularly spaced with a period equal to a. Black arrows represent the associated classical dipole moments for a state of interest. Bottom figure - probability for each atom to be excited for this state, note how the amplitudes of the dipole moments are suppressed close to the edges. (b) Frequencies (left axis) and lifetimes (right axis) of each eigenstate in the system versus the associated wavenumber, note that only a half of the Brilluoin zone is shown due to the symmetry of the problem. Bright red solid line, and dark red open circles denote the dispersions for an infinite and finite ($N = 10$) arrays, correspondingly, solid black vertical line is the lightline, blue squares are the corresponding lifetimes of all states for a finite array. The state of interest at the band edge is identified by an ellipse

Optical properties of dipole arrays arranged in one-dimensional chains have been studied extensively for a very long time already and one of the first work related to this subject touched the effect of retardation on optical properties of excitons in 1D [39]. Later on a huge interest to dipolar chains has been gained due to the promising applications in plasmonics, where arrays of

metallic nanoparticles were supposed to serve as a nanoscale waveguide for light allowing for a deep subwavelength localization of the electromagnetic field [40–42]. In this regard it became extremely important to better understand the optical properties of polarization modes in particle chains, especially the dispersion of eigenmodes, their radiative lifetimes [43–45], as well as the propagation of excitations [43; 46; 47]; many important results of these theoretical studies were exhaustively summarized in [48; 49]. It is also interesting to mention that the appearance of very narrow lattice resonances was predicted for infinite arrays of dipolar scatterers [50] as a result of calcellation of a single particle radiation losses by the imaginary part of the interaction through the radiation. Afterwards this was numerically shown for finite plasmonic nanoparticle arrays [51], and later it was experimentally confirmed that by tuning the system parameters one can control the widths of plasmonic resonances [52] owing to the aforementioned effect.

However, there is a major drawback of plasmonic systems - the presence of relatively large inevitable Ohmic losses, which can limit the applicability of them in real devices. This is why an alternative approach was also considered, for example, the one being based upon the use of optically resonant dielectric particles with high refractive index [53]. For linear arrays of such particles an efficient waveguiding with strong subwavelength transverse localization (comparable to plasmonic systems) was numerically predicted [54], as well as the possibility to exploit not only the electric dipole resonance, but also the magnetic one [55]. Waveguiding in dielectric nanoparticle chains was also shown experimentally in radiofrequencies [56], optical, and near-infrared domains [57]. One of very interesting theoretical results shown for this kind of systems was that the quality factors of guiding modes close to the edge of the Brillioun zone demonstrate a qubic growth with the system size $\sim N^3$, and it was explained through a quantum-mechanical analogy of optical guiding modes to localized states in a quantum well [30].

The interaction of dipole scatterers can be studied not only in the framework of classical physics, part of which plasmonics and nanophotonics are, but also in the area of quantum, and atomic optics. This is quite natural as all atoms of the same chemical element are identical by nature, and, moreover, when a particular dipole-allowed transition in an atom is considered, the characteristic size of an atom is much smaller than the optical wavelength. Owing to this, atomic ensembles also present an appealing subject to study. A number of theoretical studies have been devoted to quantum light-matter interactions in the simplest cases like a pair of atoms put in free space and interacting through the electromagnetic field modes [58; 59]. Later on theoretical studies of regular one-dimensional atomic arrays in free space were also conducted [60–62], with promising applications in many-body physics [63], atomic clocks [64], generation of long-

lived subradiant [6] states [65], etc. Even though atoms are quite different from classical dipoles as electrons in them obey the Fermi statistics, if one excites atoms weakly, they behave very similar to classical dipolar scatterers. In this regard, it is also worthy to mention early theoretical works by Vadim Markel [50; 66; 67] related to dielectric, and plasmonic particle arrays, which nevertheless grasp many important phenomena in such systems along with important theoretical approaches to the problem.

Despite the fact that direct confirmation of the theoretical predictions in experiment is quite challenging in atomic optics, some fascinating results were demonstrated. For instance, the interaction between two ions, and their super- and subradiance [68], as well as the collective effects like a cooperative Lamb-shift for a 1D array of Sr^+ ions of length up to 9 [69] were reported. Working with neutral atom rather than ions presents a challenging problem, especially when one wants to deterministically position them in space by loading minima of the optical potential with a single atom per site [70]. Advances in the experiments allowed to routinely create 1D [71; 72], 2D [16; 70; 73–75], and 3D [17; 76] arrays made of individual atoms as well as arbitrary 3D structures [17]. This opens up a whole plethora of possibilities in studying light-matter interaction in the quantum domain experimentally, promising many future breakthroughs yet to be demonstrated.

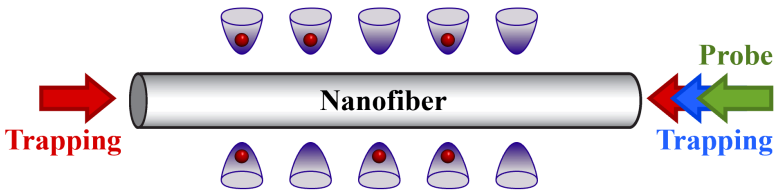

Figure 0.2 — A pictorial representation of atoms being trapped close to an optical nanofiber. Standing wave formed by a red-detuned attractive laser along with the repelling blue-detuned laser allow to create a set of periodically spaced local minima in which at most a single atom per minimum can be localized. In real experiments a perfect loading of all minima with atoms is not possible due to the collisional blockade [77]

Optical trapping of atoms is possible not only in free space, but also in the vicinity of different photonic structures. In the context of 1D systems optical nanofibers present a special interest. Compared to a common optical fiber, a nanofiber has a diameter of several hundred of nanometers, and operates in a single mode regime. Trapping atoms in the vicinity of it becomes possible by making use of two trapping lasers with opposite detunings from the atomic resonance [78; 79] ("repelling" and "attracting" lasers), due to the broken azimuthal symmetry of the field profile for specific modes [80], as well as owing to the standing waves created for the trapping laser (see Fig. 0.2), it is possible to localize atoms in all three dimensions, and fill in

each minima of the optical potential with at most one atom [81; 82]. Atoms localized close to a nanofiber present a realization of the so-called Waveguide Quantum Electrodynamical (WQED) system - a theoretical concept, which has been developed for many years already [18;83–95]. In such systems atoms, in opposition to Cavity QED, interact not with a completely localized cavity mode, but rather with a mode allowed to propagate along the waveguide. An important feature of such systems is the ability to realize long-range interactions between artificial [96] or real [22] atoms through the guided photons, allowing to observe phenomena like coherent [97], and large Bragg reflection from just a thousand atoms [20], superradiance [22], a possibility to generate single photons from a collective atomic state [21], and others. We want also to mention that in the field of WQED not only regular optical nanofibers are used, but also alternative systems like photonic crystal waveguides [98; 99], or hollow-core optical fibers, where, unlike for regular fibers, the atoms are trapped inside of the structure [100; 101].

All of the above confirms that systems of interacting quantum emitters arranged in a one-dimensional periodic chain is a very appealing object for theoretical studies as such systems can find potential applications in many areas of physics simultaneously. With regard to this particular thesis, in **the first chapter** we are going to demonstrate that by simply tuning the period of the array one can achieve a significant further increase in the lifetime of subradiant states at the edge of the Brillouin zone than was known before, and in this regime some optical properties of these modes will be noticeably modified due to the interaction between the normal modes. More specifically, we will show that the known scaling law of the inverse lifetime (or, equivalently, emission rates) does not follow the aforementioned $\sim N^{-3}$ dependence shown in many previous works [30–32; 102], but rather demonstrates a much faster decrease rate. We will also discuss how these states are manifested in the scattering cross section spectra. We are going to relate the appearance of long-lived modes to the band-edge dispersion becoming flat by considering an infinite periodic dipole chain, and we will find analytically the asymptotic value of the corresponding optimal period for which this band-edge state appears. We will also show that for such states a peculiar phenomena appears - simultaneous reduction of multipolar contributions up to a high multipole order. Additionally, we will also show that such states are preserved even in the presence of an additional interaction channel through a guided mode of the optical nanofiber (apart from the free-space dipole-dipole interaction responsible for the appearance of these subradiant states).

In **the second chapter** we will discuss some features of the system consisting of N two-level atoms, which are unidirectionally coupled with each other through a single guided mode. Namely, we will study how a single

excitation behaves in time in such a system (see Fig. 0.3 (a)), and also look at the collective emission in a single excitation domain, more precisely, we want to study sub- and superradiance (see Fig. 0.3 (b)).

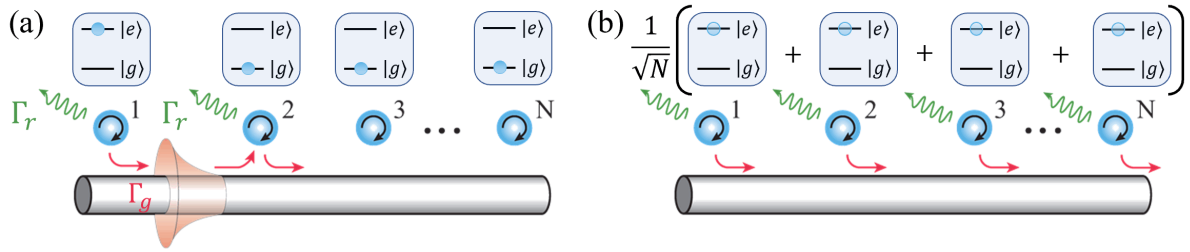

Figure 0.3 — (a) Schematic representation of a single-excitation transport problem in a chain of N two-level atoms, which are unidirectionally coupled to a guided mode propagating along the waveguide. Here Γ_g is the emission rate into the guided mode, Γ_r is for the emission rate into non-guided or radiation modes. (b) A problem of a collective emission for the same system, but now a single excitation is equivalently distributed between all N atoms

Unidirectional coupling of emitters through a guided mode presents an extreme case of asymmetric or *chiral* coupling. The asymmetry in the atom-atom coupling is a direct consequence of chirality in the atom-guided photon interaction, and the latter means that the strength of atom-photon interaction may significantly depend on the direction of photon propagation as well as the polarization of the active transition in the emitter. This asymmetry appears due to the spin-orbit interaction of light [34] or spin Hall effect of light [23], which couples the linear momentum (wavevector direction) with the local spin density (the local polarization of light). This can be superficially explained for a lightfield in a waveguide in the following way. The field in a waveguide freely propagates along it, but it is tightly confined in the transverse direction. The result of this confinement of the lightfield is that there is a phaseshift of $\pm\pi/2$ between the longitudinal and transverse components of the electric field. Such a phaseshift results in the electric field vector rotation, and this rotation, unlike in the plane wave case, happens in the plane that is not perpendicular to the propagation direction: a situation sometimes called a photonic wheel [103]. The sign of the aforementioned phaseshift simply depends on whether the field propagates in the forward or backward direction, leading to a spin-momentum locking [35], which makes the local helicity of the guided mode being dependent on the propagation direction. One can conclude that when studying the light-matter interaction, the propagation direction of light controls the way it couples with matter. Now if at a given frequency emitter has a dominant active transition with a rotating dipole moment, it turns out that its optical response is dependent on the direction from which the photon is coming, and this principle lies in the heart of a vast area of research called *chiral quantum optics* [10].

In the field of theory many novel physical effects have been predicted so far in this regard, to mention a few: an asymmetric scattering, and directional spontaneous emission [104], and the existence of a lateral Casimir-Polder force for an atom near a single mode nanofiber [105], as well as a vacuum-dielectric interface [106]; an improved spontaneous entanglement generation between the two atoms chirally coupled through the guided mode [107]; formation of dimer states in a one-dimensional chain of atoms [108], and many more.

However, such systems are of interest not just for fundamental physics, but they also promise interesting applications. When it comes to experimental realization, there are different platforms on which one can realize a chiral light-matter interface. One of such platforms is based on ultracold atomic ensembles optically trapped in the vicinity of a nanofiber [81], which we discussed previously. For such systems many application-focused results were demonstrated, including the creation of an optical circulator [12;109] from a atom-cavity-waveguides system [14], optical isolator based both on a single atom and atomic ensemble in the vicinity of a nanofiber [13], etc.

Even though ultracold atomic ensembles present an interesting and versatile tool for experimentalists in quantum optics, it is still more of a proof-of-principle platform as the complexity of the experimental set-up prevents it from being a suitable candidate for a realistic quantum nanophotonic device with the possibility of on-chip integration. For this reason alternative systems are also studied in this regard, for instance, the ones based on quantum dots rather than atoms. For this kind of set-up a control over emission direction with laser field polarization has been shown [110] for two crossed waveguides, as well as deterministic photon-emitter coupling for a quantum dot on a surface of a photonic crystal waveguide [24]. Deterministic here means that: I) the probability for an emitter to launch the photon into the guided mode is close enough to unity [111]; II) due to the directionality in the scattering process, the photon is predominantly emitted into a desired direction instead of having only 50% efficiency of this process in a non-chiral case (see Fig. 0.4). This feature is of specific importance for practical applications, for instance, a high directionality of the spontaneous emission is of big importance for the development of on-demand single photon sources.

It is also important to mention that chiral quantum optical systems present a possible realization of so-called *cascaded quantum systems* [112;113], where the output of a given system is fed into the input of the other one. This is in some sense equivalent to a unidirectional propagation as the photon scattered by an emitter is passed further to the next one, and can be re-absorbed, and re-emitted again without any back-reflection. More than that, theoretical studies of light-matter interaction in a one-dimensional case, where atoms are coupled only to a single mode [83;114;115] (sometimes referred to as a chiral

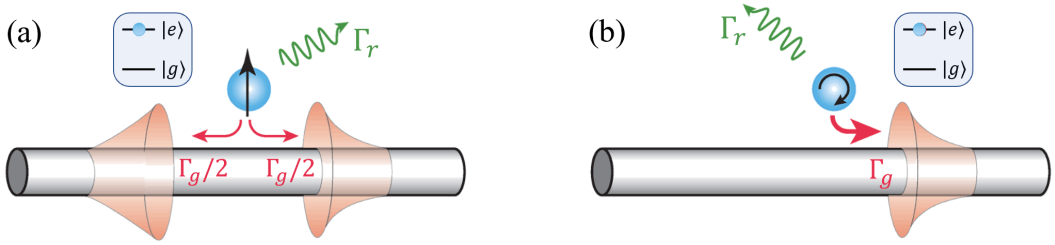

Figure 0.4 — Illustration of atom-guided mode interaction regimes. (a) A two-level atom with a linear dipole moment symmetrically couples to forward and backward propagating modes, therefore, the propability to emit a photon into a desired direction is 50%. (b) When the transition dipole moment is a rotating one, it is possible to couple selectively to a forward-propagating mode, for instance, which leads to a 100% of the radiation emitted into the guided mode to propagate into a desired direction

mode) were also of interest much before the spin-orbit interaction of light and spin-momentum locking were even discussed as such modes naturally appear after, for instance, a proper change of basis in the subspace of photonic states [87; 93; 116–118].

As was mentioned above, such a broken symmetry in the way emitter interacts with the propagating photons may alter significantly how different physical phenomena are manifested. One of such collective effects are the sub-, and superradiance, both of these phenomena were a subject of a large amount of studies for a long time both in theory [6–9; 115; 119–125] and experiments [22; 68; 126–133] for different kinds of systems. As was discussed previously by researchers [10; 134] chirality, indeed, should alter the way how a system that was initially put into a collective sub- or superradiant state decays in comparison with the case of symmetric interaction. However, this was only stated as a matter of fact, and not described neither qualitatively, nor quantitatively by finding the chiral emission rates. This is exactly what is going to be covered in the second chapter: we will derive the values of sub- and superradiant single-excitation chiral emission rates, and will explain the appearing discrepancies with the case of symmetric interaction, where appropriate.

The third chapter of this thesis is also devoted to the subject of chiral coupling. However, instead of considering how distant atoms with rotating dipole moments can be asymmetrically coupled through the electromagnetic modes of the environment, and what kind of consequences such an asymmetric interaction has, we will study chiral interaction of circularly polarized transitions inside a single quantum emitter. The interest to this problem began to raise in the scientific community with the appearance of the pioneer work by Girish Agarwal [135], where he proposed the following idea. Imagine an atom with two excited states with closely lying

transition frequencies and circularly polarized transition dipole moments (it can be a V-type atom, for example, as shown in Fig. 0.5). If such an atom is placed into free space, these two transitions are orthogonal, which means that the transition rate for an electron to be transferred from one excited state to the other is zero (Fig. 0.5, (a)). This is a direct consequence of the *isotropy* of free space, or, mathematically it can be directly linked to the fact that the classical electromagnetic local Green's tensor for the free-space is proportional to a 3×3 unit tensor. However, if one puts an atom close to an interface between two different media then the isotropy of space is broken, and, therefore, the two transitions can be coupled (Fig. 0.5, (b)). This phenomenon was named *Anisotropic Vacuum-Induced Interference (AVI)*, and the consequence of this effect is that the population can be transferred between the excited states even in the absence of any external pumping laser field.

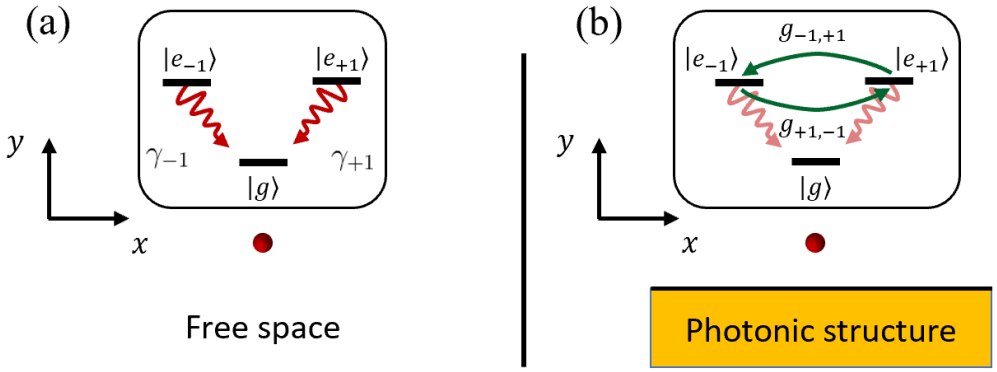

Figure 0.5 — An example of a system, where one can observe the AVI. (a) A V-type atom with two excited states $|e_{-1}\rangle, |e_{+1}\rangle$ with corresponding rotating transition dipole moments $\mathbf{d}_{\pm\mathbf{1}} = \mp\frac{|\mathbf{d}|}{\sqrt{2}}(\mathbf{e_x} \pm i\mathbf{e_y})$ that are not coupled in free space due to isotropy as x, and y directions are equivalent, only the spontaneous emission from both of the excited states is present. (b) The same V-atom, but put in the vicinity of a nanostructure. Apart from the spontaneous emission there is coupling between the states due to the AVI effect (x, and y are not equivalent anymore) characterized by constants $g_{-1,+1}, g_{+1,-1}$, and this coupling leads to the population transfer between the states. Note that it is assumed that both transition dipole moments rotate in the $x - y$ plane

After this, many theoretical works were devoted to the studies of this effect for different kinds of photonic, and plasmonic structures: AVI for an atom in a planar multilayer dielectric medium [136], a strong enhancement of the AVI effect owing to the use of left-handed materials [137] or plasmonic structures [138; 139], etc. Much later G. Agarwal along with S. Hughes [140] discussed another interesting consequence of this effect: the possibility to enhance or, more importantly, suppress the emission rate of an atom due to constructive

or destructive interference between the decay channels. AVI also led to the unusual spectral properties of a V-type emitter under the external pumping: instead of the Mollow triplet [141] appearing for a two-level atom, a much richer spectrum is observed due to the dressing of the field-driven exciting states by the electromagnetic vacuum. Even though in this paper S. Hughes, and G. Agarwal proposed a set-up with a potential experimental realization, and they have used experimentally feasible parameters in their model, to our knowledge, there is no confirmed direct observation of this phenomenon. However, we must say that the anisotropic spontaneous emission rate, for instance, has been reported by Peter Lodahl's team [142] for a quantum dot put on a two-dimensional photonic crystal. The reason for the lack of an experimental demonstration is due to the requirement to get into the strong coupling regime when the active transitions are interacting strong enough to achieve a sufficient level splitting between the dressed states, leading to the energy exchange between the bare states of the emitter. This can be realized when a quantum emitter is positioned very close to the surface of the structure compared to the corresponding resonant wavelength. However, in this case surface interactions like Casimir-Polder interactions [143; 144], surface thermal noise and etc. might play a very significant role, and make it extremely challenging to perform such an experiment.

In order to overcome these difficulties, it was proposed to enhance the AVI even when the emitter is positioned in the far-field region from the structure surface [145] by using a specifically designed array of antennas with a subwavelength size (an optical metasurface), which plays a role of a "mirror" for an emitting dipole. It was shown theoretically that in this set-up a population transfer on the order of 1% is achievable even if the emitter is positioned 20 resonant wavelengths away from the structure. Later on metasurfaces of other designs were proposed to generate spontaneous coherence between different states of excitons in novel two-dimensional materials [146], and between the ground states of a λ-type atom [147]. The metasurface mentioned above [148; 149] is a two-dimensional version of a metamaterial [150; 151] - an artificially created medium made of subwavelength optical photonic and/or plasmonic elements called meta-atoms. The use of such meta-atoms along with their proper arrangement allows to achieve optical properties not found in natural materials, for instance, the ability to shape the profile of lightfields at a deep-subwavelength scale.

In sharp contrast to previous studies, we have also shown in the third chapter that the interaction betweeen the excited states due to the AVI effect can be asymmetric, and even unidirectional - a subject that has not been discussed at all up to now. One can formulate the goal in the following way: we want the probabilities of an electron to make transitions between the excited

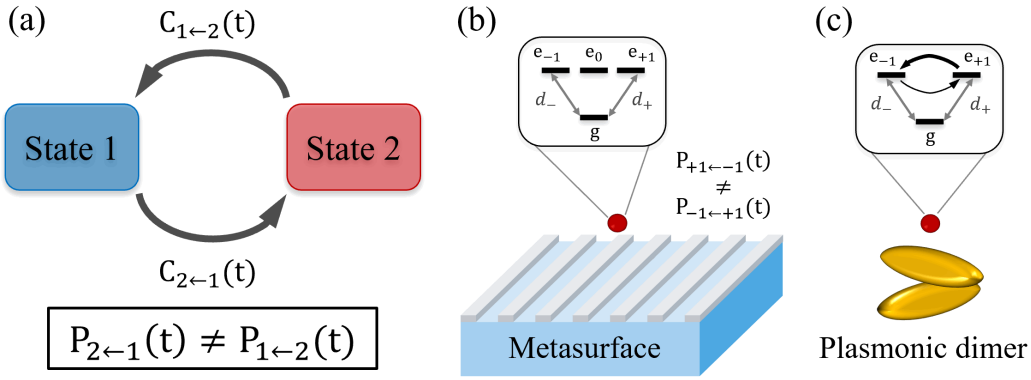

Figure 0.6 — (a) The two quantum mechanical states of the system, which are coupled due to some interaction between them. Our primary goal is to achieve inequality in the transition probabilities $P_{2\leftarrow 1} \neq P_{1\leftarrow 2}$. (b) An example of a system, where one can achieve asymmetry in transitions: a 4-level atom with a triple degeneracy in the excited state, which is placed in the vicinity of an anisotropic metasurface so that the dipole transitions become coupled due to the AVI effect. (c) Another example of a system allowing to achieve this kind of asymmetry: a V-type atom with 2 excited states, which interact through the electromagnetic modes of a structure - a plasmonic dimer made of asymmetric particles

states in one and in the opposite directions to become unequal $P_{-1,+1} \neq P_{+1,-1}$. We will demonstrate that there are at least two ways of doing so. The first way is to consider interaction with the modes of a nanophotonic structure that is locally fully anisotropic, which means that not just two, but all three directions are physically not equivalent (Fig. 0.6 (b)). Another important requirement is that one has to consider an arbitrary orientation of transition dipole moments with respect to highly symmetric directions characterizing the structure. The second way physically looks very similar to what has been discussed in the previous chapter: we will present an example of a very simple structure based on a pair of anisotropic scatterers (Fig. 0.6 (c)), which allows to completely forbid transitions of an electron in one direction, which means that the corresponding coupling constant zero: $g_{-1,+1} = 0$. We will also discuss how both of these effects can be, in principle, observed in the experiment.

1. Extreme subradiance in subdiffractional periodic dipolar chains

1.1 Single-photon scattering on a two-level atom chain in free space: theoretical framework

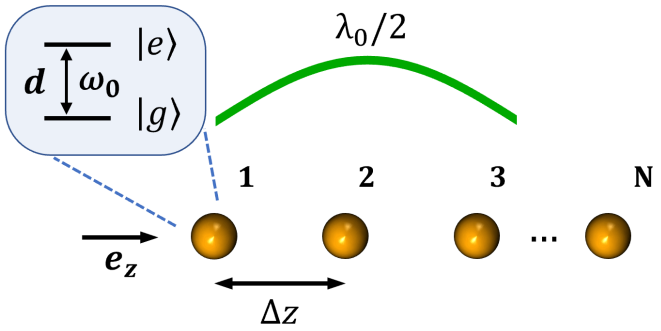

Figure 1.1 — N two-level atoms with resonance transition frequency ω_0, and transition dipole moment $\mathbf{d}$ are arranged in a periodic one-dimensional chain along the $\mathbf{e_z}$ direction. The period Δz is such that it is smaller than a half of a resonant wavelength $\lambda_0 = 2\pi c/\omega_0$, (shown in green) where c is the speed of light

In this chapter, we want to study optical properties of a very simple system (see Fig. 1.1): an ensemble of N two-level atoms, which are arranged in a one-dimensional periodic chain along a given direction (let us call it the z-axis). Atoms are characterized by transition dipole moments $\mathbf{d}$, and resonance frequency ω_0, or, equivalently, by a resonant wavelength $\lambda_0 = 2\pi c/\omega_0$. It is known [43] that there are two principally important types of modes in 1D chains of dipole scatterers: the ones with dipole moments being transverse or longitudinal to the chain axis, and we will consider only these two cases from now on. We are also going to study only the case, when the spacing between the atoms is smaller than a half of a resonance wavelength $\Delta z < \lambda_0/2$ as in this subdiffractional regime the subradiant states appear with linewidths being much smaller than that of an isolated single atom, and these subradiant states will be of special interest for us. This can be easily understood if one views this system as a diffraction grating, then with such a spacing between the atoms there are no open diffraction channels, therefore, radiation losses into the far-field can be highly suppressed.

Here we will not only study the polarization eigenmodes in such a chain, but also how they affect the spectral properties of the system, for instance, the single photon scattering cross-section. Therefore, we need to discuss how a single photon of the field mode scatters off N two-level atoms, so that the

initial, and the final states in the scattering process can be written as: $|l\rangle = |g\rangle^{\otimes N}|1_{\mu}\rangle$, $|k\rangle = |g\rangle^{\otimes N}|1_{\mu'}\rangle$. The index $\mu = (\mathbf{k}, s)$ here indicates the field mode with the wavevector $\mathbf{k}$, and polarization s, $|g\rangle^{\otimes N}$ in $|l\rangle$, and $|k\rangle$ indicates that for both initial, and final state all N atoms are in the ground state.

The process of photon scattering is described by the T-matrix, or transition matrix [4], which has the form:

$$\hat{T} = \hat{V} + \hat{V}\hat{G}(E + i0)\hat{V}, \tag{1.1}$$

where $\hat{G}(E) = \dfrac{1}{E - \hat{H}}$ is the resolvent operator of the full Hamiltonian $\hat{H}$ consisting of the unperturbed part $\hat{H}_0$, and perturbation $\hat{V}$. We consider two-level atoms with dipole-allowed $|g\rangle \leftrightarrow |e\rangle$ transition, so that the unperturbed Hamiltonian is written as $\hat{H}_0 = \sum_{\mathbf{k},s} \hbar\omega_{\mathbf{k},s}\hat{a}^{\dagger}_{\mathbf{k},s}\hat{a}_{\mathbf{k},s} + \sum_{j=1}^{N} \hbar\omega_0 \left(|g\rangle\langle g|\right)^{\otimes N-1} |e_j\rangle\langle e_j|$, and the perturbation in the dipole approximation reads as $\hat{V} = -\sum_{i=1}^{N} \hat{\mathbf{d}}_i\hat{\mathbf{E}}(\mathbf{r}_i)$, with $\hat{\mathbf{d}}_i = d_{i,eg}\hat{\sigma}^{+}_i + d_{i,ge}\hat{\sigma}^{-}_i$ being the operator of dipole moment for atom i, and $\hat{\mathbf{E}}(\mathbf{r}_i)$ here is the field operator calculated at the corresponding atomic position $\mathbf{r}_i$.

Instead of finding the resolvent operator $\hat{G}$ exactly on the whole Hilbert space of the problem, one can rather calculate the corresponding projection of this operator onto the relevant Hilbert subspace [4]:

$$\begin{aligned} \hat{P}\hat{G}(E)\hat{P} &= \hat{P}\frac{1}{E - \hat{H}_0 - \hat{\Sigma}(E)}\hat{P}, \\ \hat{\Sigma}(E) &= \hat{V}\frac{1}{E - \hat{H}}\hat{V}, \end{aligned} \tag{1.2}$$

where $\hat{P}$ is the corresponding projector, and $\hat{\Sigma}$ is the level-shift operator (also called the self-energy part). The subspace onto which the resolvent has to be projected can be easily found from the form of the initial and final states, and the outer perturbation operators $\hat{V}$ entering the definition of the T-matrix in Eq. (1.1). The right $\hat{V}$ operator absorbs the incoming photon from mode μ, and simultaneously excites one out of N atoms, while the right $\hat{V}$ operator de-excites one atom, creating an out-going photon in the mode μ'. Therefore, the projection operator is equal to: $\hat{P} = \sum_{i=1}^{N} |e_i\rangle|g\rangle^{N-1}|\{0_{\mu}\}\rangle\langle\{0_{\mu}\}|\langle g|^{\otimes N-1}\langle e_i|$.

The level-shift operator $\hat{\Sigma}$, as can be seen from Eq. (1.2), provides the modification of the unperturbed Hamiltonian spectrum $\hat{H}_0$ due to the interaction $\hat{V}$. In the lowest (2^{nd} order) of perturbation theory, this operator can be written as $\hat{\Sigma}(E) \approx \hat{V}\left(E - \hat{H}_0\right)^{-1}\hat{V}$. We also study near-resonant scattering, which means that the frequency of the incoming photon ω is very close to the resonance frequency of the corresponding atomic transition ω_0. In this regard, we can assume that $\hat{\Sigma}(E)$ is a slowly varying function of

its argument ($E = \hbar\omega \approx \hbar\omega_0$), and treat it as a quantity independent of the energy of the incoming photon, taking it at the frequency of the atomic transition $\hat{\Sigma}(E) \approx \hat{\Sigma}(\hbar\omega_0)$. One can see from Eq. (1.2) that the level-shift operator has to be also found only in the subspace of states corresponding to $\hat{P}$, where it is equal to [152; 153]:

$$\begin{aligned}\Sigma_{n,n}(\hbar\omega_0) &= \hbar\left(\Delta_{\mathrm{L}}^{\mathrm{vac}} - i\frac{\gamma_0}{2}\right)\\ \Sigma_{m,n}(\hbar\omega_0) &= -\mathbf{d}_{m,eg}\left[\frac{k_0^2 e^{ik_0R}}{R}\left(\left(1+\frac{ik_0R-1}{k_0^2R^2}\right)\mathbf{I}\right.\right.\\ &+ \left.\left.\frac{\mathbf{R}\otimes\mathbf{R}}{R^2}\cdot\frac{3-3ikR-k^2R^2}{k^2R^2}\right)\right]\mathbf{d}_{n,ge}. \qquad (1.3)\end{aligned}$$

In the above $\Delta_{\mathrm{L}}^{\mathrm{vac}}$ is the vacuum Lamb shift, $\gamma_0 = \frac{4|\mathbf{d}|^2\omega_0^3}{3\hbar c^3}$ is the spontaneous emission rate for a two-level atom put in free space, $k_0 = \omega_0/c$ is the resonant wavenumber, $\mathbf{R} = |\mathbf{r}_i - \mathbf{r}_j|$ is the distance between the atoms i and j, $\mathbf{I}$ is the 3×3 unit matrix, and $\otimes$ is the outer (dyadic) product. This is nothing else than a classical dipole-dipole interaction of atomic transitions through the electromagnetic field, which can be fully described by the classical electromagnetic Green's tensor [152]. Here $\Sigma_{n,n}$ physically corresponds to the interaction of the atomic transition with itself in a given atom, and the real part of this interaction energy $\hbar\Delta_{\mathrm{L}}^{\mathrm{vac}}$ is formally divergent as naturally comes from the properties of the vacuum classical electromagnetic Green's tensor. This quantity, as usually, is considered to be already included into the definition of the atomic transition frequency ω_0.

In free space scattering it makes sense to characterize the process by the total scattering cross section, which can be found through the optical theorem as [153]:

$$\sigma_{\mathrm{tot}} = -\frac{2\mathbb{V}}{\hbar c}\mathrm{Im}\, T_{ii}(E_i + i0), \qquad (1.4)$$

where $\mathbb{V}$ is the quantization volume. We mentioned before that $\hat{\Sigma}$ alters the eigenstates of $\hat{H}_0$, and the new eigenstates of the system are of collective nature. Therefore, it makes sense to rewrite the optical theorem so that it accounts for this fact and expresses the cross section as a sum of contributions from each eigenstate. To do this, first notice that from Eq. (1.2) it is obvious that both matrices Σ, and G have the same set of eigenvectors, as $E - H_0$ is a diagonal matrix. Let Λ_Σ be the matrix Σ in the eigenbasis, and S is the corresponding transformation matrix to this eigenspace, then $\Sigma = S\Lambda_\Sigma S^{-1}$. Having that, and the form of the electric field operator $\hat{E}(\mathbf{r}) =$

$\sum_{\mathbf{k},s} i\sqrt{\frac{2\pi\hbar\omega}{\mathbb{V}}}\left(\hat{a}_{\mathbf{k},s}\mathbf{e}_{\mathbf{k},\mathbf{s}}e^{i\mathbf{kr}} - h.c.\right)$, we can rewrite Eq. (1.4) as:

$$\sigma_{\text{tot}}(\Delta) = \sum_{j=1}^{N}\sigma_j(\Delta) = -\frac{3\pi\hbar\gamma_0}{k_0^2}\text{Im}\sum_{j=1}^{N}\frac{f_j}{\hbar\Delta - \lambda_j},$$
$$f_j = \left[\left(e^{-i\mathbf{kr_1}},...,e^{-i\mathbf{kr_N}}\right)S_{\{:,j\}}\right]\cdot\left[[S^{-1}]_{\{j,:\}}\left(e^{i\mathbf{kr_1}},...,e^{i\mathbf{kr_N}}\right)^T\right], \tag{1.5}$$

here $S_{\{:,j\}}$ denotes the j^{th} column of the matrix S, f_j is the complex-valued oscillator strength amplitude of the eigenstate j. In its definition, $\left(e^{i\mathbf{kr_1}},...,e^{i\mathbf{kr_N}}\right)$ comes from the phase that an incoming photon imprints on each atomic eigenstate (similarly for the out-going photon), therefore, f_j is proportional to the overlap between the photon and the eigenstate j. The normalization is such that $\sum_{j=1}^{N} f_j = N$, which means that there are N collective states in total. We want to note that expressions similar to those in Eq. (1.5) were first derived for a collection of classical dipole scatterers [154].

The expansion Eq. (1.5) allows to express the contribution of each eigenstate to the total cross section, and such contributions can be written as:

$$\sigma_{\text{tot}}(\Delta) = \sum_j \sigma_j(\Delta) = -\frac{3\pi\hbar\gamma_0}{k_0^2}\sum_j \frac{f_j'\lambda'' + f_j''\left(\hbar\Delta - \lambda_j'\right)}{(\hbar\Delta - \lambda_j')^2 + \lambda_j''^2}, \tag{1.6}$$

in the above prime sign indicates the real part of the quantity, while the double prime - the imaginary part. Now we can clearly see that each $\sigma_j(\Delta)$ consists of two terms: Lorentzian-shaped term proportional to f_j' (dissipative term), and asymmetric term proportional to f_j'' (dispersive term). The dispersive term appears as a result of interaction between the atoms, which can be illustrated by the following example. Consider a simple case with $N = 1$, then $f = 1$, and $f'' = 0$, so the total scattering cross section for an isolated atom takes the form $\sigma_{1a}(\Delta) = \frac{3\pi\gamma_0}{k_0^2}\frac{\gamma_0/2}{\Delta^2 + \gamma_0^2/4}$, with the resonant value equal to $\sigma_{1a}(0) = 6\pi k_0^{-2}$, as expected. The same spectral profile will be obtained if one considers a collection of non-interacting atoms (spaced very far from each other) - the cross section will be a sum of contributions from each atom $\sigma_{Na}(\Delta) = N\sigma_{1a}(\Delta)$. However, for $N > 1$, in case of interacting atoms, f_j might have both real and imaginary parts (apart from some very specific cases), therefore, leading to the appearance of asymmetrical peaks in the spectrum.

There is another reason to use the expansion presented in Eq. (1.5). As Equations (1.4), (1.2) suggest, in order to find the value of $\sigma_{\text{tot}}(\omega)$ at a particular frequency, one has to invert the operator $\hbar\omega - \hat{H}_0 - \hat{\Sigma}(\hbar\omega_0)$, which

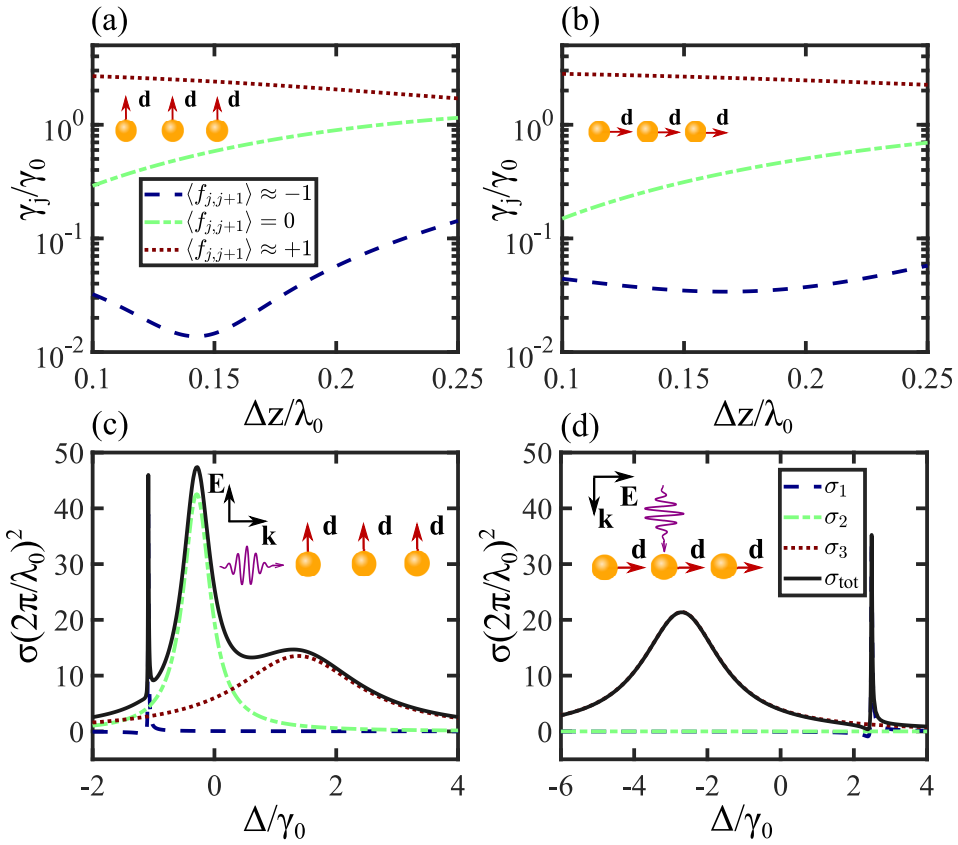

Figure 1.2 — (a), (b) Spontaneous emission rates γ_j/γ_0 for the case of $N = 3$ atoms versus the period $\Delta z/\lambda_0$. Blue dashed, green dashed-dotted, and red dotted lines correspond to three states with different values of the nearest-neighbor correlation function Eq. (1.9). (c), (d) The total cross sections as well as $\sigma_j(\Delta)$ contributions, calculated for the periods Δz giving the minimal γ_j/γ

is an $N \times N$ matrix for N two-level atoms. Instead, if one diagonalizes the Σ matrix first (finds both eigenvalues, and eigenvectors), the total cross section can be easily found with the help of Eq. (1.5). For large atomic ensembles this might be an important trick to use in order to save the computational time.

1.2 An example of $N = 3$ atoms in a chain

Now let us proceed by looking in-details at the case of $N = 3$ atoms, for which the matrix of the level-shift operator has the form:

$$\Sigma = \begin{pmatrix} -i\gamma_0/2 & \Sigma_1 & \Sigma_2 \\ \Sigma_1 & -i\gamma_0/2 & \Sigma_1 \\ \Sigma_2 & \Sigma_1 & -i\gamma_0/2 \end{pmatrix}, \tag{1.7}$$

where Σ_1 expresses the coupling of the nearest neighbors (atoms 1-2, and 2-3), while Σ_2 is related to the interaction of the next nearest neighbors (atoms 1-3). The eigenvalues for this matrix can be readily written:

$$\begin{aligned} \lambda_1 &= \frac{1}{2}\left(-i\gamma_0 + \Sigma_2 + \sqrt{8\Sigma_1^2 + \Sigma_2^2}\right), \\ \lambda_2 &= -i\gamma_0/2 - \Sigma_2, \\ \lambda_3 &= \frac{1}{2}\left(-i\gamma_0 + \Sigma_2 - \sqrt{8\Sigma_1^2 + \Sigma_2^2}\right). \end{aligned} \tag{1.8}$$

In order to characterize the corresponding eigenvectors, there is an illustrative measure introduced in [61]:

$$\langle f^j_{i,i+1} \rangle = \frac{1}{N-1} \sum_{i=1}^{N} \cos(\varphi^j_{i+1} - \varphi^j_i), \tag{1.9}$$

with $\varphi^j_i = \arg\left[c^j_i\right]$ being the phase of the probability amplitude for atom i in eigenstate j to be excited. As these probability amplitudes can be classically interpreted as the values of dipole moments, the quantity above is an average correlation between all nearest neighbors in a chain, hence the name - *nearest-neighbor correlation function*. It is equal to $+1$, when all dipole moments are parallel, and -1, when any two nearest neighbors are anti-parallel.

The spontaneous emission rates given by $\gamma_j = -2\mathrm{Im}\left[\lambda_j\right]$, as Eq. (1.9) suggests, are illustrated in Fig. 1.2 (a), and (b), where (a), and (b) correspond to the case of transition dipole moments being perpendicular or parallel to the chain (transverse, and longitudinal modes of the system [43]). Note that for the transverse case, there is a specific period Δz, for which the local minimum of γ_j/γ_0 is achieved for the mode with $\langle f_{j,j+1} \rangle \approx -1$. For the longitudinal case there is also a similar minimum, but much less pronounced, and it appears for a different value of the period. As seen from Fig. 1.2 (c), and (d), these states are present in the scattering cross section spectra as sharp asymmetric peaks, and this asymmetry is the result of an anti-symmetric part $\sim f''_j$ giving a significant contribution to the cross section.

1.3 Subradiance for larger arrays

In the previous part we observed that there is a state with a reduced emission rate achieved at a specific period of the system Δz for $N = 3$ two-level atoms, in this part we will discuss what happens as if we consider a larger

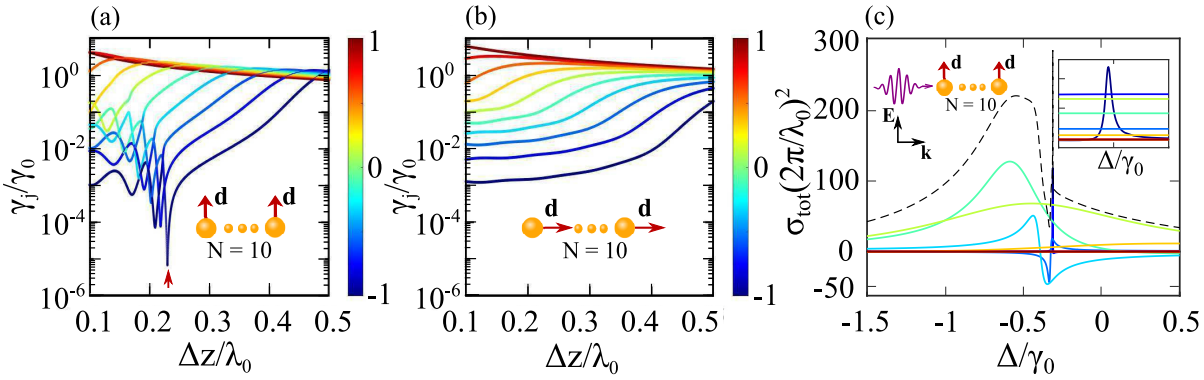

Figure 1.3 — (a), (b) Spontaneous emission rates γ_j/γ_0 for $N = 10$ different eigenstates as a function of the array period Δz for transversal (a), and longitudinal (b) modes. Red arrow points at the global minimum of the emission rate, and the corresponding optimal period. (c) The total cross section (dashed black) σ_{tot} for the transverse orientation of the dipole moments and an array period shown by the red arrow in (a), which is approximately $\Delta z \approx 0.23\lambda_0$. The inset shows the region near the most subradiant state more in-detail

number of atoms N. We can expect that as the number of atoms increases, the collective effects become more pronounced. Indeed, as can be seen from Fig. 1.3, now the relative reduction of the emission rate (subradiance) is much larger for $N = 10$ than we observed previously for $N = 3$. By comparing the Figures 1.3 (a) and (b) we can also see that for larger arrays the difference between the transverse and longitudinal modes becomes very clear: for longitudinal modes there is no such optimal period that would allow for the significant reduction of the linewidth for any mode of the system, γ_j/γ_0 as functions of Δz look rather smooth with no pecularities/dips whatsoever.

Interestingly, for transversal modes, there are many peaks corresponding to subradiant states, all of which appear for periods, roughly speaking, $\Delta z < \lambda_0/4$, while for $\lambda_0/4 < \Delta z < \lambda_0/2$ emission rates demonstrate a quite smooth behavior similarly to longitudinal modes. Obviously, for $\Delta z > \lambda_0/2$ there is no subradiance as the array is not subdiffractional anymore, and all of the collective states have significantly larger values of γ_j.

As an example, in Fig. 1.3 (c) we present cross section spectrum, and its eigenstate expansion, for a system period corresponding to a minimal possible γ_j/γ_0 (specified by a red arrow in Fig. 1.3 (a)). As in $N = 3$ case, there is a distinct sharp and quite asymmetric peak as an evidence of the subradiant state. However, we should note that a large amplitude in σ_{tot} near the spectral position of this peak is a result of several overlapping resonances, leading to a large cross section value.

One of the important characteristics of optical states with small emission rate is how does this quantity scale with the system size N. It was known already that for a subdiffraction chain of dielectric particles the modes at

the band-edge (and, therefore, the smallest value of the nearest-neighbor correlation function $\langle f_{j,j+1} \rangle$) demonstrate the quality factors scaling $\sim N^3$ [30]. During recent years this question was also revisited in the context of atomic optics, where it has been shown theoretically that the linewidths of subradiant states close to the edge of the Brillouin zone decrease as $\sim N^{-3}$ [31; 32; 155].

However, in these studies researchers did not try to optimize the emission rate, they rather tried to understand the general behavior of such states. It turns out that if one properly tunes only a single parameter - the period Δz - it immediately becomes possible to achieve a much smaller value of γ_j (as in Fig. 1.3 (a)). The emission rate scales as $\sim N^{-6.88}$ in contrast to a known $\sim N^{-3}$ scaling law, as can be seen from Fig. 1.4 (a). This faster decaying scaling law is possible to achieve due to a proper tuning of the period for each N, as seen from Fig. 1.4 (b). For large enough number of atoms $N \gg 1$, the value of this optimal period saturates, reaching the one close to $\Delta z_{\text{sub}} \approx 0.241\lambda_0$. We will clarify on why the asymptotic optimal period has this exact value, and derive it precisely later.

As we know from Eq. (1.5), in the scattering problem, apart from the eigenenergies λ_j, we also need to know the oscillator strength amplitudes f_j. As can be seen from Fig. 1.4 (c), the absolute value of this quantity $|f_j|$ follows a quite similar behavior to the observed before for $\gamma_j(N)$, but with some additional "oscillations". This difference from a simple $\sim N^\alpha$ behavior comes from a varying overlap between the incoming z-propagating photon, and the collective eigenmode as N increases. By having a closer look, one can see that the distance between the local minima of $f_j(N)$ is close to be $\Delta N = 4$ in the case of the optimized period Δz_{sub}. The reason for this can be easily understood from the following: for large enough N, as N increases further, the phase structure of a given collective mode does not change too much, however, the total phase acquired by a photon propagating along the chain grows linearly with N. Therefore, as $\Delta z_{\text{sub}} \approx 0.241\lambda_0$ for large N (as the period is close to $0.25\lambda_0$), we can expect that the oscillating part will have a half-period approximately equal to $\Delta N = 4$ as $\Delta N \Delta z_{\text{sub}}/\lambda_0 \approx \pi$.

Now that we have discussed how do different quantities vary with N, it makes sense to analyze the limit of an infinite chain $N \to \infty$, as in this case some things can be found analytically due to the periodicity of the system. Indeed, as we will show in the next part, the analysis of polarization waves dispersion will clarify certain things about the appearance of these highly subradiant states.

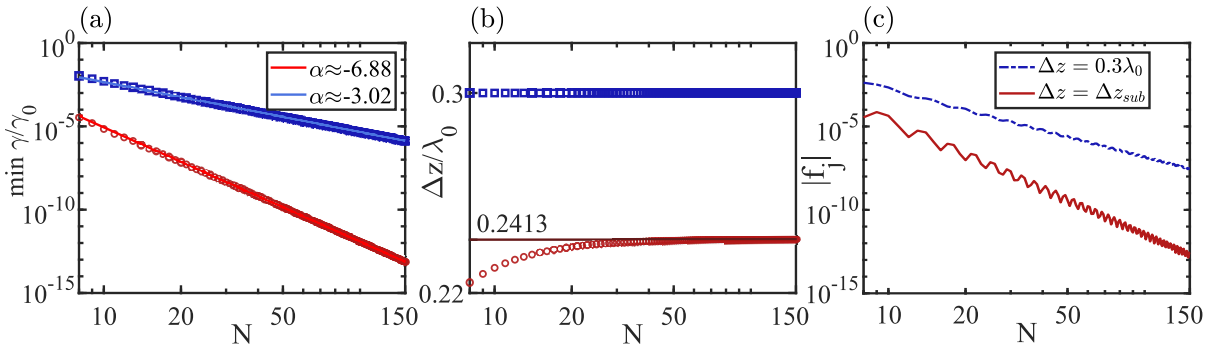

Figure 1.4 — (a) Scaling laws for the emission rates γ_j/γ_0 of the most subradiant states with the number of atoms N; blue open squares - the period of the system is fixed, and equal to $\Delta z = 0.3\lambda_0$, red open circles - the period of the system is optimized for each N, α is the coefficient specifying the characteristic scaling with N ($\gamma_j \sim N^\alpha$), light blue, and light red solid lines demonstrate the corresponding fitting curves $\sim N^\alpha$. (b) The array periods Δz used in (a) versus the number of atoms N, note that the red open circles approach the value close to $\Delta z_{\text{sub}} \approx 0.241\lambda_0$ for large $N \gg 1$. (c) The absolute value of the corresponding oscillator strength amplitude $|f_j|$. Pay attention to oscillations, and to a general behavior quite similar to γ_j/γ_0

1.4 Infinite dipole chain limit

It is very instructive to consider the limit of an infinite dipolar chain, namely, the dispersion of polarization waves in it. This problem has been studied extensively in the past [43–45; 48; 156], and the key result can be represented in the following form:

$$1 + \frac{\alpha(\omega)}{\Delta z^3}\tilde{\Sigma}(\omega, k_z) = 0,$$

$$\begin{aligned}\tilde{\Sigma}(\omega, k_z) = \mathrm{Li}_3(e^{i(k+k_z)\Delta z}) + \mathrm{Li}_3(e^{i(k-k_z)\Delta z}) - \\ ik\Delta z\left[\mathrm{Li}_2(e^{i(k+k_z)\Delta z}) + \mathrm{Li}_2(e^{i(k-k_z)\Delta z})\right] - \\ (k\Delta z)^2\left[\mathrm{Li}_1(e^{i(k+k_z)\Delta z}) + \mathrm{Li}_1(e^{i(k-k_z)\Delta z})\right], \quad (1.10)\end{aligned}$$

where $\alpha(\omega)$ is a dipole polarizability of an individual scatterer (a two-level atom in our case), $\tilde{\Sigma}(\omega, k_z)$ is a dipole sum for transversally oriented dipole moments, this sum takes into account interactions between the scatterers, k_z is the wavenumber of the polarization wave along the chain. $\mathrm{Li}_n(x)$ is a polylogarithm function. Strictly speaking, one has to numerically find self-consistent complex-valued solutions to the equation above. However,

recall that we consider two-level atoms in free space, and in this case the semiclassical polarizability can be written as [157]:

$$\alpha(\omega) = -\frac{3}{2k_0^3}\frac{\gamma_0/2}{(\omega-\omega_0)+i\gamma_0/2}. \tag{1.11}$$

This function has a very narrow peaked response in the frequency range close to ω_0, as usually for atoms $\omega_0 \gg \gamma_0$ by many orders of magnitude. Therefore, outside of this frequency range atoms respond to the external fields weakly. Mathematically, we can think of it as $\alpha(\omega)$ cuts off a very narrow spectral range around ω_0 in Eq. (1.10), while the dipole sum can be taken exactly at the resonance frequency $\tilde{\Sigma}(\omega, k_z) \approx \tilde{\Sigma}(\omega_0, k_z)$. Such an approximation assumes that $\tilde{\Sigma}(\omega, k_z)$ is a slowly varying function of ω around ω_0, and does not vary significantly in the range of several γ_0 around the resonance frequency, which is why it can be simply assumed to be constant.

Now we multiply both sides of Eq. (1.10) by $\alpha^{-1}(\omega)$, and also take the real part of the result, and after that we can finally write the explicit analytical form for the dispersion relation:

$$\begin{aligned}\frac{\Delta}{\gamma_0} = \frac{3}{4k_0^3\Delta z^3}\mathrm{Re}\Big[&\mathrm{Li}_3(e^{i(k_0+k_z)\Delta z}) + \mathrm{Li}_3(e^{i(k_0-k_z)\Delta z}) - \\ &ik_0\Delta z\left[\mathrm{Li}_2(e^{i(k_0+k_z)\Delta z}) + \mathrm{Li}_2(e^{i(k_0-k_z)\Delta z})\right] \\ &-(k_0\Delta z)^2\left[\mathrm{Li}_1(e^{i(k_0+k_z)\Delta z}) + \mathrm{Li}_1(e^{i(k_0-k_z)\Delta z})\right]\Big].\end{aligned}$$

Recall that previously we mostly concentrated on looking at the modes with $\langle f_{j,j+1}\rangle \approx -1$, which means that nearest dipole moments are almost perfectly anti-parallel. For an infinite chain it corresponds to the band edge, where $k_z = \pi/\Delta z$, so, let us expand the dispersion Equation (1.6) near this point in powers of $(\beta - \pi)$, where $\beta = k_z\Delta z$:

$$\begin{aligned}\frac{\Delta}{\gamma_0} &= c_2(\beta_0)\cdot(\beta-\pi)^2 + c_4(\beta_0)\cdot(\beta-\pi)^4 + \ldots \\ c_2(\beta_0) &= 4\mathrm{Ln}\left[2\left|\cos\left(\frac{\beta_0}{2}\right)\right|\right] + \frac{\beta_0\left(-\beta_0+\sin(\beta_0)\right)}{\cos^2\left(\frac{\beta_0}{2}\right)},\end{aligned} \tag{1.12}$$

where $\beta_0 = k_0\Delta z$. The c_2 coefficient as a function of a dimensionless parameter β_0 is plotted in Fig. (1.5) (a), from which one can see that there is a point at which $c_2 = 0$, and it corresponds to a period approximately equal to $\Delta z_{\mathrm{opt}}/\lambda_0 \approx 0.2414\ldots$. This value agrees nicely with our previous numerical finding presented in Fig. 1.4 (b).

One can compare the dispersion curves plotted in Fig. 1.5 (b) for a period of $\Delta z = 0.3\lambda_0$ (where $c_2 \neq 0$, quadratic behavior), and for the optimal

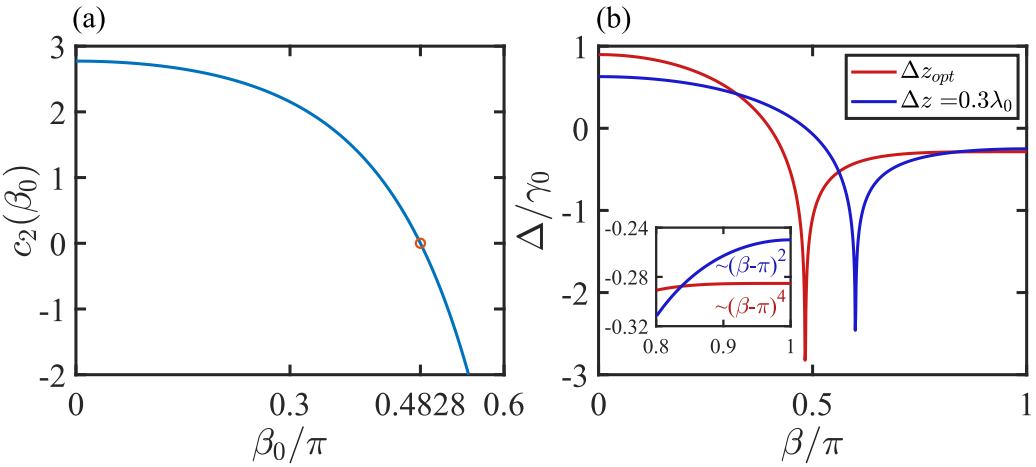

Figure 1.5 — (a) $c_2(\beta)$ coefficient from Eq. (1.12) versus $\beta_0/\pi = k_0\Delta z/\pi$. Red circle specifies the point of $c_2(\beta_0) = 0$. (b) Dispersion curves for a regular period $\Delta z = 0.3\lambda_0$ (blue line), and for an optimal period, corresponding to $c_2(\beta_0)$ coefficient being equal to zero (red line). The inset shows more in-detail the behavior of two curves near the band edge

period ($c_2 = 0$, quartic behavior). As can be seen from the inset figure, in the latter case the dispersion curve is much flatter close to the band-edge. This situation, when dispersion of waves behaves in such a way, is called Degenerate Band Edge (DBE) [33]. It was studied a lot for photonic crystals, where researchers introduced additional degrees of freedom into the system (bianisotropy of layers of the material, non-trivial unit cell, etc.) in order to achieve the regime, when the eigenmodes close to the band edge become degenerate, hence the name of the effect. However, in our system we have a single dipole in a unit cell, but unlike in photonic crystals studied in [33], where layers exchange plane-wave like lightfields, dipoles interact with each other through a dipole-dipole interaction (Eq. (1.3)), which is of more peculiar form than the interaction through the exchange of plane waves. We can speculate a little that such a peculiar behavior of the interaction potential with Δz allows one to achieve degeneracy despite the unit cell being trivial.

Even though by considering the infinite chain limit ($N \to \infty$) we were able to obtain the explicit equation for the limiting value of an optimal period, we still can not directly relate it to the reduced radiation losses. This is due to a simple fact that such an infinite subdiffractional $\Delta z < \lambda_0/2$ chain is not allowed to emit any radiation into the far-field due to the absence of open diffraction channels, which is why now we come back to the consideration of a finite dipole chain, and the analysis of the mode profile.

1.5 The eigenstate structure

Up to now we did not discuss in details how do the eigenstates of the problem look like. The reason for this is that the eigenvectors of a $N \times N$ matrix $\Sigma(\hbar\omega_0)$ from Eq. (1.3) can not be found exactly. However, it does not mean that we can not approximate them by using some ansatz. The matrix Σ is complex symmetric, and, in general, the eigenvectors are also complex-valued. Nevertheless, we can take the solution to the same problem, but with the Tight-Binding Approximation (TBA) being introduced, where only nearest-neighbor interactions are taken into account. This leads to a tridiagonal form of $\Sigma(\hbar\omega_0)$ matrix, and the following analytical form of the eigenvectors:

$$\psi_n^{(k)} = \sqrt{\frac{2}{N+1}} \sin\left(\frac{\pi k}{N+1} n\right), \tag{1.13}$$

where $k = 1..N$ enumerates the eigenstates, while $n = 1..N$ enumerates the atoms. The state with $k = 1$ corresponds to a state closest to the band center, and with the minimal corresponding wavenumber $k_z^{(1)} = \frac{\pi}{\Delta z}\frac{1}{N+1}$, while $k = N$ is related to a state which is the closest to the band-edge with $k_z^{(N)} = \frac{\pi}{\Delta z}\frac{N}{N+1}$. Even though, generally speaking, the nearest-neighbor approximation is not valid here, these functions describe the eigenstate qualitatively (not quantitatively) pretty well at least in some range of periods Δz. Probably, this is a result of the fact that dipole-dipole interaction in free space decays with the distance between the dipoles: the slowest decreasing component is the far-field one, which behaves as $\sim 1/R$ with the distance between the atoms R. However, if one analyzes the structure of the subradiant state with the minimal γ_j/γ_0, it becomes clear that it has a significantly different profile from a regular band-edge state as seen from Fig. 1.6 (a).

Further insight can be gained if one simply analyzes the structure of this state. For this, one can use the functions $\psi_n^{(k)}$ from Eq. (1.13) as an orthonormal basis, and expand any eigenstate in it. As the basis functions $\psi^{(k)}$ are purely real, then the real, and imaginary parts of the expansion coefficients are simply related to the real, and imaginary parts of the expanded eigenvector v_k. The real, and imaginary parts of the corresponding coefficients $C_k = \left(\psi^{(k)}\right)^{\mathrm{T}} \cdot v_N$ are presented in Fig. 1.6 (b), where v_N is the eigenvector of the state closest to the band-edge (the smallest $\langle f_{j,j+1}\rangle \approx -1$). As one can see, for a period $\Delta z = 0.3\lambda_0$ the real part of v_N can be very well approximated by a single function $\psi^{(N)}$, while the imaginary part of v_N does not reveal any simple structure in this basis. Moreover, $\mathrm{Re}\, C_N \approx +1$, while $\mathrm{Re}\, C_{k\neq N}$, and $\mathrm{Im}\, C_k$ are much smaller ($\ll 1$). When the system period is

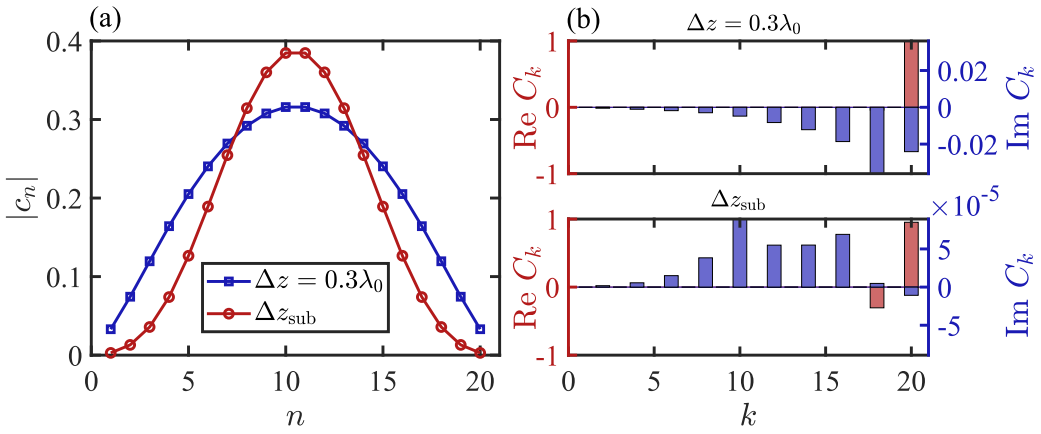

Figure 1.6 — (a) The absolute values of the probability amplitudes $|c_n|$ for atom n to be excited in a state with the smallest decay rate: blue squares - $\Delta z = 0.3\lambda_0$, red circles - $\Delta z_{\rm sub}$. The number of atoms here is $N = 20$. (b) Expansion coefficients C_k of the corresponding states in a basis of states $\psi^{(k)}$ given by Eq. (1.13). The real part is in red, while the imaginary part is in blue

equal to $\Delta z_{\rm sub}$, then there are two dominant components to the real part of v_N: C_N, and C_{N-2}. Interestingly, these two coefficients are of opposite signs, which can be interpreted as the presence of destructive interference between the contributions of these components. Indeed, one can show explicitly that the emission rate of a state $k = N$ (when the period is close to $\Delta z_{\rm sub}$) described by the eigenvector $v_N \approx C_N\psi^{(N)} + C_{N-2}\psi^{(N-2)}$ is equal to:

$$\begin{aligned}
\gamma_N &= -\tfrac{2}{\hbar}\mathrm{Im}\left[v_N^\dagger \cdot \Sigma \cdot v_N\right] \approx \tilde{\gamma}_N + \tilde{\gamma}_{N-2} + \tilde{\gamma}_{N-2,N},\\
\tilde{\gamma}_N &= -\tfrac{2}{\hbar}|C_N|^2 \left(\psi^{(N)}\right)^{\mathrm{T}} \cdot \mathrm{Im}\Sigma \cdot \psi^{(N)},\\
\tilde{\gamma}_{N-2} &= -\tfrac{2}{\hbar}|C_{N-2}|^2 \left(\psi^{(N-2)}\right)^{\mathrm{T}} \cdot \mathrm{Im}\Sigma \cdot \psi^{(N-2)},\\
\tilde{\gamma}_{N-2,N} &= -\tfrac{4}{\hbar}\mathrm{Re}\left[C_{N-2}C_N^*\right] \left(\psi^{(N)}\right)^{\mathrm{T}} \cdot \mathrm{Im}\Sigma \cdot \psi^{(N-2)},
\end{aligned} \tag{1.14}$$

where $\tilde{\gamma}_N, \tilde{\gamma}_{N-2}$ can be interpreted as contributions to the emission rate from basis states $\psi^{(N)}$, and $\psi^{(N-2)}$, and $\tilde{\gamma}_{N-2,N}$ is the interference term. One can show that from the properties of Σ it follows that $\tilde{\gamma}_N, \tilde{\gamma}_{N-2} > 0$, while for the interference term $\tilde{\gamma}_{N-2,N} < 0$ as a result of $\mathrm{Re}\left[C_{N-2}C_N^*\right] < 0$.

The question is: why do eigenstates of the system near specific values of the period turn out to have two significant components in the basis of $\psi^{(k)}$ instead of a single one? The reason for that can be understood if we revisit Fig. 1.3 (a), paying special attention to the behavior of eigenstates near these values of Δz. This is illustrated in Fig. 1.7, where in (a) one can see that as the period Δz is altered, the two modes specified by arrows approximately exchange the values of the correlation function $\langle f_{j,j+1}\rangle$. Simultaneously, from (b) it is seen that it corresponds to a region of repulsion of the corresponding energy levels. One can say that two states $k = N$, and $k = N - 2$ experience an avoided

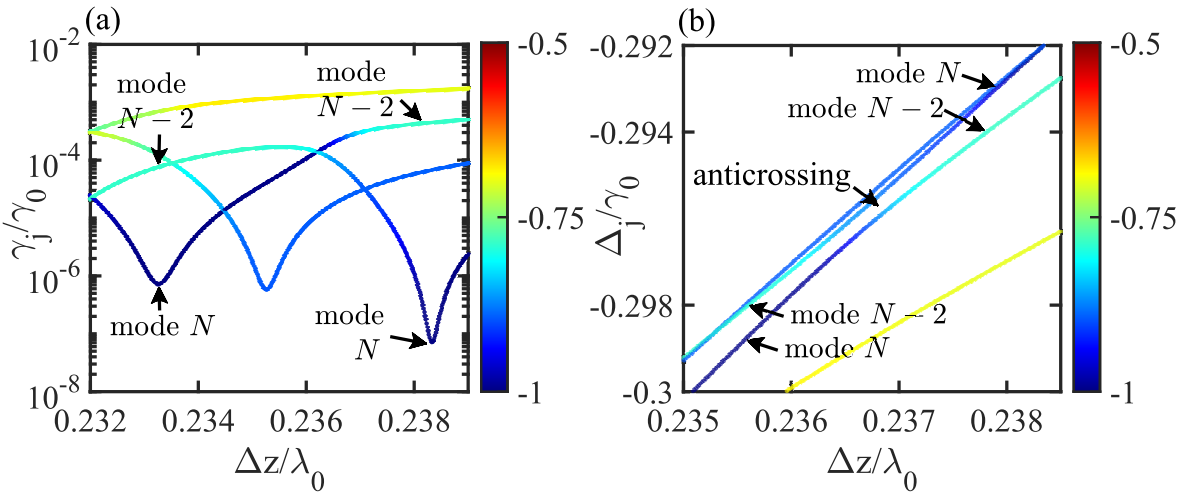

Figure 1.7 — Emission rates (a), and frequency shifts (b) for 4 modes with the smallest values $\langle f_{j,j+1} \rangle$ as a function of period $\Delta z/\lambda_0$ near the point of minimal emission rate similar to one specified in Fig. 1.3 (a). Here the number of atoms is $N = 20$

crossing (or anticrossing) [158] near Δz_{sub}, which leads to the mixing of these states. At a certain value of period Δz they are mixed in such a way that one of these states becomes extremely subradiant ($\Delta z_{\text{sub}}/\lambda_0 \geqslant 0.238$). The reason why do states N, and $N-2$ are interacting rather than $N, N-1$ is well understood. As our interaction is a symmetric dipole-dipole interaction (described by a complex symmetric matrix Σ), and as the system is periodic, then any eigenvector v_k is either symmetric or antisymmetric with respect to the reflection around the geometrical center of the system, and it is known that level repulsion during a sweep of a single parameter appears for states with the same symmetry. One can also see this from Fig. 1.6 (b), where for even band-edge state with index $N = 20$, only C_k with even k are non-zero. However, if only modes N, and $N-2$ were interacting, then we would have observed a local maximum in γ_j/γ_0 for a state $k = N-2$ near Δz_{sub} as a result of conservation of the sum of linewidths. In fact, there is a much less significant interaction with modes $N-4, N-6, ...$, but it is not evident from Fig. 1.7, and was confirmed by us numerically.

With all that being said let us also to discuss another interesting property of these states, which is related to the multipolar content of their far-field radiation.

1.6 Multipolar analysis

Let us analyze the far-fields emitted by these subradiant states. This can be done if we think about atoms as simple classical dipole scatterers as once we are provided with the eigenvector characterizing the state of interest (with label k), we can immediately assign the dipole moment to each atom according to the following simple rule: $\mathbf{d_n} = c_n^{(k)}|\mathbf{d}|$ (recall that $c_n^{(k)}$ is the probability amplitude for atom n to be excited in a state k). Now we can find the field produced by the system at point $\mathbf{r} \neq \mathbf{r_n}$ in such a state as:

$$\mathbf{E}(\mathbf{r}, \omega_0) = 4\pi k_0^2 \sum_{n=1}^{N} \mathbf{G_0}(\mathbf{r}, \mathbf{r_n}, \omega_0)\mathbf{d_n}. \tag{1.15}$$

In order to perform the spherical multipole expansion of the field $\mathbf{E}(\mathbf{r}, \omega_0)$, we can use the Green's tensor expressed through Vector Spherical Harmonics (VSH) [159]:

$$\mathbf{M}_{j,m}(\mathbf{r}, k) = \nabla \times \mathbf{r} j_j(kr) Y_{j,m}(\theta, \varphi),$$
$$\mathbf{N}_{j,m}(\mathbf{r}, k) = \frac{1}{k}\nabla \times \mathbf{M}_{j,m}(\mathbf{r}, k),$$
$$\mathbf{G_0}(\mathbf{r}, \mathbf{r}', \omega) = -\frac{\mathbf{e_r} \otimes \mathbf{e_r}}{k^2}\delta(\mathbf{r} - \mathbf{r}') + ik \sum_{j=1}^{\infty} \sum_{m=-j}^{+j} \frac{1}{j(j+1)} \times$$
$$\times \begin{cases} \mathbf{M^{(1)}_{j,m}}(k, \mathbf{r}) \otimes \mathbf{M_{j,-m}}(k, \mathbf{r}') + \mathbf{N^{(1)}_{j,m}}(k, \mathbf{r}) \otimes \mathbf{N_{j,-m}}(k, \mathbf{r}'), & \text{if } r > r', \\ \mathbf{M_{j,m}}(k, \mathbf{r}) \otimes \mathbf{M^{(1)}_{j,-m}}(k, \mathbf{r}') + \mathbf{N_{j,m}}(k, \mathbf{r}) \otimes \mathbf{N^{(1)}_{j,-m}}(k, \mathbf{r}'), & \text{if } r < r', \end{cases} \tag{1.16}$$

where $j_j(x)$ are spherical Bessel functions of order j, $Y_{j,m}(\theta, \varphi)$ are spherical harmonics, and superscript $^{(1)}$ means that spherical Bessel function $j_j(kr)$ has to be replaced with the spherical Hankel function $h^{(1)}(kr)$.

The exact expression for the Green's tensor through VSH depends upon how the field point $\mathbf{r}$ is located with respect to the source point $\mathbf{r}'$. As our goal is to compute the total power radiated into the far-field, we can say that the field point is far away from any dipole $|\mathbf{r}| \gg |\mathbf{r_n}|$, and, therefore, we can pick the corresponding form of the expansion. By plugging the chosen form of the Green's tensor into Eq. (1.15) we obtain:

$$\mathbf{E}(\mathbf{r}, \omega_0) = \sum_{j=1}^{\infty} \sum_{m=-j}^{+j} \sum_{n=1}^{N} \left(a_{j,m}^{(n)} \frac{i\mathbf{N^{(1)}_{j,m}}(k_0, \mathbf{r})}{\sqrt{j(j+1)}} + b_{j,m}^{(n)} \frac{i\mathbf{M^{(1)}_{j,m}}(k, \mathbf{r})}{\sqrt{j(j+1)}} \right), \tag{1.17}$$

where $a_{j,m}^{(n)}, b_{j,m}^{(n)}$ are the complex-valued scalars being the scalar products of right dyads entering the Green's tensor, and n^{th} particle dipole moment.

Now we proceed by calculating the period-averaged Poynting vector and the total normalized power radiated into far-field:

$$\langle \mathbf{S} \rangle = \frac{c}{8\pi} \mathrm{Re}\left[\mathbf{E}(\mathbf{r},\omega_0) \times \mathbf{H}^*(\mathbf{r},\omega_0)\right],$$
$$\Gamma = \frac{P}{P_1} = \frac{\lim\limits_{r\to\infty} \int\int \langle \mathbf{S} \rangle \cdot \mathbf{n_r}\, r^2\, d\Omega}{\lim\limits_{r\to\infty} \int\int \langle \mathbf{S_1} \rangle \cdot \mathbf{n_r}\, r^2\, d\Omega}, \tag{1.18}$$

with $P_1 = c|\mathbf{d}|^2 k_0^4/3$ being the power radiated by a single dipole $\mathbf{d}$ (c is the speed of light), integration is done over a spherical surface of radius r, and $\mathbf{n_r}$ is a unit vector normal to this spherical surface.

We can rewrite Eq. (1.18) by doing some algebraic manipulations, which will lead us to (see A.1 in Appendix for details):

$$\Gamma = \frac{3}{8\pi} \frac{1}{|\mathbf{d}|^2 k^6} \sum_{j=1}^{\infty} \sum_{m=-j}^{+j} \left(|a_{j,m}|^2 + |b_{j,m}|^2\right), \tag{1.19}$$

with $a_{j,m} = \sum\limits_{l=n}^{N} a_{j,m}^{(n)}$, $b_{j,m} = \sum\limits_{l=n}^{N} b_{j,m}^{(n)}$. Eq. (1.19) describes how does a VSH with given (j,m) contributes to the total emission rate Γ. However, in a very general case there is a problem that with increasing j the total number of harmonics grows quadratically. Therefore, one might want to rather look at contributions of harmonics with a given j: $\Gamma = \sum\limits_{j=1}^{\infty} \Gamma_j$.

We have to make one important note on the multipole expansion made above: there is a degree of freedom in choosing the coordinate system origin, and its orientation. The expansion coefficients $a_{j,m}, b_{j,m}$ depend upon this choice. Of course, it does not affect the observable quantities like Γ, but alters the contributions Γ_j, and, therefore, it has an effect on how does $\sum_{j=1}^{j_{\max}} \Gamma_j$ converge with $j_{\max}$. As our system is periodic, and quasi-1D, it makes sense to put the origin of a spherical coordinate system right at the center of our chain. Moreover, as we show in A.2, when the chain is parallel to the z-axis, only VSH with $m = -1, +1$ contribute to the emission rate. There is also a rule of thumb on how to pick the value of $j_{\max}$: as for the mode with the smallest value of nearest-neighbor correlation function $\langle f_{j,j+1} \rangle$ the neighboring dipoles are almost π out-of-phase, our $j_{\max}$ has to be at least equal to the total number of dipoles N. This is because the spherical harmonic with a given j changes sign at most j times when moving along either azimuthal or polar direction. Therefore, we have, at least, to take all spherical harmonics up to this one into account as it represents the symmetry of the state being expanded.

The result of the multipole expansion for a chain oriented along the z-axis is presented in Fig. 1.8. At each value of the period Δz we find

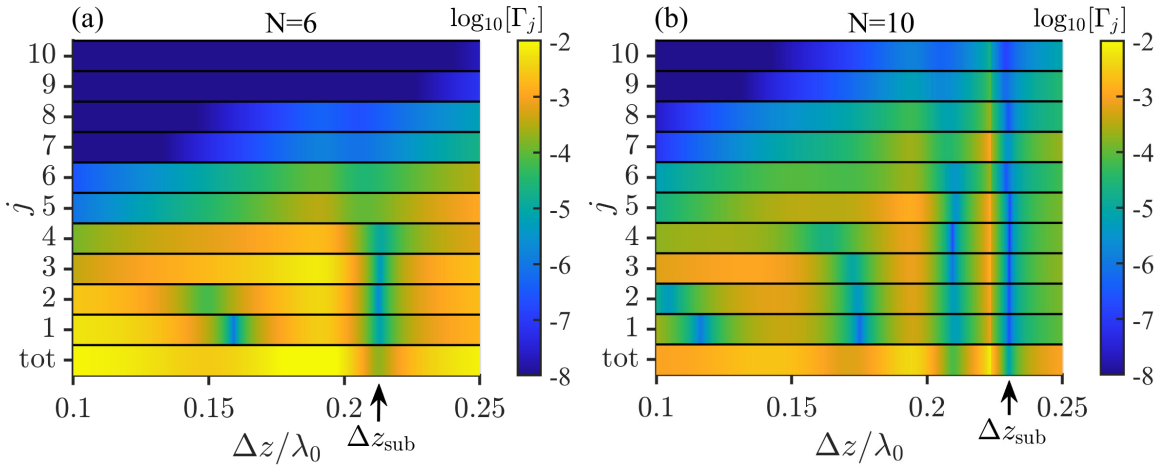

Figure 1.8 — Total value of the emission rate for a state with the smallest value of $\langle f_{j,j+1} \rangle$ function as well as contributions Γ_j of different order j versus the system period Δz for $N = 6$ (a), and $N = 10$ (b) dipole scatterers. Δz_{sub} is the period when the minimal emission rate is achieved state (identified by arrows). Note how many harmonics j have overlapping local minima very close to Δz_{sub} in case (b)

all N eigenstates, and corresponding spontaneous emission rates, then we pick the state with the smallest value of the nearest-neighbor correlation function $\langle f_{j,j+1} \rangle$. For this state we perform the multipole expansion, and plot contributions of VSH of different orders j. As one can see from Fig. 1.8 (a), for $N = 6$, when the total emission rate Γ has a minimum at Δz_{sub}, contributions from different VSH Γ_j also experience local minima in the vicinity of Δz_{sub} point, but this happens up to VSH with $j = 4$. As the number of dipoles is increased to $N = 10$, from Fig. 1.8 (b) we can see that near the Δz_{sub} point many contributions simultaneously experience minima.

This is a little bit surprising as, usually, the far-field radiation is reduced by canceling contributions from the lowest order multipoles (for instance, an electric dipole contribution might be suppressed) as they, commonly, the dominant ones. However, many multipolar contributions up to a high order tend to be minimized in our system. The reason for this can be well understood if we recall that near this point the eigenstate is well approximated by a superposition of $\psi^{(N)}$, and $\psi^{(N-2)}$ (Eq. (1.13)). For large enough values of $N \gg 1$, these two modes do not differ too much, therefore, they have quite similar multipolar contents of the radiated far-fields. Recall that the relative expansion coefficients C_N, C_{N-2} differ in phase almost by π resulting in the destructive interference not just for an overall state, and the respective emission rate, but also for every contribution Γ_j.

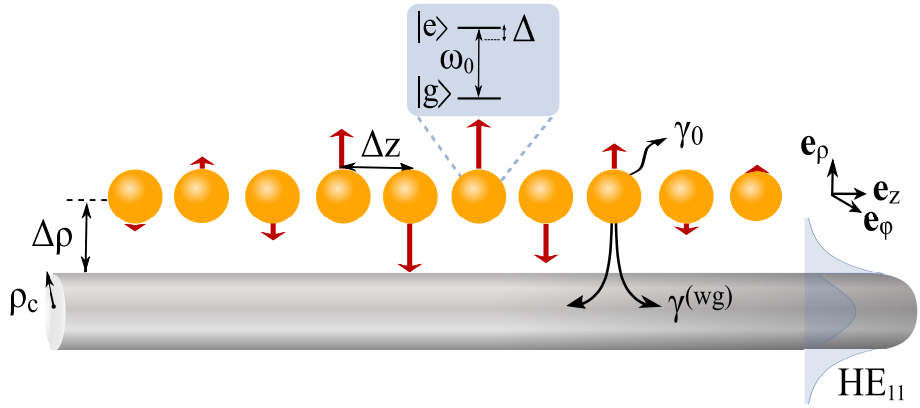

Figure 1.9 — Schematic representation of the system under consideration. 1D array of two-level atoms with period Δz at a distance $\Delta\rho$ from the nanofiber surface. The nanofiber has radius ρ_c. Red arrows represent approximately the distribution of atomic dipole moments in the subradiant mode under study. The radius ρ_c is chosen such that there is only the fundamental guided mode HE_{11} at the transition frequency ω_0

1.7 Single photon scattering for an atomic array close to an optical nanofiber: theoretical framework

Previously we studied the collective subradiant states of an atomic chain in free space, where the atom-atom interaction was only provided through the vacuum field modes. It might be interesting to see what happens if there is an additional interaction channel, for instance, atoms can interact through the guided mode of some structure, which is schematically represented in Fig. 1.9. As before, we have a periodic array of two-level atoms, but now it is placed in the vicinity of a single-mode optical nanofiber, which is one of common platforms to study light-matter interaction in the context of Waveguide Quantum Electrodynamics (WQED).

We need to modify the theoretical approach used before so that it can adequately describe the scattering in a new set-up. The scattering process, in general, can be described by the so-called S matrix given by [4]:

$$S_{kl} = \delta_{kl} - 2\pi i T_{kl}(E_l + i0)\delta(E_k - E_l), \tag{1.20}$$

where l, and k label the the asymptotic initial, and final states, correspondingly. In our problem the asymptotic scattering states are $|l\rangle = |g\rangle^{\otimes N}|1_\mu\rangle$, $|k\rangle = |g\rangle^{\otimes N}|1_{\mu'}\rangle$, where μ, μ' are fully describing the incoming, and the outgoing state of a photon. $T_{kl}(E_l + i0)$ is the matrix element of the transition matrix (1.1), which has the same form as before:

$$\hat{T} = \hat{V} + \hat{V}\hat{P}\hat{G}(E + i0)\hat{P}\hat{V} \approx \hat{V} + \hat{V}\hat{P}\frac{1}{E - \hat{H}_0 - \hat{\Sigma}(\hbar\omega_0)}\hat{P}\hat{V}. \tag{1.21}$$

This form of the transition matrix suggests the two modifications relative to the vacuum case: (I) we have to modify the matrix elements of the outer $\hat{V}$ operators as now they absorb/emit not a free space photon, but a photon of a given mode μ, μ' of the nanostructure; (II) we also have to modify the matrix of a level-shift operator $\Sigma(\hbar\omega_0)$. The latter, as is suggested in Eq. (1.3), can be found quite easily as all we have to do is to construct the scattered part of the classical electromagnetic Green's tensor for a waveguide of a circular cross-section, which can be found in A.4.

Regarding the outer $\hat{V}$ operators, we will only consider a photon from guided modes, and in order to describe the field in this case we can employ the scheme proposed in [160;161] in which the electric field operator is equal to:

$$\begin{aligned}\hat{\mathbf{E}}(\mathbf{r}) &= \textstyle\sum_{\mu} \tilde{\mathbf{E}}^{(\mu)}(\mathbf{r})\hat{a}_{\mu} + h.c.,\\ \tilde{\mathbf{E}}^{(\mu)}(\mathbf{r}) &= i\sqrt{\tfrac{2\pi\hbar\omega_{\mu}}{\mathbb{L}}}\boldsymbol{\varepsilon}^{(\mu)}(\rho,\varphi)e^{if\beta_{\mu}z+ipl\varphi}.\end{aligned} \tag{1.22}$$

where β_{μ} is the propagation constant of mode μ, and this index describes fully the eigenmode $\mu = (\eta, f, l, p)$, where η describes the mode profile, and as we study the scattering of a photon from the fundamental guided mode HE_{11}, this profile is fixed for a given set of parameters of the fiber, and we fix this index from now on, and can omit mentioning it, in principle. Here $\boldsymbol{\varepsilon}^{(\mu)}(\rho,\varphi)$ is the electric field amplitude, $\mathbb{L}$ is the quantization length, f and l label the direction of propagation ($+1$-forward,-1-backward), and the mode angular momentum (non-negative integer, for the fundamental guided mode HE_{11} from now on we fix $l = 1$, and omit this index also), respectively, while $p = \pm$ defines the direction of the electric field vector rotation (helicity). The electric field is assumed to be periodic in the z-direction, therefore, $\beta_{\mu,l}\mathbb{L} = 2\pi n_l$, where n_l is a non-negative integer number. The normalization condition for the electric field amplitude of a given mode is defined by:

$$\int_0^{2\pi}\int_0^{\infty} |\boldsymbol{\varepsilon}^{(\mu)}(\rho,\varphi)|^2 d\varphi\rho d\rho = 1. \tag{1.23}$$

Other relevant details on the mode functions are given in Appendix A.3.

Now we can write the explicit form of the outer operators $\hat{V}$ entering Eq. (1.21) as:

$$\begin{aligned}\langle e_a,\{0\}|\hat{V}|g_a,1_{\mu}\rangle &= -i\left(\mathbf{d}_{a,eg}\cdot\boldsymbol{\varepsilon}^{(\mu)}(\rho_a,\varphi_a)\right)\sqrt{\frac{2\pi\hbar\omega_{\mu}}{\mathbb{L}}}e^{if\beta_{\mu,l}z_a+ip\varphi_a}\\ \langle g_b,1_{\mu'}|\hat{V}|e_b,\{0\}\rangle &= i\left(\boldsymbol{\varepsilon}^{(\mu')*}(\rho_b,\varphi_b)\cdot\mathbf{d}_{b,ge}\right)\sqrt{\frac{2\pi\hbar\omega_{\mu'}}{\mathbb{L}}}e^{-if'\beta_{\mu',l'}z_b-ip'\varphi_b}.\end{aligned} \tag{1.24}$$

We will come back to the equations above a bit later.

Let us rewrite the definition of the scattering matrix from Eq. (1.20) by including the summation over all values of $n_{l'}$ for the final field state, and set the quantization length to infinity $\mathbb{L} \to \infty$ (but keeping it as $\mathbb{L}$ formally), making the propagation constant $\beta_{\mu'}$ continuous. Formally, this limit can be performed by the following substitution $\sum_{n_{l'}} \to \frac{\mathbb{L}}{2\pi} \int_0^\infty \frac{d\beta_{\mu',n_{l'}}}{d\omega} d\omega$. After that, the following form of the S matrix is obtained:

$$S_{f',p';f,p} = \delta_{f',p';f,p} - i \frac{\mathbb{L}}{c\hbar \cdot dk/d\beta_{\mu'}} T_{f',p';f,p}(E). \tag{1.25}$$

In order to have a nice and simple form of the S matrix we, as usually, will employ the picture of collective atomic states (eigenstates of the level-shift operator matrix $\Sigma(\hbar\omega_0)$). Previously we considered the atomic chain in the vacuum, which led to a complex symmetric matrix $\Sigma(\hbar\omega_0)$. However, when atoms interact through the surface localized modes of some nanostructure, this matrix might not be complex symmetric, in general. It means that such matrix might have different left and right eigenvectors. From now on we will simply pick the right eigenvectors:

$$\begin{gathered} \Sigma(E_0) v_j^{(r)} = \lambda_j v_j^{(r)}, \\ (S^{(r)})^{-1} \frac{1}{I\hbar\Delta - \Sigma(\hbar\omega_0)} S^{(r)} = \frac{1}{I\hbar\Delta - \Lambda_\Sigma}, \end{gathered} \tag{1.26}$$

in the above $S^{(r)}$ is the transformation matrix to the corresponding eigenspace with $v^{(r)}$ vectors as it's columns, Δ is the detuning from the bare atomic resonance frequency ω_0, and Λ_Σ is a diagonalized Σ.

Now we come back to Eq. (1.24), for which we will assume that $\mu' = \mu$ ($f' = f, l' = l, m' = m$), and that all atoms are at the same distance from the surface of the structure, and all transition dipole moments have the same orientation. In this case, all complex-valued matrix elements (1.24) have the same absolute value, but differ by phase. These matrix elements can be expressed through the spontaneous emission rate for an atom into the forward-propagating guided mode:

$$\gamma_{wg}^{(f)} = \sum_m \frac{2\pi |\mathbf{d}_{eg} \boldsymbol{\varepsilon}^{(f=+1,l=1,m)}(\rho,\varphi)|^2 k_0 \cdot d\beta/dk}{\hbar} = \sum_m \frac{3\pi |\mathbf{n}_{eg} \boldsymbol{\varepsilon}^{(f=+1,l=1,m)}(\rho,\varphi)|^2 d\beta/dk}{2k_0^2} \gamma_0,$$

and, finally, for diagonal matrix elements $S_{\mu,f,m;\mu,f,m}$, corresponding to the transmission coefficient, we can write:

$$S_{ii} = 1 - i\hbar\gamma_{wg}^{(f)} \sum_j \frac{f_j^{(t)}}{\hbar\Delta - \lambda_j}, \tag{1.27}$$

Now the scattering matrix element has a form very similar to the one obtained before for the scattering cross section in free space in Eq. (1.5), and $f_j^{(t)}$ is, again, a complex-valued constant. The assumptions mentioned before allowed us to define $f_j^{(t)}$ as dimensionless quantities. However, if atoms, for instance, have different coupling strengths to the guided mode, or atoms have multilevel structure, then Eq. (1.27) can be quite easily generalized, altering the physical meaning of $f_j^{(t)}$ constants.

Eq. (1.27) provides the coefficient, which relates the field amplitudes of an incoming, and outgoing photon. For the field intensity, we have to simply take $T = |S_{ii}|^2$, which can be expressed as:

$$\begin{aligned}
|S_{ii}|^2 &= 1 + 2\hbar\gamma_{wg}^{(f)} \sum_{j=1}^{N} \left[\frac{\eta_j^{(t)}\lambda_j'' + \xi_j^{(t)}\left(\hbar\Delta - \lambda_j'\right)}{(\hbar\Delta - \lambda_j')^2 + \lambda_j''^2} \right], \\
\eta_j^{(t)} &= f_j^{(t)\prime} - \sum_{i=1}^{N} \hbar\gamma_{wg}^{(f)} \mathrm{Im}\left[\frac{f_j^{(t)}(f_i^{(t)})^*}{\lambda_j - \lambda_i^*} \right], \\
\xi_j^{(t)} &= f_j^{(t)\prime\prime} + \sum_{i=1}^{N} \hbar\gamma_{wg}^{(f)} \mathrm{Re}\left[\frac{f_j^{(t)}(f_i^{(t)})^*}{\lambda_j - \lambda_i^*} \right],
\end{aligned} \tag{1.28}$$

where we have used a similar trick as in the derivation of Eq. (3.32). As before, the parts proportional to $\frac{f_j^{(t)}(f_i^{(t)})^*}{\lambda_j - \lambda_i}$ are related to the interference between the states i, and j.

In a very similar fashion, one can also find the reflection coefficient both for field amplitudes:

$$S_{bf} = -i\hbar\sqrt{\gamma_{wg}^{(f)}\gamma_{wg}^{(b)}} \sum_j \frac{f_j^{(r)}}{\hbar\Delta - \lambda_j}, \tag{1.29}$$

and for field intensities:

$$|S_{bf}|^2 = \sum_{i,j} \hbar^2 \gamma_{wg}^{(f)} \gamma_{wg}^{(b)} \frac{f_j^{(r)} (f_i^{(r)})^*}{(\hbar\Delta - \lambda_j)(\hbar\Delta - \lambda_i^*)} = 2\hbar\gamma_{wg}^{(f)} \sum_{j=1}^{N} \frac{\left(\eta_j^{(r)} \lambda_j'' + \xi_j^{(r)} (\hbar\Delta - \lambda_j')\right)}{(\hbar\Delta - \lambda_j')^2 + \lambda_j''^2},$$

$$\eta_j^{(r)} = -\hbar\gamma_{wg}^{(b)} \operatorname{Im} \sum_{i=1}^{N} \left[\frac{f_j^{(r)} (f_i^{(r)})^*}{\lambda_j - \lambda_i^*} \right], \xi_j^{(r)} = \hbar\gamma_{wg}^{(b)} \operatorname{Re} \sum_{i=1}^{N} \left[\frac{f_j^{(r)} (f_i^{(r)})^*}{\lambda_j - \lambda_i^*} \right]. \tag{1.30}$$

In the very beginning of this section, we defined the field operator in Eq. (1.22) for a guided mode described by the field distribution μ, direction of propagation f, orbital angular momentum l, and polarization rotation direction p. The latter assumed that we work in the basis of quasi-circularly polarized modes possessing the cylindrical symmetry of the field distribution [80]. However, by combining the two modes with opposite values of l $(+l, -l)$ with proper relative phases, one can also describe quasi-linearly polarized modes with broken azimuthal symmetry (see A.3 for details).

1.8 Decay rates and their scaling

We begin by studying how would the emission rate scaling laws of subradiant states would change if the additional interaction channel through the guided mode is present, which is shown in Fig. 1.10. Notice that the usual subradiant states studied before for the free space case are still present (type 1 states, marked by red arrows) for transverse case, but not for longitudinal case, as expected. In addition to that, there are two more local minima, which we will discuss now in brief.

Type 2 states (green arrows) are easily explainable as the corresponding period is approximately equal to $\beta_{\mathrm{HE}_{11}} \Delta z \approx \pi/2$, which is the first Bragg resonance for the fiber mode. Usually, when N two-level atoms are coupled only through a single guided mode, right at the Bragg resonance there is 1 superradiant state, and $N-1$ subradiant states [162], which are completely dark in the absence of coupling to any other modes but the guided one. However, as now there is interaction through the free space modes also, they are characterized by some finite emission rates. There are also states of type 3, which appear as a result of interference between the two interaction channels: through the free space modes and the guided mode.

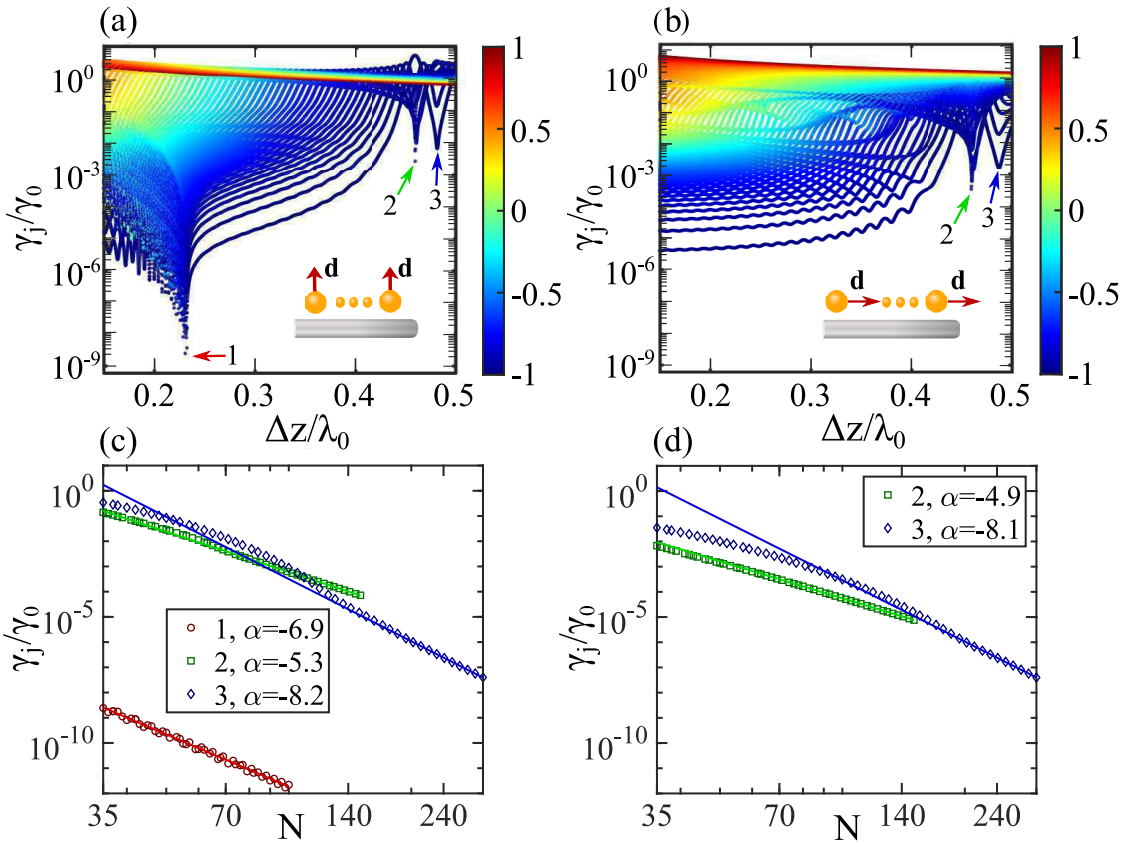

Figure 1.10 — (a), (b) Collective emission rates γ_j/γ_0 for a periodic array of $N = 75$ atoms placed near the nanofiber at a distance $\Delta\rho = \rho_c$ from the surface, where ρ_c is the fiber radius. The transition dipole moments are either perpendicular (a) or parallel (b) to the fiber axis. The relevant parameters are: $\rho_c = 0.25\lambda_0$, and $\varepsilon = 2.1$. Color, as before, specifies the values of the nearest-neighbor correlation function Eq. (1.9). (c)-(d): Scaling laws for local minima in (a)-(b) with N. Linear fits are in solid lines. In all of the calculations, only the fundamental guided mode HE_{11} was taken into account.

By inspecting the scaling laws presented in Fig. 1.10 (c), (d), we can see that type 1 states demonstrate a quite similar behavior as for the free space case with some additional "oscillations". For type 2, and 3 we can say that for sufficiently large N they follow $\sim N^{\alpha}$ law (or, at least, can be approximated by this curve in a certain range of N).

Note that in order to speed up the calculations only a single guided mode of the waveguide was taken into account, the contributions from radiation modes, and near-fields was ignored. This was done as for (c), and (d) this would be very time consuming to find the optimal periods at large N. Therefore, in (a), and (b) the regions of small Δz should not be relied upon as in this regime the ignored modes might contribute significantly.

The overall picture presented in Fig. 1.10 (a), (b) strongly depends upon the strength of atom-waveguide mode coupling $\gamma^{(wg)}$, and the value of the

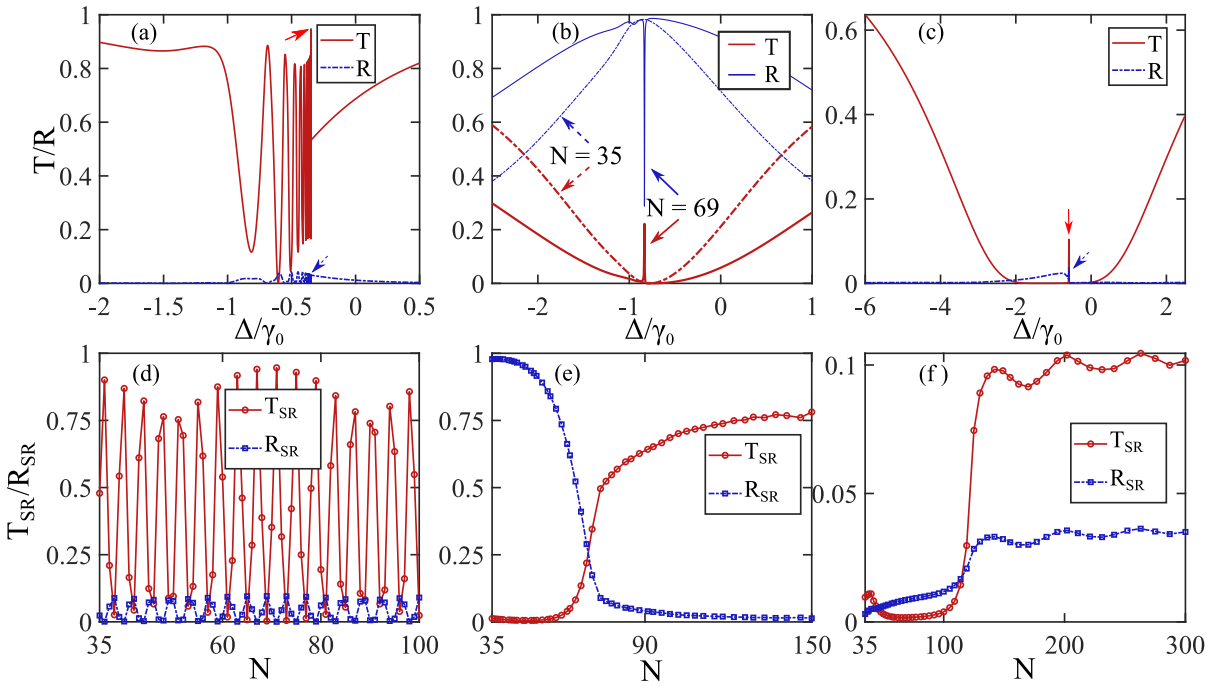

Figure 1.11 — (a), (b), (c) Transmission and reflection spectra for $N = 71$ (a), $N = 35$, $N = 69$ (b), and $N = 202$ (c). (d), (e), (f) - values of the transmission and reflection spectra $T_{\mathrm{SR}}, R_{\mathrm{SR}}$ at the corresponding subradiant state resonance frequency as functions of N. Each column corresponds to a subradiant state of a distinct type: (a), (d) - type 1, (b), (e) - type 2, and (c), (f) - type 3. The transition dipole moments of all atoms were assumed to be aligned perpendicularly to the fiber axis, and the system period Δz for each N is tuned such that the subradiant state of a given type is prominent. All other relevant parameters are the same as for Fig. 1.10

propagation constant of the guided mode $\beta_{\mathrm{HE}_{11}}$. During the calculations the parameters were chosen such that they approximately correspond to typical ones in the experiments with cold atoms and nanofibers: $\gamma^{(wg)} \ll \gamma_0$, while $\beta_{\mathrm{HE}_{11}} \approx 1.06 k_0$. This set of parameters allowed us to easily identify all three types of subradiant states discussed before.

1.9 Transmission and reflection spectra

It is also interesting to study how do these 3 types of subradiant states affect the optical response of the system. For a specific system under study, which is a quasi-1D system, the transmission and reflection spectra are of interest. This is summarized for the transverse case in Fig. 1.11.

For subradiant states of type 1 (d) the resonant values of T, R are oscillating as functions of N, and system switches from being transparent (with $T \geqslant 0.75$, and very small values of R) or opaque (with $T \leqslant 0.1$, $R \approx 0.1$). The period of these oscillations is approximately equal to $\Delta N \approx 4$, and they have the same nature as those discussed earlier in Fig. 1.4 (c) for $|f_j|$ in free space. This is due to oscillating overlap between the incoming photon, and the corresponding eigenstate. In Fig. 1.11 (a) a very sharp peak corresponding to the most subradiant state is shown by a bright red arrow, and for this figure $N = 71$ was chosen to observe the maximal possible transmission as seen from (d).

As can be seen from (b), and (e) for type 2 states the spectra look very different from the previous situation. The system period now corresponds to the first Bragg resonance, and one can expect to see a very large values of R, and very small T. Indeed, for small atom number N this is true, however, as N grows, the subradiant state becomes more and more prominent. At the corresponding resonance frequency, the system undergoes a transition from being very reflective ($R \approx 1, T \approx 0$) to partially transparent ($R \approx 0, T \approx 0.75$) more or less monotonically with growing N. In general, one can say that the spectra can be well approximated by two terms: a very broad Bragg resonance (which is a superradiant state), and a very sharp line due to the subradiant state: $T \approx 1 + T_{\text{sup}} + T_{\text{sub}}$, $R \approx R_{\text{sup}} + R_{\text{sub}}$. Therefore, for large enough number of atoms N the system switches from being reflective to partially transparent in a very narrow frequency range near the subradiant state resonance frequency. This situation is very similar to what happens under the Electromagnetically Induced Transparency (EIT) [163] conditions, but appears without use of the second (control) lightfield, here the transparency is rather a result of the destructive interference between the collective atomic modes.

For type 3 states, as can be seen from (c), and (f), right at the subradiant resonance frequency for the considered parameters both R, and T are rather small (do not exceed 0.1), and in the spectra it can be observed as a narrow peak with a relatively small amplitude.

From the above we can conclude that subradiant states discussed in this chapter do not immediately disappear if additional interaction channel through a single guided mode is present. Moreover, it allowed to make other subradiant states observable like ones at the first Bragg resonance, and a new - the third type of long-lived states.

1.10 A scientific statement

– In periodic subdiffractional chains consisting of N dipoles there exist modes with low radiation losses at a particular separation distance much smaller than the resonant wavelength of an individual dipole. This optimal period for large N can be found from the flat-band condition right at the band-edge. The radiation losses of such modes decrease as N^{α} with $\alpha < -6$, contrary to a well known N^{-3} behavior observed for non-optimal period. These extremely low radiation losses are a result of simultaneous minimization of multipolar contributions to the radiated field up to high multipolar order.

2. Chiral transport, sub- and superradiance in an array of two-level emitters unidirectionally coupled through a guided mode

In the previous chapter we discussed optical properties of one-dimensional atomic arrays in case of a symmetric dipole-dipole interaction between the atoms: be it interaction only through the free-space modes or with the additional interaction channel through a single guided mode. Now, we will switch topic to the discussion of atoms in a 1D geometry, which are *unidirectionally (chirally)* coupled through a single guided mode.

2.1 Single excitation transport in a one-dimensional array of unidirectionally coupled two-level emitters: polynomial dynamics

The goal of this chapter is to study chiral sub- and superradiance in a single excitation domain, and the natural first step is to look at the problem of a unidirectional transport of a single excitation between the two-level emitters (see Fig. 2.1).

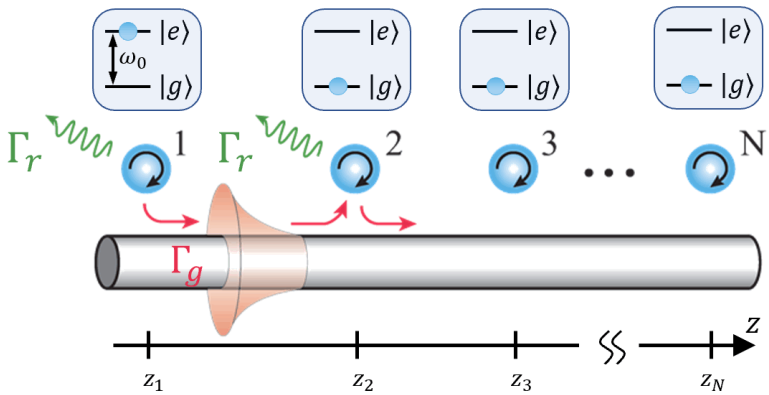

Figure 2.1 — A set of N two-level quantum emitters, which are one-way coupled through a single mode of a waveguiding structure. Each atom is assumed to be identical, characterized by its position along the waveguide z_j, and is coupled to a guided mode with the corresponding spontaneous emission rate Γ_g. However, any atom can also emit a photon into non-guided (radiation) modes, to which it is coupled with a rate Γ_r

Here we will assume that all two-level atoms are identical (have equal bare transition frequencies $\omega_j = \omega_0$), and has a coordinate z_j along the waveguide. The formal mathematical description for a problem of two-level

emitters interacting through the modes of a general dispersive, and absorptive environment has been extensively covered in the works by D.-G. Welsch with co-authors [164;165], and we are not going to cover this paritcular theory here in details. However, in the Appendix B.1 we demonstrate that by starting with the full master equation [165–168] on a density matrix $\rho_s(t)$ for the atomic subsystem, one can obtain an equivalent set of equations that we consider below.

In the weak atom-field coupling regime, a set of ordinary differential equations for the probability amplitudes for each atom j to be excited at time t is written as:

$$\dot{C}_j(t) = -\frac{\Gamma_{\text{tot}}}{2} C_j(t) + \sum_{k \neq j} G_{jk} C_k(t), \tag{2.1}$$

where $G_{jk} = i\frac{4\pi\overline{\omega}_k^2}{\hbar c^2}\mathbf{d_{eg,j}}\mathbf{G}(\mathbf{r_j}, \mathbf{r_k}, \overline{\omega}_k)\mathbf{d_{ge,k}}$ is the dipole-dipole coupling constant, $\overline{\omega}_k$ is the transition frequency of the k$^{\text{th}}$ atom with the Lamb shift included, $\mathbf{d_{eg,j}}$ is the transition dipole moment for atom j, and $\mathbf{G}(\mathbf{r_j}, \mathbf{r_k}, \overline{\omega}_k)$ is the classical electromagnetic Green's tensor of the problem, while $\Gamma_{\text{tot}} = \Gamma_{\text{g}} + \Gamma_{\text{r}}$ is the total spontaneous emission rate of an individual atom, which includes both emission into the guided mode and into the radiation modes. In case of a single guided mode to which emitters are coupled unidirectionally, we can define the emitter-emitter coupling constant as:

$$G_{jk} = \begin{cases} -\Gamma_g e^{ik^{\text{g}}|z_j - z_k|}, & \text{for } j > k, \\ 0, & \text{otherwise}, \end{cases} \tag{2.2}$$

here we assumed that all atoms are positioned at the same distance from the waveguide, so that the coupling strength of each atom with the guided mode is the same, and equal to Γ_g. k^{g} here is the propagation constant of the guided mode, and the exponent accounts for the accumulation of phase by a photon propagating from atom k to atom j.

Note that the system Eq. (2.1) can also be obtained by using the following effective non-hermitian Hamiltonian:

$$\hat{H}_{\text{eff}} = -i\sum_{j=1}^{N} \frac{\Gamma_{\text{tot}}}{2} |e_j\rangle\langle e_j| + \sum_{\substack{j,k \\ j>k}} iG_{jk}|e_j\rangle\langle e_k|, \tag{2.3}$$

by simply plugging it into the Shrodinger equation $i\hbar\frac{d|\Psi\rangle}{dt} = \hat{H}_{\text{eff}}|\Psi\rangle$, where $|\Psi\rangle = \sum_{j=1}^{N} C_j(t)|e_j\rangle$, with $|e_j\rangle = |e_j\rangle|g\rangle^{\otimes N-1}$ being the state with only atom j excited, while the rest are in the ground state.

Eq. (2.1) can be represented in a simple matrix form:

$$\dot{\mathbf{C}}(t) = \mathbf{M} \cdot \mathbf{C}(t),$$
$$\mathbf{M} = \begin{pmatrix} -\Gamma_{\text{tot}}/2 & 0 & ... & 0 \\ g e^{i\varphi_{21}} & -\Gamma_{\text{tot}}/2 & ... & 0 \\ ... & ... & ... & ... \\ g e^{i\varphi_{N1}} & g e^{i\varphi_{N2}} & ... & -\Gamma_{\text{tot}}/2 \end{pmatrix}; \quad \mathbf{C}(t) = \begin{pmatrix} C_1(t) \\ C_2(t) \\ ... \\ C_N(t) \end{pmatrix}, \quad (2.4)$$

with $g = -\Gamma_g$, $\varphi_{jk} = k^{\text{g}} |z_j - z_k|$, $\mathbf{C}$ is the column-vector with N entries of probability amplitudes of each atom to be excited, $\mathbf{M}$ is the $N \times N$ lower-triangular matrix due to the unidirectionality of interaction. The formal solution of Eq. (2.4) can be given by simply finding the matrix exponent of $\mathbf{M}$. However, this matrix is not diagonalizable as it has an eigenvalue $\lambda = -\Gamma_{\text{tot}}/2$ with the algebraic multiplicity N, while there is only a single eigenvector $\mathbf{v} = \begin{pmatrix} 0, & 0, & ..., & 1 \end{pmatrix}^T$. This eigenvector physically corresponds to a situation, when we excite the rightmost atom, and it simply exponentially decays with the decay rate of an isolated atom $P_N(t) = |C_N(t)|^2 = e^{-\Gamma_{\text{tot}} t}$ as there is no other excited atom on the left from which it can absorb the photon.

The solution to Eq. (2.4) can be written as:

$$\mathbf{C}(t) = e^{-\Gamma_{\text{tot}} t/2} e^{\mathbf{B}t} \mathbf{C_0}, \quad (2.5)$$

with $\mathbf{B} = \mathbf{M} + \dfrac{\Gamma_{\text{tot}}}{2}\mathbf{I}$, and $\mathbf{C_0}$ is the initial condition vector, which is in our case equal to $\mathbf{C_0} = \begin{pmatrix} 1, & 0, & ..., & 0 \end{pmatrix}^T$ (only the first atom is excited initially). As there is no eigendecomposition for matrix $\mathbf{M}$ (and, consequently, for matrix $\mathbf{B}$), one has to find all necessary generalized eigenvectors to span the whole $\mathbb{C}^{\mathbb{N}}$ space, and we also need to find the Jordan normal form of $\mathbf{B}$, which reads as:

$$\mathbf{J_B} = \begin{pmatrix} 0 & 1 & 0 & ... & 0 \\ 0 & 0 & 1 & ... & 0 \\ 0 & 0 & 0 & ... & 0 \\ ... & ... & ... & ... & ... \\ 0 & 0 & 0 & ... & 0 \end{pmatrix}. \quad (2.6)$$

As was pointed out before, we need to construct the full Jordan basis as soon as there is only one eigenvector for this matrix: $\mathbf{v_1} = (0, 0, ..., 1)$. The rest of the vectors needed to construct the full Jordan basis can be found by repeatedly solving $\mathbf{B f_j} = \mathbf{f_{j-1}}$, where $\mathbf{f_j}$ are the generalized eigenvectors, and $\mathbf{f_0} = \mathbf{v_1}$ is a regular eigenvector. Solving for this, we can find the following transformation matrix $\mathbf{S}$, it's inverse $\mathbf{S^{-1}}$, and the exponent of $\mathbf{B}$ in the

Jordan basis:

$$\mathbf{S} = \begin{pmatrix} 0 & 0 & 0 & ... & (-1)^{N+i+j+1} C_{N-2}^{0} e^{-i\varphi_{N,1}} \\ 0 & 0 & 0 & ... & (-1)^{N+i+j+1} C_{N-2}^{1} e^{-i\varphi_{N,2}} \\ ... & ... & ... & ... & ... \\ 0 & e^{-i\varphi_{N,N-1}} & -e^{-i\varphi_{N,N-1}} & ... & (-1)^{N+i+j+1} C_{N-2}^{N-2} e^{-i\varphi_{N,N-1}} \\ 1 & 0 & 0 & ... & 0 \end{pmatrix},$$

$$\mathbf{S^{-1}} = \begin{pmatrix} 0 & 0 & 0 & ... & 1 \\ C_{N-2}^{0} e^{i\varphi_{N,1}} & C_{N-3}^{0} e^{i\varphi_{N,2}} & C_{N-4}^{0} e^{i\varphi_{N,1}} & ... & 0 \\ ... & ... & ... & ... & ... \\ C_{N-2}^{N-2} e^{i\varphi_{N,1}} & C_{N-3}^{N-3} e^{i\varphi_{N,2}} & 0 & ... & 0 \\ C_{N-2}^{N-2} e^{i\varphi_{N,1}} & 0 & 0 & ... & 0 \end{pmatrix},$$

$$e^{gt\mathbf{J_B}} = \begin{pmatrix} 1 & gt & \frac{(gt)^2}{2!} & ... & \frac{(gt)^{N-1}}{(N-1)!} \\ 0 & 1 & gt & ... & \frac{(gt)^{N-2}}{(N-2)!} \\ ... & ... & ... & ... & ... \\ 0 & 0 & 0 & ... & gt \\ 0 & 0 & 0 & ... & 1 \end{pmatrix}, \tag{2.7}$$

where C_n^k are the binomial coefficients. For the sake of clarity one can write explicitly the matrix elements of S as:

$$S_{m,n} = \begin{cases} e^{-i\varphi_{N,m}} (-1)^{1+m+n+N} C_{n-2}^{N-1-m}, \text{ if } m \neq 1, \\ \delta_{N,m}, \text{ if } n = 1. \end{cases} \tag{2.8}$$

By substituting the above matrices into $\mathbf{C}(t) = e^{-\Gamma_{\text{tot}} t/2} \mathbf{S} e^{gt\mathbf{J_B}} \mathbf{S^{-1}} \mathbf{C_0}$, it can be found that the probability amplitude for atom N being excited as $C_N^1(t) = \frac{e^{-\Gamma_{\text{tot}} t/2} e^{i\varphi_{N,1}}}{(N-1)!} \sum_{j=0}^{N-1} L(N-1,j)(-\Gamma_g t)^j$, where $L(n,k)$ are so-called Lah numbers [169] known in combinatorics. For Lah numbers there is a relation which connects them with the generalized Laguerre polynomials of order minus one in the following way: $L_N^{(-1)}(x) = \frac{1}{N!} \sum_{j=0}^{N} L(N,j)(-x)^j$. Using this relation we can write the answer in a simple and compact form:

$$C_N^1(t) = e^{-\Gamma_{\text{tot}} t/2 + i\varphi_{N,1}} L_{N-1}^{(-1)}(\Gamma_g t). \tag{2.9}$$

The correctness of the obtained result can be easily checked by substituting this solution into the equation for the $(N+1)$-th emitter in the chain $C_{N+1}^1(t)$, and making use of the relation $\int_0^x L_N^{(\alpha)}(x)dx = L_{N+1}^{(\alpha-1)}(0) - L_{N+1}^{(\alpha-1)}(x)$.

Let us elaborate more on the physical meaning of Eq. (2.9). When looking at the probability of each atom to be excited $P_N(t) = |C_N^1(t)|^2$ the phase

factor $e^{i\varphi_{N,1}}$ vanishes, so that the behaviour of emitter N does not depend upon how exactly all emitters are located along the z-axis. Moreover, the Laguerre polynomial $L_n^{(-1)}(x)$ has n zeros on the real axis, which means that $P_N(t)$ has $N-1$ zeros (see Fig. 2.2), and, therefore, $N-1$ local maxima. This physically means that atom N undergoes $N-1$ events of the absorption with the subsequent emission.

We should note that a similar result to Eq. (2.9) was first obtained in [170] when studying the propagation of a pulse through a set of two-level atoms at the edge of a topological photonic crystal, which also allowed for unidirectionality. In this work the polynomial dynamics was imprinted on the envelope of a single photon pulse.

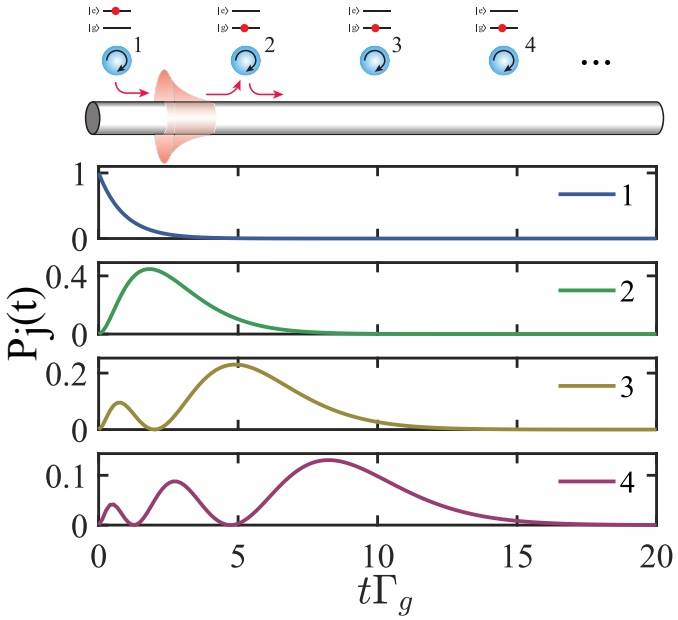

Figure 2.2 — The probabilities for different emitters to be excited $P_j(t)$ versus dimensionless time $t\Gamma_g$ shown for first $N = 4$ emitters. We set $\Gamma_g = 10$, $\Gamma_r = 1$

In this section, we have studied the problem of a single excitation transport in a chain of two-level emitters unidirectionally coupled through a guided mode. We have shown that this system shows quite a peculiar polynomial dynamics, and the number of emission/absorption cycles for each emitter is directly linked to it's ordinal number in a chain. In the next part we will use this result to study what kind of collective behavior a single excitation that is shared between all of N atoms can demonstrate in the case of sub-, and superradiance.

2.2 Collective chiral emission: sub- and superradiance in a single excitation domain

Now having Eq. (2.9), one can find the probability amplitude of the transition from a general initial state to some final state, both of which are in the single excitation domain, by calculating the following:

$$C(t) = \mathbf{C_{final}}^{\dagger}\mathbf{U(t)}\mathbf{C_{init}}, \tag{2.10}$$

here $U_{k,l}(t) = e^{-\Gamma_{\text{tot}}t/2}L_{k-l}^{(-1)}(\Gamma_g t)e^{i\varphi_{k,l}}$ for $k \geqslant l$, and $U_{k,l}(t) = 0$ otherwise:

$$\mathbf{U}(t) = e^{-\Gamma_{\text{tot}}t/2}\cdot \begin{pmatrix} L_0^{(-1)}(\Gamma_g t) & 0 & 0 & ... & 0 \\ L_1^{(-1)}(\Gamma_g t)e^{i\varphi_{2,1}} & L_0^{(-1)}(\Gamma_g t) & 0 & ... & 0 \\ L_2^{(-1)}(\Gamma_g t)e^{i\varphi_{3,1}} & L_1^{(-1)}(\Gamma_g t)e^{i\varphi_{3,2}} & L_0^{(-1)}(\Gamma_g t) & ... & 0 \\ ... & ... & ... & ... & ... \\ L_{N-1}^{(-1)}(\Gamma_g t)e^{i\varphi_{N,1}} & L_{N-2}^{(-1)}(\Gamma_g t)e^{i\varphi_{N-1,1}} & L_{N-3}^{(-1)}(\Gamma_g t)e^{i\varphi_{N-2,1}} & ... & L_0^{(-1)}(\Gamma_g t) \end{pmatrix}. \tag{2.11}$$

One can see that $\mathbf{U}(t)$ is a lower triangular matrix, it's $U_{k,l}(t)$ element represents the probability amplitude for the k-th atom to be excited at t, while initially at $t = 0$ only the l-th atom was excited; $\mathbf{C_{init}}$, and $\mathbf{C_{final}}$ are the column vectors of initial, and final states, and as we want to study the evolution of a given state in time - we set $\mathbf{C_{final}} = \mathbf{C_{init}}$. A further worthy simplification can be made if we restrict our consideration to periodic chains of emitters leading to $\varphi_{k,l} = (k-l)\varphi$, while for the initial state the phase of each probability amplitude is proportional to the respective atom number:

$$\mathbf{C_{init}} = \frac{1}{\sqrt{N}}\left(1, e^{i\psi}, e^{2i\psi}, ...e^{(N-1)i\psi}\right)^T. \tag{2.12}$$

Both φ and ψ are assumed to be real here, and their difference is responsible for how in-phase the lightfields emitted by two neighboring emitters are. In this case it can be found that:

$$C(t) = \frac{e^{-\Gamma_{\text{tot}}t/2}}{N}\sum_{k=1}^{N}(N-(k-1))e^{i(k-1)\xi}L_{k-1}^{(-1)}(\Gamma_g t), \tag{2.13}$$

with $\xi = \varphi - \psi$ (a more general solution one can find in Appendix B.2). As a next step, we find the actual probability $P(t) = |C(t)|^2$, and expand it up

to the lowest non-trivial order in t, obtaining (some details are given in B.2):

$$P(t\to 0)\approx 1-\Gamma^{(0)}t = 1-\mathrm{Re}\left[\Gamma_{\mathrm{tot}}+2\Gamma_g\frac{e^{i\xi}\left(N+e^{iN\xi}-Ne^{i\xi}-1\right)}{N\left(e^{i\xi}-1\right)^2}\right]t = 1-\Gamma_{\mathrm{tot}}-\Gamma_g\frac{N+\cos(N\xi)-1-N\cos\xi}{2N\sin^2(\xi/2)}, \tag{2.14}$$

where $\Gamma^{(0)}$ is the spontaneous emission rate at small times, which is shown as a function of ξ in Fig. 2.3 (a). First of all, this function is symmetric ($\xi\to-\xi$), and periodic (with period 2π), therefore, we can restrict our analysis to the domain $\xi\in[0,\pi]$ without loss of generality. In this domain, it has N extrema in total. When N is even, the number of maxima is equal to the number of minima, and for $\xi=\pi$ this function has the minimum (subradiance). Interestingly, that all other minima approach exactly the same value as the minimum at $\xi=\pi$. However, for odd N, $\xi=\pi$ point is the local maximum, not the minimum. As expected, for both even and odd N the point $\xi=0$ is the global maximum, corresponding to a situation when all atoms emit in-phase (superradiance).

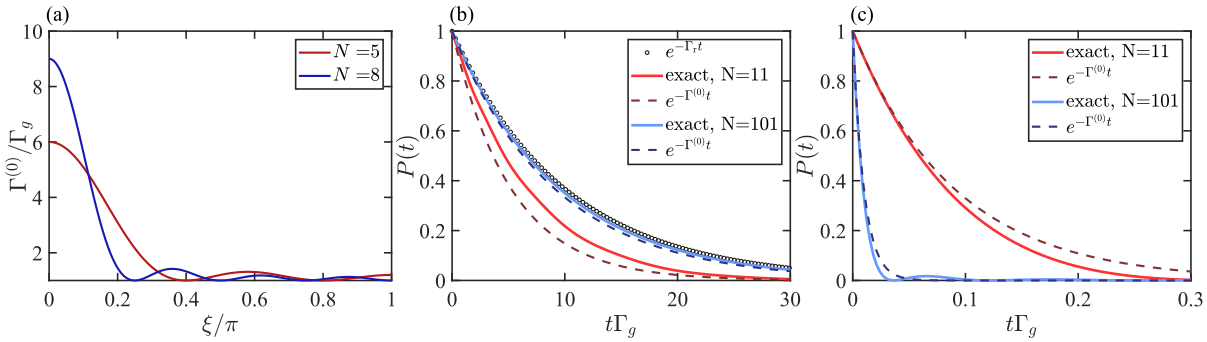

Figure 2.3 — (a) Spontaneous emission rate $\Gamma^{(0)}$ at small times defined in Eq. (2.14). Blue and red lines correspond to $N=5$, and $N=8$ cases. Here it is assumed that $\Gamma_r=\Gamma_g=1$. (b) Collective superradiant dynamics for the $\xi=\pi$ case: exact answer for $N=11$ ($N=101$) - solid light red (blue), $e^{-\Gamma^{(0)}t}$ functions for $N=11$ ($N=101$) - dashed dark red (blue). In open black circles the $e^{-\Gamma_r t}$ function is presented. (c) Same as (b), but for the case of subradiance ($\xi=0$). For (b), and (c) we took $\Gamma_r=0.1\Gamma_g$

From the above, we can say that it makes sense to consider only cases of $\xi=0$, and $\xi=\pi$ in order to obtain the maximal (superradiance), and the minimal (subradiance) possible $\Gamma^{(0)}$, correspondingly. For these two situations we have:

$$\Gamma^{(0)}=\begin{cases}\Gamma_{\mathrm{tot}}+\Gamma_g(N-1)=\Gamma_r+N\Gamma_g, & \text{if } \xi=2\pi m;\\ \Gamma_{\mathrm{tot}}-\dfrac{2N-1+(-1)^N}{2N}\Gamma_g=\Gamma_r+\dfrac{1-(-1)^N}{2N}\Gamma_g, & \text{if } \xi=\pi(2m+1).\end{cases} \tag{2.15}$$

One can recall that Γ_r is a spontaneous emission rate into non-guided modes (radiation modes), and it naturally enters the answer for $\Gamma^{(0)}$ as a separate term. The remaining part of $\Gamma^{(0)}$ is the collective emission rate into the guided mode. For the $\xi = 2\pi m$ case we obtain the same N-times enhancement of the emission rate as the original model of Dicke predicts [6]. However, for $\xi = \pi(2m+1)$ case the situation is more subtle. Once there are even number of atoms, we get $\Gamma^{(0)} = \Gamma_r$, so, the emission into a guided mode is totally suppressed. However, if N is odd, the suppression is not complete, and we have $\Gamma^{(0)} = \Gamma_r + \frac{\Gamma_g}{N}$, and the emission into a guided mode is finite, and decreses with the system size N. So, unlike the completely symmetrical case of atom-atom interaction through the guided mode, whether there are even or odd number of atoms makes a difference. Naturally, as $N \to \infty$, $\Gamma^{(0)} \to \Gamma_r$.

It is also interesting that for the in-phase case it is possible to find the dynamics of the Dicke state as a simple, and nice expression:

$$C_D(t) = \langle D|\hat{U}(t)|D\rangle = \sum_{k=1}^{N}\sum_{j=1}^{k} \frac{e^{-\Gamma_{\rm tot}t/2}}{N} L_{j-1}^{(-1)}(\Gamma_g t) = \frac{e^{-\Gamma_{\rm tot}t/2}}{N} L_{N-1}^{(1)}(\Gamma_g t), \quad (2.16)$$

where $|D\rangle = \frac{1}{\sqrt{N}}\sum_{j=1}^{N}|e_j\rangle$ is the symmetric Dicke state. In the above we have used two times the relation $\sum_{l=0}^{N} L_l^{(\alpha)}(x) = L_N^{(\alpha+1)}(x)$ mentioned before. The dynamics is again described by a generalized Laguerre polynomial, but of the order $\alpha = 1$. Needless to say that one can expand the modulus squared of this function, and obtain exactly the same value for $\Gamma^{(0)}$ in Eq. (2.15). For the subradiant emission, the simplest answer we managed to obtain is represented by Eq. (2.13): $C(t) = \frac{e^{-\Gamma_{\rm tot}t/2}}{N}\sum_{k=1}^{N}(N-(k-1))(-1)^{k+1}L_{k-1}^{(-1)}(\Gamma_g t)$.

During the derivation of these coefficients, we have implicitly used the perturbation theory in the lowest non-vanishing order in terms of emitter-emitter excitation transfer, and one may ask - was it a good approximation? Do these results make any sense? This question is especially important as from the very first obtained result (Eq. (2.9)) we understood that the dynamics of this highly degenerate system is non-exponential, but rather a polynomial one. The results presented in Fig. 2.3 (b) will help us to clarify this point. First of all, if we regard $\Gamma^{(0)}$ as a spontaneous emission rate, one may ask: whether it makes sense to approximate the probability dynamics as $P(t) = e^{-\Gamma^{(0)}t}$? Recall that we have, in general, two channels of decay in our problem: into the radiation modes, and into the guided mode. For both super-

and subradiance cases the decay into the first channel is equal to $\Gamma_{\rm r}$, while for the second one in case of subradiance we have ~ 0, and for superradiance it is $\sim N\Gamma_g$. Let us take the limit of strong radiation losses $\Gamma_r \gg N\Gamma_g > \Gamma_g$, in this case the interaction between emitters can be discarded, because if a given atom is excited, then it is much more likely that it emits a photon into the radiation modes rather then into the guided one, after which it might be absorbed by another atom. Therefore, for both super- and subradiance we will have approximately the same temporal dynamics $\approx e^{-\Gamma_r t}$, which is why we will not consider this case.

We can expect that in the opposite case, when the emission into the guided mode is dominant (so that $\Gamma_r \ll \Gamma_g < N\Gamma_g$), there might be some deviation between the exact answer in terms of generalized Laguerre polynomials, and exponential functions $e^{-\Gamma^{(0)}t}$. Indeed, as can be seen from Fig. 2.3 (b) for a rather small number of emitters $N = 11$, the difference between the exact answer and the exponential (solid bright and dashed dark red curves) is quite significant even for relatively small time arguments. However, as one increases the number of emitters to $N = 101$, this discrepancy becomes quite small, and both curves (solid bright and dark dashed blue) naturally approach the $e^{-\Gamma_{\rm r}t}$ function.

For superradiance ($\xi = 0$ case) the exponential fit is also not in a perfect agreement with the exact results. However, for both small, and large N it is at least in a good agreement for small $N\Gamma_g t$, but for large $N\Gamma_g t$ the difference is evident. Moreover, there is a region of a very small population growth in between $0.025 < t\Gamma_g < 0.1$ ($N = 101$ case, blue curves), which appears due to a small probability for the system to re-absorb the photon emitted before. From the mathematical properties of the generalized Laguerre polynomials it is known that for non-negative α, $L_N^{(\alpha)}(x)$ has N real roots on the positive x-axis, therefore, there are, actually, several local maxima, but only the first one is prominent as the outer exponent $e^{-\Gamma_{\rm tot}t}$ strongly suppresses the rest of them. Therefore, one can conclude that for a symmetric Dicke state the dynamics consists of successive emissions, and re-absorptions of the photon.

Now we can have a look at the results presented in Eq. (2.15) from a slightly different point of view, which will provide us with a simple pictorial explanation of these results.

For this let us now fix the initial state to be a symmetric Dicke state, as before, which is of the form $|\Psi_{\rm init}\rangle = |D\rangle = \dfrac{1}{\sqrt{N}} \sum\limits_{j=1}^{N} |e_j\rangle$, and derive the

probability amplitude of the excitation being only at emitter k at time Δt:

$$\langle e_k|\hat{U}(\Delta t)|\Psi_{\text{init}}\rangle = \frac{1}{\sqrt{N}}\begin{pmatrix}0\\ \dots\\ 1_k\\ \dots\end{pmatrix}^T \begin{pmatrix} 1-\frac{\Gamma_{\text{tot}}}{2}\Delta t & 0 & \dots & 0 \\ \pm\Gamma_g\Delta t & 1-\frac{\Gamma_{\text{tot}}}{2}\Delta t & \dots & 0 \\ \dots & \dots & \dots & \dots \\ \pm\Gamma_g\Delta t & -\Gamma_g\Delta t & \dots & 1-\frac{\Gamma_{\text{tot}}}{2}\Delta t \end{pmatrix}\begin{pmatrix}1\\ 1\\ \dots\\ 1\end{pmatrix} =$$

$$\begin{cases} \frac{1}{\sqrt{N}}\left(1-\frac{\Gamma_{\text{tot}}}{2}\Delta t + \ \text{mod}(k-1,2)\ \Gamma_g\Delta t\right), & \text{if } \xi = \pi(2m+1); \\ \frac{1}{\sqrt{N}}\left(1-\frac{\Gamma_{\text{tot}}}{2}\Delta t - 2(k-1)\Gamma_g\Delta t\right), & \text{if } \xi = 2\pi m. \end{cases} \tag{2.17}$$

an upper sign is for $\xi = \pi(2m+1)$ (subradiance), and a lower one is for $\xi = 2\pi m$ (superradiance). As we consider a small time argument expansion, it is also assumed that $\Gamma_{\text{tot}}\Delta t \ll 1$, so that this expansion is valid.

Through the obtained transition amplitudes, we can find the probabilities that emitter k is excited: $P_{e_k}(\Delta t) = |\langle e_k|\hat{U}(\Delta t)|\Psi_{\text{init}}\rangle|^2$, and we can expand this as $P_{e_k}(\Delta t) \approx \frac{1}{N} - \Gamma_k^{(0)}\Delta t$, where $\Gamma_k^{(0)}$ gives the contribution of the k^{th} atom to the total value of $\Gamma^{(0)} = \sum_{k=1}^{N}\Gamma_k^{(0)}$. Note that the factor $\frac{1}{N}$ in the expansion of $P_{e_k}(\Delta t)$ arises as a fact that in the initial state $|\Psi_{\text{init}}\rangle$ atom k shares only the N^{th} fraction of the exciation as $P_{|\Psi_{\text{init}}\rangle}(\Delta t) \approx \sum_{k=1}^{N} P_{e_k}(\Delta t) \approx 1 - \Gamma^{(0)}\Delta t$.

Here we also want to mention that during the time evolution of the system, excitation can be transferred between the atoms many times before being emitted into the field modes, therefore, there are many pathways of how exactly the photon can be emitted by the system. Nevertheless, in the considered case ($\Gamma_{\text{tot},g,r}\Delta t \ll 1$) it makes sense to take into account at most a single jump of the excitation from one atom to another, and after this jump the excitation is assumed to be emitted into the field subsystem. This corresponds to the mentioned before lowest non-vanishing order of perturbation theory in terms of atom-atom couplings, which is the non-diagonal part of the effective Hamiltonian in Eq. (2.3). For the sake of simplicity, we will also assume that the emission rate into non-guided modes is negligible $\Gamma_r/\Gamma_g \approx 0$ as this contribution can be trivially added as an additional term.

Now from Eq. (2.17) we can find the respective contribution of the k^{th} atom into the total emission rate $\Gamma^{(0)}$ for the case of subradiance to be equal to $\Gamma_k^{(0)} = \frac{1-2\,\text{mod}(k-1,2)}{N}\Gamma_g$. This can be rather simply explained by looking

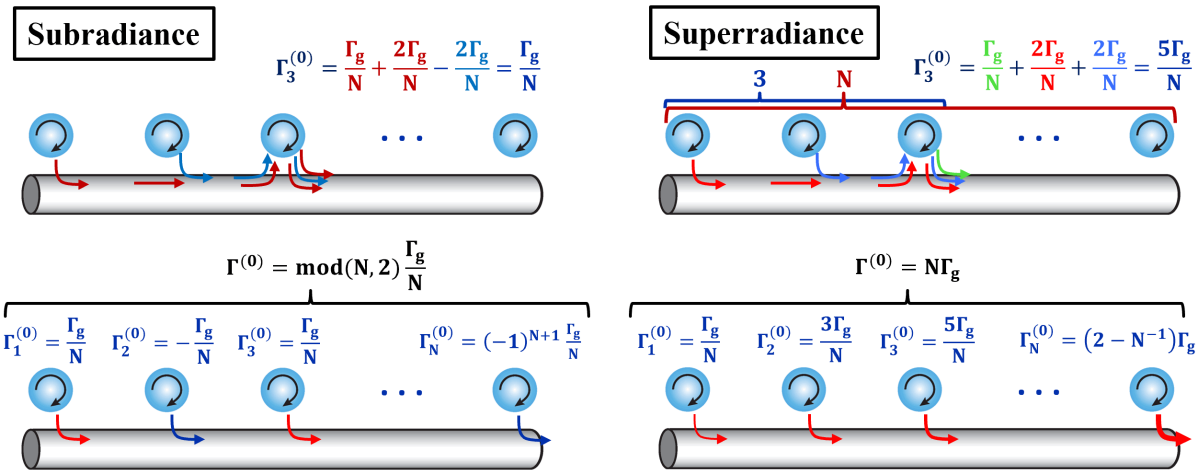

Figure 2.4 — The picture explaining chiral sub- (left) and superradiance (right). Top figures show an example of $\Gamma_3^{(0)}$, while bottom figures show all $\Gamma_k^{(0)}$, and the total value of $\Gamma^{(0)}$. Note that here it is assumed that Γ_r is negligible compared to Γ_g

at Fig. 2.4 (top left), where this value is pictorially explained for the case $k = 3$. Here one can see that $\Gamma_3^{(0)}$ consists of three contributions: 1) the first one comes from an independent spontaneous emission of atom 3, and it would be present even if this atom would not interact with any other; 2), 3) the next two contributions come from the absorption, and re-emission of the photon from atoms 1, and 2, correspondingly. However, as the initial state is a symmetric Dicke state $|D\rangle$, and as the distance between the atoms is chosen such that $\xi = (2m+1)\pi$, the latter two contributions destructively interfere, therefore, canceling each other. Clearly, the same thing happens for any other atom with an odd number, because there are even number of atoms positioned before it, which is why $\Gamma_k^{(0)} = \frac{\Gamma_g}{N}$ for odd k. For atoms with even numbers contributions from all preceding atoms would not completely cancel each other, leading to $\Gamma_k^{(0)} = \frac{\Gamma_g}{N} - \frac{2\Gamma_g}{N} = -\frac{\Gamma_g}{N}$ for even k. Therefore, one can write for any positive integer k the following: $\Gamma_k^{(0)} = \frac{1-2\mathrm{mod}(k-1,2)}{N}\Gamma_g$, so, these contributions are of the same magnitude, but of an altering sign (see Fig. 2.4, bottom left). When summing up all $\Gamma_k^{(0)}$, we obtain $\Gamma^{(0)} = \sum_{k=1}^{N}\Gamma_k^{(0)} = \mathrm{mod}(N,2)\frac{\Gamma_g}{N} = \frac{1-(-1)^N}{N}\Gamma_g$. Therefore, finite emission rate into a guided mode for odd N is simply associated with the incomplete destructive interference in the decay channels.

For $\xi = 2\pi m$ case all atoms emit photons in-phase, which is why a constructive interference appears, and one can see this from Fig. 2.4, top right. It leads to a linear growth of $\Gamma_k^{(0)}$ with the respective atom number k: $\Gamma_k^{(0)} = \frac{2k-1}{N}\Gamma_g$ (Fig. 2.4, bottom right). Obviously, this happens as the number of atoms from which atom k can receive a photon, and re-emit it later also grows linearly with k, and, effectively, atom behaves as being a

part of a chain with an effective size $\sim \frac{k}{N}$. By summing up contributions from all atoms we get $\Gamma^{(0)} = \sum_{k=1}^{N} \Gamma_k^{(0)} = N\Gamma_g$.

2.3 Strongly asymmetric single excitation transfer through a surface plasmon of a metallic nanowire

Previously, we formulated the problem by simply stating that it is possible to realize a unidirectional coupling of a rotating dipole moment to a guided mode of some structure, but we did not specified what kind of structure it was. In principle, there are many different options for that. It can be based on a glide-plane photonic crystal waveguide [24] or a nanobeam waveguide (NWG) [171;172]. The electric field of the guided mode in this case is rotating in the interface plane of the structure, and if the emitter is positioned at a proper spatial point of the waveguide, then there is an asymmetric coupling to forward and backward propagating modes. Another approach is based upon the use of a single-mode nanofiber, which is a regular dielectric waveguide with a circular cross section, and we already considered such a waveguide in the previous chapter. Such a structure has a fundamental mode of a hybrid TE-TM polarization (HE_{11} mode), which posesses a longitudinal component of the electric field being phase-shifted by $\pi/2$ [80], resulting in the electric field vector rotation, allowing for a chiral coupling [11;104], as was discussed in the beggining of this thesis.

In our further discussion we will consider a metallic nanowire rather than a dielectric nanofiber for a quite simple reason: it is more illustrative for a theoretical study as the fundamental mode of a metallic nanowire is a TM mode [173;174], which means that the electric field is rotating in the ρz-plane in any spatial point. Moreover, a propagating surface plasmon allows for an efficient emitter-guided mode coupling due to a strong confinement of the field.

First of all, we need to discuss whether high asymmetry of the coupling is achievable for a realistic structure. As shown in Fig. 2.5 (a) at sufficiently large separation distances between the emitters (at least $\Delta z > 0.1\lambda_0$) the coupling asymmetry can be, indeed, very high and exceed the value of 10. We also need to make several comments regarding this figure. One has to take into account that only the coupling through the modes of the nanowire are taken into account here for two main reasons: the free-space dipole-dipole coupling is always symmetric, and it diverges as $\Delta z \to 0$. Therefore, for very small distances the free-space coupling will dominate the coupling through the plasmon. The free-space interaction decays as $\sim |\Delta z|^{-1}$, while the interaction

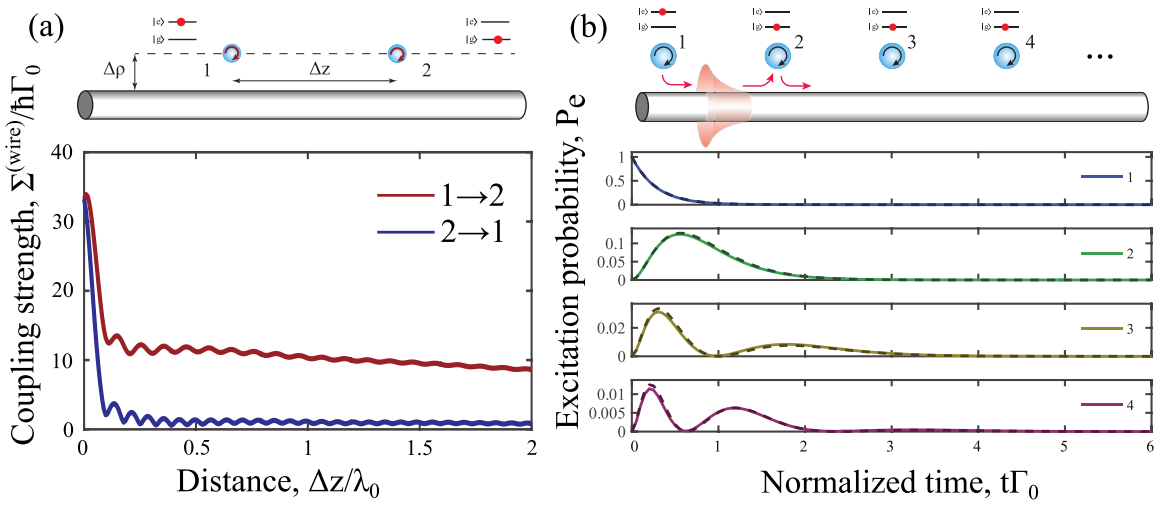

Figure 2.5 — (a) Coupling strength $\Sigma^{(\text{wire})}$ of two atoms through the modes of a nanowire, when the first (red) or the second (blue) atom is excited initially. Other relevant parameters are $\rho_c = 0.05\lambda_0$, $\Delta\rho = \rho_c$, $\varepsilon = -16.00 + 0.44i$. The chosen value of ε approximately corresponds to a silver permittivity at a wavelength $\lambda_0 \approx 600$ nm [175]. (b) Numerical (dashed) and analytical (solid) results for the excitation probabilities in a chain of $N = 4$ emitters. In the case of numerical calculations the averaging over 20 realizations of emitters' positions deviations from their regular ones along the wire was performed. The regular separation period was chosen to be $\Delta z = 2.0\lambda_0$, while the maximal deviation from a regular position is $a = \lambda_{\text{SPP}}/2$, and the deviations are assumed to be uniformly distributed

through a surface plasmon decays as $\sim e^{-k''_{\text{SPP}}|\Delta z|}$, where k_{SPP} is the imaginary part of the plasmon's wavenumber, which is non-zero due to Ohmic losses in the metal. However, for the considered parameters the Ohmic losses are quite small, resulting in a very weak exponential decay hardly seen in the Fig. 2.5 (a). Therefore, at distances $\Delta z > \lambda_0$ one can almost ignore the free-space coupling, while simultaneously having strong coupling to the wire modes ($\Gamma_{\text{plasmon}} \gg \Gamma_0$), and large asymmetry in the interaction. One can also notice that as $|\Delta z| \to 0$, the coupling constants approach the same value as in this limit the coupling constants can be interpreted as the Lamb shift and the emission rate of an atom with a circularly polarized dipole moment $\Sigma^{(wire)} = -\hbar\left(\delta^{(\text{wire})} + i\frac{\Gamma^{(\text{wire})}}{2}\right)$.

Now we can compare the results previously obtained in Fig. 2.2 with the ones calculated for the metallic nanowire. As we discussed before, for a perfect unidirectional case the transport dynamics does not depend on the emitters positions at all. However, as the interaction is not perfectly asymmetric, this might not be completely true. As can be seen from Fig. 2.5 (b), one can still describe the dynamics well enough by the previously obtained answer in Eq. (2.9). Note that for the case of a nanowire we let the emitters be

uniformly distributed around their regular positions, and then we averaged over positional disorder realizations. The details are given in Fig. 2.5 caption.

In this chapter we have discussed single excitation dynamics in a system of two-level emitters perfectly chirally coupled through a single guided mode. We did it both in the context of single excitation transport, and collective dynamics of this excitation being equally distributed among the atoms. We demonstrated that such a system demonstrates a polynomial temporal behavior, and obtained the emission rates for sub- and superradiant cases, also providing the explanation on the nature of the occuring difference with the case of a symmetric interaction between the emitters. We also discussed a more or less realistic system based on a metallic nanowire that supports a propagating surface plasmon.

2.4 A scientific statement

– For a perfectly asymmetric interaction of N two-level quantum emitters through a single guided mode, the collective spontaneous emission rate in case of superradiance is $N\Gamma_g$, while for subradiance it becomes 0 for even N, and Γ_g/N for odd N. The latter happens as a result of imperfect destructive interference between the decay channels.

3. Noninverse dynamics of the excitation transfer in many-level quantum emitter in the vicinity of a nanophotonic structure

In the previous chapter, we discussed the consequences of chiral (asymmetric) coupling of two-level emitters. In this chapter, we will elaborate on how to break the symmetry in the interaction between the dipole transitions, but inside of a single emitter with more than one excited state. We will demonstrate that this is, indeed, possible to achieve, and show at least two ways to observe such an asymmetry.

The first one is based on simultaneous use of: 1) fully locally anisotropic environment through the electromagnetic modes of which the transitions are coupled, and 2) arbitrary orientation of the respective transition dipole moments. For this we will explicitly formulate the criteria needed to be met in order to observe the asymmetry in transition dynamics, and also discuss how it affects the measurable quantities like registered temporal light intensity profile, and emitted light spectrum.

The second one will be conceptually much closer to the chiral coupling of emitters through surface localized modes - a topic covered in the previous chapter. We will show that by using a quite simple structure based on a plasmonic dimer made of two anisotropic scatterers, it is possible to realize an almost perfect unidirectional coupling of circular transitions in a V-type atom. We are also going to propose a simple scheme in which one can observe this effect in an atom under a proper external continuous wave pumping.

3.1 Theoretical framework and the case of in-plane rotating dipole moments

We begin by considering the system that is an atom with an s $\rightarrow$ p transition shown in Fig. 3.1 (a), meaning that the excited state is 3-fold degenerate with states $|e_{-1}\rangle, |e_0\rangle, |e_{+1}\rangle$, while there is only one ground state $|g\rangle$. This emitter is located in the vicinity of a photonic structure (an anisotropic metasurface in our case) and this allows for the coupling of circularly polarized transitions through the electromagnetic modes of this structure, which appears due to the Anisotropic Vacuum-Induced Interference (AVI) effect we mentioned before in the introduction [135; 140].

What we are going to look at the probability amplitudes of an atom to undergo a transition from state $|e_q\rangle$ to state $|e_{q'}\rangle$, which are given by the

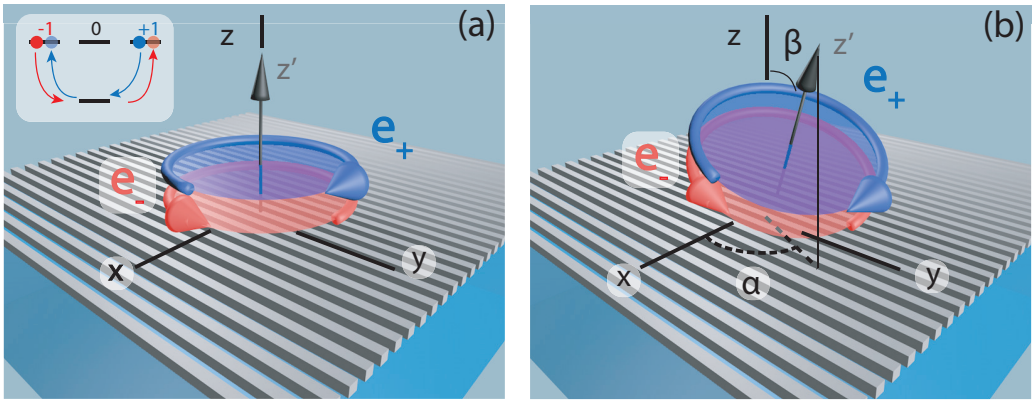

Figure 3.1 — The considered system shown schematically. (a) An atom with an s→p transition (3-fold degeneracy in the excited state) is put close to a photonic structure (anisotropic metasurface). The local atomic quantization axis z' in this scenario is parallel to the structure's normal, and to the z-axis of the introduced coordinate system, while the transitions σ^+, σ^- (in blue and red) are in the interface plane. (b) Same as (a) but with the z'-axis being rotated by angles α, β

matrix elements of the evolution operator [4]:

$$\langle e_{q'}|\hat{U}(t,0)|e_q\rangle = \int_C \frac{dz}{2\pi i} e^{-izt/\hbar}\langle e_{q'}|\hat{G}(z)|e_q\rangle, \tag{3.1}$$

where $\hat{G}(z) = (z - \hat{H})^{-1}$ is the resolvent operator of the full Hamiltonian $\hat{H} = \hat{H}_0 + \hat{V}$, which consists of the unperturbed $\hat{H}_0$ part, and perturbation $\hat{V}$. The approach we use here is similar to the one discussed in the first chapter, except that here we consider time evolution of the system rather than find the spectrum through S, and T matrices. We will briefly cover the basics of this approach below. Note that as we only consider the atomic excited states, which are discrete, there will be only pole contributions to the integral, and also note that z here is the parameter having the units of energy. The unperturbed Hamiltonian consists of parts related to the atom and the field: $\hat{H}_0 = \hat{H}_A + \hat{H}_F$. In order to describe the field, and how it interacts with the atom for a very general case of a medium with both dispersion and absorption, we use the approach introduced in [164], and mentioned in the previous chapters. In this case we can write:

$$\begin{aligned}
\hat{H}_A &= \sum_{q=-1,0,+1} \hbar\omega_0 |e_q\rangle\langle e_q|, \\
\hat{H}_F &= \int d\mathbf{r}' \int_0^\infty d\omega' \hbar\omega' \hat{\mathbf{f}}^\dagger(\mathbf{r}',\omega')\hat{\mathbf{f}}(\mathbf{r}',\omega'), \\
\hat{V} &= -\sum_q \hat{\mathbf{d}}_q \hat{\mathbf{E}}(\mathbf{r_a}),
\end{aligned} \tag{3.2}$$

where ω_0 is the resonance frequency of the atomic transition, $\hat{\mathbf{f}}^\dagger(\mathbf{r}', \omega')$ is the local field creation operator, $\hat{\mathbf{E}}(\mathbf{r_a})$ is the total electric field at the position

of the atom $\mathbf{r_a}$. The electromagnetic field operator in this case reads as $\hat{\mathbf{E}}(\mathbf{r}) = i\sqrt{4\hbar}\int d\mathbf{r}' \int_0^\infty d\omega' \frac{\omega'^2}{c^2}\sqrt{\varepsilon_I(\mathbf{r}',\omega')}\mathbf{G}(\mathbf{r},\mathbf{r}',\omega')\hat{\mathbf{f}}(\mathbf{r}',\omega') + h.c.$, where the bosonic field operators obey the commutation relation $\left[\hat{f}_i(\mathbf{r}',\omega'), \hat{f}_k^\dagger(\mathbf{r},\omega)\right] = \delta_{ik}\delta(\mathbf{r}'-\mathbf{r})\delta(\omega'-\omega)$, $\mathbf{G}(\mathbf{r},\mathbf{r}',\omega')$ is the classical electromagnetic Green's function, and $\varepsilon_I(\mathbf{r}',\omega')$ is the imaginary part of permittivity.

The resolvent operator $\hat{G}(z)$ entering Eq. (3.1) being projected onto the subspace of atomic excited states reads as:

$$\hat{P}\hat{G}(z)\hat{P} = \hat{P}\frac{1}{z - \hat{H}_0 - \hat{\Sigma}(z)}\hat{P}, \tag{3.3}$$

here $\hat{P}$ is the corresponding projector, and $\hat{\Sigma}(z)$ is the level-shift operator or self-energy part. $\hat{\Sigma}(z)$ here provides the energy shifts to the unperturbed eigenstates of $\hat{H}_0$ due to the interaction of the atom with electromagnetic field modes of the structure, and it has the form:

$$\hat{\Sigma}(z) = \hat{V} + \hat{V}\hat{G}(z)\hat{V} \approx \hat{V} + \hat{V}\hat{G}_0(z = \hbar\omega_0)\hat{V}, \tag{3.4}$$

where the last transition implied two approximations: (1) near resonant case, which ignores possible dependence of $\hat{\Sigma}(z)$ on z, also called the flat spectrum approximation; (2) $\hat{\Sigma}(z)$ is calculated up to the second order in $\hat{V}$. The former one is related to the Markov approximation, and the absence of memory effects in the system. The latter is related to the fact that transitions are coupled through the dipole-dipole interaction, which is a second-order process in terms of the photon absorption/emission [152]. The corresponding matrix elements can be represented in a rather simple form:

$$\Sigma_{q',q}(\hbar\omega_0) = -4\pi k_0^2 \mathbf{d}^*_{\mathbf{q}'}\mathbf{G}(\mathbf{r_a},\mathbf{r_a},\omega_0)\mathbf{d_q}, \tag{3.5}$$

where $k_0 = \omega_0/c$, $\mathbf{d_q}$ is the transition dipole moment from $|g\rangle$ to $|e_q\rangle$. This can be alternatively written as $\mathbf{\Sigma} = \mathbf{S}^\dagger\mathbf{\Sigma}_{\text{Cart}}\mathbf{S}$, where:

$$\mathbf{S} = \frac{1}{\sqrt{2}}\begin{pmatrix} +1 & 0 & -1 \\ -i & 0 & -i \\ 0 & \sqrt{2} & 0 \end{pmatrix}, \tag{3.6}$$

is the matrix of Cartesian components of rank-1 spherical tensors $\mathbf{S} = \left(\mathbf{n_{-1}}, \mathbf{n_0}, \mathbf{n_{+1}}\right)$ as its columns ($\mathbf{n_0} = \mathbf{e_z}, \mathbf{n_{\pm 1}} = \mp\frac{1}{\sqrt{2}}\left(\mathbf{e_x} \pm i\mathbf{e_y}\right)$), while $\mathbf{\Sigma}_{\text{Cart}}$ is related to the couplings of linear dipole moments aligned along x, y, and z axes. The latter assumes that we introduced a Cartesian coordinate system with some origin that we fix.

Essentially, if one has the total electromagnetic Green's tensor $\mathbf{G}(\mathbf{r_a}, \mathbf{r_a}, \omega_0)$, the problem is immediately solved. As we discussed above, we consider that the emitter is placed in the vicinity of an anisotropic metasurface, which basically presents a planar interface of infinitely small thickness described by a surface conductivity tensor:

$$\sigma(\omega) = \begin{pmatrix} \sigma_{xx}(\omega) & 0 \\ 0 & \sigma_{yy}(\omega) \end{pmatrix}, \tag{3.7}$$

here the diagonal elements have a form of the Lorenzians [176] $\sigma_{jj}(\omega) = A_j \dfrac{ic}{4\pi} \dfrac{\omega}{\omega^2 - \Omega_j^2 + i\gamma_j \omega}$ with A_j being the normalization factor, Ω_j - frequency of the resonance, and γ_j is the damping constant. We will also note that it is assumed here that the x, y axes of the previously introduced Cartesian coordinate system are parallel to the principal axes of $\sigma(\omega)$, while z axis is normal to the interface plane. Once we know the surface conductivity tensor, and the permittivity of the upper, and lower half-spaces we can derive the classical electromagnetic Green's tensor of the problem, the details of the derivation are described in Appendix C.1.

For the case when rotating dipole moments are in the interface plane of the structure, the matrix elements of $\hat{\Sigma}$ on states $|e_{+1}\rangle$, $|e_{-1}\rangle$ are given by:

$$\begin{aligned} \Sigma_{-,+}(\hbar\omega_0) = 4\pi k_0 \frac{|\mathbf{d}|^2}{2} \begin{pmatrix} 1 & i & 0 \end{pmatrix} \begin{pmatrix} G_{xx} & 0 & 0 \\ 0 & G_{yy} & 0 \\ 0 & 0 & G_{zz} \end{pmatrix} \begin{pmatrix} 1 \\ i \\ 0 \end{pmatrix} = \\ 2\pi k_0^2 |\mathbf{d}|^2 \left(G_{xx} - G_{yy}\right) = \Sigma_{+,-}(\hbar\omega_0), \\ \Sigma_{-,-}(\hbar\omega_0) = 4\pi k_0 \frac{|\mathbf{d}|^2}{2} \begin{pmatrix} 1 & i & 0 \end{pmatrix} \begin{pmatrix} G_{xx} & 0 & 0 \\ 0 & G_{yy} & 0 \\ 0 & 0 & G_{zz} \end{pmatrix} \begin{pmatrix} 1 \\ -i \\ 0 \end{pmatrix} = \\ 2\pi k_0^2 |\mathbf{d}|^2 \left(G_{xx} + G_{yy}\right) = \Sigma_{+,+}(\hbar\omega_0). \end{aligned} \tag{3.8}$$

One can already notice that the coupling of transitions $\Sigma_{-,+}(\hbar\omega_0) = \Sigma_{+,-}(\hbar\omega_0) \neq 0$ is present only if the structure is anisotropic $G_{xx} \neq G_{yy}$, as expected, and this holds true if the corresponding surface conductivities are not equal $\sigma_{xx}(\omega_0) \neq \sigma_{yy}(\omega_0)$. Also note that states $|e_{+1}\rangle, |e_{-1}\rangle$ are decoupled from $|e_0\rangle$, and if the atom is in spin-polarized state initially $|e_{\pm 1}\rangle$, then excitation is only transferred between $|e_{+1}\rangle, |e_{-1}\rangle$.

The excitation transfer probability has the following explicit form:

$$\begin{aligned} P_{\mp 1,-1}(t,0) = \left| \langle e_{\mp} | \hat{U}(t,0) | e_{-} \rangle \right|^2 = \\ \frac{1}{2} e^{2\mathrm{Im}[g_{-,-}]t} \left(\cos(2\mathrm{Re}[g_{-,+}]t) \pm \cosh(2\mathrm{Im}[g_{-,+}]t) \right), \end{aligned} \tag{3.9}$$

where $g_{i,j} = \Sigma_{i,j}/\hbar$, and also note that $g_{-,-} = g_{+,+}$, $g_{-,+} = g_{+,-}$ in the considered case. This result was first obtained in [165] in the context of two distant two-level atoms interacting through the modes of some photonic structure.

The oscillating part of this solution is related to the energy exchange between the levels $|e_-\rangle, |e_+\rangle$, and the frequency of these oscillations is naturally proportional to the energy splitting due to the coupling of transitions $2\mathrm{Re}\,[g_{-,+}]$. How well these oscillations are pronounced depends on the parameter $-\dfrac{|\mathrm{Re}\,[g_{-,+}]|}{\mathrm{Im}\,[g_{-,-}]}$. If $|\mathrm{Re}\,[g_{-,+}]| > -\mathrm{Im}\,[g_{-,-}]$, then the population oscillations are underdumpled, which corresponds to a *strong coupling regime*, while in the opposite case it is a *weak coupling regime* with overdumped oscillations.

In order to demonstrate these two regimes we will consider one specific example. In general, the local Green's function of a metasurface includes integrals (see Appendix C.1). However, we can consider the case, when metasurface is strongly anisotropic, and lossless: $\sigma_{xx} \to 0i$, and $\sigma_{yy} \to \infty i$. One can think about it as the structure being perfectly conducting in y-direction, while simultaneously being an isolator in x-direction. This allows us to write the local Green's function $\mathbf{G_{sc}}(\mathbf{r_a}, \mathbf{r_a}, \omega_0)$ in a form of a simple explicit expression (some details are presented in Appendix C.1):

$$
\begin{aligned}
G^{sc}_{xx}(\mathbf{r_a}, \mathbf{r_a}, \omega) &= e^{2ik\Delta z}\frac{1}{32\pi k^2 \Delta z^3}, \\
G^{sc}_{yy}(\mathbf{r_a}, \mathbf{r_a}, \omega) &= e^{2ik\Delta z}\frac{-1 + 2ik\Delta z + 4k^2\Delta z^2}{32\pi k^2 \Delta z^3}, \\
G^{sc}_{zz}(\mathbf{r_a}, \mathbf{r_a}, \omega) &= e^{2i\Delta z k}\frac{1 - ik\Delta z}{16\pi k^2 \Delta z^3},
\end{aligned}
\tag{3.10}
$$

where Δz is the atom-interface distance, which is asummed to be positive, and the relevant coupling constants can be readily found:

$$
\begin{aligned}
\hbar g_{-,+} = -4\pi k_0^2 \mathbf{d}^*_{-1}\mathbf{G}(\mathbf{r_a}, \mathbf{r_a}, \omega_0)\mathbf{d}_{+1} = 4\pi k_0^2 |\mathbf{d}|^2 \frac{G_{xx} - G_{yy}}{2} = \\
\left(\frac{1 - ik\Delta z - 2k^2\Delta z^2}{4\Delta z^3}\right)|\mathbf{d}|^2 e^{ik2\Delta z}, \\
\hbar g_{-,-} = -4\pi k_0^2 \mathbf{d}^*_{-1}\mathbf{G}(\mathbf{r_a}, \mathbf{r_a}, \omega_0)\mathbf{d}_{-1} = -4\pi k_0^2 |\mathbf{d}|^2 \frac{G_{xx} + G_{yy}}{2} = \\
-\left(\frac{ik\Delta z + 2k^2\Delta z^2}{4\Delta z^3}\right)|\mathbf{d}|^2 e^{ik2\Delta z}.
\end{aligned}
\tag{3.11}
$$

Now we can look at two typical profiles of Eq. (3.9), which are presented in Fig. 3.2 (a). It can be seen that for atom-surface distance $\Delta z = 0.1\lambda_0$ this function is purely decaying, which corresponds to a weak coupling of

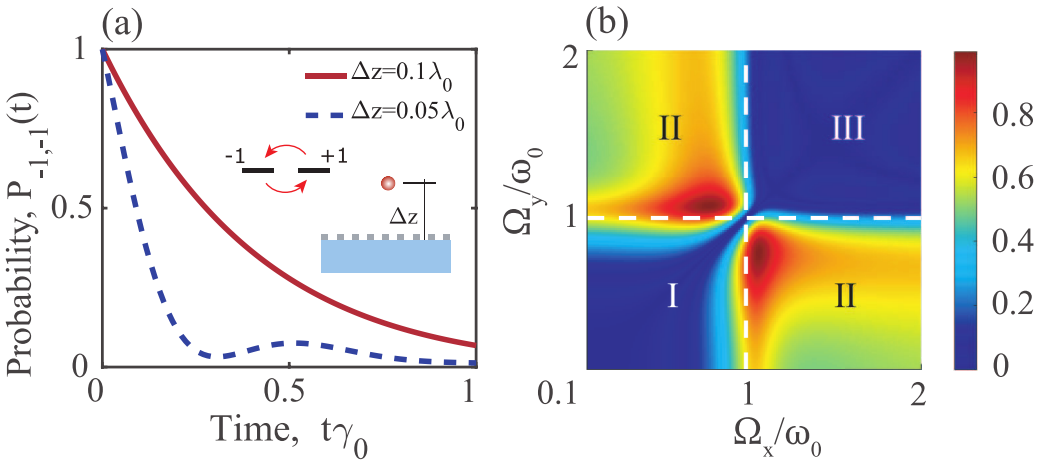

Figure 3.2 — a) Probability function $P_{-,-}(t)$ when a strongly aisotropic metasurface is considered. The regime of strong coupling is reached for an atom-interface distance $\Delta z = 0.05\lambda_0$, which manifests itself in the presence of oscillations. b) Color plot of the strong coupling parameter $-|\mathrm{Re}[g_{-,+}]|/\mathrm{Im}[g_{-,-}]$ as a function of frequencies Ω_x, Ω_y. There are three regions specified, these regions correspond to three regimes: I) inductive ($\mathrm{Im}[\sigma_{xx}], \mathrm{Im}[\sigma_{yy}] > 0$), II) hyperbolic ($\mathrm{Im}[\sigma_{xx}] \cdot \mathrm{Im}[\sigma_{yy}] < 0$), and III) capacitive ($\mathrm{Im}[\sigma_{xx}], \mathrm{Im}[\sigma_{yy}] < 0$) regimes. Other relevant parameters are: atom-metasurface distance is $\Delta z = 0.05\lambda_0$, the damping rates for surface conductivities $\gamma_x = \gamma_y = 0.1\omega_0$, substrate permittivity is $\varepsilon_{subs} = 1$, and the normalization constants are $A_x = A_y = 1$

$|e_{-1}\rangle, |e_{+1}\rangle$ states (solid red line). But as emitter becomes closer to the surface, the energy level splitting becomes larger, and the strong coupling regime appears ($\Delta z = 0.05\lambda_0$, dashed blue line). We want to note that going into deep subwavelength atom-surface distances $\Delta z \leqslant 0.01\lambda_0$ might lead to the breakdown of the purely resonant form of dipole-dipole coupling of transitions (see Eq. (3.5)) as the near-fields of the structure will play an important role through non-resonant Casimir-Polder interactions [143; 144]. This particular mechanism of coupling will not be discussed in here, and further.

The considered above limit of a strong anisotropy allows for the explicit analytical solution of the excitation transfer problem. However, for a metasurface described by Lorenz-like surface conductivities it can be also analyzed if we simply plot the strong coupling parameter $-\dfrac{|\mathrm{Re}\,[g_{-,+}]|}{\mathrm{Im}\,[g_{-,-}]}$ versus two resonance frequencies Ω_x, Ω_y, which is shown in Fig. 3.2 (b). As can be seen, the regions of this parameter being sufficiently larger than zero are the areas, where the transition frequency lies in-between the Ω_x, Ω_y frequencies, which is commonly called the hyperbolic regime of operation [151; 176; 177] of metasurfaces.

In this section, we discussed how it is possible to couple circular transitions in an atom put close to an anisotropic metasurface. However, for the situation when dipole moments are rotating in the interface plane, the symmetry in transitions between the excited states is preserved. In the next part we will show how the arbitrary orientation of dipole moments will help us to break this symmetry.

3.2 Rotation of dipole moments, and broken symmetry in transitions

As a straightforward generalization of the problem under consideration, we let the local quantization axis (z'-axis) of the atom be arbitrarily oriented in space. Formally, this boils down to the transformation of the form:

$$\tilde{\mathbf{\Sigma}} = \mathbf{S}^{\dagger}\mathbf{M}^{\dagger}\mathbf{\Sigma}_{\mathrm{Cart}}\mathbf{M}\mathbf{S} = \mathbf{T}^{\dagger}\mathbf{\Sigma}_{\mathrm{Cart}}\mathbf{T}, \tag{3.12}$$

where $\mathbf{M}$ is the rotation matrix on Euler angles $\boldsymbol{\alpha}, \boldsymbol{\beta}, \boldsymbol{\gamma}$. We need also to fix the following conventions: we will use active representation (rotation of the objects, not of the coordinate axes), right-hand rule (according to which the rotation is performed), $z'' - y' - z$ convention (which defines the order of rotation axes).

The transofmation matrices have the following explicit forms:

$$\mathbf{M} = \begin{pmatrix} \cos(\boldsymbol{\alpha})\cos(\boldsymbol{\beta})\cos(\boldsymbol{\gamma}) - \sin(\boldsymbol{\alpha})\sin(\boldsymbol{\gamma}) & -\cos(\boldsymbol{\gamma})\sin(\boldsymbol{\alpha}) - \cos(\boldsymbol{\alpha})\cos(\boldsymbol{\beta})\sin(\boldsymbol{\gamma}) & \cos(\boldsymbol{\alpha})\sin(\boldsymbol{\beta}) \\ \cos(\boldsymbol{\alpha})\sin(\boldsymbol{\gamma}) + \cos(\boldsymbol{\beta})\cos(\boldsymbol{\gamma})\sin(\boldsymbol{\alpha}) & \cos(\boldsymbol{\alpha})\cos(\boldsymbol{\gamma}) - \cos(\boldsymbol{\beta})\sin(\boldsymbol{\alpha})\sin(\boldsymbol{\gamma}) & \sin(\boldsymbol{\alpha})\sin(\boldsymbol{\beta}) \\ -\cos(\boldsymbol{\gamma})\sin(\boldsymbol{\beta}) & \sin(\boldsymbol{\beta})\sin(\boldsymbol{\gamma}) & \cos(\boldsymbol{\beta}) \end{pmatrix},$$

$$\mathbf{T} = \begin{pmatrix} \frac{e^{i\boldsymbol{\gamma}}}{\sqrt{2}}\left(\cos(\boldsymbol{\alpha})\cos(\boldsymbol{\beta}) + i\sin(\boldsymbol{\alpha})\right) & \cos(\boldsymbol{\alpha})\sin(\boldsymbol{\beta}) & \frac{e^{-i\boldsymbol{\gamma}}}{\sqrt{2}}\left(-\cos(\boldsymbol{\alpha})\cos(\boldsymbol{\beta}) + i\sin(\boldsymbol{\alpha})\right) \\ \frac{e^{i\boldsymbol{\gamma}}}{\sqrt{2}}\left(-i\cos(\boldsymbol{\alpha}) + \cos(\boldsymbol{\beta})\sin(\boldsymbol{\alpha})\right) & \sin(\boldsymbol{\alpha})\sin(\boldsymbol{\beta}) & \frac{e^{-i\boldsymbol{\gamma}}}{\sqrt{2}}\left(-i\cos(\boldsymbol{\alpha}) - \cos(\boldsymbol{\beta})\sin(\boldsymbol{\alpha})\right) \\ -\frac{e^{i\boldsymbol{\gamma}}}{\sqrt{2}}\sin(\boldsymbol{\beta}) & \cos(\boldsymbol{\beta}) & \frac{e^{-i\boldsymbol{\gamma}}}{\sqrt{2}}\sin(\boldsymbol{\beta}) \end{pmatrix}. \tag{3.13}$$

There is an important point to make: when rotating the local quantization axis of the atom, we change the orientation of the respective transition dipole moments. However, the eigenvalues of $\mathbf{\Sigma}$ and $\tilde{\mathbf{\Sigma}}$ are, obviously, the same, which means that the transition frequencies, and linewidths of the eigenstates are also the same before, and after the rotation. Nevertheless, rotation changes the projections of atomic transition dipole moments on the introduced Cartesian coordinate system axes.

The consequences of this can be illustrated by the following: let us consider the probability amplitude of a transition from state q to q'. It has the simplest

form in the eigenstate basis, and can be found to be:

$$U_{q',q}(t,0) = \sum_{j=x,y,z} C_j^{(q',q)} e^{-ig_j t}, \quad q,q' = \{-1,0,+1\}, \tag{3.14}$$

where g_j are the complex-valued eigenvalues of $\tilde{\mathbf{\Sigma}}/\hbar$, and $C_j^{(q',q)} = \left(\mathrm{T}^{-1}\right)_{q',j} \mathrm{T}_{j,q}$. The physical meaning of this constant is simple - it is related to how each eigenstate j contributes to the dynamics. As the nanostructure under consideration is the planar anisotropic conducting interface, the eigenstates of the system correspond to three linear dipole moments oriented along highly symmetric directions of this structure (principal axes of the nanostructure). The three axes of high symmetry are: the normal to the interface (z-axis), and two orthogonal axes in which the surface conductivity tensor becomes diagonal. We want to note that in this coordinate system the local Green's tensor $\mathbf{G}(\mathbf{r},\mathbf{r},\omega_0)$ is also diagonal. Therefore, we can state that $\hbar g_j = -4\pi k_0^2 \mathbf{d}_\mathbf{j}^\dagger \mathbf{G}(\mathbf{r_a},\mathbf{r_a},\omega)\mathbf{d_j}$ are the self-energies of three linear dipole moments oriented along x, y, and z directions.

Now let us inspect the explicit form of coefficients $C_j^{(q',q)}$ for the specific case of the transition $|e_{+1}\rangle \rightarrow |e_{-1}\rangle$:

$$\begin{aligned} C_x^{(-1,+1)} &= -\tfrac{e^{-2i\gamma}}{2}\left(\cos(\alpha)\cos(\beta) - i\sin(\alpha)\right)^2, \\ C_y^{(-1,+1)} &= \tfrac{e^{-2i\gamma}}{2}\left(\cos(\alpha) - i\cos(\beta)\sin(\alpha)\right)^2, \\ C_z^{(-1,+1)} &= -\tfrac{e^{-2i\gamma}}{2}\sin^2(\beta). \end{aligned} \tag{3.15}$$

One can notice that all three coefficients have a common phase factor $e^{-2i\gamma}$. As a quantity of interest is the transition probability $|U_{-1,+1}(t,0)|^2$, this phase factor will vanish, which means that the last rotation around the new $\mathbf{e_{z'}}$-axis on angle $\boldsymbol{\gamma}$ is redundant as it does not affect the dynamics, and, therefore, we can proceed with $\boldsymbol{\gamma} = 0$ without loss of generality.

Also note that the transformation matrix $\mathbf{T}$ is unitary, from which follows the property of these coefficients: $C_j^{(+,-)} = (C_j^{(-,+)})^*$. We can expect that for general values of $\boldsymbol{\alpha},\boldsymbol{\beta}$ this phase difference can lead to noninverse dynamics between these two states, and to broken symmetry between the transitions $|e_{-1}\rangle \rightarrow |e_{+1}\rangle$, and $|e_{+1}\rangle \rightarrow |e_{-1}\rangle$.

Now let us compute the transition probabilities as $P_{q',q}(t) = |U_{q',q}(t,0)|^2$, and obtain the following quantity, which is the asymmetry in transfer probabilities $P_{-,+}(t) - P_{+,-}(t)$:

$$\begin{aligned} P_{-,+}(t) - P_{+,-}(t) &= f(\alpha,\beta) \sum_{(k,l)}^{(x,y),(y,z),(z,x)} e^{(g_k''+g_l'')t} \sin\left(\left(g_k' - g_l'\right)t\right), \\ f(\alpha,\beta) &= \tfrac{1}{8}\sin(2\alpha)\sin(2\beta)\sin(\beta), \end{aligned} \tag{3.16}$$

where $g_j = g'_j + ig''_j$. From Eq. (3.16) one can see that there are two separate conditions, which are necessary for this quantity to be non-zero:

$$\begin{cases} (I) \quad f(\alpha,\beta) \neq 0 \quad \rightarrow \quad \alpha \neq \frac{\pi}{2}m, \quad \beta \neq \frac{\pi}{2}m', \\ (II) \quad g'_k \neq g'_l, \quad \text{for any pair of eigenstates } k,l. \end{cases} \tag{3.17}$$

The first condition is a purely geometrical condition, and is related to the respective orientation of transition dipole moments, and to principal axes of the nanostructure. It simply states that the z' quantization axis of the atom should not lie in a plane formed by any two principal axes. The second statement, however, is electrodynamical, and can be formulated as: the eigenstates of the system, formed due to the interaction through the nanostructure modes, should not be degenerate.

A further insight into the physical nature of the effect can be gained if one looks at the explicit form of the transition probability:

$$P_{q',q}(t) = \sum_{k=x,y,z} P^{(k)}_{q',q}(t) + \sum_{(k,l)}^{(x,y),(y,z),(z,x)} P^{(k,l)}_{q',q}(t) = \\ \sum_{k=x,y,z} C^{(q',q)}_{k,k} e^{2g''_j t} + \sum_{(k,l)}^{(x,y),(y,z),(z,x)} 2\left|C^{(q',q)}_{k,l}\right| \cos\left[(g'_k - g'_l)t - \varphi^{(q',q)}_{k,l}\right] e^{(g''_k+g''_l)t}, \tag{3.18}$$

where $C^{(q',q)}_{k,l} = C^{(q',q)}_{k}(C^{(q',q)}_{l})^*$, and $\varphi^{(q',q)}_{k,l} = \arg\left(C^{(q',q)}_{k,l}\right)$. The origin of the two terms above is simple: the first one is simply each term from Eq. (3.14) being squared, while the second part is responsible for the interference of different eigenstates, leading not only to the exponential decay, but also to the oscillations due to this interference. And in the oscillating part, there is an initial phase $\varphi^{(q',q)}_{k,l}$, which has opposite signs for the forward $|e_q\rangle \rightarrow |e_{q'}\rangle$, and backward $|e_{q'}\rangle \rightarrow |e_q\rangle$ processes $\varphi^{(q',q)}_{k,l} = -\varphi^{(q,q')}_{k,l}$, as it can be clearly seen from it's definition. Therefore, we can conclude, that this effect is, essentially, the *phase interference effect*. This can be easily illustrated by considering the mentioned before limit of strong anisotropy ($\sigma_{xx} \rightarrow 0i, \sigma_{yy} \rightarrow \infty i$). As one can see from Fig. 3.3 (a), when both conditions from Eq. (3.17) are satisfied, then, indeed, $P_{-,+}(t) \neq P_{+,-}(t)$, and this discrepancy is a result of difference in the corresponding interference components entering the second part of Eq. (3.18), which are shown in Fig. 3.3 (b). Also notice that in Fig. 3.3 (b) both $P_{-,+}(t)$, and $P_{+,-}(t)$ at sufficiently large times start to behave identical. This happens as a result of interference components, which oscillate, being completely suppressed, and the dynamics is only described by a collection of the decaying exponents (the first part of Eq. (3.18)).

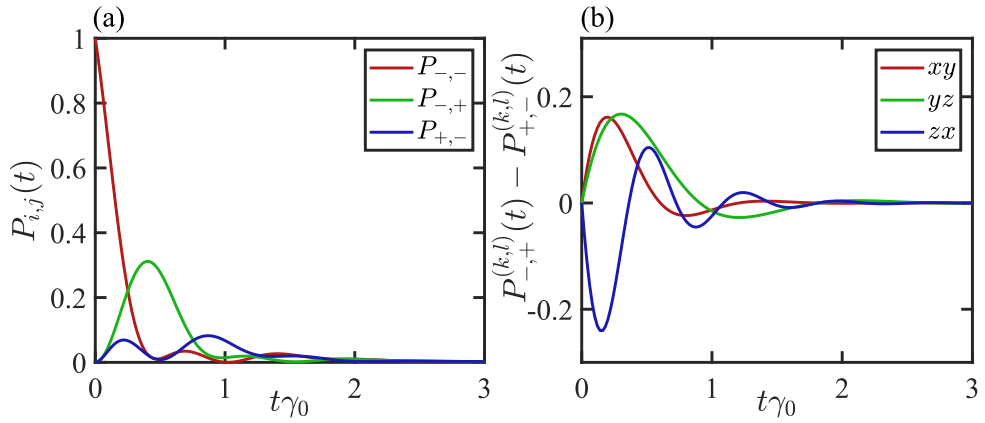

Figure 3.3 — (a) Different transition probabilities $P_{i.j}(t)$ versus normalized time $t\gamma_0$. (b) Difference between the three interference terms entering as the second part of Eq. (3.18) for forward, and backward transition probabilities. The parameters are: $\Delta z = 0.05\lambda_0$, $\alpha = \beta = \pi/4$

From Eq. (3.18) one can also derive the conditions in Eq. (3.17). Let us do this for the first condition from Eq. (3.17). Notice that if $\varphi^{(\pm,\mp)}_{k,l} = 0$ or $\varphi^{(\pm,\mp)}_{k,l} = \pi$, then $P_{+,-}(t) = P_{-,+}(t)$ as a result of $\cos(x - \pi) = \cos(x + \pi)$. Therefore, the effect is absent when $C^{\pm,\mp}_{k,l}$ are purely real. We can inspect the imaginary parts of these coefficients, which turn out to be equal:

$$\mathrm{Im}\, C^{+,-}_{x,y} = \mathrm{Im}\, C^{+,-}_{y,z} = \mathrm{Im}\, C^{+,-}_{z,x} = \frac{1}{8}\sin(2\alpha)\sin(2\beta)\sin(\beta), \tag{3.19}$$

which is equal to zero if either α or β is an integer multiple of $\dfrac{\pi}{2}$.

Now we can discuss the second condition from Eq. (3.17). Let us imagine that two eigenstates turn out to be degenerate, meaning that $g_x = g_y = g_{||}$. Clearly, in this case $P^{(x,y)}_{-,+}(t) = P^{(x,y)}_{+,-}(t)$ as the interference term does not oscillate, and it can be thought of a constant factor having the property $\cos(-\varphi^{(-,+)}_{x,y}) = \cos(-\varphi^{(+,-)}_{x,y})$. For other two terms we have:

$$\begin{aligned}
P^{(y,z)}_{-,+}(t) &= 2\left|C^{(-,+)}_{y,z}\right| \cos\left[(g'_{||} - g'_z)t - \varphi^{(-,+)}_{y,z}\right] e^{(g''_{||}+g''_z)t},\\
P^{(z,x)}_{-,+}(t) &= 2\left|C^{(-,+)}_{z,x}\right| \cos\left[(g'_z - g'_{||})t - \varphi^{(-,+)}_{z,x}\right] e^{(g''_z+g''_{||})t},\\
P^{(y,z)}_{+,-}(t) &= 2\left|C^{(+,-)}_{y,z}\right| \cos\left[(g'_{||} - g'_z)t - \varphi^{(+,-)}_{y,z}\right] e^{(g''_{||}+g''_z)t},\\
P^{(z,x)}_{+,-}(t) &= 2\left|C^{(+,-)}_{z,x}\right| \cos\left[(g'_z - g'_{||})t - \varphi^{(+,-)}_{z,x}\right] e^{(g''_z+g''_{||})t}.
\end{aligned} \tag{3.20}$$

It should be true that $P^{(y,z)}_{-,+}(t) + P^{(z,x)}_{-,+}(t) - P^{(y,z)}_{+,-}(t) - P^{(z,x)}_{+,-}(t) = 0$, but at the first glance this does not seem to be so. Recall that $\left|C^{(-,+)}_{y,z}\right| = \left|C^{(+,-)}_{y,z}\right|$, $\left|C^{(-,+)}_{z,x}\right| = \left|C^{(+,-)}_{z,x}\right|$, $\varphi^{(-,+)}_{y,z} = -\varphi^{(+,-)}_{y,z}$, $\varphi^{(-,+)}_{z,x} = -\varphi^{(+,-)}_{z,x}$. With this in mind

let's rewrite the above:

$$P_{-,+}^{(y,z)}(t) + P_{-,+}^{(z,x)}(t) - P_{+,-}^{(y,z)}(t) - P_{+,-}^{(z,x)}(t) = 2\Big(\big|C_{y,z}^{(-,+)}\big| \sin\Big[\Big(g'_{||} - g'_z\Big)\, t\Big] \sin\big(\varphi_{y,z}^{-,+}\big) + \big|C_{z,x}^{(-,+)}\big| \sin\Big[\Big(g'_z - g'_{||}\Big)\, t\Big] \sin\big(\varphi_{z,x}^{-,+}\big)\Big) e^{(g''_z + g''_{||})t} = \frac{1}{4}\sin(2\alpha)\sin(2\beta)\sin(\beta)\Big(\sin\Big[\Big(g'_{||} - g'_z\Big)\, t\Big] + \sin\Big[\Big(g'_z - g'_{||}\Big)\, t\Big]\Big) = 0, \tag{3.21}$$

in the above we have used the facts that $|C_{i,j}^{(q',q)}| \sin(\varphi_{i,j}^{(q',q)}) = \mathrm{Im}\left[C_{i,j}^{(q',q)}\right]$, and, as we know from Eq. (3.19), these coefficients are equal for fixed q',q, and any i,j.

To conclude, we have demonstrated that by coupling a multilevel $s \to p$ quantum emitter with the electromagnetic modes of an anisotropic metasurface, it is possible to break the symmetry in electron transitions between the excited states: $P_{q',q}(t) \neq P_{q,q'}(t)$. We derived analytically the criteria needed to be satisfied in order to observe this effect, and also identified that it has a nature of a phaseshift appearing as a result of interference between the eigenstates of the system.

3.3 Effect on the observables: detected temporal intensity, and the total emitted light spectrum.

Previously, we derived the conditions under which the excitation probability function between the states $P_{q',q}(t)$ will be different for forward, and backward processes. However, we are not able to observe directly the transition of an atom from one excited state to another. Therefore, we need to consider experimentally measurable quantities, that are simultaneously related to the results that were obtained already.

In order to do this, we can begin by considering the temporal dynamics of the emitted light intensity. The set-up of the problem will be similar: the atom is initially assumed to be in the excited state $|e_{q_0}\rangle$, and we measure the time-dependency of the light intensity registered at the position of the detector $\mathbf{r_d}$ put in the far-field, which can be found to be [178]:

$$I_{q_0}(t) = \langle\psi(t)|\hat{\mathbf{E}}^{(-)}(\mathbf{r_d})\hat{\mathbf{E}}^{(+)}(\mathbf{r_d})|\psi(t)\rangle = \left|\sum_{q'} 4k_0^2 \int_0^t dt' C_{q',q_0}(t') \int_0^\infty d\omega\, \mathrm{Im}\left[\mathbf{G}(\mathbf{r_d},\mathbf{r_a},\omega)\right] \mathbf{d}_{\mathbf{q}'} e^{-i(\omega-\omega_0)(t-t')}\right|^2. \tag{3.22}$$

As we want to find the intensity registered in the far-field zone, we need to replace the full Green's tensor with its far-field part $\mathbf{G}(\mathbf{r_d}, \mathbf{r_a}, \omega) \rightarrow \mathbf{G^{FF}}(\mathbf{r_d}, \mathbf{r_a}, \omega)$. Owing to a superposition principle [159; 179] this far-field Green's tensor can be written as a sum of free space and scattered contributions: $\mathbf{G^{FF}}(\mathbf{r_d}, \mathbf{r_a}, \omega) = \mathbf{G^{FF,0}}(\mathbf{r_d}, \mathbf{r_a}, \omega) + \mathbf{G^{FF,sc}}(\mathbf{r_d}, \mathbf{r_a}, \omega)$ or, more precisely:

$$\mathbf{G^{FF}}(\mathbf{r_d}, \mathbf{r_a}, \omega) = \mathbf{f^0}(\mathbf{r_d}, \mathbf{r_a}, \omega) e^{ikR_-} + \mathbf{f^{sc}}(\mathbf{r_d}, \mathbf{r_a}, \omega) e^{ikR_+}, \tag{3.23}$$

where $R_\pm = \sqrt{(x_d - x_a)^2 + (y_d - y_a)^2 + (z_d \pm z_a)^2}$. Eq. (3.23) simply states that the scattered part of the field emitted by a dipole can be represented as a sum of two kinds of outgoing spherical waves. The first one would be present even if there was no photonic structure nearby, it is a direct term, which is just a far-field emitted by an isolated dipole $\mathbf{f^0}(\mathbf{r_d}, \mathbf{r_a}, \omega) e^{ikR_-}$, while the second term represents the field scattered off the photonic environment $\mathbf{f^{sc}}(\mathbf{r_d}, \mathbf{r_a}, \omega) e^{ikR_+}$. The difference in the exponential factors is quite clear - it appears as these two contributions are generated by two different dipoles: one is located at the position $\mathbf{r_a}$, and the other one is its mirror image located at $\left(x_a, y_a, -z_a\right)$.

As we want to couple emitter's transitions through the modes of the structure, we put atom close to the structure surface ($z_a/\lambda_0 \ll 1$), then we can ignore the fact that the atom itself, and its image have different locations $R_- \approx R_+ = R$. This will allow us to write the far-field Green's tensor as $\mathbf{G^{FF}}(\mathbf{r_d}, \mathbf{r_a}, \omega) \approx \mathbf{f} e^{ikR}$, and, by using the fact that $\mathrm{Im}\left[\mathbf{f}(\mathbf{r_d}, \mathbf{r_a}, \omega) e^{ikR}\right] = \mathrm{Re}\left[\mathbf{f}(\mathbf{r_d}, \mathbf{r_a}, \omega)\right] \sin(kR) + \mathrm{Im}\left[\mathbf{f}(\mathbf{r_d}, \mathbf{r_a}, \omega)\right] \cos(kR)$, and making the expansion of the wavenumber near the atomic resonance frequency $k(\omega) \approx k(\omega_0) + k'(\omega_0)(\omega - \omega_0)$, we can finally perform the integration over the frequency in Eq. (3.22). The function $\mathbf{f}(\mathbf{r_d}, \mathbf{r_a}, \omega)$, which is a sum $\mathbf{f^0}() + \mathbf{f^{sc}}()$, in our case can be thought of as a slowly varying function of frequency, and taken outside of the ω integral calculated at the resonance atomic frequency ω_0. We want to note that the approximation used here can be considered as a Markovianity in a weak sense, which means that we took into account the dispersion of a photon propagating in the far-field, and it led to a finite propagation time from atomic position $\mathbf{r_a}$ to the detector $\mathbf{r_d}$ for a lightfield.

Now we can finally take care of the ω integral, and arrive at the following result:

$$I_{q_0}(t) \approx \left| \frac{4\pi k_0^2}{i} \sum_{q'} C_{q',q_0}(t - R/c) \mathbf{G^{FF}}(\mathbf{r_d}, \mathbf{r_a}, \omega_0) \mathbf{d_{q'}} \right|^2. \tag{3.24}$$

Note that the transition dipole moments $\mathbf{d_{q'}}$ here are the rotated ones, and can be written as: $\mathbf{d_{q'}} = |\mathbf{d}|\mathbf{M}\mathbf{S}_{:,q'}$, where matrices $\mathbf{M}$, and $\mathbf{S}$ are given by Eqs. (3.13), (3.6), correspondingly.

This result can be interpreted in a quite simply way. The atom is initially pumped in state $|e_{q_0}\rangle$, but due to the coupling of transitions, other excited states also can be populated. Each transition can be viewed as a dipole $\mathbf{d_{q'}}$, which produces the field at $\mathbf{r_d}$ proportional to $4\pi k_0^2 \mathbf{G^{FF}}(\mathbf{r_d}, \mathbf{r_a}, \omega_0)\mathbf{d_{q'}}$ and this field is multiplied by the corresponding probability amplitude $C_{q',q_0}(t - R/c)$ of the atom being in state $|e_{q'}\rangle$ at the retarded time $t - R/c$. These fields, independently produced by, in general, all three transition dipole moments are summed up, and squared.

Another view on the equation above can be performed if one substitutes Eq. (3.14) in it:

$$I_{q_0}(\tau) \approx |4\pi k_0^2 \mathbf{d}|^2 \left| \sum_j \mathbf{f_j} e^{-ig_j\tau} \right|^2, \tag{3.25}$$

where $\tau = (t - R/c)$ is the retarded time, $\mathbf{f_j} = \mathbf{G^{FF}_{:,j}}(\mathbf{r_d}, \mathbf{r_a}, \omega_0)\,(\mathbf{MS}_{j,q_0})$ is related to the electric field produced at the position of the detector $\mathbf{r_d}$, and $\mathbf{G^{FF}_{:,j}}(\mathbf{r_d}, \mathbf{r_a}, \omega_0)$ is the j$^{\text{th}}$ column of the far-field classical Green's tensor of the system. The difference between Eq. (3.24), and Eq. (3.25) is that the former one is written in the basis of bare atomic excited states, while the latter one is expressed in the eigenstate picture.

The manifestation of the effect under study can be observed by making the comparison of the intensity dynamics for two initial conditions ($q_0 = -1$ and $q_0 = +1$), when the structure is isotropic, and anisotropic. The results of this comparison are presented in Fig. 3.4 (a). Note that in a general case the orientation of the local atomic quantization axis, and the position of the detector relative to the location of the atom are not correlated. In order to reduce the total amount of degrees of freedom in the system, we enforce that the detector position is given by $\mathbf{r_d} || \mathbf{M}\hat{z}$, which means that the orientation of the local atomic quantization axis, and location of the detector are given by the angles α, β. As can be seen from Fig. 3.4 (a) for isotropic case (Case A: dark red solid line, and bright red open circles) the intensity profiles are the same for both initial conditions, while for anisotropic case (Case B: blue dash-dotted, and blue dotted lines) they differ noticeably.

Previously we had a look at how the phenomenon under study affects the intensity profile. It might be also interesting to consider what happens with the spectral properties of the system, which can be described by the far-field total emitted light spectrum. This quantity in the Markov approximation can be found to be [165]:

$$S_{q_0}(\omega) = \int_0^\infty dt_2 \int_0^\infty dt_1 \left[e^{-i\omega(t_2 - t_1)} \langle \hat{\mathbf{E}}^{(-)}(\mathbf{r}, t_2) \hat{\mathbf{E}}^{(+)}(\mathbf{r}, t_1) \rangle \right] = \left| \sum_{q'} \int_0^\infty dt' C_{q',q_0}(t') e^{i(\omega - \omega_{q'})t'} \mathbf{F^{q'}}(\mathbf{r_d}, \mathbf{r_a}) \right|^2, \tag{3.26}$$

where $\omega_{q'}$ is the corresponding transition frequency, $C_{q',q_0}(t')$ is the probability amplitude of the system to be in the excite state $|e_{q'}\rangle$ at time t', while being initially in q_0 state, and $\mathbf{F}^{\mathbf{q}'}(\mathbf{r_d}, \mathbf{r_a})$ is given by:

$$\mathbf{F}^{\mathbf{q}'}(\mathbf{r_d}, \mathbf{r_a}) = 4\frac{\omega_{q'}^2}{c^2}\int' d\omega' \mathrm{Im}[\mathbf{G}(\mathbf{r_d}, \mathbf{r_a}, \omega')]\mathbf{d_{q'}}\zeta(\omega_{q'} - \omega') = \mathbf{\Gamma}(\mathbf{r_d}, \mathbf{r_a})\mathbf{d_{q'}}, \tag{3.27}$$

with $\zeta(x) = i\mathrm{P}\frac{1}{x} + \pi\delta(x)$. We want to note that during further derivations we only take into account the part proportional to $\pi\delta(x)$. Despite the fact that the principal value part of the integral above is, generally, not zero, we will ignore this as this will simplify further calculations significantly, but will not affect the results qualitatively with regard to the studied effect. Finally, for this quantity we have:

$$\mathbf{F}^{\mathbf{q}'}(\mathbf{r_d}, \mathbf{r_a}) \approx 4\pi\frac{\omega_{q'}^2}{c^2}\mathrm{Im}\left[\mathbf{G}(\mathbf{r_d}, \mathbf{r_a}, \omega_{q'})\right]\mathbf{d_{q'}}. \tag{3.28}$$

In the definition of the emitted light spectrum Eq. (3.26) we put bare transition frequencies $\omega_{q'} = \omega_0$ without the Lamb shift included in contrast to how it was done in the original paper [165]. Formally, it means that the bare transition frequency has to be replaced with the corrected value. For instance, transition frequency enters as an argument in the Green's tensor of the problem, but in our problem Green's tensor varies significantly on the scale $\sim \omega_0$, while the corrections are on the order of a bare atomic linewidth $\sim \gamma_0 \ll \omega_0$, therefore, these corrections will not lead to any significant deviations.

Now we can proceed with the calculation of the spectrum by carrying out the time integral in Eq. (3.26):

$$\begin{aligned} S_{q_0}(\omega) = \left|\sum_j \frac{i\sum_{q'}\mathbf{F}_{\mathbf{q}'}(\mathbf{r_d}, \mathbf{r_a})C_j^{(q',q_0)}}{(\delta - g_j)}\right|^2 = \left|\sum_j \frac{i\sum_{q'}\mathbf{\Gamma}(\mathbf{r_d}, \mathbf{r_a})\mathbf{d_{q'}}C_j^{(q',q_0)}}{(\delta - g_j)}\right|^2 = \\ \left|\sum_j \frac{i\sum_{q'}|\mathbf{d}|\mathbf{\Gamma}(\mathbf{r_d}, \mathbf{r_a})\mathbf{MS}_{:,q'}\left[(\mathbf{MS})^{-1}\right]_{q',j}(\mathbf{MS})_{j,q_0}}{(\delta - g_j)}\right|^2 = \\ \left|\sum_j \frac{i|\mathbf{d}|\mathbf{\Gamma}_{:,j}(\mathbf{r_d}, \mathbf{r_a})(\mathbf{MS})_{j,q_0}}{(\delta - g_j)}\right|^2 = \left|\sum_j \frac{\boldsymbol{f}_j^{q_0}(\mathbf{r_d}, \mathbf{r_a})}{(\delta - g_j)}\right|^2, \end{aligned} \tag{3.29}$$

where we introduced the detuning $\delta = \omega - \omega_0$. In the above we have also used Eq. (3.14) for $C_{q',q_0}(t')$, and the fact that $C_j^{(q',q_0)}$ is just equal to $\left[(\mathbf{MS})^{-1}\right]_{q',j}(\mathbf{MS})_{j,q_0}$ by definition. Essentially, Eq. (3.29) is all we need, and it physically expresses the contribution to the spectrum of each eigenstate j with complex-valued eigenfrequency $g_j = g_j' + ig_j''$, which produces the field $\boldsymbol{f}_j^{q_0}(\mathbf{r_d}, \mathbf{r_a})$ at the position of the detector.

There is also another way of representing the spectrum, which can be obtained if we use the same trick we have used already in the first chapter:

$$\sum_{j=1}^{N}\sum_{i=1}^{N}\frac{(\boldsymbol{f}_i^{q_0})^\dagger \boldsymbol{f}_j^{q_0}}{(\delta-g_j)(\delta-g_i^*)}=\sum_{j=1}^{N}\sum_{i=1}^{N}\frac{(\boldsymbol{f}_i^{q_0})^\dagger \boldsymbol{f}_j^{q_0}}{g_j-g_i^*}\left[\frac{1}{\delta-g_j}-\frac{1}{\delta-g_i^*}\right]=$$
$$\sum_{j=1}^{N}\sum_{i=1}^{N}2\mathrm{Re}\left[\frac{(\boldsymbol{f}_i^{q_0})^\dagger \boldsymbol{f}_j^{q_0}}{g_j-g_i^*}\frac{1}{\delta-g_j}\right]=\sum_{j=1}^{N}\sum_{i=1}^{N}2\mathrm{Re}\left[\frac{(\boldsymbol{f}_i^{q_0})^\dagger \boldsymbol{f}_j^{q_0}(\delta-g_j^*)}{g_j-g_i^*}\right]\frac{1}{|\delta-g_j|^2}, \tag{3.30}$$

where in transition from the 2nd to the 3rd equation the interchange $i \leftrightarrow j$ was made for the second term. Now we can define the following two quantities:

$$\xi_j=+2\mathrm{Re}\left[\sum_i\frac{(\boldsymbol{f}_i^{q_0})^\dagger \boldsymbol{f}_j^{q_0}}{g_j-g_i^*}\right],\eta_j=-2\mathrm{Im}\left[\sum_i\frac{(\boldsymbol{f}_i^{q_0})^\dagger \boldsymbol{f}_j^{q_0}}{g_j-g_i^*}\right], \tag{3.31}$$

and, at last, arrive at the following:

$$S_{q_0}(\delta)=\left|\sum_j\frac{\boldsymbol{f}_j^{q_0}(\mathbf{r_d},\mathbf{r_a})}{(\delta-g_j)}\right|^2=\sum_j\frac{\left(\xi_j(\delta-g_j')+\eta_j g_j''\right)}{(\delta-g_j')^2+g_j''^2}, \tag{3.32}$$

Now let us discuss this form of the spectrum once more. First of all, notice, that there are two principally different contributions to it. The one proportional to $\sim \xi_j$ has a simple Lorenzian lineshape described by the spectral position of the line g_j', and spectral width g_j''. The other contribution is antisymmetrical with respect to $\delta-g_j' \to -(\delta-g_j')$ and it gives asymmetry to each spectral line. The reason for the presence of this asymmetry is that even though the spectrum is described in the picture of eigenstates, these eigenstates are not orthogonal, in general, this leads to the interference between the eigenstates. Eq. (3.32) presented above is absolutely identical to the one we derived in the first chapter for total scattering cross-section (Eq. (1.6)), transmission (Eq. (1.28)), and reflection (Eq. (1.30)) for an ensemble of atoms.

Now let us come back to the discussion of the effect, for this, let us have a look at the Fig. 3.4 (b). As expected, for isotropic metasurface (Case A: dark red solid line, and bright red open circles) the spectra for two initial conditions ($q_0=-1$, and $q_0=+1$) are identical, but once the structure is anisotropic (Case B: blue dash-dotted, and blue dotted lines) the spectra become different. The presence of the phaseshift can be seen explicitly, if one recalls that $\boldsymbol{f}_j^{q_0}(\mathbf{r_d},\mathbf{r_a})=i|\mathbf{d}|\boldsymbol{\Gamma}_{:,j}(\mathbf{r_d},\mathbf{r_a})(\mathbf{MS})_{j,q_0}$, and, as clearly seen from Eq. (3.13), the normalized rotated dipole moments obey the following:

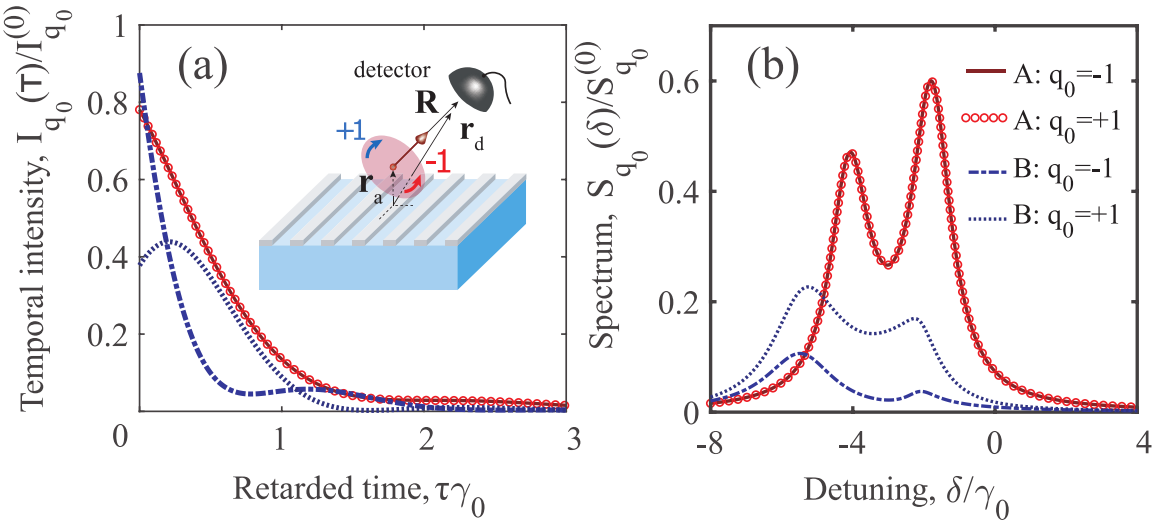

Figure 3.4 — a) Field intensity registered at the position of the detector $\mathbf{r_d}$ as a function of time $\tau\gamma_0 = (t - R/c)\gamma_0$. $\tau = 0$ time is when the light emitted by the atom reaches the detector position. The emitter is assumed to be in a state $|e_{q_0}\rangle$ initially. We consider the two following cases: A - isotropic ($\Omega_x = \Omega_y = 1.5k_0$), and B - anisotropic ($\Omega_x = 1.5k_0, \Omega_y = 1.1k_0$) metasurface. We also study two possible initial conditions, hence, 4 cases in total: isotropic metasurface - $A : q_0 = -1$, and $A : q_0 = +1$ (solid dark red line, and bright red circles); anisotropic metasurface - $B : q_0 = -1$, and $B : q_0 = +1$ (blue dash-dotted, and dotted lines). The parameters are the following: $\gamma_x = \gamma_y = 0.1k_0$, $\varepsilon_{\text{subs}} = 1.0$, $\Delta z = 0.05\lambda_0$, $\mathbf{r_a} = (0, 0, \Delta z)$, $\mathbf{r_d} = R(\cos(\alpha)\sin(\beta), \sin(\alpha)\sin(\beta), \cos(\beta))$, $R = 100\lambda_0$, $\alpha = \pi/4$, $\beta = \pi/4$. Normalization constant $I^{(0)}_{q_0}$ is the intensity registered at $\tau = 0$ when the atom is in free space. b) The total emitted light spectra. All relevant parameters, and the studied cases are the same as in Fig. 3.4 (a), $S^{(0)}_{q_0}$ is the value of the total emitted light spectrum for an atom in free space at it's resonance frequency. We provide comments on how to pick the parameters (Ω_x, Ω_y) for cases A, and B in Appendix C.4

$[\text{MS}]^*_{:,1} = -[\text{MS}]_{:,3}$, which leads to $\left(\boldsymbol{f}_j^{q_0=-1}\right)^* = -\left(\boldsymbol{f}_j^{q_0=+1}\right)$. Similarly to temporal dynamics, this phase difference will affect the interference terms in the total spectrum Eq. (3.29).

There is one more important point that we want to discuss. In the beginning we derived the explicit expressions for the excitation transfer amplitudes $U_{q',q}(t,0)$ (Eq. (3.14)), and the respective probabilities $P_{q',q}(t)$ (Eq. (3.18)), both of which depend on the orientation of the local quantization axis through α, β angles, and also on the parameters of the nanostructure as well as the position of the emitter through the complex eigenfrequencies (g_j). However, as we introduced the detector, and calculated either the intensity dynamics $I_{q_0}(t)$ (Eq. (3.22)) or the total emitted light spectrum $S_{q_0}(\omega)$ (Eq.

(3.26)), we brought new degrees of freedom into the problem. Even though we put detector into the far-field area, and linked it's position $\mathbf{r_d}$ to the orientation of the quantization axis, this problem is quite different from the one where we simply considered the transition probabilities $P_{q',q}(t)$, and it can be illustrated by the following example.

When calculating results for Fig. 3.4, for the sake of simplicity we used the fact that the materials of the lower, and the upper half-space media are of the same kind, namely, that both of them are vacuum. Now imagine that we set $\alpha = \beta = 0$, so that the transition dipole moments $\mathbf{d_{-1}}, \mathbf{d_{-1}}$ are parallel to the interface plane, while the detector is located right above the atom at $\mathbf{r_d} = (0, 0, R)$. For this set-up we compare two cases: $\varepsilon_{\text{subs}} = 1.0$, and $\varepsilon_{\text{subs}} \neq 1.0$, where $\varepsilon_{\text{subs}}$ is the dielectric constant of a lower medium (the substrate). Results of this comparison can be seen in Fig. 3.5 (a), (b). Interestingly, once the substrate is present, it turns out that despite the orientation of transition dipole moments, $S_{-1}(\omega) \neq S_{+1}(\omega)$ still holds true. It is quite clear that this happens not due to the studied effect as for $\alpha = \beta = \gamma = 0$ we have: $C_x^{(-1,+1)} = C_x^{(+1,-1)} = -\frac{1}{2}$, $C_y^{(-1,+1)} = C_y^{(+1,-1)} = +\frac{1}{2}$, while $C_z^{(-1,+1)} = C_z^{(+1,-1)} = 0$. So, there is no phaseshift, which means that $P_{q',q}(t) = P_{q,q'}(t)$ for this set of parameters. However, as can be seen from definitions Eq. (3.24), and Eq. (3.29), apart from transition probability amplitudes $\sim U_{q',q_0}(t,0)$, there is also a field produced by each eigenstate $\boldsymbol{f}_j^{q_0}(\mathbf{r_d}, \mathbf{r_a}) = i|\mathbf{d}|\mathbf{\Gamma}_{:,j}(\mathbf{r_d}, \mathbf{r_a})(\mathbf{MS})_{j,q_0}$, which is related to the far-field Green's tensor $\mathbf{G^{FF}}(\mathbf{r_d}, \mathbf{r_a}, \omega_0)$. For the parameters considered in Fig. 3.5 (a) ($\varepsilon_{\text{subs}} = 1.0$), we can write the following:

$$\mathbf{\Gamma}(\mathbf{r_d}, \mathbf{r_a}) = \begin{pmatrix} \Gamma_{xx} & 0 & 0 \\ 0 & \Gamma_{yy} & 0 \\ 0 & 0 & 0 \end{pmatrix},$$

$$\left(\boldsymbol{f}_x^{\pm}(\mathbf{r_d}, \mathbf{r_a}),\ \ \boldsymbol{f}_y^{\pm}(\mathbf{r_d}, \mathbf{r_a}),\ \ \boldsymbol{f}_z^{\pm}(\mathbf{r_d}, \mathbf{r_a})\right) = \frac{i|\mathbf{d}|}{\sqrt{2}} \begin{pmatrix} \mp\Gamma_{xx} & 0 & 0 \\ 0 & -i\Gamma_{yy} & 0 \\ 0 & 0 & 0 \end{pmatrix}. \quad (3.33)$$

As can be seen, $\mathbf{\Gamma}$ is a diagonal matrix in this case with $\Gamma_{zz} = 0$. The latter is true as both atom, and detector are located on the z-axis (as $\alpha = \beta = 0$), and z-oriented dipole moment does not radiate into the far-field along the direction of it's orientation. As a consequence of this, only $\boldsymbol{f}_x^{q_0}(\mathbf{r_d}, \mathbf{r_a})$, $\boldsymbol{f}_y^{q_0}(\mathbf{r_d}, \mathbf{r_a})$ are non-zero. These vector quantities in our set-up obey the following properties: $\left[\boldsymbol{f}_j^{-1}\right]_x = -\left[\boldsymbol{f}_j^{+1}\right]_x$, $\left[\boldsymbol{f}_j^{-1}\right]_y = \left[\boldsymbol{f}_j^{+1}\right]_y$, so only x-components flip their overall phase by π, when we change $q_0 = +1 \to q_0 = -1$. However, as seen from Eq. (3.33), these quantities have zero overlap $(\boldsymbol{f}_x^{q_0})^{\dagger} \cdot \boldsymbol{f}_y^{q_0} = 0$, leading to a fact that such a phaseshift does affect the

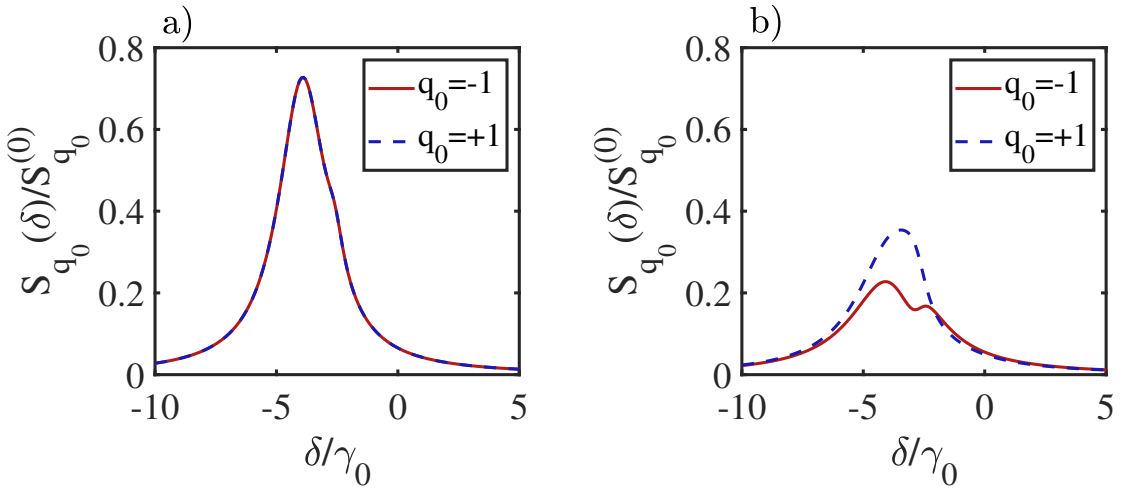

Figure 3.5 — (a) The total emitted light spectra in the case of the absent substrate $\varepsilon_{\text{subs}} = 1$, and for $\alpha = \beta = 0$. Solid red, and dashed blue lines are for $q_0 = -1$, and $q_0 = +1$ cases, correspondingly. (b) Same as (a), but for $\varepsilon_{\text{subs}} = 2.2$. Here we take the following resonance frequencies for surface conductivity tensor components: $\Omega_x = 0.6k_0$, $\Omega_y = 1.0k_0$. All other relevant parameters are the same as for Fig. 3.4

spectrum as:

$$S_{q_0}(\delta) = \left| \sum_j \frac{\boldsymbol{f}_x^{q_0}(\mathbf{r_d}, \mathbf{r_a})}{(\delta - g_x)} + \frac{\boldsymbol{f}_y^{q_0}(\mathbf{r_d}, \mathbf{r_a})}{(\delta - g_y)} \right|^2 = \left| \frac{\boldsymbol{f}_x^{q_0}(\mathbf{r_d}, \mathbf{r_a})}{(\delta - g_x)} \right|^2 + \left| \frac{\boldsymbol{f}_y^{q_0}(\mathbf{r_d}, \mathbf{r_a})}{(\delta - g_y)} \right|^2, \tag{3.34}$$

and there are no cross-terms related to the interference of eigenstates x, and y. As a result, $S_{-1}(\delta) = S_{+1}(\delta)$.

Now let us inspect the case from Fig. 3.5 (b) ($\varepsilon_{\text{subs}} = 2.2$), when we have:

$$\mathbf{\Gamma}(\mathbf{r_d}, \mathbf{r_a}) = \begin{pmatrix} \Gamma_{xx} & \Gamma_{xy} & 0 \\ \Gamma_{xy} & \Gamma_{yy} & 0 \\ 0 & 0 & 0 \end{pmatrix},$$

$$\left(\boldsymbol{f}_x^{\pm}(\mathbf{r_d}, \mathbf{r_a}),\ \ \boldsymbol{f}_y^{\pm}(\mathbf{r_d}, \mathbf{r_a}),\ \ \boldsymbol{f}_z^{\pm}(\mathbf{r_d}, \mathbf{r_a})\right) = \frac{i|\mathbf{d}|}{\sqrt{2}} \begin{pmatrix} \mp\Gamma_{xx} & \mp\Gamma_{xy} & 0 \\ -i\Gamma_{xy} & -i\Gamma_{yy} & 0 \\ 0 & 0 & 0 \end{pmatrix}, \tag{3.35}$$

now the situation is different as we have non-diagonal components of $\mathbf{\Gamma}$ matrix. Now the fields generated by eigenstates associated with $x-$, and y-oriented dipoles interfere $(\boldsymbol{f}_x^{q_0})^\dagger \cdot \boldsymbol{f}_y^{q_0} \neq 0$, and this phaseflip for the x-component of $\boldsymbol{f}_j^{q_0}$ affects the total spectrum, leading to $S_{-1}(\delta) \neq S_{+1}(\delta)$. Note that this is a purely electrodynamical effect, and has nothing to do with the phenomenon under study, as, again, in the situation described above $\alpha = \beta = 0$, which means that the transition probabilities are equal $P_{-1,+1}(t) = P_{+1,-1}(t)$ even though the spectra are different $S_{-1}(\delta) \neq S_{+1}(\delta)$.

3.4 Chiral coupling of excited states in a V-type atom: analysis of the coupling constants

In the previous sections of this chapter in order to break the symmetry in transitions $|e_{q'}\rangle \rightarrow |e_q\rangle$, and $|e_q\rangle \rightarrow |e_{q'}\rangle$ we allowed the transition dipole moments $\mathbf{d_q}$ to be arbitrarily oriented in space. We also allowed the nanostructure in the vicinity of which the emitter is placed to be fully locally anisotropic, which means that the components of a Green's tensor are pairwise non-identical: $G_{xx}(\mathbf{r_0},\mathbf{r_0},\omega_0) \neq G_{yy}(\mathbf{r_0},\mathbf{r_0},\omega_0)$, $G_{yy}(\mathbf{r_0},\mathbf{r_0},\omega_0) \neq G_{zz}(\mathbf{r_0},\mathbf{r_0},\omega_0)$, $G_{zz}(\mathbf{r_0},\mathbf{r_0},\omega_0) \neq G_{xx}(\mathbf{r_0},\mathbf{r_0},\omega_0)$. It led to the phaseshift in the interference components in the time-dependent transition rates under the exchange of the initial, and final states $q' \leftrightarrow q$. However, this did not allow us to make the system completely asymmetric such that, for instance, $P_{q',q}(t) = 0$, while $P_{q,q'}(t) \neq 0$. Let us now try to understand how we can make this happen.

First of all, let us simplify a problem by making it quasi-2D: instead of considering an $s \rightarrow p$ atom with triple digeneracy in the excited state, we will take a look at an atom with V-type structure of levels (see Fig. 3.6 (a)) with excited states $|e_{-1}\rangle$, $|e_{+1}\rangle$ only. As we will see later, this will significantly simplify the analysis. Let us review the respective coupling constants for the most general nanostructure:

$$\Sigma^{-,+}_{+,-}(\hbar\omega_0) = 4\pi k_0 \frac{|\mathbf{d}|^2}{2}(\mp)\begin{pmatrix}1 & \pm i & 0\end{pmatrix}\begin{pmatrix}G_{xx} & G_{xy} & G_{xz}\\ G_{yx} & G_{yy} & G_{yz}\\ G_{zx} & G_{zy} & G_{zz}\end{pmatrix}\begin{pmatrix}1\\ \pm i\\ 0\end{pmatrix} =$$
$$2\pi k_0^2|\mathbf{d}|^2\left(G_{xx} - G_{yy} \pm i\left(G_{xy} + G_{yx}\right)\right),$$
$$\Sigma^{+,+}_{-,-}(\hbar\omega_0) = 4\pi k_0 \frac{|\mathbf{d}|^2}{2}\begin{pmatrix}1 & \mp i & 0\end{pmatrix}\begin{pmatrix}G_{xx} & G_{xy} & G_{xz}\\ G_{yx} & G_{yy} & G_{yz}\\ G_{zx} & G_{zy} & G_{zz}\end{pmatrix}\begin{pmatrix}1\\ \pm i\\ 0\end{pmatrix} =$$
$$2\pi k_0^2|\mathbf{d}|^2\left(G_{xx} + G_{yy} \pm i\left(G_{xy} - G_{yx}\right)\right), \qquad (3.36)$$

where we have assumed that the transition dipole moments lie in the xy-plane, and that $G_{ij}(\mathbf{r},\mathbf{r},\omega_0) \neq 0$ for all i,j.

As one can see from the above, we can obtain $\Sigma_{-,+} \neq \Sigma_{+,-}$ only if we have $G_{xy}(\mathbf{r_0},\mathbf{r_0},\omega_0) + G_{yx}(\mathbf{r_0},\mathbf{r_0},\omega_0) \neq 0$, so, the local Green's tensor has to be at least non-diagonal, and the sum of off-diagonal elements should not be equal to zero. For typical photonic structures like semi-infinite planar dielectric interface, dielectric/metal spherical nanoparticle, or conventional dielectric/plasmonic waveguide the local Green's tensor turns out to be diagonal.

One of the first naive ideas is to break time-reversal symmetry in the system, which can be done by making use of the external static (DC) magnetic field. This magnetic field can magnetize the electronic plasma in the material leading to the appearance of non-diagonal Hall conductivities σ_{xy}, σ_{yx}. However, these conductivities obey the relation $\sigma_{xy} = -\sigma_{yx}$ as a direct consequence of the Onsager principle (see this happen [180] for graphene, for instance). This symmetry of the conductivity tensor components will be reflected in the local Green's tensor leading to $G_{xy} + G_{yx} = 0$. Therefore, breaking the time-reversal symmetry would not help to achieve the asymmetric coupling. Needless to say that a strong DC magnetic field lifts the degeneracy in the excited states due to the Zeeman effect, and lowers the spectral overlap of the levels, leading to smaller values of coupling constants [152]. However, as Eq. (3.36) shows, the use of magnetic field makes $\Sigma_{-,-} \neq \Sigma_{+,+}$. It means that the Lamb shifts, and the spontaneous emission rates for states of opposite helicities differ in this case, but we will not discuss this as it does not affect the transition rates between the states.

From now on we will assume that the local Green's tensor components have the property $G_{xy} - G_{yx} = 0$, leading to $\Sigma_{+,+} = \Sigma_{-,-}$. If we study the free dynamics (in the absence of the external pumping field) of an initially excited atom, we can find the evolution operator matrix elements as:

$$\mathbf{U}(t,0) = \begin{pmatrix} U_{-,-}(t) & U_{-,+}(t) \\ U_{+,-}(t) & U_{+,+}(t) \end{pmatrix} = e^{-ig_e t} \begin{pmatrix} \cosh\left(\sqrt{g_{-,+}g_{+,-}}t\right) & -i\sqrt{\frac{g_{-,+}}{g_{+,-}}}\sinh\left(\sqrt{g_{-,+}g_{+,-}}t\right) \\ -i\sqrt{\frac{g_{+,-}}{g_{-,+}}}\sinh\left(\sqrt{g_{-,+}g_{+,-}}t\right) & \cosh\left(\sqrt{g_{-,+}g_{+,-}}t\right) \end{pmatrix}, \quad (3.37)$$

where $g_{i,j} = \Sigma_{i,j}/\hbar$, as before. The respective transition probabilities can be found to be:

$$P^{-,+}_{+,-}(t) = \frac{e^{-\gamma_e t}}{2}\left|\frac{g_{-,+}}{g_{+,-}}\right| \cdot \left(\cosh\left(2\,\mathrm{Re}\left[\sqrt{g_{-,+}g_{+,-}}\right]t\right) - \cos\left(2\mathrm{Im}\left[\sqrt{g_{-,+}g_{+,-}}\right]t\right)\right), \quad (3.38)$$

The transition rate $P_{q,q'}$ is simply proportional to the ratio $\left|\frac{g_{q,q'}}{g_{q',q}}\right|$. Now we can see explicitly that having $g_{-,+} \neq g_{+,-}$ is not enough to obtain $P_{q,q'}(t) \neq P_{q',q}(t)$, we rather need difference in the absolute values of the coupling constants $|g_{-,+}| \neq |g_{+,-}|$. This is of importance as in some cases it might be that the couplings differ by an overall phase (in the simplest case they differ in sign $g_{-,+} = -g_{+,-}$), and, as the result above suggests, this will keep transition probabilities being equal $P_{-,+}(t) = P_{+,-}(t)$.

We can also look at the limit of an extreme asymmetry of interaction, for example, let us consider the limit $g_{+,-} \to 0$, then Eq. (3.38) becomes:

$$P_{+,-}(t) = e^{-\gamma_e t} |g_{+,-}|^2 t^2,$$
$$P_{-,+}(t) = 0. \tag{3.39}$$

Note that this answer is identical to the one obtained for a transport in a chain of two-level atoms unidirectionally coupled through a guided mode (see Eq. (2.9)), if we just set the number of atoms to $N = 2$. This is quite natural as the problem of two coupled transitions in a single atom is mathematically identical to the case of two interacting two-level atoms, if one stays in a single excitation domain. Now we will switch our discussion to a particular example of a system, where one can realize such an asymmetric coupling.

3.5 Example of a system allowing for chiral coupling: qualitative analysis

As was discussed previously, breaking the time-reversal symmetry does not help to achieve the desired effect. Another possible option is to do something with the parity of the system. Indeed, if one breaks certain geometric symmetries in the photonic structure, one can achieve *optical* or *electromagnetic chirality* [181]. Actually, there are, at least, several ways through which one can achieve optical chirality: for instance, one can use electromagnetic coupling. However, for now we will focus on a particular way, which is based on altering the geometry of the system.

The simplest model for chiral nanophotonic structure is based on a Born-Kuhn model [36;37], which was used to describe the natural optical activity in a system of two coupled oscillators, which are displaced in a vertical direction [38]. Let us quickly demonstrate that this simple model will also work for our purposes.

In order to do that, let us consider two strongly anisotropic dipolar scatterers as presented in Fig. 3.6 (b), which are located in two parallel planes, both of which are perpendicular to the z-axis of the introduced coordinate system. By strongly anisotropic we mean that they are predominantly polarized along a given direction which we will call the long axis of a scatterer, and this long axis for both of them is always perpendicular to z-axis. If we start from a given scatterer being aligned along the x-axis, then it's polarizability is given by:

$$\alpha(\omega) = S(\varphi_0) \cdot \mathrm{diag}(\alpha_{||}(\omega),\ \ 0,\ \ 0) \cdot S^{-1}(\varphi_0), \tag{3.40}$$

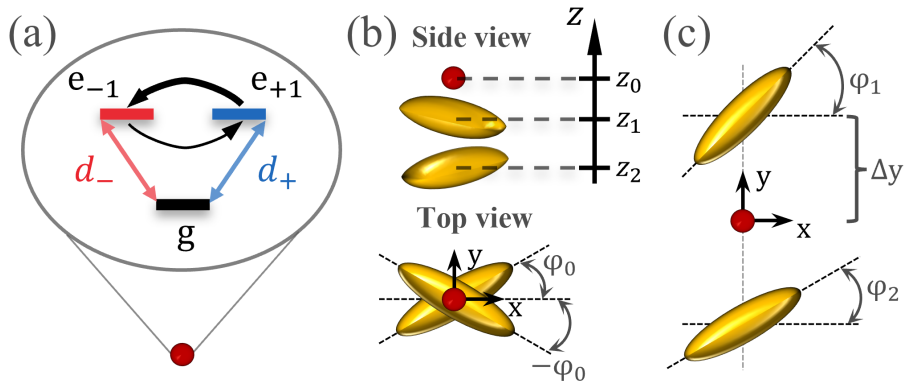

Figure 3.6 — (a) A level scheme of a V-type emitter. (b) A scheme based on the Born-Kuhn model similar to the one used in [38]. The centers of two ellipsoidal scatterers, and the atom are located on the z-axis at positions z_1, z_2, and z_0, correspondingly, while the long axes of both ellipsoids are perpendicular to z-axis. (c) An alternative scheme, where centers of both scatterers, and the atom are in the xy-plane, on the y-axis

where φ_0 defines the angle between the long axis of a scatterer and the positive x-direction, and $S(\varphi_0)$ is a rotation matrix around the z-axis. We want to note that such a form of polarizability is only chosen for a qualitative analysis, later we will use another model.

If we want to find the local Green's tensor of two point dipolar scatterers (in order to analyze the coupling constants), we can do that by using the Dyson equation [2; 182]:

$$\mathbf{G}_{\text{tot}}(\mathbf{r}, \mathbf{r_0}) = \mathbf{G_0}(\mathbf{r}, \mathbf{r_0}) + 4\pi k^2 \Big(\mathbf{G_0}(\mathbf{r}, \mathbf{r_1}) \boldsymbol{\alpha_1} \mathbf{G}_{\text{tot}}(\mathbf{r_1}, \mathbf{r_0}) + \mathbf{G_0}(\mathbf{r}, \mathbf{r_2}) \boldsymbol{\alpha_2} \mathbf{G}_{\text{tot}}(\mathbf{r_2}, \mathbf{r_0}) \Big), \quad (3.41)$$

where α_1, α_2 are the respective polarizabilities of both scatterers, $\mathbf{r_1}, \mathbf{r_2}$ are their locations. The values of the total Green's tensor at field points $\mathbf{r_1}$, and $\mathbf{r_2}$ can be found by setting $\mathbf{r}$ to be equal to $\mathbf{r_1}$, and $\mathbf{r_2}$, excluding the appearing self-interaction terms $\mathbf{G_0}(\mathbf{r_1}, \mathbf{r_1})$, $\mathbf{G_0}(\mathbf{r_2}, \mathbf{r_2})$, and by solving the resulting system of equations for $\mathbf{G}_{\text{tot}}(\mathbf{r_1}, \mathbf{r_0})$, $\mathbf{G}_{\text{tot}}(\mathbf{r_2}, \mathbf{r_0})$. The details of this can be found in Appendix C.5.

If we assume that the atom is also on the z-axis, and that scatterer 1 is rotated on angle φ_0, while 2 - on $-\varphi_0$, then the conditions for $|g_{-,+}| \neq |g_{+,-}|$ in this particular set-up are the following:

$$\begin{cases} |z_0 - z_1| \neq |z_0 - z_2|, \\ \varphi_0 \neq \frac{\pi}{4} m, \ \ m \in \mathbb{Z}. \end{cases} \quad (3.42)$$

This is not that surprising that we were able to achieve chiral coupling for this specific system as it is geometrically chiral, and geometrical chirality

leads to the optical chirality with respect to plane wave scattering [181]. As the dipole field is of more complex profile than a usual plane wave, we can naturally expect the system to allow for chiral coupling of circular transitions. However, the question is, whether or not it is possible to achieve the same result, but for the system with simpler geometry? The answer is yes.

In order to demonstrate that, let us allow for both dipole scatterers and the atom to be in the same plane (xy-plane, for instance), and, moreover, on the same axis (let it be y-axis) as shown in Fig. 3.6 (c). We will also put the atom right in between the scatterers, and let the long axes of both scatterers be parallel, and defined by angle φ_0 in order to simplify the problem as much as possible. In this set-up, if we will also set $\varphi_1 = \varphi_2 = \varphi_0$ we will have $G_{xy} \neq 0$ if:

$$\varphi_0 \neq \frac{\pi}{2} m, \;\; m \in \mathbb{Z}. \tag{3.43}$$

Indeed, even though the described system, clearly, has a reflection plane (at least the xy-plane), and geometrically is achiral, it allows for chiral coupling of circularly polarized transitions. In the next section we will switch to a more realistic description of the system, and show some quantitative rather than qualitative results.

3.6 Example of a system allowing for chiral coupling: quantitative results

One of the simplest shapes of anisotropic scatterers, which simultaneously has an analytical explicit form of a polarizability is based on a prolate ellipsoid, the quasi-static polarizability of which can be written as [183; 184]:

$$\boldsymbol{\alpha}^{-1}(\omega) = \frac{4\pi}{V}\left[(4\pi\boldsymbol{\varepsilon}(\omega) - 1)^{-1}\,\mathbf{I} + \mathbf{L}\right] - i\frac{2}{3}k^3\mathbf{I}, \tag{3.44}$$

where $\boldsymbol{\varepsilon}(\omega)$ is a dielectric permittivity tensor of the ellipsoid material, $V = 4\pi a_x a_y a_z/3$ is the ellipsoid volume, a_j are it's semiaxes, and $\mathbf{L} = \mathrm{diag}\,(N_x, N_y, N_y)$ is the depolarization matrix with N_j being the related elliptic integrals [184]. For a prolate ellipsoid $a_x > a_y = a_z$ one can write $N_x = \frac{1-e^2}{2e^3}\left(\ln\left(\frac{1+e}{1-e} - 2e\right)\right)$, $N_y = N_z = (1 - N_x)/2$, where $e = \sqrt{1 - a_y^2/a_x^2}$.

When describing the optical response of the metal out of which the scatterers are made, we can use the Drude model [185]: $\varepsilon_{\mathrm{D}}(\omega) = \varepsilon_\infty + \frac{\omega_p}{\omega(\omega+i\gamma)}$, where ε_∞ is a high-frequency permittivity, ω_p, γ are the plasma

frequency, and electron damping rate. However, the Drude model has its limitations, and one can rather use table data from [175; 186], for instance.

As Eq. (3.38) suggests, $|g_{i,j}|/|g_{j,i}|$ defines the asymmetry of transition probabilities, but if the coupling strength will be too weak realative to γ_e, for instance, it will be impossible to observe this asymmetry in any measurable quantity. Therefore, we need to look at both of these quantities, and in Fig. 3.7 we show the results for the set-up from Fig. 3.6 (b). We note that the atomic resonance frequency ω_0 is always asummed to be tuned to the longitudinal surface plasmon resonance (with dipole moment being parallel to the long axis of a scatterer), which we define through the condition on maximal $\mathrm{Im}\,[\tilde{\alpha}_{xx}(\omega)]$, and the corresponding vacuum wavelength is defined as $\lambda_{||} = \dfrac{2\pi c}{\omega_0}$.

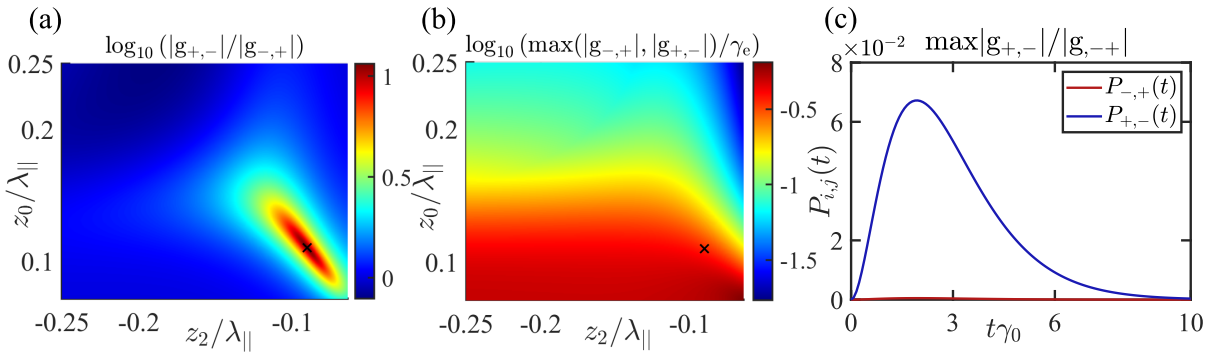

Figure 3.7 — (a) Coupling asymmetry, and (b) coupling strength versus positions of the second emitter z_2, and atom z_0. The first scatterer is assumed to be located at the origin of the introduced coordinate system. (c) Excitation transfer probabilities between the excited states for parameters z_0, z_2 specified by the black cross. The parameters are: $a_x = 2a_y = 2a_z = 30$ nm, $\lambda_{||} \approx 470$ nm, ε is taken from [186], $\varphi_0 = \pi/8$

As we discussed previously, there is no asymmetry $\frac{|g_{+,-}|}{|g_{-,+}|} = 1$ if the rotation angle is $\varphi_0 = \frac{\pi}{4}m$. Therefore, as a consequence of the problem's symmetry, we can expect that the maximal coupling asymmetry will be at $\varphi_0 = \pi/8$, and we fix this parameter. By tuning the respective positions of one of the scatterers z_2, and the atom z_0, we observe a region with a quite high value of the asymmetry parameter (red region in Fig. 3.7(a)). Interestingly, for the parameters chosen, it lies very close to a region of a large coupling strength (see lower right part of Fig. 3.7(b)). Fig. 3.7 (c) demonstrates that, indeed, the high asymmetry regime is achieved as $P_{-,+}(t)$ is almost zero at any time, while $P_{+,-}(t)$ achieves a peak value of ~ 0.06.

In Fig. 3.8 the same quantities are presented for the situation from Fig. 3.6 (c): when we put the emitter, and both scatterers in the xy-plane, fix the emitter-scatterers distance Δy, but vary φ_1, φ_2. Interestingly, as seen from (a), one can easily switch from $|g_{-,+}| \gg |g_{+,-}|$ to $|g_{+,-}| \gg |g_{-,+}|$ by

a relatively slight change of φ_1, φ_2. From Fig. 3.8 (b) one realizes that the angles allowing for the maximal coupling asymmetry do not quite correspond to the maximal coupling constants. Despite this, as Fig. 3.8 (c) demonstrates, such coupling strengths is enough to achieve a perfectly asymmetric transfer of $\sim +10\%$ of the excitation.

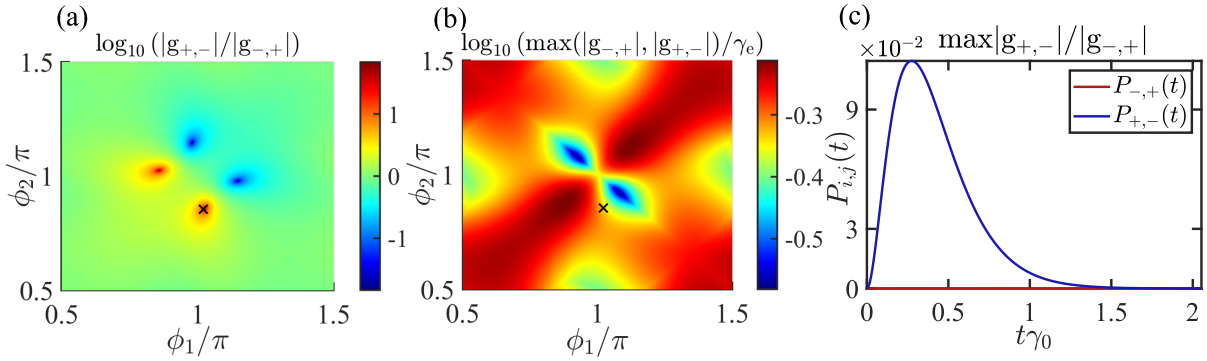

Figure 3.8 — (a) Coupling asymmetry, and (b) coupling strength versus the rotation angles of long axes of both emitters φ_1, φ_2. The atom is located at the origin, while both scatterers are symmetrically displaced along the y-axis. (c) Excitation transfer probabilities between the excited states for the point with the maximal asymmetry in (a) that is marked by a black cross. All relevant parameters are the same as in Fig. 3.7, while the distance atom-scatterer is chosen to be $\Delta y = a_x + \lambda_{||}/20$

In this section we demonstrated the possibility of almost perfectly chiral coupling of levels on the example of an initially excited V-atom in one of its excited states by looking at the transfer probabilities. However, instantaneous level populations for the initially excited atom are not the quantities which can be measured directly in the experiment, and one might rather want to look at a scheme with, for instance, a continuous external pumping by a laser field. This situation we are going to cover in the next section.

3.7 Chiral coupling in the presence of an external pumping field

The approach used in the previous sections - the calculation of the evolution operator matrix elements, and the respective probabilities - can not include simultaneously dissipative processes like spontaneous emission, and the interaction with the pumping field. We need to rather use the full master equation on the density matrix for the emitter. However, the conventional Lindblad equation, which can be found, for instance, in Ref. [140] is not suitable here, in the case of chiral interactions, and one has to rather use a

more general form [165; 187]:

$$\dot{\hat{\rho}}_s(t) = i\sum_i \Delta\omega_i \left[\hat{\sigma}_{ii}, \hat{\rho}_s(t)\right] - \frac{i}{\hbar}\left[\hat{H}_p, \hat{\rho}_s(t)\right] + \hat{\mathcal{L}}\hat{\rho}_s(t),$$

$$\hat{\mathcal{L}}\hat{\rho}_s(t) = \sum_i \frac{\Gamma_{ii}}{2}\left(2\hat{\sigma}_{g,i}\hat{\rho}_s(t)\hat{\sigma}_{i,g} - \hat{\sigma}_{i,i}\hat{\rho}_s(t) - \hat{\rho}_s(t)\hat{\sigma}_{i,i}\right) +$$

$$\sum_{i,j}^{i\neq j} \frac{\Gamma_{ij}}{2}\left(\left[\hat{\sigma}_{g,j}\hat{\rho}_s(t), \hat{\sigma}_{i,g}\right] + \left[\hat{\sigma}_{g,i}, \hat{\rho}_s(t)\hat{\sigma}_{j,g}\right]\right),$$

$$\sum_{i,j}^{i\neq j} \delta_{ij}\left(-i\left[\hat{\sigma}_{g,j}\hat{\rho}_s(t), \hat{\sigma}_{i,g}\right] + i\left[\hat{\sigma}_{g,i}, \hat{\rho}_s(t)\hat{\sigma}_{j,g}\right]\right),$$

$$-\frac{i}{\hbar}\left[\hat{H}_p, \hat{\rho}_s(t)\right] = -\frac{i}{2}\Big(\left[\hat{\sigma}_{g,+}, \hat{\rho}_s(t)\right]\Omega_+ e^{i\varphi_+} + \left[\hat{\sigma}_{+,g}, \hat{\rho}_s(t)\right]\Omega_+ e^{-i\varphi_+} +$$

$$\left[\hat{\sigma}_{g,-}, \hat{\rho}_s(t)\right]\Omega_- e^{i\varphi_-} + \left[\hat{\sigma}_{-,g}, \hat{\rho}_s(t)\right]\Omega_- e^{-i\varphi_-}\Big), \tag{3.45}$$

where detuning of the laser ω_L from the atomic transition frequency corrected for the Lamb shift $\omega_{0,i} - \delta_{ii}$ is given by $\Delta\omega_i = \omega_L - \omega_{0,i} + \delta_{ii}$, $\hat{H}_p = \hat{\sigma}_{g,+}\Omega_+ e^{i\varphi_+} + \hat{\sigma}_{g,-}\Omega_- e^{i\varphi_-} + \text{h.c.}$ is responsible for the interaction of the atom with the laser field, $\Omega_\pm$ are the respective Rabi frequencies, $e^{i\varphi_\pm}$ are related to the relative phases between the transition dipole moments, and the external laser field, $\hat{\mathcal{L}}$ is the Lindblad superoperator, and $\delta_{ij} = 4\pi k_{0,j}^2 \mathbf{d_i^\dagger} \text{Re}\left[\mathbf{G}(\mathbf{r_0}, \mathbf{r_0}, \omega_{0,j})\right]\mathbf{d_j}/\hbar$, $\Gamma_{ij} = 8\pi k_{0,j}^2 \mathbf{d_i^\dagger} \text{Im}\left[\mathbf{G}(\mathbf{r_0}, \mathbf{r_0}, \omega_{0,j})\right]\mathbf{d_j}/\hbar$.

As $\hat{\rho}_s(t)$ is the reduced density matrix of the system of interest (V-atom), then we have 9 equations in total, and the system Eq. (3.45) can be re-written as $\dot{x}_\rho(t) = \mathbf{M}_\rho \cdot x_\rho(t)$, where $x_\rho(t)$ is a vector of 9×1 size containing all components of the density matrix, and $\mathbf{M}_\rho$ is a 9×9 matrix. Now our point in the beginning of the chapter is clear: if we took a more relistic $s \to p$ atom with 4 levels, then $\mathbf{M}_\rho$ would be 16×16 in size. However, this simplification does not allow us to obtain analytical solutions even for some extreme cases, and the system in Eq. (3.45) has to be solved numerically. Nevertheless, the reduced number of states will help us in the future when analyzing the stationary solutions.

In order to demonstrate the presence of chirality, we can do the following. Imagine that there is a plane wave of a general polarization impinging on the system. The polarization should be chosen such that the total field (consisting of the incident one, and the scattered one off the nanostructure) should be linearly polarized at the atomic position $\mathbf{r_0}$. This means that the Rabi frequencies for both transitions will be equal in strength, so $\Omega_- = \Omega_+$. However, as the interaction between the transitions is chiral, then the populations of the excited states will be unequal $\rho_{++}(t) \neq \rho_{--}(t)$ despite the equal pumping rates. We will concentrate on the case presented in Fig. 3.7 (c),

and, for the sake of simplicity, assume that the incident field is propagating along the $-z$ direction, and is given by:

$$\mathbf{E}_{\mathrm{inc}}(\mathbf{r}) = \frac{\mathrm{E}_{\mathrm{inc},0}}{\sqrt{1+\xi^2}} \begin{pmatrix} 1 \\ \xi e^{i\varphi_{\mathrm{inc}}} \\ 0 \end{pmatrix} e^{i\mathbf{k}_{\mathrm{inc}}\mathbf{r}}, \tag{3.46}$$

where $\mathrm{E}_{\mathrm{inc},0}$ is the electric field strength of the incoming plane wave, and $\xi, \varphi_{\mathrm{inc}}$ define it's polarization. After tuning the atom-scatterer distance Δy, and rotation angles φ_1, φ_2 (we assume using the geometry presented in Fig. 3.6 (c)) in order to obtain $|g_{+,-}| \gg |g_{-,+}|$, we alter the incident wave parameters $\xi, \varphi_{\mathrm{inc}}$ such that $\Omega_- = \Omega_+$. However, in this scenario we do not have full control over the values of phases φ_-, φ_+, but the effect of these phases on the dynamics will not be discussed here.

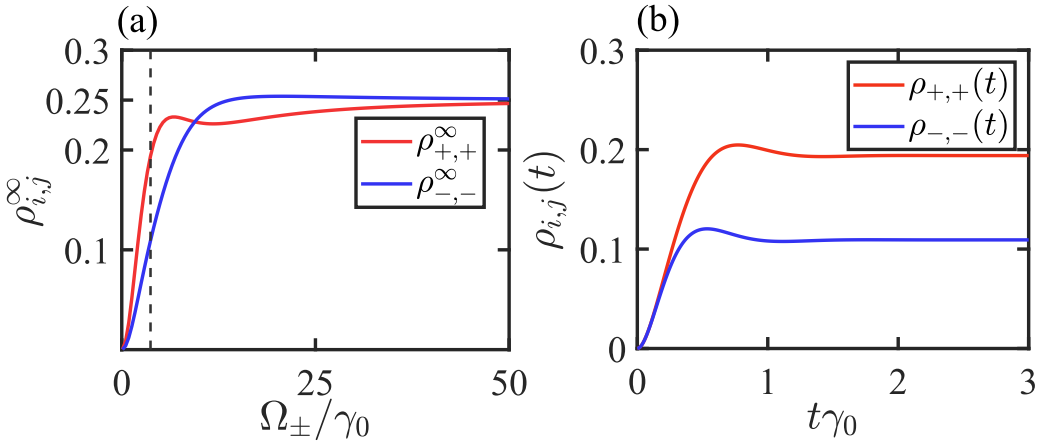

Figure 3.9 — (a) Stationary values of excited state populations versus the Rabi frequencies for both transitions $\Omega_- = \Omega_+$. The dashed black line indicates the point of the maximal difference between the populations $|\rho^{\infty}_{+,+} - \rho^{\infty}_{-,-}|$. (b) Populations of excited states as a function of time for the field strength allowing for a maximal stationary population difference from (a)

Under the external excitation, after the transient processes take place, the density matrix elements approach the stationary values, therefore, it makes sense to look at how the stationary populations vary with the strength of the external field, which is presented in Fig. 3.9 (a). First of all notice that as $\Omega_-, \Omega_+ \to \infty$, the population difference expectably vanishes as the values of the coupling constants $|g_{-,+}|, |g_{+,-}|$, and the asymmetry between them do not play any role in this regime. However, for some specific value of the field strength, the maximal population difference is achieved (indicated by the vertical dashed line). The population dynamics for this parameter is shown in Fig. 3.9 (b), notice that the stationary populations vary by the factor of 2.

Another possible way to demonstrate chirality is to consider selective optical pumping of a given transition $\Omega_- \gg \Omega_+$ ($\Omega_+ \gg \Omega_-$), and looking at

the excited state population on the orthogonal transition $\rho_{+,+}(t)$ ($\rho_{-,-}(t)$). Selective pumping of each transition can be done by properly tuning the ξ, φ_{inc} parameters, as we have done previously. In case of symmetric coupling $g_{-,+} = g_{+,-}$, these populations would be equal $\rho_{-,-}(t) = \rho_{+,+}(t)$, and once the system is chiral, there will be difference between them. First of all, similarly, we analyze the stationary values for the two situations discussed above as functions of the dominant Rabi frequency. From Fig. 3.10 (a) one can see that, unlike in the symmetric pumping case (Fig. 3.9 (a)), for $\Omega_{\pm} \gg |g_{\pm,\mp}|$, the stationary values approach zero, as here we look at the population on the orthogonal transition, and the emitter does not have a chance to undergo a transition due to the dipole-dipole coupling of levels before the pumping field de-excites it. Secondly, as here $|g_{+,-}| \gg |g_{-,+}|$, if we pump the σ^+ transition, then our system effectively behaves as a simple two-level atom, and level $|e_-\rangle$ is never populated (blue dashed line). However, if we pump σ^- transition, we can obtain a substantial population $\rho^{\infty}_{+,+}$ (solid red line) for a properly chosen strength of the external field Ω_- (indicated by a vertical dashed line). Indeed, as Fig. 3.10 (b) confirms, $|e_-\rangle$ does not get populated at all, while $|e_+\rangle$ does.

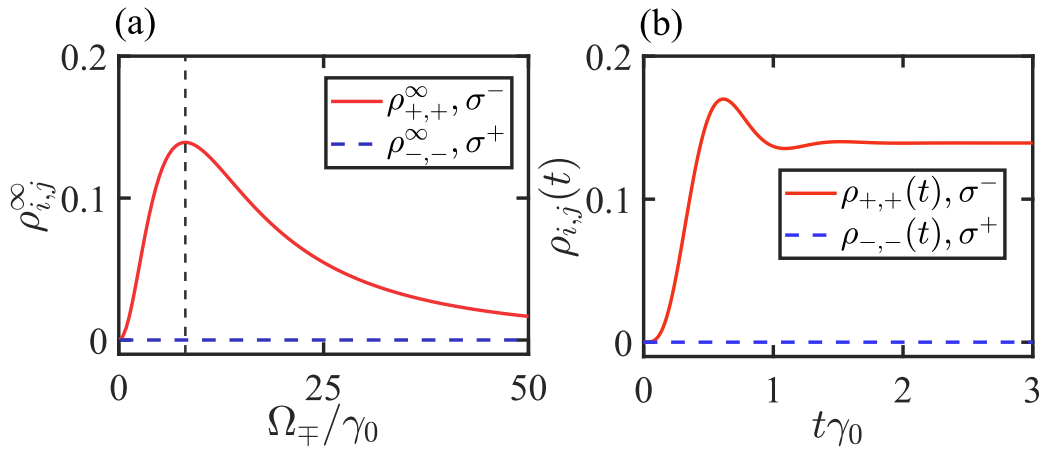

Figure 3.10 — (a) Stationary values of excited state populations $\rho^{\infty}_{+,+}$ ($\rho^{\infty}_{-,-}$) versus the Rabi frequency Ω_- (Ω_+) in solid red (dashed blue). The dashed black line indicates the point of the maximal population $\rho^{\infty}_{+,+}$ for σ^- pumping. Note that here $|g_{+,-}| \gg |g_{-,+}|$, therefore, $\rho^{\infty}_{-,-} \approx 0$. (b) Populations of excited states as functions of time for the field strength allowing for a maximal stationary population from (a). Solid red line is for $\rho_{+,+}(t)$, when $\Omega_- \neq 0, \Omega_+ = 0$, dashed blue line - $\rho_{-,-}(t)$ for $\Omega_+ \neq 0, \Omega_- = 0$

As this scenario is a kind of an extreme case, where the chiral nature of coupling is most prominent, we can obtain the stationary solution of Eq. (3.45) analytically. Let us fix that $g_{-,+} = \Omega_+ = 0$, and $\Delta\omega_- = 0$ (the external field is exactly in resonance with the Lamb-shift corrected transition

frequency), then we can find that:

$$\begin{aligned}
\rho^{\infty}_{+,+} &= \frac{8\Omega_-^2|g_{+,-}|^2}{2\gamma_e^4+5\gamma_e^2\Omega_-^2+2\Omega_-^4+8\Omega_-^2|g_{+-}|^2},\\
\rho^{\infty}_{g,g} &= \frac{\left(\gamma_e^2+\Omega_-^2\right)\left(2\gamma_e^2+\Omega_-^2\right)}{2\gamma_e^4+5\gamma_e^2\Omega_-^2+2\Omega_-^4+8\Omega_-^2|g_{+-}|^2},\\
\rho^{\infty}_{-,-} &= \frac{\Omega_-^2\left(2\gamma_e^2+\Omega_-^2\right)}{2\gamma_e^4+5\gamma_e^2\Omega_-^2+2\Omega_-^4+8\Omega_-^2|g_{+,-}|^2},\\
\rho^{\infty}_{-,+} &= \frac{i4\gamma_e\Omega_-^2 g^*_{+,-}}{2\gamma_e^4+5\gamma_e^2\Omega_-^2+2\Omega_-^4+8\Omega_-^2|g_{+,-}|^2},\\
\rho^{\infty}_{+,g} &= \frac{-2g_{+,-}\Omega_-\left(2\Gamma_e^2-\Omega_-^2\right)}{2\gamma_e^4+5\gamma_e^2\Omega_-^2+2\Omega_-^4+8\Omega_-^2|g_{+,-}|^2},\\
\rho^{\infty}_{-,g} &= \frac{-i\gamma_e\Omega_-\left(2\gamma_e^2+\Omega_-^2\right)}{2\gamma_e^4+5\gamma_e^2\Omega_-^2+2\Omega_-^4+8\Omega_-^2|g_{+,-}|^2}.
\end{aligned} \tag{3.47}$$

Notice from the above, that the populations $\rho^{\infty}_{g,g}, \rho^{\infty}_{-,-}$ contain $g_{+,-}$ only in the denominator, while $\rho^{\infty}_{+,+}$ has it both in numerator, and denominator, and, more importantly, in the same power. It means that, in principle, by tuning the parameters one can achieve population inversion on the $|e_-\rangle \leftrightarrow |e_g\rangle$ transition, if the condition $8\Omega_-^2|g_{+,-}|^2 \gg \left(\gamma_e^2+\Omega_-^2\right)\left(2\gamma_e^2+\Omega_-^2\right)$ is satisfied. However, as one can see from the form of $\rho^{\infty}_{+,g}$, if we simply go into the limit $|g_{+,-}| \gg \Omega_-, \gamma_e$, then the corresponding coherence tends to be zero $\rho^{\infty}_{+,g} \to 0$, as expected.

In this part of the chapter we demonstrated that it is possible to achieve a strongly asymmetric coupling of circular transitions in a V-type quantum emitter by making use of a quite simple structure based on just a pair of asymmetric dipole scatters. We have shown that the asymmetry is achievable both with the Born-Kuhn type arrangement of scatteres, and also for a system that is geometrically achiral. We also suggested a scheme with the external continuous wave pumping, which might allow to observe chiral coupling through unequal stationary populations of the excited states.

3.8 Scientific statements

– When coupling the transitions in a multilevel quantum emitter through the modes of an anisotropic metasurface, it is possible to achieve asymmetry in the excitation transfer dynamics. This asymmetry appears only if the quantization axis is tilted with respect to high-symmetry planes, and if the dressed states of the emitter are not

degenerate. The effect arises from the phaseshift in the interference part of the temporal dynamics, and it is prominent in both detected temporal intensity or the total emitted light spectrum, making them dependent on the spin orientation of the initially excited state.

– By using a plasmonic dimer structure consisting of two anisotropic dipole scatterers (prolate ellipsoidal particles), one can achieve an asymmetric coupling of circularly polarized transitions in a single V-type quantum emitter. This coupling asymmetry results in an uneven steady-state populations of the excited states even when pumping strengths for both transitions are equal, and it also makes the optical response of the system being strongly dependent on the local helicity of the total field at the atomic position.

Conclusion

In the presented work we have considered, and solved several theoretical problems in which one observes the manifestation of the interference effect in the interaction of light with matter from a quantum optical perspective. Here are **the highlights of the most important results of this work**:

1. In the first chapter we have discussed the appearance of strongly subradiant states at the edge of a Brilluoin zone in subdiffractional periodic chains of two-level atoms, where the enhancement in lifetimes of such states was possible due to the mixing of eigenmodes, and the consequent destructive interference of their constituents. This led to several distinct features of such states as much faster decrease of the emission rate with the system size ($\sim N^{-6.8}$ instead of a regular $\sim N^{-3}$ dependency), as well as a better eigenstate localization due to the suppression of dipole moments at the edges of a chain. More than that, the aforementioned destructive interference is found to lead to a simultaneous reduction of many multipolar contributions into the far-field radiation for this kind of subradiant state. We also demonstrated that the presence of an additional interaction channel, apart from the vacuum dipole-dipole interaction, does not necessarily lead to the disappearance of this effect, and we have shown this for the case of atomic chain near a single-mode optical nanofiber.
2. In the second chapter we have revealed a peculiar polynomial temporal behavior of a single excitation transport in a one-dimensional chain of atoms, which are unidirectionally coupled through a guided mode. We have solved the problem analytically for arbitrary system sizes, and based on this result, we have also estimated the approximate collective sub-, and superradiant emission rates. For subradiance it was found to be different from the case of symmetrically coupled atoms, which is given by the Dicke theory. In order to reveal the reason for this discrepancy to appear, we have analyzed the single-excitation dynamics in the lowest non-vanishing order of perturbation theory, and found that it happens due to the imperfect destructive interference.
3. In the third chapter we have demonstrated how, by using an anisotropic photonic structure (metasurface), and by controlling the orientation of transition dipole moments in an $s \rightarrow p$ atom, one can break the symmetry of forward, and backward quantum-mechanical processess related to the probabilities for an electron to make a transition from one excited states to another. We derived analytically the requirements for the observation of this phenomenon, and also attributed it to the

interference of the eigenstates, which appear as a result of emitter's interaction with the electromagnetic modes of the environment. It is demonstrated that this interference gives rise to a phaseshift in the transition probability dynamics. We have also shown how these unequal transition probabilities in such a system affect the measurable quantities: detected light intensity dynamics, and total emitted light spectrum.

4. In the third chapter we have also proposed another way to break this symmetry in transitions by using a simple plasmonic structure - a dimer made of two asymmetric dipolar matallic scatterers. By properly tuning the geometry of the system, we have shown that it is possible to almost completely forbid transitions of an electron in one direction between the excited states with circularly polarized dipole moments in a V-type atom. We have also analyzed the dynamics of the system under the external continuous-wave pumping, and demonstrated that, for instance, the steady-state populations of excited states can be unequal due to their asymmetric coupling despite the Rabi frequencies for corresponding transitions being equal. More than that, it is shown that in this case the response of the system strongly depends on the local helicity of the total field at the position of the atom.

To conclude, we want to pay a special attention that this thesis was mostly concentrated on studying the very basics of the effects considered, clarifying the mechanisms of their appearance, and specifying how they affect different optical properties of the systems. An interesting future direction of research can be to consider possible applications in different branches of quantum physics: be it general quantum technologies, quantum computations, quantum metrology or sensing. This is of interest as the effects studied can play an important role in the development of concepts for future quantum nanophotonic devices operating at the level of one or few quanta.

List of figures

References

1. *Scully Marlan O., Zubairy M. Suhail.* Quantum Optics. — Cambridge University Press, 1997.

2. *Novotny Lukas, Hecht Bert.* Principles of Nano-Optics. — 2 edition. — Cambridge University Press, 2012.

3. *Glauber Roy J.* Quantum theory of optical coherence: selected papers and lectures. — John Wiley & Sons, 2007.

4. *Claude Cohen-Tannoudji, Dupont-Roc Jacques, Grynberg Gilbert.* Atom-Photon Interactions. — Wiley-VCH Verlag GmbH & Co. KGaA, 2004. — P. 660. — URL: papers2://publication/uuid/794705AA-C281-47AF-9096-8CEF65BE1820.

5. *Haroche Serge, Raimond Jean Michel.* Exploring the Quantum: Atoms, Cavities, and Photons. — Oxford: Oxford Univ. Press, 2006. — URL: https://cds.cern.ch/record/993568.

6. *Dicke R. H.* Coherence in Spontaneous Radiation Processes // *Phys. Rev.* — 1954. — Jan. — Vol. 93. — Pp. 99–110. — URL: https://link.aps.org/doi/10.1103/PhysRev.93.99.

7. *Scully Marlan O, Svidzinsky Anatoly A.* The super of superradiance // *Science.* — 2009. — Vol. 325, no. 5947. — Pp. 1510–1511.

8. Directed spontaneous emission from an extended ensemble of N atoms: Timing is everything / Marlan O Scully, Edward S Fry, CH Raymond Ooi, Krzysztof Wódkiewicz // *Physical review letters.* — 2006. — Vol. 96, no. 1. — P. 010501.

9. *Scully Marlan O.* Collective Lamb shift in single photon Dicke superradiance // *Physical review letters.* — 2009. — Vol. 102, no. 14. — P. 143601.

10. Chiral quantum optics / Peter Lodahl, Sahand Mahmoodian, Søren Stobbe et al. // *Nature.* — 2017. — Vol. 541, no. 7638. — Pp. 473–480. — URL: https://doi.org/10.1038/nature21037.

11. *Petersen Jan, Volz Jürgen, Rauschenbeutel Arno.* Chiral nanophotonic waveguide interface based on spin-orbit interaction of light // *Science.* — 2014. — Vol. 346, no. 6205. — Pp. 67–71. — URL: https://science.sciencemag.org/content/346/6205/67.

12. Quantum optical circulator controlled by a single chirally coupled atom / Michael Scheucher, Adèle Hilico, Elisa Will et al. // *Science*. — 2016. — Vol. 354, no. 6319. — Pp. 1577–1580. — URL: https://science.sciencemag.org/content/354/6319/1577.

13. Nanophotonic Optical Isolator Controlled by the Internal State of Cold Atoms / Clément Sayrin, Christian Junge, Rudolf Mitsch et al. // *Phys. Rev. X*. — 2015. — Dec. — Vol. 5. — P. 041036. — URL: https://link.aps.org/doi/10.1103/PhysRevX.5.041036.

14. Fiber-Optical Switch Controlled by a Single Atom / Danny O'Shea, Christian Junge, Jürgen Volz, Arno Rauschenbeutel // *Phys. Rev. Lett.* — 2013. — Nov. — Vol. 111. — P. 193601. — URL: https://link.aps.org/doi/10.1103/PhysRevLett.111.193601.

15. Atom-by-atom assembly of defect-free one-dimensional cold atom arrays / Manuel Endres, Hannes Bernien, Alexander Keesling et al. // *Science*. — 2016. — Vol. 354, no. 6315. — Pp. 1024–1027. — URL: https://science.sciencemag.org/content/354/6315/1024.

16. Single-Atom Trapping in Holographic 2D Arrays of Microtraps with Arbitrary Geometries / F. Nogrette, H. Labuhn, S. Ravets et al. // *Phys. Rev. X*. — 2014. — May. — Vol. 4. — P. 021034. — URL: https://link.aps.org/doi/10.1103/PhysRevX.4.021034.

17. Synthetic three-dimensional atomic structures assembled atom by atom / Daniel Barredo, Vincent Lienhard, Sylvain de Léséleuc et al. // *Nature*. — 2018. — Sep. — Vol. 561, no. 7721. — Pp. 79–82. — URL: https://doi.org/10.1038/s41586-018-0450-2.

18. *Zheng Huaixiu, Gauthier Daniel J., Baranger Harold U.* Waveguide-QED-Based Photonic Quantum Computation // *Phys. Rev. Lett.* — 2013. — Aug. — Vol. 111. — P. 090502. — URL: https://link.aps.org/doi/10.1103/PhysRevLett.111.090502.

19. Microwave photonics with superconducting quantum circuits / Xiu Gu, Anton Frisk Kockum, Adam Miranowicz et al. // *Physics Reports*. — 2017. — Vol. 718-719. — Pp. 1 – 102. — Microwave photonics with superconducting quantum circuits. URL: http://www.sciencedirect.com/science/article/pii/S0370157317303290.

20. Large Bragg Reflection from One-Dimensional Chains of Trapped Atoms Near a Nanoscale Waveguide / Neil V. Corzo, Baptiste Gouraud, Aveek Chandra et al. // *Phys. Rev. Lett.* — 2016. — Sep. — Vol. 117.

— P. 133603. — URL: https://link.aps.org/doi/10.1103/PhysRevLett.117.133603.

21. Waveguide-coupled single collective excitation of atomic arrays / Neil V. Corzo, Jérémy Raskop, Aveek Chandra et al. // *Nature*. — 2019. — Vol. 566, no. 7744. — Pp. 359–362. — URL: https://doi.org/10.1038/s41586-019-0902-3.

22. Super-radiance reveals infinite-range dipole interactions through a nanofiber / P. Solano, P. Barberis-Blostein, F. K. Fatemi et al. // *Nature Communications*. — 2017. — Vol. 8, no. 1. — P. 1857. — URL: https://doi.org/10.1038/s41467-017-01994-3.

23. *Bliokh Konstantin Y., Smirnova Daria, Nori Franco*. Quantum spin Hall effect of light // *Science*. — 2015. — Vol. 348, no. 6242. — Pp. 1448–1451. — URL: https://science.sciencemag.org/content/348/6242/1448.

24. Deterministic photon-emitter coupling in chiral photonic circuits / Immo Söllner, Sahand Mahmoodian, Sofie Lindskov Hansen et al. // *Nature Nanotechnology*. — 2015. — Vol. 10, no. 9. — Pp. 775–778. — URL: https://doi.org/10.1038/nnano.2015.159.

25. Colloquium: Excitons in atomically thin transition metal dichalcogenides / Gang Wang, Alexey Chernikov, Mikhail M. Glazov et al. // *Reviews of Modern Physics*. — 2018. — Vol. 90, no. 2. — P. 21001. — URL: https://doi.org/10.1103/RevModPhys.90.021001.

26. Nanoscale chiral valley-photon interface through optical spin-orbit coupling / Gong Su-Hyun, Filippo Alpeggiani, Beniamino Sciacca et al. // *Science*. — 2018. — Vol. 359, no. January. — Pp. 443–447.

27. Room Temperature Chiral Coupling of Valley Excitons with Spin-Momentum Locked Surface Plasmons / Thibault Chervy, Stefano Azzini, Etienne Lorchat et al. // *ACS Photonics*. — 2018. — Vol. 5, no. 4. — Pp. 1281–1287.

28. Nanoscale chiral valley-photon interface through optical spin-orbit coupling / Su Hyun Gong, Filippo Alpeggiani, Beniamino Sciacca et al. // *Science*. — 2018. — Vol. 359, no. 6374. — Pp. 443–447.

29. Coherent steering of nonlinear chiral valley photons with a synthetic Au–WS2 metasurface / Guangwei Hu, Xuanmiao Hong, Kai Wang et al. // *Nature Photonics*. — 2019. — URL: http://www.nature.com/articles/s41566-019-0399-1.

30. Guiding optical modes in chains of dielectric particles / Gail S. Blaustein, Michael I. Gozman, Olga Samoylova et al. // *Opt. Express*. — 2007. — Dec. — Vol. 15, no. 25. — Pp. 17380–17391. — URL: http://www.opticsexpress.org/abstract.cfm?URI=oe-15-25-17380.

31. Exponential Improvement in Photon Storage Fidelities Using Subradiance and "Selective Radiance" in Atomic Arrays / A. Asenjo-Garcia, M. Moreno-Cardoner, A. Albrecht et al. // *Phys. Rev. X*. — 2017. — Aug. — Vol. 7. — P. 031024. — URL: https://link.aps.org/doi/10.1103/PhysRevX.7.031024.

32. *Zhang Yu-Xiang, Mølmer Klaus*. Theory of Subradiant States of a One-Dimensional Two-Level Atom Chain // *Phys. Rev. Lett.* — 2019. — May. — Vol. 122. — P. 203605. — URL: https://link.aps.org/doi/10.1103/PhysRevLett.122.203605.

33. *Figotin Alex, Vitebskiy Ilya*. Gigantic transmission band-edge resonance in periodic stacks of anisotropic layers // *Phys. Rev. E*. — 2005. — Sep. — Vol. 72. — P. 036619. — URL: https://link.aps.org/doi/10.1103/PhysRevE.72.036619.

34. Spin-orbit interactions of light / K. Y. Bliokh, F. J. Rodríguez-Fortuño, F. Nori, A. V. Zayats // *Nature Photonics*. — 2015. — Dec. — Vol. 9, no. 12. — Pp. 796–808. — URL: https://doi.org/10.1038/nphoton.2015.201.

35. *Mechelen Todd Van, Jacob Zubin*. Universal spin-momentum locking of evanescent waves // *Optica*. — 2016. — Feb. — Vol. 3, no. 2. — Pp. 118–126. — URL: http://www.osapublishing.org/optica/abstract.cfm?URI=optica-3-2-118.

36. *Born M.* Über die natürliche optische Aktivität von Flüssigkeiten und Gasen // *Phys. Z.* — 1915. — Vol. 16. — Pp. 251–258.

37. *Kuhn Werner*. Quantitative Verhältnisse und Beziehungen bei der natürlichen optischen Aktivität // *Zeitschrift für Physikalische Chemie*. — 1929. — Vol. 4, no. 1. — Pp. 14–36.

38. Interpreting chiral nanophotonic spectra: the plasmonic Born–Kuhn model / Xinghui Yin, Martin Schäferling, Bernd Metzger, Harald Giessen // *Nano letters*. — 2013. — Vol. 13, no. 12. — Pp. 6238–6243.

39. *Agranovich V. M., A. Dubovskii O.* Driving a quantum system with the output field from another driven quantum system // *JETP*. — 1966. — May. — Vol. 3. — P. 233. — URL: http://www.jetpletters.ac.ru/ps/1618/article_24767.pdf.

40. Electromagnetic energy transport via linear chains of silver nanoparticles / M. Quinten, A. Leitner, J. R. Krenn, F. R. Aussenegg // *Opt. Lett.* — 1998. — Sep. — Vol. 23, no. 17. — Pp. 1331–1333. — URL: http://ol.osa.org/abstract.cfm?URI=ol-23-17-1331.

41. Plasmonics—a route to nanoscale optical devices / Stefan A Maier, Mark L Brongersma, Pieter G Kik et al. // *Advanced materials.* — 2001. — Vol. 13, no. 19. — Pp. 1501–1505.

42. *Maier Stefan A., Kik Pieter G., Atwater Harry A.* Observation of coupled plasmon-polariton modes in Au nanoparticle chain waveguides of different lengths: Estimation of waveguide loss // *Applied Physics Letters.* — 2002. — Vol. 81, no. 9. — Pp. 1714–1716. — URL: https://doi.org/10.1063/1.1503870.

43. *Weber W. H., Ford G. W.* Propagation of optical excitations by dipolar interactions in metal nanoparticle chains // *Phys. Rev. B.* — 2004. — Sep. — Vol. 70. — P. 125429. — URL: https://link.aps.org/doi/10.1103/PhysRevB.70.125429.

44. *Citrin D. S.* Plasmon-polariton transport in metal-nanoparticle chains embedded in a gain medium // *Opt. Lett.* — 2006. — Jan. — Vol. 31, no. 1. — Pp. 98–100. — URL: http://ol.osa.org/abstract.cfm?URI=ol-31-1-98.

45. *Koenderink A. Femius, Polman Albert.* Complex response and polariton-like dispersion splitting in periodic metal nanoparticle chains // *Phys. Rev. B.* — 2006. — Jul. — Vol. 74. — P. 033402. — URL: https://link.aps.org/doi/10.1103/PhysRevB.74.033402.

46. *Citrin D. S.* Coherent Excitation Transport in Metal-Nanoparticle Chains // *Nano Letters.* — 2004. — Vol. 4, no. 9. — Pp. 1561–1565. — URL: https://doi.org/10.1021/nl049679l.

47. *Markel Vadim A., Sarychev Andrey K.* Propagation of surface plasmons in ordered and disordered chains of metal nanospheres // *Phys. Rev. B.* — 2007. — Feb. — Vol. 75. — P. 085426. — URL: https://link.aps.org/doi/10.1103/PhysRevB.75.085426.

48. *Shore Robert A., Yaghjian Arthur D.* Complex waves on periodic arrays of lossy and lossless permeable spheres: 1. Theory // *Radio Science.* — 2012. — Vol. 47, no. 2. — URL: https://agupubs.onlinelibrary.wiley.com/doi/abs/10.1029/2011RS004859.

49. *Shore Robert A., Yaghjian Arthur D.* Complex waves on periodic arrays of lossy and lossless permeable spheres: 2. Numerical results // *Radio Science*. — 2012. — Vol. 47, no. 2. — URL: https://agupubs.onlinelibrary.wiley.com/doi/abs/10.1029/2011RS004860.

50. *Markel V. A.* Coupled-dipole Approach to Scattering of Light from a One-dimensional Periodic Dipole Structure // *Journal of Modern Optics*. — 1993. — Vol. 40, no. 11. — Pp. 2281–2291. — URL: https://doi.org/10.1080/09500349314552291.

51. *Zou Shengli, Janel Nicolas, Schatz George C.* Silver nanoparticle array structures that produce remarkably narrow plasmon lineshapes // *The Journal of Chemical Physics*. — 2004. — Vol. 120, no. 23. — Pp. 10871–10875. — URL: https://doi.org/10.1063/1.1760740.

52. Controlling Plasmon Line Shapes through Diffractive Coupling in Linear Arrays of Cylindrical Nanoparticles Fabricated by Electron Beam Lithography / Erin M. Hicks, Shengli Zou, George C. Schatz et al. // *Nano Letters*. — 2005. — Vol. 5, no. 6. — Pp. 1065–1070. — PMID: 15943444. URL: https://doi.org/10.1021/nl0505492.

53. Optically resonant dielectric nanostructures / Arseniy I. Kuznetsov, Andrey E. Miroshnichenko, Mark L. Brongersma et al. // *Science*. — 2016. — Vol. 354, no. 6314. — URL: https://science.sciencemag.org/content/354/6314/aag2472.

54. Dielectric-based extremely-low-loss subwavelength-light transport at the nanoscale: An alternative to surface-plasmon-mediated waveguiding / Junjie Du, Shiyang Liu, Zhifang Lin et al. // *Phys. Rev. A*. — 2011. — Mar. — Vol. 83. — P. 035803. — URL: https://link.aps.org/doi/10.1103/PhysRevA.83.035803.

55. All-dielectric optical nanoantennas / Alexander E. Krasnok, Andrey E. Miroshnichenko, Pavel A. Belov, Yuri S. Kivshar // *Opt. Express*. — 2012. — Aug. — Vol. 20, no. 18. — Pp. 20599–20604. — URL: http://www.opticsexpress.org/abstract.cfm?URI=oe-20-18-20599.

56. Subwavelength waveguides composed of dielectric nanoparticles / Roman S. Savelev, Alexey P. Slobozhanyuk, Andrey E. Miroshnichenko et al. // *Phys. Rev. B*. — 2014. — Jan. — Vol. 89. — P. 035435. — URL: https://link.aps.org/doi/10.1103/PhysRevB.89.035435.

57. Resonant Light Guiding Along a Chain of Silicon Nanoparticles / Reuben M. Bakker, Ye Feng Yu, Ramón Paniagua-Domínguez et al. //

Nano Letters. — 2017. — Vol. 17, no. 6. — Pp. 3458–3464. — PMID: 28463510. URL: https://doi.org/10.1021/acs.nanolett.7b00381.

58. *Milonni P. W., Knight P. L.* Retardation in the resonant interaction of two identical atoms // *Phys. Rev. A*. — 1974. — Oct. — Vol. 10. — Pp. 1096–1108. — URL: http://link.aps.org/doi/10.1103/PhysRevA.10.1096.

59. *Dung Ho Trung, Ujihara Kikuo*. Analytic solution for retardation in two-atom systems // *Phys. Rev. A*. — 1999. — Mar. — Vol. 59. — Pp. 2524–2527. — URL: http://link.aps.org/doi/10.1103/PhysRevA.59.2524.

60. *Nienhuis G, Schuller F*. Spontaneous emission and light scattering by atomic lattice models // *Journal of Physics B: Atomic and Molecular Physics*. — 1987. — Vol. 20, no. 1. — P. 23.

61. *Bettles Robert J., Gardiner Simon A., Adams Charles S.* Cooperative eigenmodes and scattering in one-dimensional atomic arrays // *Phys. Rev. A*. — 2016. — Oct. — Vol. 94. — P. 043844. — URL: https://link.aps.org/doi/10.1103/PhysRevA.94.043844.

62. *Sutherland R. T., Robicheaux F.* Collective dipole-dipole interactions in an atomic array // *Phys. Rev. A*. — 2016. — Jul. — Vol. 94. — P. 013847. — URL: https://link.aps.org/doi/10.1103/PhysRevA.94.013847.

63. Long-Range Interacting Many-Body Systems with Alkaline-Earth-Metal Atoms / B. Olmos, D. Yu, Y. Singh et al. // *Phys. Rev. Lett.* — 2013. — Apr. — Vol. 110. — P. 143602. — URL: https://link.aps.org/doi/10.1103/PhysRevLett.110.143602.

64. *Krämer S., Ostermann L., Ritsch H.* Optimized geometries for future generation optical lattice clocks // *EPL (Europhysics Letters)*. — 2016. — Apr. — Vol. 114, no. 1. — P. 14003. — URL: https://doi.org/10.1209/0295-5075/114/14003.

65. *Jen H. H., Chang M.-S., Chen Y.-C.* Cooperative single-photon subradiant states // *Phys. Rev. A*. — 2016. — Jul. — Vol. 94. — P. 013803. — URL: https://link.aps.org/doi/10.1103/PhysRevA.94.013803.

66. *Markel V. A.* Scattering of Light from Two Interacting Spherical Particles // *Journal of Modern Optics*. — 1992. — Vol. 39, no. 4. — Pp. 853–861. — URL: https://doi.org/10.1080/09500349214550851.

67. *Markel Vadim A.* Divergence of dipole sums and the nature of non-Lorentzian exponentially narrow resonances in one-dimensional periodic arrays of nanospheres // *Journal of Physics B: Atomic, Molecular and Optical Physics*. — 2005. — Vol. 38, no. 7. — P. L115.

68. *DeVoe R. G., Brewer R. G.* Observation of Superradiant and Subradiant Spontaneous Emission of Two Trapped Ions // *Phys. Rev. Lett.* — 1996. — Mar. — Vol. 76. — Pp. 2049–2052. — URL: https://link.aps.org/doi/10.1103/PhysRevLett.76.2049.

69. Cooperative Lamb Shift in a Mesoscopic Atomic Array / Z. Meir, O. Schwartz, E. Shahmoon et al. // *Phys. Rev. Lett.* — 2014. — Nov. — Vol. 113. — P. 193002. — URL: https://link.aps.org/doi/10.1103/PhysRevLett.113.193002.

70. Rapid Production of Uniformly Filled Arrays of Neutral Atoms / Brian J. Lester, Niclas Luick, Adam M. Kaufman et al. // *Phys. Rev. Lett.* — 2015. — Aug. — Vol. 115. — P. 073003. — URL: https://link.aps.org/doi/10.1103/PhysRevLett.115.073003.

71. An atom-sorting machine / Yevhen Miroshnychenko, Wolfgang Alt, Igor Dotsenko et al. // *Nature*. — 2006. — Jul. — Vol. 442, no. 7099. — Pp. 151–151. — URL: https://doi.org/10.1038/442151a.

72. Atom-by-atom assembly of defect-free one-dimensional cold atom arrays / Manuel Endres, Hannes Bernien, Alexander Keesling et al. // *Science*. — 2016. — Vol. 354, no. 6315. — Pp. 1024–1027. — URL: https://science.sciencemag.org/content/354/6315/1024.

73. An atom-by-atom assembler of defect-free arbitrary two-dimensional atomic arrays / Daniel Barredo, Sylvain de Léséleuc, Vincent Lienhard et al. // *Science*. — 2016. — Vol. 354, no. 6315. — Pp. 1021–1023. — URL: https://science.sciencemag.org/content/354/6315/1021.

74. In situ single-atom array synthesis using dynamic holographic optical tweezers / Hyosub Kim, Woojun Lee, Han-gyeol Lee et al. // *Nature Communications*. — 2016. — Oct. — Vol. 7, no. 1. — P. 13317. — URL: https://doi.org/10.1038/ncomms13317.

75. Defect-Free Assembly of 2D Clusters of More Than 100 Single-Atom Quantum Systems / Daniel Ohl de Mello, Dominik Schäffner, Jan Werkmann et al. // *Phys. Rev. Lett.* — 2019. — May. — Vol. 122. — P. 203601. — URL: https://link.aps.org/doi/10.1103/PhysRevLett.122.203601.

76. *Nelson Karl D., Li Xiao, Weiss David S.* Imaging single atoms in a three-dimensional array // *Nature Physics*. — 2007. — Aug. — Vol. 3, no. 8. — Pp. 556–560. — URL: https://doi.org/10.1038/nphys645.

77. *Schlosser N., Reymond G., Grangier P.* Collisional Blockade in Microscopic Optical Dipole Traps // *Phys. Rev. Lett.* — 2002. — Jun. — Vol. 89. — P. 023005. — URL: https://link.aps.org/doi/10.1103/PhysRevLett.89.023005.

78. *Dowling Jonathan P., Gea-Banacloche Julio.* Evanescent Light-Wave Atom Mirrors, Resonators, Waveguides, and Traps / Ed. by Benjamin Bederson, Herbert Walther. — Academic Press, 1996. — Vol. 37 of *Advances In Atomic, Molecular, and Optical Physics*. — Pp. 1 – 94. — URL: http://www.sciencedirect.com/science/article/pii/S1049250X08600981.

79. *Le Kien Fam, Balykin V. I., Hakuta K.* Atom trap and waveguide using a two-color evanescent light field around a subwavelength-diameter optical fiber // *Phys. Rev. A*. — 2004. — Dec. — Vol. 70. — P. 063403. — URL: https://link.aps.org/doi/10.1103/PhysRevA.70.063403.

80. Field intensity distributions and polarization orientations in a vacuum-clad subwavelength-diameter optical fiber / Fam Le Kien, J.Q. Liang, K. Hakuta, V.I. Balykin // *Optics Communications*. — 2004. — Vol. 242, no. 4. — Pp. 445 – 455. — URL: http://www.sciencedirect.com/science/article/pii/S0030401804008739.

81. Optical Interface Created by Laser-Cooled Atoms Trapped in the Evanescent Field Surrounding an Optical Nanofiber / E. Vetsch, D. Reitz, G. Sagué et al. // *Phys. Rev. Lett.* — 2010. — May. — Vol. 104. — P. 203603. — URL: https://link.aps.org/doi/10.1103/PhysRevLett.104.203603.

82. Demonstration of a State-Insensitive, Compensated Nanofiber Trap / A. Goban, K. S. Choi, D. J. Alton et al. // *Phys. Rev. Lett.* — 2012. — Jul. — Vol. 109. — P. 033603. — URL: https://link.aps.org/doi/10.1103/PhysRevLett.109.033603.

83. *Yudson VI.* Dynamics of the integrable one-dimensional system "photons+ two-level atoms // *Physics Letters A*. — 1988. — Vol. 129, no. 1. — Pp. 17–20.

84. *Makarov AA, Letokhov VS.* Spontaneous decay in a system of two spatially separated atoms (one-dimensional case) // *Journal of Experimental and Theoretical Physics.* — 2003. — Vol. 97, no. 4. — Pp. 688–701.

85. *Shen Jung-tsung, Fan Shanhui.* Coherent photon transport from spontaneous emission in one-dimensional waveguides // *Optics letters.* — 2005. — Vol. 30, no. 15. — Pp. 2001–2003.

86. *Shen Jung-Tsung, Fan Shanhui.* Coherent Single Photon Transport in a One-Dimensional Waveguide Coupled with Superconducting Quantum Bits // *Phys. Rev. Lett.* — 2005. — Nov. — Vol. 95. — P. 213001. — URL: https://link.aps.org/doi/10.1103/PhysRevLett.95.213001.

87. *Shen Jung-Tsung, Fan Shanhui.* Strongly Correlated Two-Photon Transport in a One-Dimensional Waveguide Coupled to a Two-Level System // *Phys. Rev. Lett.* — 2007. — Apr. — Vol. 98. — P. 153003. — URL: https://link.aps.org/doi/10.1103/PhysRevLett.98.153003.

88. Controllable Scattering of a Single Photon inside a One-Dimensional Resonator Waveguide / Lan Zhou, Z. R. Gong, Yu-xi Liu et al. // *Phys. Rev. Lett.* — 2008. — Sep. — Vol. 101. — P. 100501. — URL: https://link.aps.org/doi/10.1103/PhysRevLett.101.100501.

89. *Yudson V. I., Reineker P.* Multiphoton scattering in a one-dimensional waveguide with resonant atoms // *Phys. Rev. A.* — 2008. — Nov. — Vol. 78. — P. 052713. — URL: https://link.aps.org/doi/10.1103/PhysRevA.78.052713.

90. *Zheng Huaixiu, Gauthier Daniel J., Baranger Harold U.* Waveguide QED: Many-body bound-state effects in coherent and Fock-state scattering from a two-level system // *Phys. Rev. A.* — 2010. — Dec. — Vol. 82. — P. 063816. — URL: https://link.aps.org/doi/10.1103/PhysRevA.82.063816.

91. *Witthaut Dirk, Sørensen A Søndberg.* Photon scattering by a three-level emitter in a one-dimensional waveguide // *New Journal of Physics.* — 2010. — Vol. 12, no. 4. — P. 043052.

92. Entanglement of Two Qubits Mediated by One-Dimensional Plasmonic Waveguides / A. Gonzalez-Tudela, D. Martin-Cano, E. Moreno et al. // *Phys. Rev. Lett.* — 2011. — Jan. — Vol. 106. — P. 020501. — URL: https://link.aps.org/doi/10.1103/PhysRevLett.106.020501.

93. *Rephaeli Eden, Kocabaş Şükrü Ekin, Fan Shanhui.* Few-photon transport in a waveguide coupled to a pair of colocated two-level atoms // *Phys. Rev. A.* — 2011. — Dec. — Vol. 84. — P. 063832. — URL: https://link.aps.org/doi/10.1103/PhysRevA.84.063832.

94. Cavity QED with atomic mirrors / Darrick E Chang, L Jiang, AV Gorshkov, HJ Kimble // *New Journal of Physics.* — 2012. — Vol. 14, no. 6. — P. 063003.

95. *Fang Yao-Lung L, Zheng Huaixiu, Baranger Harold U.* One-dimensional waveguide coupled to multiple qubits: photon-photon correlations // *EPJ Quantum Technology.* — 2014. — Vol. 1, no. 1. — P. 3.

96. Photon-Mediated Interactions Between Distant Artificial Atoms / Arjan F. van Loo, Arkady Fedorov, Kevin Lalumière et al. // *Science.* — 2013. — Vol. 342, no. 6165. — Pp. 1494–1496. — URL: https://science.sciencemag.org/content/342/6165/1494.

97. Coherent Backscattering of Light Off One-Dimensional Atomic Strings / H. L. Sørensen, J.-B. Béguin, K. W. Kluge et al. // *Phys. Rev. Lett.* — 2016. — Sep. — Vol. 117. — P. 133604. — URL: https://link.aps.org/doi/10.1103/PhysRevLett.117.133604.

98. Nanowire photonic crystal waveguides for single-atom trapping and strong light-matter interactions / S.-P. Yu, J. D. Hood, J. A. Muniz et al. // *Applied Physics Letters.* — 2014. — Vol. 104, no. 11. — P. 111103. — URL: https://doi.org/10.1063/1.4868975.

99. Atom-light interactions in photonic crystals / A. Goban, C.-L. Hung, S.-P. Yu et al. // *Nature Communications.* — 2014. — May. — Vol. 5, no. 1. — P. 3808. — URL: https://doi.org/10.1038/ncomms4808.

100. Trapping of ultracold atoms in a hollow-core photonic crystal fiber / Caleb A. Christensen, Sebastian Will, Michele Saba et al. // *Phys. Rev. A.* — 2008. — Sep. — Vol. 78. — P. 033429. — URL: https://link.aps.org/doi/10.1103/PhysRevA.78.033429.

101. Efficient All-Optical Switching Using Slow Light within a Hollow Fiber / M. Bajcsy, S. Hofferberth, V. Balic et al. // *Phys. Rev. Lett.* — 2009. — May. — Vol. 102. — P. 203902. — URL: https://link.aps.org/doi/10.1103/PhysRevLett.102.203902.

102. Subradiant states of quantum bits coupled to a one-dimensional waveguide / Andreas Albrecht, Loïc Henriet, Ana Asenjo-Garcia et al. // *New Journal of Physics.* — 2019. — Vol. 21, no. 2. — P. 025003.

103. From transverse angular momentum to photonic wheels / Andrea Aiello, Peter Banzer, Martin Neugebauer, Gerd Leuchs // *Nature Photonics*. — 2015. — Dec. — Vol. 9, no. 12. — Pp. 789–795. — URL: https://doi.org/10.1038/nphoton.2015.203.

104. *Le Kien Fam, Rauschenbeutel A.* Anisotropy in scattering of light from an atom into the guided modes of a nanofiber // *Phys. Rev. A*. — 2014. — Aug. — Vol. 90. — P. 023805. — URL: https://link.aps.org/doi/10.1103/PhysRevA.90.023805.

105. Directional spontaneous emission and lateral Casimir-Polder force on an atom close to a nanofiber / Stefan Scheel, Stefan Yoshi Buhmann, Christoph Clausen, Philipp Schneeweiss // *Phys. Rev. A*. — 2015. — Oct. — Vol. 92. — P. 043819. — URL: https://link.aps.org/doi/10.1103/PhysRevA.92.043819.

106. *Oude Weernink Ricardo R. Q. P. T., Barcellona Pablo, Buhmann Stefan Yoshi.* Lateral Casimir-Polder forces by breaking time-reversal symmetry // *Phys. Rev. A*. — 2018. — Mar. — Vol. 97. — P. 032507. — URL: https://link.aps.org/doi/10.1103/PhysRevA.97.032507.

107. Chiral route to spontaneous entanglement generation / Carlos Gonzalez-Ballestero, Alejandro Gonzalez-Tudela, Francisco J. Garcia-Vidal, Esteban Moreno // *Phys. Rev. B*. — 2015. — Oct. — Vol. 92. — P. 155304. — URL: https://link.aps.org/doi/10.1103/PhysRevB.92.155304.

108. Quantum Spin Dimers from Chiral Dissipation in Cold-Atom Chains / Tomás Ramos, Hannes Pichler, Andrew J. Daley, Peter Zoller // *Phys. Rev. Lett.* — 2014. — Dec. — Vol. 113. — P. 237203. — URL: https://link.aps.org/doi/10.1103/PhysRevLett.113.237203.

109. All-optical routing of single photons by a one-atom switch controlled by a single photon / Itay Shomroni, Serge Rosenblum, Yulia Lovsky et al. // *Science*. — 2014. — Vol. 345, no. 6199. — Pp. 903–906. — URL: https://science.sciencemag.org/content/345/6199/903.

110. Optical control of the emission direction of a quantum dot / I. J. Luxmoore, N. A. Wasley, A. J. Ramsay et al. // *Applied Physics Letters*. — 2013. — Vol. 103, no. 24. — P. 241102. — URL: https://doi.org/10.1063/1.4845975.

111. Near-Unity Coupling Efficiency of a Quantum Emitter to a Photonic Crystal Waveguide / M. Arcari, I. Söllner, A. Javadi et al. // *Phys.*

Rev. Lett. — 2014. — Aug. — Vol. 113. — P. 093603. — URL: https://link.aps.org/doi/10.1103/PhysRevLett.113.093603.

112. *Carmichael H. J.* Quantum trajectory theory for cascaded open systems // *Phys. Rev. Lett.* — 1993. — Apr. — Vol. 70. — Pp. 2273–2276. — URL: https://link.aps.org/doi/10.1103/PhysRevLett.70.2273.

113. *Gardiner C. W.* Driving a quantum system with the output field from another driven quantum system // *Phys. Rev. Lett.* — 1993. — Apr. — Vol. 70. — Pp. 2269–2272. — URL: https://link.aps.org/doi/10.1103/PhysRevLett.70.2269.

114. *Rupasov VI.* Contribution to the Dicke superradiance theory. Exact solution of the quasi-one-dimensional quantum model // *Sov. Phys. JETP.* — 1982. — Vol. 56, no. 5.

115. *Rupasov VI, Yudson VI.* Exact Dicke superradiance theory: Bethe wavefunctions in the discrete atom model // *Zh. Eksp. Teor. Fiz.* — 1984. — Vol. 86. — P. 825.

116. *Eckle H-P, Johannesson Henrik, Stafford Charles A.* Kondo resonance in a mesoscopic ring coupled to a quantum dot: Exact results for the Aharonov-Bohm-Casher effects // *Physical Review Letters.* — 2001. — Vol. 87, no. 1. — P. 016602.

117. *Shen Jung-Tsung, Fan Shanhui.* Strongly correlated multiparticle transport in one dimension through a quantum impurity // *Physical Review A.* — 2007. — Vol. 76, no. 6. — P. 062709.

118. *Fan Shanhui, Kocabaş Şükrü Ekin, Shen Jung-Tsung.* Input-output formalism for few-photon transport in one-dimensional nanophotonic waveguides coupled to a qubit // *Physical Review A.* — 2010. — Vol. 82, no. 6. — P. 063821.

119. *Rehler Nicholas E, Eberly Joseph H.* Superradiance // *Physical Review A.* — 1971. — Vol. 3, no. 5. — P. 1735.

120. *MacGillivray Jeffrey Charles, Feld MS.* Theory of superradiance in an extended, optically thick medium // *Physical Review A.* — 1976. — Vol. 14, no. 3. — P. 1169.

121. *Andreev Anatolii V, Emel'yanov Vladimir I, Il'inskiĭ Yu A.* Collective spontaneous emission (Dicke superradiance) // *Soviet Physics Uspekhi.* — 1980. — Vol. 23, no. 8. — P. 493.

122. *Gross Michel, Haroche Serge.* Superradiance: An essay on the theory of collective spontaneous emission // *Physics Reports.* — 1982. — Vol. 93, no. 5. — Pp. 301–396.

123. *Svidzinsky Anatoly A, Chang Jun-Tao, Scully Marlan O.* Cooperative spontaneous emission of N atoms: Many-body eigenstates, the effect of virtual Lamb shift processes, and analogy with radiation of N classical oscillators // *Physical Review A.* — 2010. — Vol. 81, no. 5. — P. 053821.

124. *Bienaimé Tom, Piovella Nicola, Kaiser Robin.* Controlled Dicke subradiance from a large cloud of two-level systems // *Physical Review Letters.* — 2012. — Vol. 108, no. 12. — P. 123602.

125. *Scully Marlan O.* Single photon subradiance: quantum control of spontaneous emission and ultrafast readout // *Physical Review Letters.* — 2015. — Vol. 115, no. 24. — P. 243602.

126. Observation of Dicke superradiance in optically pumped HF gas / N Skribanowitz, IP Herman, JC MacGillivray, MS Feld // *Physical Review Letters.* — 1973. — Vol. 30, no. 8. — P. 309.

127. Superradiance of quantum dots / Michael Scheibner, Thomas Schmidt, Lukas Worschech et al. // *Nature Physics.* — 2007. — Vol. 3, no. 2. — Pp. 106–110.

128. Single-photon superradiance in cold atoms / Rafael A de Oliveira, Milrian S Mendes, Weliton S Martins et al. // *Physical Review A.* — 2014. — Vol. 90, no. 2. — P. 023848.

129. Superradiance for atoms trapped along a photonic crystal waveguide / A Goban, C-L Hung, JD Hood et al. // *Physical Review Letters.* — 2015. — Vol. 115, no. 6. — P. 063601.

130. *Guerin William, Araújo Michelle O, Kaiser Robin.* Subradiance in a large cloud of cold atoms // *Physical Review Letters.* — 2016. — Vol. 116, no. 8. — P. 083601.

131. Superradiance in a large and dilute cloud of cold atoms in the linear-optics regime / Michelle O Araújo, Ivor Krešić, Robin Kaiser, William Guerin // *Physical Review Letters.* — 2016. — Vol. 117, no. 7. — P. 073002.

132. Observation of single-photon superradiance and the cooperative Lamb shift in an extended sample of cold atoms / SJ Roof, KJ Kemp, MD Havey, IM Sokolov // *Physical Review Letters.* — 2016. — Vol. 117, no. 7. — P. 073003.

133. A subradiant optical mirror formed by a single structured atomic layer / Jun Rui, David Wei, Antonio Rubio-Abadal et al. // *Nature*. — 2020. — Jul. — Vol. 583, no. 7816. — Pp. 369–374. — URL: https://doi.org/10.1038/s41586-020-2463-x.

134. *Le Kien Fam, Rauschenbeutel A.* Nanofiber-mediated chiral radiative coupling between two atoms // *Phys. Rev. A*. — 2017. — Feb. — Vol. 95. — P. 023838. — URL: https://link.aps.org/doi/10.1103/PhysRevA.95.023838.

135. *Agarwal G. S.* Anisotropic Vacuum-Induced Interference in Decay Channels // *Phys. Rev. Lett.* — 2000. — Jun. — Vol. 84. — Pp. 5500–5503. — URL: https://link.aps.org/doi/10.1103/PhysRevLett.84.5500.

136. *Li Gao-xiang, Li Fu-li, Zhu Shi-yao.* Quantum interference between decay channels of a three-level atom in a multilayer dielectric medium // *Phys. Rev. A*. — 2001. — Jun. — Vol. 64. — P. 013819. — URL: https://link.aps.org/doi/10.1103/PhysRevA.64.013819.

137. Quantum Interference Enhancement with Left-Handed Materials / Yaping Yang, Jingping Xu, Hong Chen, Shiyao Zhu // *Phys. Rev. Lett.* — 2008. — Jan. — Vol. 100. — P. 043601. — URL: https://link.aps.org/doi/10.1103/PhysRevLett.100.043601.

138. *Yannopapas Vassilios, Paspalakis Emmanuel, Vitanov Nikolay V.* Plasmon-Induced Enhancement of Quantum Interference near Metallic Nanostructures // *Phys. Rev. Lett.* — 2009. — Aug. — Vol. 103. — P. 063602. — URL: https://link.aps.org/doi/10.1103/PhysRevLett.103.063602.

139. Surface-Plasmon-Induced Modification on the Spontaneous Emission Spectrum via Subwavelength-Confined Anisotropic Purcell Factor / Ying Gu, Luojia Wang, Pan Ren et al. // *Nano Letters*. — 2012. — Vol. 12, no. 5. — Pp. 2488–2493. — PMID: 22512860. URL: https://doi.org/10.1021/nl300655n.

140. *Hughes Stephen, Agarwal Girish S.* Anisotropy-induced quantum interference and population trapping between orthogonal quantum dot exciton states in semiconductor cavity systems // *Physical review letters*. — 2017. — Vol. 118, no. 6. — P. 063601.

141. *Mollow B. R.* Power Spectrum of Light Scattered by Two-Level Systems // *Phys. Rev.* — 1969. — Dec. — Vol. 188. — Pp. 1969–1975. — URL: https://link.aps.org/doi/10.1103/PhysRev.188.1969.

142. Highly anisotropic decay rate of single quantum dots in photonic crystal membranes / Q. Wang, S. Stobbe, H. Thyrrestup et al. // Conference on Lasers and Electro-Optics 2010. — Optical Society of America, 2010. — P. CMFF5. — URL: http://www.osapublishing.org/abstract.cfm?URI=CLEO-2010-CMFF5.

143. *Buhmann Stefan Yoshi.* Dispersion Forces I: Macroscopic quantum electrodynamics and ground-state Casimir, Casimir–Polder and van der Waals forces. — Springer, 2013. — Vol. 247.

144. *Buhmann Stefan.* Dispersion Forces II: Many-Body Effects, Excited Atoms, Finite Temperature and Quantum Friction. — Springer, 2013. — Vol. 248.

145. Metasurface-Enabled Remote Quantum Interference / Pankaj K. Jha, Xingjie Ni, Chihhui Wu et al. // *Phys. Rev. Lett.* — 2015. — Jul. — Vol. 115. — P. 025501. — URL: https://link.aps.org/doi/10.1103/PhysRevLett.115.025501.

146. Spontaneous Exciton Valley Coherence in Transition Metal Dichalcogenide Monolayers Interfaced with an Anisotropic Metasurface / Pankaj K. Jha, Nir Shitrit, Xuexin Ren et al. // *Phys. Rev. Lett.* — 2018. — Sep. — Vol. 121. — P. 116102. — URL: https://link.aps.org/doi/10.1103/PhysRevLett.121.116102.

147. Long-lifetime coherence in a quantum emitter induced by a metasurface / Emmanuel Lassalle, Philippe Lalanne, Syed Aljunid et al. // *Phys. Rev. A.* — 2020. — Jan. — Vol. 101. — P. 013837. — URL: https://link.aps.org/doi/10.1103/PhysRevA.101.013837.

148. *Kildishev Alexander V, Boltasseva Alexandra, Shalaev Vladimir M.* Planar photonics with metasurfaces // *Science.* — 2013. — Vol. 339, no. 6125.

149. *Yu Nanfang, Capasso Federico.* Flat optics with designer metasurfaces // *Nature Materials.* — 2014. — Vol. 13, no. 2. — Pp. 139–150.

150. *Cai Wenshan, Shalaev Vladimir M.* Optical metamaterials. — Springer, 2010. — Vol. 10.

151. Hyperbolic metamaterials / Alexander Poddubny, Ivan Iorsh, Pavel Belov, Yuri Kivshar // *Nature Photonics.* — 2013. — Vol. 7, no. 12. — Pp. 948–957. — URL: https://doi.org/10.1038/nphoton.2013.243.

152. *Dung Ho Trung, Knöll Ludwig, Welsch Dirk-Gunnar.* Intermolecular energy transfer in the presence of dispersing and absorbing media // *Phys. Rev. A.* — 2002. — Apr. — Vol. 65. — P. 043813. — URL: https://link.aps.org/doi/10.1103/PhysRevA.65.043813.

153. Cooperative light scattering on an atomic system with degenerate structure of the ground state / A. S. Sheremet, A. D. Manukhova, N. V. Larionov, D. V. Kupriyanov // *Phys. Rev. A.* — 2012. — Oct. — Vol. 86. — P. 043414. — URL: https://link.aps.org/doi/10.1103/PhysRevA.86.043414.

154. *Markel Vadim A.* Antisymmetrical optical states // *J. Opt. Soc. Am. B.* — 1995. — Oct. — Vol. 12, no. 10. — Pp. 1783–1791. — URL: http://josab.osa.org/abstract.cfm?URI=josab-12-10-1783.

155. *Tsoi T. S., Law C. K.* Quantum interference effects of a single photon interacting with an atomic chain inside a one-dimensional waveguide // *Phys. Rev. A.* — 2008. — Dec. — Vol. 78. — P. 063832. — URL: https://link.aps.org/doi/10.1103/PhysRevA.78.063832.

156. *Alù Andrea, Engheta Nader.* Theory of linear chains of metamaterial/-plasmonic particles as subdiffraction optical nanotransmission lines // *Phys. Rev. B.* — 2006. — Nov. — Vol. 74. — P. 205436. — URL: https://link.aps.org/doi/10.1103/PhysRevB.74.205436.

157. *Loudon Rodney, Barnett Stephen M.* Theory of the linear polarizability of a two-level atom // *Journal of Physics B: Atomic, Molecular and Optical Physics.* — 2006. — Vol. 39, no. 15. — P. S555.

158. *Landau Lev Davidovich, Lifshitz Evgenii Mikhailovich.* Quantum mechanics: non-relativistic theory. — Elsevier, 2013. — Vol. 3.

159. *Chew Weng Cho.* Waves and fields in inhomogeneous media. — Wiley-IEEE Press, 1999. — P. 632. — URL: http://ieeexplore.ieee.org/xpl/bkabstractplus.jsp?bkn=5270998.

160. *Loudon Rodney.* The quantum theory of light. — OUP Oxford, 2000.

161. *Minogin V. G., Chormaic Síle Nic.* Manifestation of the van der Waals surface interaction in the spontaneous emission of atoms into an optical nanofiber // *Laser Physics.* — 2010. — Vol. 20, no. 1. — Pp. 32–37. — URL: https://doi.org/10.1134/S1054660X09170137.

162. *Haakh Harald R., Faez Sanli, Sandoghdar Vahid.* Polaritonic normal-mode splitting and light localization in a one-dimensional nanoguide //

Phys. Rev. A. — 2016. — Nov. — Vol. 94. — P. 053840. — URL: https://link.aps.org/doi/10.1103/PhysRevA.94.053840.

163. *Kocharovskaya A, Khanin Ya I.* Population trapping and coherent bleaching of a three-level medium by a periodic train of ultrashort pulses // *Zh. Eksp. Teor. Fiz.* — 1986. — Vol. 90. — Pp. 1610–1618.

164. *Knoll Ludwig, Scheel Stefan, Welsch Dirk-Gunnar.* QED in dispersing and absorbing media // *arXiv preprint quant-ph/0006121.* — 2000.

165. *Dung Ho Trung, Knöll Ludwig, Welsch Dirk-Gunnar.* Resonant dipole-dipole interaction in the presence of dispersing and absorbing surroundings // *Phys. Rev. A.* — 2002. — Dec. — Vol. 66. — P. 063810. — URL: https://link.aps.org/doi/10.1103/PhysRevA.66.063810.

166. *Lindblad Goran.* On the generators of quantum dynamical semigroups // *Communications in Mathematical Physics.* — 1976. — Vol. 48, no. 2. — Pp. 119–130.

167. *Gorini Vittorio, Kossakowski Andrzej, Sudarshan E. C. G.* Completely positive dynamical semigroups of N-level systems // *Journal of Mathematical Physics.* — 1976. — Vol. 17, no. 5. — Pp. 821–825. — URL: https://aip.scitation.org/doi/abs/10.1063/1.522979.

168. *Agarwal G. S.* Quantum electrodynamics in the presence of dielectrics and conductors. IV. General theory for spontaneous emission in finite geometries // *Phys. Rev. A.* — 1975. — Oct. — Vol. 12. — Pp. 1475–1497. — URL: https://link.aps.org/doi/10.1103/PhysRevA.12.1475.

169. *Riordan John.* Introduction to Combinatorial Analysis. — Princeton University Press, 1958.

170. *Ringel Matous, Pletyukhov Mikhail, Gritsev Vladimir.* Topologically protected strongly correlated states of photons // *New Journal of Physics.* — 2014. — Vol. 16, no. 11. — P. 113030.

171. Chirality of nanophotonic waveguide with embedded quantum emitter for unidirectional spin transfer / R. J. Coles, D. M. Price, J. E. Dixon et al. // *Nature Communications.* — 2016. — Mar. — Vol. 7, no. 1. — P. 11183. — URL: https://doi.org/10.1038/ncomms11183.

172. Spin–photon interface and spin-controlled photon switching in a nanobeam waveguide / Alisa Javadi, Dapeng Ding, Martin Hayhurst Appel et al. // *Nature Nanotechnology.* — 2018. — May. — Vol. 13, no. 5. — Pp. 398–403. — URL: https://doi.org/10.1038/s41565-018-0091-5.

173. Strong coupling of single emitters to surface plasmons / D. E. Chang, A. S. Sørensen, P. R. Hemmer, M. D. Lukin // *Phys. Rev. B.* — 2007. — Jul. — Vol. 76. — P. 035420. — URL: https://link.aps.org/doi/10.1103/PhysRevB.76.035420.

174. *Dzsotjan David, Sørensen Anders S., Fleischhauer Michael.* Quantum emitters coupled to surface plasmons of a nanowire: A Green's function approach // *Phys. Rev. B.* — 2010. — Aug. — Vol. 82. — P. 075427. — URL: https://link.aps.org/doi/10.1103/PhysRevB.82.075427.

175. *Johnson P. B., Christy R. W.* Optical Constants of the Noble Metals // *Phys. Rev. B.* — 1972. — Dec. — Vol. 6. — Pp. 4370–4379. — URL: https://link.aps.org/doi/10.1103/PhysRevB.6.4370.

176. Hybrid waves localized at hyperbolic metasurfaces / O. Y. Yermakov, A. I. Ovcharenko, M. Song et al. // *Phys. Rev. B.* — 2015. — Jun. — Vol. 91. — P. 235423. — URL: https://link.aps.org/doi/10.1103/PhysRevB.91.235423.

177. *Gomez-Diaz JS, Tymchenko M, Alù A.* Hyperbolic metasurfaces: surface plasmons, light-matter interactions, and physical implementation using graphene strips // *Optical Materials Express.* — 2015. — Vol. 5, no. 10. — Pp. 2313–2329. — URL: http://www.osapublishing.org/ome/abstract.cfm?URI=ome-5-10-2313.

178. *Dung Ho Trung, Knöll Ludwig, Welsch Dirk-Gunnar.* Spontaneous decay in the presence of dispersing and absorbing bodies: General theory and application to a spherical cavity // *Phys. Rev. A.* — 2000. — Oct. — Vol. 62. — P. 053804. — URL: https://link.aps.org/doi/10.1103/PhysRevA.62.053804.

179. *Tai Chen-To.* Dyadic Green functions in electromagnetic theory. — IEEE Press Series on Electromagnetic Waves, 1994. — P. 343. — URL: http://www.getcited.org/pub/103091504.

180. *Gusynin VP, Sharapov SG, Carbotte JP.* Magneto-optical conductivity in graphene // *Journal of Physics: Condensed Matter.* — 2006. — Vol. 19, no. 2. — P. 026222.

181. *Caloz C., Sihvola A.* Electromagnetic Chirality, Part 1: The Microscopic Perspective [Electromagnetic Perspectives] // *IEEE Antennas and Propagation Magazine.* — 2020. — Vol. 62, no. 1. — Pp. 58–71.

182. *Martin Olivier J. F., Dereux Alain, Girard Christian.* Iterative scheme for computing exactly the total field propagating in dielectric structures

of arbitrary shape // *J. Opt. Soc. Am. A.* — 1994. — Mar. — Vol. 11, no. 3. — Pp. 1073–1080. — URL: http://josaa.osa.org/abstract.cfm?URI=josaa-11-3-1073.

183. *Hadad Y, Steinberg Ben Z.* Magnetized spiral chains of plasmonic ellipsoids for one-way optical waveguides // *Physical review letters.* — 2010. — Vol. 105, no. 23. — P. 233904.

184. *Sihvola Ari H.* Electromagnetic mixing formulas and applications. No. 47. — Iet, 1999.

185. Modelling the optical response of gold nanoparticles / Viktor Myroshnychenko, Jessica Rodriguez-Fernandez, Isabel Pastoriza-Santos et al. // *Chemical Society Reviews.* — 2008. — Vol. 37, no. 9. — Pp. 1792–1805.

186. Plasmonic films can easily be better: rules and recipes / Kevin M McPeak, Sriharsha V Jayanti, Stephan JP Kress et al. // *ACS photonics.* — 2015. — Vol. 2, no. 3. — Pp. 326–333.

187. *Gangaraj S. Ali Hassani, Hanson George W., Antezza Mauro.* Robust entanglement with three-dimensional nonreciprocal photonic topological insulators // *Phys. Rev. A.* — 2017. — Jun. — Vol. 95. — P. 063807. — URL: https://link.aps.org/doi/10.1103/PhysRevA.95.063807.

188. *Fuller K. A.* Scattering and absorption cross sections of compounded spheres. I. Theory for external aggregation // *J. Opt. Soc. Am. A.* — 1994. — Dec. — Vol. 11, no. 12. — Pp. 3251–3260. — URL: http://josaa.osa.org/abstract.cfm?URI=josaa-11-12-3251.

189. Higher-order modes of vacuum-clad ultrathin optical fibers / Fam Le Kien, Thomas Busch, Viet Giang Truong, Síle Nic Chormaic // *Phys. Rev. A.* — 2017. — Aug. — Vol. 96. — P. 023835. — URL: https://link.aps.org/doi/10.1103/PhysRevA.96.023835.

190. *Lakhtakia Akhlesh.* Green's functions and Brewster condition for a half-space bounded by an anisotropic impedance plane // *International Journal of Infrared and Millimeter Waves.* — 1992. — Feb. — Vol. 13, no. 2. — Pp. 161–170. — URL: https://doi.org/10.1007/BF01010651.

191. *Mandel Leonard, Wolf Emil.* Optical Coherence and Quantum Optics. — Cambridge University Press, 1995.

192. *Yaghjian A. D.* Electric dyadic Green's functions in the source region // *Proceedings of the IEEE.* — 1980. — Feb. — Vol. 68, no. 2. — Pp. 248–263.

Acknowledgements:

Here I wanted to personally thank everyone, with whom I collaborated during my PhD studies, among them:

- my scientific supervisor Mihail Petrov for helping to develop the topics, all the continuous provided support, motivation, guidance, and shared knowledge on different kinds of subjects;
- Ivan Iorsh, who literally co-supervised my PhD studies, and participated actively in, at least, half of the works presented in this thesis. I would like to thank him especially for an immediate response on any of my questions;
- Alexandra Sheremet, my previous scientific supervisor during my Bachelor's programme, with whom I continued to collaborate during my Master's, and PhD;
- Roman Savelev as a collaborator, expert in nanophotonics, and numerical modelling, who always asked the right questions, and by this provoked a further study of the subject;
- Julien Laurat from Laboratoire Kastler-Brossel, Sorbonne University for hospitality and supervision during my visit;
- Síle Nic Chormaic, Thomas Busch, Emi Nakamura, Fam Le Kien from OIST Graduate University for their endless hospitality during two of my visits in Okinawa, and for their cooperation on research;
- Zarina Sadrieva, for her invaluable help with the paperwork during the PhD defense preparations.

A. Additional materials for Chapter 1

A.1 Expanding the emission rate of a collection of dipole scatterers in terms of Vector Spherical Harmonics

Our primary goal in this appendix is to expand the emission rate in terms of contributions of different Vector Spherical Harmonics (VSH), which have the following explicit form:

$$\mathbf{M}_{j,m}(k,\mathbf{r}) = \begin{pmatrix} 0 \\ \frac{im}{\sin\theta} j_j(kr) Y_{j,m}(\theta,\varphi) \\ -j_j(kr)\frac{\partial Y_{j,m}(\theta,\varphi)}{\partial\theta} \end{pmatrix},$$
$$\mathbf{N}_{j,m}(k,\mathbf{r}) = \frac{1}{kr}\begin{pmatrix} j_j(kr)j(j+1)Y_{j,m}(\theta,\varphi) \\ \frac{\partial(rj_j(kr))}{\partial r}\frac{\partial Y_{j,m}(\theta,\varphi)}{\partial\theta} \\ \frac{\partial(rj_j(kr))}{\partial r}\frac{im}{\sin\theta}Y_{j,m}(\theta,\varphi) \end{pmatrix}. \tag{A.1}$$

We start from the definitions of a period-averaged Poynting vector, electric, and magnetic fields, which read as:

$$P = \lim_{r\to\infty}\int\int\langle\mathbf{S}\rangle\cdot\mathbf{n}_\mathbf{r}\, r^2\, d\Omega, \quad \langle\mathbf{S}\rangle = \frac{c}{8\pi}\mathrm{Re}\left[\mathbf{E}(\mathbf{r},\omega)\times\mathbf{H}^*(\mathbf{r},\omega)\right],$$
$$\mathbf{E}(\mathbf{r},\omega) = \sum_{j=0}^{\infty}\sum_{m=-j}^{+j}\frac{ia_{j,m}}{\sqrt{j(j+1)}}\mathbf{N}^{(1)}_{\mathbf{j},\mathbf{m}}(k,\mathbf{r}) + \frac{ib_{j,m}}{\sqrt{j(j+1)}}\mathbf{M}^{(1)}_{\mathbf{j},\mathbf{m}}(k,\mathbf{r}),$$
$$\mathbf{H}(\mathbf{r},\omega) = \sum_{j=0}^{\infty}\sum_{m=-j}^{+j}\frac{a_{j,m}}{\sqrt{j(j+1)}}\mathbf{M}^{(1)}_{\mathbf{j},\mathbf{m}}(k,\mathbf{r}) + \frac{b_{j,m}}{\sqrt{j(j+1)}}\mathbf{N}^{(1)}_{\mathbf{j},\mathbf{m}}(k,\mathbf{r}). \tag{A.2}$$

When plugging the expressions of $\mathbf{E}(\mathbf{r},\omega), \mathbf{H}(\mathbf{r},\omega)$ into the definition of $\langle\mathbf{S}\rangle$ there are two types of terms appearing: the direct ones (proportional to $a_{j,m}a^*_{j',m'}$, and $b_{j,m}b^*_{j',m'}$), and the cross-terms ($a_{j,m}b^*_{j',m'}$, and $b_{j,m}a^*_{j',m'}$). Let us first look at the direct terms in $\left[\mathbf{E}(\mathbf{r},\omega)\times\mathbf{H}^*(\mathbf{r},\omega)\right]_r$ (it can be shown that the cross terms will give zero contribution to the radiated power):

$$\sum_{j=1}^{\infty}\sum_{m=-j}^{+j}\sum_{j'=1}^{\infty}\sum_{m'=-j'}^{+j'}\left(\frac{ia_{j,m}a^*_{j',m'}}{\sqrt{jj'(j+1)(j'+1)}}\left[\mathbf{N}^{(1)}_{\mathbf{j},\mathbf{m}}(k,\mathbf{r})\times\mathbf{M}^{(1),*}_{\mathbf{j}',\mathbf{m}'}(k,\mathbf{r})\right]_r + \right.$$
$$\left.\frac{ib_{j,m}b^*_{j',m'}}{\sqrt{jj'(j+1)(j'+1)}}\left[\mathbf{M}^{(1)}_{\mathbf{j},\mathbf{m}}(k,\mathbf{r})\times\mathbf{N}^{(1),*}_{\mathbf{j}',\mathbf{m}'}(k,\mathbf{r})\right]_r\right),$$

$$\left[\mathbf{N}^{(1)}_{\mathbf{j},\mathbf{m}}(k,\mathbf{r})\times\mathbf{M}^{(1),*}_{\mathbf{j'},\mathbf{m'}}(k,\mathbf{r})\right]_r=-\frac{\partial(krh^{(1)}_j(kr))}{\partial(kr)}\frac{h^{(1),*}_{j'}(kr)}{kr}\cdot$$
$$\left(\frac{\partial Y_{j,m}(\theta,\varphi)}{\partial\theta}\frac{\partial Y^*_{j',m'}(\theta,\varphi)}{\partial\theta}+\frac{mm'}{\sin^2(\theta)}Y_{j,m}(\theta,\varphi)Y^*_{j',m'}(\theta,\varphi)\right),$$

$$\left[\mathbf{M}^{(1)}_{\mathbf{j},\mathbf{m}}(k,\mathbf{r})\times\mathbf{N}^{(1),*}_{\mathbf{j'},\mathbf{m'}}(k,\mathbf{r})\right]_r=\frac{\partial(krh^{(1),*}_{j'}(kr))}{\partial(kr)}\frac{h^{(1)}_j(kr)}{kr}\cdot$$
$$\left(\frac{\partial Y_{j,m}(\theta,\varphi)}{\partial\theta}\frac{\partial Y^*_{j',m'}(\theta,\varphi)}{\partial\theta}+\frac{mm'}{\sin^2(\theta)}Y_{j,m}(\theta,\varphi)Y^*_{j',m'}(\theta,\varphi)\right), \quad (A.3)$$

With the help of the identity [188]:

$$\int\int\left(\frac{\partial Y_{j,m}(\theta,\varphi)}{\partial\theta}\frac{\partial Y^*_{j',m'}(\theta,\varphi)}{\partial\theta}+\frac{mm'}{\sin^2(\theta)}Y_{j,m}(\theta,\varphi)Y^*_{j',m'}(\theta,\varphi)\right)\cdot$$
$$\sin\theta d\theta d\varphi=j(j+1)\delta_{m,m'}\delta_{j,j'}, \quad (A.4)$$

we can find that:

$$\int\int\left[\mathbf{N}^{(1)}_{\mathbf{j},\mathbf{m}}(k,\mathbf{r})\times\mathbf{M}^{(1),*}_{\mathbf{j'},\mathbf{m'}}(k,\mathbf{r})\right]_r r^2 sin\theta d\theta d\varphi=$$
$$-\frac{\partial(krh^{(1)}_j(kr))}{\partial(kr)}\frac{h^{(1),*}_{j'}(kr)}{kr}j(j+1)r^2\delta_{j,j'}\delta_{m,m'},$$
$$\int\int\left[\mathbf{M}^{(1)}_{\mathbf{j},\mathbf{m}}(k,\mathbf{r})\times\mathbf{N}^{(1),*}_{\mathbf{j'},\mathbf{m'}}(k,\mathbf{r})\right]_r r^2\sin\theta d\theta d\varphi=$$
$$\frac{\partial(krh^{(1),*}_{j'}(kr))}{\partial(kr)}\frac{h^{(1)}_j(kr)}{kr}j(j+1)r^2\delta_{j,j'}\delta_{m,m'}. \quad (A.5)$$

After the integration was done, we can take the limit ($\lim_{r\to\infty}...$), taking into account that $\lim_{kr\to+\infty}\xi^*_j(kr)\xi'_j(kr)=i$ (with $\xi_j(kr)=krh^{(1)}_j(kr)$), we can get rid of the integrals:

$$P=\frac{c}{8\pi}\frac{1}{k^2}\sum_{j=1}^{\infty}\sum_{m=-j}^{+j}\left(|a_{j,m}|^2+|b_{j,m}|^2\right). \quad (A.6)$$

However, one might want to normalize the above expression with respect to the everage power radiated by a single dipole scatterer with dipole moment $\mathbf{d}$: $P_1(t)=\frac{c|\mathbf{d}|^2k^4}{3}$. This brings us to the final result:

$$\overline{\Gamma}=\frac{P}{P_1}=\frac{3}{8\pi}\frac{1}{|\mathbf{d}|^2k^6}\sum_{j=1}^{\infty}\sum_{m=-j}^{+j}\left(|a_{j,m}|^2+|b_{j,m}|^2\right). \quad (A.7)$$

A.2 Case of the atomic chain along the z-axis

As we discussed in the maintext, one is free to choose how exactly to position the system of dipole scatterers in order to perform the multipolar expansion, this will not affect the final results, but will affect how many multipolar orders j one needs to take into account to have a reliable result. As we are studying the emission rates of a linear periodic chain of dipoles, it makes sense to position it so that the center of the chain coincides with the center of the introduced spherical coordinate system. We will also consider that the total number of dipoles N is even, but this can be easily generalized for the N-odd case.

Moreover, we will align the chain along the z-direction, and as we will show later, that will reduce the number of VSHs needed to be taken into account significantly. In this set-up the spherical coordinates of a given dipole n are given by:

$$\begin{aligned} r_n &= \left((n-1) - \frac{N-1}{2}\right)\Delta z, \\ \theta_n &= \begin{cases} 0, & \text{for } z > 0, \\ \pi, & \text{for } z < 0, \end{cases} \\ \varphi_n &= 0, \end{aligned} \tag{A.8}$$

where we were free to chose any fixed value for φ_n as all dipoles are on the z-axis, where φ-coordinate is undefined. The dipole moments for the eigenmodes of interest are trasverse to the chain axis, so we can set them to be parallel to the x-axis (θ-axis in the spherical coordinates). This means that we care only about θ components of VSHs. From the form of VSHs one can see that as all dipoles are located on the z-axis, a special care needed with the term $Y_{j,m}(\theta,\varphi)/\sin(\theta)$ appearing for $b_{j,m}$ coefficients. Recalling that $Y_{j,m} \sim P_n^m(\cos\theta)\sin^{|m|}\theta$, we can say that for the θ's considered only the coefficients $b_{j,+1}, b_{j,-1}$ are non-zero.

Similarly, for coefficients $a_{j,m}$ we inspect the angular part:

$$\begin{aligned} \left.\frac{\partial Y_{j,-m}(\theta,\varphi)}{\partial\theta}\right|_{\substack{\theta=0(\pi)\\ \varphi=0}} = \\ \frac{1}{2}\Big(Y_{j,-m+1}(0(\pi),0)\sqrt{(j+m)(j-m+1)} - \\ Y_{j,-m-1}(0(\pi),0)\sqrt{(j-m)(j+m+1)}\Big). \end{aligned}$$

From the above one can see that the only coefficints of relevance are, again, the ones with $|m| = \pm 1$: $a_{j,+1}, a_{j,-1}$.

Below we also provide helpful relations for the spherical harmonics, and their derivatives with respect to θ:

$$\begin{aligned}
\left.\frac{Y_{j,\pm1}(\theta,\varphi)}{\sin\theta}\right|_{\substack{\theta=0\\ \varphi=0}} &= \mp\frac{1}{2}\sqrt{\frac{2j+1}{4\pi}}\sqrt{j(j+1)},\\
\left.\frac{Y_{j,\pm1}(\theta,\varphi)}{\sin\theta}\right|_{\substack{\theta=\pi\\ \varphi=0}} &= \pm(-1)^j\frac{1}{2}\sqrt{\frac{2j+1}{4\pi}}\sqrt{j(j+1)},\\
\left.\frac{\partial Y_{j,\pm1}(\theta,\varphi)}{\partial\theta}\right|_{\substack{\theta=0\\ \varphi=0}} &= \mp\frac{1}{2}\sqrt{\frac{2j+1}{4\pi}}\sqrt{j(j+1)},\\
\left.\frac{\partial Y_{j,\pm1}(\theta,\varphi)}{\partial\theta}\right|_{\substack{\theta=\pi\\ \varphi=0}} &= \mp(-1)^j\frac{1}{2}\sqrt{\frac{2j+1}{4\pi}}\sqrt{j(j+1)}.
\end{aligned} \tag{A.9}$$

A.3 Description of the fundamental guided mode

Following the [80; 104; 189] papers we define the field functions for the modes of a waveguide with a circular cross-section in the following way:

$$\boldsymbol{\varepsilon}^{(f,l,p)} = \boldsymbol{e}_{\rho}\varepsilon_{\rho} + \boldsymbol{e}_{\varphi}\varepsilon_{\varphi} + \boldsymbol{e}_{z}\varepsilon_{z}, \tag{A.10}$$

where index $f = \pm$ defines the direction of propagation, l - azimuthal mode order or orbital momentum of the mode, $p = \pm$ defines the direction of the field vector rotation, $\mathbf{e_j}$ are the unit vectors along the corresponding directions, ε_j are the scalar functions of the corresponding field components, we will define them later.

There are two fundamental bases in which one can define the field functions: quasicircularly, and quasilinearly polarized:

$$\begin{aligned}
\mathbf{E}^{(\mathbf{f},\mathbf{l},\mathbf{p})} &= \boldsymbol{\varepsilon}^{(f,l,p)}e^{if\beta z+ilp\varphi},\\
\mathbf{E}^{(\mathbf{f},\mathbf{l},\mathbf{p},\varphi_0)} &= \frac{1}{\sqrt{2}}\left(\mathbf{E}^{(\mathbf{f},\mathbf{l},+1)}e^{-i\varphi_0} + \mathbf{E}^{(\mathbf{f},\mathbf{l},-1)}e^{+i\varphi_0}\right),
\end{aligned} \tag{A.11}$$

where β is a propagation constant (wavenumber along the waveguide), φ_0 parameter defines the symmetry axis of the electric field strength of quasilinearly polarized modes, as light intensity for these modes, unlike for the quasicircular ones, loses a complete cylindrical symmetry. The propagation constant of a particular guided mode can be found from the

following equation:

$$\left[\frac{J_l'(h\rho_c)}{haJ_l(h\rho_c)}+\frac{K_l'(q\rho_c)}{q\rho_c K_l(q\rho_c)}\right]\left[\frac{n_1^2 J_l'(q\rho_c)}{h\rho_c J_l(h\rho_c)}+\frac{n_2^2 K_l'(q\rho_c)}{q\rho_c K_l(q\rho_c)}\right]= l^2\left(\frac{1}{h^2\rho_c^2}+\frac{1}{q^2\rho_c^2}\right)\frac{\beta^2}{k^2}, \quad \text{(A.12)}$$

where $J_l(x), K_l(x)$ are the Bessel, and modified Bessel functions, respectively, $h = \sqrt{n_1^2 k^2 - \beta^2}, q = \sqrt{\beta^2 - n_2^2 k^2}$ with n_1, n_2 being refractive indeces inside, and outside of the waveguide, $k = \omega/c$ - vacuum wavenumber.

The modes with $l = 0$ are either TE or TM modes, while $l \neq 0$ modes have a hybrid nature (HE, EH modes), which means that, generaly, all three field components are non-zero for such modes. It turns out that for a dielectric waveguide the fundamental guided mode HE_{11} is of hybrid nature. As we study the scattering of a single photon from this fundamental mode in the maintext, we will provide explicit expressions for the field functions only for this mode. For $\rho < \rho_c$ they read as:

$$\begin{aligned}
\varepsilon_\rho &= iA\frac{q}{h}\frac{K_1(q\rho_c)}{J_1(h\rho_c)}\left((1-s)J_0(h\rho)-(1+s)J_2(h\rho)\right),\\
\varepsilon_\varphi &= -A\frac{q}{h}\frac{K_1(q\rho_c)}{J_1(h\rho_c)}\left((1-s)J_0(h\rho)+(1+s)J_2(h\rho)\right),\\
\varepsilon_z &= A\frac{2q}{h}\frac{K_1(q\rho_c)}{J_1(h\rho_c)}J_1(h\rho),
\end{aligned} \quad \text{(A.13)}$$

while for $\rho \geqslant \rho_c$:

$$\begin{aligned}
\varepsilon_\rho &= iA\left((1-s)K_0(q\rho)+(1+s)K_2(q\rho)\right),\\
\varepsilon_\varphi &= -A\left((1-s)K_0(q\rho)-(1+s)K_2(q\rho)\right),\\
\varepsilon_z &= A\frac{2q}{h}K_1(q\rho),
\end{aligned} \quad \text{(A.14)}$$

where A is a normalization constant, which is defined through the condition $\int_0^{2\pi} d\varphi \int_0^{+\infty} n^2(\rho)|\boldsymbol{\varepsilon}|\rho d\rho = 1$. The parameter s is defined as:

$$s = \frac{h^{-2}\rho_c^{-2}+q^{-2}\rho_c^{-2}}{J_1'(h\rho_c)/h\rho_c J_1(h\rho_c)+K_1'(q\rho_c)/q\rho_c K_1(q\rho_c)}. \quad \text{(A.15)}$$

Expressions for field functions for other guided modes can be found in Ref. [189].

A.4 Green's tensor of a circular waveguide

The classical electromagnetic Green's tensor for the system under study can be found from the vector Helmholtz equation:

$$\left[-\frac{\omega^2}{c^2}\varepsilon(\mathbf{r},\omega) + \nabla\times\nabla\times\right]\mathbf{G}(\mathbf{r},\mathbf{r}',\omega) = \mathbf{I}\delta(\mathbf{r}-\mathbf{r}'), \tag{A.16}$$

where $\varepsilon(\mathbf{r},\omega)$ is the complex dielectric permittivity, and $\mathbf{I}$ is the unit 3×3 matrix (rank-2 tensor). In the maintext we consider a dielectic cylindrical waveguide of a radius ρ_c, and dielectric permittivity ε, which is assumed to be constant inside the cylindrical waveguide. To find the solution of the equation above, we first apply the scattering superposition method [159;179] that allows to expand the total Green's tensor into a sum of the homogeneous, and inhomogeneous parts:

$$\mathbf{G}(\mathbf{r},\mathbf{r}',\omega) = \mathbf{G}_0(\mathbf{r},\mathbf{r}',\omega) + \mathbf{G}_s(\mathbf{r},\mathbf{r}',\omega). \tag{A.17}$$

The case of interest for us is when both source, and field points $\mathbf{r},\mathbf{r}'$ are outside the cylindrical waveguide. For this case the homogeneous term is non-zero, and it describes the field that is directly generated at the point $\mathbf{r}$ by the source placed at the point $\mathbf{r}'$, and this term is present even if there is no waveguide. This term can be found analytically from the Green's tensor written in Cartesian coordinates by making use of the transformation from Cartesian to cylindrical coordinate system $\mathbf{S}(\varphi)\mathbf{G}_0^{\text{Cart}}(\mathbf{r},\mathbf{r}',\omega)\mathbf{S}^T(\varphi')$, where $\mathbf{G}_0^{\text{Cart}}$ is given by the following analytic expression [2]:

$$\mathbf{G}_0^{\text{Cart}}(\mathbf{r},\mathbf{r}',\omega) = \left(\mathbf{I} + \frac{1}{k^2}\nabla\otimes\nabla\right) G_0(\mathbf{r},\mathbf{r}',\omega), \tag{A.18}$$

here $G_0(\mathbf{r},\mathbf{r}',\omega)$ is the scalar Green's function, which is the solution to the scalar Helmholtz equation.

The scattering part of the Green's tensor can be constructed by exploiting the integral representation of the homogeneous part. In order to obtain this representation we need apply the method of Vector Wave Functions (VWF), which is explained in details in Ref. [159;179]. However, below we will only describe the basic idea, and provide the final answer. In order to find the solution of the vector Helmholtz equation (A.16), we can first look at the solution to a scalar Helmholtz equation in the cylindrical coordinate system that is given by:

$$\begin{aligned}&\nabla^2\varphi(\mathbf{k},\mathbf{r}) + k^2\varphi(\mathbf{k},\mathbf{r}) = 0,\\ &\varphi_n(k_z,\mathbf{r}) = J_n(k_\rho\rho)e^{in\theta+ik_z z},\end{aligned} \tag{A.19}$$

here $\mathbf{r} = (\rho,\theta,z)$ is a vector of cylindrical coordinates, $J_n(x)$ is the Bessel function of the first kind, and k_ρ, k_z are the projections of the wavevector $\mathbf{k}$ onto the corresponding directions.

The solution of the vector equation may be written in terms of the following vector wavefunctions (VWFs):

$$\begin{aligned} \mathbf{M}_n(k_z,\mathbf{r}) &= \nabla \times [\varphi_n(k_z,\mathbf{r})\mathbf{e_z}], \\ \mathbf{N}_n(k_z,\mathbf{r}) &= \frac{1}{k}\nabla \times \mathbf{M}_n(k_z,\mathbf{r}), \end{aligned} \tag{A.20}$$

where $\mathbf{e_z}$ is called the pilot vector, it is just a unit vector pointing in the z direction in this case. These VWFs $\mathbf{M_n}(k_z,\mathbf{r})$, $\mathbf{N_n}(k_z,\mathbf{r})$ correspond to transverse electric/magnetic (TE/TM) modes of the field.

It is possible to demonstrate [159] that the homogeneous part of the Green's function can also be represented in terms of these VWFs, and this expansion has the following form:

$$\mathbf{G}_0(\mathbf{r},\mathbf{r}',\omega) = -\frac{\mathbf{e}_\rho\mathbf{e}_\rho}{k_0^2}\delta(\mathbf{r}-\mathbf{r}') + \frac{i}{8\pi}\sum_{n=-\infty}^{\infty}\int_{-\infty}^{\infty}\frac{dk_z}{k_{0\rho}^2}\mathbf{F}_n(k_z,\mathbf{r},\mathbf{r}'), \tag{A.21}$$

where the $\mathbf{F}_n(k_z,\mathbf{r},\mathbf{s})$ function is given by:

$$\mathbf{F}_n(k_z,\mathbf{r},\mathbf{s}) = \begin{cases} \mathbf{M}_n^{(1)}(k_z,\mathbf{r})\overline{\mathbf{M}}_n(k_z,\mathbf{r}') + \mathbf{N}_n^{(1)}(k_z,\mathbf{r})\overline{\mathbf{N}}_n(k_z,\mathbf{r}'), \\ \mathbf{M}_n(k_z,\mathbf{r})\overline{\mathbf{M}}_n^{(1)}(k_z,\mathbf{r}') + \mathbf{N}_n(k_z,\mathbf{r})\overline{\mathbf{N}}_n^{(1)}(k_z,\mathbf{r}'). \end{cases} \tag{A.22}$$

In the above the first line is used for the case $\rho_r > \rho_{r'}$, while the second one is for $\rho_r < \rho_{r'}$, and $k_0 = \omega/c$ is the vacuum wavenumber, $k_{0\rho} = \sqrt{k_0^2 - k_z^2}$ is it's projection onto the $\mathbf{e}_\rho$ direction, and the superscript (1) in VWFs indicates that the Bessel functions of the first kind $J_n(k_\rho\rho)$ should be replaced with the Hankel functions of the first kind $H_n^{(1)}(k_\rho\rho)$, as the latter corresponds to the out-going wave, satisfying the Sommerfeld radiation condition. Below we

provide the explicit expressions for WVFs:

$$\begin{aligned}
\mathbf{M}_n(k_z,\mathbf{r}) &= \begin{pmatrix} \frac{in}{\rho} J_n(k_{0\rho}\rho) \\ -k_{0\rho}(J_n(k_{0\rho}\rho))' \\ 0 \end{pmatrix} e^{in\theta+ik_z z}, \\
\mathbf{N}_n(k_z,\mathbf{r}) &= \begin{pmatrix} \frac{ik_z k_{0\rho}}{k}(J_n(k_{0\rho}\rho))' \\ -\frac{nk_z}{\rho k} J_n(k_{0\rho}\rho) \\ \frac{k_{0\rho}^2}{k} J_n(k_{0\rho}\rho) \end{pmatrix} e^{in\theta+ik_z z} \\
\overline{\mathbf{M}}_n(k_z,\mathbf{r}') &= \begin{pmatrix} -\frac{in}{\rho'} J_n(k_{0\rho}\rho') \\ -k_{0\rho}(J_n(k_{0\rho}\rho'))' \\ 0 \end{pmatrix}^T e^{-in\theta'-ik_z z'}, \\
\overline{\mathbf{N}}_n(k_z,\mathbf{r}') &= \begin{pmatrix} -\frac{ik_z k_{0\rho}}{k}(J_n(k_{0\rho}\rho'))' \\ -\frac{nk_z}{\rho' k} J_n(k_{0\rho}\rho') \\ \frac{k_{0\rho}^2}{k} J_n(k_{0\rho}\rho') \end{pmatrix}^T e^{-in\theta'-ik_z z'}
\end{aligned} \tag{A.23}$$

where $J_n(k_\rho\rho)'$ denotes the derivative of the expression with respect to the dimensionless argument $k_\rho\rho$.

Now with the help of the integral representation for the homogeneous part of the Green's tensor, we can construct the scattering term $\mathbf{G}_s(\mathbf{r},\mathbf{r}',\omega)$ in a similar way. Let us label the medium outside the dielectric waveguide as 1, and the medium inside as 2. An exact form of the Green's tensor depends on whether the source point $\mathbf{r}'$ is inside or outside the waveguide. As soon as we are interested in a situation when both source, and field points are outside the structure (atoms in the maintext are in the vicinity of a waveguide), and in the latter we consider only the second case. Therefore, the total Green's tensor can be written as:

$$\begin{cases} \mathbf{G}^{11}(\mathbf{r},\mathbf{r}',\omega) = \mathbf{G}_0^{11}(\mathbf{r},\mathbf{r}',\omega) + \mathbf{G}_s^{11}(\mathbf{r},\mathbf{r}',\omega), \\ \mathbf{G}^{21}(\mathbf{r},\mathbf{r}',\omega) = \mathbf{G}_s^{21}(\mathbf{r},\mathbf{r}',\omega), \end{cases} \tag{A.24}$$

here the two superscripts denote the positions of the field, and the source points, respectively. The two scattering parts of the Green's tensor can be written as:

$$\begin{aligned}
\mathbf{G}_s^{11}(\mathbf{r},\mathbf{r}',\omega) &= \frac{i}{8\pi} \sum_{n=-\infty}^{\infty} \int_{-\infty}^{\infty} \frac{dk_z}{k_{\rho 1}^2} \mathbf{F}_{\mathbf{M};n,1}^{11(1)}(k_z,\mathbf{r}) \overline{\mathbf{M}}_{n,1}^{(1)}(k_z,\mathbf{r}') \\
&+ \mathbf{F}_{\mathbf{N};n,1}^{11(1)}(k_z,\mathbf{r}) \overline{\mathbf{N}}_{n,1}^{(1)}(k_z,\mathbf{r}'), \\
\mathbf{F}_{\mathbf{M};n,1}^{11(1)}(k_z,\mathbf{r}) &= R_{MM}^{11} \mathbf{M}_{n,1}^{(1)}(k_z,\mathbf{r}) + R_{NM}^{11} \mathbf{N}_{n,1}^{(1)}(k_z,\mathbf{r}), \\
\mathbf{F}_{\mathbf{N};n,1}^{11(1)}(k_z,\mathbf{r}) &= R_{MN}^{11} \mathbf{M}_{n,1}^{(1)}(k_z,\mathbf{r}) + R_{NN}^{11} \mathbf{N}_{n,1}^{(1)}(k_z,\mathbf{r}).
\end{aligned} \tag{A.25}$$

$$\begin{aligned}
\mathbf{G}_s^{21}(\mathbf{r},\mathbf{r}',\omega) &= \frac{i}{8\pi}\sum_{n=-\infty}^{\infty}\int_{-\infty}^{\infty}\frac{dk_z}{k_{\rho 1}^2}\mathbf{F}_{\mathbf{M};n,2}^{21}(k_z,\mathbf{r})\overline{\mathbf{M}}_{n,1}^{(1)}(k_z,\mathbf{r}') \\
&+ \mathbf{F}_{\mathbf{N};n,1}^{21}(k_z,\mathbf{r})\overline{\mathbf{N}}_{n,1}^{(1)}(k_z,\mathbf{r}'), \\
\mathbf{F}_{\mathbf{M};n,2}^{21}(k_z,\mathbf{r}) &= R_{MM}^{21}\mathbf{M}_{n,2}(k_z,\mathbf{r}) + R_{NM}^{21}\mathbf{N}_{n,2}(k_z,\mathbf{r}), \\
\mathbf{F}_{\mathbf{N};n,2}^{21}(k_z,\mathbf{r}) &= R_{MN}^{21}\mathbf{M}_{n,2}(k_z,\mathbf{r}) + R_{NN}^{21}\mathbf{N}_{n,2}(k_z,\mathbf{r}),
\end{aligned} \tag{A.26}$$

here the Fresnel coefficients R_{AB}^{ij} are introduced, and the second subscript in the VWFs identifies that wavenumber k, and the corresponding projection of the wavevector k_ρ have to be replaced with their values inside the corresponding medium $k_i = \sqrt{\varepsilon_i(\mathbf{r},\omega)}k_0$, $k_{\rho i} = \sqrt{k_i^2 - k_z^2}$. We want to notice that unlike the case of the homogeneous term (vacuum Green's tensor), here we have cross-terms - products of $\mathbf{M}$ and $\mathbf{N}$ VWFs, which is due to the fact that the normal modes in our case have a hybrid nature. It simply means that a cylindrical TE(TM) mode can be converted into a cylindrical TM(TE) after either reflection or transmission through the structure.

Now the only thing we need to find are the Fresnel coefficients, which can be derived by imposing the boundary conditions on the Green's tensor at the waveguide surface:

$$\begin{cases}
\mathbf{e}_\rho \times [\mathbf{G}^{11}(\mathbf{r},\mathbf{r}',\omega) - \mathbf{G}^{21}(\mathbf{r},\mathbf{r}',\omega)]|_{\rho_r=\rho_c} = 0, \\
\mathbf{e}_\rho \times \nabla_{\mathbf{r}} \times [\mathbf{G}^{11}(\mathbf{r},\mathbf{r}',\omega) - \mathbf{G}^{21}(\mathbf{r},\mathbf{r}',\omega)]|_{\rho_r=\rho_c} = 0.
\end{cases} \tag{A.27}$$

By solving the above system of algebraic equations, we can find the explicit expressions for the Fresnel coefficients R_{AB}^{ij} and, finally, construct the scattering part of the Green's tensor $\mathbf{G}_s(\mathbf{r},\mathbf{r}',\omega)$. Below we provide the expressions for the Fresnel coefficients:

$$DT(k_z) = -\left(\frac{1}{k_{\rho 2}^2} - \frac{1}{k_{\rho 1}^2}\right)^2 k_z^2 n^2 + \left(\frac{(J_n(k_{\rho 2}\rho_c))'}{k_{\rho 2} J_n(k_{\rho 2}\rho_c)} - \frac{(H_n^{(1)}(k_{\rho 1}\rho_c))'}{k_{\rho 1} H_n^{(1)}(k_{\rho 1}\rho_c)}\right) \cdot \left(\frac{(J_n(k_{\rho 2}\rho_c))' k_2^2}{k_{\rho 2} J_n(k_{\rho 2}\rho_c)} - \frac{(H_n^{(1)}(k_{\rho 1}\rho_c))' k_1^2}{k_{\rho 1} H_n^{(1)}(k_{\rho 1}\rho_c)}\right) \rho_c^2,$$

$$R_{MM}^{11}(k_z) = \frac{1}{DT(k_z)} \frac{J_n(k_{\rho 1}\rho_c)}{H_n^{(1)}(k_{\rho 1}\rho_c)} \left[\left(\frac{1}{k_{\rho 2}^2} - \frac{1}{k_{\rho 1}^2}\right)^2 k_z^2 n^2 - \left(\frac{(J_n(k_{\rho 2}\rho_c))'}{k_{\rho 2} J_n(k_{\rho 2}\rho_c)} - \frac{(J_n(k_{\rho 1}\rho_c))'}{k_{\rho 1} J_n(k_{\rho 1}\rho_c)}\right) \left(\frac{(J_n(k_{\rho 2}\rho_c))' k_2^2}{k_{\rho 2} J_n(k_{\rho 2}\rho_c)} - \frac{(H_n^{(1)}(k_{\rho 1}\rho_c))' k_1^2}{k_{\rho 1} H_n^{(1)}(k_{\rho 1}\rho_c)}\right) \rho_c^2\right],$$

$$R_{NM}^{11}(k_z) = \frac{J_n(k_{\rho 1}\rho_c)}{H_n^{(1)}(k_{\rho 1}\rho_c)} \frac{1}{k_{\rho 1}} \left(\frac{1}{k_{\rho 1}^2} - \frac{1}{k_{\rho 2}^2}\right) \cdot \left(\frac{(J_n(k_{\rho 1}\rho_c))'}{J_n(k_{\rho 1}\rho_c)} - \frac{(H_n^{(1)}(k_{\rho 1}\rho_c))'}{H_n^{(1)}(k_{\rho 1}\rho_c)}\right) \frac{k_1 k_z n \rho_c}{DT(k_z)},$$

$$R_{MN}^{11}(k_z) = R_{NM}^{11},$$

$$R_{NN}^{11}(k_z) = \frac{1}{DT(k_z)} \frac{J_n(k_{\rho 1}\rho_c)}{H_n^{(1)}(k_{\rho 1}\rho_c)} \left[\left(\frac{1}{k_{\rho 2}^2} - \frac{1}{k_{\rho 1}^2}\right)^2 k_z^2 n^2 - \left(\frac{(J_n(k_{\rho 2}\rho_c))'}{k_{\rho 2} J_n(k_{\rho 2}\rho_c)} - \frac{(H_n^{(1)}(k_{\rho 1}\rho_c))'}{k_{\rho 1} H_n^{(1)}(k_{\rho 1}\rho_c)}\right) \left(\frac{(J_n(k_{\rho_2}\rho_c))' k_2^2}{k_{\rho 2} J_n(k_{\rho 2}\rho_c)} - \frac{(J_n(k_{\rho 1}\rho_c))' k_1^2}{k_{\rho 1} J_n(k_{\rho 1}\rho_c)}\right) \rho_c^2\right]. \tag{A.28}$$

Note that the integral representations in Eq. (A.26) include integration over the whole range of k_z values, which means that it takes into account all present modes: radiation (leaky), guided, near-field modes. Of special interest are the guided modes, and mathematically their contribution is in the poles of the Fresnel coefficients, which lie on the real k_z axis (for the lossless dielectric medium) between k_0 (vacuum wavenumber), and k_2 (dielectric wavenumber). In a single-mode regime, when there is only the fundamental guided mode in a waveguide, and one can extract it's contribution to the Green's tensor easily. In order to do that, one needs to take the common denominator of all of the Fresnel coefficients, and expand it near the corresponding $\beta_{\mathrm{HE}_{11}}$ point up to the first order: $DT(k_z) \approx \left.\frac{\partial DT(k_z)}{\partial k_z}\right|_{k_z=\beta_{\mathrm{HE}_{11}}} (k_z - \beta_{\mathrm{HE}_{11}}) + \ldots$. Then one needs to calculate the pole contribution to the integral by using the residue theorem, provided the value of $\beta_{\mathrm{HE}_{11}}$ is found from the dispersion relation from Eq. (A.12).

B. Additional materials for Chapter 2

B.1 Derivation of the effective Schrodinger equation from the master equation

Here we want to prove that for the problem considered (dynamics of a single excitation in an ensemble of coupled two-level systems) we can use the Schrodinger equation with the effective Hamiltonian (Eq. (2.3)) rather than use the full master equation on a density matrix. The latter for the considered case (dipole-dipole coupled atoms with asymmetric interaction) has the following form [165; 187]:

$$\begin{aligned}
\dot{\hat{\rho}}_s(t) &= i\sum_k \Delta\omega_k \left[\hat{\sigma}_k^+\hat{\sigma}_k^-, \hat{\rho}_s(t)\right] + \hat{\mathcal{L}}\hat{\rho}_s(t), \\
\hat{\mathcal{L}}\hat{\rho}_s(t) &= \sum_k \frac{\Gamma_{kk}}{2}\left(2\hat{\sigma}_k^-\hat{\rho}_s(t)\hat{\sigma}_k^+ - \hat{\sigma}_k^+\hat{\sigma}_k^-\hat{\rho}_s(t) - \hat{\rho}_s(t)\hat{\sigma}_k^+\hat{\sigma}_k^-\right) + \\
&\sum_{k,l}^{k\neq l} \frac{\Gamma_{kl}}{2}\left(\left[\hat{\sigma}_l^-\hat{\rho}_s(t), \hat{\sigma}_k^+\right] + \left[\hat{\sigma}_k^-, \hat{\rho}_s(t)\hat{\sigma}_l^+\right]\right) + \\
&\sum_{k,l}^{k\neq l} \delta_{kl}\left(-i\left[\hat{\sigma}_l^-\hat{\rho}_s(t), \hat{\sigma}_k^+\right] + i\left[\hat{\sigma}_k^-, \hat{\rho}_s(t)\hat{\sigma}_l^+\right]\right),
\end{aligned} \tag{B.1}$$

where $\Delta\omega_k = -\omega_{0,k} + \delta_{kk}$, with $\omega_{0,k}$ - transition frequency for atom k, $\hat{\mathcal{L}}$ is the Lindblad superoperator accounting for the dissipative dynamics, and $\delta_{ij} = 4\pi k_{0,j}^2 \mathrm{Re}\left[\mathbf{d_i^\dagger G}(\mathbf{r_0}, \mathbf{r_0}, \omega_{0,j})\mathbf{d_j}\right]/\hbar$, $\Gamma_{ij} = 8\pi k_{0,j}^2 \mathrm{Im}\left[\mathbf{d_i^\dagger G}(\mathbf{r_0}, \mathbf{r_0}, \omega_{0,j})\mathbf{d_j}\right]/\hbar$, which are responsible for the coherent, and dissipative coupling of atoms.

Our primal interest is to find the probability that each atom is excited at time t, given by the respective component of the density matrix $\langle e_k|\hat{\rho}_s(t)|e_k\rangle = \rho_{k,k}(t)$, where $|e_k\rangle = |e_k\rangle|g\rangle^{\otimes N-1}$. Therefore, by calculating

the average value from the operator equation above, one finds that:

$$\dot{\rho}_{m,m}(t) = -\Gamma_{m,m}\rho_{m,m}(t) + \sum_{k\neq m}\Gamma_{k,k}\rho_{mk,mk}(t) + \sum_{k,l;k\neq l}^{k\neq m,l\neq m}\left(-i\delta_{k,l} + \frac{\Gamma_{k,l}}{2}\right)\rho_{ml,mk}(t) + \sum_{l,l\neq m}\left(i\delta_{m,l} - \frac{\Gamma_{m,l}}{2}\right)\rho_{l,m}(t) + \sum_{k,l;k\neq l}^{k\neq m,l\neq m}\left(i\delta_{k,l} + \frac{\Gamma_{k,l}}{2}\right)\rho_{mk,ml}(t) + \sum_{l,l\neq m}\left(-i\delta_{m,l} - \frac{\Gamma_{m,l}}{2}\right)\rho_{m,l}(t), \quad \text{(B.2)}$$

where double subscript means that two atoms out of N are excited $\rho_{ml,mk} = \langle e_m|\langle e_l|\langle g|^{\otimes N-2}\hat{\rho}_s(t)|g\rangle^{\otimes N-2}|e_l\rangle|e_m\rangle$, and due to the definition, the order in each pair of indeces does not matter $\rho_{mk,ml} = \rho_{km,ml} = \rho_{mk,lm} = \rho_{km,lm}$. One can see that the second, the third, and the fifth terms in the righthand side are expressing how the states from two-excitation domain interact with the states in a single excitation domain. However, as we want to study single excitation transport we can ignore these terms, and we end up with the following reduced system:

$$\dot{\rho}_{m,m}(t) = -\Gamma_{m,m}\rho_{m,m}(t) + \sum_{l,l\neq m}\left(i\delta_{m,l} - \frac{\Gamma_{m,l}}{2}\right)\rho_{l,m}(t) + \sum_{l,l\neq m}\left(-i\delta_{m,l} - \frac{\Gamma_{m,l}}{2}\right)\rho_{m,l}(t). \quad \text{(B.3)}$$

We can now make the following formal substitution $\rho_{l,m}(t) = C_l(t)C_m^*(t)$, plug it in the equation above, and gather together the terms with common multipliers:

$$\mathrm{Re}\left[C_m^*(t)\left(\dot{C}_m(t) + \frac{\Gamma_{m,m}}{2}C_m(t) - \sum_{l,l\neq m}C_l(t)\left(i\delta_{m,l} - \frac{\Gamma_{m,l}}{2}\right)\right)\right] = 0. \quad \text{(B.4)}$$

It is easily seen that the expression in round brackets should always be equal to zero, even if the corresponding $C_m^*(t) = 0$ for a given m. One can immediately identify that the expression in the round brackets is identical to a Schrodinger equation that can be obtained with the effective Hamiltonian.

Here, an important note has to be made. Even though the substitution $\rho_{l,m}(t) = C_l(t)C_m^*(t)$ looks like a standard expression of a density matrix through the components of a state vector $\rho(t) = |\Psi(t)\rangle\langle\Psi(t)|$, in our problem, strictly speaking, we do not have a state vector for the full Hilbert space of the problem. This is why we called this substitution formal.

Let us proceed with a system consisting of just a pair of asymmetrically coupled two-level atoms, one of which is excited initially. One can formulate

this in terms of a density matrix as:

$$\dot{\boldsymbol{\rho}}(t) = \mathbf{M}_{\rho} \cdot \boldsymbol{\rho}(t),$$
$$\mathbf{M}_{\rho} = \begin{pmatrix} -\Gamma & G_{12}^{*} & G_{12} & 0 \\ G_{21}^{*} & -\Gamma & 0 & G_{12} \\ G_{21} & 0 & -\Gamma_{e} & G_{12}^{*} \\ 0 & G_{21} & G_{21}^{*} & -\Gamma \end{pmatrix}, \boldsymbol{\rho}(t) = \begin{pmatrix} \rho_{1,1}(t) \\ \rho_{1,2}(t) \\ \rho_{2,1}(t) \\ \rho_{2,2}(t) \end{pmatrix}, \tag{B.5}$$

where in the above we assumed that both atoms have equal emission rates $\Gamma_{11} = \Gamma_{22} = \Gamma$, and Lamb-shifts $\delta_{11} = \delta_{22}$, and $G_{ij} = i\delta_{ij} - \Gamma_{ij}/2$. All we need to do is to find the matrix exponent $\exp(\mathbf{M}_{\rho} \cdot t)$, and then multiply it by initial condition vector $\boldsymbol{\rho}(t = 0)$ from the right. However, as we assume that initially atom 1 is excited $\rho_{1,1}(t = 0) = 1$, we will provide below only the first column of the matrix exponent:

$$[\exp(\mathbf{M}_{\rho} \cdot t)]_{:,1} = e^{-\Gamma t} \begin{pmatrix} \cosh(\sqrt{G_{12}G_{21}}t)\cosh(\sqrt{G_{12}^{*}G_{21}^{*}}t) \\ \sqrt{\frac{G_{21}^{*}}{G_{12}^{*}}}\cosh(\sqrt{G_{12}G_{21}}t)\sinh(\sqrt{G_{12}^{*}G_{21}^{*}}) \\ \sqrt{\frac{G_{21}}{G_{12}}}\cosh(\sqrt{G_{12}^{*}G_{21}^{*}}t)\sinh(\sqrt{G_{12}G_{21}}t) \\ \sqrt{\frac{G_{21}}{G_{12}}\frac{G_{21}^{*}}{G_{12}^{*}}}\sinh(\sqrt{G_{12}G_{21}}t)\sinh(\sqrt{G_{12}G_{21}}t) \end{pmatrix}. \tag{B.6}$$

Now we can write a similar system, but in terms of probability amplitudes for each atom to be excited:

$$\dot{\mathbf{C}}(t) = \mathbf{M}_{\mathbf{C}} \cdot \mathbf{C}(t),$$
$$\mathbf{M}_{\mathbf{C}} = \begin{pmatrix} -\Gamma/2 & G_{12} \\ G_{21} & \Gamma/2 \end{pmatrix}, \mathbf{C}(t) = \begin{pmatrix} C_1(t) \\ C_2(t) \end{pmatrix}, \tag{B.7}$$

and the matrix exponent for this system is equal to:

$$\exp(\mathbf{M}_{\mathbf{C}}t) = e^{-\Gamma t/2} \begin{pmatrix} \cosh(\sqrt{G_{12}G_{21}}t) & \sqrt{\frac{G_{12}}{G_{21}}}\sinh(\sqrt{G_{12}G_{21}}t) \\ \sqrt{\frac{G_{21}}{G_{12}}}\sinh(\sqrt{G_{12}G_{21}}t) & \cosh(\sqrt{G_{12}G_{21}}t) \end{pmatrix}. \tag{B.8}$$

One can easily see that the two answers obtained above are identical. Moreover, with the help of the following identities:

$$\begin{aligned} \cosh(X) &= i\sinh(X')\sin(X'') + \cosh(X')\cos(X''), \\ \sinh(X) &= \cosh(X')\cos(X'') + i\cosh(X')\sin(X''), \\ \cosh(X)\cosh(X^{*}) &= \frac{1}{2}\left(\cosh(2X') + \cos(2X'')\right), \\ \sinh(X)\sinh(X^{*}) &= \frac{1}{2}\left(\cosh(2X') - \cos(2X'')\right), \end{aligned} \tag{B.9}$$

with $X = X' + iX''$, one can obtain results presented in the maintext in Chapter 3, where the coupling of two excited states in a single emitter is discussed, as this problem is mathematically equivalent to the case of two interacting two-level atoms in a single excitation domain.

B.2 Chiral collective emission rate

As we mentioned in the maintext (see Eq. (2.10)), the emission rate of a collective state can be found by calculating the following:

$$C_{|\Psi\rangle}(t) = A^2 \begin{pmatrix} e^{-i\psi_1^*} \\ e^{-i\psi_2^*} \\ \dots \\ e^{-i\psi_N^*} \end{pmatrix}^T \begin{pmatrix} e^{i\varphi_{1,1}}F_0(t) & 0 & \dots & 0 \\ e^{i\varphi_{2,1}}F_1(t) & e^{i\varphi_{2,2}}F_0(t) & \dots & 0 \\ \dots & \dots & \dots & \dots \\ e^{i\varphi_{N,1}}F_{N-1}(t) & e^{i\varphi_{N,2}}F_{N-2}(t) & \dots & e^{i\varphi_{N,N}}F_0(t) \end{pmatrix} \begin{pmatrix} e^{i\psi_1} \\ e^{i\psi_2} \\ \dots \\ e^{i\psi_N} \end{pmatrix}, \tag{B.10}$$

here A is the normalization factor assumed to be real, and both $\varphi_{i,j}$ and ψ_j can be complex, in general. Let us define these phases in the following way: $\varphi_{l,k} = (l-k)\varphi \quad (\varphi = \varphi' + i\varphi'')$, and $\psi_j = (j-1)\psi \quad (\psi = \psi' + i\psi'')$. For propagation phases $\varphi_{l,k}$ this corresponds to the case, when emitters are regularly spaced, while the imaginary part of $\varphi_{l,k}$ accounts for the decay of the propagating waveguide mode arising due to the presence material losses. The phases ψ_j entering the state vectors are introduced to compensate for this propagation phases, which will allow for both in-phase, and out-of-phase emission of neighboring emitters. Due to the periodicity of the system, we are able to write that $F_{s-1}(t) = e^{-\Gamma_{\text{tot}}t/2}L_{s-1}^{(-1)}(\Gamma_g(t-(s-1)\tau))\Theta(t-(s-1)\tau)$ as now the retardation time between any two emitters can be written in terms of photon flight time between the neighboring ones τ. Moreover, in this case, the normalization constant A can be readily found: $A^{-2} = e^{\psi''(1-N)}\text{csch}(\psi'')\sinh(N\psi'')$, where $\text{csch}(x)$ and $\sinh(x)$ are cosecant hyperbolic, and sine hyperbolic functions, respectively.

The product can be written as $\mathbf{C}^\dagger\mathbf{U}\mathbf{C}$, where $C_k = e^{i(k-1)\psi}$, $U_{l,k} = A^2 e^{i(l-k)\varphi}F_{l-k}(t)\Theta_{l,k}$, $C_l^\dagger = e^{-i(l-1)\psi^*}$, where $\Theta_{l,k}$ is a discrete analogue of a Heaviside function given by $\Theta_{l,k} = 1$ for $l \geqslant k$, and equal to 0 otherwise. $(\mathbf{U}\mathbf{C})_l = \sum_{k=1}^{l} U_{l,k}C_k = \sum_{k=1}^{l} e^{i(l-k)\varphi}F_{l-k}(t)e^{i(k-1)\psi} = \sum_{k=1}^{l} F_{l-k}(t)e^{ik(\psi-\varphi)}e^{il\varphi-i\psi}$; $\sum_{l=1}^{N} C_l^\dagger(\mathbf{U}\mathbf{C})_l =$

$$\sum_{l=1}^{N} e^{-i(l-1)\psi^*} \sum_{k=1}^{l} F_{l-k}(t) e^{ik(\psi-\varphi)} e^{il\varphi - i\psi} =$$
$$\sum_{l=1}^{N} \sum_{k=1}^{l} e^{i(l-k)(\varphi'-\psi')+2\psi''-(l+k)\psi''-(l-k)\varphi''} F_{l-k}(t).$$

The final general answer can be written as:

$$C_{|\Psi\rangle}(t) = A^2 \sum_{l=1}^{N} \sum_{k=1}^{l} e^{i(l-k)(\varphi'-\psi')+2\psi''-(l+k)\psi''-(l-k)\varphi''} F_{l-k}(t) =$$
$$A^2 \sum_{s=1}^{N} e^{i(s-1)(\varphi'-\psi')-(s-1)\varphi''} e^{2\psi''} \sum_{j=1}^{N-(s-1)} e^{-(s-1)\psi''} e^{-2j\psi''} F_{s-1}(t). \quad \text{(B.11)}$$

Now let us ignore the retardation effects $\tau \to 0$, and expand $e^{-\Gamma_{\rm tot} t/2} L_{s-1}^{(-1)}(\Gamma_g t)$ to the first order in t:

$$e^{-\Gamma_{\rm tot} t/2} L_{s-1}^{(-1)}(\Gamma_g t) = \begin{cases} 1 - \Gamma_{\rm tot} t, & \text{if } s = 1; \\ -\Gamma_g t, & \text{if } s > 1. \end{cases} \quad \text{(B.12)}$$

For the case of complex-valued φ, ψ phases, the form of the expansion looks quite cumbersome. Instead, let us from now on consider that both ψ, and φ are real, while the normalization constant is equal to $A = 1/\sqrt{N}$ (a single excitation is equally distributed between all atoms), and in this case one can obtain:

$$C(t \to 0) \sim 1 + \left[-\frac{\Gamma_{\rm tot}}{2} - \Gamma_g \frac{e^{i\xi} \left(N + e^{iN\xi} - N e^{i\xi} - 1 \right)}{N \left(e^{i\xi} - 1 \right)^2} \right] t \sim$$
$$P(t \to 0) = |C(t \to 0)|^2 \sim 1 - \Gamma^{(0)} t, \quad \text{(B.13)}$$

where $\xi = \varphi' - \psi'$, and the modified spontaneous emission rate at small times is equal to:

$$\Gamma^{(0)} = 2{\rm Re} \left[\frac{\Gamma_{\rm tot}}{2} + \Gamma_g \frac{e^{i\xi} \left(N + e^{iN\xi} - N e^{i\xi} - 1 \right)}{N \left(e^{i\xi} - 1 \right)^2} \right] =$$
$$\Gamma_{\rm tot} + \Gamma_{\rm g} \frac{N + \cos(N\xi) - 1 - N\cos(\xi)}{2N \sin^2(\xi/2)}. \quad \text{(B.14)}$$

It is natural to proceed by considering the two extreme cases: each two neighbouring emitters are emitting photons in- (superradiance), and out of phase (subradiance), which corresponds to $\xi = 2\pi m$, and $\xi = \pi(2m+1)$. For these two cases we can rewrite the expression above as:

$$\Gamma^{(0)} = \begin{cases} \Gamma_{\rm r} + N\Gamma_g, & \text{if } \xi = 2\pi m; \\ \Gamma_{\rm r} + \Gamma_g \dfrac{1 + (-1)^N}{2N}, & \text{if } \xi = \pi(2m+1), \end{cases} \quad \text{(B.15)}$$

which is then discussed in the maintext. Pay attention that for superradiance, and subradiance with N being even the answers are the same as for the symmetric interaction case. However, for odd N subradiant emission into the guided mode is not perfectly suppressed, and the deviation from zero decreases with the system size as $\Gamma_{\rm g}^{(0)} = \Gamma^{(0)} - \Gamma_{\rm r} = \Gamma_{\rm g}/N$.

B.3 The effect of retardation

In the maintext (Chapter 2) as well as in the previous Appendix section we assumed that the retardation time due to the photon time of flight from one emitter to another is negligible. However, one can ask a question of how the answers obtained so far are modified due to this when the system size is so large that the retardation effects can not be ignored?

The way how retardation affects the atom-atom interaction through the electromagnetic field was studied in Ref. [58;59], for instance. One can write the following modification of the system in Eq. (2.1) in a form:

$$\dot{C}_n(t) = -i\Omega C_n(t) + \sum_{m=1}^{n-1} G_{nm} C_n(t - \Delta\tau_{n,m})\Theta(t - \Delta\tau_{n,m}), \tag{B.16}$$

where $\Delta\tau_{nm} = (z_n - z_m)/v_{gr}$ are the flight times for a photon traveling from emitter m to emitter n, and $\Theta(t)$ is a unit step Heaviside function.

Let us proceed with examination of Eq. (B.16) for the first three emitters:

$$\begin{gathered} C_1 = e^{-\Gamma_{\rm tot} t/2}, \\ C_2 = (t - \Delta\tau_{2,1}) G_{21} e^{-\Gamma_{\rm tot}(t-\Delta\tau_{2,1})/2}\Theta(t - \Delta\tau_{2,1}), \\ C_3 = \left(G_{32}G_{21}\frac{(t - \Delta\tau_{3,1})^2}{2} + G_{31}(t - \Delta\tau_{3,1}) \right) e^{-\Gamma_{\rm tot}(t-\Delta\tau_{3,1})/2}\Theta(t - \Delta\tau_{3,1}). \end{gathered} \tag{B.17}$$

One can easily deduce that it has a form quite close to that in the absence of retardation, and, indeed, for the interaction constant of the form $G_{nm} = -\Gamma_g e^{ik^g(z_n - z_m)}$, the answer can be given by:

$$C_N^1(t) = e^{-\Gamma_{\rm tot}(t-\Delta\tau_{N,1})/2 + i\varphi_{N,1}} L_{N-1}^{(-1)}(\Gamma_g(t - \Delta\tau_{N,1}))\Theta(t - \Delta\tau_{N,1}). \tag{B.18}$$

The reason why this answer looks almost the same as Eq. (2.9) is, again, in the fact that the system is unidirectional, and there is no back-reflection. One can consider different ways of how excitation can jump from the first emitter to emitter N, and while it is transferred from one atom to another, it is only allowed to make jumps in one direction. This leads to the fact that any of the

considered pathways has the same length equal to $z_N - z_1$, and, hence, the same propagation time $\Delta\tau_{N,1}$. The term $\Theta(t - \Delta\tau_{N,1})$ appears for the same reason, as from $t = 0$ it takes $\Delta\tau_{N,1}$ time for the photon to reach atom N. We want to note that a similar result was first obtained in Ref. [170], where the authors studied the propagation of photon pulses through a chain of two-level emitters, which were embedded in the topological photonic structure with one-way propagating edge mode.

We mentioned in Appendix B.2 that from Eq. (B.18) one can find how does any state in the single excitation domain evolve. This will involve summation over all pairs of emitters, and the collective behavior will be altered due to the fact that each time the photon emitted by one atom hits another one, the time evolution of the latter will be affected. This can be viewed as the field produced by the first atom plays a role of, roughly speaking, an external driving field for the second one. But one should not make a direct connection here to the external pumping field (a laser field in a coherent state) as it was emitted by another atom spontaneously.

C. Additional materials for Chapter 3

C.1 Green's function of a metasurface

For the derivation of the Green's tensor of a metasurface characterized by a surface conductivity tensor $\sigma(\omega)$, we basically follow the procedure outlined in [190]. It is assumed that the interface lies in the xy-plane with $z = 0$. First, let us introduce useful notations.

For the wavevector of a wave propagating in medium j in the positive or negative direction along z we write:

$$\mathbf{k_{j,\pm}} = \begin{pmatrix} \kappa_x \\ \kappa_y \\ \pm k_{j,z} \end{pmatrix}, \quad \kappa = \sqrt{\kappa_x^2 + \kappa_y^2}, \quad k_{j,z} = \sqrt{k_j^2 - \kappa^2}. \tag{C.1}$$

For TE, and TM modes:

$$\mathbf{t_{j,\pm}} = \frac{1}{\kappa} \begin{pmatrix} -\kappa_y \\ \kappa_x \\ 0 \end{pmatrix}, \quad \mathbf{p_{j,\pm}} = \frac{1}{k_j} \begin{pmatrix} \mp k_{j,z}\kappa_x/\kappa \\ \mp k_{j,z}\kappa_y/\kappa \\ \kappa \end{pmatrix}, \tag{C.2}$$

$$\mathbf{t^{\perp}_{j,\pm}} = \mathbf{e_z} \times \mathbf{t_{j,\pm}} = \frac{1}{\kappa} \begin{pmatrix} -\kappa_x \\ -\kappa_y \\ 0 \end{pmatrix}; \quad \mathbf{p^{\perp}_{j,\pm}} = \mathbf{e_z} \times \mathbf{p_{j,\pm}} = \frac{k_{1,z}}{k_1 \kappa} \begin{pmatrix} \pm\kappa_y \\ \mp\kappa_x \\ 0 \end{pmatrix}, \tag{C.3}$$

$$\begin{gathered} \mathbf{t_{j,\pm}} = -\mathbf{k_{j,\pm}} \times \mathbf{p_{j,\pm}}/k_j, \\ \mathbf{p_{j,\pm}} = +\mathbf{k_{j,\pm}} \times \mathbf{t_{j,\pm}}/k_j, \\ \nabla \times [\mathbf{t_{j,\pm}} e^{i\mathbf{k_{j,\pm}}\mathbf{r}}] = i\mathbf{k_{j,\pm}} \times \mathbf{t_{j,\pm}} e^{i\mathbf{k_{j,\pm}}\mathbf{r}} = ik_j \mathbf{p_{j,\pm}} e^{i\mathbf{k_{j,\pm}}\mathbf{r}}, \\ \nabla \times [\mathbf{p_{j,\pm}} e^{i\mathbf{k_{j,\pm}}\mathbf{r}}] = i\mathbf{k_{j,\pm}} \times \mathbf{p_{j,\pm}} e^{i\mathbf{k_{j,\pm}}\mathbf{r}} = -ik_j \mathbf{t_{j,\pm}} e^{i\mathbf{k_{j,\pm}}\mathbf{r}}. \end{gathered} \tag{C.4}$$

Let us label the upper medium as 1, while the lower one as 2. Below we will consider only the situation, when the source point $\mathbf{r}$ is always in medium 1. According to a superposition principle [159;179], the total Green's function can be decomposed into the free space part and the scattered part, as usual:

$$\mathbf{G^{ij}}(\mathbf{r}, \mathbf{r}', \omega) = \mathbf{G_0}(\mathbf{r}, \mathbf{r}', \omega) + \mathbf{G^{ij}_{sc}}(\mathbf{r}, \mathbf{r}', \omega), \tag{C.5}$$

where $i(j)$ labels the medium in which the field (source) point is located. The relevant Green's tensors are of the form:

$$\begin{aligned}
\mathbf{G_0}(\mathbf{r},\mathbf{r}',\omega) &= -\mathbf{e_z}\mathbf{e_z}\delta(\mathbf{R}) + \frac{i}{8\pi^2}\int\int d\kappa_x d\kappa_y \frac{1}{k_{1z}}\big[\mathbf{t_{1\pm}}\mathbf{t_{1\pm}} + \\
&\qquad \mathbf{p_{1\pm}}\mathbf{p_{1\pm}}\big]\exp(i\mathbf{k_{1\pm}}\mathbf{R}), \\
\mathbf{G_{sc}^{11}}(\mathbf{r},\mathbf{r}',\omega) &= \frac{i}{8\pi^2}\int\int \frac{d\kappa_x d\kappa_y}{k_{1,z}}\Big[R_{tt}^{11}\mathbf{t}_{\mathbf{1},+}\mathbf{t}_{\mathbf{1},-} + R_{tp}^{11}\mathbf{t}_{\mathbf{1},+}\mathbf{p}_{\mathbf{1},-} + \\
&\qquad R_{pt}^{11}\mathbf{p}_{\mathbf{1},+}\mathbf{t}_{\mathbf{1},-} + R_{pp}^{11}\mathbf{p}_{\mathbf{1},+}\mathbf{p}_{\mathbf{1},-}\Big] \times \\
&\qquad \exp(i\mathbf{k}_{\mathbf{1},+}\mathbf{r} - i\mathbf{k}_{\mathbf{1},-}\mathbf{r}'), \\
\mathbf{G_{sc}^{21}}(\mathbf{r},\mathbf{r}',\omega) &= \frac{i}{8\pi^2}\int\int \frac{d\kappa_x d\kappa_y}{k_{1,z}}\Big[R_{tt}^{21}\mathbf{t}_{\mathbf{2},-}\mathbf{t}_{\mathbf{1},-} + R_{tp}^{21}\mathbf{t}_{\mathbf{2},-}\mathbf{p}_{\mathbf{1},-} + \\
&\qquad R_{pt}^{21}\mathbf{p}_{\mathbf{2},-}\mathbf{t}_{\mathbf{1},-} + R_{pp}^{21}\mathbf{p}_{\mathbf{2},-}\mathbf{p}_{\mathbf{1},-}\Big] \times \\
&\qquad \exp(i\mathbf{k}_{\mathbf{2},-}\mathbf{r} - i\mathbf{k}_{\mathbf{1},-}\mathbf{r}'),
\end{aligned} \tag{C.6}$$

here $\mathbf{R} = \mathbf{r} - \mathbf{r}'$. For the free-space Green's tensor the upper (lower) superscripts correspond to $z > z'$ ($z < z'$). In the equations above we also introduced the Fresnel coefficients R_{kl}^{ij} accounting for the scattering from mode l to mode k. Note that due to the structure being, generally, anisotropic in the xy-plane, there are hybrid modes, which is why there are the cross terms present involving the products of $\mathbf{t_{j,\pm}}$, and $\mathbf{p_{j,\pm}}$. The dyads required for the calculation of $\mathbf{G_{sc}^{11}}(\mathbf{r},\mathbf{r}',\boldsymbol{\omega})$ are listed below:

$$\begin{aligned}
\frac{\mathbf{t}_{\mathbf{1},+}\mathbf{t}_{\mathbf{1},-}}{k_{1,z}} &= \begin{pmatrix} \frac{\kappa_y^2}{\kappa^2 k_{1,z}} & -\frac{\kappa_x\kappa_y}{\kappa^2 k_{1,z}} & 0 \\ -\frac{\kappa_x\kappa_y}{\kappa^2 k_{1,z}} & \frac{\kappa_x^2}{\kappa^2 k_{1,z}} & 0 \\ 0 & 0 & 0 \end{pmatrix}, \ \frac{\mathbf{t}_{\mathbf{1},+}\mathbf{p}_{\mathbf{1},-}}{k_{1,z}} = \begin{pmatrix} -\frac{\kappa_x\kappa_y}{k_1\kappa^2} & -\frac{\kappa_y^2}{k_1\kappa^2} & -\frac{\kappa_y}{k_1 k_{1,z}} \\ \frac{\kappa_x^2}{k_1\kappa^2} & \frac{\kappa_x\kappa_y}{k_1\kappa^2} & \frac{\kappa_x}{k_1 k_{1,z}} \\ 0 & 0 & 0 \end{pmatrix}, \\
\frac{\mathbf{p}_{\mathbf{1},+}\mathbf{t}_{\mathbf{1},-}}{k_{1,z}} &= \begin{pmatrix} \frac{\kappa_x\kappa_y}{k_1\kappa^2} & -\frac{\kappa_x^2}{k_1\kappa^2} & 0 \\ \frac{\kappa_y^2}{k_1\kappa^2} & -\frac{\kappa_x\kappa_y}{k_1\kappa^2} & 0 \\ -\frac{\kappa_y}{k_1 k_{1,z}} & \frac{\kappa_x}{k_1 k_{1,z}} & 0 \end{pmatrix}, \ \frac{\mathbf{p}_{\mathbf{1},+}\mathbf{p}_{\mathbf{1},-}}{k_{1,z}} = \begin{pmatrix} -\frac{\kappa_x^2 k_{1,z}}{k_1^2\kappa^2} & -\frac{\kappa_x\kappa_y k_{1,z}}{k_1^2\kappa^2} & -\frac{\kappa_x}{k_1^2} \\ -\frac{\kappa_x\kappa_y k_{1,z}}{k_1^2\kappa^2} & -\frac{\kappa_y^2 k_{1,z}}{k_1^2\kappa^2} & -\frac{\kappa_y}{k_1^2} \\ \frac{\kappa_x}{k_1^2} & \frac{\kappa_y}{k_1^2} & \frac{\kappa^2}{k_1^2 k_{1,z}} \end{pmatrix}.
\end{aligned} \tag{C.7}$$

In order to find the Fresnel coefficients, we need to satisfy the boundary conditions at the interface plane:

$$\begin{cases} \mathbf{e_z} \times (\mathbf{E_1} - \mathbf{E_2}) = 0, \\ \mathbf{e_z} \times (\mathbf{H_1} - \mathbf{H_2}) = \dfrac{4\pi}{c}\sigma\mathbf{E_{1,2}}, \end{cases} \tag{C.8}$$

where $\sigma = \begin{pmatrix} \sigma_{xx} & \sigma_{xy} \\ \sigma_{yx} & \sigma_{yy} \end{pmatrix}$ is a surface conductivity tensor.

Even though the boundary conditions on electric, and magnetic fields have to be considered together, by looking only at the condition on the electric field, and taking into account that ($\mathbf{t}^{\perp}_{\mathbf{i},+} = \mathbf{t}^{\perp}_{\mathbf{i},-} = \mathbf{t}^{\perp}_{\mathbf{j},+}$, $\mathbf{p}^{\perp}_{\mathbf{i},+} = -\mathbf{p}^{\perp}_{\mathbf{i},-}$, $\mathbf{p}^{\perp}_{\mathbf{i},+} = \frac{k_i k_{j,z}}{k_{i,z} k_j} \mathbf{p}^{\perp}_{\mathbf{j},+}$), we obtain:

$$\begin{cases} 1 + R^{11}_{tt} = R^{21}_{tt}, \\ R^{11}_{pt} \dfrac{k_{1,z}}{k_1} = -R^{21}_{pt} \dfrac{k_{2,z}}{k_2}, \\ R^{11}_{tp} = R^{21}_{tp}, \\ -1 + R^{11}_{pp} = -R^{21}_{pp} \dfrac{k_{2,z} k_1}{k_2 k_{1,z}}. \end{cases} \tag{C.9}$$

From the boundary conditions for the magnetic fields we have 2 systems of 2x2 equations:

$$\begin{pmatrix} M_{11} & M_{12} \\ M_{21} & M_{22} \end{pmatrix} \begin{pmatrix} R^{11}_{tt} \\ R^{11}_{pt} \end{pmatrix} = \begin{pmatrix} B^{(1)}_1 \\ B^{(1)}_2 \end{pmatrix}, \\ \begin{pmatrix} M_{11} & M_{12} \\ M_{21} & M_{22} \end{pmatrix} \begin{pmatrix} R^{11}_{tp} \\ R^{11}_{pp} \end{pmatrix} = \begin{pmatrix} B^{(2)}_1 \\ B^{(2)}_2 \end{pmatrix}, \tag{C.10}$$

$$R^{11}_{tt} = \frac{B^{(1)}_1 M_{22} - B^{(1)}_2 M_{12}}{M_{11} M_{22} - M_{12} M_{21}}, R^{11}_{pt} = \frac{B^{(1)}_2 M_{11} - B^{(1)}_1 M_{21}}{M_{11} M_{22} - M_{12} M_{21}}, \\ R^{11}_{tp} = \frac{B^{(2)}_1 M_{22} - B^{(2)}_2 M_{12}}{M_{11} M_{22} - M_{12} M_{21}}, R^{11}_{pp} = \frac{B^{(2)}_2 M_{11} - B^{(2)}_1 M_{21}}{M_{11} M_{22} - M_{12} M_{21}}, \tag{C.11}$$

where:

$$
\begin{aligned}
M_{11} &= -\frac{4\pi}{c\kappa}\left(-\kappa_y\sigma_{xx}+\kappa_x\sigma_{xy}\right)+\frac{\kappa_y}{k_0\kappa}\left(k_{1,z}+k_{2,z}\right),\\
M_{21} &= -\frac{4\pi}{c\kappa}\left(-\kappa_y\sigma_{yx}+\kappa_x\sigma_{yy}\right)-\frac{\kappa_x}{k_0\kappa}\left(k_{1,z}+k_{2,z}\right),\\
M_{12} &= \frac{4\pi}{c}\frac{k_{1,z}k_2}{k_{2,z}k_1}\frac{k_{2,z}}{k_2\kappa}\left(\kappa_x\sigma_{xx}+\kappa_y\sigma_{xy}\right)+\frac{\kappa_x}{k_0\kappa}\left(k_1+\frac{k_{1,z}k_2^2}{k_1k_{2,z}}\right),\\
M_{22} &= \frac{4\pi}{c}\frac{k_{1,z}k_2}{k_{2,z}k_1}\frac{k_{2,z}}{k_2\kappa}\left(\kappa_x\sigma_{yx}+\kappa_y\sigma_{yy}\right)+\frac{\kappa_y}{k_0\kappa}\left(k_1+\frac{k_{1,z}k_2^2}{k_1k_{2,z}}\right),\\
B_1^{(1)} &= \frac{4\pi}{c}\frac{1}{\kappa}\left(-\kappa_y\sigma_{xx}+\kappa_x\sigma_{xy}\right)+\frac{\kappa_y}{k_0\kappa}\left(k_{1,z}-k_{2,z}\right),\\
B_2^{(1)} &= \frac{4\pi}{c}\frac{1}{\kappa}\left(-\kappa_y\sigma_{yx}+\kappa_x\sigma_{yy}\right)+\frac{\kappa_x}{k_0\kappa}\left(-k_{1,z}+k_{2,z}\right),\\
B_1^{(2)} &= \frac{4\pi}{c}\frac{k_{1,z}k_2}{k_1k_{2,z}}\frac{k_{2,z}}{\kappa k_2}\left(\kappa_x\sigma_{xx}+\kappa_y\sigma_{xy}\right)+\frac{\kappa_x}{k_0\kappa}\left(-k_1+\frac{k_{1,z}k_2^2}{k_1k_{2,z}}\right),\\
B_2^{(2)} &= \frac{4\pi}{c}\frac{k_{1,z}k_2}{k_{2,z}k_1}\frac{k_{2,z}}{k_2\kappa}\left(\kappa_x\sigma_{yx}+\kappa_y\sigma_{yy}\right)+\frac{\kappa_y}{k_0\kappa}\left(-k_1+\frac{k_{1,z}k_2^2}{k_1k_{2,z}}\right).
\end{aligned}
\tag{C.12}
$$

We want to note that the double integral in Eq. (C.6) $\int\int d\kappa_x d\kappa_y$ is better to carry out in cylindrical coordinates as one of the integration domains becomes finite. This can be done by a simple transformation $\kappa_x \to \kappa\cos(\varphi)$, $\kappa_y \to \kappa\sin(\varphi)$.

A very general explicit form of the Fresnel's coefficients is quite complicated, however, we can consider some specific cases, for which we can at least make some analysis.

C.1.1 The case of: $\varepsilon_1 \neq \varepsilon_2$, $\sigma_{ij} = 0$ for $i \neq j$

In case of the presence of the optical contrast between upper (1), and lower (2) media ($\varepsilon_1 \neq \varepsilon_2 = 1$), and vanishing non-diagonal surface conductivity tensor components ($\sigma_{xy} = \sigma_{yx} = 0$), we can have a closer look at the components of the Green's tensor.

First, let us introduce the following notations:

$$
\begin{aligned}
k_z^+ &= k_{1,z} + k_{2,z},\\
k_z^- &= k_{1,z} - k_{2,z},\\
K_{12}^+ &= k_{1,z}k_2^2 + k_{2,z}k_1^2,\\
K_{12}^- &= k_{1,z}k_2^2 - k_{2,z}k_1^2.
\end{aligned}
\tag{C.13}
$$

Now we will present each Fresnel coefficients in the form $R_{ij}^{11} = \frac{\text{Num}\left[R_{ij}^{11}\right]}{\text{Det}}$, where Num[...] stands for numerator, and Det is the determinant of the corresponding system Eq. (C.11).

$$\text{Det} = \frac{k_z^+ K_{12}^+}{k_0^2 k_1 k_{2,z}} + \frac{4\pi}{c}\frac{1}{k_0 k_1 k_{2,z}}\Bigg[k_{1,z}k_{2,z}k_z^+\left(\sigma_{xx}\cos^2(\varphi)+\sigma_{yy}\sin^2(\varphi)\right)+ K_{12}^+\left(\sigma_{yy}\cos^2(\varphi)+\sigma_{xx}\sin^2(\varphi)\right)\Bigg] + \left(\frac{4\pi}{c}\right)^2\frac{k_{1,z}\left(\sigma_{xx}\sigma_{yy}\right)}{k_1}. \quad \text{(C.14)}$$

As can be seen, in this case the determinant is symmetric with respect to $\pi+\varphi \to \pi-\varphi$ transformation. And inside both of domains $\varphi \in [0,\pi]$, and $\varphi \in [\pi, 2\pi]$ the determinant is symmetric with respect to the domain's central point ($\pi/2$, and $3\pi/2$, correspondingly).

Now let us have a look at the numerators:

$$\text{Num}(R_{tt}^{11}) = \frac{1}{c^2 k_0^2 k_1 k_{2,z}}\Bigg[c^2 k_z^- K_{12}^+ - 2ck_0\left(K_{12}^+ - k_{1,z}k_{2,z}k_z^-\right)\pi(\sigma_{xx}+\sigma_{yy}) - 16k_0^2 k_{1,z}k_{2,z}\pi^2\sigma_{xx}\sigma_{yy} + 2ck_0\left(K_{12}^+ + k_{1,z}k_{2,z}k_z^-\right)\pi(\sigma_{xx}-\sigma_{yy})\cos(2\varphi)\Bigg],$$

$$\text{Num}(R_{pt}^{11}) = \frac{4k_{1,z}\pi}{ck_0}\left(\sigma_{yy}-\sigma_{xx}\right)\sin(2\varphi),$$

$$\text{Num}(R_{tp}^{11}) = \frac{4k_{1,z}\pi}{ck_0}(\sigma_{xx}-\sigma_{yy})\sin(2\varphi),$$

$$\text{Num}(R_{pp}^{11}) = \frac{1}{c^2 k_0^2 k_1 k_{2,z}}\Bigg(c^2 k_z^+ K_{12}^- + 2ck_0\left(k_{1,z}k_{2,z}k_z^+ - K_{12}^-\right)\pi\left(\sigma_{xx}+\sigma_{yy}\right) + 16k_0^2 k_{1,z}k_{2,z}\pi^2\sigma_{xx}\sigma_{yy} + 2ck_0\Big(-K_{12}^- + k_{1,z}k_{2,z}k_z^+\Big)\pi\left(\sigma_{xx}-\sigma_{yy}\right)\cos(2\varphi)\Bigg). \quad \text{(C.15)}$$

For this case R_{tt}^{11}, and R_{pp}^{11} are of the same angular symmetry as the denominator (as they contain only $\sim\cos(2\varphi)$ part). However, R_{tp}^{11}, and R_{pt}^{11} are both anti-symmetric inside of domains $\varphi \in [0,\pi]$, $\varphi \in [\pi, 2\pi]$ with respect to their central points.

In the maintext, we are interested mostly in the local Green's tensor, $\mathbf{G_{sc}^{11}}(\mathbf{r},\mathbf{r},\omega)$. For equal source, and field points, the exponential factor in Eq. (C.6) turns into:

$$\exp(i\mathbf{k_{1,+}}\mathbf{r} - i\mathbf{k_{1,-}}\mathbf{r}) = \exp\left(i2k_{1,z}z\right), \quad \text{(C.16)}$$

where, as usual, $z > 0$ condition is assumed. One can see that this factor does not contain the angular part at all. Therefore, whether or not some component of the local Green's tensor is equal to zero, can be understood by looking at the products of corresponding dyad's component with the related Fresnel coefficient. The dyads entering the local Green's tensor can be written in the cylindrical coordinates as:

$$\frac{\mathbf{t_1},_+\mathbf{t_1},_-}{k_{1,z}} = \begin{pmatrix} \frac{sin^2(\varphi)}{k_{1,z}} & -\frac{sin(2\varphi)}{2k_{1,z}} & 0 \\ -\frac{sin(2\varphi)}{2k_{1,z}} & \frac{cos^2(\varphi)}{k_{1,z}} & 0 \\ 0 & 0 & 0 \end{pmatrix},$$

$$\frac{\mathbf{t_1},_+\mathbf{p_1},_-}{k_{1,z}} = \begin{pmatrix} -\frac{sin(2\varphi)}{2k_1} & -\frac{sin^2(\varphi)}{k_1} & -\frac{\kappa sin(\varphi)}{k_1 k_{1,z}} \\ \frac{cos^2(\varphi)}{k_1} & \frac{sin(2\varphi)}{2k_1} & \frac{\kappa cos(\varphi)}{k_1 k_{1,z}} \\ 0 & 0 & 0 \end{pmatrix},$$

$$\frac{\mathbf{p_1},_+\mathbf{t_1},_-}{k_{1,z}} = \begin{pmatrix} \frac{sin(2\varphi)}{2k_1} & -\frac{cos^2(\varphi)}{k_1} & 0 \\ \frac{sin^2(\varphi)}{k_1} & -\frac{sin(2\varphi)}{2k_1} & 0 \\ -\frac{\kappa sin(\varphi)}{k_1 k_{1,z}} & \frac{\kappa cos(\varphi)}{k_1 k_{1,z}} & 0 \end{pmatrix},$$

$$\frac{\mathbf{p_1},_+\mathbf{p_1},_-}{k_{1,z}} = \begin{pmatrix} -\frac{cos^2(\varphi)k_{1,z}}{k_1^2} & -\frac{sin(2\varphi)k_{1,z}}{2k_1^2} & -\frac{\kappa cos(\varphi)}{k_1^2} \\ -\frac{sin(2\varphi)k_{1,z}}{2k_1^2} & -\frac{sin^2(\varphi)k_{1,z}}{k_1^2} & -\frac{\kappa sin(\varphi)}{k_1^2} \\ \frac{\kappa cos(\varphi)}{k_1^2} & \frac{\kappa sin(\varphi)}{k_1^2} & \frac{\kappa^2}{k_1^2 k_{1,z}}. \end{pmatrix}. \tag{C.17}$$

One can easily analyze the symmetry of each component, and quickly understand that in the considered case the local Green's tensor is diagonal. This is, essentially, a result of the surface conductivity tensor being diagonal $\sigma_{xy} = \sigma_{yx} = 0$. In the next subsection we will demonstrate the appearance of these components explicitly.

C.1.2 The case of: $\varepsilon_1 = \varepsilon_2 = 1$, $\sigma_{ij} \neq 0$ for all $i,j = x,y$

This is the simplest situation, where one can observe that non-diagonal components of the local Green's tensor do not vanish. For this case we have

$K_{12}^{-}=0$, $k_z^{-}=0$, $k_z^{+}=2k_z$, $K_{12}^{+}=2k_zk_0^2$, and can write that:

$$\begin{aligned}\mathrm{Det}=&-\frac{16\pi^2}{c^2}\frac{k_z}{k_0}\left[\sigma_{xy}\sigma_{yx}-\sigma_{xx}\sigma_{yy}\right]+\\&\frac{8\pi}{k_0^2c}\Big[k_0^2\left(\sin^2(\varphi)\sigma_{xx}-\cos(\varphi)\sin(\varphi)(\sigma_{xy}+\sigma_{yx})+\cos^2(\varphi)\sigma_{yy}\right)+\\k_z^2&\left(\cos^2(\varphi)\sigma_{xx}+\cos(\varphi)\sin(\varphi)(\sigma_{xy}+\sigma_{yx})+\sin^2(\varphi)\sigma_{yy}\right)\Big]+4\frac{k_z}{k_0}.\end{aligned}\quad(C.18)$$

The numerators of the Fresnel coefficients are given by:

$$\begin{aligned}\mathrm{Num}\left[R_{tt}^{11}\right]=&-\frac{8\pi}{c^2k_0}\Big(ck_0\big(\sin^2(\varphi)\sigma_{xx}-\cos(\varphi)\sin(\varphi)\left(\sigma_{xy}+\sigma_{yx}\right)+\\&\cos^2(\varphi)\sigma_{yy}\big)-2k_z\pi\left(\sigma_{xy}\sigma_{yx}-\sigma_{xx}\sigma_{yy}\right)\Big),\\\mathrm{Num}\left[R_{pt}^{11}\right]=&\frac{8k_z\pi\left(\cos^2(\varphi)\sigma_{xy}-\sin^2(\varphi)\sigma_{yx}+\cos(\varphi)\sin(\varphi)\left(\sigma_{yy}-\sigma_{xx}\right)\right)}{ck_0},\\\mathrm{Num}\left[R_{tp}^{11}\right]=&\frac{8k_z\pi\left(\sin^2(\varphi)\sigma_{xy}-\cos^2(\varphi)\sigma_{yx}+\cos(\varphi)\sin(\varphi)\left(\sigma_{xx}-\sigma_{yy}\right)\right)}{ck_0},\\\mathrm{Num}\left[R_{pp}^{11}\right]=&\frac{8\pi k_z}{c^2k_0^2}\Big(ck_z\big(\cos^2(\varphi)\sigma_{xx}+\cos(\varphi)\sin(\varphi)\left(\sigma_{xy}+\sigma_{yx}\right)+\\&\sin^2(\varphi)\sigma_{yy}\big)+2k_0\pi\left(\sigma_{xx}\sigma_{yy}-\sigma_{xy}\sigma_{yx}\right)\Big).\end{aligned}\quad(C.19)$$

Notice, that for all of the Fresnel coefficients the angular symmetry is now more peculiar than in the previously considered case. Now they are neither symmetric nor antisymmetric with respect to $\varphi=\pi/2$, and $\varphi=3\pi/2$ points in the corresponding domains ($\varphi\in[0,\pi]$, and $\varphi\in[\pi,2\pi]$). However, nothing happened to the angular symmetry of dyads entering the Green's tensor. Therefore, one can expect that the local Green's tensor is now non-diagonal.

C.2 Far-field Green's tensor

At some point, we will require the far-field part of the scattered Green's tensor. For the case of both source, and field points being located in medium 1, the i,j component of the Green's tensor scattered part for a single-interface planar nanostructure has the following form:

$$G_{ij}^{11,sc}(\mathbf{r},\mathbf{r}',\omega)=\frac{i}{8\pi^2}\int\int g_{ij}^{11,sc}(\kappa_x,\kappa_y)e^{i(\kappa_xX+\kappa_yY+k_zZ)}d\kappa_xd\kappa_y,\quad(C.20)$$

where $X = x - x', Y = y - y', Z = z + z', \mathbf{R} = \left(X, Y, Z\right), R = |\mathbf{R}|$. The "+" sign in Z appears as the scattered field is generated by a mirror image of a source dipole. We also implied that the medium 1 has $\varepsilon_1 = 1$ for simplicity.

By taking the limit $kR \to \infty$, one can obtain [191]:

$$G_{ij}^{11,scFF} = \frac{1}{4\pi}\frac{kZ}{R}\frac{e^{ikR}}{R} g_{ij}^{11,sc}\left(k\frac{X}{R}, k\frac{Y}{R}\right). \tag{C.21}$$

For the case of an interface: $X = x - x0, Y = y - y0, Z = z + z0, \mathbf{R} = \left(X, Y, Z\right), R = |\mathbf{R}|$.

C.3 Extreme anisotropy case

Clearly, the Green's function of anistoropic metasurface can be written only in the form of double integrals $\int\int d\kappa_x d\kappa_y$. However, it is possible to obtain the explicit form of the local Green's function $G^{11,sc}(\mathbf{r}, \mathbf{r}, \omega)$, when there is no substrate ($\varepsilon_2 = 1$), and when the following limit is taken: $\sigma_{yy} \to i\infty, \sigma_{xx} \to i0$. In this work the phenomenological Lorenz model for surface conductivity tensor components is used rather than some ab-initio calculation of it:

$$\sigma_{jj}(\omega) = A_j \frac{ic}{4\pi}\frac{\omega}{\omega^2 - \Omega_j^2 + i\gamma_j\omega}, \tag{C.22}$$

here A_j is the normalization factor, Ω_j - frequency of the corresponding resonance, γ_j is the damping constant, c is the speed of light. The aforementioned limit corresponds to considering an almost or perfectly lossless case ($\gamma_j \approx 0$), and ω is chosen such that the resonance condition is satisfied for one component of the tensor (in this case $\omega \approx \Omega_y$, and, therefore $\sigma_{yy} \to i\infty$), while for the other component this frequency is far from the resonance ($\omega \gg \Omega_x$ or $\omega \ll \Omega_x$, leading to $\sigma_{xx} \to 0i$). In a physical sense it means that the system for this set of parameters presents a perfect electric conductor along the y direction, and a perfect isolator along the x direction.

In this regime of strong anisotropy, and in the absence of the substrate, the Fresnel coefficients take the following form:

$$\begin{aligned}
R_{tt}^{11} &= -\frac{\cos^2(\varphi)}{\frac{k_z^2}{k^2}\sin^2(\varphi) + \cos^2(\varphi)}, \quad & R_{pt}^{11} &= +\frac{\sin(\varphi)\cos(\varphi)\frac{k_z}{k}}{\frac{k_z^2}{k^2}\sin^2(\varphi) + \cos^2(\varphi)}, \\
R_{tp}^{11} &= -\frac{\sin(\varphi)\cos(\varphi)\frac{k_z}{k}}{\frac{k_z^2}{k^2}\sin^2(\varphi) + \cos^2(\varphi)}, \quad & R_{pp}^{11} &= +\frac{\frac{k_z^2}{k_0^2}\sin^2(\varphi)}{\frac{k_z^2}{k^2}\sin^2(\varphi) + \cos^2(\varphi)},
\end{aligned} \tag{C.23}$$

where the transformation from Cartesian to cylindrical coordinates is assumed to be made. The components of the local Green's tensor then take the form:

$$
\begin{aligned}
G_{xx}^{sc,11}(\mathbf{r},\mathbf{r},\omega) &= -\int\int \frac{i}{8\pi^2}\frac{\sin^2(\varphi)\cos^2(\varphi)}{\frac{k_z^2}{k^2}\sin^2(\varphi)+\cos^2(\varphi)}\frac{k_\rho^5}{k_z k^4}e^{i2k_z\Delta z}dk_\rho d\varphi,\\
G_{yy}^{sc,11}(\mathbf{r},\mathbf{r},\omega) &= \int\int \frac{i}{8\pi^2}\left(\frac{k_z^2}{k^2}\sin^2(\varphi)+\cos^2(\varphi)\right)\frac{k_\rho}{k_z}e^{i2k_z\Delta z}dk_\rho d\varphi,\\
G_{zz}^{sc,11}(\mathbf{r},\mathbf{r},\omega) &= \int\int \frac{i}{8\pi^2}\frac{\sin^2(\varphi)}{\frac{k_z^2}{k^2}\sin^2(\varphi)+\cos^2(\varphi)}\frac{k_\rho^3 k_z}{k^4}e^{i2k_z\Delta z}dk_\rho d\varphi,
\end{aligned}
\tag{C.24}
$$

where it is assumed that the atom is located at $\Delta z > 0$ distance from the metasurface.

The three double integrals above can be carried out by first performing the integration over φ, and then integration over k_ρ. Finally, we arrive at the following:

$$
\begin{aligned}
G_{xx}^{sc}(\mathbf{r},\mathbf{r},\omega) &= e^{2ik\Delta z}\frac{1}{32\pi k^2\Delta z^3},\\
G_{yy}^{sc}(\mathbf{r},\mathbf{r},\omega) &= e^{2ik\Delta z}\frac{-1+2ik\Delta z+4k^2\Delta z^2}{32\pi k^2\Delta z^3},\\
G_{zz}^{sc}(\mathbf{r},\mathbf{r},\omega) &= e^{2ik\Delta z}\frac{1-ik\Delta z}{16\pi k^2\Delta z^3}.
\end{aligned}
\tag{C.25}
$$

The functions derived above are visualized in Fig. C.1. Let us analyze how do these functions behave in the limit of a small emitter-interface distance ($k\Delta z \ll 1$):

$$
\begin{aligned}
&\mathrm{Re}\left[G_{xx}^{sc}(\mathbf{r},\mathbf{r},\omega)\right] \approx \frac{k}{32\pi(k\Delta z)^3}, \qquad \mathrm{Im}\left[G_{xx}^{sc}(\mathbf{r},\mathbf{r},\omega)\right] \approx \frac{k}{16\pi(k\Delta z)^2},\\
&\mathrm{Re}\left[G_{yy}^{sc}(\mathbf{r},\mathbf{r},\omega)\right] \approx -\frac{k}{32\pi(k\Delta z)^3}, \qquad \mathrm{Im}\left[G_{yy}^{sc}(\mathbf{r},\mathbf{r},\omega)\right] \approx \frac{k}{6\pi},\\
&\mathrm{Re}\left[G_{zz}^{sc}(\mathbf{r},\mathbf{r},\omega)\right] \approx -\frac{k}{16\pi(k\Delta z)^3}, \qquad \mathrm{Im}\left[G_{zz}^{sc}(\mathbf{r},\mathbf{r},\omega)\right] \approx \frac{k}{16\pi(k\Delta z)^2}.
\end{aligned}
\tag{C.26}
$$

As seen, the real parts diverge as $\sim (k\Delta z)^{-3}$ as a result of dipole interacting with its mirror image through the near fields (quasi-static interaction). This is a quite typical behavior, and can be also found, for instance, for a dipole put close to a planar half-space [2]. The behavior of the imaginary parts is more peculiar: for xx, and zz components the imaginary parts diverge as $\sim (k\Delta z)^{-2}$, while for yy-component it is finite, and is equal

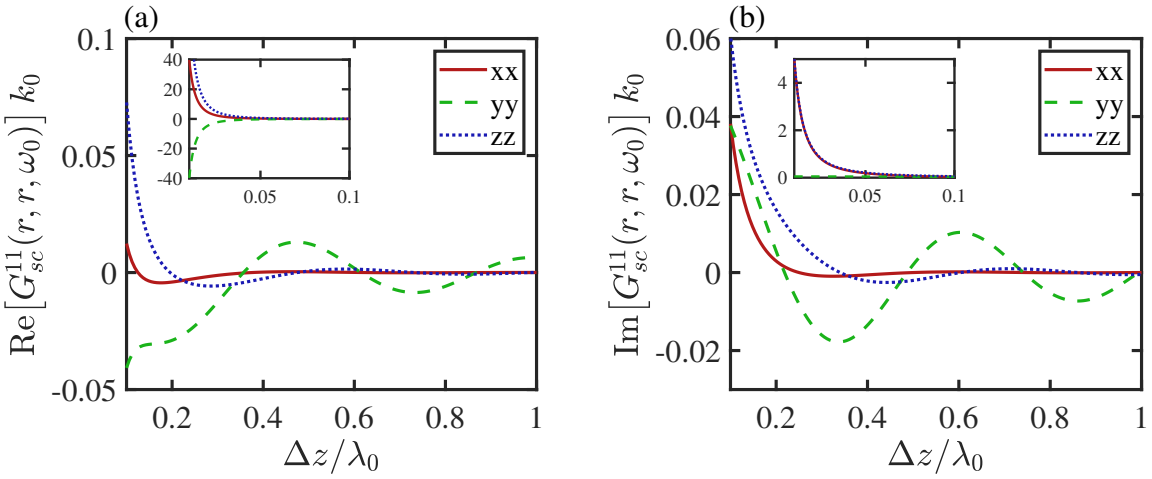

Figure C.1 — Real (a), and Imaginary (b) parts of the local Green's tensor given by Eq. (C.25) as a function of dipole-interface distance $\Delta z/\lambda_0$. Red solid, green dashed, blue dotted lines correspond to xx, yy, and zz components. The insets show more in detail the region $0.01 \leqslant \Delta z/\lambda_0 \leqslant 0.1$

to the same value, as for the vacuum Green's tensor ($k/(6\pi)$). The latter is easily interpretable: the dipole is oriented along the y-direction, and as $\sigma_{yy} \to i\infty$, it behaves as if it was in the vicinity of a half-space made of a perfect electric conductor, and the dipole field constructively interferes with the field of the image dipole, leading to the enhancement of the emission rate by the factor of two. However, the divergence of the other two components is not that easily explainable. This might be a result of the inconsistency of the model, as here we have an infinitely thin layer of a material, which is conducting in one direction, and isolating in the orthogonal direction, while being described as a continuous medium. One might view this system as a set of infinitely thin metallic wires aligned along the y-direction. Such wires would have had a microscopic structure, and the near fields would vary significantly when moving perpendicularly to their alignment axis. This model does not take into account this microscopic structure of the constituent elements of the metasurface. This might be only considered a speculation rather than explanation, and might require some additional analysis as well as the comparison with full-wave modelling, which we do not present here.

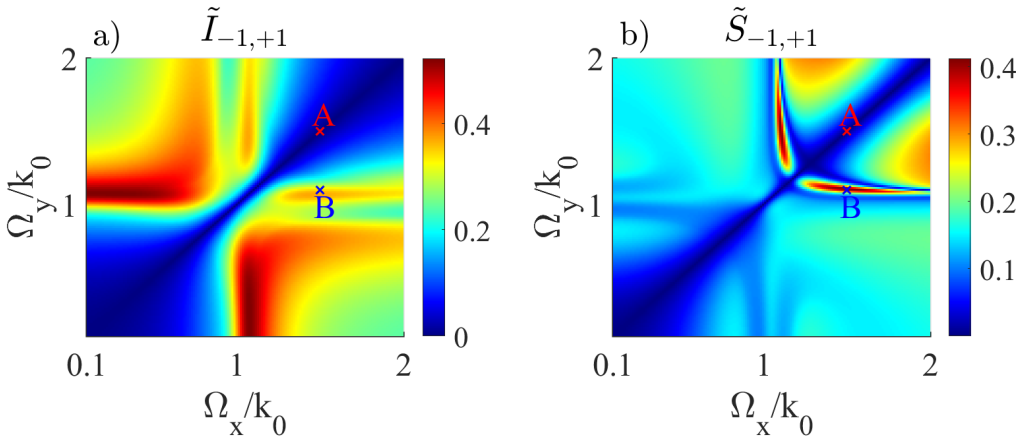

Figure C.2 — Colorplots of quantities $\tilde{I}_{-1,+1}$, and $\tilde{S}_{-1,+1}$ defined by Eq. (C.27), and Eq. (C.28) as functions of resonance frequencies Ω_x, Ω_y. Other relevant parameters are the same as the ones used in Fig. 3.4. The two specified points correspond to isotropic (A: $\Omega_x = \Omega_y = 1.5k_0$), and anisotropic ($\Omega_x = 1.5k_0$, $\Omega_y = 1.1k_0$) metasurface

C.4 A measure of the discrepancy in the intensity, and spectral profiles

Imagine that we set all the relevant parameters, and plotted intensity dynamics $I_{q_0}(\tau)$ as well as the spectrum $S_{q_0}(\delta)$. We want to introduce some measure, which quantifies how much these functions are different for initial conditions $q_0 = -1$, and $q_0 = +1$. For the sake of simplicity, we will predefine the angles α, β responsible for the orientation of the local quantization axis as well as the position of the detector. Now we introduce the following two quantities:

$$\tilde{I}_{-1,+1} = \frac{\int_0^\infty |I_{-1}(\tau) - I_{+1}(\tau)|\, d\tau}{\int_0^\infty (I_{-1}(\tau) + I_{+1}(\tau))\, d\tau}, \tag{C.27}$$

$$\tilde{S}_{-1,+1} = \frac{\int_{-\infty}^\infty |S_{-1}(\delta) - S_{+1}(\delta)|\, d\delta}{\int_{-\infty}^\infty (S_{-1}(\delta) + S_{+1}(\delta))\, d\delta}. \tag{C.28}$$

The two functions defined above are, clearly, always between 0 and 1, and they can be used to measure how much the two functions are similar or different. Therefore, we can plot the maps of these quantities in Eq. (C.27), and Eq. (C.28) versus frequencies Ω_x, Ω_y, which are presented in Fig. C.2

(a), (b). Note that once $\Omega_x = \Omega_y$ the metasurface is isotropic in the interface plane, and both quantities $\tilde{I}_{-1,+1}$, $\tilde{S}_{-1,+1}$ are equal to zero. It can be seen that the local maxima of these two functions $\tilde{I}_{-1,+1}$, and $\tilde{S}_{-1,+1}$ do not overlap. However, one can easily spot a region on these maps, where both of them are close to being equal to $\sim 0.2 - 0.3$, which might be sufficient in order to observe the discrepancy for $q_0 = -1, +1$ cases. Indeed, as seen from Fig. 3.4 (a), and (b), this set of parameters allows to achieve the primary goal.

C.5 Green's tensor of two anisotropic dipole scatterers

We want to construct a Green's tensor for the system consisting of two dipolar scatterers characterized by polarizabilities $\boldsymbol{\alpha_{1,2}}$, this can be done with the help of Dyson equation [2; 182]:

$$\mathbf{G}_{\text{tot}}(\mathbf{r}, \mathbf{r_0}) = \mathbf{G_0}(\mathbf{r}, \mathbf{r_0}) + 4\pi k^2 \Big(\mathbf{G_0}(\mathbf{r}, \mathbf{r_1}) \boldsymbol{\alpha_1} \mathbf{G}_{\text{tot}}(\mathbf{r_1}, \mathbf{r_0}) + \mathbf{G_0}(\mathbf{r}, \mathbf{r_2}) \boldsymbol{\alpha_2} \mathbf{G}_{\text{tot}}(\mathbf{r_2}, \mathbf{r_0}) \Big), \tag{C.29}$$

where α_1, α_2 are electric dipole polarizabilities of the scatterers. In order to find $\mathbf{G}_{\text{tot}}(\mathbf{r_1}, \mathbf{r_0})$, $\mathbf{G_F}(\mathbf{r_2}, \mathbf{r_0})$ we make the two following substitutions: $\mathbf{r} = \mathbf{r_1}$, and $\mathbf{r} = \mathbf{r_2}$ into Eq. (C.29). This will lead to the algebraic system:

$$\mathbf{M}(\mathbf{r_1}, \mathbf{r_2}) \cdot \mathbf{X}(\mathbf{r_1}.\mathbf{r_2}, \mathbf{r_0}) = \mathbf{B}(\mathbf{r_1}, \mathbf{r_2}, \mathbf{r_0}), \tag{C.30}$$

where:

$$\mathbf{M}(\mathbf{r_1}, \mathbf{r_2}) = \begin{pmatrix} \mathbf{I} & -4\pi k^2 \mathbf{G_0}(\mathbf{r_1}, \mathbf{r_2}) \boldsymbol{\alpha_2} \\ -4\pi k^2 \mathbf{G_0}(\mathbf{r_2}, \mathbf{r_1}) \boldsymbol{\alpha_1} & \mathbf{I} \end{pmatrix};$$
$$\mathbf{B}(\mathbf{r_1}, \mathbf{r_2}, \mathbf{r_0}) = \begin{pmatrix} \mathbf{G_0}(\mathbf{r_1}, \mathbf{r_0}) \\ \mathbf{G_0}(\mathbf{r_2}, \mathbf{r_0}) \end{pmatrix}; \quad \mathbf{X}(\mathbf{r_1}.\mathbf{r_2}, \mathbf{r_0}) = \begin{pmatrix} \mathbf{G}_{\text{tot}}(\mathbf{r_1}, \mathbf{r_0}) \\ \mathbf{G}_{\text{tot}}(\mathbf{r_2}, \mathbf{r_0}) \end{pmatrix}. \tag{C.31}$$

Note that during the derivation of this system, the self-interaction terms $\mathbf{G_0}(\mathbf{r_1}, \mathbf{r_1})$, and $\mathbf{G_0}(\mathbf{r_2}, \mathbf{r_2})$ were put to zero as point dipolar scatterers do not polarize themselves, unless there are additional boundaries on which dipole field can scatter off, and be reflected back. This would occur (but only for the scattered fields) if one introduces a substrate, for instance. It is important to note that these divergent self-interaction terms appear as Eq. (C.29) is, strictly speaking, valid only in the region which is free from the current sources [182; 192], and can not be used to describe the field generated at the position of any of the dipole scatterers.

Our real interest is in the total local Green's tensor of the system $\mathbf{G}_{\text{tot}}(\mathbf{r_0}, \mathbf{r_0})$, and now we will consider several specific cases. First, for the sake of simplicity, we will consider the case, when both scatterers are identical, and their polarizabilities correspond to ones of an ellipsoid:

$$\tilde{\boldsymbol{\alpha}}_\mathbf{1} = \tilde{\boldsymbol{\alpha}}_\mathbf{2} = \begin{pmatrix} \alpha_{||} & 0 & 0 \\ 0 & \alpha_\perp & 0 \\ 0 & 0 & \alpha_\perp \end{pmatrix}, \tag{C.32}$$

where tilde indicates that these are the polarizabilities in a specific orientation of the scatterers with respect to the introduced reference frame: principal axes of the particle are parallel to the coordinate axes. Now we want to rotate those particles on angles $+\varphi_0, -\varphi_0$ in the xy-plane, so there is some angle between their principal axes; this can be done trivially: $\boldsymbol{\alpha}_\mathbf{1} = \mathbf{S}(\varphi_0)\tilde{\boldsymbol{\alpha}}_\mathbf{1}\mathbf{S}^{-\mathbf{1}}(\varphi_0)$, $\boldsymbol{\alpha}_\mathbf{2} = \mathbf{S}(-\varphi_0)\tilde{\boldsymbol{\alpha}}_\mathbf{2}\mathbf{S}^{-\mathbf{1}}(-\varphi_0)$.

C.5.1 $\mathbf{r_0}, \mathbf{r_1}, \mathbf{r_2}$ are on the z-axis

Now let us set all relevant position vectors on the z-axis:

$$\mathbf{r_0} = \begin{pmatrix} 0 \\ 0 \\ z_0 \end{pmatrix}, \ \mathbf{r_1} = \begin{pmatrix} 0 \\ 0 \\ z_1 \end{pmatrix}, \ \mathbf{r_2} = \begin{pmatrix} 0 \\ 0 \\ z_2 \end{pmatrix}, \tag{C.33}$$

as a result, we have the following:

$$\begin{aligned}
\mathbf{G_0}(\mathbf{r_1}, \mathbf{r_0}) = \mathbf{G_0}(\mathbf{r_0}, \mathbf{r_1}) &= \begin{pmatrix} G^\perp_{0,10} & 0 & 0 \\ 0 & G^\perp_{0,10} & 0 \\ 0 & 0 & G^{||}_{0,10} \end{pmatrix}, \\
\mathbf{G_0}(\mathbf{r_2}, \mathbf{r_0}) = \mathbf{G_0}(\mathbf{r_0}, \mathbf{r_2}) &= \begin{pmatrix} G^\perp_{0,20} & 0 & 0 \\ 0 & G^\perp_{0,20} & 0 \\ 0 & 0 & G^{||}_{0,20} \end{pmatrix}, \\
\mathbf{G_0}(\mathbf{r_1}, \mathbf{r_2}) = \mathbf{G_0}(\mathbf{r_2}, \mathbf{r_1}) &= \begin{pmatrix} G^\perp_{0,12} & 0 & 0 \\ 0 & G^\perp_{0,12} & 0 \\ 0 & 0 & G^{||}_{0,12} \end{pmatrix},
\end{aligned} \tag{C.34}$$

which is due to the form of the free-space Green's tensor.

General expressions for xx, yy components of $\mathbf{G}_{\text{tot}}(\mathbf{r_0}, \mathbf{r_0})$ are quite cumbersome, but we are more interested in the non-diagonal term, which

is rather simple:

$$\begin{aligned}
&\mathrm{Num}\left[G_{\mathrm{sc},xy}(\mathbf{r_0},\mathbf{r_0})\right] = \mathrm{Num}\left[G_{\mathrm{sc},yx}(\mathbf{r_0},\mathbf{r_0})\right] = \\
&2\pi k^2\left(\alpha_{||}-\alpha_{\perp}\right)\left(\left[G^{\perp}_{0,10}\right]^2-\left[G^{\perp}_{0,20}\right]^2\right)\left(1-16\pi^2k^4\alpha_{||}\alpha_{\perp}\left[G^{\perp}_{0,12}\right]^2\right)\sin\left(2\varphi_0\right) \\
&\mathrm{Den}\left[G_{\mathrm{sc},ij}\right] = 1-8\pi^2k^4\left(\alpha_{||}+\alpha_{\perp}\right)^2\left[G^{\perp}_{0,12}\right]^2+256\pi^4k^8\alpha_{||}^2\alpha_{\perp}^2\left[G^{\perp}_{0,12}\right]^4- \\
&\qquad 8\pi^2k^4\left(\alpha_{||}-\alpha_{\perp}\right)^2\left[G^{\perp}_{0,12}\right]^2\cos\left(4\varphi_0\right),
\end{aligned}$$

where Num[...], Den[...] stand for numerator, and denominator, respectively, and $\mathbf{G}_{\mathrm{sc}}$ is defined as: $\mathbf{G}_{\mathrm{tot}} = \mathbf{G}_0 + \mathbf{G}_{\mathrm{sc}}$.

One can see that the condition $G_{sc,xy} = 0$ is satisfied when:

$$\begin{cases}
\alpha_{||} = \alpha_{\perp} \\
G^{\perp}_{0,10} = G^{\perp}_{0,20} \\
16\pi^2k^4\alpha_{||}\alpha_{\perp}\left[G^{\perp}_{0,12}\right]^2 = 1 \\
\varphi_0 = \dfrac{\pi}{2}m,\ m\in\mathbb{Z}.
\end{cases} \tag{C.35}$$

The first condition is obvious - in case of isotropic scatterers, there should be no chirality, as expected. The second condition in this configuration is equivalent to $|z_1 - z_0| \neq |z_2 - z_0|$, so as $z_1 \neq z_2$, then it means that the atom should not be right in between the scatterers. The third condition menifests interference of the fields generated by both particles, but this condition is unlikely to be satisfied as $\alpha_{||}, \alpha_{\perp}, G^{\perp}_{0,12} \in \mathbb{C}$. The last condition is related to the respective orientation of the scatterers principal axes: it means that once the long axes of scatterers are collinear or perpendicular - there is no chirality.

It is also instructive to consider the case of a strongly anisotropic scatterer $\alpha_{\perp} = 0$ as it is discussed in the maintext. In this regime we have:

$$\begin{aligned}
\mathrm{Den}\left[G_{\mathrm{sc},ij}\right] &= 1-8\pi^2k^4\alpha_{||}^2\left[G^{\perp}_{0,12}\right]^2\left(1+\cos(4\varphi_0)\right), \\
\mathrm{Num}\left[G_{\mathrm{sc},xy}\right] &= 2\pi k^2\alpha_{||}\left(\left[G^{\perp}_{0,10}\right]^2-\left[G^{\perp}_{0,20}\right]^2\right)\sin(2\varphi_0), \\
\mathrm{Num}\left[G_{\mathrm{sc},xx}\right] &= 4\pi k^2\alpha_{||}\big(\left[G^{\perp}_{0,10}\right]^2+\left[G^{\perp}_{0,20}\right]^2+ \\
&\quad 8\pi k^2\alpha_{||}G^{\perp}_{0,10}G^{\perp}_{0,20}G^{\perp}_{0,12}\cos(2\varphi_0)\big)\cos^2(\varphi_0), \\
\mathrm{Num}\left[G_{\mathrm{sc},yy}\right] &= 4\pi k^2\alpha_{||}\big(\left[G^{\perp}_{0,10}\right]^2+\left[G^{\perp}_{0,20}\right]^2- \\
&\quad 8\pi k^2\alpha_{||}G^{\perp}_{0,10}G^{\perp}_{0,20}G^{\perp}_{0,12}\cos(2\varphi_0)\big)\sin^2(\varphi_0).
\end{aligned} \tag{C.36}$$

Unlike in the previous case, here one can see more clearly that for $\varphi_0 = \pi/4$, $G_{sc,xx} = G_{sc,yy}$, therefore, for this rotation angle $g_{-,+} = -g_{+,-}$, and there is no asymmetry in the transition probabilities $P_{-,+}(t) = P_{+,-}(t)$.

Another option discussed in the maintext is that both scatterers, and the atom are in the xy-plane, more specifically, they all lie on the y-axis, and

the atom is right in-between the scatterers:

$$\mathbf{r_0} = \begin{pmatrix} 0 \\ 0 \\ 0 \end{pmatrix}, \ \mathbf{r_1} = \begin{pmatrix} 0 \\ +y \\ 0 \end{pmatrix}, \ \mathbf{r_2} = \begin{pmatrix} 0 \\ 0 \\ -y \end{pmatrix}. \tag{C.37}$$

We will also let the long axes of both scatterers to be parallel, so that $\boldsymbol{\alpha_1} = \boldsymbol{\alpha_2} = \mathbf{S}(\varphi_0) \cdot \mathrm{diag}\left(\alpha_{||}, \alpha_\perp, \alpha_\perp\right) \cdot \mathbf{S^{-1}}(\varphi_0)$. The required vacuum Green's tensors in this situation are given by:

$$\begin{aligned} \mathbf{G_0}(\mathbf{r_1}, \mathbf{r_0}) = \mathbf{G_0}(\mathbf{r_2}, \mathbf{r_0}) = \mathbf{G_0}(\mathbf{r_0}, \mathbf{r_1}) = \mathbf{G_0}(\mathbf{r_0}, \mathbf{r_2}) = \\ \begin{pmatrix} G^{\perp}_{0,20} & 0 & 0 \\ 0 & G^{||}_{0,20} & 0 \\ 0 & 0 & G^{\perp}_{0,20} \end{pmatrix}, \\ \mathbf{G_0}(\mathbf{r_1}, \mathbf{r_2}) = \mathbf{G_0}(\mathbf{r_2}, \mathbf{r_1}) = \begin{pmatrix} G^{\perp}_{0,12} & 0 & 0 \\ 0 & G^{||}_{0,12} & 0 \\ 0 & 0 & G^{\perp}_{0,12} \end{pmatrix}, \end{aligned} \tag{C.38}$$

In this case we have the following components of the Green's tensor:

$$\begin{aligned} \mathrm{Den}\left[G_{\mathrm{sc},ij}\right] = 1 - 2\pi k^2(\alpha_{||} + \alpha_\perp)(G^{||}_{0,12} + G^{\perp}_{0,12}) + \\ 16\pi^2 k^4 \alpha_{||}\alpha_\perp G^{||}_{0,12} G^{\perp}_{0,12} + 2\pi k^2(\alpha_{||} - \alpha_\perp)(G^{||}_{0,12} - G^{\perp}_{0,12})\cos(2\varphi_0), \\ \mathrm{Num}\left[G_{\mathrm{sc},xy}\right] = 4\pi k^2(\alpha_{||} - \alpha_\perp) G^{||}_{0,20} G^{\perp}_{0,20} \sin(2\varphi_0), \\ \mathrm{Num}\left[G_{\mathrm{sc},xx}\right] = 4\pi k^2 \left[G^{\perp}_{0,20}\right]^2 \big(\alpha_{||} + \alpha_\perp - 8\pi k^2 \alpha_{||}\alpha_\perp G^{||}_{0,12} + \\ (\alpha_{||} - \alpha_\perp)\cos(2\varphi_0)\big), \\ \mathrm{Num}\left[G_{\mathrm{sc},yy}\right] = 4\pi k^2 \left[G^{||}_{0,20}\right]^2 \big(\alpha_{||} + \alpha_\perp - 8\pi k^2 \alpha_{||}\alpha_\perp G^{\perp}_{0,12} + \\ (\alpha_\perp - \alpha_{||})\cos(2\varphi_0)\big). \end{aligned} \tag{C.39}$$

One can see that $G_{sc,xy} = 0$ if:

$$\begin{cases} \alpha_{||} = \alpha_\perp, \\ \varphi_0 = \dfrac{\pi}{2} m, \ \ m \in \mathbb{Z}. \end{cases} \tag{C.40}$$

However, unlike in the previous case of $\mathbf{r_0}, \mathbf{r_1}, \mathbf{r_2} || \mathbf{e_z}$, the conditions for having $G_{sc,xx} = G_{sc,yy}$ can not be formulated that straightforwardly, and, probably, this happens only accidentally for a very specific choice of many system's parameters.

D. (mandatory) Texts of author's publications

PHYSICAL REVIEW A **100**, 063832 (2019)

Extremely subradiant states in a periodic one-dimensional atomic array

D. F. Kornovan,[1,*] N. V. Corzo,[2,3] J. Laurat,[2] and A. S. Sheremet[2,4,†]

[1]*Department of Nanophotonics and Metamaterials, ITMO University, St. Petersburg 197101, Russia*
[2]*Laboratoire Kastler Brossel, Sorbonne Université, CNRS, ENS–Université PSL, Collège de France, 4 place Jussieu, 75005 Paris, France*
[3]*Centro de Investigación y de Estudios Avanzados del I.P.N. Unidad Querétaro, Libramiento Norponiente 2000, 76230 Querétaro, Mexico*
[4]*Russian Quantum Center, Novaya 100, 143025 Skolkovo, Moscow Region, Russia*

(Received 24 June 2019; published 19 December 2019)

We study the subradiant collective states of a periodic chain of two-level atoms with either transversal or longitudinal transition dipole moments with respect to the chain axis. We show that long-lived subradiant states can be obtained for the transversal polarization by properly choosing the chain period for a given number of atoms in the case of no open diffraction channels. While not being robust against the positional disorder along the chain, these highly subradiant states have a linewidth that decreases with the number of atoms much faster than it was shown previously. In addition, our paper shows that similar states are present even if there are additional interaction channels between the atoms, i.e., they interact via the waveguide mode of an optical nanofiber, for instance. We develop a theoretical framework allowing us to describe the spectral properties of the system in terms of contributions from each collective eigenstate and we show that subradiant states manifest themselves in the transmission and reflection spectra, allowing us to observe interaction-induced transparency in a very narrow spectral range. Such long-lived collective states may find potential applications in nanophotonics and quantum optics.

DOI: 10.1103/PhysRevA.100.063832

I. INTRODUCTION

Cooperative effects in spatially dense atomic ensembles have generated large interest in recent years due to the significant induced modifications to the optical properties of the system [1–11]. These effects come from strong dipole-dipole interaction in a collection of quantum emitters with a subwavelength average separation. Recent experimental advances in trapping techniques have made it possible to create one-dimensional (1D) [12,13], two-dimensional [14–17], and three-dimensional (3D) [18,19] spatially ordered atomic configurations where such collective effects can play a very important role. The most prominent phenomenon is superradiance [20–24], i.e., the enhancement of the collective spontaneous emission rate that can be explained as a constructive interference between the emission pathways of N closely located dipoles. Contrary to this effect, the subradiance [6,25–30] is the suppression of the collective emission rate due to the destructive interference between dipoles. Being interesting due to their enhanced lifetimes, these states are, however, hard to observe experimentally because of their weak coupling to the light field and strong sensitivity to additional nonradiative decay channels. Nevertheless, such states have been observed for a pair of trapped ions [31], ultracold molecules [32], polymer nanostructures [33], atomic gases [27,34], and thermal light sources [35].

At the same time, one-dimensional systems recently gained special attention as a possible platform for quantum light-matter interfaces due to the strong transverse confinement of the light field and the possibility of infinite-range atom-atom interaction [36,37]. Such a system is a versatile platform for achieving efficient light-atom coupling due to the collective nature of atomic interaction with the evanescent field of the guided mode [38]. The strong coupling of an atomic ensemble with such a nanophotonic waveguide provides opportunities to further develop the emerging field of waveguide QED [11,39–41], in which many remarkable results were recently demonstrated not only in the field of theoretical research [40,42–53] but also in experiments [54–60], including observation of subradiant states [61].

From these perspectives subradiant states in quasi-one-dimensional atomic chains are of interest for the development of new approaches in quantum technologies. In particular, generation of a periodic one-dimensional atomic chain in the subdiffractional regime, where the period of the system is smaller than half of the resonant wavelength, can bring new effects that cannot be achieved in free space because of the limited mode matching between light and the atomic system [51,52].

Optical properties of 1D systems containing a large number of scatterers were studied previously in different contexts from arrays of nanoparticles [62–65] to cold atoms [7,66]. In this paper, we study the subradiant effects occurring in a periodic one-dimensional atomic chain in the subwavelength regime, when the period of the system is smaller than $\lambda_0/2$, with $\lambda_0 = 2\pi c/\omega_0$ being the resonant radiation wavelength. We consider a regular 1D chain of two-level atoms coupled to a single-mode nanofiber including free-space spontaneous emission with inherent dipole-dipole coupling, as shown in Fig. 1. In order to study the effect of subradiance, we have

*d.kornovan@metalab.ifmo.ru
†alexandra.sheremet@lkb.upmc.fr

extended the formalism developed in our previous work [49] introducing the eigenstate picture [67], and calculated transmission and reflection coefficients for each eigenstate. In our theoretical formalism, we consider the full Green's tensor of the electromagnetic field taking into account all of the field modes (free-space, radiation, guided, and near-field modes) without applying the paraxial regime as it was done in [53]. As a reference point, we first study suppression of the spontaneous emission rate for the atomic chain in vacuum using a microscopic approach of light scattering. In a further step, we extend our system considering atoms trapped near a single-mode nanofiber. In such a system in addition to the collective coupling to the 3D free-space vacuum modes, the nanofiber structure introduces an additional channel of virtually infinite-range dipole-dipole coupling. In this paper we aim to find conditions required for manifestation of a highly subradiant state with the collective emission rate less than the known N^{-3} scaling.

The paper is organized as follows. In Sec. II we first review the theoretical framework for the case of a periodic chain in free space and discuss different quantities relative to the studied collective effect. For the sake of intuitive understanding, we start by considering $N = 3$ atoms and then increase the number of atoms in the system. In Sec. III we discuss the modification of the theory for the case of the waveguide mode scattering and demonstrate a similar expansion to the one developed in Sec. II. We show that the long-lived dark states are present even for atoms coupled not only by a vacuum dipole-dipole interaction but also through a guided mode.

II. LIGHT SCATTERING IN AN ATOMIC ARRAY IN VACUUM

In this section, we consider single-photon scattering in a one-dimensional array of N two-level atoms with a period Δz in vacuum (see Fig. 1). A single photon with a near-resonant atomic frequency induces electric dipoles in each atom of the array. The strength of the atomic response on the incident photon drastically depends on the interatomic distance. Thus, atoms with a large distance between their neighbors Δz behave as independent scatters, while closely located atoms bring a collective response. The key point of this collective behavior is that each atom is driven not only by the incident photon but also by the field emitted by all other atoms in the array. The resulting dipole-dipole interaction between atoms significantly modifies their scattering properties.

In quantum theory, the scattering process can be described in terms of the scattering matrix, which can be linked to observable variables such as transmittance and reflectance. Moreover, the cooperative nature of the interaction can be roughly characterized by the resonance widths of the total cross-section spectra or the decay rates of the collective states.

In this section, we investigate collective effects by studying the eigenvalues of the system. These characteristics allow us to find decay rates for each collective state and cross-section spectrum. The emergence of the collective effects strongly depends on the interatomic distance Δz, thus illustrating the role of dipole-dipole interaction in the formation of subradiant states.

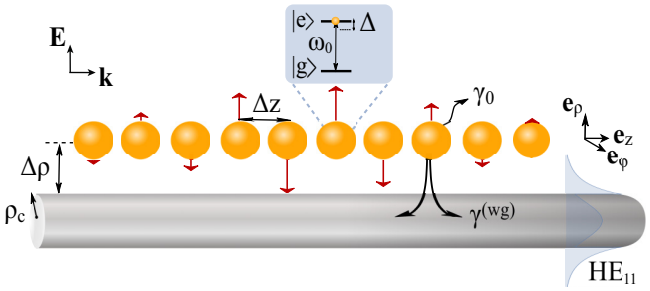

FIG. 1. Light scattering on the 1D array of two-level atoms separated by a distance Δz and trapped at a distance $\Delta\rho$ from the surface of an optical nanofiber with radius ρ_c and permittivity ε. The fiber radius ρ_c is less than the atomic resonant wavelength, so only the fundamental mode HE_{11} can be guided. The red arrows indicate the eigenvector components of the subradiant state for $N = 10$ atoms.

A. General theoretical formalism

In order to simplify the theoretical description, let us consider the single-photon scattering process, where the initial and the final states of the decoupled atom-photon system can be represented as $|l\rangle = |g\rangle^{\otimes N}|1_\mu\rangle$, $|k\rangle = |g\rangle^{\otimes N}|1_{\mu'}\rangle$, where the index μ describes a particular field mode $\mu = (\mathbf{k}, s)$, where $\mathbf{k}$ is the wave vector, $s = 1, 2$ denotes two orthogonal polarizations, and $|g\rangle^{\otimes N}$ means that all N atoms are in the ground state $|g\rangle$.

The scattering process can be described by the scattering matrix S [68] that transforms the asymptotic states from the initial l to the final system state k and has the following form:

$$S_{kl} = \delta_{kl} - 2\pi i T_{kl}(E_l + i0)\delta(E_k - E_l). \tag{2.1}$$

Here the T matrix has the standard form [68]:

$$\hat{T} = \hat{V} + \hat{V}\hat{G}(E + i0)\hat{V}, \tag{2.2}$$

where $\hat{G}(E) = (E - \hat{H})^{-1}$ is the resolvent operator of the total Hamiltonian $\hat{H} = \hat{H}_0 + \hat{V}$. In the dipole approximation the interaction operator $\hat{V}$ has the form $\hat{V} = -\sum_{i=1}^{N} \hat{\mathbf{d}}_i \hat{\mathbf{E}}(\mathbf{r}_i)$, where $\hat{\mathbf{d}}_i = d_{i,eg}\hat{\sigma}^+ + d_{i,ge}\hat{\sigma}^-$ is the dipole moment operator of the ith atom, and $\hat{\mathbf{E}}(\mathbf{r}_i)$ is the field operator at the atomic position $\mathbf{r}_i$. In the rotating-wave approximation the matrix elements of the operator $\hat{T}$ can be found as a projection onto the Hilbert subspace of the vacuum state for the electromagnetic field and the single excited state for the atomic subsystem [68]:

$$\hat{P}\hat{G}(E)\hat{P} = \hat{P}\frac{1}{E - \hat{H}_0 - \hat{\Sigma}(E)}\hat{P},$$
$$\hat{\Sigma}(E) = \hat{V}\frac{1}{E - \hat{H}}\hat{V}, \tag{2.3}$$

where the projector operator can be defined as $\hat{P} = \sum_{i=1}^{N} |g_1, \ldots, e_i, \ldots g_N; \{0_\mu\}\rangle\langle\{0_\mu\}; g_1, \ldots e_i, \ldots, g_N|$, and the level-shift operator has the form $\hat{\Sigma}(E) \approx \hat{V}(E - \hat{H}_0)^{-1}\hat{V}$ in second-order perturbation theory.

We now apply the resonant approximation, where the scattering photon frequency ω can be considered close to the atomic transition frequency ω_0. In this approximation the level-shift operator $\hat{\Sigma}(E)$ can be assumed to be a slowly

varying function of the argument as $\hat{\Sigma} \approx \hat{\Sigma}(E_0 = \hbar\omega_0)$. The single- and double-particle contributions to the level-shift operator can be written as

$$\Sigma^{(nn)}(E_0) = \hbar\left(\Delta_{\mathrm{L}}^{\mathrm{vac}} - i\frac{\gamma_0}{2}\right),$$

$$\Sigma^{(mn)}(E_0) = -\mathbf{d}_{m,eg}\left\{\frac{k_0^2 e^{ik_0R}}{R}\left[\left(1 + \frac{ik_0R - 1}{k_0^2R^2}\right)\mathbf{I} + \frac{\mathbf{R}\otimes\mathbf{R}}{R^2}\cdot\frac{3 - 3ikR - k^2R^2}{k^2R^2}\right]\right\}\mathbf{d}_{n,ge}, \quad (2.4)$$

where $\Delta_{\mathrm{L}}^{\mathrm{vac}}$ is the vacuum Lamb shift, $\gamma_0 = \frac{4|\mathbf{d}|^2\omega_0^3}{3\hbar c^3}$ is the free-space spontaneous emission rate for a two-level atom, $k_0 = \omega_0/c$ is the resonant wave number, $\mathbf{R} = |\mathbf{r}_i - \mathbf{r}_j|$ is the distance between an atom i and an atom j, $\mathbf{I}$ is the unit dyad, and $\otimes$ stands for the outer product. Note that Eq. (2.4) is written in CGS units, and it will be used from now on. Here the single-particle contribution is responsible for the vacuum Lamb shift (and it is considered to be already included into the definition of the transition frequency ω_0) and the finite lifetime of the atomic excited state, while the double-particle contribution describes the excitation transfer between atoms and takes into account the dipole-dipole interaction.

In general, the scattering process in free space is characterized by *the total cross section*, which can be found using the optical theorem [69]:

$$\sigma_{\mathrm{tot}} = -\frac{2\mathbb{V}}{\hbar c}\mathrm{Im}\, T_{ii}(E_i + i0), \quad (2.5)$$

where $\mathbb{V}$ is the quantization volume. Since the dipole-dipole interaction alters the eigenstates of the system, it is convenient to expand the total cross section Eq. (2.5) into a sum, where each term will correspond to a particular collective eigenstate of the system. From Eq. (2.3) one can see that both $\Sigma(\omega_0)$ and $[E - H_0 - \Sigma(\omega_0)]^{-1}$ share the same set of eigenvectors, while their eigenstates are simply shifted by $E - H_0$. Therefore, we can rewrite the total cross section taking into account the form of the vacuum field operator $\hat{E}(\mathbf{r}) = \sum_{\mathbf{k},s} i\sqrt{\frac{2\pi\hbar\omega}{\mathbb{V}}}(\hat{a}_{\mathbf{k},s}\mathbf{e}_{\mathbf{k},s}e^{i\mathbf{kr}} - \mathrm{H.c.})$ as

$$\sigma_{\mathrm{tot}}(\Delta) = \sum_{j=1}^{N}\sigma_j(\Delta) = -\frac{3\pi\hbar\gamma_0}{k_0^2}\mathrm{Im}\sum_{j=1}^{N}\frac{f_j}{\hbar\Delta - \lambda_j}, \quad (2.6)$$

where $\Delta = \omega - \omega_0$ is the detuning, and $f_j = [(e^{-i\mathbf{kr_1}}, \ldots, e^{-i\mathbf{kr_N}})S_{[:,j]}] \times [[S^{-1}]_{\{j,:\}}(e^{i\mathbf{kr_1}}, \ldots, e^{i\mathbf{kr_N}})^T]$ with S being the transformation matrix to the eigenspace of $\Sigma(\omega_0)$ with corresponding eigenvectors $S_{[:,j]}$ as its columns. The parameter f_j corresponds to a complex-valued oscillator strength amplitude associated with a particular collective eigenstate and for a collection of N two-level atoms $\sum_{j=1}^{N} f_j = N$. The physical meaning of the factor f_j, as can be seen from the definition above, is that it is related to the overlap between the photon and the jth eigenstates of the system. Furthermore from a mathematical point of view, the expansion in Eq. (2.6) essentially simplifies the process of finding the total cross section. Thus, instead of inversion of a $N \times N$ matrix for each frequency point for Eq. (2.5), it is enough to diagonalize the problem only once for a given configuration and then to find the spectrum analytically [Eq. (2.6)]. This property is very important for a large number of atoms N. Note that similar decomposition was introduced in [67] to expand the scattering cross section for a collection of classical dipoles.

We can rewrite the total cross section Eq. (2.6) in the following form:

$$\sigma_{\mathrm{tot}}(\Delta) \sim \mathrm{Im}\sum_{j=1}^{N}\left[\frac{f_j}{\hbar\Delta - \lambda_j}\right] = \sum_{j=1}^{N}\frac{f_j'\lambda'' + f_j''(\hbar\Delta - \lambda_j')}{(\hbar\Delta - \lambda_j')^2 + \lambda_j''^2}, \quad (2.7)$$

where prime and double prime indicate real and imaginary parts, respectively. One can see that each contribution $\sigma_j(\Delta)$ to the total cross section consists of two terms: a dissipative term, which is proportional to f_j' and has a Lorentzian shape, and a dispersive term, proportional to f_j'', which introduces asymmetries. Note that by analogy with the level-shift operator Eq. (2.4), here the first term, corresponding to the single-particle contribution, is always present, while the second term appears in the system of interacting atoms. As the second term in Eq. (2.7) is antisymmetric, the area under a partial cross section $\sigma_j(\Delta)$ is proportional to f_j': $\int_{-\alpha}^{\alpha}\sigma_j(\Delta)d\Delta \sim f_j'$, which provides the contribution of a particular eigenstate to the total cross section. Note that for $\alpha \to \infty$ the corresponding integral $\int_{-\alpha}^{\alpha}\sigma_j(\Delta)d\Delta$ formally diverges, which is a well-known problem of the Cauchy distribution having no finite moments of order greater than or equal to 1. However, we can integrate over a symmetric region with a sufficiently large and physically meaningful parameter α. There is also another reason to consider a finite value of α: integration over the whole frequency might not be consistent with the Markov approximation $[\hat{\Sigma} \approx \hat{\Sigma}(E_0 = \hbar\omega_0)]$ in some specific situations.

B. Collective effects in the array of $N = 3$ atoms

In order to present the effect of subradiance in more details, we now analytically solve the problem of light scattering in an array of $N = 3$ two-level atoms, which has also been studied before in the context of super-radiance [70] and cooperative scattering [66].

The matrix of the level-shift operator Eq. (2.4) can be rewritten in terms of coupling constants, which are related to dipole-dipole interaction between atoms as follows:

$$\Sigma = \begin{pmatrix} g_{\mathrm{self}} & g_1 & g_2 \\ g_1 & g_{\mathrm{self}} & g_1 \\ g_2 & g_1 & g_{\mathrm{self}} \end{pmatrix}, \quad (2.8)$$

where $g_{\mathrm{self}} = -i\gamma_0/2$, g_1 is the matrix element related to the interaction between the atoms being one period apart $(1 - 2, 2 - 3)$, and g_2 is for atoms two periods away from each other $(1 - 3)$. In this context, the corresponding eigenvalues

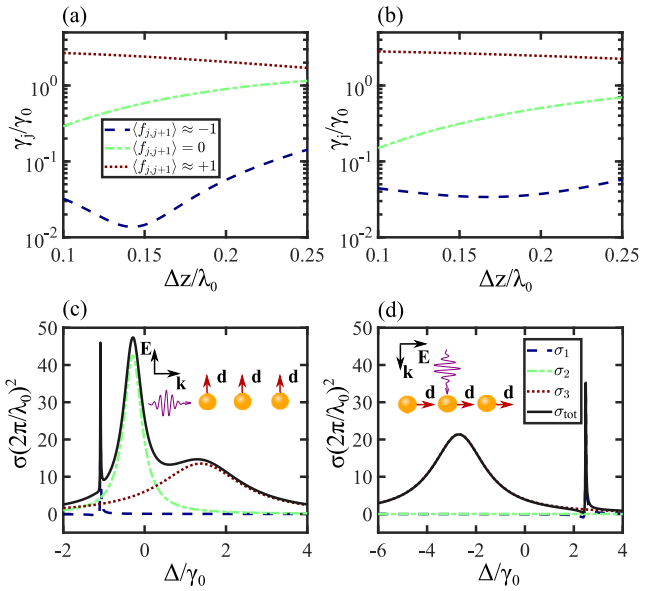

FIG. 2. Scattering of a photon propagating along (left column) and perpendicular (right column) to the chain axis. (a, b) Normalized spontaneous emission rates γ_j for the eigenstates of the regular array of $N = 3$ atoms as a function of the period Δz. Blue dashed, green dash-dotted, and red dotted lines correspond to three states with different values of the nearest-neighbor correlation function Eq. (2.10). (c, d) The partial σ_j and the total σ_{tot} scattering cross sections in the array of $N = 3$ atoms with the period Δz giving the minimal γ_j.

of this matrix can be easily found in the following forms:

$$\lambda_1 = \tfrac{1}{2}\left(2g_{\text{self}} + g_2 + \sqrt{8g_1^2 + g_2^2}\right),$$
$$\lambda_2 = g_{\text{self}} - g_2,$$
$$\lambda_3 = \tfrac{1}{2}\left(2g_{\text{self}} + g_2 - \sqrt{8g_1^2 + g_2^2}\right). \tag{2.9}$$

In Figs. 2(a) and 2(b) we provide the spontaneous decay rates of these three states for the transversal and longitudinal photon polarizations, respectively. In Fig. 2(a) we can see that for a state corresponding to λ_1 (blue dashed line) it is possible to achieve a strong suppression of the emission rate for some array period Δz. Indeed, for the array of $N = 3$ atoms with $\Delta z \approx 0.14\lambda_0$ the imaginary part of λ_1 is more than an order of magnitude smaller than the linewidths of the two other states.

Additionally, in order to characterize the collective effects of the system, we can introduce a *nearest-neighbor correlation function* [66]:

$$\left\langle f_{i,i+1}^j \right\rangle = \frac{1}{N-1}\sum_{i=1}^{N} \cos\left(\phi_{i+1}^j - \phi_i^j\right), \tag{2.10}$$

as shown in Fig. 2 by color grading. Here a phase angle of the ith component of the jth eigenvector $\phi_i^j = \arg[c_i^j]$ corresponds to a probability amplitude c_i^j to have the excited atom i for the eigenstate j. The function Eq. (2.10) gives the information about the phase correlation between neighboring dipoles: it is equal to $+1$ for the neighboring dipoles with the same phases, and -1 for the neighboring dipoles with opposite phases [66]. As one can see from Fig. 2, this correlation function provides useful information for a few-atoms case, and allows distinguishing states with different symmetry. We also note that the state with the smallest value of $\langle f_{i,i+1}^j \rangle$ also possesses the smallest emission rate γ_j due to the state symmetry; by further tuning Δz it is possible to achieve a very small γ_j as seen from Fig. 2(a).

In Figs. 2(c) and 2(d) we show the partial $\sigma_j(\Delta)$ and the total $\sigma_{\text{tot}}(\Delta)$ cross sections of the photon for two cases: when atoms have transverse [Figs. 2(a) and 2(c)] and longitudinal [Figs. 2(b) and 2(d)] dipole moments with respect to the chain axis. The cross-section profile of the subradiant state $\sigma_1(\Delta)$ is asymmetric due to the significant non-Lorentzian part $\sim f_j''$, as it appears in Eq. (2.7).

In this simple and already studied example we have shown that there exists a specific interatomic spacing that allows us to strongly suppress the emission rate of the system. In the next section we demonstrate what happens in an array with a larger number of atoms.

C. Collective effects in an array of N two-level atoms: Highly subradiant states

In this subsection we apply the developed formalism to the case of N two-level atoms in vacuum. Increasing the number of atoms leads to significant manifestation of collective effects. The difference between transverse and longitudinal cases becomes thereby more evident: the transverse one shows a variety of highly subradiant states for different lattice periods Δz as shown in Fig. 3(a). The difference in the behavior between transverse and longitudinal dipolar chains has been studied before in the context of optical properties of 1D nanoparticle arrays [62,66].

The arrangement of atoms in a 1D chain with a subdiffractional period leads to a strong subradiance. Figures 3(a) and 3(b) show the collective decay rates for an array of $N = 10$ atoms for various periods Δz. One can see that the strong subradiance appears only for transverse polarization. Moreover, this effect can be obtained for different atomic periods, as indicated by arrows in Fig. 3(a). Furthermore, from Fig. 3(b) it can be seen that interaction of an array of atoms with longitudinally polarized dipole moments leads to subradiance as well. But the dependence of the eigenvalue decay rate in this case is rather smooth and without any special features. To understand the difference of collective effects for different polarization in more details, let us compare the dipole-dipole coupling constants for these two cases:

$$g^{\perp} = -\frac{3}{4}\hbar\gamma_0 e^{ik_0\Delta z}\left[\frac{1}{(k_0\Delta z)} + \frac{i}{(k_0\Delta z)^2} - \frac{1}{(k_0\Delta z)^3}\right],$$
$$g^{\parallel} = -\frac{3}{2}\hbar\gamma_0 e^{ik_0\Delta z}\left[-\frac{i}{(k_0\Delta z)^2} + \frac{1}{(k_0\Delta z)^3}\right]. \tag{2.11}$$

Now one can gain a physical intuition about the subradiance for different polarizations: there is no *far-field* contribution in the dipole-dipole coupling constant in the case of the longitudinal polarization [Eq. (2.11)]. Therefore, the strong subradiance results from an interplay between different types of fields: near, intermediate, and, importantly, far fields.

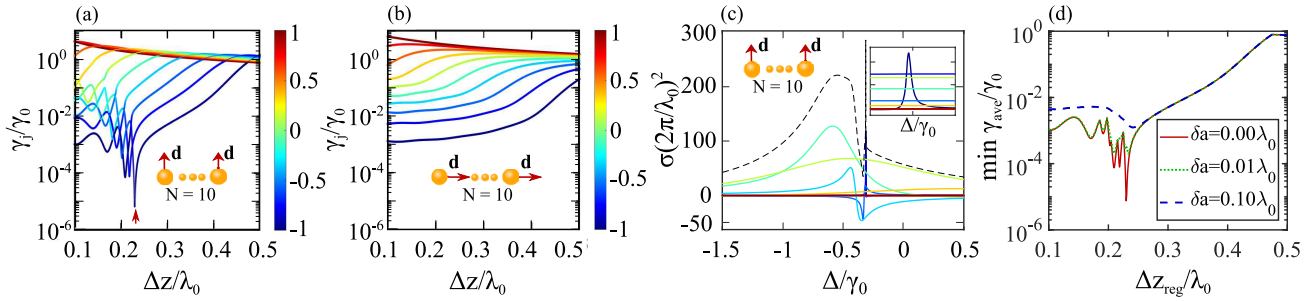

FIG. 3. Normalized spontaneous emission rates γ_j of eigenstates as a function of the array period Δz for $N = 10$ atoms. All atomic dipole moments are either purely transversal (a) or longitudinal (b). The color grade specifies the nearest-neighbor correlation function value; the bright red arrow points out the global minimum of the decay rate. (c) The total (black dashed) and the partial (color solid) cross sections (σ_{tot} and σ_j) for the specific case of the transverse polarization and an array period $\Delta z \approx 0.23\lambda_0$, shown by the red arrow in (a). The inset shows the region near the most subradiant state. (d) The effect of position disorder on a minimal collective decay rate γ_j for an atomic array with a period Δz_{reg}. The position of each atom is slightly fluctuating according to a uniform distribution and it is plotted for different maximal deviations δa.

Furthermore, comparison of Figs. 2(a) and 3(a) reveals that the subradiant states appear at different atomic periods and with different spontaneous emission rates, which depend on the number of atoms N in the chain.

In Fig. 3(c) we also show the total cross section for the system period Δz_{sub}, which allows us to achieve the minimal possible emission rate γ_j [red arrow in Fig. 3(a)]. One can see that for $N = 10$ the subradiant state appears in the spectrum as a sharp and asymmetric peak. It can be explained as a result of several overlapping resonances which contribute to the total cross section in this area [see inset of Fig. 3(c)] leading to a large total cross-section value in this spectral region.

Another feature of these dark states is their sensitivity to position disorder, when the atomic array is not perfectly periodic. In Fig. 3(d) we show the dependence of the average minimal collective emission rate γ_{ave} on the regular atomic array period introducing small fluctuation with uniform distribution and the maximal deviation δa. We see that even with small fluctuations $\delta a = 0.01\lambda_0$ in the atomic positions the resonances are almost smeared out, while a larger disorder induces a slight reduction of the emission rate in the range of regular system periods $0.20\lambda_0 < \Delta z_{\text{reg}} < 0.25\lambda_0$.

D. Emission rate scaling with atom number N

It is also interesting to understand how the emission rate of this highly subradiant state depends on the number of atoms N in the chain. Previously, in [71], it has been shown that in a subdiffractional chain of dielectric particles the quality factor of most bound modes scales as $\approx N^3$. Recently this question was also studied in the context of atomic chains, where the spontaneous emission rate for most subradiant states decreases as $\approx N^{-3}$ [51,72] at least in some range of periods.

In our subdiffractional atomic array with the lattice period Δz_{sub} taken from Fig. 3, the value of the collective spontaneous emission rate scales as $\approx N^{-6.88}$, as shown in Fig. 4(a). A much faster decrease of the emission rate with number of atoms N in comparison with the aforementioned studies [51,71,72] happens due to a proper choice of the system period Δz_{sub}, which allows us to achieve a better destructive interference between scattering channels. We can see in Fig. 4(b) that this value is saturated to $\Delta z_{\text{sub}} \sim 0.24\lambda_0$ for a large number of atoms N.

Another physically important quantity is the oscillator strength amplitude of the corresponding collective eigenstate f_j. We can see from Figs. 4(a) and 5(a) that $|f_j(N)|$ basically follows the same behavior as γ_j, but involves additional oscillations. This can be explained if one considers the overlap between the eigenstate j with the z-propagating photon. In most cases, the "darker" the collective state is (and the smaller the corresponding decay rate γ_j is), the smaller this overlap with the photon. Also we note that the distance between two neighboring local minima of $|f_j(N)|$ caused by the aforementioned oscillations is close to $\Delta N \approx 4$. These oscillations are induced by a bigger or smaller overlap between the atomic collective eigenstate and the z-propagating photon. In Fig. 5(b) one can also see how the total scattering cross section [Eq. (2.7)] for the system period Δz_{sub} varies with atom number N: for sufficiently large N subradiant states manifest themselves as a set of very sharp peaks; however, their relative contribution to the spectrum becomes less pronounced.

Finally, we address the scaling of the subradiant state emission rate in the presence of disorder in the atomic positions.

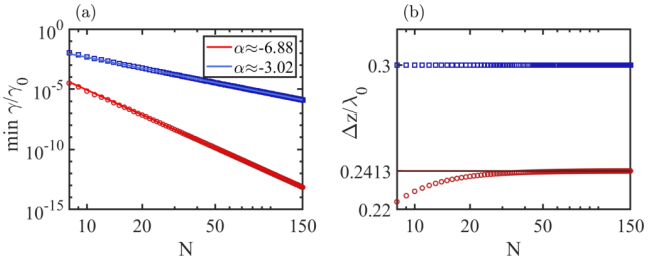

FIG. 4. (a) Collective emission rates for the most subradiant state as a function of the number of atoms N: blue open squares and red open circles correspond to $\Delta z = 0.3\lambda_0$ and Δz_{sub}, respectively; α specifies the characteristic scaling with the number of atoms, $\gamma_j \sim N^{\alpha}$, and the corresponding fitting curves are specified by light blue and light red solid lines. In order to find α we used only data points for which $N \geqslant 20$. (b) The corresponding array periods Δz vs number of atoms N for which the subradiant state with the decay rate γ_j can be achieved; note that the red open circles approach the value close to $\Delta z_{\text{sub}} \approx 0.24\lambda_0$ for large N.

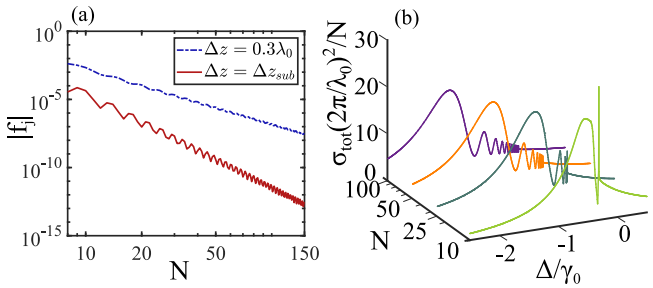

FIG. 5. (a) Dependence of the complex oscillator strength $|f_j|$ on the number of atoms N; blue dash-dotted and red solid lines are for a fixed period ($\Delta z = 0.3\lambda_0$) and $\Delta z_{\rm sub}$ from Fig. 4(b), correspondingly. (b) The normalized total cross section $\sigma_{\rm tot}(2\pi/\lambda_0)^2/N$ for different N. For each N we choose the lattice period to be equal to $\Delta z_{\rm sub}$.

In Fig. 6 we provide the emission rate scaling as a function of the number of atoms N for two different disorders in the position of an atom j: $z_j = z_{{\rm reg},j} + 2\delta a U(0,1)$. Here $z_{{\rm reg},j} = (j-1)\Delta z_{\rm reg}$ is the atomic position for a regular chain and U(0, 1) stands for a uniformly distributed pseudo random real number between 0 and 1.

From Fig. 6 one can see that disorder leads to a significantly slower decrease rate $\approx N^{-3.7}$ and this happens even for relatively small deviations from perfect periodicity ($2\delta a = 10^{-3}\lambda_0$). However, increasing the number of atoms N in the chain results in a transition to another regime, where a decrease of the emission rate is even slower. Numerical estimations show that in this region the scaling is on the order of $\approx N^{-0.3}$–$N^{-0.4}$. The main reason for this transition is related to disorder which induces localization of states. It can be estimated by calculating the inverse participation ratio (IPR) [73]: ${\rm IPR}^{-1} = \sum_{j=1}^{N} |c_j^{(k)}|^4$, where k is the label of a state of interest and $c_j^{(k)}$ is the probability amplitude

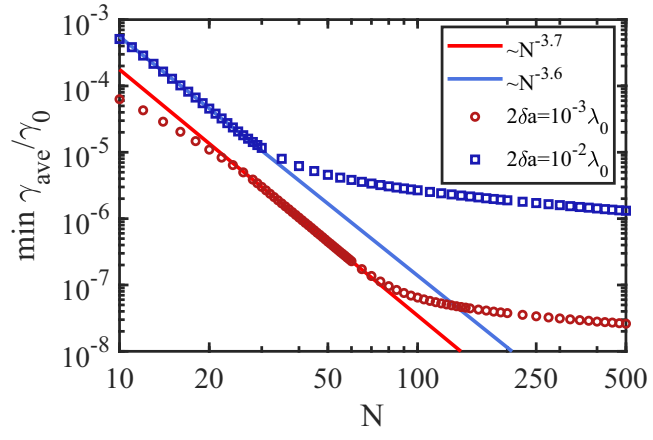

FIG. 6. Average minimal emission rate, corresponding to the most subradiant state, vs the atom number N for the case of a uniform disorder of atomic z positions. Two maximal position deviations are considered: $2\delta a = 10^{-3}\lambda_0$ (open dark red circles) and $2\delta a = 10^{-2}\lambda_0$ (open dark blue squares). Note that for both cases there are distinct regions of a $\approx N^{\alpha}$ behavior in the region of small N, where the linear fit in the double-log plot was performed, which is shown in solid bright red and solid bright blue lines, correspondingly.

that the atom j is excited in a state k. For instance, for a positional disorder $2\delta a = 10^{-2}\lambda_0$, and for a number of atoms $N = 20$ (the region of min $\gamma_{\rm ave}/\gamma_0 \sim N^{-3.7}$ scaling), the average IPR of the corresponding subradiant state is equal to IPR ≈ 7.7, while for $N = 200$ (where the scaling switches to min $\gamma_{\rm ave}/\gamma_0 \sim N^{-0.36}$) IPR ≈ 9.7. With this, one can see that for a sufficiently large atom number $N \gg 1$ the subradiant states become strongly localized (IPR $\ll N$), and extension of the atomic chain does not modify the min $\gamma_{\rm ave}/\gamma_0$ significantly, contrary to the case of perfect periodicity.

III. LIGHT SCATTERING ON AN ARRAY OF ATOMS TRAPPED IN THE VICINITY OF AN OPTICAL NANOFIBER

So far we have studied the collective subradiance of an atomic array in vacuum. It is known that the light-atoms interaction can be significantly enhanced by placing the atomic system near a nanoscale object. Indeed, trapping atoms in the vicinity of an optical nanofiber dramatically changes the character of the atomic interaction and provides long-range dipole-dipole coupling between atoms not only via vacuum but also through the nanofiber guided mode. In this section we study modification of coupling effects coming from the scattering of the guided mode on an atomic chain trapped near the nanofiber surface (Fig. 1).

A. Theoretical framework of the light scattering process for an atomic array trapped near an optical nanofiber

In this subsection we modify the developed formalism of light scattering in free space by introducing additional interaction via the nanofiber guided mode. Foremost, we need to modify the outer operators $\hat{V}$ in Eq. (2.2), which are responsible for absorption of the incoming guided photon and emission of the photon back into the same field mode. Furthermore, we are interested only in guided field modes of the outer operators $\hat{V}$. However, the operator $\hat{\Sigma}(E_0)$ introduced in Eq. (2.4) for free space should include now all possible modes. The field subsystem in this configuration can be described using the quantization scheme proposed in [74], where the quantized electric field of the nanofiber guided mode can be written as

$$\hat{\mathbf{E}}(\mathbf{r}) = \sum_{\mu} \mathbf{E}_{\mu}(\mathbf{r})\hat{a}_{\mu} + {\rm H.c.}, \tag{3.1}$$

where $\mathbf{E}_{\mu}$ is the electric field of the guided mode μ given by

$$\mathbf{E}_{\mu}(\mathbf{r}) = i\sqrt{\frac{2\pi\hbar\omega_{\mu}}{\mathbb{L}}}\tilde{\mathbf{E}}_{\mu}(\rho,\phi)e^{if\beta_{\mu}z+im\phi}. \tag{3.2}$$

Here β_{μ} is the propagation constant, $\tilde{\mathbf{E}}_{\mu}(\rho,\phi)$ is the amplitude of the electric field, $\mathbb{L}$ is the quantization length, and f and m define the direction of propagation and the mode angular momentum, respectively. The electric field is periodic in the z direction with $\beta_l\mathbb{L} = 2\pi l$, where l is a positive integer, and the electric-field amplitude is normalized according to

$$\int_0^{2\pi}\int_0^{\infty} |\tilde{\mathbf{E}}_{\mu}(\rho,\phi)|^2 d\phi\rho d\rho = 1. \tag{3.3}$$

For simplicity, we assume that all atoms are located at the same distance $\Delta\rho$ from the nanofiber surface. All matrix elements of the outer operator $\hat{V}$ have, therefore, the same absolute values and differ only by phases. The outer operators $\hat{V}$ presented in the matrix T in Eq. (2.2) can finally be written as

$$\begin{aligned}&\langle e_a, \{0\}|\hat{V}|g_a, 1_{\mu'}\rangle \\ &\quad = -i(\mathbf{d}_{a,eg}\cdot\tilde{\mathbf{E}}_{\mu'}(\rho_a,\phi_a))\sqrt{\frac{2\pi\hbar\omega_{\mu'}}{\mathbb{L}}}e^{i\beta_{\mu'}z_a+i\phi_a}, \\ &\langle g_b, 1_{\mu''}|\hat{V}|e_b, \{0\}\rangle \\ &\quad = i(\tilde{\mathbf{E}}^*_{\mu''}(\rho_b,\phi_b)\cdot\mathbf{d}_{b,ge})\sqrt{\frac{2\pi\hbar\omega_{\mu''}}{\mathbb{L}}}e^{-i\beta_{\mu''}z_b-i\phi_b}\end{aligned} \tag{3.4}$$

where β_μ is the propagation constant of the guided mode μ.

In the next step, we calculate the matrix elements of the operator $\hat{\Sigma}$ in the presence of the nanofiber. The theoretical description of excitation transfer between atoms through the radiation into vacuum and nanofiber guided modes was done in [75]. Using this formalism, the Hamiltonian of our system can be written as

$$\begin{aligned}\hat{H}_0 &= \sum_n \hbar\omega_0\hat{\sigma}_n^+\hat{\sigma}_n^- + \int d\mathbf{r}'\int_0^\infty d\omega'\hbar\omega'\hat{\mathbf{f}}^\dagger(\mathbf{r}',\omega')\hat{\mathbf{f}}(\mathbf{r}',\omega'), \\ \hat{V} &= -\sum_n \hat{\mathbf{d}}_n\hat{\mathbf{E}}(\mathbf{r}_n),\end{aligned} \tag{3.5}$$

where ω_0 is the atomic transition frequency. $\hat{\mathbf{E}}(\mathbf{r}_n)$ is the total electric field and $\hat{\mathbf{f}}(\mathbf{r}',\omega')$ and $\hat{\mathbf{f}}^\dagger(\mathbf{r}',\omega')$ are the bosonic vector local-field operators, which obey the following commutation relations:

$$\begin{aligned}&[\hat{f}_i(\mathbf{r}',\omega'), \hat{f}_k^\dagger(\mathbf{r},\omega)] = \delta_{ik}\cdot\delta(\mathbf{r}'-\mathbf{r})\cdot\delta(\omega'-\omega), \\ &[\hat{f}_i(\mathbf{r}',\omega'), \hat{f}_k(\mathbf{r},\omega)] = 0.\end{aligned} \tag{3.6}$$

The positive-frequency part of the total electric field has the following form:

$$\begin{aligned}&\hat{\mathbf{E}}^+(\mathbf{r}) \\ &\quad = i\sqrt{4\hbar}\int d\mathbf{r}'\int_0^\infty d\omega'\frac{\omega'^2}{c^2}\sqrt{\epsilon_I(\mathbf{r}',\omega')}\mathbf{G}(\mathbf{r},\mathbf{r}',\omega')\cdot\hat{\mathbf{f}}(\mathbf{r}',\omega'),\end{aligned} \tag{3.7}$$

where $\epsilon_I(\mathbf{r}',\omega')$ is the imaginary part of the dielectric permittivity of the media and $\mathbf{G}(\mathbf{r},\mathbf{r}',\omega')$ is the classical Green's tensor of the electric field. In the presence of the optical nanofiber the Green's tensor can be expanded into

$$\mathbf{G}(\mathbf{r},\mathbf{r}',\omega) = \mathbf{G}_0(\mathbf{r},\mathbf{r}',\omega) + \mathbf{G}_s(\mathbf{r},\mathbf{r}',\omega), \tag{3.8}$$

where $\mathbf{G}_0$ is the vacuum Green's tensor, and $\mathbf{G}_s$ is the Green's tensor corresponding to light scattering from the nanofiber. The scattering term of the Green's tensor can be expanded into the vector wave functions (VWFs) and the details of these calculations are given in Appendix A. In the lowest nonvanishing order, the matrix elements of the level-shift operator can be written as

$$\langle f|\hat{\Sigma}(E)|i\rangle = \sum_{|\alpha\rangle,|\beta\rangle}\langle f|\hat{V}|\alpha\rangle\langle\alpha|\frac{1}{E-\hat{H}_0+i\eta}|\beta\rangle\langle\beta|\hat{V}|i\rangle, \tag{3.9}$$

where $|i\rangle$ and $|f\rangle$ are the initial and final states of the system, respectively; $|\alpha\rangle$ and $|\beta\rangle$ are the two possible intermediate states with a single elementary excitation for the field subsystem. Both atoms are either in the excited or the ground state:

$$|e_n, e_m\rangle\times\hat{\mathbf{f}}^\dagger(\mathbf{r}',\omega')|\{0\}\rangle, \quad |g_n, g_m\rangle\times\hat{\mathbf{f}}^\dagger(\mathbf{r}',\omega')|\{0\}\rangle. \tag{3.10}$$

Further details on the derivation of the matrix elements of the level-shift operator Eq. (3.9) can be found in [76] and here we provide only the final expression:

$$\langle f|\hat{\Sigma}(E)|i\rangle = -4\pi\frac{\omega_0^2}{c^2}\mathbf{d}_{m,eg}\cdot\mathbf{G}(\mathbf{r}_m,\mathbf{r}_n,\omega_0)\mathbf{d}_{n,ge}. \tag{3.11}$$

The matrix $\hat{\Sigma}(E)$ can be found using Eq. (3.11). Note that the scattering matrix Eq. (2.1) is also valid in the presence of the nanofiber. In the field quantization scheme that we use here one should include summation over final states into Eq. (2.1), going into the limit $\mathbb{L}\to\infty$, which means that the propagation constant β can now be continuous. This limit is equivalent to $\sum_{n_\beta}\to\frac{\mathbb{L}}{2\pi}\int_0^\infty\frac{d\beta}{d\omega}d\omega$. In the end we seek the expression for the scattering matrix:

$$S_{f',p';fp} = \delta_{f',p';fp} - i\frac{\mathbb{L}}{c\hbar\cdot dk/d\beta}T_{f',p';fp}(E), \tag{3.12}$$

which can be also found in [53].

B. *S* matrix in the eigenstate picture

Let us now analyze the scattering process considering the eigenstates of the system. For this, we need to diagonalize the matrix $\Sigma(\omega_0)$, which is responsible for the coupling of different atomic states through the field modes. We should mention that in the case of a reciprocal problem Σ is a symmetric matrix, while in a nonreciprocal one (when, for example, a magnetic field is applied to separate the σ^+ and σ^- transitions, making only one of them active at a given frequency) Σ is not symmetric anymore, and it has different right and left eigenvectors. However, the diagonalization of the problem can be simply done by choosing the right eigenvectors, for instance,

$$\begin{aligned}\Sigma(E_0)v_j^{(r)} &= \lambda_j v_j^{(r)}, \\ (S^{(r)})^{-1}\frac{1}{I\hbar\Delta-\Sigma(E_0)}S^{(r)} &= \frac{1}{I\hbar\Delta-\Lambda},\end{aligned} \tag{3.13}$$

where the matrix $S^{(r)}$ is the transformation matrix to the eigenspace the columns of which are the right eigenvectors $v^{(r)}$ of $\Sigma(E_0)$, Δ is the photon detuning from the atomic resonance, and Λ is a diagonal matrix having the corresponding eigenvalues λ_j as its entries.

In order to simplify the final expression for the scattering matrix, we can express the product of two outer $\hat{V}$ matrix elements Eq. (3.5) using the known relations for the spontaneous

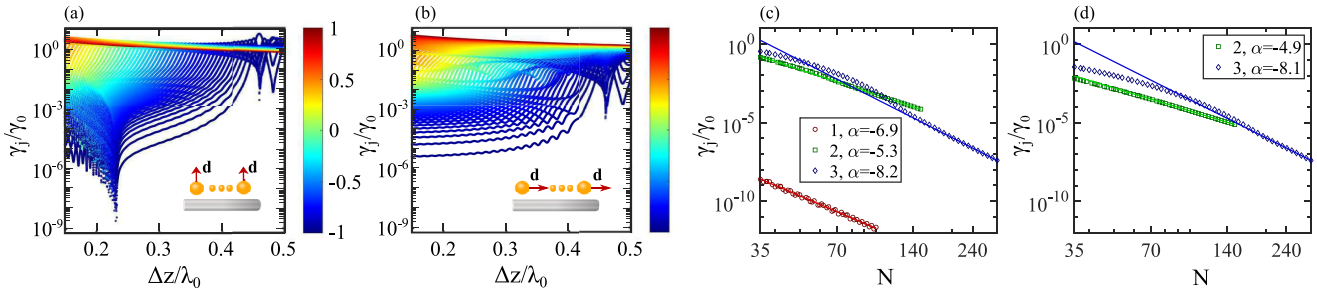

FIG. 7. (a) Spontaneous emission rates γ_j/γ_0 of the eigenstates j for a periodic chain of $N = 75$ atoms placed near the nanofiber at a distance $\Delta\rho = \rho_c$ from the surface. The dipole moments of all atoms are aligned along the $\mathbf{e}_\rho$ direction. The nanofiber has radius $\rho_c = 0.25\lambda_0$ and $\epsilon = 2.1$. (b) Same as in (a), but for dipole moments aligned along the axis $\mathbf{e_z}$. Color grade in (a) and (b) corresponds to values of the nearest-neighbor correlation function Eq. (2.10) for each collective eigenstate. (c, d) Local minima of the subradiant states in (a) and (b) with the number of atoms N. The solid lines correspond to linear approximations. Only the fundamental mode HE_{11} was taken into account for these calculations.

emission rate into the forward-propagating guided modes:

$$\gamma_{wg}^{(f)} = \sum_m \frac{3\pi |\mathbf{n}_{eg}\tilde{\mathbf{E}}_{f=+1,m}|^2 d\beta/dk}{2k_0^2}\gamma_0$$
$$= \sum_m \frac{2\pi |\mathbf{d}_{eg}\tilde{\mathbf{E}}_{f=+1,m}|^2 k_0 \cdot d\beta/dk}{\hbar}. \quad (3.14)$$

In this special symmetry we can push the coupling constant to the forward-propagating guided mode $\gamma_{wg}^{(f)}$ outside of the sum over the eigenstates and finally rewrite the S matrix element corresponding to forward scattering as

$$S_{ii} = 1 - i\hbar\gamma_{wg}^{(f)} \sum_j \frac{f_j^{(t)}}{\hbar\Delta - \lambda_j}, \quad (3.15)$$

which has a form similar to Eq. (2.6) with $f_j^{(t)}$ being complex-valued constants. We observe that indeed considering equal coupling strengths for all of the atoms is clear: in this case coefficients $f_j^{(t)}$ are dimensionless and carry information only about the phase. However, it is possible to rewrite it for a general situation, but the meaning of $f_j^{(t)}$ will be slightly different and it will take into account the couplings of individual atoms to the guided mode.

The light scattering in a one-dimensional configuration can be characterized by a transmission coefficient $t = |S_{ii}|^2$, which can be written in the following form, as shown in Appendix B:

$$|S_{ii}|^2 = 1 + 2\hbar\gamma_{wg}^{(f)} \sum_{j=1}^{N} \left[\frac{\eta_j^{(t)}\lambda_j'' + \xi_j^{(t)}(\hbar\Delta - \lambda_j')}{(\hbar\Delta - \lambda_j')^2 + \lambda_j''^2}\right],$$
$$\eta_j^{(t)} = f_j^{(t)\prime} - \sum_{i=1}^{N} \hbar\gamma_{wg}^{(f)} \mathrm{Im}\left[\frac{f_j^{(t)}(f_i^{(t)})^*}{\lambda_j - \lambda_i^*}\right],$$
$$\xi_j^{(t)} = f_j^{(t)\prime\prime} + \sum_{i=1}^{N} \hbar\gamma_{wg}^{(f)} \mathrm{Re}\left[\frac{f_j^{(t)}(f_i^{(t)})^*}{\lambda_j - \lambda_i^*}\right]. \quad (3.16)$$

One can see that the transmission, as with the cross section for the vacuum case Eq. (2.7), includes Lorentzian and non-Lorentzian terms. However, the respective dimensionless coefficients $\xi_j^{(t)}$ and $\eta_j^{(t)}$ differ: apart from $f_j^{(t)\prime}$ and $f_j^{(t)\prime\prime}$ there are also terms expressed through $\frac{f_j^{(t)}(f_i^{(t)})^*}{\lambda_j - \lambda_i}$, which can be associated with the interference of i and j resonances.

Similarly, we can expand the reflection coefficient and the corresponding reflectance as

$$S_{bf} = -i\hbar\sqrt{\gamma_{wg}^{(f)}\gamma_{wg}^{(b)}} \sum_j \frac{f_j^{(r)}}{\hbar\Delta - \lambda_j},$$
$$|S_{bf}|^2 = \sum_{i,j} \hbar^2\gamma_{wg}^{(f)}\gamma_{wg}^{(b)} \frac{f_j^{(r)}(f_i^{(r)})^*}{(\hbar\Delta - \lambda_j)(\hbar\Delta - \lambda_i^*)}$$
$$= 2\hbar\gamma_{wg}^{(f)} \sum_{j=1}^{N} \frac{\left[\eta_j^{(r)}\lambda_j'' + \xi_j^{(r)}(\hbar\Delta - \lambda_j')\right]}{(\hbar\Delta - \lambda_j')^2 + \lambda_j''^2},$$
$$\eta_j^{(r)} = -\hbar\gamma_{wg}^{(b)} \mathrm{Im} \sum_{i=1}^{N} \left[\frac{f_j^{(r)}(f_i^{(r)})^*}{\lambda_j - \lambda_i^*}\right],$$
$$\xi_j^{(r)} = \hbar\gamma_{wg}^{(b)} \mathrm{Re} \sum_{i=1}^{N} \left[\frac{f_j^{(r)}(f_i^{(r)})^*}{\lambda_j - \lambda_i^*}\right]. \quad (3.17)$$

We analyze the subradiance in the presence of a nanoscale waveguide in the next subsection.

C. Highly subradiant states and atom number scaling in the presence of a nanofiber

We now apply the developed formalism to the perfectly periodic 1D array of atoms trapped near a nanofiber. Similarly to the free-space configuration, in Fig. 7 we show the spontaneous emission rate of each eigenstate of the periodic chain of $N = 75$ atoms into the fundamental nanofiber mode HE_{11}, as well as the dependence of the spontaneous emission minima on the number of atoms N.

The third subradiant resonance at $\Delta z \approx 0.48\lambda_0$ can be explained as a result of interference between the two interaction channels: the vacuum modes and the guided mode. In Figs. 7(c) and 7(d) we show the scaling of these minima with

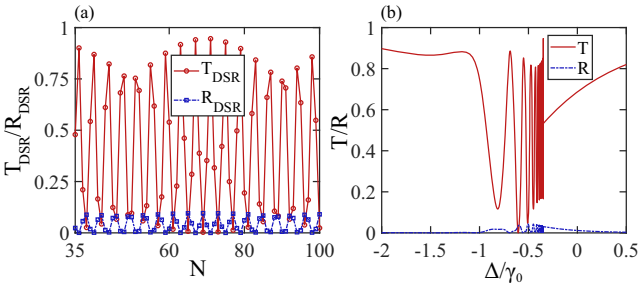

FIG. 8. (a) Transmission (red circles, solid line) and reflection (blue squares, dash-dotted line) of guided light in a 1D array of N trapped atoms with a lattice period $\Delta z = \Delta z_{\text{sub}}$ corresponding to the dark state. (b) Transmission (red solid line) and reflection (blue dash-dotted line) spectra for $N = 71$, which corresponds to the highest T_{DSR} in (a). All fiber parameters are the same as for Fig. 7.

the number of atoms N. One can see that for sufficiently large N all three curves follow to $\approx N^{\alpha}$ dependency.

D. Subradiant states in the transmission and reflection spectra

In the context of the specific 1D configuration of the system, it is interesting to study the transmission and reflection coefficients at the subradiant resonance condition.

In Fig. 8(a) we show the dependence of the transmission and the reflection coefficients on the number of trapped atoms N for the first subradiant state. One can see that these coefficients have oscillating behavior making the system either transparent with $T \geqslant 0.75$ and $R \sim 0$ or opaque with $T \leqslant 0.10$ and $R \approx 0.10$. A corresponding spectrum in the first subradiant state range of Δz is shown in Fig. 8(b) for $N = 71$ atoms, where one can see many distinct subradiant states and a very sharp resonance with $T \approx 0.90$. The nature of such oscillations in T_{DSR} and R_{DSR} is the same as was discussed for the scattering of a photon on a transverse chain in vacuum: it appears due to an oscillating value of the overlap between the atomic eigenstate and the photon, and these oscillations have the same distance between the local minima of $\Delta N = 4$.

The transmission and reflection for the second subradiant state that appears at the Bragg resonance condition for the fundamental guided mode are shown in Fig. 9. One can see that at the second subradiant state the atom-atom interaction

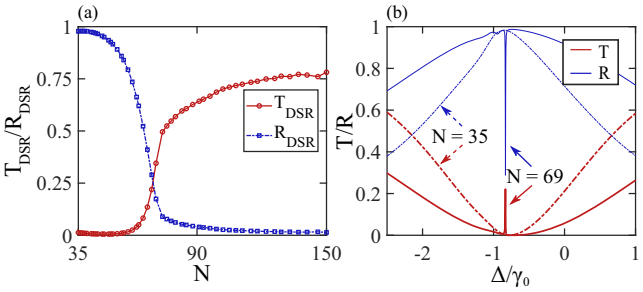

FIG. 9. (a) Same as in Fig. 8(a), but at the second subradiant resonance condition. (b) Transmission (red) and reflection (blue) spectra for $N = 35$ (dash-dotted line) and $N = 69$ (solid line) atoms. All other relevant parameters are the same as for Fig. 7.

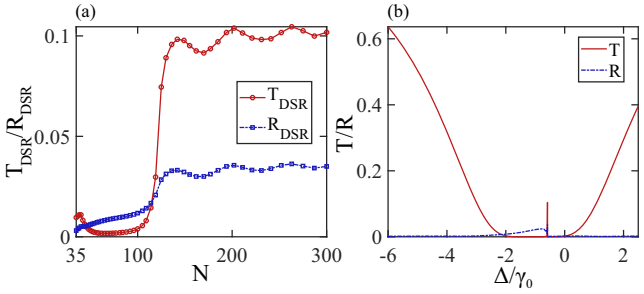

FIG. 10. (a) Same as in Fig. 8(a), but for the third subradiant resonance condition. (b) Transmission (red solid line) and reflection (blue dash-dotted line) spectra for $N = 202$. All other relevant parameters are the same as for Fig. 7.

has different behavior. Effectively, one can say that the total spectrum mainly consists of the super-radiant and a very long-lived subradiant state $T = |S_{ii}|^2 = 1 + T^{\text{BS}} + T^{\text{DS}}$, where BS and DS correspond to bright and dark states [77]. Futhermore, increasing the number of atoms N makes this dark state more distinguishable and leads to an increase of the transmission and reduction of the reflection [see Fig. 9(a)]. At the same time, the system can be purely transparent or purely reflective for a small number of atoms at this resonance condition and can have a very narrow transparency window near $\Delta/\gamma_0 \approx -1$ for the large number of atoms, as it is shown in Fig. 9(b).

The third subradiant state, which is the result of interaction between the vacuum and the nanofiber guided modes, does not show any particularly interesting behavior: both the transmission and the reflection are small (less than 0.1) for the considered number of atoms N, as shown in Fig. 10(a). At the same time, the subradiant state manifests itself as a sharp resonance with a small amplitude of both the transmission T and the reflection R [see Fig. 10(b)].

IV. CONCLUSION

In conclusion, we have studied the subradiant collective states for a periodic array of two-level atoms with a given dipole moment transition in the subdiffractional regime. We considered the atomic array both in free space and trapped in the vicinity of an optical nanofiber. Trapping atoms with transversal dipole moments in a one-dimensional array with specific lattice periods Δz provides a significant reduction of the collective emission rate; the emission rate can be decreased further by taking a bigger number of atoms N. Importantly, we have shown that this dependency on the number of atoms is $\approx N^{-6}$–N^{-7}, unlike the known so far $\approx N^{-3}$ scaling. We have found that the corresponding period has an asymptotic value $\Delta z \approx 0.24\lambda_0$ for a large number of atoms N in vacuum. In addition, we studied the scaling of the collective emission rate in the presence of positional disorder along the chain. We have shown that the introduction of disorder in the system leads to a slower decrease of the emission rate up to $\approx N^{-3.6}$. There is also a transition to a significantly slower decrease rate after a certain number of atoms N, which happens due to disorder-induced localization of states.

Moreover, we have studied the subradiant states when the interaction between the atoms is also provided by the fundamental guided mode of an optical nanofiber. We showed that in this scenario there are extremely subradiant states similar to those mentioned before for the vacuum case and they affect the optical properties of the system like transmittance and reflectance leading to the presence of very sharp peaks in the spectra. We found that in the corresponding resonance frequency the system becomes either highly transparent or opaque depending upon the number of atoms N.

There are also two other types of subradiant states that appear in the presence of a nanofiber. These states are present for both transverse and longitudinal cases: one can be observed on the first Bragg resonance for the nanofiber guided mode and the other one is the result of an interplay between the vacuum and guided mode interaction channels. The former one allows the subradiant state on the first Bragg resonance to be visible in the transmission or reflection spectra opening a very narrow window of a partial transparency for sufficiently large N. The latter is weakly pronounced in the spectra at least for the considered set of parameters.

Extremely subradiant states studied in this paper may find applications in both atomic optics and quantum information science in relation to the problem of quantum memory, for instance [51]. We also want to note that such states might be studied in the context of not only cold atoms physics but also nanophotonics, e.g., 1D arrays of dielectric or plasmonic nanoparticles. In this field of research long-lived states might be exploited in order to create tunable discrete waveguides, where the optical properties of an overall system are defined by characteristics of individual elements and their arrangement.

ACKNOWLEDGMENTS

D.F.K. acknowledges support from the Embassy of France in Russia via the Ostrogradski scholarship, and support from Basis Foundation. This work was supported by the European Research Council (Starting Grant HybridNet), Sorbonne Université (PERSU program), the French National Research Agency (NanoStrong project), the Ile-de-France DIM Sirteq, and Russian Science Foundation (Project No. 19-72-10129). A.S.S. is supported by the European Union (Marie Curie fellowship NanoArray).

APPENDIX A

The classical electromagnetic Green's tensor of our system can be found from the vector Helmholtz equation:

$$\left[-\frac{\omega^2}{c^2}\varepsilon(\mathbf{r},\omega)+\nabla\times\nabla\times\right]\mathbf{G}(\mathbf{r},\mathbf{r}',\omega)=\mathbf{I}\delta(\mathbf{r}-\mathbf{r}'), \tag{A1}$$

where $\varepsilon(\mathbf{r},\omega)$ is the complex dielectric function and $\mathbf{I}$ is the unit dyad. In our case we consider a dielectric cylindrical waveguide of radius ρ_c and dielectric permittivity ε being constant inside the cylinder. To find the solution we apply the scattering superposition method [78,79], which allows us to expand the Green's tensor into homogeneous and inhomogeneous terms:

$$\mathbf{G}(\mathbf{r},\mathbf{r}',\omega)=\mathbf{G}_0(\mathbf{r},\mathbf{r}',\omega)+\mathbf{G}_s(\mathbf{r},\mathbf{r}',\omega). \tag{A2}$$

As soon as we consider dielectric particles in the vicinity of the waveguide, so that $\mathbf{r}$ and $\mathbf{r}'$ are outside the cylinder, the homogeneous term is always present and describes the field directly generated at the field point $\mathbf{r}$ by the source placed at the point $\mathbf{r}'$. This term can be obtained analytically from the Green's tensor written in Cartesian coordinates using the transformation from Cartesian to cylindrical coordinates $\mathbf{S}(\phi)\mathbf{G}_0^{\mathrm{Cart}}(\mathbf{r},\mathbf{r}',\omega)\mathbf{S}^T(\phi')$, where $\mathbf{G}_0^{\mathrm{Cart}}$ has an analytic expression [80] and is given by

$$\mathbf{G}_0^{\mathrm{Cart}}(\mathbf{r},\mathbf{r}',\omega)=\left(\mathbf{I}+\frac{1}{k^2}\nabla\otimes\nabla\right)G_0(\mathbf{r},\mathbf{r}',\omega), \tag{A3}$$

where $G_0(\mathbf{r},\mathbf{r}',\omega)$ is the Green's function of the scalar Helmholtz equation.

The scattering term can be calculated via the integral representation of the homogeneous part. To obtain this representation we apply the method of VWFs explained in details in [78,79], here we cover only the basic ideas and provide the final expressions. To find the solution of the vector Helmholtz equation (A1), we introduce the scalar Helmholtz equation and the solution of this equation in the cylindrical coordinates:

$$\nabla^2\phi(\mathbf{k},\mathbf{r})+k^2\phi(\mathbf{k},\mathbf{r})=0,\quad \phi_n(k_z,\mathbf{r})=J_n(k_\rho\rho)e^{in\theta+ik_z z}, \tag{A4}$$

where $J_n(x)$ is the Bessel function of the first kind, $\mathbf{r}=(\rho,\theta,z)$ are the cylindrical coordinates and k_ρ and k_z are the projections of the wave vector $\mathbf{k}$. The solution of the vector Helmholtz equation may be written in terms of the following vector wave functions:

$$\begin{aligned}\mathbf{M}_n(k_z,\mathbf{r})&=\nabla\times[\phi_n(k_z,\mathbf{r})\mathbf{e_z}],\\ \mathbf{N}_n(k_z,\mathbf{r})&=\frac{1}{k}\nabla\times\mathbf{M}_n(k_z,\mathbf{r})\end{aligned} \tag{A5}$$

where $\mathbf{e_z}$ is the so-called pilot vector, the unit vector pointing in the z direction. These VWFs $\mathbf{M_n}(k_z,\mathbf{r})$ and $\mathbf{N_n}(k_z,\mathbf{r})$ correspond to TE and TM modes of the field.

One can show [78] that the homogeneous part of the Green's function can be expanded in terms of these vector wave functions in the following way:

$$\begin{aligned}\mathbf{G}_0(\mathbf{r},\mathbf{r}',\omega)=&-\frac{\mathbf{e}_\rho\mathbf{e}_\rho}{k_0^2}\delta(\mathbf{r}-\mathbf{r}')\\ &+\frac{i}{8\pi}\sum_{n=-\infty}^{\infty}\int_{-\infty}^{\infty}\frac{dk_z}{k_{0\rho}^2}\mathbf{F}_n(k_z,\mathbf{r},\mathbf{r}')\end{aligned} \tag{A6}$$

and the $\mathbf{F}_n(k_z,\mathbf{r},\mathbf{s})$ function is given by

$$\begin{aligned}&\mathbf{M}_n^{(1)}(k_z,\mathbf{r})\overline{\mathbf{M}}_n(k_z,\mathbf{r}')+\mathbf{N}_n^{(1)}(k_z,\mathbf{r})\overline{\mathbf{N}}_n(k_z,\mathbf{r}')\\ &\mathbf{M}_n(k_z,\mathbf{r})\overline{\mathbf{M}}_n^{(1)}(k_z,\mathbf{r}')+\mathbf{N}_n(k_z,\mathbf{r})\overline{\mathbf{N}}_n^{(1)}(k_z,\mathbf{r}')\end{aligned} \tag{A7}$$

where the first line holds for $\rho_r>\rho_{r'}$ while the second one holds for $\rho_r<\rho_{r'}$, and $k_0=\omega/c$, $k_{0\rho}=\sqrt{k_0^2-k_z^2}$, and the superscript (1) in vector wave functions denotes that the Bessel function of the first kind $J_n(k_\rho\rho)$ should be replaced with the Hankel function of the first kind $H_n^{(1)}(k_\rho\rho)$. Here we

provide the explicit form of VWFs:

$$\mathbf{M}_n(k_z,\mathbf{r})=\begin{pmatrix}\frac{in}{\rho}J_n(k_{0\rho}\rho)\\ -k_{0\rho}(J_n[k_{0\rho}\rho)]'\\ 0\end{pmatrix}e^{in\theta+ik_zz},$$

$$\mathbf{N}_n(k_z,\mathbf{r})=\begin{pmatrix}\frac{ik_zk_{0\rho}}{k}[J_n(k_{0\rho}\rho)]'\\ -\frac{nk_z}{\rho k}J_n(k_{0\rho}\rho)\\ \frac{k_{0\rho}^2}{k}J_n(k_{0\rho}\rho)\end{pmatrix}e^{in\theta+ik_zz},$$

$$\overline{\mathbf{M}}_n(k_z,\mathbf{r}')=\begin{pmatrix}-\frac{in}{\rho}J_n(k_{0\rho}\rho')\\ -k_{0\rho}[J_n(k_{0\rho}\rho')]'\\ 0\end{pmatrix}^T e^{-in\theta'-ik_zz'},$$

$$\overline{\mathbf{N}}_n(k_z,\mathbf{r}')=\begin{pmatrix}-\frac{ik_zk_{0\rho}}{k}[J_n(k_{0\rho}\rho')]'\\ -\frac{nk_z}{\rho'k}J_n(k_{0\rho}\rho')\\ \frac{k_{0\rho}^2}{k}J_n(k_{0\rho}\rho')\end{pmatrix}^T e^{-in\theta'-ik_zz'} \tag{A8}$$

where $J_n(k_\rho\rho)'$ corresponds to the derivative with respect to the dimensionless argument.

Now having the integral representation of the homogeneous term of the Green's function, we can construct the scattering term in a similar fashion. Let us denote the medium outside the dielectric cylinder as 1 and the medium inside as 2. The particular form of the Green's tensor depends on the position of a source point $\mathbf{r}'$: whether it is inside or outside the cylinder. We are interested in a situation when both source and receiver are outside the cylinder, and in the latter we consider only the second case. Thus, the total Green's tensor can be written as

$$\begin{aligned}\mathbf{G}^{11}(\mathbf{r},\mathbf{r}',\omega)&=\mathbf{G}_0^{11}(\mathbf{r},\mathbf{r}',\omega)+\mathbf{G}_s^{11}(\mathbf{r},\mathbf{r}',\omega),\\ \mathbf{G}^{21}(\mathbf{r},\mathbf{r}',\omega)&=\mathbf{G}_s^{21}(\mathbf{r},\mathbf{r}',\omega),\end{aligned} \tag{A9}$$

where the two superscripts denote the positions of the receiver and the source point, respectively, and the two scattering parts of the Green's tensor have the following forms:

$$\begin{aligned}\mathbf{G}_s^{11}(\mathbf{r},\mathbf{r}',\omega)&=\frac{i}{8\pi}\sum_{n=-\infty}^{\infty}\int_{-\infty}^{\infty}\frac{dk_z}{k_{\rho1}^2}\mathbf{F}_{\mathbf{M};n,1}^{11(1)}(k_z,\mathbf{r})\overline{\mathbf{M}}_{n,1}^{(1)}(k_z,\mathbf{r}')\\ &\quad+\mathbf{F}_{\mathbf{N};n,1}^{11(1)}(k_z,\mathbf{r})\overline{\mathbf{N}}_{n,1}^{(1)}(k_z,\mathbf{r}'),\\ \mathbf{F}_{\mathbf{M};n,1}^{11(1)}(k_z,\mathbf{r})&=R_{MM}^{11}\mathbf{M}_{n,1}^{(1)}(k_z,\mathbf{r})+R_{NM}^{11}\mathbf{N}_{n,1}^{(1)}(k_z,\mathbf{r}),\\ \mathbf{F}_{\mathbf{N};n,1}^{11(1)}(k_z,\mathbf{r})&=R_{MN}^{11}\mathbf{M}_{n,1}^{(1)}(k_z,\mathbf{r})+R_{NN}^{11}\mathbf{N}_{n,1}^{(1)}(k_z,\mathbf{r}),\end{aligned} \tag{A10}$$

$$\begin{aligned}\mathbf{G}_s^{21}(\mathbf{r},\mathbf{r}',\omega)&=\frac{i}{8\pi}\sum_{n=-\infty}^{\infty}\int_{-\infty}^{\infty}\frac{dk_z}{k_{\rho1}^2}\mathbf{F}_{\mathbf{M};n,2}^{21}(k_z,\mathbf{r})\overline{\mathbf{M}}_{n,1}^{(1)}(k_z,\mathbf{r}')\\ &\quad+\mathbf{F}_{\mathbf{N};n,1}^{21}(k_z,\mathbf{r})\overline{\mathbf{N}}_{n,1}^{(1)}(k_z,\mathbf{r}'),\\ \mathbf{F}_{\mathbf{M};n,2}^{21}(k_z,\mathbf{r})&=R_{MM}^{21}\mathbf{M}_{n,2}(k_z,\mathbf{r})+R_{NM}^{21}\mathbf{N}_{n,2}(k_z,\mathbf{r}),\\ \mathbf{F}_{\mathbf{N};n,2}^{21}(k_z,\mathbf{r})&=R_{MN}^{21}\mathbf{M}_{n,2}(k_z,\mathbf{r})+R_{NN}^{21}\mathbf{N}_{n,2}(k_z,\mathbf{r}),\end{aligned} \tag{A11}$$

where the scattering Fresnel coefficients R_{AB}^{ij} are introduced and the second subscript in the VWFs denotes that k and k_ρ should be replaced with their values inside the corresponding media $k_i=\varepsilon_i(\mathbf{r},\omega)k_0$, $k_{\rho i}=\sqrt{k_i^2-k_z^2}$. We should notice that, unlike the case of the homogeneous term, here we have products of **M** and **N**, which is due to the fact that the normal modes in our case have hybrid natures.

The form of the Fresnel coefficients mentioned above can be found by imposing the boundary conditions on the Green's tensor at the surface of the cylinder:

$$\mathbf{e}_\rho\times[\mathbf{G}^{11}(\mathbf{r},\mathbf{r}',\omega)-\mathbf{G}^{21}(\mathbf{r},\mathbf{r}',\omega)]|_{\rho_r=\rho_c}=0,\quad \mathbf{e}_\rho\times\nabla_{\mathbf{r}}\times[\mathbf{G}^{11}(\mathbf{r},\mathbf{r}',\omega)-\mathbf{G}^{21}(\mathbf{r},\mathbf{r}',\omega)]|_{\rho_r=\rho_c}=0. \tag{A12}$$

Solving for this, we can find the Fresnel coefficients R_{AB}^{ij} and, finally, construct the scattering part of the Green's tensor $\mathbf{G}_s(\mathbf{r},\mathbf{r}',\omega)$. We provide the explicit expressions for the Fresnel coefficients below:

$$\begin{aligned}DT(k_z)&=-\left(\frac{1}{k_{\rho2}^2}-\frac{1}{k_{\rho1}^2}\right)^2k_z^2n^2+\left(\frac{[J_n(k_{\rho2}\rho_c)]'}{k_{\rho2}J_n(k_{\rho2}\rho_c)}-\frac{[H_n^{(1)}(k_{\rho1}\rho_c)]'}{k_{\rho1}H_n^{(1)}(k_{\rho1}\rho_c)}\right)\times\left(\frac{[J_n(k_{\rho2}\rho_c)]'k_2^2}{k_{\rho2}J_n(k_{\rho2}\rho_c)}-\frac{[H_n^{(1)}(k_{\rho1}\rho_c)]'k_1^2}{k_{\rho1}H_n^{(1)}(k_{\rho1}\rho_c)}\right)\rho_c^2,\\ R_{MM}^{11}(k_z)&=\frac{J_n(k_{\rho1}\rho_c)}{H_n^{(1)}(k_{\rho1}\rho_c)}\left[\left(\frac{1}{k_{\rho2}^2}-\frac{1}{k_{\rho1}^2}\right)^2k_z^2n^2-\left(\frac{[J_n(k_{\rho2}\rho_c)]'}{k_{\rho2}J_n(k_{\rho2}\rho_c)}-\frac{[J_n(k_{\rho1}\rho_c)]'}{k_{\rho1}J_n(k_{\rho1}\rho_c)}\right)\right.\\ &\quad\left.\times\left(\frac{[J_n(k_{\rho2}\rho_c)]'k_2^2}{k_{\rho2}J_n(k_{\rho2}\rho_c)}-\frac{[H_n^{(1)}(k_{\rho1}\rho_c)]'k_1^2}{k_{\rho1}H_n^{(1)}(k_{\rho1}\rho_c)}\right)\rho_c^2\right]\frac{1}{DT(k_z)},\\ R_{NM}^{11}(k_z)&=\frac{J_n(k_{\rho1}\rho_c)}{H_n^{(1)}(k_{\rho1}\rho_c)}\frac{1}{k_{\rho1}}\left(\frac{1}{k_{\rho1}^2}-\frac{1}{k_{\rho2}^2}\right)\left(\frac{[J_n(k_{\rho1}\rho_c)]'}{J_n(k_{\rho1}\rho_c)}-\frac{[H_n^{(1)}(k_{\rho1}\rho_c)]'}{H_n^{(1)}(k_{\rho1}\rho_c)}\right)\frac{k_1k_zn\rho_c}{DT(k_z)},\\ R_{MN}^{11}(k_z)&=R_{NM}^{11}\\ R_{NN}^{11}(k_z)&=\frac{J_n(k_{\rho1}\rho_c)}{H_n^{(1)}(k_{\rho1}\rho_c)}\left[\left(\frac{1}{k_{\rho2}^2}-\frac{1}{k_{\rho1}^2}\right)^2k_z^2n^2-\left(\frac{[J_n(k_{\rho2}\rho_c)]'}{k_{\rho2}J_n(k_{\rho2}\rho_c)}-\frac{[H_n^{(1)}(k_{\rho1}\rho_c)]'}{k_{\rho1}H_n^{(1)}(k_{\rho1}\rho_c)}\right)\right.\\ &\quad\left.\times\left(\frac{[J_n(k_{\rho_2}\rho_c)]'k_2^2}{k_{\rho2}J_n(k_{\rho2}\rho_c)}-\frac{[J_n(k_{\rho1}\rho_c)]'k_1^2}{k_{\rho1}J_n(k_{\rho1}\rho_c)}\right)\rho_c^2\right]\frac{1}{DT(k_z)}.\end{aligned} \tag{A13}$$

In order to extract the fundamental guided mode contribution to the Green's tensor, one needs to take the common denominator of all of the Fresnel coefficients and expand it near the corresponding $\beta_{\mathrm{HE}_{11}}$ value up to the first order: $DT(k_z) \approx \frac{\partial DT(k_z)}{\partial k_z}\Big|_{k_z=\beta_{\mathrm{HE}_{11}}} (k_z - \beta_{\mathrm{HE}_{11}}) + \ldots$. Then one needs to calculate the pole contribution to the integral by using the residue theorem and finding the value of $\beta_{\mathrm{HE}_{11}}$ from the dispersion relation.

APPENDIX B

Starting from Eq. (3.15), where $S_{ii} = 1 - i\hbar\gamma_{wg}^{(f)} \sum_j \frac{f_j^{(t)}}{\hbar\Delta - \lambda_j}$, we want to express the transmission spectra $t = |S_{ii}|^2$ in a convenient way. For this, let us consider different kinds of terms:

$$|S_{ii}|^2 = 1 + \sum_{j=1}^{N} \left(\left| \hbar\gamma_{wg}^{(f)} \frac{f_j^{(t)}}{\hbar\Delta - \lambda_j} \right|^2 + 2\hbar\gamma_{wg}^{(f)} \mathrm{Im} \frac{f_j^{(t)}}{\hbar\Delta - \lambda_j} + (\hbar\gamma_{wg}^{(f)})^2 \sum_{i=1, i\neq j}^{N} \frac{f_j^{(t)} (f_i^{(t)})^*}{(\hbar\Delta - \lambda_j)(\hbar\Delta - \lambda_i^*)} \right). \tag{B1}$$

The second term can be simply written into a form similar to Eq. (2.7):

$$\mathrm{Im} \frac{f_j^{(t)\prime} + i f_j^{(t)\prime\prime}}{\hbar\Delta - \lambda_j' - i\lambda_j''} = \frac{f_j^{(t)\prime}\lambda_j'' + f_j^{(t)\prime\prime}(\hbar\Delta - \lambda_j')}{(\hbar\Delta - \lambda_j')^2 + \lambda_j''^2}. \tag{B2}$$

The last term contains cross products of contributions from different eigenstates having different eigenvalues and we want to rewrite it in a similar way, which can be done through a sequence of the following transformations:

$$\begin{aligned}
&\sum_{j=1}^{N} \sum_{i=1, i\neq j}^{N} \frac{f_j^{(t)} (f_i^{(t)})^*}{(\hbar\Delta - \lambda_j)(\hbar\Delta - \lambda_i^*)} \\
&= \sum_{j=1}^{N} \sum_{i=1, i\neq j}^{N} \frac{f_j^{(t)} (f_i^{(t)})^*}{\lambda_j - \lambda_i^*} \left[\frac{1}{\hbar\Delta - \lambda_j} - \frac{1}{\hbar\Delta - \lambda_i^*} \right] \\
&= \sum_{j=1}^{N} \sum_{i=1, i\neq j}^{N} \frac{f_j^{(t)} (f_i^{(t)})^*}{\lambda_j - \lambda_i^*} \left(\frac{1}{\hbar\Delta - \lambda_j} \right) - \sum_{i=1}^{N} \sum_{j=1, j\neq i}^{N} \frac{f_j^{(t)} (f_i^{(t)})^*}{\lambda_j - \lambda_i^*} \left(\frac{1}{\hbar\Delta - \lambda_i^*} \right) = |i \leftrightarrow j \text{ for the second term}| \\
&= \sum_{i\neq j} 2\mathrm{Re} \frac{f_j^{(t)} (f_i^{(t)})^*}{\lambda_j - \lambda_i^*} \frac{1}{\hbar\Delta - \lambda_j} \\
&= \sum_{i\neq j} 2\mathrm{Re} \left[\frac{f_j^{(t)} (f_i^{(t)})^*}{\lambda_j - \lambda_i^*} (\hbar\Delta - \lambda_j^*) \right] \frac{1}{(\hbar\Delta - \lambda_j')^2 + \lambda_j''^2} \\
&= \sum_{i\neq j} \left\{ 2\mathrm{Re} \left[\frac{f_j^{(t)} (f_i^{(t)})^*}{\lambda_j - \lambda_i^*} \right] (\hbar\Delta - \lambda_j') - 2\mathrm{Im} \left[\frac{f_j^{(t)} (f_i^{(t)})^*}{\lambda_j - \lambda_i^*} \right] \lambda_j'' \right\} \frac{1}{(\hbar\Delta - \lambda_j')^2 + \lambda_j''^2}.
\end{aligned} \tag{B3}$$

Finally, by combining all terms together we seek Eq. (3.16). Similarly to this, Eq. (3.17) for the reflection coefficient can be obtained.

[1] R. Dicke, Coherence in spontaneous radiation processes, Phys. Rev. **93**, 99 (1954).

[2] R. H. Lehmberg, Radiation from an N-atom system, Phys. Rev. A **2**, 883 (1970).

[3] A. V. Andreev, V. I. Emel'yanov, and Yu. A. Ill'inski, Collective spontaneous emission (Dicke superradiance), Sov. Phys. Usp. **23**, 493 (1980).

[4] M. Gross and S. Haroche, Superradiance: An essay on the theory of collective spontaneous emission, Phys. Rep. **93**, 301 (1982).

[5] I. M. Sokolov, M. D. Kupriyanova, D. V. Kupriyanov, and M. D. Havey, Light scattering from a dense and ultracold atomic gas, Phys. Rev. A **79**, 053405 (2009).

[6] D. Plankensteiner, L. Ostermann, H. Ritsch, and C. Genes, Selective protected state preparation of coupled dissipative quantum emitters, Sci. Rep. **5**, 16231 (2015).

[7] R. T. Sutherland and F. Robicheaux, Collective dipole-dipole interactions in an atomic array, Phys. Rev. A **94**, 013847 (2016).

[8] W. Guerin, M. T. Rouabah, and R. Kaiser, Light interaction with atomic ensembles: Collective, cooperative and mesoscopic effects, J. Mod. Opt. **64**, 895 (2016).

[9] D. V. Kupriyanov, I. M. Sokolov, and M. D. Havey, Mesoscopic coherence in light scattering from cold, optically dense and disordered atomic systems, Phys. Rep. **671**, 1 (2017).

[10] A. S. Kuraptsev and I. M. Sokolov, Spontaneous decay of an atom excited in a dense and disordered atomic ensemble: Quantum microscopic approach, Phys. Rev. A **90**, 012511 (2014).

[11] D. E. Chang, J. S. Douglas, A. González-Tudela, C.-L. Hung, and H. J. Kimble, Colloquium: Quantum matter built from nanoscopic lattices of atoms and photons, Rev. Mod. Phys. **90**, 031002 (2018).

[12] Y. Miroshnychenko, W. Alt, I. Dotsenko, L. Förster, M. Khudaverdyan, D. Meschede, D. Scharader, and A. Rauschenbeutel, An atom-sorting machine, Nature (London) **442**, 151 (2006).

[13] M. Endres, H. Bernien, A. Keesling, H. Levine, E. R. Anschuetz, and A. Krajenbrink, Atom-by-atom assembly of defect-free one-dimensional cold atom arrays, Science **354**, 1024 (2016).

[14] F. Nogrette, H. Labuhn, S. Ravets, D. Barredo, L. Béguin, A. Vernier, T. Lahaye, and A. Browaeys, Single-Atom Trapping in Holographic 2D Arrays of Microtraps with Arbitrary Geometries, Phys. Rev. X **4**, 021034 (2014).

[15] D. Barredo, S. de Léséleuc, V. Lienhard, T. Lahaye, and A. Browaeys, An atom-by-atom assembler of defect-free arbitrary two-dimensional atomic arrays, Science **354**, 1021 (2016).

[16] H. Kim, W. Lee, H.-G. Lee, H. Jo, Y. Song, and J. Ahn, In situ single-atom array synthesis using dynamic holographic optical tweezers, Nat. Commun. **7**, 13317 (2016).

[17] D. Ohl de Mello, D. Schäffner, J. Werkmann, T. Preuschoff, L. Kohfahl, M. Schlosser, and G. Birkl, Defect-Free Assembly of 2D Clusters of More Than 100 Single-Atom Quantum Systems, Phys. Rev. Lett. **122**, 203601 (2019).

[18] K. D. Nelson, M. Müller, I. Lesanovsky, P. Zoller, and H. P. Büchler, A Rydberg quantum simulator, Nat. Phys. **3**, 556 (2007).

[19] D. Barredo, V. Lienhard, S. de Léséleuc, T. Lahaye, and A. Browaeys, Synthetic three-dimensional atomic structures assembled atom by atom, Nature (London) **561**, 79 (2018).

[20] R. A. de Oliveira, M. S. Mendes, W. S. Martins, P. L. Saldanha, J. W. R. Tabosa, and D. Felinto, Single-photon superradiance in cold atoms, Phys. Rev. A **90**, 023848 (2014).

[21] A. Goban, C.-L. Hung, J. D. Hood, S.-P. Yu, J. A. Muniz, O. Painter, and H. J. Kimble, Superradiance for Atoms Trapped Along a Photonic Crystal Waveguide, Phys. Rev. Lett. **115**, 063601 (2015).

[22] S. L. Bromley, B. Zhu, M. Bishof, X. Zhang, T. Bothwell, J. Schachenmayer, T. L. Nicholson, R. Kaiser, S. F. Yelin, M. D. Lukin, A. M. Rey, and J. Ye, Collective atomic scattering and motional effects in a dense coherent medium, Nat. Commun. **7**, 11039 (2016).

[23] M. O. Araújo, I. Kresić, R. Kaiser, and W. Guerin, Superradiance in a Large and Dilute Cloud of Atoms in the Linear-Optics Regime, Phys. Rev. Lett. **117**, 073002 (2016).

[24] S. J. Roof, K. J. Kemp, M. D. Havey, and I. M. Sokolov, Observation of Single-Photon Superradiance and the Cooperative Lamb Shift in an Extended Sample of Cold Atoms, Phys. Rev. Lett. **117**, 073003 (2016).

[25] T. Bienaimé, N. Piovella, and R. Kaiser, Controlled Dicke Subradiance from a Large Cloud of Two-Level Systems, Phys. Rev. Lett. **108**, 123602 (2012).

[26] M. O. Scully, Single Photon Subradiance: Quantum Control of Spontaneous Emission and Ultrafast Readout, Phys. Rev. Lett. **115**, 243602 (2015).

[27] W. Guerin, M. O. Araújo, and R. Kaiser, Subradiance in a Large Cloud of Cold Atoms, Phys. Rev. Lett. **116**, 083601 (2016).

[28] H. H. Jen, M.-S. Chang, and Y.-C. Chen, Cooperative single-photon subradiant states, Phys. Rev. A **94**, 013803 (2016).

[29] Y.-X. Zhang and K. Mølmer, Theory of Subradiant States of a One-Dimensional Two-Level Atom Chain, Phys. Rev. Lett. **122**, 203605 (2019).

[30] Y.-X. Zhang, C. Yu, and K. Mølmer, Subradiant dimer excited states of atom chains coupled to a 1D waveguide, arXiv:1908.01818.

[31] R. G. DeVoe, and R. G. Brewer, Observation of Superradiant and Subradiant Spontaneous Emission of two Trapped Ions, Phys. Rev. Lett. **76**, 2049 (1996).

[32] B. H. McGuyer, M. McDonald, G. Z. Iwata, M. G. Tarallo, W. Skomorowski, R. Moszynski, and T. Zelevinsky, Precise study of asymptotic physics with subradiant ultracold molecules, Nat. Phys. **11**, 32 (2015).

[33] M. D. Barnes, P. S. Krstic, P. Kumar, A. Mehta, and J. C. Wells, Far-field modulation of fluorescence decay rates in pairs of oriented semiconducting polymer nanostructures, Phys. Rev. B **71**, 241303(R) (2005).

[34] P. Weiss, M. O. Araújo, R. Kaiser, and W. Guerin, Subradiance and radiation trapping in cold atoms, New J. Phys. **20**, 063024 (2018).

[35] D. Bhatti, R. Schneider, S. Oppel, and J. von Zanthier, Directional Dicke Subradiance with Nonclassical and Classical Light Sources, Phys. Rev. Lett. **120**, 113603 (2018).

[36] D. E. Chang, V. Vuletic, and M. D. Lukin, Quantum nonlinear optics: Photon by photon, Nat. Photon. **8**, 685 (2014).

[37] H. Pichler, T. Ramos, A. J. Daley, and P. Zoller, Quantum optics of chiral spin networks, Phys. Rev. A **91**, 042116 (2015).

[38] V. I. Balykin, K. Hakuta, F. L. Kien, J. Q. Liang, and M. Morinaga, Atom trapping and guiding with a subwavelength-diameter optical fiber, Phys. Rev. A **70**, 011401(R) (2004).

[39] H. Zheng, D. J. Gauthier, and H. U. Baranger, Waveguide-QED-Based Photonic Quantum Computation, Phys. Rev. Lett. **111**, 090502 (2013).

[40] J.-T. Shen and S. Fan, Strongly Correlated Two-Photon Transport in a One-Dimensional Waveguide Coupled to a Two-Level System, Phys. Rev. Lett. **98**, 153003 (2007).

[41] X. Gu, A. F. Kockum, A. Miranowicz, Y.-X. Liu, and F. Nori, Microwave Photonics with Superconducting Quantum Circuits, Phys. Rep. **718–719**, 1 (2017).

[42] X. Qi, B. Q. Baragiola, P. S. Jessen, and I. H. Deutsch, Dispersive response of atoms trapped near the surface of an optical nanofiber with applications to quantum nondemolition measurement and spin squeezing, Phys. Rev. A **93**, 023817 (2016).

[43] Z. Liao, M. Al-Amri, and M. S. Zubairy, Measurement of deep-subwavelength emitter separation in waveguide-QED system, Opt. Express **25**, 31997 (2017).

[44] Z. Liao, X. Zeng, S.-Y. Zhu, and M. S. Zubairy, Single-photon transport through an atomic chain coupled to a one-dimensional nanophotonic waveguide, Phys. Rev. A **92**, 023806 (2015).

[45] D. Roy, C. M. Wilson, and O. Firstenberg, Colloquium: Strongly interacting photons in one-dimensional continuum, Rev. Mod. Phys. **89**, 021001 (2017).

[46] S. Mahmoodian, M. Čepulkovskis, S. Das, P. Lodahl, K. Hammerer, and A. S. Sørensen, Strongly Correlated Photon

Transport in Waveguide QED with Weakly Coupled Emitters, Phys. Rev. Lett. **121**, 143601 (2018).

[47] A. González-Tudela, V. Paulisch, H. J. Kimble, and J. I. Cirac, Efficient Multiphoton Generation in Waveguide Quantum Electrodynamics, Phys. Rev. Lett. **118**, 213601 (2017).

[48] V. Paulisch, H. J. Kimble, and A. Gonzáles-Tudela, Universal quantum computation in waveguide QED using decoherence free subspaces, New J. Phys. **18**, 043041 (2016).

[49] D. F. Kornovan, A. S. Sheremet, and M. I. Petrov, Collective polaritonic modes in an array of two-level quantum emitters coupled to an optical nanofiber, Phys. Rev. B **94**, 245416 (2016).

[50] D. F. Kornovan, M. I. Petrov, and I. V. Iorsh, Transport and collective radiance in a basic quantum chiral optical model, Phys. Rev. B **96**, 115162 (2017).

[51] A. Asenjo-Garcia, M. Moreno-Cardoner, A. Albrecht, H. J. Kimble, and D. E. Chang, Exponential Improvement in Photon Storage Fidelities Using Subradiance and Selective Radiance in Atomic Arrays, Phys. Rev. X **7**, 031024 (2017).

[52] H. R. Haakh, S. Faez, and V. Sandoghdar, Polaritonic normal-mode splitting and light localization in a one-dimensional nanoguide, Phys. Rev. A **94**, 053840 (2016).

[53] V. A. Pivovarov, A. S. Sheremet, L. V. Gerasimov, V. M. Porozova, N. V. Corzo, J. Laurat, and D. V. Kupriyanov, Light scattering from an atomic array trapped near a one-dimensional nanoscale waveguide: A microscopic approach, Phys. Rev. A **97**, 023827 (2018).

[54] E. Vetsch, D. Reitz, G. Sagué, R. Schmidt, S. T. Dawkins, and A. Rauschenbeutel, Optical Interface Created by Laser-Cooled Atoms Trapped in the Evanescent Field Surrounding an Optical Nanofiber, Phys. Rev. Lett. **104**, 203603 (2010).

[55] A. Goban, K. S. Choi, D. J. Alton, D. Ding, C. Lacroûte, M. Pototschnig, T. Thiele, N. P. Stern, and H. J. Kimble, Demonstration of a State-Insensitive, Compensated Nanofiber Trap, Phys. Rev. Lett. **109**, 033603 (2012).

[56] B. Gouraud, D. Maxein, A. Nicolas, O. Morin, and J. Laurat, Demonstration of a Memory for Tightly Guided Light in an Optical Nanofiber, Phys. Rev. Lett. **114**, 180503 (2015).

[57] N. V. Corzo, B. Gouraud, A. Chandra, A. Goban, A. S. Sheremet, D. V. Kupriyanov, and J. Laurat, Large Bragg Reflection from One-Dimensional Chains of Trapped Atoms Near a Nanoscale Waveguide, Phys. Rev. Lett. **117**, 133603 (2016).

[58] H. L. Sørensen, J.-B. Béguin, K. W. Kluge, I. Iakoupov, A. S. Sørensen, J. H. Müller, E. S. Polzik, and J. Appel, Coherent Backscattering of Light Off One-Dimensional Atomic Strings, Phys. Rev. Lett. **117**, 133604 (2016).

[59] J.-B. Béguin, J. H. Müller, J. Appel, and E. S. Polzik, Observation of Quantum Spin Noise in a 1D Light-Atoms Quantum Interface, Phys. Rev. X **8**, 031010 (2018).

[60] N. V. Corzo, J. Raskop, A. Chandra, A. S. Sheremet, B. Gouraud, and J. Laurat, Waveguide-coupled single collective excitation of atomic arrays, Nature (London) **566**, 359 (2019).

[61] P. Solano, P. Barberis-Blostein, F. K. Fatemi, L. A. Orozco, and S. L. Rolston, Superradiance reveals infinite-range interactions through a nanofiber, Nat. Commun. **8**, 1857 (2017).

[62] W. H. Weber and G. W. Ford, Propagation of optical excitations by dipolar interactions in metal nanoparticle chains, Phys. Rev. B **70**, 125429 (2004).

[63] I. Rasskazov, S. Karpov, and V. Markel, Waveguiding properties of short linear chains of nonspherical metal nanoparticles, J. Opt. Soc. Am. B **31**, 2981 (2014).

[64] V. A. Markel, Coupled-dipole approach to scattering of light from a one-dimensional periodic dipole structure, J. Mod. Opt. **40**, 2281 (1993).

[65] V. A. Markel, Divergence of dipole sums and the nature of non-Lorentzian exponentially narrow resonances in one-dimensional periodic arrays of nanospheres, J. Phys. B **38**, L115 (2005).

[66] R. J. Bettles, S. A. Gardiner, and C. S. Adams, Cooperative eigenmodes and scattering in one-dimensional atomic arrays, Phys. Rev. A **94**, 043844 (2016).

[67] V. A. Markel, Antisymmetrical optical states, J. Opt. Soc. Am. B **12**, 1783 (1995).

[68] C. Cohen-Tannoudji, J. Dupont-Roc, and G. Grynberg, *Atom-Photon Interactions Basic Processes and Applications* (Wiley, New York, 1992).

[69] A. S. Sheremet, A. D. Manukhova, N. V. Larionov, and D. V. Kupriyanov, Cooperative light scattering on an atomic system with degenerate structure of the ground state, Phys. Rev. A **86**, 043414 (2012).

[70] W. Feng, Y. Li, and S.-Y. Zhu, Cooperative spontaneous emission of three identical atoms, Phys. Rev. A **88**, 033856 (2013).

[71] G. S. Blaustein, M. I. Gozman, O. Samoylova, I. Y. Polishchuk, and A. L. Burin, Guiding optical modes in chains of dielectric particles, Opt. Express **15**, 17380 (2007).

[72] T. S. Tsoi and C. K. Law, Quantum interference effects of a single photon interacting with an atomic chain inside a one-dimensional waveguide, Phys. Rev. A **78**, 063832 (2008)

[73] B. Kramer and A. MacKinnon, Localization: Theory and experiment, Rep. Prog. Phys. **56**, 1469 (1993)

[74] V. G. Minogin and S. Nic Chormaic, Manifestation of the van der Waals surface interaction in the spontaneous emission of atoms into an optical nanofiber, Laser Phys. **20**, 32 (2010).

[75] T. Gruner and D.-G. Welsch, Green-function approach to the radiation-field quantization for homogeneous and inhomogeneous Kramers-Kronig dielectrics, Phys. Rev. A **53**, 1818 (1996).

[76] H. T. Dung, L. Knöll, and D.-G. Welsch, Resonant dipole-dipole interaction in the presence of dispersing and absorbing surroundings, Phys. Rev. A **66**, 063810 (2002).

[77] D. Plankensteiner, C. Sommer, H. Ritsch, and C. Genes, Cavity Antiresonance Spectroscopy of Dipole Coupled Subradiant Arrays, Phys. Rev. Lett. **119**, 093601 (2017).

[78] W. C. Chew, *Waves and Fields in Inhomogeneous Media* (Wiley-IEEE Press, New York, 1999).

[79] C. T. Tai, *Dyadic Green's Functions in Electromagnetic Theory*, 2nd ed. (IEEE, New York, 1994).

[80] L. Novotny and B. Hecht, *Principles of Nano-Optics* (Cambridge University Press, Cambridge, England, 2012).

PHYSICAL REVIEW A **100**, 033840 (2019)

Noninverse dynamics of a quantum emitter coupled to a fully anisotropic environment

Danil Kornovan, Mihail Petrov, and Ivan Iorsh
ITMO University, Saint Petersburg 197101, Russia

(Received 11 April 2019; published 30 September 2019)

Anisotropic nanophotonic structures can couple the levels of a quantum emitter through the quantum interference effect. In this paper we study the coupling of quantum emitter excited states through the modes of a fully anisotropic structure, a structure for which all directions are physically nonequivalent. We consider an anisotropic metasurface as an illustrative example of such a structure. We point out another degree of freedom in controlling the temporal dynamics and spectral profiles of quantum emitters; namely, we show that a combination of the metasurface anisotropy and tilt of the emitter quantization axis with respect to the metasurface normal results in nonsymmetric dynamics between the transitions of electrons from the left-circular state to the right-circular state and in the inverse process. Our findings give an additional mechanism for control over light emission by quantum systems and can be utilized for probing active transitions of quantum emitters.

DOI: 10.1103/PhysRevA.100.033840

I. INTRODUCTION

The field of nanophotonics provides unique opportunities for controlling the polarization state of light that governs light-matter interaction. For example, the nonzero transverse optical spin momentum density of the electric field localized close to structure interfaces allows for achieving artificial chirality of light-matter interactions [1]. Considered for the first time decades ago [2,3], chiral quantum optics has acquired an experimental platform for the observation of the chiral coupling of light with individual quantum emitters (QEs) in photonic crystal waveguides [4,5], nanofiber systems [6–8], bottle microresonators [9], and planar grating systems [10]. The nonsymmetric interaction of quantum emitters with photonic modes propagating in opposite directions allows one to achieve, for instance, incremental spontaneous entanglement generation [11], unidirectional quantum transport [12,13], unusual optomechanics [14,15], and modified radiative collective properties of quantum emitter ensembles [12,16]. An alternative to atoms and quantum dots, semiconducting two-dimensional materials are a promising source of quantum chirality [17] due to circular optical transitions related to the spin states of valley electrons. Important progress has been recently demonstrated in coupling excitons in two-dimensional materials with plasmonic waveguides [18] and metasurfaces (MSs) [18–22]. The latter are naturally considered as photonic counterparts to two-dimensional semiconductor materials. Metasurfaces have already demonstrated unprecedented flexibility in the engineering of the polarization state of reflected and transmitted light [23] as well as localized surface waves [24–26], and the enhancement of the spontaneous emission rate of quantum sources [24].

Another intriguing feature of light-matter interactions in nanophotonics is that the intrinsic anisotropy of a nanostructure's interface results in the coupling of quantum transitions [27,28] due to the quantum interference effect [29]. Recently, it has been demonstrated that the coupling of orthogonal chiral states in two-dimensional materials with MS modes leads to the formation of strongly coupled exciton-polariton states [19], and coherence buildup during spontaneous transition was predicted [30]. The possibility of an effective coupling of chiral transitions through the MSs motivated us to study the dynamics of transitions between two states with different total angular momentum projections, which become coupled due to the quantum interference enabled by the anisotropy of a MS [see Fig. 1(a)]. We consider the coupling of transitions with opposite helicities through the anisotropic MS, including the hyperbolic regimes. We predict that one can achieve noninverse dynamics in transitions between the states by tilting the local quantization axis of the emitter. Control over the orientation of the emitter quantization axis can be achieved, for example, by applying a magnetic [31] or electric field, which can be utilized in field sensing [32]. Moreover, it has been shown that orientation of a weak external magnetic field can control the spontaneous emission process from a multilevel atom into the modes of the structure [33,34]. The orientation of transition dipole moments can be also controlled by the strains induced in quantum dots, which has been demonstrated experimentally [35]. The results proposed in this paper open a way for the reconstruction of the initially excited spin state of a quantum emitter based on its optical response, thus realizing the optical tomography of quantum states with fully anisotropic structures.

II. METASURFACE INDUCED QUANTUM INTERFERENCE

We start with a QE having optically allowed transition with three degenerate excited states $|e_{-1}\rangle$, $|e_0\rangle$, and $|e_{+1}\rangle$ and a single ground state $|g\rangle$. The corresponding transition dipole moments are denoted by $\mathbf{d_{-1}}$, $\mathbf{d_0}$, and $\mathbf{d_{+1}}$ and their directions are given by the corresponding vectors $\mathbf{e_{-1}} = +(\mathbf{e_x} - i\mathbf{e_y})/\sqrt{2}$, $\mathbf{e_0} = \mathbf{e_z}$, and $\mathbf{e_{+1}} = -(\mathbf{e_x} + i\mathbf{e_y})/\sqrt{2}$, while the amplitudes are assumed to be equal to $|\mathbf{d_{-1}}| = |\mathbf{d_0}| = |\mathbf{d_{+1}}| = d$. Note that at this stage $\mathbf{d_{-1}}$ and $\mathbf{d_{+1}}$ are in the interface plane, while $\mathbf{d_0}$ is parallel to a normal of the structure. Having different angular momentum projections, these states are

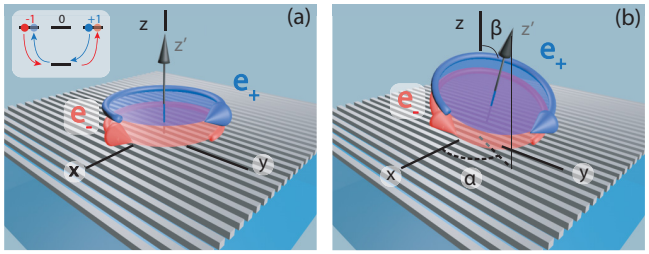

FIG. 1. General scheme of the setup. (a) A four-level atom with an $s \rightarrow p$ transition placed near an anisotropic metasurface. The rotating transition dipole moments of the atom lie in the interface plane. The x and y axes are chosen in such a way that the surface conductivity tensor σ is diagonal. (b) The same setup but with the local quantization axis z' rotated by angles α and β.

orthogonal in the vacuum due to its isotropy, but if placed in an anisotropic environment these states may couple with each other via anisotropy induced quantum interference [29]. An anisotropic metasurface is an example of such a nanophotonic system, breaking the isotropy in all three directions. The anisotropic response of the metasurface can be well described [25] with the use of the effective conductivity tensor $\hat{\sigma}(\omega)$. In the coordinate system (*laboratory frame*) coinciding with the main axes of the conductivity tensor, one obtains

$$\hat{\sigma}(\omega) = \begin{pmatrix} \sigma_{xx}(\omega) & 0 \\ 0 & \sigma_{yy}(\omega) \end{pmatrix},$$

where the diagonal entries are modeled with the Lorentzians $\sigma_{jj}(\omega) = A_j \frac{ic}{4\pi} \frac{\omega}{\omega^2 - \Omega_j^2 + i\gamma_j\omega}$ with A_j being the normalization factor, Ω_j the resonance frequency, and γ_j the damping rate. Note that from now on we will use CGS units rather than SI.

The in-plane anisotropy of the metasurface allows for coupling between the two transitions with opposite helicities [Fig. 1(a)]. Indeed, the interaction between the states is described by the coupling constant $g_{-,+}$, which acquires a nonvanishing value: $g_{-,+} = -4\pi k_0^2 \mathbf{d}_{-1}^* \mathbf{G}(\mathbf{r_a}, \mathbf{r_a}, \omega_0)\mathbf{d}_{+1}/\hbar \sim G_{xx}(\mathbf{r_a}, \mathbf{r_a}, \omega_0) - G_{yy}(\mathbf{r_a}, \mathbf{r_a}, \omega_0)$, where k_0 is the wave number and $\mathbf{G}(\mathbf{r_a}, \mathbf{r_a}, \omega_0)$ is the electromagnetic Green's tensor. The total Green's tensor consists of the vacuum and scattered contributions, $\mathbf{G} = \mathbf{G_0} + \mathbf{G_{SC}}$; it is known that for equal field and source points the real part of the vacuum contribution diverges. However, we will only take into account the imaginary part of it and consider the vacuum Lamb shift as being already included into the definition of the emitter's bare transition frequency ω_0.

The nonzero coupling between the states results in the redistribution of the quantum excitation if the system was initially pumped in any of the excited states. The temporal dynamics of the system is governed by the evolution operator $\hat{U}(t, 0)$ [36], which gives the probability $P_{e_f,e_i}(t) = |U_{e_f,e_i}(t, 0)|^2$ for the atom to be in the excited state $|e_f\rangle$ at time t given that it was in the state $|e_i\rangle$ initially. This allows us to implicitly reduce our attention to the subspace of the excited states only.

The evolution operator can be expressed as

$$\langle e_f|\hat{U}(t, 0)|e_i\rangle = \int_C \frac{dz}{2\pi i} e^{-izt/\hbar} \langle e_f|\hat{G}(z)|e_i\rangle, \tag{1}$$

where $\hat{G}(z) = (z - \hat{H})^{-1}$ is the resolvent operator of the full Hamiltonian $\hat{H} = \hat{H}_0 + \hat{V}$, consisting of the unperturbed $\hat{H}_0$ part and perturbation $\hat{V}$, and $|e_i\rangle$ and $|e_f\rangle$ are the initial and final states, respectively.

The unperturbed Hamiltonian consists of the atomic and field parts $\hat{H}_0 = \hat{H}_A + \hat{H}_F$. In order to describe the field itself and its interaction with the atom for a very general case of a medium with, possibly, dispersion and absorption, we employ the approach introduced in Ref. [37]. In this case we can write

$$\begin{aligned} \hat{H}_A &= \sum_{q=-1,0,+1} \hbar\omega_0 |e_q\rangle\langle e_q|, \\ \hat{H}_F &= \int d\mathbf{r}' \int_0^\infty d\omega' \hbar\omega' \hat{\mathbf{f}}^\dagger(\mathbf{r}', \omega')\hat{\mathbf{f}}(\mathbf{r}', \omega'), \\ \hat{V} &= -\sum_q \hat{\mathbf{d}}_q \hat{\mathbf{E}}(\mathbf{r_a}), \end{aligned} \tag{2}$$

where ω_0 is the resonance frequency of the atomic transition, $\hat{\mathbf{f}}^\dagger(\mathbf{r}', \omega')$ is the local-field creation operator, and $\hat{\mathbf{E}}(\mathbf{r_a})$ is the total electric field at the position of the atom $\mathbf{r_a}$. The electromagnetic field operator in this case reads as $\hat{\mathbf{E}}(\mathbf{r}) = i\sqrt{4\hbar} \int d\mathbf{r}' \int_0^\infty d\omega' \frac{\omega'^2}{c^2} \sqrt{\varepsilon_I(\mathbf{r}', \omega')}\mathbf{G}(\mathbf{r}, \mathbf{r}', \omega')\hat{\mathbf{f}}(\mathbf{r}', \omega') + \text{H.c.}$, where the bosonic field operators obey the commutation relation $[\hat{f}_i(\mathbf{r}', \omega'), \hat{f}_k^\dagger(\mathbf{r}, \omega)] = \delta_{ik}\delta(\mathbf{r}' - \mathbf{r})\delta(\omega' - \omega)$, $\mathbf{G}(\mathbf{r}, \mathbf{r}', \omega')$ is the classical electromagnetic Green's function, and $\epsilon_I(\mathbf{r}', \omega')$ is the imaginary part of permittivity.

The resolvent operator $\hat{G}(z)$ projected onto the subspace of interest reads as

$$\hat{P}\hat{G}(z)\hat{P} = \hat{P}\frac{1}{z - \hat{H}_0 - \hat{\Sigma}(z)}\hat{P}, \tag{3}$$

where $\hat{P}$ is the projector onto the subspace of emitter excited states, $\hat{H}_0$ is the unperturbed Hamiltonian, and $\hat{\Sigma}(z)$ is the level-shift operator or self-energy part. $\hat{\Sigma}(z)$ here provides the energy shifts to the unperturbed eigenstates of $\hat{H}_0$ due to the interaction and has the form

$$\hat{\Sigma}(z) = \hat{V} + \hat{V}\hat{G}(z)\hat{V} \approx \hat{V} + \hat{V}\hat{G}_0(z = \hbar\omega_0)\hat{V}, \tag{4}$$

where the last equation implies the two approximations. The first one is the near resonant case, which ignores possible dependence of $\hat{\Sigma}(z)$ on z, also called the flat spectrum approximation. The second one is the case that $\hat{\Sigma}(z)$ is calculated up to the second order in $\hat{V}$.

The matrix elements of $\Sigma_{q',q}(\hbar\omega_0) = \langle e_{q'}|\hat{\Sigma}(\hbar\omega_0)|e_q\rangle$ represent the coupling of excited states through the modes of the field and can be found in Ref. [38]: $\Sigma_{q',q}(\hbar\omega_0) = -4\pi k_0^2 \mathbf{d}_{\mathbf{q}'}^* \mathbf{G}(\mathbf{r_a}, \mathbf{r_a}, \omega_0)\mathbf{d_q}$, where $k_0 = \omega_0/c$ and $\mathbf{d_q}$ is the transition dipole moment.

Once we construct the Green's tensor (see Appendix A) of a metasurface, we can compute the coupling elements $\Sigma_{q'q}(\hbar\omega_0)$ and solve for the dynamics of the atomic state populations. In the setup considered [Fig. 2(a)] the states $|e_{-1}\rangle$ and $|e_{+1}\rangle$ are mutually coupled while both being decoupled from $|e_0\rangle$ as a consequence of the Green's tensor $\mathbf{G}(\mathbf{r_a}, \mathbf{r_a}, \omega)$ being diagonal. Therefore, when studying the interaction between the states $|e_{+1}\rangle$ and $|e_{-1}\rangle$, we can ignore $|e_0\rangle$ and immediately find the probability for the system to be

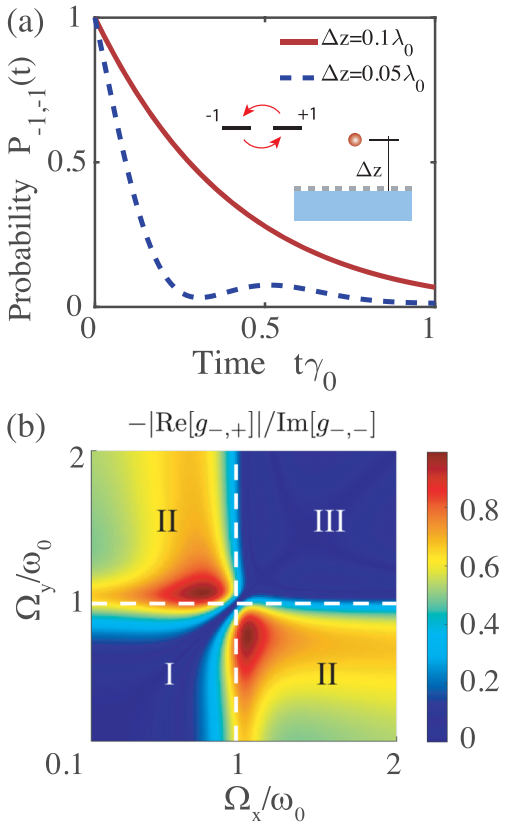

FIG. 2. (a) Excited-state probability $P_{-,-}(t)$ in the extreme anisotropy limit [see Eq. (6)]. The strong-coupling regime appears for an atom-metasurface distance $\Delta z = 0.05\lambda_0$. (b) 2D map of the strong-coupling parameter $-|\mathrm{Re}[g_{-,+}]|/\mathrm{Im}[g_{-,-}]$ as a function of Ω_x, Ω_y. The three specified regions correspond to (I) inductive ($\mathrm{Im}[\sigma_{xx}]$, $\mathrm{Im}[\sigma_{yy}] > 0$), (II) hyperbolic ($\mathrm{Im}[\sigma_{xx}] \cdot \mathrm{Im}[\sigma_{yy}] < 0$), and (III) capacitive ($\mathrm{Im}[\sigma_{xx}]$, $\mathrm{Im}[\sigma_{yy}] < 0$) regimes. Other relevant parameters are $\Delta z = 0.05\lambda_0$, $\gamma_x = \gamma_y = 0.1\omega_0$, $\varepsilon_{\mathrm{subs}} = 1$.

in the state $|e_{-1}\rangle$ explicitly:

$$P_{-1,-1}(t,0) = \tfrac{1}{2}e^{2\mathrm{Im}[g_{-,-}]t}\{\cos(2\mathrm{Re}[g_{-,+}]t) + \cosh(2\mathrm{Im}[g_{-,+}]t)\}. \quad (5)$$

$g_{-,-}$ and $g_{-,+}$ represent the diagonal and nondiagonal entries of $\Sigma(\hbar\omega_0)/\hbar$, respectively. The expression describing the dynamics of quantum states consists of two parts: a purely decaying term and an oscillatory part. If one can achieve $\mathrm{Re}[g_{-,+}] \geqslant -\mathrm{Im}[g_{-,-}]$ then the oscillations will be underdamped, which corresponds to a *strong coupling* of states $|e_{+1}\rangle$ and $|e_{-1}\rangle$ through the modes of the structure.

It is illustrative to consider the case of the extreme anisotropy, when $\sigma_{xx} \to 0i$ and $\sigma_{yy} \to \infty i$, which corresponds to the ideal conductance in the y direction and isolation in the x direction. This gives us a very simple analytical result for the coupling constants:

$$\hbar g_{-,+} = \left(\frac{1 - ik\Delta z - 2k^2\Delta z^2}{4\Delta z^3}\right)|\mathbf{d}|^2 e^{ik2\Delta z},$$
$$\hbar g_{-,-} = -\left(\frac{ik\Delta z + 2k^2\Delta z^2}{4\Delta z^3}\right)|\mathbf{d}|^2 e^{ik2\Delta z}. \quad (6)$$

In Fig. 2(a) we plot the dynamics of the initially excited state for the case of strong anisotropy in the absence (red solid) and the presence (blue dashed) of strong coupling. However, for a more realistic case of finite loss and $\gamma_j \neq 0$, Fig. 2(b), the strong-coupling regime can *almost* be achieved for the considered atom-surface distance $\Delta z = 0.05\lambda_0$ when at least one of the quantities Ω_x and Ω_y is close to the atomic transition frequency ω_0 only. One of the simplest ways to achieve strong coupling is to consider smaller atom-surface distances Δz; however, at some point it might be necessary to consider also the Casimir-Polder interactions [39] with the modes of the nanostructure.

The requirement for the strong-coupling regime ($\mathrm{Re}[g_{-,+}] \geqslant -\mathrm{Im}[g_{-,-}]$) derived from Eq. (5) makes sense for the case of two interacting transitions. However, as we will show in the next section, it is still possible to achieve not only a measurable population transfer between the states but also nonequivalent dynamics for $|e_{-1}\rangle \to |e_{+1}\rangle$ and $|e_{+1}\rangle \to |e_{-1}\rangle$ processes. This can be done if the transition dipole moments are arbitrarily oriented and all three of them are coupled.

III. NONINVERSE DYNAMICS OF THE FOUR-LEVEL EMITTER

The dynamics of the system is fully defined by the electromagnetic properties of the MS through the coupling constants $g_{q',q}$ and is given by Eq. (5). The asymmetry in the quantum dynamics, i.e., when the dynamics of a transition from $|e_{+1}\rangle \to |e_{-1}\rangle$ and $|e_{-1}\rangle \to |e_{+1}\rangle$ will be different, is also defined by the same coupling constants g. Thus, in order to obtain the asymmetry in the dynamics one should achieve $g_{-,+} \neq g_{+,-}$. From the Green's-function perspective the coupling constants read as $g_{+,-}^{-,+} \sim G_{yy} - G_{xx} \mp i(G_{xy} + G_{yx})$. One can expect that applying a strong magnetic field along the z axis should break the time-reversal symmetry, making the conductivity tensor σ nondiagonal and antisymmetric [40]. This results in nonzero nondiagonal components of the Green's tensors G_{xy} and G_{yx}; however, they have opposite signs $G_{xy} = -G_{yx}$ in this case, which still makes the coupling constants equal, $g_{-+} = g_{+-}$.

However, there is another less direct way of breaking the symmetry between the $|e_{-1}\rangle$ and $|e_{+1}\rangle$ states, if one considers the atomic quantization axis to be tilted with respect to the laboratory axis $\mathbf{e_z}$ at an arbitrary angle as shown in Fig. 1(b). Mathematically, this can be described by considering the level-shift operator in the metasurface frame after the rotation of the quantization axis:

$$\tilde{\mathbf{\Sigma}}(\hbar\omega_0) = \mathbf{S}^\dagger\mathbf{M}^\dagger\mathbf{\Sigma}(\hbar\omega_0)\mathbf{M}\mathbf{S} = \mathbf{T}^\dagger\mathbf{\Sigma}(\hbar\omega_0)\mathbf{T}.$$

Here $\mathbf{S}$ is the matrix of Cartesian components of the spherical tensors of rank 1 as columns; $\mathbf{M}$ is the rotation matrix on Euler angles α, β, and γ (active representation, right-hand rule, z''-y'-z convention), and $\mathbf{T} = \mathbf{MS}$ is the composition of these transformations.

All of the information about the dynamics of the system is contained in the eigenvalues and eigenstates of $\tilde{\mathbf{\Sigma}}(\hbar\omega_0)$. Note that the rotation of the quantization axis does not change the eigenvalues, but alters the eigenstates of the system, and the

evolution matrix can be expressed as

$$U_{q'q}(t,0)=\sum_{j=x,y,z} C_j^{(q',q)} e^{-ig_j t};\quad q,q'=\{-1,0,+1\}, \tag{7}$$

where g_j are the complex eigenvalues of $\mathbf{\Sigma}$, and $C_j^{(q',q)}=(T^{-1})_{q',j}T_{j,q}$. We should note that, since our nanostructure is the planar conducting interface, the physical meaning of eigenstates of the system is that they correspond to three linear dipole moments aligned along highly symmetric directions of the environment (main axes of the nanostructure); therefore, $\hbar g_j=-4\pi k_0^2 \mathbf{d_j^\dagger G}(\mathbf{r_a},\mathbf{r_a},\omega)\mathbf{d_j}$ are the self-couplings of three linear dipole moments oriented along x, y, and z.

The coefficients $C_j^{(q',q)}$ for the case of the excitation transfer from $|e_{+1}\rangle \to |e_{-1}\rangle$ have the following explicit form:

$$\begin{aligned} C_x^{(-1,+1)} &= -\frac{e^{-2i\gamma}}{2}[\cos(\alpha)\cos(\beta)-i\sin(\alpha)]^2,\\ C_y^{(-1,+1)} &= \frac{e^{-2i\gamma}}{2}[\cos(\alpha)-i\cos(\beta)\sin(\alpha)]^2,\\ C_z^{(-1,+1)} &= -\frac{e^{-2i\gamma}}{2}\sin^2(\beta). \end{aligned} \tag{8}$$

First, one can notice that since γ enters as an overall phase for all of the coefficients $C_j^{(q',q)}$ it does not affect the population dynamics $P_{q',q}(t,0)=|U_{q',q}(t,0)|^2$. This means that the last rotation around the new $\mathbf{e}'_\mathbf{z}$ axis by angle γ is redundant and without loss of generality we can set $\gamma=0$. From the unitarity of $\mathbf{T}(\alpha,\beta,\gamma)$ it follows that $C_j^{(+,-)}=(C_j^{(-,+)})^*$. This fact immediately gives us a straightforward result that for arbitrary values of α and β one can achieve noninverse dynamics between the two transitions as the coefficients are not equal anymore. Indeed, the asymmetry in the excitation transport between the states manifests itself in the following way:

$$\begin{aligned} &P_{-,+}(t)-P_{+,-}(t)\\ &\quad=f(\alpha,\beta)\sum_{(k,l)}^{(x,y),(y,z),(z,x)} e^{(g_k''+g_l'')t}\sin[(g_k'-g_l')t], \end{aligned} \tag{9}$$

where $g_j=g_j'+ig_j''$ and $f(\alpha,\beta)=\frac{1}{8}\sin(2\alpha)\sin(2\beta)\sin(\beta)$. Equation (9) is the central result of the paper, and it has several important consequences. First, one can see that the difference vanishes in two cases: (i) when $f(\alpha,\beta)=0$ or, equivalently, when either α or β is an integer multiple of $\pi/2$; and (ii) when any two directions are equivalent, so that $g_k=g_l$. Thus, to obtain the noninverse dynamics of the excitation we need to have both the atomic system quantization axis tilted at an arbitrary angle relative to the metasurface and full anisotropy of the environment.

We want to stress that this effect can be observed for the process involving any pair of states with $q,q'=\{-1,0,+1\}$, not only the processes coupling $|e_{-1}\rangle$ and $|e_{+1}\rangle$. It is also important to mention that from the form of transport asymmetry (9) one can formulate the explicit way to describe the difference of $P_{-1,+1}(t)$ and $P_{+1,-1}(t)$. Indeed, we can calculate the actual probabilities given by $P_{q',q}(t)=|U_{q',q}(t,0)|^2$:

$$\begin{aligned} P_{q',q}(t)=&\sum_{k=x,y,z} C_{k,k}^{(q',q)} e^{2g_j' t}+\sum_{(k,l)}^{(x,y),(y,z),(z,x)} 2\left|C_{k,l}^{(q',q)}\right|\\ &\times\cos\left[(g_k'-g_l')t-\varphi_{k,l}^{(q',q)}\right]e^{(g_k''+g_l'')t}, \end{aligned} \tag{10}$$

where g_j are, as in Eq. (7), the eigenvalues of $\Sigma_{q',q}(\hbar\omega_0)/\hbar$ (self-couplings of linear dipoles along x, y, and z); $C_{k,l}^{(q',q)}=C_k^{(q',q)}(C_l^{(q',q)})^*$; and $\varphi_{k,l}^{(q',q)}=\arg(C_{k,l}^{(q',q)})$. Note that the second sum is responsible for the interference of contributions from different eigenstates. From the property $C_{k,l}^{(q',q)}=(C_{k,l}^{(q,q')})^*$ it immediately follows that $\varphi_{k,l}^{(q',q)}=-\varphi_{k,l}^{(q,q')}$, which means that the difference in population transfer probabilities $P_{q',q}(t)$ and $P_{q,q'}(t)$ manifests itself as the *phase delay* in the interference part of the dynamics.

In this section we described the physical origin of the effect under study in terms of internal degrees of freedom of the emitter-transition probabilities $P_{q',q}(t)$. In the next section we proceed by considering how the observable quantities like detected light intensity or emitted spectrum are affected, which might be of special interest if one keeps in mind a possible experimental verification.

IV. THE EFFECT ON THE MEASURABLE OBSERVABLES

A. Far-field intensity dynamics

The temporal dynamics can be detected by measuring the far-field radiation generated by the atom. Basing on the results presented in Refs. [41,42], we will obtain the detected light intensity, the temporal profile of which is given by Ref. [42]:

$$\begin{aligned} I_{q_0}(t)=\Bigg|\sum_{q'}4k_0^2\int_0^t dt' C_{q',q_0}(t')\int_0^\infty d\omega\,\mathrm{Im}[\mathbf{G}(\mathbf{r_d},\mathbf{r_a},\omega)]\mathbf{d_{q'}}\\ e^{-i(\omega-\omega_0)(t-t')}\Bigg|^2, \end{aligned} \tag{11}$$

with $\mathbf{r_d}$ and $\mathbf{r_a}$ being the positions of the detector and atom, respectively, and $C_{q',q_0}(t)$ the probability amplitude that state q' is excited at time t, while initially the system was in the q_0 state.

If we want to find the intensity detected in the far-field zone, we need to replace the full Green's tensor with its far-field part $\mathbf{G}(\mathbf{r_d},\mathbf{r_a},\omega)\to\mathbf{G^{FF}}(\mathbf{r_d},\mathbf{r_a},\omega)$. According to a superposition principle [43,44] this far-field Green's tensor can be written as a sum of free-space and scattered parts: $\mathbf{G^{FF}}(\mathbf{r_d},\mathbf{r_a},\omega)=\mathbf{G^{FF,0}}(\mathbf{r_d},\mathbf{r_a},\omega)+\mathbf{G^{FF,sc}}(\mathbf{r_d},\mathbf{r_a},\omega)$ or

$$\mathbf{G^{FF}}(\mathbf{r_d},\mathbf{r_a},\omega)=\mathbf{f^0}(\mathbf{r_d},\mathbf{r_a},\omega)e^{ikR_-}+\mathbf{f^{SC}}(\mathbf{r_d},\mathbf{r_a},\omega)e^{ikR_+}, \tag{12}$$

where $R_\pm=\sqrt{(x_d-x_a)^2+(y_d-y_a)^2+(z_d\pm z_a)^2}$. The phases in the exponent differ as these two contributions are created by two dipoles: one is located at the position $\mathbf{r_a}$ and the other one is its mirror image located at $(x_a,y_a,-z_a)$. However, if we put a dipole very close to a surface so that $z_0/\lambda_0\ll 1$ then we can ignore this discrepancy and set $R_-=R_+=R$, obtaining that

$\mathbf{G^{FF}}(\mathbf{r_d}, \mathbf{r_a}, \omega) \approx \mathbf{f}e^{ikR}$. Now using $\mathrm{Im}[\mathbf{f}(\mathbf{r_d}, \mathbf{r_a}, \omega)e^{ikR}] = \mathrm{Re}[\mathbf{f}(\mathbf{r_d}, \mathbf{r_a}, \omega)]\sin(kR) + \mathrm{Im}[\mathbf{f}(\mathbf{r_d}, \mathbf{r_a}, \omega)]\cos(kR)$ and making the expansion near the resonance frequency $k(\omega) \approx k(\omega_0) + k'(\omega_0)(\omega - \omega_0)$, we can proceed by taking the frequency integral in Eq. (11). The $\mathbf{f}(\mathbf{r_d}, \mathbf{r_a}, \omega)$ function in our case can be regarded as a slowly varying function of frequency and put in front of the ω integral taken at resonance frequency ω_0. Then we can perform the ω integral and arrive at the following result:

$$I_{q_0}(t) \approx \left| \frac{4\pi k_0^2}{i} \sum_{q'} C_{q',q_0}(t - R/c)\mathbf{G^{FF}}(\mathbf{r_d}, \mathbf{r_a}, \omega_0)\mathbf{d}_{q'} \right|^2. \quad (13)$$

One should note that this form naturally expresses the total amplitude as a sum of contributions from three dipole moments associated with each active transition $q' = (-1, 0, +1)$ multiplied by the probability amplitude of the corresponding excited state at the retarded time $\tau = t - R/c$. We can rewrite Eq. (13) by making use of the $\mathbf{d_q}$ definition and Eq. (7) in the form

$$I_{q_0}(\tau) \approx |4\pi k_0^2 \mathbf{d}|^2 \left| \sum_j \mathbf{f_j} e^{-ig_j\tau} \right|^2, \quad (14)$$

where $\tau = (t - R/c)$, c is the speed of light, $\mathbf{f_j} = \mathbf{G^{FF}_{:,j}}(\mathbf{r_d}, \mathbf{r_a}, \omega_0)(\mathbf{M}\mathbf{S}_{j,q_0})$ is related to the field generated at the detector's position $\mathbf{r_d}$, $\mathbf{r}_a$ is the position of a QE, and $\mathbf{G^{FF}_{:,j}}(\mathbf{r_d}, \mathbf{r_a}, \omega_0)$ is the jth column of the far-field classical Green's tensor of the system. It is clear that the temporal dynamics described by Eq. (7) is directly mapped onto this quantity.

In order to observe the manifestation of the effect it is convenient to compare the intensity dynamics for the two initial conditions (an atom being in $|e_{-1}\rangle$ and $|e_{+1}\rangle$ initially) in the case of isotropic and anisotropic metasurfaces. The results are presented in Fig. 3(a). Notice that the position of the detector is rotated with respect to the axis origin in the same way as the atomic local quantization z axis is rotated: it is simply $\mathbf{r_d}||\mathbf{M}\hat{z}$. This keeps the number of degrees of freedom constant as the orientations of atomic quantization axis and detector position relative to an atom are now related and described only by (α, β). One can notice in Fig. 3(a) that for the setup considered for the anisotropic metasurface there is a difference in temporal dynamics of the detected field intensity $I_{q_0}(\tau)$ for initially excited states with opposite helicities A, $q_0 = -1$ (blue dash-dotted), and A, $q_0 = +1$ (blue dotted). For the isotropic case the difference between the B, $q_0 = -1$ (solid dark red line), and B, $q_0 = +1$ (bright red circles), intensity profiles vanishes, as expected.

It is also important to mention that it might be natural to consider a hyperbolic regime for a metasurface when it comes to studying light-matter interactions as the surface-plasmon polariton (SPP) modes are prominent in this case. Despite the fact that the SPPs might have a very strong local field (leading to the increase of $\mathrm{Re}[g_j]$), they also carry the energy away from the system due to strongly enhanced spontaneous emission (and, therefore, high $-\mathrm{Im}[g_j]$). One can conclude that for the problem considered in our paper the *near field modes* which are forbidden to propagate in any direction are of interest, but not the propagating modes.

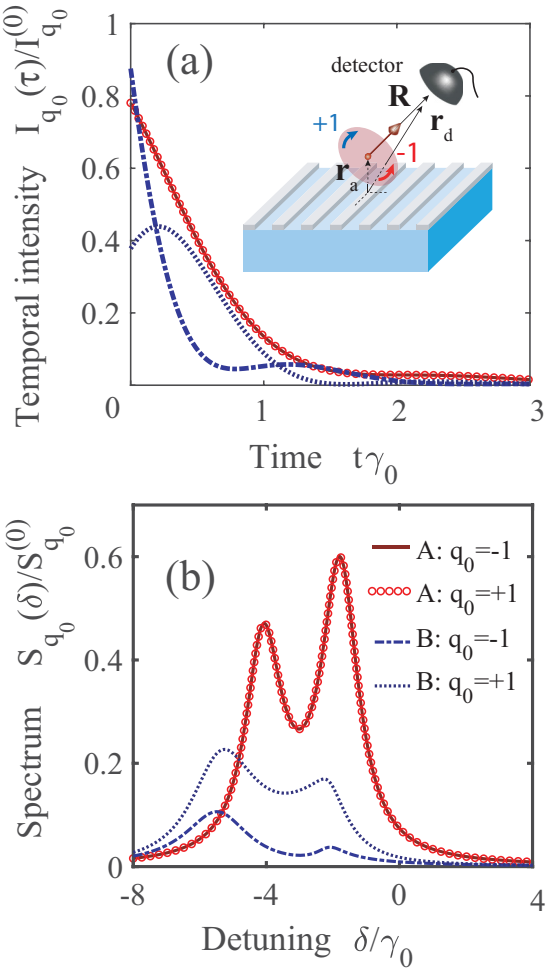

FIG. 3. (a) Local-field intensity registered at the detector position $\mathbf{r_d}$ vs time $\tau = t - R/c$ measured in the units of an inverse of a free-space emission rate γ_0. Zero time corresponds to a moment when the emitted light reaches the detector. The atom is initially in the $|e_{q_0}\rangle$ state. Two cases are studied: case A, an isotropic metasurface ($\Omega_x = \Omega_y = 1.5k_0$); and case B, an anisotropic metasurface ($\Omega_x = 1.5k_0$, $\Omega_y = 1.1k_0$). There are also two initial conditions considered with four cases in total: isotropic case A, $q_0 = -1$ and $+1$ (solid dark red line and bright red circles, respectively); and anisotropic case B, $q_0 = -1$ and $+1$ (blue dash-dotted and dotted line, respectively). The parameters are $\Omega_x = 0.6k_0$, $\Omega_y = 1.0k_0$, $\gamma_x = \gamma_y = 0.1k_0$, $\epsilon_{\mathrm{subs}} = 1.0$, $\Delta z = 0.05\lambda_0$, $\mathbf{r_a} = (0, 0, \Delta z)$, $\mathbf{r_d} = R(\cos(\alpha)\sin(\beta), \sin(\alpha)\sin(\beta), \cos(\beta))$, $R = 100\lambda_0$, $\alpha = \pi/4$, and $\beta = \pi/4$. Normalization factor $I_{q_0}^{(0)}$ is the intensity detected at moment $t = R/c$ in the absence of a metasurface. (b) The total emitted light spectra. The relevant parameters and the cases considered are the same as for Fig. 3(a). $S_{q_0}^{(0)}$ is the resonant value of the total emitted light spectrum for an atom in the vacuum. Comments on how we choose parameters for cases A and B are given in Appendix B.

B. Far-field emitted light spectrum

In the previous section we studied how the temporal intensity profile is affected by the described phenomenon. In order

to obtain insight into the spectral manifestation of the aforementioned asymmetry, we calculate the far-field spectrum of the initially excited atom. According to Ref. [42] one can find the emitted light spectrum in the Markov approximation:

$$S_{q_0}(\omega) = \left| \sum_{q'} \int_0^\infty dt' C_{q',q_0}(t') e^{i(\omega-\omega_{q'})t'} \mathbf{F}^{\mathbf{q}'}(\mathbf{r_d}, \mathbf{r_a}) \right|^2, \quad (15)$$

where $\omega_{q'}$ is the transition frequency $|g\rangle \to |e_{q'}\rangle$, $C_{q',q_0}(t')$ is the excited-state $|e_{q'}\rangle$ probability amplitude (with q_0 being the initial state) given by (7), and $\mathbf{F}^{\mathbf{q}'}(\mathbf{r_d}, \mathbf{r_a})$ is

$$\begin{aligned} \mathbf{F}^{\mathbf{q}'}(\mathbf{r_d}, \mathbf{r_a}) &= 4\frac{\omega_{q'}^2}{c^2} \int' d\omega' \mathrm{Im}[\mathbf{G}(\mathbf{r_d}, \mathbf{r_a}, \omega')] \mathbf{d}_{\mathbf{q}'} \zeta(\omega_{q'} - \omega') \\ &= \mathbf{\Gamma}(\mathbf{r_d}, \mathbf{r_a}) \mathbf{d}_{\mathbf{q}'}, \end{aligned} \quad (16)$$

with $\zeta(x) = i\mathrm{P}\frac{1}{x} + \pi\delta(x)$.

The unrotated transition dipole moments are given by $\mathbf{d}_{\mathbf{q}'} = |\mathbf{d}|\mathbf{S}_{:,q'}$, where $\mathbf{S} = [\mathbf{e}_{-1}, \mathbf{e}_0, \mathbf{e}_{+1}]$ is the matrix, where each column is a spherical tensor in Cartesian coordinates. We need to rotate each vector written in Cartesian coordinates on Euler angles using the matrix $\mathbf{M}(\alpha, \beta, \gamma)$, so the rotated vectors are $\mathbf{MS}_{:,\mathbf{q}'}$.

Also, unlike in Ref. [42], to make our paper more coherent we consider that the unperturbed Hamiltonian does not take into account the Lamb shift for each excited state and we account for it in $\mathbf{\Sigma}_{\mathrm{rot}}$. Formally, this means that in the Green's-function argument ω_0 has to be replaced by the corrected atomic transition frequency with the Lamb shift included. We need to note that this cannot lead to any significant changes as the corresponding corrections are on the order of $\sim\gamma_0$, while we consider that $\omega_0 \gg \gamma_0$ and the Green's tensor in our problem varies significantly in the frequency range on the order of ω_0.

We also take only the $\pi\delta(x)$ part of $\zeta(x)$ in (16) for the sake of simplicity. Even though the principal value part can be significant, it will not affect the result qualitatively.

Now, taking the integral over t' in (15) we arrive at the following result:

$$\begin{aligned} S_{q_0}(\omega) &= \left| \sum_j \frac{i\sum_{q'} \mathbf{F}_{\mathbf{q}'}(\mathbf{r_d}, \mathbf{r_a}) C_j^{(q',q_0)}}{(\delta - g_j)} \right|^2 = \left| \sum_j \frac{i\sum_{q'} \mathbf{\Gamma}(\mathbf{r_d}, \mathbf{r_a}) \mathbf{d}_{\mathbf{q}'} C_j^{(q',q_0)}}{(\delta - g_j)} \right|^2 \\ &= \left| \sum_j \frac{i\sum_{q'} |\mathbf{d}| \mathbf{\Gamma}(\mathbf{r_d}, \mathbf{r_a}) \mathbf{MS}_{:,q'} [(\mathbf{MS})^{-1}]_{q',j} (\mathbf{MS})_{j,q_0}}{(\delta - g_j)} \right|^2 = \left| \sum_j \frac{i|\mathbf{d}| \mathbf{\Gamma}_{:,j}(\mathbf{r_d}, \mathbf{r_a}) (\mathbf{MS})_{j,q_0}}{(\delta - g_j)} \right|^2 = \left| \sum_j \frac{\boldsymbol{f}_j^{q_0}(\mathbf{r_d}, \mathbf{r_a})}{(\delta - g_j)} \right|^2, \end{aligned} \quad (17)$$

where we used the fact that $C_j^{(q',q_0)}$ is nothing but $[(\mathbf{MS})^{-1}]_{q',j}(\mathbf{MS})_{j,q_0}$. Another way of representing the total spectrum can be obtained as follows:

$$\begin{aligned} \sum_{j=1}^N \sum_{i=1}^N \frac{\left(\boldsymbol{f}_i^{q_0}\right)^\dagger \boldsymbol{f}_j^{q_0}}{(\delta - g_j)(\delta - g_i^*)} &= \sum_{j=1}^N \sum_{i=1}^N \frac{\left(\boldsymbol{f}_i^{q_0}\right)^\dagger \boldsymbol{f}_j^{q_0}}{g_j - g_i^*} \left[\frac{1}{\delta - g_j} - \frac{1}{\delta - g_i^*} \right] \\ &= \sum_{j=1}^N \sum_{i=1}^N 2\,\mathrm{Re}\left[\frac{\left(\boldsymbol{f}_i^{q_0}\right)^\dagger \boldsymbol{f}_j^{q_0}}{g_j - g_i^*} \frac{1}{\delta - g_j} \right] = \sum_{j=1}^N \sum_{i=1}^N 2\,\mathrm{Re}\left[\frac{\left(\boldsymbol{f}_i^{q_0}\right)^\dagger \boldsymbol{f}_j^{q_0} (\delta - g_j^*)}{g_j - g_i^*} \right] \frac{1}{|\delta - g_j|^2}, \end{aligned} \quad (18)$$

where in the transition from the first to the second line the interchange $i \leftrightarrow j$ in the second term is made.

We can define the following two quantities:

$$\xi_j = +2\mathrm{Re}\left[\sum_i \frac{\left(\boldsymbol{f}_i^{q_0}\right)^\dagger \boldsymbol{f}_j^{q_0}}{g_j - g_i^*} \right], \quad \eta_j = -2\mathrm{Im}\left[\sum_i \frac{\left(\boldsymbol{f}_i^{q_0}\right)^\dagger \boldsymbol{f}_j^{q_0}}{g_j - g_i^*} \right], \quad (19)$$

and, finally, we obtain the following:

$$S_{q_0}(\delta) \approx \left| \sum_j \frac{\boldsymbol{f}_j^{q_0}(\mathbf{r_d}, \mathbf{r_a})}{(\delta - g_j)} \right|^2 = \sum_j \frac{(\xi_j(\delta - g_j') + \eta_j g_j'')}{(\delta - g_j')^2 + g_j''^2}. \quad (20)$$

The last part of Eq. (20) simply shows that the spectrum for three eigenstates can be decomposed into three symmetric Lorentzian lines $\sim\eta_j$ and three antisymmetric parts $\sim\xi_j$, and depending upon their values the line shape can vary significantly.

Here we also want to note that it is easy to calculate the emitted spectrum of a certain polarization. Formally, this can be done by replacing the vector $\boldsymbol{f}_j^{q_0}(\mathbf{r_d}, \mathbf{r_a})$ with a scalar $f_j^{q_d,q_0}(\mathbf{r_d}, \mathbf{r_a}) = \mathbf{e}_{\mathbf{q_d}}^\dagger \cdot \boldsymbol{f}_j^{q_0}(\mathbf{r_d}, \mathbf{r_a})$, where q_d is a polarization to which the detector is sensitive, and $\mathbf{e}_{\mathbf{q_d}}^\dagger$ is the corresponding normalized polarization vector. In this case the total emitted light spectrum is simply $S_{q_0}(\delta) = \sum_{q_d} S_{q_d,q_0}(\delta)$ as a result of the completeness relation $\sum_{q_d} \mathbf{e}_{\mathbf{q_d}} \otimes \mathbf{e}_{\mathbf{q_d}}^\dagger = \mathbf{1}$.

As expected, the total emitted light spectra also differ for two initially excited states of opposite helicities in the case of an anisotropic structure, and with the tilted atomic quantization axis [see Fig. 3(b)]. It should be stressed that tilting the quantization axis is not the only way to observe the difference between $S_{-1}(\delta)$ and $S_{+1}(\delta)$. Namely, the introduction of the substrate with $\varepsilon_{\mathrm{subs}} \neq 1$ leads to a similar result. However, this happens not due to different populations of atomic energy levels but rather due to the mixing of the fields emitted by different eigenstates. The details can be found in Appendix C.

The described effect opens a route towards the optical tomography of the internal state of a quantum emitter. Namely, placing an isolated emitter or an array of them in the vicinity of the structure would allow the reconstruction of the symmetry axes of the nanosized object by the scattering spectra or intensity dynamics. The effect under study is also of importance for spectroscopy and has to be taken into account.

V. CONCLUSION

We have shown that the combined effect of the metasurface anisotropy and the tilt of the quantum emitter quantization axis leads to an observable difference both in temporal dynamics and in spectral properties of the emitter initially pumped into states of opposite helicities. This is a somewhat counterintuitive result since it states that optical activity can emerge due to the anisotropy of the system and it originates through the quantum interference of the multiple decay channels of the emitter.

The results presented here are applicable not only for metasurfaces but for any structure that is fully anisotropic, for example, planar cavities with in-plane anisotropy, elliptical micropillar cavities [45], or an ensemble of ultracold atoms trapped near the optical nanofiber [8]. Moreover, in the case of a cavity it should be enhanced by the order of the quality factor while the field localization is usually smaller for the case of cavities than for metasurfaces or waveguide structures. These findings not only open avenues towards the engineering of quantum optical systems at the nanoscale but can be readily used for the relatively simple optical tomography of nano-objects.

ACKNOWLEDGMENTS

We thank for fruitful discussions A. A. Bogdanov, L. E. Golub, M. M. Glazov, and O. E. Yermakov. This work was supported by the Russian Foundation for Basic Research (Projects No. 18-32-00691 and No. 17-02-01234). D.K. and M.P. acknowledge support from Basis Foundation. I.I. acknowledges the support of the Grants of the Ministry of Science of Russian Federation No. 3.1365.2017/4.6, No. 14.Y26.31.0015, and the Grant of the President of Russian Federation MK-6248.2018.2. The dynamics of the quantum emitter was modelled in the framework of RFBR (Projects No. 17-02-01234, No. 18-32-00691), and the electrodynamics response of the anisotropic metasurfaces was supported by Russian Scientific Foundation (Project No. 19-72-10129). D.K. and M.P. also acknowledge support from the Foundation for the Advancement of Theoretical Physics and Mathematics "BASIS".

APPENDIX A: GREEN'S TENSOR OF A METASURFACE

According to a superposition principle [43,44], the total Green's tensor of the problem can be expanded into the following sum:

$$\mathbf{G^{ij}}(\mathbf{r},\mathbf{r}',\omega)=\mathbf{G_0}(\mathbf{r},\mathbf{r}',\omega)+\mathbf{G^{ij}_{SC}}(\mathbf{r},\mathbf{r}',\omega), \tag{A1}$$

where $\mathbf{G_0}(\mathbf{r},\mathbf{r}',\omega)$ is the free-space Green's tensor and $\mathbf{G_{SC}}(\mathbf{r},\mathbf{r}',\omega)$ is the scattered part, which contains all the information about the modes of the structure. The superscripts i and j describe the position of the field and the source points with respect to the interface of the structure. We label the upper half space as 1 and the lower one as 2. We are especially interested in constructing the $\mathbf{G^{11}}(\mathbf{r},\mathbf{r}',\omega)$ tensor, and we also want to find $\mathbf{G^{21}}(\mathbf{r},\mathbf{r}',\omega)=\mathbf{G^{21}_{SC}}(\mathbf{r},\mathbf{r}',\omega)$ to satisfy the boundary conditions on the interface.

In order to find the scattered part we want to use the approach described in Ref. [46] and begin by introducing the following vector functions, corresponding to TE and TM modes:

$$\mathbf{t_{j,\pm}}=\frac{1}{\kappa}\begin{pmatrix}-\kappa_y\\ +\kappa_x\\ 0\end{pmatrix},\quad \mathbf{p_{j,\pm}}=\frac{1}{k_j}\begin{pmatrix}\mp k_{j,z}\kappa_x/\kappa\\ \mp k_{j,z}\kappa_y/\kappa\\ \kappa\end{pmatrix}, \tag{A2}$$

where $\kappa=\sqrt{\kappa_x^2+\kappa_y^2}$ and $k_{j,z}=\sqrt{k_j^2-\kappa^2}$. The first subscript (in $\mathbf{t}$ and $\mathbf{p}$ functions $_j$) labels the media, while the $\pm$ sign defines the propagation direction along the z axis.

The expansions for both free and scattered parts have the form

$$\mathbf{G_0}(\mathbf{r},\mathbf{r}',\omega)=-\mathbf{e_z}\mathbf{e_z}\delta(\mathbf{R})+\frac{i}{8\pi^2}\iint d\kappa_x d\kappa_y\frac{1}{k_{1z}}[\mathbf{t_{1\pm}}\mathbf{t_{1\pm}}+\mathbf{p_{1\pm}}\mathbf{p_{1\pm}}]\exp(i\mathbf{k_{1\pm}}\mathbf{R}),$$

$$\mathbf{G^{11}_{SC}}(\mathbf{r},\mathbf{r}',\omega)=\frac{i}{8\pi^2}\iint\frac{d\kappa_x d\kappa_y}{k_{1,z}}\left[R^{11}_{tt}\mathbf{t_{1,+}}\mathbf{t_{1,-}}+R^{11}_{tp}\mathbf{t_{1,+}}\mathbf{p_{1,-}}+R^{11}_{pt}\mathbf{p_{1,+}}\mathbf{t_{1,-}}+R^{11}_{pp}\mathbf{p_{1,+}}\mathbf{p_{1,-}}\right]\exp(i\mathbf{k_{1,+}}\mathbf{r}-i\mathbf{k_{1,-}}\mathbf{r}'),$$

$$\mathbf{G^{21}_{SC}}(\mathbf{r},\mathbf{r}',\omega)=\frac{i}{8\pi^2}\iint\frac{d\kappa_x d\kappa_y}{k_{1,z}}\left[R^{21}_{tt}\mathbf{t_{2,-}}\mathbf{t_{1,-}}+R^{21}_{tp}\mathbf{t_{2,-}}\mathbf{p_{1,-}}+R^{21}_{pt}\mathbf{p_{2,-}}\mathbf{t_{1,-}}+R^{21}_{pp}\mathbf{p_{2,-}}\mathbf{p_{1,-}}\right]\exp(i\mathbf{k_{2,-}}\mathbf{r}-i\mathbf{k_{1,-}}\mathbf{r}'), \tag{A3}$$

where $\mathbf{R}=\mathbf{r}-\mathbf{r}'$. In $\mathbf{G_0}(\mathbf{r},\mathbf{r}',\omega)$ the upper (lower) signs in the field vector functions are for the case $z>z'$ ($z<z'$). Here we also introduced the Fresnel coefficients R^{ij}_{kl} accounting for the scattering of the mode "l" into the mode "k." Note that since our structure is, in general, anisotropic in the xy plane, there are modes of a hybrid nature which can be identified by the cross terms involving products of $\mathbf{t_{j,\pm}}$ and $\mathbf{p_{j,\pm}}$.

The coefficients R^{ij}_{kl} can be found by satisfying the boundary conditions for both electric and magnetic fields:

$$\begin{cases}\mathbf{e_z}\times(\mathbf{E_1}-\mathbf{E_2})=0,\\ \mathbf{e_z}\times(\mathbf{H_1}-\mathbf{H_2})=\dfrac{4\pi}{c}\sigma\mathbf{E_{1,2}},\end{cases} \tag{A4}$$

where σ is a surface conductivity tensor. The first condition on the electric field allows one to relate different Fresnel

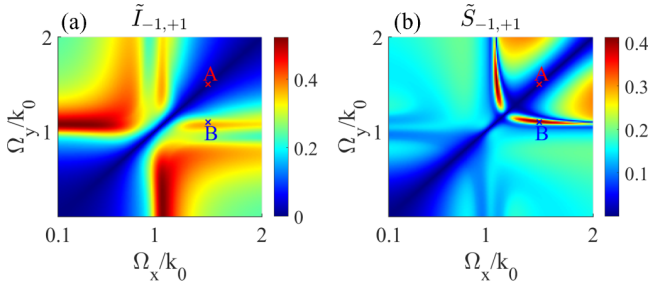

FIG. 4. $\tilde{I}_{-1,+1}$ and $\tilde{S}_{-1,+1}$ parameters defined by (B1) and (B2) vs metasurface resonance frequencies Ω_x and Ω_y. All other parameters are the same as in Fig. 3. The two specific points correspond to isotropic (A, $\Omega_x = \Omega_y = 1.5k_0$) and anisotropic ($\Omega_x = 1.5k_0$, $\Omega_y = 1.1k_0$) cases.

coefficients to each other in a rather simple form:

$$\begin{aligned} 1 + R^{11}_{tt} &= R^{21}_{tt}, \\ R^{11}_{pt}\frac{k_{1,z}}{k_1} &= -R^{21}_{pt}\frac{k_{2,z}}{k_2}, \\ R^{11}_{tp} &= R^{21}_{tp}, \\ -1 + R^{11}_{pp} &= -R^{21}_{pp}\frac{k_{2,z}k_1}{k_2 k_{1,z}}. \end{aligned} \tag{A5}$$

By using this along with the second line of (A4) we can find the rest of the coefficients.

The optical properties of such a metasurface can be characterized by effective surface conductivity tensor σ, which can be chosen to be diagonal in some reference frame. To describe the optical properties of a metasurface we use the effective conductivity described by Ref. [25]:

$$\sigma = \begin{pmatrix} \sigma_{xx} & 0 \\ 0 & \sigma_{yy} \end{pmatrix}, \quad \sigma_{jj} = A_j \frac{ic}{4\pi}\frac{\omega}{\omega^2 - \Omega_j^2 + i\gamma_j\omega}, \tag{A6}$$

where A_j is the normalization constant, Ω_j is the resonance frequency, and γ_j is the bandwidth.

In the absence of a substrate ($\epsilon_1 = \epsilon_2$) and in the case of a strong anisotropy ($\sigma_{yy} \to i\infty, \sigma_{xx} \to i0$), we can perform the double integral in Eq. (A3) and obtain $\mathbf{G^{11}_{SC}}(\mathbf{r}, \mathbf{r}, \omega)$ analytically:

$$\begin{aligned} G^{sc,11}_{xx}(\mathbf{r}, \mathbf{r}, \omega) &= \frac{1}{32\pi k^2 \Delta z^3} e^{ik2\Delta z}, \\ G^{sc,11}_{yy}(\mathbf{r}, \mathbf{r}, \omega) &= \frac{-1 + 2ik\Delta z + 4k^2\Delta z^2}{32\pi k^2 \Delta z^3} e^{ik2\Delta z}, \\ G^{sc,11}_{zz}(\mathbf{r}, \mathbf{r}, \omega) &= \frac{1 - ik\Delta z}{16\pi \Delta z^3 k^2} e^{ik2\Delta z}. \end{aligned} \tag{A7}$$

APPENDIX B: A MEASURE OF THE DISCREPANCY BETWEEN THE INTENSITY AND SPECTRAL PROFILES

As we are interested in both intensity $I_{q_0}(\tau)$ and spectrum $S_{q_0}(\delta)$ for two initial conditions ($q_0 = -1, +1$), it is good to study how the difference between these two cases depends upon the metasurface parameters. For this we need to fix the orientation of the local quantization z axis (angles α and β)

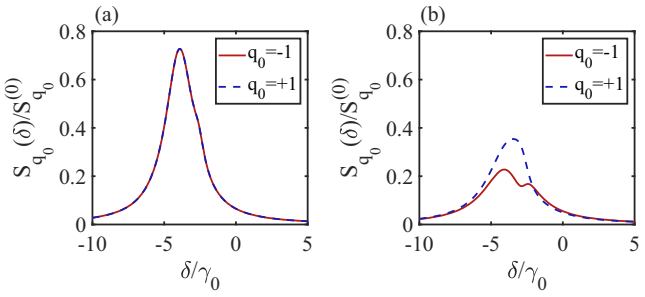

FIG. 5. The total emitted light spectra for two initial conditions: $q_0 = -1$ (solid red lines) and $q_0 = +1$ (dashed blue lines) in the case of an absent substrate $\varepsilon_{\text{subs}} = 1$ (a) and with substrate $\varepsilon_{\text{subs}} = 2.2$ (b) for the in-plane situation ($\alpha = \beta = 0$). The other relevant parameters are the same as in Fig. 3. $S^{(0)}_{q_0}$ is the resonant value of the total emitted light spectrum for an atom in the vacuum.

and introduce the following two quantities:

$$\tilde{I}_{-1,+1} = \frac{\int_0^\infty |I_{-1}(\tau) - I_{+1}(\tau)| d\tau}{\int_0^\infty [I_{-1}(\tau) + I_{+1}(\tau)] d\tau}, \tag{B1}$$

$$\tilde{S}_{-1,+1} = \frac{\int_{-\infty}^\infty |S_{-1}(\delta) - S_{+1}(\delta)| d\delta}{\int_{-\infty}^\infty [S_{-1}(\delta) + S_{+1}(\delta)] d\delta}. \tag{B2}$$

Clearly, these two quantities are always between 0 and 1 and can be used to measure how much the two graphs are similar or different. Therefore, we can plot the map of (B1) and (B2) versus resonance frequencies Ω_x and Ω_y presented in Figs. 4(a) and 4(b). Note that for $\Omega_x = \Omega_y$ the metasurface is isotropic and both $\tilde{I}_{-1,+1}$ and $\tilde{S}_{-1,+1}$ are equal to zero. Even though the local maxima of $\tilde{I}_{-1,+1}$ and $\tilde{S}_{-1,+1}$ do not overlap, there is a region where both of these quantities exceed the value of ≈0.2–0.3, which is sufficient in order to observe the discrepancy for $q_0 = -1$ and $+1$ cases [see Figs. 4(a) and 4(b)].

APPENDIX C: EMITTED LIGHT INTENSITY AND SPECTRUM IN THE CASE OF A SUBSTRATE

One major difference between observing the probabilities of some processes $P_{e_f,e_i}(t)$ and looking at either detected intensity $I_{q_0}(t)$ or spectrum $S_{q_0}(\delta)$ is that in the latter two cases the position of the detector with respect to the atom and nanostructure is involved. One can consider the case when $\mathbf{d_{-1}}$ and $\mathbf{d_{+1}}$ rotate in the interface plane ($\alpha = \beta = 0$) and put the detector right above the atom in the far-field zone so that it has the position $\mathbf{r_d} = (0, 0, R)$. Note that in this scenario the eigenstate with the associated z-oriented dipole moment does not contribute to the result as it does not have the far-field term. If there is no substrate $\epsilon_{\text{subs}} = 1$ then the corresponding Green's tensor $\mathbf{G^{FF}}(\mathbf{r_d}, \mathbf{r_a}, \omega_0)$ is diagonal and the two relevant contributions in Eqs. (14) and (20) from x and y dipole moments do not interfere with each other. However, if one introduces the substrate $\epsilon_{\text{subs}} \neq 1$ then there are nonzero components of the Green's tensor $\mathbf{G^{FF}_{xy}}(\mathbf{r_d}, \mathbf{r_a}, \omega_0) = \mathbf{G^{FF}_{yx}}(\mathbf{r_d}, \mathbf{r_a}, \omega_0) \neq 0$, which leads to the mixing of the fields generated by x and y dipoles resulting in the observable difference in $S_{-1}(\delta)$ and $S_{+1}(\delta)$. However, one should not

confuse this with the effect described in the main text as in this case the transition probabilities will be equal: $P_{-,+}(t) = P_{+,-}(t)$.

Indeed, as can be seen from Fig. 5, the presence of the substrate leads to an observable difference in the emitted light spectra, for instance.

[1] P. Lodahl, S. Mahmoodian, S. Stobbe, A. Rauschenbeutel, P. Schneeweiss, J. Volz, H. Pichler, and P. Zoller, Chiral quantum optics, Nature (London) **541**, 473 (2017).

[2] C. W. Gardiner, Driving a Quantum System with the Output Field from Another Driven Quantum System, Phys. Rev. Lett. **70**, 2269 (1993).

[3] H. J. Carmichael, Quantum Trajectory Theory for Cascaded Open Systems, Phys. Rev. Lett. **70**, 2273 (1993).

[4] I. Söllner, S. Mahmoodian, S. L. Hansen, L. Midolo, A. Javadi, G. Kiršanskė, T. Pregnolato, H. El-Ella, E. H. Lee, J. D. Song, S. Stobbe, and P. Lodahl, Deterministic photon-emitter coupling in chiral photonic circuits, Nat. Nanotechnol. **10**, 775 (2015).

[5] R. J. Coles, D. M. Price, J. E. Dixon, B. Royall, E. Clarke, P. Kok, M. S. Skolnick, A. M. Fox, and M. N. Makhonin, Chirality of nanophotonic waveguide with embedded quantum emitter for unidirectional spin transfer, Nat. Commun. **7**, 11183 (2016).

[6] N. V. Corzo, B. Gouraud, A. Chandra, A. Goban, A. S. Sheremet, D. V. Kupriyanov, and J. Laurat, Large Bragg Reflection from One-Dimensional Chains of Trapped Atoms Near a Nanoscale Waveguide, Phys. Rev. Lett. **117**, 133603 (2016).

[7] H. L. Sørensen, J.-B. Béguin, K. W. Kluge, I. Iakoupov, A. S. Sørensen, J. H. Müller, E. S. Polzik, and J. Appel, Coherent Backscattering of Light off One-Dimensional Atomic Strings, Phys. Rev. Lett. **117**, 133604 (2016).

[8] R. Mitsch, C. Sayrin, B. Albrecht, P. Schneeweiss, and A. Rauschenbeutel, Quantum state-controlled directional spontaneous emission of photons into a nanophotonic waveguide, Nat. Commun. **5**, 5713 (2014).

[9] C. Junge, D. O'Shea, J. Volz, and A. Rauschenbeutel, Strong Coupling between Single Atoms and Nontransversal Photons, Phys. Rev. Lett. **110**, 213604 (2013).

[10] F. Spitzer, A. N. Poddubny, I. A. Akimov, V. F. Sapega, L. Klompmaker, L. E. Kreilkamp, L. V. Litvin, R. Jede, G. Karczewski, M. Wiater, T. Wojtowicz, D. R. Yakovlev, and M. Bayer, Routing the emission of a near-surface light source by a magnetic field, Nat. Phys. **14**, 1043 (2018).

[11] C. Gonzalez-Ballestero, A. Gonzalez-Tudela, F. J. Garcia-Vidal, and E. Moreno, Chiral route to spontaneous entanglement generation, Phys. Rev. B **92**, 155304 (2015).

[12] D. Kornovan, M. Petrov, and I. Iorsh, Transport and collective radiance in a basic quantum chiral optical model, Phys. Rev. B **96**, 115162 (2017).

[13] C. A. Downing, J. C. L. Carreño, F. P. Laussy, E. Del Valle, and A. I. Fernández-Domínguez, Quasichiral Interactions between Quantum Emitters at the Nanoscale, Phys. Rev. Lett. **122**, 057401 (2019).

[14] R. R. Q. P. T. Oude Weernink, P. Barcellona, and S. Y. Buhmann, Lateral Casimir-Polder forces by breaking time-reversal symmetry, Phys. Rev. A **97**, 032507 (2018).

[15] F. Le Kien, D. F. Kornovan, S. Sahar S. Hejazi, V. G. Truong, M. I. Petrov, S. N. Chormaic, and T. Busch, Force of light on a two-level atom near an ultrathin optical fiber, New J. Phys. **20**, 093031 (2018).

[16] F. Le Kien and A. Rauschenbeutel, Nanofiber-mediated chiral radiative coupling between two atoms, Phys. Rev. A **95**, 023838 (2017).

[17] G. Wang, A. Chernikov, M. M. Glazov, T. F. Heinz, X. Marie, T. Amand, and B. Urbaszek, *Colloquium*: Excitons in atomically thin transition metal dichalcogenides, Rev. Mod. Phys. **90**, 021001 (2018).

[18] S.-H. Gong, F. Alpeggiani, B. Sciacca, E. C. Garnett, and L. Kuipers, Nanoscale chiral valley-photon interface through optical spin-orbit coupling, Science **359**, 443 (2018).

[19] T. Chervy, S. Azzini, E. Lorchat, S. Wang, Y. Gorodetski, J. A. Hutchison, S. Berciaud, T. W. Ebbesen, and C. Genet, Room temperature chiral coupling of valley excitons with spin-momentum locked surface plasmons, ACS Photonics **5**, 1281 (2018).

[20] S. Guddala, R. Bushati, M. Li, A. B. Khanikaev, and V. M. Menon, Valley selective optical control of excitons in 2D semiconductors using chiral metasurface, Opt. Mater. Exp. **9**, 536 (2018).

[21] E. Lassalle, P. Lalanne, S. Aljunid, P. Genevet, B. Stout, T. Durt, and D. Wilkowski, Long-lifetime coherence in a quantum emitter induced by a metasurface, arXiv:1909.02409v1.

[22] G. Hu, X. Hong, K. Wang, J. Wu, H.-X. Xu, W. Zhao, W. Liu, S. Zhang, F. Garcia-Vidal, B. Wang, P. Lu, and C.-W. Qiu, Coherent steering of nonlinear chiral valley photons with a synthetic Au-WS2 metasurface, Nat. Photonics **13**, 467 (2019).

[23] S. B. Glybovski, S. A. Tretyakov, P. A. Belov, Y. S. Kivshar, and C. R. Simovski, Metasurfaces: From microwaves to visible, Phys. Rep. **634**, 1 (2016).

[24] J. S. Gomez-Diaz, M. Tymchenko, and A. Alù, Hyperbolic Plasmons and Topological Transitions Over Uniaxial Metasurfaces, Phys. Rev. Lett. **114**, 233901 (2015).

[25] O. Y. Yermakov, A. I. Ovcharenko, M. Song, A. A. Bogdanov, I. V. Iorsh, and Yu. S. Kivshar, Hybrid waves localized at hyperbolic metasurfaces, Phys. Rev. B **91**, 235423 (2015).

[26] O. Y. Yermakov, A. I. Ovcharenko, A. A. Bogdanov, I. V. Iorsh, K. Y. Bliokh, and Y. S. Kivshar, Spin control of light with hyperbolic metasurfaces, Phys. Rev. B **94**, 075446 (2016).

[27] S. Hughes and G. S. Agarwal, Anisotropy-Induced Quantum Interference and Population Trapping between Orthogonal Quantum Dot Exciton States in Semiconductor Cavity Systems, Phys. Rev. Lett. **118**, 063601 (2017).

[28] P. K. Jha, X. Ni, C. Wu, Y. Wang, and X. Zhang, Metasurface-Enabled Remote Quantum Interference, Phys. Rev. Lett. **115**, 025501 (2015).

[29] G. S. Agarwal, Anisotropic Vacuum-Induced Interference in Decay Channels, Phys. Rev. Lett. **84**, 5500 (2000).

[30] P. K. Jha, N. Shitrit, X. Ren, Y. Wang, and X. Zhang, Spontaneous Exciton Valley Coherence in Transition Metal Dichalcogenide Monolayers Interfaced with an Anisotropic Metasurface, Phys. Rev. Lett. **121**, 116102 (2018).

[31] J. H. Oh, K. J. Chang, G. Ihm, and S. J. Lee, Electronic structure of three-dimensional quantum dots in tilted magnetic fields, Phys. Rev. B **50**, 15397 (1994).

[32] J. Koepsell, T. Thiele, J. Deiglmayr, A. Wallraff, and F. Merkt, Measuring the polarization of electromagnetic fields using Rabi-rate measurements with spatial resolution: Experiment and theory, Phys. Rev. A **95**, 053860 (2017).

[33] F. Le Kien and K. Hakuta, Effect of the orientation of a weak magnetic field on the radiative decay of a cesium atom near a nanofiber, Phys. Rev. A **78**, 063803 (2008).

[34] F. Le Kien, S. S. S. Hejazi, T. Busch, V. G. Truong, and S. N. Chormaic, Channeling of spontaneous emission from an atom into the fundamental and higher-order modes of a vacuum-clad ultrathin optical fiber, Phys. Rev. A **96**, 043859 (2017).

[35] X. Yuan, F. Weyhausen-Brinkmann, J. Martín-Sánchez, G. Piredda, V. Krápek, Y. Huo, H. Huang, C. Schimpf, O. G. Schmidt, J. Edlinger, G. Bester, R. Trotta, and A. Rastelli, Uniaxial stress flips the natural quantization axis of a quantum dot for integrated quantum photonics, Nat. Commun. **9**, 3058 (2018).

[36] C. Cohen-Tannoudji, J. Dupont-Roc, and G. Grynberg, *Atom-Photon Interactions* (Wiley, New York, 2004).

[37] L. Knoll, S. Scheel, and D.-G. Welsch, QED in dispersing and absorbing media, arXiv:quant-ph/0006121.

[38] H. T. Dung, L. Knöll, and D.-G. Welsch, Intermolecular energy transfer in the presence of dispersing and absorbing media, Phys. Rev. A **65**, 043813 (2002).

[39] S. Y. Buhmann, *Dispersion Forces II: Many-Body Effects, Excited Atoms, Finite Temperature and Quantum Friction* (Springer-Verlag, Berlin, 2012).

[40] V. P. Gusynin, S. G. Sharapov, and J. P. Carbotte, Magneto-optical conductivity in graphene, J. Phys.: Condensed Matter **19**, 026222 (2006).

[41] H. T. Dung, L. Knöll, and D.-G. Welsch, Spontaneous decay in the presence of dispersing and absorbing bodies: General theory and application to a spherical cavity, Phys. Rev. A **62**, 053804 (2000).

[42] H. T. Dung, L. Knöll, and D.-G. Welsch, Resonant dipole-dipole interaction in the presence of dispersing and absorbing surroundings, Phys. Rev. A **66**, 063810 (2002).

[43] W. C. Chew, *Waves and Fields in Inhomogeneous Media* (Wiley, New York, 1999).

[44] C.-T. Tai, *Dyadic Green Functions in Electromagnetic Theory*, IEEE Press Series on Electromagnetic Waves (IEEE, New York, 1994).

[45] Y.-M. He, H. Wang, S. Gerhardt, K. Winkler, J. Jurkat, Y. Yu, M.-C. Chen, X. Ding, S. Chen, J. Qian *et al.*, Polarized indistinguishable single photons from a quantum dot in an elliptical micropillar, arXiv:1809.10992.

[46] A. Lakhtakia, Green's functions and brewster condition for a halfspace bounded by an anisotropic impedance plane, Int. J. Infrared Millimeter Waves, **13**, 161 (1992).

12th International Congress on Artificial Materials for Novel Wave Phenomena - Metamaterials 2018
Espoo, Finland, Aug. 27$^{\text{th}}$ - Sept. 1$^{\text{st}}$ 2018

Strong coupling and non-reciprocity in the dynamics of a V-atom placed near an anisotropic metasurface.

D. F. Kornovan[1], M. I. Petrov[1,2], and I. V. Iorsh[1]

[1]ITMO University , Nanophotonics and Metamaterials Department, Birjevaja line V.O., 14, 199034, St. Petersburg, Russian Federation
[2] University of Eastern Finland, Yliopistokatu 7, FI-80101 Joensuu, Finland
d.kornovan@metalab.ifmo.ru

***Abstract* – In this work we focus on studying the temporal dynamics of a V-type quantum emitter with two excited states, which allows to observe an interplay between different spontaneous emission channels. We show that the presence of an anisotropic metasurface enables an interaction between the two active transitions and makes it possible to achieve a strong coupling regime. We also show that if the rotation plane of the transition dipole moments is arbitrarily oriented with respect to the metasurface interface, it is possible to observe a non-reciprocal behavior.**

I. Introduction

The subject of anisotropic vacuum has been attracting a lot of attention since the proposal by G. Agarwal [1], where the idea of exploiting the interference between different emission channels was considered for the first time. A major interest was in trying different photonic systems in order to control this effect and allow for the suppression of the emission rate due to destructive interference between the decay channels [2].

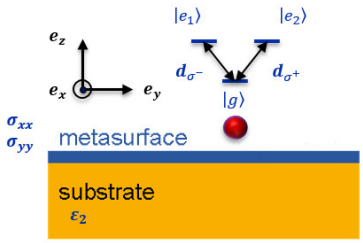

Fig. 1: System under consideration: a V-type atom with two rotating transition dipole moments placed near an anisotropic metasurface.

II. Theoretical Framework and Results

In this work we investigate the time evolution of a three level V-type atom with two excited states $|e_1\rangle$, $|e_2\rangle$ with the corresponding transition dipole moments $\mathbf{d}_{\sigma+}$ and $\mathbf{d}_{\sigma-}$ (Fig. 1). The two orthogonal dipole moments are decoupled in the isotropic media, but they can interact with each other via the electromagnetic modes of some photonic/plasmonic structure, for example, an anisotropic metasurface. The optical properties of such a metasurface can be characterized by the tensor of the effective surface conductivity σ, which can be chosen to be diagonal in some reference frame. To describe the optical properties of a metasurface we use the effective conductivity described by [3]:

$$\sigma = \begin{pmatrix} \sigma_{xx} & 0 \\ 0 & \sigma_{yy} \end{pmatrix}, \quad \sigma_{jj} = A_{jj} \frac{ic}{4\pi} \frac{\omega}{\omega^2 - \Omega_{jj}^2 + i\gamma_{jj}\omega}, \tag{1}$$

where A_{jj} is the normalization constant, Ω_{jj} is the resonance frequency, γ_{jj} is the bandwidth.

In order to solve for the temporal dynamics of the emitter we employ the approach of the resolvent operator [4, 5], when it is possible to find the matrix elements of the evolution operator $\hat{U}(t,0)$ using:

$$\langle e_f|\hat{U}(t,0)|e_i\rangle = \int_C dz/(2\pi i)e^{-izt/\hbar}\langle e_f|\hat{G}(z)|e_i\rangle, \tag{2}$$

where $\hat{G}(z) = (z-\hat{H})^{-1}$ is the resolvent operator of the full Hamiltonian $\hat{H}$. Using this relation we can find probabilities for the atom to be in the excited state $|e_f\rangle$ at time t given that it was in the state $|e_i\rangle$ initially by simply calculating $P_{e_f}(t) = |U_{e_f e_i}(t,0)|^2$.

We should note that here we work in the single excitation domain since we are studying the excited states evolution of a single atom. In this single excitation subspace of a Hilbert space the resolvent can be found to be:

$$\langle e_f|\hat{G}(z)|e_i\rangle = \langle e_f|\left[z-\hat{H}_0-\hat{\Sigma}(z)\right]^{-1}|e_i\rangle \approx \left[(z-\hbar\omega_0)\,\delta_{e_f e_i} + 4\pi k_0^2 \mathbf{d}^*_{\mathbf{e_f}}\mathbf{G}(\mathbf{r_0},\mathbf{r_0},\omega_0)\mathbf{d}_{\mathbf{e_i}}\right]^{-1}, \tag{3}$$

here $\hat{H}_0$ is the unperturbed Hamiltonian and $\Sigma(z)$ is the level shift operator, δ_{ij} is the Kronecker delta. The level-shift operator in the latter expression is written within two approximations: near-resonant interaction of the states ($z=\hbar\omega_0$) and taking into account only proccesses of the second order [6], leading to a form of a classical dipole-dipole coupling constants. From now on we will notate the diagonal matrix elements of $\Sigma_{e_j e_j}(\hbar\omega_0) = g_{nd} = \hbar\left(\Delta_{e_i} - i\gamma_{e_i}/2\right)$ and non-diagonal as $\Sigma_{e_k e_l}(\hbar\omega_0) = g_{nd} = \hbar\left(\Delta_{e_k e_l} - i\gamma_{e_k e_l}/2\right)$, where $\Delta_{e_k}, \gamma_{e_k}$ are the Lamb shift and the total decay rate of the state $|e_k\rangle$, and $\Delta_{e_k e_l}, \gamma_{e_k e_l}$ are the coherent and dissipative parts of the interaction constant of levels $|e_k\rangle, |e_l\rangle$. All of these parameters can be expressed via classical electromagnetic Green's function $\Sigma_{e_f e_i} = -4\pi k_0^2 \mathbf{d}^*_{\mathbf{e_f}}\mathbf{G}(\mathbf{r_0},\mathbf{r_0},\omega_0)\mathbf{d}_{\mathbf{e_i}}$. Therefore, in order to describe the interaction of the emitter with the electromagnetic modes of the field we only need to construct the Green's function of a metasurface, which can be done by following the procedure outlined in [7].

We begin by studying the interaction of the two excited states of a quantum emitter in the case, when transition dipole moments rotate in the plane of the interface of the structure considered. In this case the dynamics of the excited states can be found to be:

$$\begin{aligned} |U_{e_1 e_1}(t,0)|^2 &= e^{-\gamma_{e_1} t}\left[cosh\left(\gamma_{e_1 e_2} t\right) + cos\left(2\Delta_{e_1 e_2} t\right)\right]/2, \\ |U_{e_2,e_1}(t,0)|^2 &= e^{-\gamma_{e_1} t}\left[cosh\left(\gamma_{e_1 e_2} t\right]\right) - cos\left(2\Delta_{e_1 e_2} t\right)\right]/2 \end{aligned} \tag{4}$$

The solutions (4) consist of two parts: purely exponentially decaying and the oscillating one, which accounts for the population exchange between the states. From the answers above one can conclude that in order to obtain a strong coupling between orthogonal transitions one needs to achive a regime, when the coherent coupling strength between the states *exceeds* the dissipations, which in our case takes the form: $|\text{Re}[g_{nd}]| > \text{Im}[g_d]$ or equivalently $\xi = 2|\Delta_{e_1 e_2}|/\gamma_{e_1} > 1$, where ξ is the strong coupling parameter. From Fig. 2, a) one can see that for given parameters, this condition can be satisfied when the atom-surface distance is about $\Delta z \approx \lambda_{xx}/20$, where $\lambda_{xx} = 2\pi c/\Omega_{xx}$. Fig. 2, b) shows that the probabilities $P_{e_1 e_1}(t)$ and $P_{e_2 e_1}(t)$ clearly undergo oscillations as a signature of a strong coupling regime. We should note that this strong coupling is not due to the surface plasmon modes of a metasurface [3], but rather due to the radiation modes and near-fields as surface plasmons as propagating modes lead to the energy dissipation in this system.

Another interesting phenomena appears if we let the quantization axis (the new $\mathbf{e_{z'}}$ axis) to point into an arbitrary direction), which means that the rotation transition dipole moments $\mathbf{d_{e_1}}, \mathbf{d_{e_2}}$ rotate in the plane, which generally does not coincide with the metasurface interface. This can be formally done by considering the level-shift operator matrix in the Cartesian coordinate system $\Sigma_{Cart}(\hbar\omega_0)$, which physically expresses the coupling of linear dipoles $\mathbf{d_j}, j = x, y, z$ and then using a transformation matrix S: $S^\dagger \Sigma_{Cart} S$, which first make the transformation from the Cartesian coordinate system into the basis of spherical tensors $\mathbf{e_j}, j = \sigma^-, \pi,$, and then rotate the spherical tensors with Wigner matrix $D_1^{mm'}(\alpha,\beta,\gamma)$, where α,β,γ are the Euler angles. In this case the dynamics can be described by a rather general form:

$$P_{e_1 e_2}(t) = \sum_j C^{(jj)}_{e_1 e_2} e^{-\gamma_{jj} t} + \sum_{i,j;i\neq j} C^{(ij)}_{e_1 e_2} 2cos\left(\left[\Delta_{ii} - \Delta_{jj}\right] t - \phi^{(ij)}_{e_1 e_2}\right) e^{-(\gamma_{ii}+\gamma_{jj})t/2}, \tag{5}$$

12th International Congress on Artificial Materials for Novel Wave Phenomena - Metamaterials 2018
Espoo, Finland, Aug. 27th - Sept. 1st 2018

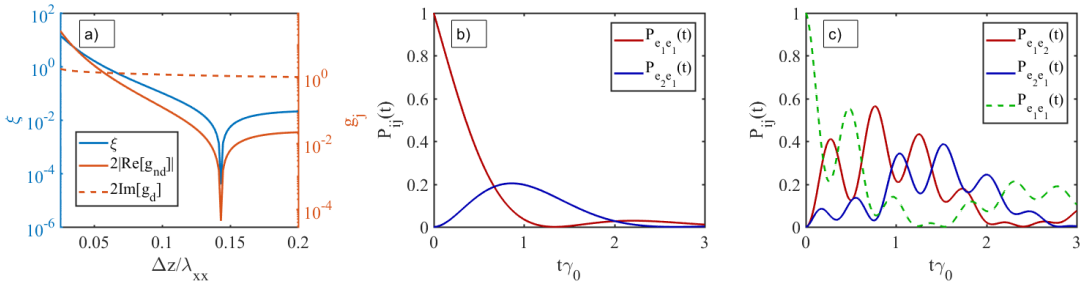

Fig. 2: a) Strong coupling parameter ξ (blue) and both real and imaginary parts of $2g_{nd}$ and $2g_d$ (orange), respectively, versus emitter-interface distance Δz measured in $\lambda_{xx} = 2\pi c/\Omega_{xx}$. b) Population dynamics for the initially excited state $|e_1\rangle$, and for the state $|e_2\rangle$, when the emitter-surface distance is $\Delta z/\lambda_{xx} = 0.05$. Here γ_0 is a free-space spontaneous emission rate from $|e_1\rangle/|e_2\rangle$ to the ground state. c) Excitation transfer from e_1 to e_2 and vice versa along with the initially excited state population. The parameters for both figures are: $A_{xx} = A_{yy} = 1$, $\Omega_{xx} = 1$, $\Omega_{yy} = 3$, $\gamma_{xx} = \gamma_{yy} = 0.01$, $\varepsilon_2 = 4$, $k_0 = 0.5$. Note that the strong coupling regime is achieved at $\Delta z/\lambda_{xx} \approx 0.06$. The dip at $\Delta z/\lambda_{xx} \approx 0.15$ is due to the destructive interference between different modes of the structure. for c) the rotation angles were $\alpha = \beta = \pi/4, \gamma = 0$.

here $i, j = x, y, z$, $C^{(ij)}_{e_k e_l}$ are some real-valued constant pre-factors, $-4\pi k_0^2 \mathbf{d_i^*} \mathbf{G}(\mathbf{r_0}, \mathbf{r_0}, \omega_0)\mathbf{d_i} = \hbar \left[\Delta_{ii} - i\frac{\gamma_{ii}}{2}\right]$, and $\phi^{(ij)}_{e_1 e_2}$ are the phaseshifts. Note that both $C^{(ij)}_{e_k e_l}$ and $\phi^{(ij)}_{e_1 e_2}$ depend only upon the Euler angles and that for constant pre-factors it does not matter whether we study the population transfer from $|e_1\rangle$ to $|e_2\rangle$ or vice versa: $C^{(ij)}_{e_k e_l} = C^{(ij)}_{e_l e_k}$. However, this is not the case for the phase factors: $\phi^{(ij)}_{e_1 e_2} = -\phi^{(ij)}_{e_2 e_1}$, which leads to a phase delay in the oscillatory part of the dynamics, making the transfer non-reciprocal even though the time reversal symmetry is preserved (see Fig. 2, c)).

III. Conclusion

In this work we study the dynamics of a V-type quantum emitter with two excited states being initially excited. We show the possibility to achieve a strong coupling between the excited states via electromagnetic modes of a nanostructe, which in our case was an anisotropic metasurface. We also demonstrate that in the case, when quantization has an arbitrary orientation then it is possible to observe a non-reciprocity, which manifests itself in a phase delay in the oscillating part of the dynamics.

References

[1] G. S. Agarwal, "Anisotropic vacuum-induced interference in decay channels", Phys. Rev. Lett., vol. 84, p. 5500-5503, (Jun 2000).
[2] S. Hughes, and G. S. Agarwal, "Anisotropy-Induced Quantum Interference and Population Trapping between Orthogonal Quantum Dot Exciton States in Semiconductor Cavity Systems", Phys. Rev. Lett., vol. 118, p. 063601, (Feb. 2017).
[3] O. Y. Yermakov, and A. I. Ovcharenko, and M. Song, and A. A. Bogdanov, and I. V. Iorsh, and Yu. S. Kivshar, "Hybrid waves localized at hyperbolic metasurfaces", Phys. Rev. B, vol. 91, p. 235423, (Jun. 2015).
[4] C. Cohen-Tannoudji, and J. Dupont-Roc, and G. Grynberg, *Atom-Photon Interactions: Basic Processes and Applications*, Wiley-VCH Verlag GmbH & Co. KGaA, 2004.
[5] D. F. Kornovan, and M. I. Petrov, and I. V. Iorsh, "Transport and collective radiance in a basic quantum chiral optical model", Phys. Rev. B, vol. 96, p. 115162, (Sep. 2017).
[6] H. T. Dung, and L. Knöll, and D.-G. Welsch, "Resonant dipole-dipole interaction in the presence of dispersing and absorbing surroundings", Phys Rev A, vol. 66, p. 063810, (2002).
[7] A. Lakhtakia, "Green's functions and Brewster condition for a halfspace bounded by an anisotropic impedance plane", International Journal of Infrared and Millimeter Waves, vol. 13, p. 161-170, (Feb. 1992).

Journal of Physics: Conference Series

Temporal dynamics of a quantum emitter with multiple excited states in the vicinity of an anisotropic metasurface

METANANO 2018 IOP Publishing
IOP Conf. Series: Journal of Physics: Conf. Series **1092** (2018) 012063 doi:10.1088/1742-6596/1092/1/012063

Temporal dynamics of a quantum emitter with multiple excited states in the vicinity of an anisotropic metasurface

D. F. Kornovan[1], I. D. Toftul[1], A. V. Chebykin[1], M. I. Petrov[1,2], and I. V. Iorsh[1]

[1] ITMO University , Nanophotonics and Metamaterials Department, Birjevaja line V.O., 14, 199034, St. Petersburg, Russian Federation
[2] University of Eastern Finland, Yliopistokatu 7, FI-80101 Joensuu, Finland

E-mail: d.kornovan@metalab.ifmo.ru

Abstract. In this work we focus on studying the temporal dynamics of a quantum emitter with few (3) excited states, which allows to observe an interplay between different spontaneous emission channels. We show that if the quantization axis is being rotated with respect to the normal of a metasurface it is possible to observe a difference in the transfer dynamics from one state to another and vice versa.

1. Introduction

The topic of anisotropic vacuum has been attracting a lot of attention since the first time it was discussed in [1] by G. Agarwal. The author proposed an idea that one can exploit the interference between different emission channels of a quantum emitter due to the anisotropy of the surrounding. An interesting manifestation of this effect is that it is possible to suppress the total emission rate due to destructive interference between the decay channels, which was studied in [2]. In this paper we want to study further the topic of coupling the orthogonal transitions of a single quantum emitter through the field modes of a metasurface.

2. Theoretical Framework and results

In this work we investigate the time evolution of a four level inverse tripod-type atom with a single ground state $|g\rangle$ and three excited states $|e_{-1}\rangle$, $|e_0\rangle$, $|e_+\rangle$ with the corresponding transition dipole moments $\mathbf{d_{-1}}$, $\mathbf{d_0}$, and $\mathbf{d_{+1}}$ as shown in Fig. 1, (a). These three dipole moment vectors form an orthonormal set in $\mathbb{R}^3$, which leads to the fact that the three corresponding excited states are decoupled in the isotropic environment. However, they might interact with each other via the modes supported by a photonic or plasmonic structure. From this perspective a metasurface presents an interesting system to consider, since it can be anisotropic in the interface plane. The optical properties of it can be characterized by the tensor of the effective surface conductivity σ, which can be chosen to be diagonal in some coordinate system. To describe the optical properties of a metasurface we use the effective conductivity described by [3]:

METANANO 2018 IOP Publishing
IOP Conf. Series: Journal of Physics: Conf. Series **1092** (2018) 012063 doi:10.1088/1742-6596/1092/1/012063

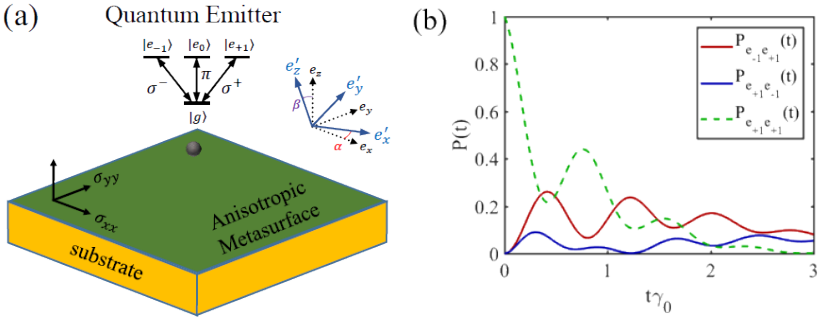

Figure 1. a) Schematic picture of the system: an atom with 3 excited states in the vicinity of an anisotropic metasurface. The dotted arrows represent the lab coordinate system, the blue solid arrows - the rotated on 2 Euler angles. b) Excitation transfer from e_1 to e_2 and vice versa along with the initially excited state population. The parameters are: $A_{xx} = A_{yy} = 1$, $\Omega_{xx} = 1$, $\Omega_{yy} = 3$, $\gamma_{xx} = \gamma_{yy} = 0.01$, $k_0 = 0.65\Omega_{xx}/c$, the rotation angles were $\alpha = \beta = \pi/4, \gamma = 0$. The substrate was considered as an infinite dielectric half-space with $\epsilon_2 = 4$. The atom-surface distance is $\Delta z = 0.05\, c/\Omega_{xx}$.

$$\sigma = \begin{pmatrix} \sigma_{xx} & 0 \\ 0 & \sigma_{yy} \end{pmatrix}, \quad \sigma_{jj} = A_{jj} \frac{ic}{4\pi} \frac{\omega}{\omega^2 - \Omega_{jj}^2 + i\gamma_{jj}\omega}, \tag{1}$$

where A_{jj} is the normalization constant, Ω_{jj} is the resonance frequency, γ_{jj} is the bandwidth of the corresponding resonance.

In order to solve for temporal dynamics of the emitter's states we employ the approach of the resolvent operator [4, 5], when it is possible to find the matrix elements of the evolution operator $\hat{U}(t, 0)$ using:

$$\langle e_f|\hat{U}(t,0)|e_i\rangle = \int_C \frac{dz}{2\pi i} e^{-izt/\hbar} \langle e_f|\hat{G}(z)|e_i\rangle, \tag{2}$$

where $\hat{G}(z) = (z - \hat{H})^{-1}$ is the resolvent operator of the full Hamiltonian $\hat{H}$. Using this relation we can find probabilities for the atom to be in the excited state $|e_f\rangle$ at time t given that it was in the state $|e_i\rangle$ initially by simply finding $P_{e_f}(t) = |U_{e_f e_i}(t, 0)|^2$.

We should note that here we work in the single excitation domain since we are studying the excited states evolution of a single atom. In this single excitation subspace of a Hilbert space the resolvent can be found to be:

$$\langle e_f|\hat{G}(z)|e_i\rangle = \langle e_f| \left[z - \hat{H}_0 - \hat{\Sigma}(z)\right]^{-1} |e_i\rangle \approx \left[(z - \hbar\omega_0)\, \delta_{e_f e_i} + 4\pi k_0^2 \mathbf{d}^*_{\mathbf{e_f}} \mathbf{G}(\mathbf{r_0}, \mathbf{r_0}, \omega_0) \mathbf{d}_{\mathbf{e_i}}\right]^{-1}, \tag{3}$$

here $\hat{H}_0$ is the unperturbed Hamiltonian and $\Sigma(z)$ is the level shift operator, δ_{ij} is the Kronecker delta. The level-shift operator in the latter expression is written within two approximations: near-resonant interaction of the states ($z = \hbar\omega_0$) and taking into account only proccesses of the second order [6], leading to a form of a classical dipole-dipole coupling constants: $\Sigma_{e_f e_i} = -4\pi k_0^2 \mathbf{d}^*_{\mathbf{e_f}} \mathbf{G}(\mathbf{r_0}, \mathbf{r_0}, \omega_0) \mathbf{d}_{\mathbf{e_i}}$. Therefore, in order to describe the interaction of the emitter with the electromagnetic modes of the field we only need to construct the Green's function of a metasurface, which can be done by following the procedure outlined in [7].

METANANO 2018 IOP Publishing
IOP Conf. Series: Journal of Physics: Conf. Series **1092** (2018) 012063 doi:10.1088/1742-6596/1092/1/012063

Now we want to rotate the transition dipole moments $\mathbf{d_q}$ with respect to the original coordinate system, in which σ tensor is diagonal. The rotation of dipole moments will alter the way excited states couple with each other, therefore, altering the time dynamics. Formally this can be done by first considering the level-shift operator matrix in the Cartesian coordinate system $\Sigma_{Cart}(\hbar\omega_0)$, which expresses the couplings of linear dipoles d_j, $j = x, y, z$. Then we can use the transformation matrix S, which transforms the Σ from the Cartesian coordinate system into the spherical tensor basis $\mathbf{d_q}$, $q = +1, 0, -1$. Finally, we can simply rotate the spherical tensors written in Cartesian coordinates with rotation matrix $M(\alpha, \beta, \gamma)$ (active representation, right-hand rule, $z'' - y' - z$ convention), where α, β, γ are the Euler angles:

$$\begin{aligned} \Sigma'_{Sph} &= T^{-1}(\alpha, \beta, \gamma)\Sigma_{Cart}T(\alpha, \beta, \gamma), \\ T(\alpha, \beta, \gamma) &= M(\alpha, \beta, \gamma)S. \end{aligned} \tag{4}$$

After performing this, we can express the evolution operator matrix elements (2) through the matrix elements of $T(\alpha, \beta, \gamma)$, and the diagonal entries of Σ_{Cart} as:

$$U_{kl}(t, 0) = \sum_{j=1}^{3} T^*_{j,k}T_{j,l}e^{-i\Sigma_{jj}t/\hbar} = \sum_{j=1}^{3} C_j^{(kl)}e^{-i\Sigma_{jj}t/\hbar}, \tag{5}$$

Note that for Σ_{Cart} index j labels the Cartesian coordinates as $1 - x, 2 - y, 3 - z$, and for the case of spherical basis - $1 - (-1), 2 - (0), 3 - (+1)$.

Let us focus on the case, when we study how excitation is transferred between the two excited states: $|\mathbf{e_{+1}}\rangle \to |\mathbf{e_{-1}}\rangle$ and the inverse process $|\mathbf{e_{-1}}\rangle \to |\mathbf{e_{+1}}\rangle$. For them we can write explicitly the corresponding coefficients before the exponents:

$$\begin{aligned} C_1^{(13)} &= -\frac{e^{2i\gamma}}{2}\left(cos(\alpha)cos(\beta) - isin(\alpha)\right)^2, \\ C_2^{(13)} &= \frac{e^{2i\gamma}}{2}\left(cos(\alpha) - icos(\beta)sin(\alpha)\right)^2, \\ C_3^{(13)} &= -\frac{e^{2i\gamma}}{2}sin^2(\beta), \end{aligned} \tag{6}$$

and for the inverse process we have $C_j^{(31)} = (C_j^{(13)})^*$. One can notice from (6) that the Euler angle γ enters as an overall phase factor, therefore, the probabilities given by $|U_{kl}(t, 0)|^2$ are independent of it. This is natural since γ represents the rotation around the new quantization axis $\mathbf{e'_z}$ and such a rotation should not change the behavior of the system. It is also important to note that in a general situation, for arbitrary α and β, the coefficients $C_k^{(ij)}$ are complex. It means that when finding the probabilities $|U_{kl}(t, 0)|^2$, the $e^{-i\Sigma_{jj}t/\hbar}$ terms will interfere in such a way that the oscillating parts of the dynamics for $|e_{+1}\rangle \to |e_{-1}\rangle$ and $|e_{-1}\rangle \to |e_{+1}\rangle$ will have different initial phases as can be seen in Fig. 1, (b). Indeed,

$$P_{e_{-1}e_{+1}}(t) = \sum_j \xi^{(jj)}_{e_{-1}e_{+1}}e^{-\gamma_{jj}t} + \sum_{i<j} 2\xi^{(ij)}_{e_{-1}e_{+1}}cos\left(\left[\Delta_{ii} - \Delta_{jj}\right]t - \phi^{(ij)}_{e_{-1}e_{+1}}\right)e^{-(\gamma_{ii}+\gamma_{jj})t/2}, \tag{7}$$

where $\Delta_{ii} = \mathrm{Re}[\Sigma_{ii}]$, $\gamma_{ii} = -2\mathrm{Im}[\Sigma_{ii}]$, $\xi^{(ij)}_{e_{-1}e_{+1}}$ are some real-valued constants, $\phi^{(ij)}_{e_{-1}e_{+1}}$ are the initial phases of oscillations. Notice that both $\xi^{(ij)}_{e_{-1}e_{+1}}$ and $\phi^{(ij)}_{e_{-1}e_{+1}}$ depend only upon the Euler

angles and have the following properties: $\xi^{(ij)}_{e_{-1}e_{+1}} = \xi^{(ij)}_{e_{+1}e_{-1}}$, but $\phi^{(ij)}_{e_{-1}e_{+1}} = -\phi^{(ij)}_{e_{+1}e_{-1}}$. The latter leads to a *phaseshift* in the oscillatory dynamics for the probabilities of the two processes under study. Also notice from (7) that in order to observe this effect the anisotropy of the structure is needed as if $\Delta_{ii} = \Delta_{jj}$, then the contributions from the phaseshifts can be simply absorbed in the definition of the constant $\xi^{(ij)}_{e_1e_3}$ and there will be no difference in the dynamics.

3. Conclusion

In our work we studied the dynamical behavior of an inverse-tripod type quantum emitter with three excited states interacting though the modes of an anisotropic metasurface. We demonstrated that if the quantization axis has an arbitrary orientation then it is possible to observe a non-reciprocity, which manifests itself in a phase delay in the oscillating part of the dynamics arising from the anisotropic properties of the structure.

4. Acknoledgements

This work was supported by the Russian Foundation for Basic Research (proj. # 18-32-00691). D. K. and M.P. acknowledge the support from Basis Foundation.

References

[1] Agarwal G S, 2000 Anisotropic vacuum-induced interference in decay channels, *Phys. Rev.* Lett., vol. **84**, p. 5500-5503.
[2] Hughes S and Agarwal G S 2017 Anisotropy-Induced Quantum Interference and Population Trapping between Orthogonal Quantum Dot Exciton States in Semiconductor Cavity Systems *Phys. Rev.* Lett., vol. **118**, p. 063601.
[3] Yermakov O Y, Ovcharenko A I, Song M, Bogdanov A A, Iorsh I V and Kivshar Yu S 2015 Hybrid waves localized at hyperbolic metasurfaces *Phys. Rev.* B, vol. **91**, p. 235423.
[4] Cohen-Tannoudji C, Dupont-Roc J and Grynberg G 2004 *Atom-Photon Interactions: Basic Processes and Applications*, Wiley-VCH Verlag GmbH & Co. KGaA.
[5] Kornovan D F, Petrov M I and Iorsh I V, 2017 Transport and collective radiance in a basic quantum chiral optical model, *Phys. Rev.* B, vol. **96**, p. 115162.
[6] Dung H T, Knöll L and Welsch D-G 2002 Resonant dipole-dipole interaction in the presence of dispersing and absorbing surroundings, *Phys. Rev.* A, vol. **66**, p. 063810.
[7] Lakhtakia A, 1992 Green's functions and Brewster condition for a halfspace bounded by an anisotropic impedance plane, *International Journal of Infrared and Millimeter Waves*, vol. **13**, p. 161-170.

PHYSICAL REVIEW B **96**, 115162 (2017)

Transport and collective radiance in a basic quantum chiral optical model

D. F. Kornovan,[1,*] M. I. Petrov,[1,2] and I. V. Iorsh[1]
[1]*ITMO University, Birzhevaya liniya 14, 199034 St.-Petersburg, Russia*
[2]*University of Eastern Finland, Yliopistokatu 7, FI-80101 Joensuu, Finland*
(Received 7 February 2017; revised manuscript received 2 September 2017; published 29 September 2017)

In our work, we theoretically study the dynamics of a single excitation in a one-dimensional array of two-level systems, which are chirally coupled through a single mode waveguide. The chirality is achieved owing to a strong optical spin-locking effect, which in an ideal case gives perfect unidirectional excitation transport. We obtain a simple analytical solution for a single excitation dynamics in the Markovian limit, which directly shows the tolerance of the system with respect to the fluctuations of emitters position. We also show that the Dicke state, which is well known to be superradiant, has twice lower emission rate in the case of unidirectional quantum interaction. Our model is supported and verified with the numerical computations of quantum emitters coupled via surface plasmon modes in a metallic nanowire. The obtained results are based on a very general model and can be applied to any chirally coupled system that gives a new outlook on quantum transport in chiral nanophotonics.

DOI: 10.1103/PhysRevB.96.115162

I. INTRODUCTION

The recently emerged field of *chiral quantum optics* [1] promises new prospectives for manipulation and control of quantum states of matter. The chiral coupling of quantum sources with photonic excitations can be implemented, for example, through the interaction with topological edge states [2,3]. However, one of the most simple routes for chiral coupling is employment of transverse spin angular momentum of light (SAM), which has recently attracted significant research interest [4,5]. In the simplest setup of an electromagnetic surface or a waveguide mode, the nonzero optical SAM density emerges due to the $\pi/2$ phase shift between the electric field projections onto the interface plane and to its normal [4]. An important feature of the electromagnetic waves carrying transverse SAM is the spin-momentum locking: the spin projection is defined by the propagation direction of the wave [6,7]. This effect, which can be regarded as spin-orbit coupling, has been studied both theoretically and experimentally in many applications related to nano-optomechanics [8–10], topological photonics with surface waves [11], electromagnetic routing [12], and electromagnetically assisted unidirectional spin transfer [13] and others. Moreover, the spin-orbit coupling in quasi-one-dimensional photonic structures can be used to engineer a new class of quantum information networks [14–16]. The basic model under consideration is a one-dimensional array of two-level systems (TLS) coupled to a quasi-one-dimensional photonic nanostructure (see Fig. 1). The current technology allows for measuring light scattering on such one-dimensional TLS arrays consisting of thousands of cooled atoms trapped near an optical nanofiber [17]. Moreover, in Refs. [18,19] it was shown that the chiral coupling of an atom with nanofiber mode leads to strong modification of Bragg reflection spectrum as well as the modification of the collective emission of two atoms near the nanofiber was demostrated theoretically [20].

In this prospective the inherent spin-orbit coupling of light in conjunction with the chiral light-matter coupling (which can be achieved to be, e.g., transverse magnetic field) can allow deterministic transfer of the initial quantum state of the TLS unidirectionally along the channel. Such an approach allows for the engineering of the large scale cascaded quantum networks [21], which are immensely in demand in quantum information processing. Despite the importance of this field, the dynamical picture of the excitation transport in a unidirectionally coupled system has not been studied before.

In this work we focus on the spatiotemporal dynamics of the excited state in such a chiral chain. We adopt the formalism of the Green's function which was proven to be a powerful tool for the studies of quantum dynamics in open systems [22]. We reveal that under certain approximation the problem of finding the excited states probability amplitude dynamics allows an elegant yet simple analytical solution which agrees well with the rigorous numerical calculations.

II. SINGLE MODE COUPLING

We begin by considering an ensemble consisting of N two-level systems (TLS) forming a one-dimensional linear chain placed parallel to a surface of a photonic/plasmonic nanostructure supporting a single fundamental guided mode. Assuming that coupling is mediated by the guided mode only in the strong spin-locking regime, we formulate the equations descibing the dynamics of the system [23]:

$$\dot{C}_n(t) = -i\Omega C_n(t) + \sum_{m=1}^{n-1} G_{nm} C_n(t), \tag{1}$$

where $C_n(t)$ is the complex probability amplitude of the n-th TLS to be excited at time t, the diagonal parameter $\Omega = \Delta_L + i\gamma_{\text{tot}}/2$ contains Δ_L which is the Lamb shift and γ_{tot} which is the total spontaneous emission rate consisting of two contributions: emission into radiation and guided modes ($\gamma_{\text{tot}} = \gamma_r + \gamma_g$). The single mode coupling coefficients G_{nm} between the TLSs with numbers m and n can be written as $G_{nm} = -\frac{\gamma_g}{2} e^{i\phi_{nm}}$, where $\gamma_g/2$ is the coupling strength, $\phi_{nm} = k^g(z_n - z_m)$ is the phase acquired by the photon due to the propagation from emitter m to emitter n, and k^g is the corresponding propagation constant of the guided mode. We assume strong spin-locking regime, which leads to a unidirectional coupling, i.e., $G_{nm} \neq 0$ only for $n > m$. The

*newparadigm.dk@gmail.com

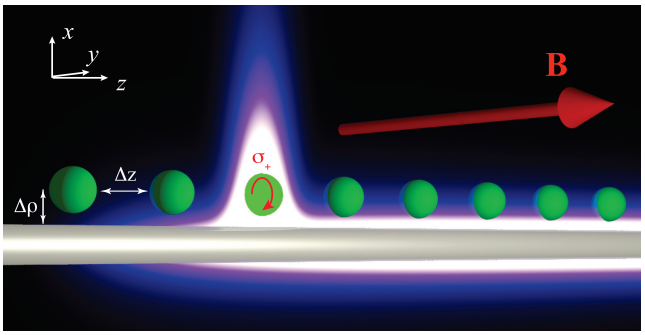

FIG. 1. Schematic image of the periodic chain of two level systems on top of a waveguide. Initially, only one two level system is excited. The excitation can be transferred either by symmetric short range dipole-dipole or radiative coupling, or by asymmetric long-range coupling via the waveguide mode. The transverse magnetic field **B** breaks the symmetry of coupling of the two-level system to left- and right-propagating waveguide mode.

system of equations (1) can be formulated in the matrix form $\dot{\mathbf{C}}(t) = \hat{\mathbf{M}}\mathbf{C}(t)$, with $\hat{\mathbf{M}}$ being a lower triangular matrix, which means that the problem is already diagonalized and, moreover, it is degenerate. All quantum oscillators have equal transition frequencies and lifetimes and, therefore, the system has only one eigenstate in which the last atom is excited. For this state the corresponding eigenfrequency is complex and a single excitation is not transferred between the atoms; it can only decay to the field modes due to the spontaneous emission process, which is significantly different from the case of symmetric coupling [24,25].

We focus on the problem of the excitation transport through the TLS chain, and for that we consider the initial condition in which the first atom is excited, while all the rest are in the ground state: $C_1(0) = 1$, $C_n(0) = 0, n \geqslant 2$. Exploiting the triangular form of the matrix $\hat{\mathbf{M}}$ and the given form of the initial condition, one can build an exact solution of the problem, which in its compact form can be written as (see Appendix A for the details)

$$C_n^1(t) = e^{-i\Omega t + i\phi_{n1}} L_{n-1}^{(-1)}(\gamma_g t/2), \tag{2}$$

where $C_n^1(t)$ is the probability amplitude of the n-th emitter to be excited at time t and superscript 1 means that this solution holds only for the case when the first emitter is excited initially; $L_n^{(\alpha)}(x)$ are the generalized Laguerre polynomials of degree n,α. This simple solution gives all the insights on the one-directional transport in quantum chains, which we would like to briefly discuss here. First, as expected, in the case of lossless guided mode the excitation dynamics is *irrelevant* of the spatial distribution of the emitters along the z coordinate as $|e^{i\phi_{mn}}| = 1$. This makes this system tolerant with respect to positional fluctuations, which is a consequence of the perfect one-way transport: the phase of the excitation transported between two emitters, the 1st and n-th always sums up giving the total phase $k^g(z_n - z_1)$. However, this irrelevance of the distribution of the quantum emitters on the final result is also due to the enforced initial condition that only a single (the first) emitter is excited. If we impose a very general initial condition $\mathbf{C}(t = 0) = (c_1; c_2; c_3; \ldots; c_N)$,

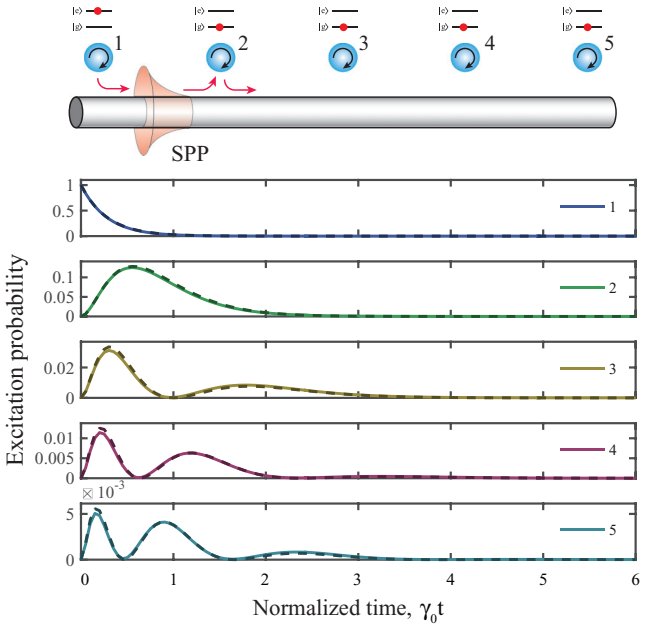

FIG. 2. Probabilities for different emitters to be excited at particular time moments $P_n(t)$ for a chain of $N = 5$ emitters; time is measured in the units of $\gamma_0 t$, where γ_0 is the free-space spontaneous emission rate for a single emitter. The solid and dashed lines are for the numerical and analytical results, correspondingly. For the numerical case the probabilities were averaged over 20 distributions of emitters around their regular positions and the distribution is uniform. The regular separation $\Delta z = 2.0\lambda_0$, where λ_0 is the resonant wavelength of the transition, and the maximal deviation from regular positions $a = \lambda_{\mathrm{SPP}}/2$. The parameters for the numerical case: nanowire radius is $\rho_c = 0.05\lambda_0$, $\varepsilon \approx -16.00 + 0.44i$, and $\Delta\rho = \rho_c$.

which corresponds to the case when a single excitation is distributed among different atoms meaning that $\sum_{i=1}^{N} |c_i|^2 = 1$, the answer will depend on the atomic positions. Secondly, the time evolution of the n-th atom excitation probability $P_n^1(t) = |C_n^1(t)|^2$ has trivial exponentially decaying factor $e^{-\gamma_{\mathrm{tot}} t}$, where $\gamma_{\mathrm{tot}} = \mathrm{Im}\,\Omega$, and the stationary solution in such system is zero. Finally, the nontrivial temporal dynamics of the n-th emiter's excitation depends on the amplitude of the coupling constant γ_g through the corresponding Laguerre polynomial. According to Laguerre's polynomial properties [26] the number of local excitation maxima for a particular emitter n equals the number of emitters positioned before it. This dynamics is shown in Fig. 2 (solid lines) for a chain consisting of $N = 5$ emitters.

III. METALLIC NANOWIRE

The analytical model we have proposed is based on the interaction of TLSs via arbitrary guided mode. To support these results we consider the interaction of dipole emitters through the plasmonic modes of a nanowire. We adopt the exact solution of this problem in terms of the Green's function approach. We are interested in the probabilities of excitation being transferred from the first emitter of a chain to the n-th $P_{n1} = |\langle e_n|\hat{U}(t,0)|e_1\rangle|^2$ as before. Here $\hat{U}(t,0)$ is the evolution operator for our system and $|e_n\rangle$ are the

states, where only the n-th emitter is excited initially, while all the rest are in the ground state. We can rewrite the matrix elements of the evolution operator according to [27]:

$$\langle e_n|\hat{U}(t,0)|e_1\rangle = \int_C \frac{dp}{2\pi i} e^{-ipt/\hbar}\langle e_n|\hat{G}(p)|e_1\rangle, \quad (3)$$

where $\hat{G}(p) = (p - \hat{H})^{-1}$ is the resolvent operator of the Hamiltonian $\hat{H}$ and the contour C here is traversed in the counterclockwise direction and encloses all complex poles of the resolvent (since we consider a subspace containing only discrete states). The total Hamiltonian $\hat{H}$ can be expanded in a sum of unperturbed part $\hat{H}_0$ and the interaction term $\hat{V}$ such that $\hat{H} = \hat{H}_0 + \hat{V}$:

$$\hat{H}_0 = \sum_n \hbar\omega_0 \hat{\sigma}_n^+ \hat{\sigma}_n^- + \int d\mathbf{r} \int_0^\infty d\omega\, \hbar\omega \hat{\mathbf{f}}^\dagger(\mathbf{r},\omega)\hat{\mathbf{f}}(\mathbf{r},\omega), \quad (4)$$

$$\hat{V} = -\sum_n \hat{\mathbf{d}}_n \hat{\mathrm{E}}(\mathbf{r}_n), \quad (5)$$

where ω_0 is the atomic transition frequency and $\hat{\sigma}_n^+ = |e_n\rangle\langle g_n|$ and $\hat{\sigma}_n^- = |g_n\rangle\langle e_n|$ are raising and lowering atomic operators. Here the interaction part of the Hamiltonian $\hat{V}$ is considered in the dipole approximation, where $\hat{\mathbf{E}}(\mathbf{r}_n) = \hat{\mathbf{E}}^+(\mathbf{r}_n) + \hat{\mathbf{E}}^-(\mathbf{r}_n)$ is the total electric field and $\hat{\mathbf{d}}_n$ is the transition dipole moment operator of the n-th atom. We employ the Green's function approach proposed in Ref. [28] in order to quantize the radiation field in the case of absorptive and dispersive media. The electromagnetic field operator in this case reads as $\hat{\mathbf{E}}^+(\mathbf{r}) = i\sqrt{4\hbar}\int d\mathbf{r}' \int_0^\infty d\omega' \frac{\omega'^2}{c^2}\sqrt{\mathrm{Im}(\varepsilon(\mathbf{r}',\omega'))}\mathbf{G}(\mathbf{r},\mathbf{r}',\omega')\hat{\mathbf{f}}(\mathbf{r}',\omega')$, where the bosonic field operators obey the commutation relation $[\hat{f}_i(\mathbf{r}',\omega'), \hat{f}_k^\dagger(\mathbf{r},\omega)] = \delta_{ik}\delta(\mathbf{r}' - \mathbf{r})\delta(\omega' - \omega)$; $\mathbf{G}(\mathbf{r},\mathbf{r}',\omega')$ is the classical electromagnetic Green's function. The local field operators define the photon energy part in the unperturbed Hamiltonian in Eq. (4).

We then find the projections of the resolvent operator on states with a single atomic excitation which are given by [27]

$$\hat{P}\hat{G}(p)\hat{P} = \hat{P}\frac{1}{p - \hat{H}_0 - \hat{\Sigma}(p)}\hat{P}, \quad (6)$$

$$\hat{\Sigma}(p) = \hat{V} + \hat{V}\hat{G}(p)\hat{V} \approx \hat{V} + \hat{V}\hat{G}_0(p = \hbar\omega_0)\hat{V}, \quad (7)$$

where $\hat{P} = \sum_{j=1}^N |e_j\rangle\langle e_j|$ is the projection operator onto the corresponding subspace and $\hat{\Sigma}(p)$ is the level-shift operator [27], also known as self-energy part, which provides us with the correction to the unperturbed Hamiltonian $\hat{H}_0$ due to the interaction between the quantum emitters.

By inverting the operator standing in the denominator of Eq. (6) one can obtain the projection of the resolvent operator and, consequently, build the dynamics of the system according to Eq. (3). We impose two approximations in Eq. (7): (i) we limit ourselves in the calculation of the self-energy only up to the second order in $\hat{V}$; (ii) we consider a near-resonant interaction between TLS computing $\hat{G}$ at the resonant frequency $p = \hbar\omega_0$. Within these approximations the matrix elements $\langle e_k|\hat{\Sigma}(p)|e_l\rangle = \Sigma_{kl}(p)$ show the coupling strength of two emitters with numbers k and l. It is defined by the electromagnetic Green's function of the system [29] and reads as $\Sigma_{kl}(\omega_0) = -4\pi k_0^2 \mathbf{d}_k^* \mathbf{G}(\mathbf{r}_k,\mathbf{r}_l,\omega_0)\mathbf{d}_l$, where $k_0 = \omega_0/c$ and $\mathbf{d}_k$ is the transition dipole moment. By taking the exact

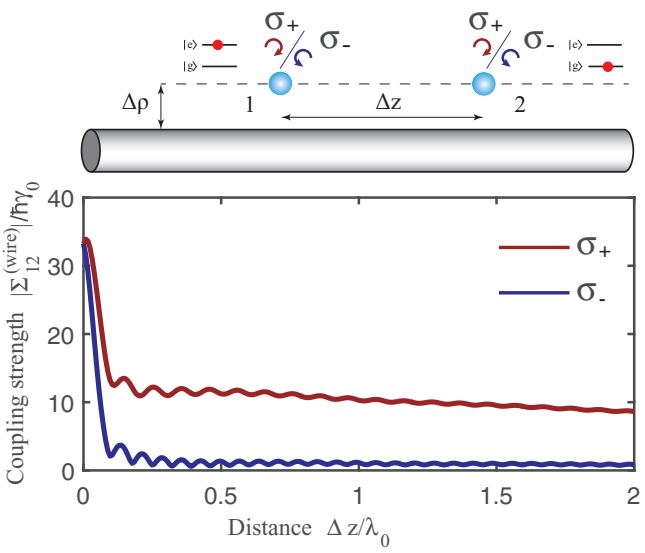

FIG. 3. Absolute values of the coupling strength $\Sigma_{kl}^{(\mathrm{wire})}(\hbar\omega_0)$ through the nanowire modes for two atoms spaced by Δz and placed at a distance $\Delta\rho$ from the surface of the metallic nanowire measured in $\hbar\gamma_0$. The quantization axis is chosen to be $\mathbf{e}_y$, therefore, $\mathbf{e}_{\sigma_+} = -(i\mathbf{e}_x + \mathbf{e}_z)/\sqrt{2}$, $\mathbf{e}_{\sigma_-} = -\mathbf{e}_{\sigma_+}^*$. The parameters ρ_c, $\Delta\rho$, and ε are the same as for Fig. 2.

Green's function of a metallic nanowire (see Appendix B), we have studied the interaction strength between two emitters mediated by the propagating surface plasmon-polariton modes (SPP). One can expand the Green's function $\mathbf{G} = \mathbf{G_0} + \mathbf{G_s}$ into a sum of vacuum part $\mathbf{G_0}$ and scattered part $\mathbf{G_s}$, which includes the interaction through the structure. This allows for introducing the parameter of coupling strength through the nanowire $\Sigma_{kl}^{(\mathrm{wire})}(\omega_0) = -4\pi k_0^2 \mathbf{d}_k^* \mathbf{G_s}(\mathbf{r}_k,\mathbf{r}_l,\omega_0)\mathbf{d}_l$. By introducing an external magnetic field along y axis one can achieve efficient coupling of the emitters with circular transitions only with dipole moment $\mathbf{d}_{\sigma_+} = -d_0(i\mathbf{e}_x + \mathbf{e}_z)/\sqrt{2}$ or $\mathbf{d}_{\sigma_-} = d_0(-i\mathbf{e}_x + \mathbf{e}_z)/\sqrt{2}$. Due to the spin-locking two σ_+ atoms are coupled well through the SPP mode for positive distance between them Δz, while two σ_- atoms have much weaker coupling Fig. 3. For negative values of Δz the picture will be opposite. The considered nanowire has $\varepsilon(\omega_0) \approx -16 + 0.44i$, which corresponds to the silver permittivity at $\lambda_0 = 2\pi\frac{c}{\omega_0} = 600$ nm [30], the nanowire radius $\rho_c = 0.05\lambda_0 \approx 30$ nm, and the distance from the fiber surface is $\Delta\rho = \rho_c$. As the distance between the TLS increases, the interaction through the guided mode of the wire plays the dominant role. Any visible oscillations occur due to the interference between the fundamental guided mode and higher-order radiation modes. As can be seen clearly in Fig. 3, for such a thin fiber, supporting only one fundamental guided mode with radial eigenvalue $n = 0$, the interaction strength is very different for the transition dipole moments rotating in the opposite directions (σ_+ and σ_-). The perfect spin-orbit coupling requires exact circular polarization of the SPP mode, which can be achieved at the resonance [31], when $\mathrm{Re}(\varepsilon) = -1$ and the z component of the wave vector goes to infinity. Though the TLS transition frequency is far from the SPP

resonance, the asymmetry of the coupling strength is of the order of 10 as shown in Fig. 3. Thus the interaction is not perfectly unidirectional and there is a finite probability for the excitation to propagate backwards. The property of a complete independence of the dynamics upon the distribution of emitters along z does not hold in this case. But due to the strong asymmetry, it can be still quite robust to positional disorder. In order to take it into account for the numerical calculation we perform averaging over 20 distributions of emitters along z near their regular positions (regular separation between the neighboring emitters Δz). The distribution is taken to be uniform and the maximal deviation from the regular positions into a given direction is $\lambda_p/2$ (λ_p is the plasmon wavelength), allowing for a full phase randomization due to the plasmon propagation between emitters. This allows us to apply the unidirectional model and compare this to the solution of the numerical one; the latter is shown in Fig. 2 (solid lines). We get almost perfect correspondence between our simplified model (dashed line) and the obtained numerical solution (solid line), which confirms that all the unique properties of the unidirectional transport formulated before can be observed in realistic structures.

We also plot the excitation probability versus both time t and emitter number N. One can observe that there are excitation waves propagating in the chain, which can be indicated by tracking the positions of zeros in dynamics; the fronts of these waves can be described with the help of an asymptotic relation connecting the Laguerre polynomials and the Bessel functions for large n and fixed time t: $L_N^{(\alpha)}(\gamma_g t/2) \approx N^{\alpha/2} e^{\frac{\gamma_g t}{4}} \frac{J_\alpha(2\sqrt{N\gamma_g t/2})}{(\gamma_g t/2)^{\alpha/2}}$, and zeros of this function were plotted for the case of continuous N in Fig. 4 with blue lines. Defining the argument of the Bessel function as a phase of the probability oscillation, one can think of negative phase velocity as for a larger emitter number N zeros appear at earlier time moments.

IV. COLLECTIVE EMISSION

In the previous chapters we have considered the redistribution of a single excitation initially localized at the first atom in the chain. However, the physical mechanisms lying beyond the emission of specially prepared states attracts much interest. One of the common cases is the Dicke state having superradiant property. The collective emission of excitation in the case of unidirectional coupling can significantly differ from symmetrical coupling.

For such a collective state in the absence of retardation the dynamics can be found as

$$C(t) = \mathbf{C}_{\text{final}}{}^{\dagger}\mathbf{U}(\mathbf{t})\mathbf{C}_{\text{init}}, \tag{8}$$

with $U_{k,l}(t) = e^{-i\Omega t} L_{k-l}^{(-1)}(\gamma_g t/2) e^{i\phi_{k,l}}$ being a lower triangular matrix, this matrix represents probability amplitudes for kth atom to be excited at time t, while initially at $t = 0$ only the lth atom was excited, and it has a form similar to (2); $\mathbf{C}_{\text{init}}$ and $\mathbf{C}_{\text{final}}$ are the column vectors for the final and initial states of the system, correspondingly. Since we are interested in the decay of a particular initial state we set $C_{\text{final},l} = C_{\text{init},l} = \frac{e^{i\psi_l}}{\sqrt{N}}$. We proceed by considering that atoms in our chain are spaced regularly $\phi_{k,l} = (k-l)\phi$ and that $\psi_l = (l-1)\psi$. Here both ϕ and ψ are purely real and denote the phase acquired by the SPP mode propagating between the neighboring atoms and the phase difference in probability amplitudes between them in the initial state. In this case it can be found that $C(t) = \frac{e^{-i\Omega t}}{N} \sum_{k=1}^{N} (N-(k-1)) e^{i(k-1)\xi} L_{k-1}^{(-1)}(\gamma_g t/2)$ with $\xi = \phi - \psi$ (a more general solution one can find in Appendix C). Next, we consider sufficiently small times and expand $C(t)$ to the

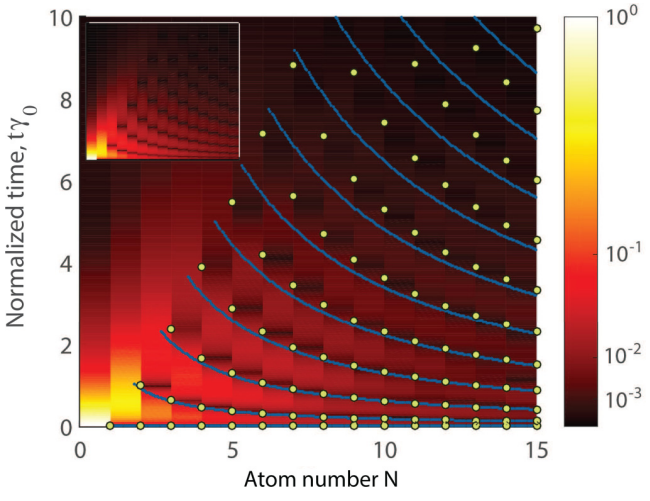

FIG. 4. Distribution of excitation between different emitter n in a chain of total $N = 15$ emitters. In a computational model parameters Δz, $\Delta\rho$, ρ_c, and ε are the same as for Fig. 2. Yellow circles correspond to exact positions of zeros in dynamics for each emitter for the case of a perfect unidirectionality, while the dark blue lines are zeros of $J_1(2\sqrt{N\gamma_g t/2})$. The inset figure shows analytical results calculated with Eq. (2).

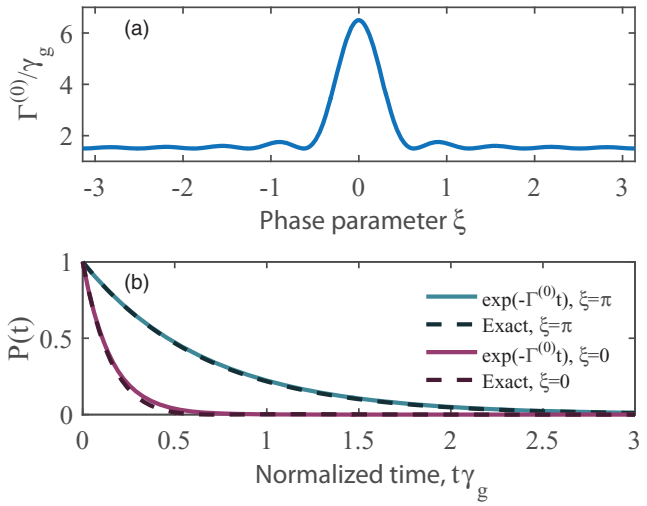

FIG. 5. (a) Dependence of the initial spontaneous emission rate $\Gamma^{(0)}$ on phase difference parameter ξ for a chain of $N = 10$ atoms, when $\gamma_g = \gamma_r$. (b) Dynamics for the case of out of phase (blue) and in phase (purple) neighboring emitters. Solid lines represent the exact solution and dashed exponential with $\Gamma^{(0)}$ given by (9). The parameters are the same as for (a).

first order in t finally obtaining

$$C(t \to 0) \sim 1 - \left[i\Omega + \frac{\gamma_g}{2} \frac{e^{i\xi}(N + e^{iN\xi} - Ne^{i\xi} - 1)}{N(e^{i\xi} - 1)^2} \right] t \sim 1 - \frac{\Gamma^{(0)}}{2} t, \tag{9}$$

where $\Gamma^{(0)}$ is the initial spontaneous emission rate being a real part of the expression in square brackets. Its dependence upon ξ is illustrated in Fig. 5(a).

It is reasonable to proceed by considering the two cases corresponding to the situations when the neighboring atoms are emitting photons in and out of phase:

$$\frac{\Gamma^{(0)}}{2} = \begin{cases} -i\Omega - \frac{\gamma_g}{2} \frac{(N-1)}{2}, & \text{if } \xi = 2\pi m, \\ -i\Omega + \frac{\gamma_g}{2} \frac{(2N-1+e^{iN\pi})}{4N}, & \text{if } \xi = \pi(2m+1). \end{cases} \tag{10}$$

Notice that for even N in the second case the coefficient $\Gamma^{(0)}$ reaches its absolute minimum. In the limit of strong coupling with the guided mode $\gamma_g \gg \gamma_r$ and large emitter number $N \gg 1$ for the $\xi = 2\pi m$ case $\Gamma^{(0)} = N\gamma_g/2$ unlike the $N\gamma_g$ factor known for the emission of the symmetric Dicke superradiant state [32]. For the out-of-phase case when $\xi = 2\pi(m+1)$ the initial decay rate is $\Gamma^{(0)} = \gamma_g/2$. The dynamics for both situations are illustrated in Fig. 5(b).

V. CONCLUSION

Concluding, we have proposed a simple analytical model of the unidirectional quantum transport mediated by spin-locked coupling to an arbitrary waveguide mode. We have obtained the exact analytical solution, showing that the dynamics of the TLS is described by the Laguerre polynomials. The behavior of the chiral TLS system is fully defined by the amplitude of the coupling coefficient of a single emitter with the waveguide mode. From the obtained solution it immediately follows that the unidirectional system possesses the tolerance with respect to the positional disorder. Our model also predicts that, for systems with perfectly asymmetric coupling, the symmetric Dicke superradiant state in a special case of phase-matched positions of the emitters has the emission rate equal to $N\gamma_g/2$, contrary to a value $N\gamma_g$ typical for systems with symmetrical interaction. In order to verify our model of the excitation quantum transport, we have performed the simulation through SPP mode of a metallic nanowire, constructing the evolution operator, based on the exact electromagnetic Green's function of the system. The simulations have shown a good agreement with the proposed analytical model, which allows its application for describing any chiral quantum system unidirectionally coupled to a waveguide mode.

ACKNOWLEDGMENTS

We are grateful to Mikhail Glazov, Andrey Bogdanov, and Yuri Kivshar for helpful discussions. The work was supported by the Russian Foundation for Basic Research (Projects No. 16-32-60167, No. 16-32-60123, and No. 17-02-01234), Russian Ministry of Education and Science (Projects No. 3.1365.2017/4.6 and No. 3.8884.2017/8.9), and Mega-Grant No. 14.Y26.31.0015. M.I.P. also acknowledges the support from BASIS foundation.

APPENDIX A: SOLUTION FOR THE UNIDIRECTIONAL TRANSPORT PROBLEM

In order to study the transfer of an excitation in a chain of coupled two-level systems we can formulate our problem (1) in the main text in the matrix form $\dot{\mathbf{C}}(t) = \hat{\mathbf{M}}\mathbf{C}(t)$, where $\hat{\mathbf{M}}$ is given by

$$\hat{\mathbf{M}} = \begin{pmatrix} -i\Omega & 0 & \cdots & 0 \\ ge^{i\phi_{21}} & -i\Omega & \cdots & 0 \\ \cdots & \cdots & \cdots & \cdots \\ ge^{i\phi_{N1}} & ge^{i\phi_{N2}} & \cdots & -i\Omega \end{pmatrix}. \tag{A1}$$

One of the possible ways to solve this system of equations is to find the matrix exponent of $\hat{\mathbf{M}}$ using the Jordan decomposition. Our problem, as can be seen from (A1), is diagonalized and degenerate, meaning that it has only one eigenvector, which is due to all diagonal elements being the same. Since our matrix has N dimensions and only a single eigenvalue $-i\Omega$ of the N-th order, the solution is of the form

$$\mathbf{C}(t) = e^{-i\Omega t}(\mathbf{C_0} + \mathbf{C_1}t + \mathbf{C_2}t^2 + \cdots + \mathbf{C_{N-1}}t^{N-1}) = e^{-i\Omega t} \sum_{j=0}^{N-1} \mathbf{C_j} t^j, \tag{A2}$$

where C_j are the column vectors. Substituting it in the equation we can find that

$$(\hat{\mathbf{M}} - \hat{\mathbf{I}}(-i\Omega))\mathbf{C_j} = (j+1)\mathbf{C_{j+1}}, \mathbf{C_j} = \frac{(\hat{\mathbf{M}} - \hat{\mathbf{I}}(-i\Omega))^j}{j!}\mathbf{C_0},$$

$$\mathbf{C}(t) = e^{-i\Omega t} \sum_{j=0}^{N-1} \frac{1}{j!} (\hat{\mathbf{M}} + i\Omega\hat{\mathbf{I}})^j t^j \mathbf{C_0}. \tag{A3}$$

Here $\hat{\mathbf{I}}$ is the identity matrix; $\mathbf{C_0}$ is the vector of the initial condition. Since our two-level system is one-way coupled, the addition of TLSs to the system does not affect the dynamics of all the previous oscillators in the chain, and we can set $N \to \infty$ and obtain a formal solution $\mathbf{C}(t) = e^{-i\Omega t} e^{(\hat{\mathbf{M}} + i\Omega\hat{\mathbf{I}})t} \mathbf{C_0}$. We need then to find the exponent of the following matrix:

$$\hat{\mathbf{B}} = \hat{\mathbf{M}} + i\Omega\hat{\mathbf{I}} = \begin{pmatrix} 0 & 0 & 0 & \cdots & 0 \\ gte^{i\phi_{2,1}} & 0 & 0 & \cdots & 0 \\ gte^{i\phi_{3,1}} & gte^{i\phi_{3,2}} & 0 & \cdots & 0 \\ \cdots & \cdots & \cdots & \cdots & \cdots \\ gte^{i\phi_{N,1}} & gte^{i\phi_{N,2}} & gte^{i\phi_{N,3}} & \cdots & 0 \end{pmatrix}. \tag{A4}$$

This matrix has only one eigenvalue $\lambda = 0$ and the Jordan normal form of this matrix is equal to

$$\hat{\mathbf{J}}_{\hat{\mathbf{M}}} = \begin{pmatrix} 0 & 1 & 0 & \cdots & 0 \\ 0 & 0 & 1 & \cdots & 0 \\ 0 & 0 & 0 & \cdots & 0 \\ \cdots & \cdots & \cdots & \cdots & \cdots \\ 0 & 0 & 0 & \cdots & 0 \end{pmatrix}. \tag{A5}$$

As can be seen from the form of matrix $\hat{\mathbf{J}}_{\hat{\mathbf{M}}}$, we need to construct the full Jordan basis as soon as there is only one eigenvector for this matrix: $\mathbf{v_1} = (0,0,\ldots,1)$. The rest of the vectors needed to construct the full Jordan basis

can be found by consistently solving $\hat{\mathbf{B}}\mathbf{f_j} = \mathbf{f_{j-1}}$, where $\mathbf{f_j}$ are the generalized eigenvectors and $\mathbf{f_0} = \mathbf{v_1}$ is a regular eigenvector. Solving for this, we can find transformation matrix $\hat{\mathbf{S}}$:

$$\hat{\mathbf{S}} = \begin{pmatrix} 0 & 0 & 0 & \dots & (-1)^{N+i+j+1} C^0_{N-2} e^{-i\phi_{N,1}} \\ 0 & 0 & 0 & \dots & (-1)^{N+i+j+1} C^1_{N-2} e^{-i\phi_{N,2}} \\ \dots & \dots & \dots & \dots & \dots \\ 0 & e^{-i\phi_{N,N-1}} & -e^{-i\phi_{N,N-1}} & \dots & (-1)^{N+i+j+1} C^{N-2}_{N-2} e^{-i\phi_{N,N-1}} \\ 1 & 0 & 0 & \dots & 0 \end{pmatrix},$$

$$\hat{\mathbf{S}}^{-1} = \begin{pmatrix} 0 & 0 & 0 & \dots & 1 \\ C^0_{N-2} e^{i\phi_{N,1}} & C^0_{N-3} e^{i\phi_{N,2}} & C^0_{N-4} e^{i\phi_{N,1}} & \dots & 0 \\ \dots & \dots & \dots & \dots & \dots \\ C^{N-2}_{N-2} e^{i\phi_{N,1}} & C^{N-3}_{N-3} e^{i\phi_{N,2}} & 0 & \dots & 0 \\ C^{N-2}_{N-2} e^{i\phi_{N,1}} & 0 & 0 & \dots & 0 \end{pmatrix}, \quad e^{gt\hat{\mathbf{J}}} = \begin{pmatrix} 1 & gt & \frac{(gt)^2}{2!} & \dots & \frac{(gt)^{N-1}}{(N-1)!} \\ 0 & 1 & gt & \dots & \frac{(gt)^{N-2}}{(N-2)!} \\ \dots & \dots & \dots & \dots & \dots \\ 0 & 0 & 0 & \dots & gt \\ 0 & 0 & 0 & \dots & 1 \end{pmatrix}, \tag{A6}$$

where C^k_n are the binomial coefficients. By substituting into $\mathbf{C}(t) = e^{-i\Omega t}\hat{\mathbf{S}} e^{gt\hat{\mathbf{J}}_{\mathrm{M}}} \hat{\mathbf{S}}^{-1}\mathbf{C_0}$, it can be found that $C^1_N(t) = \frac{e^{-i\Omega t} e^{i\phi_{N,1}}}{(N-1)!} \sum_{j=0}^{N-1} L(N-1,j)(-\gamma_g t/2)$, where $g = -\gamma_g/2$ and $L(n,k)$ are so-called Lah numbers [33] known in combinatorics. For Lah numbers there is a relation which interconnects them with the generalized Laguerre polynomials of order minus one according to $L^{(-1)}_N(x) = \frac{1}{N!}\sum_{j=0}^{N} L(N,j)(-x)^j$. By making use of this relation we can write the final answer in a simple and compact form

$$C^1_N(t) = e^{-i\Omega t + i\phi_{N,1}} L^{(-1)}_{N-1}(\gamma_g t/2). \tag{A7}$$

The correctness of the obtained result can be easily checked by substituting this solution into the equation for the $(N+1)$th emitter in the chain $C^1_{N+1}(t)$ and making use of the relation $\int_0^x L^{(\alpha)}_N(x)dx = L^{(\alpha-1)}_{N+1}(0) - L^{(\alpha-1)}_{N+1}(x)$.

APPENDIX B: GREEN'S TENSOR

In order to obtain the Σ^{mn} matrix elements we need to construct the Green's tensor of the system, which can be found from

$$\left[-\frac{\omega^2}{c^2}\varepsilon(\mathbf{r},\omega) + \nabla\times\nabla\times\right]\mathbf{G}(\mathbf{r},\mathbf{r}',\omega) = \mathbf{I}\delta(\mathbf{r}-\mathbf{r}'), \tag{B1}$$

where $\varepsilon(\mathbf{r},\omega)$ is the complex dielectric function and $\mathbf{I}$ is the unit dyad. In our case we consider a dielectric cylindrical waveguide of radius ρ_c and dielectric permittivity ε being constant inside the cylinder. To find the solution we apply the scattering superposition method [34,35], which allows us to expand the Green's tensor into the homogeneous and inhomogeneous terms:

$$\mathbf{G}(\mathbf{r},\mathbf{r}',\omega) = \mathbf{G}_0(\mathbf{r},\mathbf{r}',\omega) + \mathbf{G}_s(\mathbf{r},\mathbf{r}',\omega). \tag{B2}$$

As soon as we consider atomic dipoles in the vicinity of the waveguide, so that $\mathbf{r},\mathbf{r}'$ are outside the cylinder, the homogeneous term is always present and describes the field generated directly by the source placed at the point $\mathbf{r}'$ at the field point $\mathbf{r}$. This term can be obtained analytically from the Green tensor written in Cartesian coordinates using the transformation from Cartesian to cylindrical coordinates $\mathbf{S}(\phi)\mathbf{G}^{\mathrm{Cart}}_0(\mathbf{r},\mathbf{r}',\omega)\mathbf{S}^T(\phi)$, where $\mathbf{G}^{\mathrm{Cart}}_0$ has an analytic expression [36] and is given by

$$\mathbf{G}^{\mathrm{Cart}}_0(\mathbf{r},\mathbf{r}',\omega) = \left(\mathbf{I} + \frac{1}{k^2}\nabla\otimes\nabla\right)G_0(\mathbf{r},\mathbf{r}',\omega). \tag{B3}$$

Here $G_0(\mathbf{r},\mathbf{r}',\omega)$ is the Green's function of the scalar Helmholtz equation.

The scattering term can be calculated via the integral representation of the homogeneous part. To obtain this representation we apply the method of VWF explained in details in Refs. [34,35]; here we cover only the basic ideas and provide the final expressions. To find the solution of the vector Helmholtz equation (B1) we introduce the scalar Helmholtz equation and the solution of this equation in the cylindrical coordinates:

$$\begin{aligned} &\nabla^2\phi(\mathbf{k},\mathbf{r}) + k^2\phi(\mathbf{k},\mathbf{r}) = 0, \\ &\phi_n(k_z,\mathbf{r}) = J_n(k_\rho\rho)e^{in\theta + ik_z z}. \end{aligned} \tag{B4}$$

Here $J_n(x)$ is the Bessel function of the first kind, $\mathbf{r} = (\rho,\theta,z)$ are the cylindrical coordinates, and k_ρ, k_z are the projections of the wave vector $\mathbf{k}$. The solution of the vector Helmholtz equation may be written in terms of the following vector wave functions:

$$\begin{aligned} \mathbf{M}_n(k_z,\mathbf{r}) &= \nabla\times[\phi_n(k_z,\mathbf{r})\mathbf{e_z}], \\ \mathbf{N}_n(k_z,\mathbf{r}) &= \frac{1}{k}\nabla\times\mathbf{M}_n(k_z,\mathbf{r}), \end{aligned} \tag{B5}$$

where $\mathbf{e_z}$ is the so-called pilot vector, the unit vector pointing in the z direction. These WVFs $\mathbf{M}$, $\mathbf{N}$ correspond to TE/TM modes of the field.

One can show [34] that the homogeneous part of the Green's function can be expanded in terms of these vector wave functions in the following way:

$$\begin{aligned} \mathbf{G}_0(\mathbf{r},\mathbf{r}',\omega) = &-\frac{\mathbf{e}_\rho\mathbf{e}_\rho}{k_0^2}\delta(\mathbf{r}-\mathbf{r}') \\ &+\frac{i}{8\pi}\sum_{n=-\infty}^{\infty}\int_{-\infty}^{\infty}\frac{dk_z}{k^2_{0\rho}}\mathbf{F}_n(k_z,\mathbf{r},\mathbf{r}') \end{aligned} \tag{B6}$$

and the $\mathbf{F}_n(k_z,\mathbf{r},\mathbf{s})$ function is given by

$$\begin{aligned} &\mathbf{M}^{(1)}_n(k_z,\mathbf{r})\overline{\mathbf{M}}_n(k_z,\mathbf{r}') + \mathbf{N}^{(1)}_n(k_z,\mathbf{r})\overline{\mathbf{N}}_n(k_z,\mathbf{r}'), \\ &\mathbf{M}_n(k_z,\mathbf{r})\overline{\mathbf{M}}^{(1)}_n(k_z,\mathbf{r}') + \mathbf{N}_n(k_z,\mathbf{r})\overline{\mathbf{N}}^{(1)}_n(k_z,\mathbf{r}'). \end{aligned} \tag{B7}$$

Here the first line holds for $\rho_r > \rho_{r'}$ while the second one for $\rho_r < \rho_{r'}$, and $k_0 = \omega/c$, $k_{0\rho} = \sqrt{k_0^2 - k_z^2}$, and the superscript (1) in vector wave functions denotes that the Bessel function of the first kind $J_n(k_\rho\rho)$ should be replaced with the Hankel function of the first kind $H_n^{(1)}(k_\rho\rho)$. Here we provide the explicit form of WVF:

$$\begin{aligned}
\mathbf{M}_n(k_z,\mathbf{r}) &= \begin{pmatrix} \frac{in}{\rho} J_n(k_{0\rho}\rho) \\ -k_{0\rho}(J_n(k_{0\rho}\rho))' \\ 0 \end{pmatrix} e^{in\theta + ik_z z}, \\
\mathbf{N}_n(k_z,\mathbf{r}) &= \begin{pmatrix} \frac{ik_z k_{0\rho}}{k}(J_n(k_{0\rho}\rho))' \\ -\frac{nk_z}{\rho k} J_n(k_{0\rho}\rho) \\ \frac{k_{0\rho}^2}{k} J_n(k_{0\rho}\rho) \end{pmatrix} e^{in\theta + ik_z z}, \\
\overline{\mathbf{M}}_n(k_z,\mathbf{r}') &= \begin{pmatrix} -\frac{in}{\rho'} J_n(k_{0\rho}\rho') \\ -k_{0\rho}(J_n(k_{0\rho}\rho'))' \\ 0 \end{pmatrix}^T e^{-in\theta' - ik_z z'}, \\
\overline{\mathbf{N}}_n(k_z,\mathbf{r}') &= \begin{pmatrix} -\frac{ik_z k_{0\rho}}{k}(J_n(k_{0\rho}\rho'))' \\ -\frac{nk_z}{\rho' k} J_n(k_{0\rho}\rho') \\ \frac{k_{0\rho}^2}{k} J_n(k_{0\rho}\rho') \end{pmatrix}^T e^{-in\theta' - ik_z z'},
\end{aligned} \tag{B8}$$

where $J_n(k_\rho\rho)'$ means derivative with respect to the dimensionless argument.

Now having the integral representation of the homogeneous term of the Green's function, we can construct the scattering term in a similar fashion. Let us denote the medium outside the dielectric cylinder as 1 and the medium inside as 2. The particular form of the Green's tensor depends on the position of a source point $\mathbf{r}'$: whether it is inside or outside the cylinder. As soon as we are interested in a situation, when both source and receiver are outside the cylinder and in the latter we consider only the second case. Thus the total Green's tensor can written as

$$\begin{aligned}
\mathbf{G}^{11}(\mathbf{r},\mathbf{r}',\omega) &= \mathbf{G}_0^{11}(\mathbf{r},\mathbf{r}',\omega) + \mathbf{G}_s^{11}(\mathbf{r},\mathbf{r}',\omega), \\
\mathbf{G}^{21}(\mathbf{r},\mathbf{r}',\omega) &= \mathbf{G}_s^{21}(\mathbf{r},\mathbf{r}',\omega).
\end{aligned} \tag{B9}$$

Here two superscripts denote position of the receiver and the source point, respectively, and the two scattering parts of the Green's tensor have the following form:

$$\begin{aligned}
\mathbf{G}_s^{11}(\mathbf{r},\mathbf{r}',\omega) &= \frac{i}{8\pi}\sum_{n=-\infty}^{\infty}\int_{-\infty}^{\infty}\frac{dk_z}{k_{\rho 1}^2}\mathbf{F}_{\mathbf{M};n,1}^{11(1)}(k_z,\mathbf{r})\overline{\mathbf{M}}_{n,1}^{(1)}(k_z,\mathbf{r}') \\
&\quad + \mathbf{F}_{\mathbf{N};n,1}^{11(1)}(k_z,\mathbf{r})\overline{\mathbf{N}}_{n,1}^{(1)}(k_z,\mathbf{r}'), \\
\mathbf{F}_{\mathbf{M};n,1}^{11(1)}(k_z,\mathbf{r}) &= R_{MM}^{11}\mathbf{M}_{n,1}^{(1)}(k_z,\mathbf{r}) + R_{NM}^{11}\mathbf{N}_{n,1}^{(1)}(k_z,\mathbf{r}), \\
\mathbf{F}_{\mathbf{N};n,1}^{11(1)}(k_z,\mathbf{r}) &= R_{MN}^{11}\mathbf{M}_{n,1}^{(1)}(k_z,\mathbf{r}) + R_{NN}^{11}\mathbf{N}_{n,1}^{(1)}(k_z,\mathbf{r}). \\
\mathbf{G}_s^{21}(\mathbf{r},\mathbf{r}',\omega) &= \frac{i}{8\pi}\sum_{n=-\infty}^{\infty}\int_{-\infty}^{\infty}\frac{dk_z}{k_{\rho 1}^2}\mathbf{F}_{\mathbf{M};n,2}^{21}(k_z,\mathbf{r})\overline{\mathbf{M}}_{n,1}^{(1)}(k_z,\mathbf{r}') \\
&\quad + \mathbf{F}_{\mathbf{N};n,1}^{21}(k_z,\mathbf{r})\overline{\mathbf{N}}_{n,1}^{(1)}(k_z,\mathbf{r}'), \\
\mathbf{F}_{\mathbf{M};n,2}^{21}(k_z,\mathbf{r}) &= R_{MM}^{21}\mathbf{M}_{n,2}(k_z,\mathbf{r}) + R_{NM}^{21}\mathbf{N}_{n,2}(k_z,\mathbf{r}), \\
\mathbf{F}_{\mathbf{N};n,2}^{21}(k_z,\mathbf{r}) &= R_{MN}^{21}\mathbf{M}_{n,2}(k_z,\mathbf{r}) + R_{NN}^{21}\mathbf{N}_{n,2}(k_z,\mathbf{r}).
\end{aligned} \tag{B10}$$

Here the scattering Fresnel coefficients R_{AB}^{ij} are introduced and the second subscript in the VWFs denotes that k and k_ρ should be replaced with their values inside the corresponding media $k_i = \varepsilon_i(\mathbf{r},\omega)k_0$, $k_{\rho i} = \sqrt{k_i^2 - k_z^2}$. We should notice that unlike the case of the homogeneous term, here we have products of $\mathbf{M}$ and $\mathbf{N}$, which are due to the fact that the normal modes in our case have hybrid nature.

The form of the Fresnel coefficients mentioned above can be found by imposing the boundary conditions on the Green's tensor at the surface of the cylinder,

$$\begin{aligned}
&\mathbf{e}_\rho \times [\mathbf{G}^{11}(\mathbf{r},\mathbf{r}',\omega) - \mathbf{G}^{21}(\mathbf{r},\mathbf{r}',\omega)]|_{\rho_r=\rho_c} = 0, \\
&\mathbf{e}_\rho \times \nabla_{\mathbf{r}} \times [\mathbf{G}^{11}(\mathbf{r},\mathbf{r}',\omega) - \mathbf{G}^{21}(\mathbf{r},\mathbf{r}',\omega)]|_{\rho_r=\rho_c} = 0.
\end{aligned} \tag{B11}$$

Solving for this, we can find the Fresnel coefficients R_{AB}^{ij} and, finally, construct the scattering part of the Green's tensor $\mathbf{G}_s(\mathbf{r},\mathbf{r}',\omega)$.

APPENDIX C: COLLECTIVE EMISSION

According to Eq. (6) from the main text, the collective emission can be studied by considering $C_{|\Psi\rangle} = \mathbf{C}_{\text{init}}^\dagger \mathbf{U}(\mathbf{t})\mathbf{C}_{\text{init}}$:

$$C_{|\Psi\rangle}(t) = A^2 e^{-i\Omega t}\begin{pmatrix} e^{-i\psi_1^*} \\ e^{-i\psi_2^*} \\ \cdots \\ e^{-i\psi_N^*} \end{pmatrix}^T \begin{pmatrix} e^{i\phi_{1,1}}F_0(t) & 0 & \cdots & 0 \\ e^{i\phi_{2,1}}F_1(t) & e^{i\phi_{2,2}}F_0(t) & \cdots & 0 \\ \cdots & \cdots & \cdots & \cdots \\ e^{i\phi_{N,1}}F_{N-1}(t) & e^{i\phi_{N,2}}F_{N-2}(t) & \cdots & e^{i\phi_{N,N}}F_0(t) \end{pmatrix} \begin{pmatrix} e^{i\psi_1} \\ e^{i\psi_2} \\ \cdots \\ e^{i\psi_N} \end{pmatrix}. \tag{C1}$$

Here A is defined from the normalization condition. Notice that both $\phi_{i,j}$ and ψ_j can be complex. Let $\phi_{l,k} = (l-k)\phi$ ($\phi = \phi' + i\phi''$) and $\psi_j = (j-1)\psi$ ($\psi = \psi' + i\psi''$). Therefore, the normalization constant can be found to be $A^{-2} = e^{\psi''(1-N)}\text{csch}(\psi'')\sinh(N\psi'')$, where $\text{csch}(x)$ and $\sinh(x)$ are cosecant and sine hyperbolic.

The product can be written as $\mathbf{C}^\dagger\mathbf{B}\mathbf{C}$, where $C_k = e^{i(k-1)\psi}$, $B_{l,k} = e^{i(l-k)\phi}F_{l-k}(t)\Theta_{l,k}$, $C_l^\dagger = e^{-i(l-1)\psi^*}$, where $\Theta_{l,k} = 1$ for $l \geqslant k$ and zero otherwise.

$$\begin{aligned}
(\mathbf{BC})_l &= \sum_{k=1}^{l} B_{l,k}C_k = \sum_{k=1}^{l} e^{i(l-k)\phi}F_{l-k}(t)e^{i(k-1)\psi} = \sum_{k=1}^{l} F_{l-k}(t) \times e^{ik(\psi-\phi)}e^{il\phi - i\psi}, \\
\sum_{l=1}^{N} C_l^\dagger(\mathbf{BC})_l &= \sum_{l=1}^{N} e^{-i(l-1)\psi^*}\sum_{k=1}^{l} F_{l-k}(t)e^{ik(\psi-\phi)}e^{il\phi - i\psi} = \sum_{l=1}^{N}\sum_{k=1}^{l} e^{i(l-k)(\phi'-\psi')+2\psi''-(l+k)\psi''-(l-k)\phi''}F_{l-k}(t).
\end{aligned}$$

Finally, we have

$$C_{|\Psi\rangle}(t) = A^2 \sum_{l=1}^{N}\sum_{k=1}^{l} e^{i(l-k)(\phi'-\psi')+2\psi''-(l+k)\psi''-(l-k)\phi''} F_{l-k}(t)$$
$$= A^2 \sum_{s=1}^{N} e^{i(s-1)(\phi'-\psi')-(s-1)\phi''} e^{2\psi''} \sum_{j=1}^{N-(s-1)} e^{-(s-1)\psi''} e^{-2j\psi''} F_{s-1}(t). \tag{C2}$$

Here $F_{s-1}(t) = e^{-i\Omega t} L_{s-1}^{(-1)}(\gamma_g t/2)\Theta(t-(s-1)\tau)$, and we expand $e^{-i\Omega t} L_{s-1}^{(-1)}(\gamma_g t/2)$ to the first order in t:

$$e^{-i\Omega t} L_{s-1}^{(-1)}(\gamma_g t/2) = \begin{cases} 1 - i\Omega t, & \text{if } s = 1, \\ -\gamma_g t/2, & \text{if } s > 1. \end{cases} \tag{C3}$$

A very general form of the expansion looks cumbersome, however, for a specific case when both ψ and ϕ are real the answer has the following form:

$$C(t \to 0) \sim 1 + \left[-i\Omega - \frac{\gamma_g}{2}\frac{e^{i\xi}(N + e^{iN\xi} - Ne^{i\xi} - 1)}{N(e^{i\xi}-1)^2}\right] t \sim 1 - \frac{\Gamma^{(0)}}{2} t, \tag{C4}$$

where $\xi = \phi' - \psi'$ and $\Gamma^{(0)} = -\mathrm{Re}[-i\Omega - \frac{\gamma_g}{2}\frac{e^{i\xi}(N+e^{iN\xi}-Ne^{i\xi}-1)}{N(e^{i\xi}-1)^2}]$ is the modified initial spontaneous emission rate. Following the main text we proceed by considering the two cases: the neighboring emitters are emitting photons in and out of phase:

$$\frac{\Gamma^{(0)}}{2} = \begin{cases} -i\Omega - \frac{\gamma_g}{2}\frac{(N-1)}{2}, & \text{if } \xi = 2\pi m, \\ -i\Omega + \frac{\gamma_g}{2}\frac{(2N-1+e^{iN\pi})}{4N}, & \text{if } \xi = \pi(2m+1). \end{cases} \tag{C5}$$

In order to have a simple interpretation of these results we can consider our initial state to be a symmetric Dicke superradiant state $|\Psi_{\text{init}}\rangle = |D\rangle = \frac{1}{\sqrt{N}}\sum_{j=1}^{N}|e_j\rangle|\{0\}\rangle$ and have a look at two situations: when the propagation phase acquired by the photon between the neighboring atoms is $\phi = 2\pi m$ or $2\pi(m+1)$ for all j. We can find out a probability amplitude of every k emitter to be excited at some later time Δt,

$$\langle e_k|\hat{U}(\Delta t)|\Psi_{\text{init}}\rangle = \frac{1}{\sqrt{N}}\begin{pmatrix} 0 \\ \cdots \\ 1_k \\ \cdots \end{pmatrix}^T \begin{pmatrix} 1-\frac{\gamma_{\text{tot}}}{2}\Delta t & 0 & \cdots & 0 \\ \pm\frac{\gamma_g}{2}\Delta t & 1-\frac{\gamma_{\text{tot}}}{2}\Delta t & \cdots & 0 \\ \cdots & \cdots & \cdots & \cdots \\ \pm\frac{\gamma_{\text{tot}}}{2}\Delta t & -\frac{\gamma_{\text{tot}}}{2}\Delta t & \cdots & 1-\frac{\gamma_{\text{tot}}}{2}\Delta t \end{pmatrix}\begin{pmatrix} 1 \\ 1 \\ \cdots \\ 1 \end{pmatrix}$$
$$= \begin{cases} \frac{1}{\sqrt{N}}\left(1 - \frac{\gamma_{\text{tot}}}{2}\Delta t + (1 - k \bmod 2)\frac{\gamma_g}{2}\Delta t\right), & \text{if } \phi = \pi(2m+1), \\ \frac{1}{\sqrt{N}}\left(1 - \frac{\gamma_{\text{tot}}}{2}\Delta t - (k-1)\frac{\gamma_g}{2}\Delta t\right), & \text{if } \phi = 2\pi m, \end{cases} \tag{C6}$$

where we have replaced $-i\Omega$ with $-\gamma_{\text{tot}}/2$, T stands for transpose, an upper sign is for $\phi = \pi(2m+1)$ and a lower is for $\phi = 2\pi m$, and we also consider N to be even for simplicity, which does not affect the answer in the limit of large N. Here Δt is some sufficiently small time, meaning that $\mathrm{Im}[\Omega]\Delta t,\ \gamma_g \Delta t \ll 1$.

Now we can calculate the probability for every emitter to be excited at Δt as $P_{|e_k\rangle}(\Delta t) = |\langle e_k|\hat{U}(\Delta t)|\Psi_{\text{init}}\rangle|^2$. We should note that an excitation in principle might jump many times between the atoms before escaping the atomic subsystem and, therefore, there are a lot of ways how our system can emit a photon. However, for small times Δt it is reasonable to consider only a single jump of the excitation from one emitter to another, after which it goes into the field subsystem. Therefore, we can find the probability that excitation is not in the atomic subsystem as $1 - \sum_{k=1}^{N} P_{|e_k\rangle}(\Delta t)$ keeping only terms with the first power of Δt. The corresponding coefficient before Δt can be thought of as the modified initial spontaneous emission rate $\Gamma^{(0)}$ we have discussed before,

$$\Gamma^{(0)} = \begin{cases} \gamma_{\text{tot}} + \frac{N-1}{2}\gamma_g \xrightarrow[N\to\infty]{\gamma_g \gg \gamma_r} \frac{N}{2}\gamma_g, & \text{if } \phi = 2\pi m, \\ \gamma_{\text{tot}} - \frac{N \,\text{div}\, 2}{N}\gamma_g \xrightarrow[N\to\infty]{\gamma_g \gg \gamma_r} \frac{\gamma_g}{2}, & \text{if } \phi = \pi(2m+1), \end{cases} \tag{C7}$$

where div means integer division.

There is also another way to interpret the $(N+1)\gamma_g/2$ result for the in-phase initial spontaneous emission rate $\Gamma^{(0)}$. By making use of the relation $\sum_{l=0}^{N} L_l^{(\alpha)}(x) = L_N^{(\alpha+1)}(x)$ we can find the probability amplitude of the kth emitter to be excited $C_k(t)$ like in Eq. (C6), but without making a small

argument expansion

$$C_k(t) = \langle k|\hat{U}(t)|D\rangle = \sum_{j=1}^{k} \frac{e^{-i\Omega t}}{\sqrt{N}} L_{j-1}^{(-1)}(\gamma_g t/2) = \frac{e^{-i\Omega t}}{\sqrt{N}} L_{k-1}^{(0)}(\gamma_g t/2), \tag{C8}$$

and then we can take $\frac{d|C_k(t)|^2}{dt}|_{t\to 0} \approx (\frac{1}{N} - \Gamma_k^{(0)} t)$ and make the coupling to the guided mode strong $\Omega = -i\gamma_g/2$, obtaining $\Gamma_k^{(0)} = \frac{k}{N}\gamma_g$. Here a factor of $\frac{1}{N}$ simply arises from the fact that since the initial state is $|D\rangle = \sum_{j=1}^{N} |e_j\rangle \times |\{0\}\rangle$, an individual atom shares N-th fraction of an initial excitation. The obtained result tells us that emitters in a chain have a position dependent emission rate. The reason for that is also due to the perfect unidirectionality: each emitter simply behaves itself as it would as a part of a chain which is efficiently a $\frac{k}{N}$th fraction of the original one, since an emitter "senses" only other emitters positioned before it.

Now it can be seen that the emission rate of the Dicke superradiant state itself for the in-phase emission is a simple arithmetic sum of the emission rates of individual emitters: $\sum_{k=1}^{N} \Gamma_k^{(0)} = \frac{1}{N}\sum_{k=1}^{N} k\gamma_g = \frac{N+1}{2}\gamma_g$.

We also want to note that when studying the emission of a Dicke superradiant state itself for the in-phase emission, the dynamics in our toy model can be found exactly:

$$C_D(t) = \langle D|\hat{U}(t)|D\rangle = \sum_{k=1}^{N}\sum_{j=1}^{k} \frac{e^{-i\Omega t}}{N} L_{j-1}^{(-1)}(\gamma_g t/2) = \frac{e^{-i\Omega t}}{N} L_{N-1}^{(1)}(\gamma_g t/2), \tag{C9}$$

where we applied the aforementioned relation for the sum of Laguerre polynomials two times. At small times it gives, of course, the same expressions as in the top line of Eq. (C7) for the initial spontaneous emission rate.

[1] P. Lodahl, S. Mahmoodian, S. Stobbe, A. Rauschenbeutel, P. Schneeweiss, J. Volz, H. Pichler, and P. Zoller, Nature (London) **541**, 473 (2017).
[2] B. L. Altshuler, I. L. Aleiner, and V. I. Yudson, Phys. Rev. Lett. **111**, 086401 (2013).
[3] M. Ringel, M. Pletyukhov, and V. Gritsev, New J. Phys. **16**, 113030 (2014).
[4] K. Bliokh, F. Rodríguez-Fortuño, F. Nori, and A. V. Zayats, Nat. Photon. **9**, 796 (2015).
[5] K. Y. Bliokh, D. Smirnova, and F. Nori, Science **348**, 1448 (2015).
[6] F. J. Rodríguez-Fortuño, G. Marino, P. Ginzburg, D. O'Connor, A. Martínez, G. A. Wurtz, and A. V. Zayats, Science (N.Y.) **340**, 328 (2013).
[7] T. Van Mechelen and Z. Jacob, Optica **3**, 118 (2016).
[8] F. J. Rodríguez-Fortuño, N. Engheta, A. Martínez, and A. V. Zayats, Nat. Commun. **6**, 8799 (2015).
[9] A. Hayat, J. P. B. Mueller, and F. Capasso, Proc. Natl. Acad. Sci. USA **112**, 13190 (2015).
[10] M. I. Petrov, S. V. Sukhov, A. A. Bogdanov, A. S. Shalin, and A. Dogariu, Laser Photon. Rev. **10**, 116 (2016).
[11] J. Yuen-Zhou, S. K. Saikin, T. Zhu, M. C. Onbasli, C. A. Ross, V. Bulovic, and M. A. Baldo, Nat. Commun. **7**, 11783 (2016).
[12] P. V. Kapitanova, P. Ginzburg, F. J. Rodríguez-Fortuño, D. S. Filonov, P. M. Voroshilov, P. A. Belov, A. N. Poddubny, Y. S. Kivshar, G. A. Wurtz, and A. V. Zayats, Nat. Commun. **5**, 3226 (2014).
[13] R. J. Coles, D. M. Price, J. E. Dixon, B. Royall, E. Clarke, P. Kok, M. S. Skolnick, A. M. Fox, and M. N. Makhonin, Nat. Commun. **7**, 11183 (2016).
[14] H. Pichler, T. Ramos, A. J. Daley, and P. Zoller, Phys. Rev. A **91**, 042116 (2015).
[15] T. Ramos, B. Vermersch, P. Hauke, H. Pichler, and P. Zoller, Phys. Rev. A **93**, 062104 (2016).
[16] S. Hughes and G. S. Agarwal, Phys. Rev. Lett. **118**, 063601 (2017).
[17] D. Chang, V. Vuletic, and M. Lukin, Nat. Photon. **8**, 685 (2014).
[18] N. V. Corzo, B. Gouraud, A. Chandra, A. Goban, A. S. Sheremet, D. V. Kupriyanov, and J. Laurat, Phys. Rev. Lett. **117**, 133603 (2016).
[19] H.L. Sørensen, J.-B. Béguin, K.W. Kluge, I. Iakoupov, A. S. Sørensen, J. H. Müller, E. S. Polzik, and J. Appel, Phys. Rev. Lett. **117**, 133604 (2016).
[20] F. L. Kien and A. Rauschenbeutel, Phys. Rev. A **95**, 023838 (2017).
[21] H. J. Carmichael, Phys. Rev. Lett. **70**, 2273 (1993).
[22] A. N. Poddubny, I. V. Iorsh, and A. A. Sukhorukov, Phys. Rev. Lett. **117**, 123901 (2016).
[23] D.-G. Welsch, H. Dung, and L. Knoll, Fortschr. Phys. **51**, 255 (2003).
[24] D. F. Kornovan, A. S. Sheremet, and M. I. Petrov, Phys. Rev. B **94**, 245416 (2016).
[25] G. Angelatos and S. Hughes, Optica **3**, 370 (2016).
[26] G. Arfken, *Mathematical Methods for Physicists* (Academic Press, New York, 1972), p. 642.
[27] C. Cohen-Tannoudji, J. Dupont-Roc, and G. Grynberg, Atom-Photon Interactions: Basic Process and Applications (Wiley, New York, 1992), Vol. I.
[28] T. Gruner and D.-G. Welsch, Phys. Rev. A **53**, 1818 (1996).
[29] H. T. Dung, L. Knöll, and D.-G. Welsch, Phys. Rev. A **66**, 063810 (2002).
[30] P. B. Johnson and R. W. Christy, Phys. Rev. B **6**, 4370 (1972).
[31] D. O'Connor, P. Ginzburg, F. J. Rodríguez-Fortuño, G. A. Wurtz, and A. V. Zayats, Nat. Commun. **5**, 5327 (2014).
[32] R. H. Dicke, Phys. Rev. **93**, 99 (1954).
[33] J. Riordan, *Introduction to Combinatorial Analysis* (Princeton University Press, Princeton, NJ, 1958).
[34] W. C. Chew, *Waves and Fields in Inhomogeneous Media* (Wiley-IEEE Press, New York, 1999), p. 632.
[35] C.-T. Tai, *Dyadic Green Functions in Electromagnetic Theory* (IEEE Press Series on Electromagnetic Waves, New York, 1994), p. 343.
[36] L. Novotny and B. Hecht, *Principles of Nano-Optics* (Cambridge University Press, Cambridge, UK, 2012), p. 578.

11th International Congress on Engineered Material Platforms for Novel Wave Phenomena - Metamaterials 2017
Marseille, France, Aug. 28th - Sept. 2nd 2017

Light interaction and quantum transport in atomic chain chirally coupled to a waveguide

D. F. Kornovan[1], A.S. Sheremet[1], I.V. Iorsh[1], and M.I. Petrov[1]

[1] ITMO University, Department of Nanophotonics and Metamaterials, Birzhevaya linia 14, 199034, Saint-Petersburg, Russia
email: newparadigm.dk@gmail.com, trisha.petrov@gmail.com,

***Abstract* – In this work we considered light interaction with two-level quantum systems chirally coupled to a single guided mode with account for a spin-locking effect. The chiral coupling allows achieving asymmetric interaction between the two-level systems, which strongly affects the light scattering of a guided mode of an optical nanofiber by one-dimensional atomic chain. We have also build an analytical model of unidirectional transport of quantum excitation and verified it with modelling of atoms coupled with surface plasmon polariton mode of a metallic nanowire. In particularly, we showed the tolerance of the unidirectionally coupled systems over the positional disorder of the two-level systems.**

I. Introduction

Controlling the interaction of quantum emitters with optical nanostructures at the single-photon level is a key tool for the realization of quantum technologies [1]. It is supported by the recent experimental progress in coupling single quantum sources to surface plasmon polaritons [2], and to photonic crystal waveguide modes [3], as well as by the results in neutral atoms trapping in the vicinity of an optical nanofiber [4, 5]. All of these realizations are characterized by interaction of quantum system with an evanescent guided mode of nanophotonic structure. In recent years attention of researches is paid also paid to optical spin properties of evanescent guided modes: in such systems the direction of optical spin is not parallel to the direction of electromagnetic wave propagation [6]. The presence of the transverse optical spin component opens a possibility to control the direction of propagation by means of the so called spin-locking effect [7]. In this case the polarization of an active transition of the quantum source of light defines the direction of surface-localized wave propagation. Theoretical studies on possible applications as well as experimental realization were demonstrated for both plasmonic and photonic nanostructures [8, 9]. Fascinating effects were also observed for quantum systems including a single atom near whispering-gallery mode microresonator[10], a large bragg reflection from an array of just 2000 ultracold atoms trapped near an optical nanofiber [11]. These achievements make the fundamental studies of quantum systems with chiral unidirectional coupling highly important and timely.

II. Results

We consider a one-dimensional (1D) array of N two-level atoms with a period Δz and in the vicinity of 1D cylindrical waveguide (see Fig. 1 (a)). We consider both dielectric nanofiber to study the process of light scattering, and plasmonic nanowire to achieve strong spin-locking effect and unidirectional transport of a single quantum excitation.

A. Light scattering with account for chiral coupling

In the first turn, we have considered [12] single-photon scattering by the atomic chain in the regimes of symmetric coupling to the guided mode, and asymmetric (chiral) coupling. We compared scattering of the incident photon on atoms with (i) radial component of the dipole moment $\mathbf{d_0}$ and (ii) σ_+ polarized dipole having both radial $\mathbf{d}_\rho$ and z-component $\mathbf{d}_z$ (see Fig. 1 (b)). In the latter case the two components have $\pi/2$ phase shift but the absolute dipole moment equals $|-\mathbf{d}_\rho + i\mathbf{d}_z|/\sqrt{2} = d_0$. Contrary to radially polarized atom the σ_+ atoms has a strong asymmetry in coupling with the forward and backward propagating fiber mode [7]. We have made the calculation

11^{th} *International Congress on Engineered Material Platforms for Novel Wave Phenomena - Metamaterials 2017*
Marseille, France, Aug. 28^{th} - Sept. 2^{nd} 2017

for the fiber backscattering regime, when the symmetry should be conserved for linearly polarized atom, but not for the circularly polarized atom. In Fig.1 the normalized scattering losses spectra are shown for the case of the first and second fiber Bragg resonance in the case of radially polarized atoms (dashed line) and in the case of σ_+ atoms. We see the pronounced switching from the Lorentzian spectral shape to a notched shape. For the first fiber Bragg condition $\Delta z = 0.5\lambda_f$, see Fig.1 (a), one can see sharp peaks in the center of the band due to scattering by the long-lived collective atomic states. In the case of the second Bragg resonance, see Fig.1 (b) there the sharp peaks are smeared out as all the polaritonic states are above light cone and, thus, have high losses.

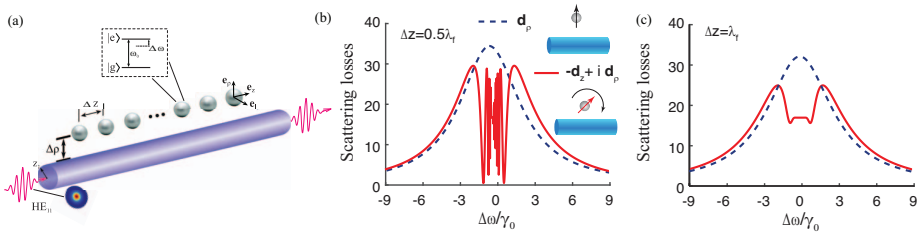

Fig. 1: (a) The general view of the considered problem. λ_f is the wavelength of the fiber mode at the atomic transition frequency. (b,c) the spectrum of scattering losses in case of symmetric (dashed line) and asymmetric (solid line) shown for two periods of an atomic chain.

B. Unidirectional quantum transport

Further on, we have analyzed spatial and temporal dynamics of quantum excitation propagation in chiral coupled atomic chain, which allows achieving unidirectional transport due to the spin-locking effect. Assuming that coupling is mediated by the guided mode only in the strong spin-locking regime, we formulate the equations describing the dynamics of the system [13]:

$$\dot{C}_n(t) = -i\Omega C_n(t) + \sum_{m=1}^{n-1} G_{nm} C_m(t), \tag{1}$$

where $C_n(t)$ is the complex probability amplitude of the n-th TLS to be excited at time t, the diagonal parameter $\Omega = \Delta_L + i\gamma_{tot}/2$ contians Δ_L, which is the Lamb Shift and γ_{tot}, which is the total spontaneous emission rate (total damping rate) comprising two contributions: emission into radiation and guided modes ($\gamma_{tot} = \gamma_r + \gamma_g$). The single mode coupling cefficients G_{nm} between the TLSs with number m and n and can be written as $G_{nm} = -(\gamma_g/2)e^{i\phi_{nm}}$, where $\gamma_g/2$ is the coupling strength, $\phi_{nm} = k^g(z_n - z_m)$ is the phase acquired by the photon due to the propagation from emitter m to emitter n, and k^g is the corresponding propagation constant of the guided mode. We assume strong spin-locking regime, which leads to unidirectional coupling, i.e. $G_{nm} \neq 0$ only for $n > m$. The system of equations (1) can be formulated in the matrix form $\dot{\mathbf{C}}(t) = \hat{\mathbf{M}}\mathbf{C}(t)$, with $\hat{\mathbf{M}}$ being a lower triangular matrix, which means that the problem is already diagonalized and moreover, it is degenerate. All quantum oscillators have equal transition frequencies and lifetimes and, therefore, the system has only one eigenstate in which the last atom is excited, which significantly differs from the case of symmetric coupling [12].

We focus on the problem of the excitation transport through the chain of TLSs, and for that we consider the initial condition in which the first atom is excited, while all other are in the ground states: $C_1(0) = 1$, $C_n(0) = 0, n \geq 2$. We have build an exact solution of the problem, which in its compact form can be written as:

$$C_n^1(t) = e^{-i\Omega t + i\phi_{n1}} L_{n-1}^{(-1)}(\gamma_g t/2) \tag{2}$$

here $L_n^{(\alpha)}(x)$ is the generalized Laguerre polynomials of degree n, α. This simple solution gives all the insights on the one-directional transport in quantum chains: (i) *irrelevannce* of the spatial distribution of the emitters along the z-coordinate; (ii) the time evolution of the n-th atom excitation probability has trivial exponentially decaying factor $e^{-\gamma t}$; (iii) finally, the number of local excitation maxima for a particular emitter n equals to the number of emitters positioned before it according to Laguerre's polynomials properties. This dynamics is clearly shown in

11th International Congress on Engineered Material Platforms for Novel Wave Phenomena - Metamaterials 2017
Marseille, France, Aug. 28th - Sept. 2nd 2017

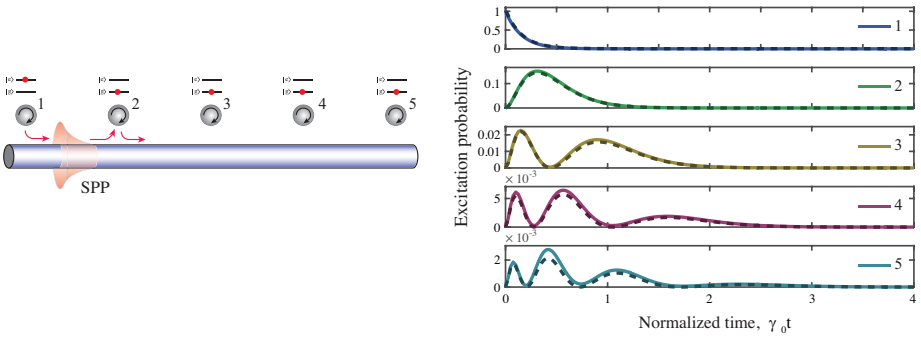

Fig. 2: The probabilities for different emitters to be excited at particular time moments for a chain of $N = 5$ emitters. The solid and dashed lines are for the numerical and analytical results, correspondingly. In the numerical case the parameters are: $\Delta z = 3.75\lambda_{pl}$, $a = \lambda_{pl}$, where λ_{pl} is the wavelength of surface plasmon polariton mode. For the numerical case the probabilities were averaged over 20 distributions of emitters and the distribution is uniform.

Fig. 2 (solid lines) for a chain consisting of $N = 5$ emmiters separated with equal distance Δz and coupled to surface plasmon polariton mode (SPP) of metallic nanowire. The dashed lines correspond to the results obtained with exact numerical model based on a Green's function approach. Good coincidence between two approaches supports the obtained analytical results.

III. Conclusion

In this work we have shown that the chiral coupling significantly influences the properties of light scattering on a chain of two-level quantum systems, resulting in the changing of the scattering losses spectrum. We have obtained the exact analytical solution, showing that the dynamics of single quantum excitation in chirally coupled system is described by the Laguerre polynomials. The behaviour of the chiral TLS system is fully defined by the amplitude of the coupling coefficient of a single emitter with the waveguide mode. From the obtained solution it immediately follows, that unidirectional system possesses the tolerance with respect to the positional disorder.

Acknowledgement

The work was supported by the Russian Foundation for Basic Research projects mol-a-dk 16-32-60167, and mol-a-dk 16-32-60123.

References

[1] H. J. Kimble, *Nature* 453, 1023 (2008).
[2] S. J. P. Kress, F. V. Antolinez, P. Richner, S. V. Jayanti, D. K. Kim, F. Prins, A. Riedinger, M. P. C. Fischer, S. Meyer, K. M. McPeak, D. Poulikakos, and D. J. Norris, *Nano Letters* 15, 6267 (2015).
[3] R. J. Coles, D. M. Price, J. E. Dixon, B. Royall, E. Clarke, P. Kok, M. S. Skolnick, A. M. Fox, and M. N. Makhonin, *Nature Communications* 7, 1 (2016).
[4] F. L. Kien, J. Q. Liang, K. Hakuta, and V. I. Balykin, *Optics Communications* 242, 445 (2004).
[5] E. Vetsch, D. Reitz, G. Sague, R. Schmidt, S. T. Dawkins, and A. Rauschenbeutel, *Physical Review Letters* 104, 203603 (2010).
[6] K. Bliokh, D. Smirnova, and F. Nori, *Science* 348, 6242, 1448-1451 (2015).
[7] T. Mechelen, J. Zubin *Optica* 3, 12, 118–126 (2015).
[8] J. Petersen, J. Volz, A. Rauschenbeutel *Science* 346, 12, 67-71 (2014).
[9] M. Petrov, S. Sukhov, A. Bogdanov, A. Shalin, A. Dogariu *Laser & Photonics Reviews* 10, 1, 116-122, (2016).
[10] D. O'Shea, C. Junge, J. Volz, A. Rauschenbeutel *Phys. Rev. Lett.* 111, 19, 193601 (2013).
[11] N. Corzo, B. Gouraud, A. Changra, J. Laurat *Phys. Rev. Lett.* 117, 13, 133603 (2016).
[12] D. Kornovan, A. Sheremet, M. Petrov *Phys. Rev. B* 94, 245416, 2016 .
[13] D.-G. Welsch, H. Dung, and L. Knoll, *Fortschritte der Physik* 51, 255 (2003)

PHYSICAL REVIEW B **94**, 245416 (2016)

Collective polaritonic modes in an array of two-level quantum emitters coupled to an optical nanofiber

D. F. Kornovan,[1,2,*] A. S. Sheremet,[1,3] and M. I. Petrov[1,2,4]
[1]*ITMO University, Birzhevaya liniya 14, 199034 St. Petersburg*
[2]*St. Petersburg Academic University, 8/3 Khlopina str., 194021 St. Petersburg, Russia*
[3]*Russian Quantum Center, Novaya str. 100, 143025 Skolkovo, Moscow Region, Russia*
[4]*University of Eastern Finland, Yliopistokatu 7, FI-80101 Joensuu, Finland*
(Received 14 August 2016; revised manuscript received 22 November 2016; published 13 December 2016)

In this paper we develop a microscopic analysis of the light scattering on a periodic two-level atomic array coupled to an optical nanofiber. We extend the scattering matrix approach for two-level system interaction with nanofiber fundamental guided mode HE_{11}, which allows us to model the scattering spectra. We support these results by considering the dispersion of the polaritonic states formed by the superposition of the fundamental mode of light HE_{11} and the atomic chain states. To illustrate our approach we start by considering a simple model of light scattering over an atomic array in free space. We discuss Bragg diffraction in the atomic array and show that the scattering spectrum is defined by the nonsymmetric coupling of a two-level system with nanofiber and vacuum modes. The proposed method allows consideration of two-level system interactions with a full account of dipole-dipole interactions via both near fields and long-range interaction owing to nanofiber mode coupling.

DOI: 10.1103/PhysRevB.94.245416

I. INTRODUCTION

Controlling interactions of quantum emitters with optical nanostructures at the single-photon level is a key tool for the realization of quantum technologies [1,2]. Most experimental efforts focus on the reversible mapping of quantum states between light and matter and the implementation of quantum networking protocols using this interaction [3,4]. In this context localization of photonic modes at the nanoscale object opens a feasible route for on-chip quantum communication [5,6] and allows implementation of quantum networking protocols [7,8]. At the same time the evanescent character of the electromagnetic field manifested near a nano-object reveals fundamentally new features of light-matter interactions [9,10]. It is supported by the recent experimental progress in coupling single quantum sources to surface plasmon polaritons [11] and to photonic crystal waveguide modes [12], as well as by the results in neutral atoms trapped in the vicinity of an optical nanofiber [13–15]. The latter system is a versatile platform for achieving efficient light-atom coupling due to the collective nature of atomic interaction with an evanescent field of the single-photon mode [16]. This provides an exceptional opportunity to develop new approaches to the study of optical interactions of quantum many-body systems at the nanoscale level.

From this perspective the interaction between a two-level system and the evanescent field of the photonic mode yields to the formation of mixed polaritonic states with a modified dispersion relation [17,18]. Strong modification of dispersion is observed in a system of coupled plasmonic or dielectric resonators [19–22], which manifest themselves as classically coupled dipole-dipole particles. Nevertheless, considering the cold-atomic system trapped in the vicinity of an optical nanofiber the origin of the polaritonic states and their dispersion is significantly overlooked. The existing theoretical approaches are based on reflection and transmission spectroscopy of an incident fiber mode [23]. Theoretical predictions [24,25], and experimental verification [14] have shown that the spectral distribution of atomic fluorescence is strongly affected by the presence of the nanofiber. This has been experimentally examined [26,27] by detecting Bragg diffraction in the atomic chain. Despite its universality and technical convenience this approach does not clarify the exact picture of atom-atom interaction in the presence of a nanofiber, as it omits the exact details of dipole-dipole coupling. This paper aims to eliminate this gap by considering the eigenstates of the atomic array coupled to the nanofiber modes, which manifest themselves as polaritonic states. We apply the T-matrix method to study the scattering of the nanofiber mode over the constructed polaritonic states. Contrary to the reflectance and transmittance spectroscopy approach, this method can be universally extended to an arbitrary dense atomic array. In order to expose the full picture of the atom-photon interaction, we start our consideration with single-photon scattering at the atomic chain in vacuum and identifying the polaritonic states.

The paper is organized as follows: in Sec. II we describe in detail the theoretical approach to the considered problem in the case of an atomic chain in vacuum and in the vicinity of a nanofiber; in Sec. III we discuss the calculated scattering cross sections and interpret them using a polaritonic band diagram; and in Sec. IV we extend the approach to the case of the nanofiber and observe strong backscattering into the nanofiber mode when the Bragg condition is satisfied.

*newparadigm.dk@gmail.com

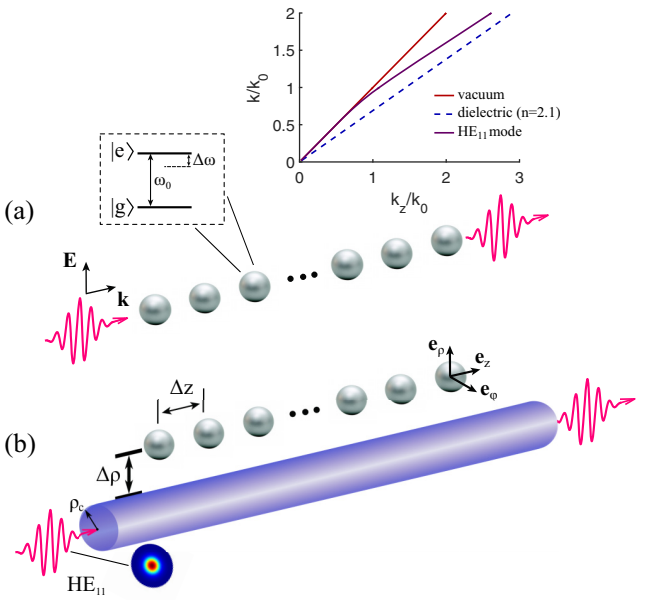

FIG. 1. Light scattering on the 1D array of two-level atoms with period Δz. (a) A single photon with the polarization vector parallel to the dipole moment of the atomic transition scatters and propagates along the atomic chain axis. (b) The scattering of a quasicircularly polarized single photon from the fundamental guided mode HE_{11} on the array of atoms trapped in the vicinity of the optical nanofiber. All atoms are positioned at the same distance $\Delta\rho$ from the fiber surface. Inset: Dispersion of a photon in vacuum (solid red line), dielectric with $n = 2.1$ (dashed blue line), and HE_{11} mode dispersion (solid purple line).

II. THEORETICAL APPROACH

We consider light scattering on a one-dimensional (1D) array of N two-level atoms with period Δz and compare this process for two systems: (i) the atomic chain in vacuum [see Fig. 1(a)] and (ii) the atomic chain in the vicinity of an optical silica nanofiber ($n = 2.1$) [see Fig. 1(b)]. In the first case we consider single-photon scattering with a wave vector directed along the atomic chain, and in the presence of a nanofiber we consider the propagation of a guided light field in the fundamental mode HE_{11} [Fig. 1(b)]. All atoms are placed at the same distance $\Delta\rho = 0.3\lambda_0$ from the fiber surface with radius $\rho_c = 0.25\lambda_0$, which is a typical value for such systems realized experimentally [15,28]. Here λ_0 is the wavelength of the atomic transition.

A. Interaction of a single photon with an atomic chain in a vacuum

In microscopic quantum theory the light scattering process can be described using the standard T-matrix formalism [29]. The total Hamiltonian $\hat{H}$ describing the interaction between propagating light and the atomic chain can be expanded as the sum of the nonperturbed part $\hat{H}_0$ and the interaction term $\hat{V}$ such that $\hat{H} = \hat{H}_0 + \hat{V}$, where

$$\hat{H}_0 = \sum_n \hbar\omega_0 \hat{\sigma}_n^+ \hat{\sigma}_n^- + \sum_\mu \hbar\omega_k \hat{a}_\mu^\dagger \hat{a}_\mu,$$
$$\hat{V} = -\sum_n \hat{\mathbf{d}}_n \hat{\mathbf{E}}(\mathbf{r}_n). \quad (1)$$

Here the interaction part of the Hamiltonian $\hat{V}$ is considered in the dipole approximation, where $\hat{\mathbf{d}}_n$ is the transition dipole moment operator of the nth atom, $\hat{\sigma}_n^+ = |e_n\rangle\langle g_n|$ and $\hat{\sigma}_n^- = |g_n\rangle\langle e_n|$ are raising and lowering atomic operators, $\hat{a}_\mu^\dagger$ ($\hat{a}_\mu$) are the bosonic creation (annihilation) operators, the index μ describes a particular field mode $\mu = (\mathbf{k},s)$, where $\mathbf{k}$ is the wave vector, $s = 1,2$ denotes two orthogonal polarizations, and $\hat{\mathbf{E}}(\mathbf{r}_n)$ is the total microscopic electric-field operator, which can be written as

$$\hat{\mathbf{E}}(\mathbf{r}) = \sum_\mu \sqrt{\frac{2\pi\hbar\omega_k}{\mathbb{V}}}(i\mathbf{e}_\mu \hat{a}_\mu e^{i\mathbf{kr}} + \text{H.c.}), \quad (2)$$

where $\mathbb{V}$ is the quantization volume and $\mathbf{e}_\mu$ is the unit polarization vector.

The T matrix then can be written in the form [29]

$$\hat{T} = \hat{V} + \hat{V}\hat{G}(E + i0)\hat{V}, \quad (3)$$

where $\hat{G}(z) = (z - \hat{H})^{-1}$ is the resolvent operator of the total Hamiltonian. In accordance with the rotating-wave approximation the matrix elements of the $\hat{T}$ operator can be found as a projection onto the Hilbert subspace of the vacuum state for the field subsystem and the single excited state for the atomic subsystem,

$$\hat{P}\hat{G}(E)\hat{P} = \hat{P}\,\frac{1}{E - \hat{H}_0 - \hat{\Sigma}(E)}\,\hat{P}, \quad (4)$$

where we have defined the projector operator as follows:

$$\hat{P} = \sum_{n=1}^{N} |g_1,\ldots,e_n,\ldots,g_N;\{0_\mu\}\rangle\langle\{0_\mu\};g_1,\ldots,e_n,\ldots,g_N|. \quad (5)$$

In Eq. (4) we introduced the level-shift operator $\hat{\Sigma}$ [29]. The form of this operator can be found as perturbative series in powers of $\hat{V}$.

At the lowest order of the perturbation theory the operator $\hat{\Sigma}$ can be described by two contributions corresponding to single-particle and the double-particle interactions [30]. The single-particle contribution leads to the Lamb shift and the finite lifetime of the atomic excited state, while the double-particle contribution is responsible for the excitation transfer between atoms.

Here we work in the resonant approximation, which allows consideration of the scattering of a photon with a carrier frequency ω close to the atomic transition frequancy ω_0. In this approximation $\hat{\Sigma}(E)$ is assumed to be a slowly varying function of the argument so that $\hat{\Sigma}(E) \approx \hat{\Sigma}(E_0)$. The single- and

double-particle contributions can be written as

$$\Sigma^{(nn)}(E_0) = \hbar\Big(\Delta_L - i\frac{\gamma_0}{2}\Big),$$
$$\Sigma^{(mn)}(E_0) = -\mathbf{d}_m^*\Bigg[\frac{e^{ikR}}{R}\Bigg(\Big(1+\frac{ikR-1}{k^2R^2}\Big)\mathbf{I} + \frac{\mathbf{R}\otimes\mathbf{R}}{R^2}\cdot\frac{3-3ikR-k^2R^2}{k^2R^2}\Bigg)\Bigg]\mathbf{d}_n, \quad (6)$$

where Δ_L is the Lamb shift, γ_0 is the spontaneous emission rate, $k=\omega/c$ is the wave number of a vacuum photon, $R=|\mathbf{r_m}-\mathbf{r_n}|$ is the distance between atom m and atom n, $\mathbf{I}$ is the unit dyad, and $\otimes$ stands for the outer product.

Once the operator matrix $\hat{\Sigma}$ is computed we can construct the denominator in (4) and, by inverting it, obtain the matrix for the projected resolvent and the T matrix. We are interested in the scattering of the photon back into the same field mode, which is an elastic scattering channel, corresponding to the diagonal matrix element of the T matrix $T_{ii}(E)$.

In the case of a vacuum, this matrix element is connected to the total scattering cross section according to the optical theorem [30,31]: $\sigma_{\text{tot}}(E)\sim \text{Im}T_{ii}(E)$. In the presence of a nanofiber this exact formula for the total scattering cross section is not applicable. We introduce the quantity, which shows the enhancement of the scattered energy in a chain of N atoms, compared to the maximal energy scattered on a single atom,

$$\sigma_N(E) = \frac{\text{Im}\ T_{ii}^{(N)}(E)}{\text{Im}\ T_{ii}^{(1)}(E_{\text{res}})}, \quad (7)$$

where $\text{Im}T_{ii}^{(1)}(E_{\text{res}})$ corresponds to a resonant value of the T matrix for a single photon scattering off a single atom.

B. Interaction of a guided light with an atomic chain in the presence of a nanofiber

However, to correctly take into account the optical fiber we need to modify the approach discussed in Sec. II A, and we do this in two steps. First, we need to modify the "outer" operators $\hat{V}$ in Eq. (3), which are responsible for the absorption of the incoming guided photon and emission of the photon back into the same field mode. To describe the field subsystem at this step we use the quantization scheme proposed in [32], where the quantized electric field of the guided mode of the nanofiber can be written as

$$\hat{\mathbf{E}}(\mathbf{r}) = \sum_\mu \mathbf{E}_\mu(\mathbf{r})\hat{a}_\mu + \text{H.c.}, \quad (8)$$

where $\mathbf{E}_\mu$ is the electric field of the guided mode μ:

$$\mathbf{E}_\mu(\mathbf{r}) = i\sqrt{\frac{2\pi\hbar\omega_\mu}{\mathbb{L}}}\tilde{\mathbf{E}}_\mu(\rho,\phi)e^{if\beta_\mu z+im\phi}. \quad (9)$$

Here β_μ is the propagation constant, $\tilde{\mathbf{E}}_\mu(\rho,\phi)$ is the amplitude of the electric field, $\mathbb{L}$ is the quantization length, the index $\mu=(\beta_l,f,m)$ describes a particular guided mode, and f and m define the direction of propagation $(+1/-1)$ and the mode angular momentum $(+1/-1)$, respectively. The electric field is periodic in the z direction and the periodicity condition can be written as $\beta_l\mathbb{L}=2\pi l$, where l is a positive integer number. The electric-field amplitude is normalized according to

$$\int_0^{2\pi}\int_0^\infty |\tilde{\mathbf{E}}_\mu(\rho,\phi)|^2 d\phi\rho d\rho = 1. \quad (10)$$

At the next step, we need to calculate the matrix elements of the operator $\hat{\Sigma}$ in the presence of a nanofiber. To account for the excitation transfer between atoms through the radiation of vacuum modes and modes of the nanofiber, we need to introduce the proper quantum-electrodynamical description of the electromagnetic field, which was developed by Welsch *et al.* in Ref. [33]. Using this formalism we can modify Hamiltonian (1) to describe our system as

$$\hat{H}_0 = \sum_n \hbar\omega_0\hat{\sigma}_n^+\hat{\sigma}_n^- + \int d\mathbf{r}'\int_0^\infty d\omega'\hbar\omega'\hat{\mathbf{f}}^\dagger(\mathbf{r}',\omega')\hat{\mathbf{f}}(\mathbf{r}',\omega'),$$
$$\hat{V} = -\sum_n \hat{\mathbf{d}}_n\hat{\mathbf{E}}(\mathbf{r}_n), \quad (11)$$

where ω_0 is the atomic transition frequency, $\hat{\mathbf{E}}(\mathbf{r}_n)$ is the total electric field, and $\hat{\mathbf{f}}(\mathbf{r}'\omega')$ and $\hat{\mathbf{f}}^\dagger(\mathbf{r}',\omega')$ are the bosonic vector local-field operators, which obey the following commutation relations:

$$[\hat{f}_i(\mathbf{r}',\omega'),\hat{f}_k^\dagger(\mathbf{r},\omega)] = \delta_{ik}\delta(\mathbf{r}'-\mathbf{r})\delta(\omega'-\omega),$$
$$[\hat{f}_i(\mathbf{r}',\omega'),\hat{f}_k(\mathbf{r},\omega)] = 0. \quad (12)$$

The positive-frequency part of the total electric field has the form

$$\hat{\mathbf{E}}^+(\mathbf{r}) = i\sqrt{4\hbar}\int d\mathbf{r}'\int_0^\infty d\omega'\frac{\omega'^2}{c^2}\sqrt{\varepsilon_I(\mathbf{r}',\omega')} \times \mathbf{G}(\mathbf{r},\mathbf{r}',\omega')\hat{\mathbf{f}}(\mathbf{r}',\omega'), \quad (13)$$

where $\varepsilon_I(\mathbf{r}',\omega')$ is the imaginary part of the dielectric permittivity of the media and $\mathbf{G}(\mathbf{r},\mathbf{r}',\omega')$ is the classical Green's tensor of the electric field. In the presence of the optical fiber the Green's tensor can be expanded into

$$\mathbf{G}(\mathbf{r},\mathbf{r}',\omega) = \mathbf{G}_0(\mathbf{r},\mathbf{r}',\omega) + \mathbf{G}_s(\mathbf{r},\mathbf{r}',\omega), \quad (14)$$

where $\mathbf{G}_0$ is the vacuum Green's tensor and $\mathbf{G}_s$ is the Green's tensor corresponding to the light scattering from the fiber. The scattering term of the Green's tensor can be expanded into the vector wave functions (WVFs), and the details of these calculations are given in the Appendix. At the lowest nonvanishing order the matrix elements of the level-shift operator in this case can be written as

$$\langle f|\hat{\Sigma}(E)|i\rangle = \sum_{|\alpha\rangle,|\beta\rangle}\langle f|\hat{V}|\alpha\rangle\langle\alpha|\frac{1}{E-\hat{H}_0+i\eta}|\beta\rangle\langle\beta|\hat{V}|i\rangle, \quad (15)$$

where $|i\rangle$ and $|f\rangle$ are the initial and final states of the system, respectively, $|\alpha\rangle$ and $|\beta\rangle$ are the two possible intermediate states with a single elementary excitation for the field subsystem, and both atoms are in either the excited or the ground state:

$$|e_n,e_m\rangle\times\hat{\mathbf{f}}^\dagger(\mathbf{r}',\omega')|\{0\}\rangle,$$
$$|g_n,g_m\rangle\times\hat{\mathbf{f}}^\dagger(\mathbf{r}',\omega')|\{0\}\rangle. \quad (16)$$

The derivation of these matrix elements of the level-shift operator can be found elsewhere [34,35] and here we provide only the final expression:

$$\langle f|\hat{\Sigma}(E)|i\rangle = -4\pi\frac{\omega_0^2}{c^2}\mathbf{d}_m^*\mathbf{G}(\mathbf{r}_m,\mathbf{r}_n,\omega_0)\mathbf{d}_n. \quad (17)$$

We should note that in the case of a single-particle contribution, where $|i\rangle = |f\rangle$ and, thus, $\mathbf{r}_n = \mathbf{r}_m$, the homogeneous part of the Green's function has a singularity in the real part $\mathrm{Re}[\mathbf{G}_0(\mathbf{r}_n,\mathbf{r}_n,\omega_0)] \to \infty$ which corresponds to the infinite Lamb shift due to the interaction with the vacuum modes. This term is renormalized and can be thought of as already incorporated into the definition of the transition frequency of atomic dipoles ω_0. However, $\mathrm{Re}[\mathbf{G}_s(\mathbf{r}_n,\mathbf{r}_n,\omega_0)]$ is finite and it leads to the presence of a Lamb shift due to the interaction of the excited atom with the fiber modes.

Now using (17) we can find the matrix $\Sigma(E)$, the T-matrix elements, and, consequently, the normalized scattering losses $\sigma_N(E)$. In this case when calculating the denominator of Eq. (7) the atom is placed at the same distance $\Delta\rho$ from the fiber surface as atoms in our periodic chain. Also, we note that E_{res} now differs from $\hbar\omega_0$ because of the Lamb shift.

III. RESULTS: ATOMIC CHAIN IN A VACUUM

We consider photon scattering in an atomic chain in vacuum in the geometry shown in Fig. 1(a). In this case we assume that the dipole moments of the atoms are aligned parallel to photon polarization.

We have applied the T-matrix approach to plot the spectra of the scattering cross section for different interatomic distances. The scattering intensity is shown in Fig. 2. One can note that it changes in a nonmonotonous way as the distance between the atoms varies. The most pronounced changes are observed when the period is approximately $m\lambda_0/2$, where m is an integer. For instance, changing the interatomic distance from $\Delta z = 0.49\lambda_0$ to $\Delta z = 0.55\lambda_0$ results in a decrease in the intensity and a widening of the peak. A similar but much weaker effect is observed when the distance is changed from $0.95\lambda_0$ to $1.05\lambda_0$. This behavior is related to the opening of the diffraction channels each time the Bragg condition is satisfied. On the other hand, this process can be easily understood by analyzing the eigenstates of the atomic system, which manifest themselves in polaritonic states.

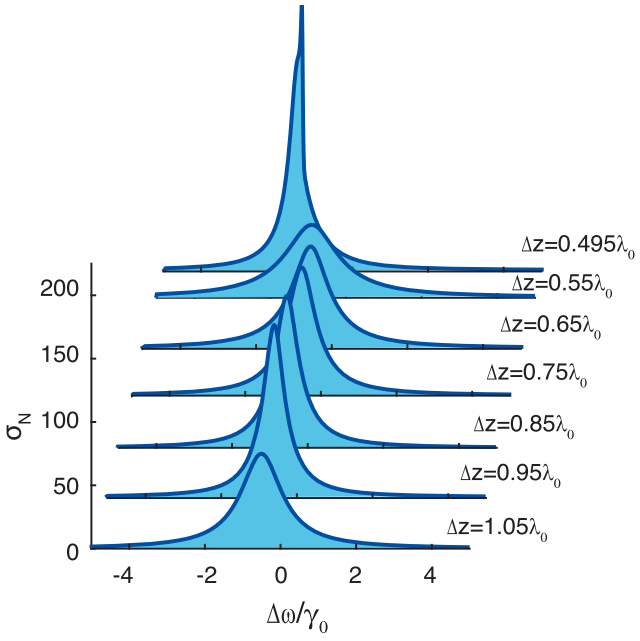

FIG. 2. Normalized total scattering cross section's dependence on photon frequency detuning $\Delta\omega = \omega - \omega_0$ for different periods of chain Δz in vacuum. The dipole transition is oriented parallel to the field polarization $\mathbf{d}||\mathbf{E}$. The number of atoms is $N = 100$.

A. Polaritonic states in an atomic chain

Polaritonic states can be constructed by defining the eigenstates of the level-shift operator, which is, in our approximation, the operator of dipole-dipole atomic coupling. In the limit of resonant excitation the eigenproblem can be formulated as follows:

$$\Sigma(\omega_0)\mathbf{v} = \mathcal{E}\mathbf{v}. \quad (18)$$

Here $\Sigma(\omega_0)$ is the matrix representation of the level-shift operator. The solution of this equation gives us N complex eigenvalues $\mathcal{E}_i = \hbar\omega_i$ and column eigenvectors $\mathbf{v}_i$, which are the energies and eigenstates of the system described in the basis of states with a single atomic excitation. We utilize the solution of a finite eigensystem to plot the dispersion curve for an infinite chain [19,36]. A problem of this type was also considered for one- and two-dimensional structures with excitons in [37], but formulated in a self-consistent way, where the energy dependence of $\Sigma(\omega)$ is kept. In our case, we calculate $\Sigma(\omega)$ at frequency ω_0, which is a simplification giving adequate results [4,36].

For this we correlate the eigenvector with the corresponding wave number k_z enumerating the eigenstates in accordance with the number of nodes l in the profile of the eigenmode $\mathbf{v_i}$. Then we can assign the corresponding wave number k_z to each mode according to

$$\frac{k_z^{(l)}}{K} = \frac{(l+1)}{2N}, \quad (19)$$

where $K = 2\pi/\Delta z$ is the reciprocal lattice vector of a periodic chain and $l = 0,1,2,\ldots$ is the mode number. For $l = 0$ relation (19) gives $\lambda_l = 2Nd$, so there is a single antinode in the profile of this fundamental mode, while for $l = N-1$ we have $\lambda_l = 2d$, and therefore, the neighboring atoms are exactly out of phase for this mode.

This procedure allows us to plot both the real and the imaginary parts of the eigenfrequencies of our system as functions of k_z, where the real part accounts for the dispersion of normal modes and the imaginary part describes radiative losses or the inverse lifetimes of the eigenstates.

In order to support the scattering cross-section spectra shown in Fig. 2 we illustrate the light interaction with the atomic chain by plotting the dispersion curves for transversal ($\mathbf{d} \perp \mathbf{e_z}$) polaritonic states (see Fig. 3). We consider subdiffractional ($K > 2k_0$) [Fig. 3(a)] and diffractional ($K < 2k_0$) [Fig. 4(b)] regimes, where the first Bragg condition is satisfied. The light line, which is vertical on the scale of the polaritonic bandwidth as $\gamma_0 \ll \omega_0$, divides the states into radiative and

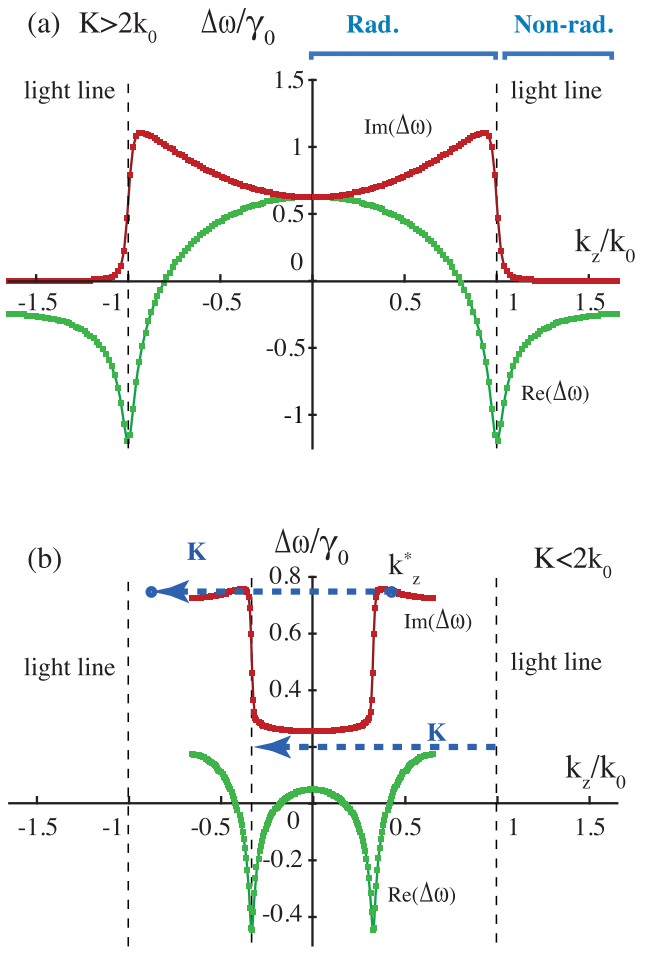

FIG. 3. Real (green curve) and imaginary (red curve) parts of the eigenfrequencies of the transversal polaritonic states with $\mathbf{d} \perp \mathbf{e_z}$ versus the corresponding k_z values for (a) the sub-diffractional case $K > 2k_0$ ($\Delta z = 0.3\lambda_0$) and (b) the diffractional case $K < 2k_0$ ($\Delta z = 0.75\lambda_0$). The dispersions of the vacuum photon modes (light line) are shown by dashed horizontal lines. Regions of radiative and nonradiative states are marked.

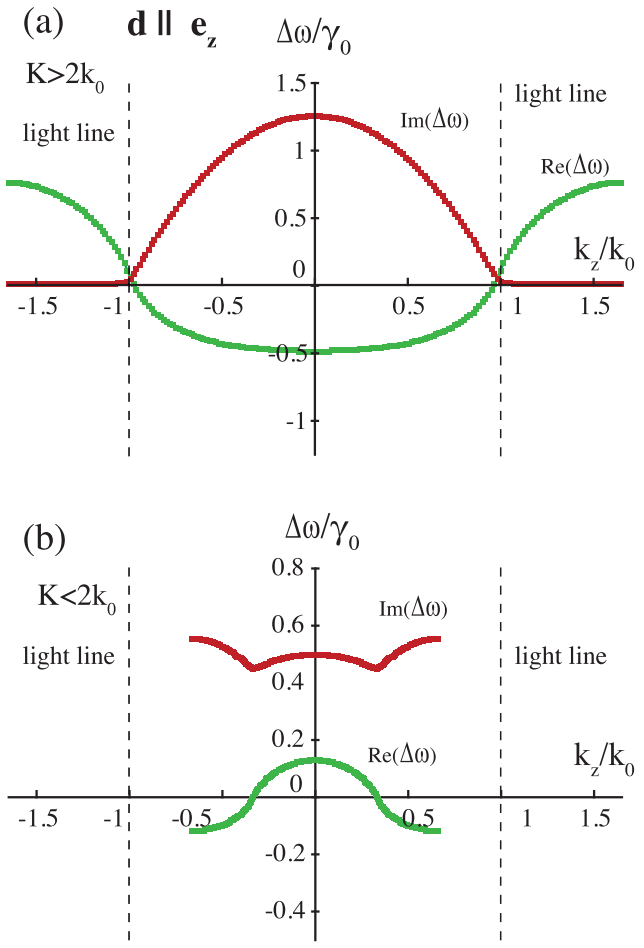

FIG. 4. Real (green curve) and imaginary (red curve) parts of the eigenfrequencies of the longitudinal polaritonic states with $\mathbf{d} \parallel \mathbf{e_z}$ versus the corresponding k_z values for (a) the subdiffractional case $K > 2k_0$ ($\Delta z = 0.3\lambda_0$) and (b) the diffractional case $K < 2k_0$ ($\Delta z = 0.75\lambda_0$). The dispersions of the vacuum photon modes (light line) are shown by dashed horizontal lines.

nonradiative ones. In the vicinity of point $k_z = k_0$ the atomic states undergo hybridization with vacuum photon modes. For the diffractional case [see Fig. 3(b)], all the eigenmodes become radiative as they appear above the light line. However, one should note that hybridization features are preserved but are shifted from the light line for quantity K, as the wave vector k_z is a quasivector of the polaritonic state and is conserved up to a reciprocal vector. Moreover, states near the band edges ($k_z > K - k_0$) become more radiative than states in the band center, as they have two channels of radiation: they can emit (i) a photon with $k_z^{\mathrm{ph}} = k_z^*$ and (ii) a photon with $k_z^{\mathrm{ph}} = k_z^* - K$.

The dispersion of the longitudinal modes ($\mathbf{d} \parallel \mathbf{e_z}$), similarly to the transversal modes, can also be divided into radiative and nonradiative regions (see Fig. 4). However, hybridization with the vacuum modes in the vicinity of the light line is not observed due to polarization mismatch: the vacuum modes have transversal polarization and the polaritonic excitations are longitudinal.

B. Bragg diffraction

The plotted dispersion curves clarify the character of the cross-section spectra shown in Fig. 2, in particular, the opening of the first Bragg diffraction channel when the period changes from $\Delta z = 0.49\lambda_0$ to $\Delta z = 0.51\lambda_0$. The k_z component of the incident photon equals k_0 according to Fig. 1(a), and for the subdiffractional regime the scattering occurs on states near the light line $k_z \approx k_0$ [see Fig. 5(b)]. In the subdiffractional regime, when $k_0 \lesssim K/2$ these states have low losses, which generates a narrow cross-section spectrum shape [see solid line in Fig. 5(a)]. After switching to the diffractional regime $k_0 \gtrsim K/2$ the incident photon scatters off states with $k_z = k_0 - K$ (umklapp process) as shown in Fig. 5(c). Due to the high radiative losses connected to free-space diffraction the cross-section spectrum is wide [see dashed line in Fig. 5(a)].

IV. RESULTS: ATOMIC CHAIN IN THE VICINITY OF AN OPTICAL NANOFIBER

The presence of an optical nanofiber changes the character of atomic interaction and allows long-range dipole-dipole

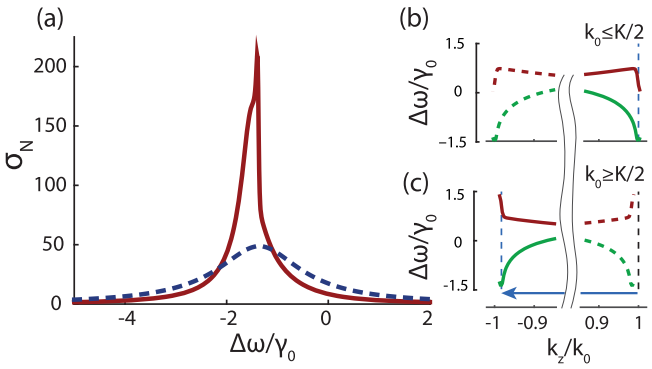

FIG. 5. Illustration of the diffraction channel opening in the photon scattering on a two-level atomic array in vacuum. (a) Scattering cross sections for two chain periods: $K \gtrsim 2k_0$ ($\Delta z = 0.49\lambda_0$) (solid red line) and $K \lesssim 2k_0$ ($\Delta z = 0.51\lambda_0$) (dashed blue line). (b, c) Dispersion curves (green) and inverse lifetimes (red curves) of these states in the region close to the situations shown in (a). The number of atoms is $N = 100$.

coupling between atoms not only via the vacuum, but also through the guided mode. To study this effect and its influence on the scattering of the guided mode over an atomic chain, we have applied the T-matrix method. In contrast to the commonly used transfer matrix method, where the interaction of the guiding mode with each atom is treated individually [26,38], here we consider the scattering on collective polaritonic states taking account of the full atomic dipole-dipole interaction and splitting their energy levels. For this we start by building the eigenstate picture of the atomic system with an optical nanofiber.

A. Dispersion of polaritonic states

The polaritonic dispersion relation in the presence of an optical nanofiber can be found from the eigenstates of the system, (18), but with the corrected level-shift operator, which includes interaction with the nanofiber by means of the scattering Green's function in Eq. (14). The real and imaginary parts of eigenfrequencies versus the corresponding k_z values are plotted in Fig. 6 for transverse $\mathbf{d} \parallel \mathbf{e}_\rho$ modes. The parameters of the nanofiber are chosen in such a way that it supports only one fundamental mode HE_{11} at the frequency of the atomic transition ω_0. The fiber mode dispersion curve is shown by the dash-dotted line in Fig. 6, in addition to the vacuum photon line, shown by the dashed line. In the subdiffractional regime $K > 2k_0$ the nanofiber interaction channel gives an anticrossing-like feature in the polaritonic dispersion in the vicinity of $k_z = k_0^f$, where k_0^f denotes the wave vector of the wave guiding photon having frequency ω_0. The nanofiber modifies the nonradiative atomic states and forms nanofiber coupled polaritonic states [see Fig. 6(a)]. These states are situated close to radiative states as the wave vector of the fundamental guided mode is close to the wave vector of the vacuum photon $|k_0 - k_0^f| \ll k_0$ (see Fig. 1). The peak in the spectrum of the imaginary frequency at $k_z = k_0^f$ is related to the leakage of the state through the fiber mode. For the diffractional regime $K < 2k_0$ [see Fig. 6(b)], all states

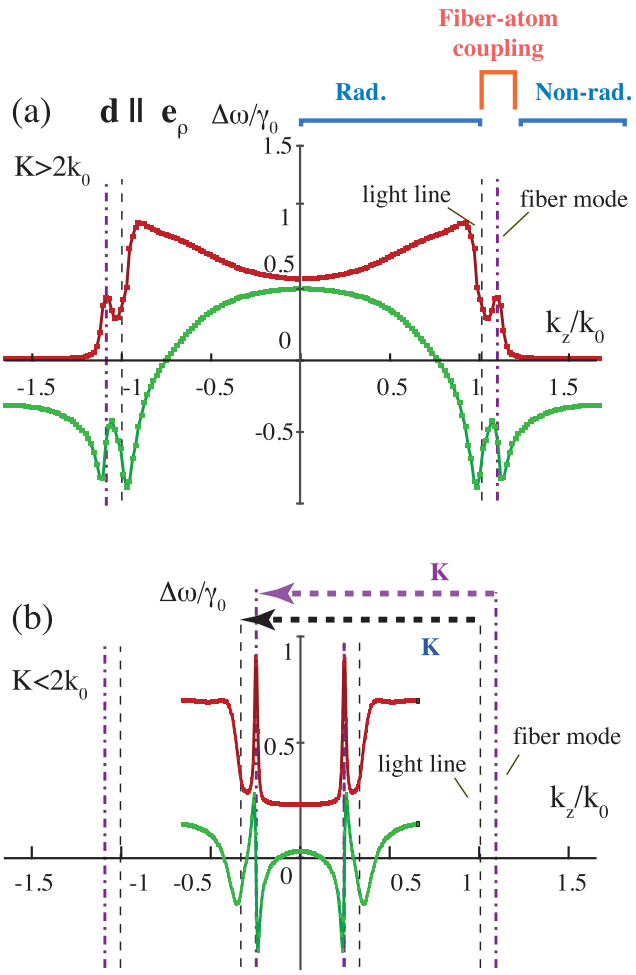

FIG. 6. Real (green curve) and imaginary (red curve) parts of the eigenfrequencies of the transversal polaritonic states with $\mathbf{d} \parallel \mathbf{e}_\rho$ versus the corresponding k_z values for (a) the subdiffractional case $K > 2k_0$ ($\Delta z = 0.3\lambda_0$) and (b) the diffractional case $K < 2k_0$ ($\Delta z = 0.75\lambda_0$). The dispersion of vacuum photon modes (light line) are shown by dashed black lines. The dispersion of the nanofiber fundamental mode HE_{11} is shown by the dash-dotted purple line. Regions of radiative, nonradiative, and strong coupling to the nanofiber mode states are shown. The number of atoms is $N = 100$, the nanofiber radius is $\rho_c = \lambda_0/4$, and the distance from the fiber surface is $\Delta\rho = 0.3\lambda_0$.

become radiative and there is resonant anticrossing coupling to the guided mode of the fiber at $\pm k_0^f \mp K$ along with the vacuum mode coupling at $\pm k_0 \mp K$.

The field of the fundamental fiber mode HE_{11} has all three components of the electric field, thus, in general all of them contribute to the dipole-dipole interaction. For completeness of consideration we have plotted the other two polarizations of the dipole moments of the atomic transition: the azimuthal transversal ($\mathbf{d} \parallel \mathbf{e}_\varphi$) and longitudinal ($\mathbf{d} \parallel \mathbf{e}_z$) polarizations are shown in Fig. 7. The dispersion of azimuthal modes is similar to that of radial modes but has a weaker interaction with the fiber mode due to the weaker amplitude of the azimuthal component of the electrical field in the fiber mode. The longitudinal modes fully resemble the longitudinal modes in

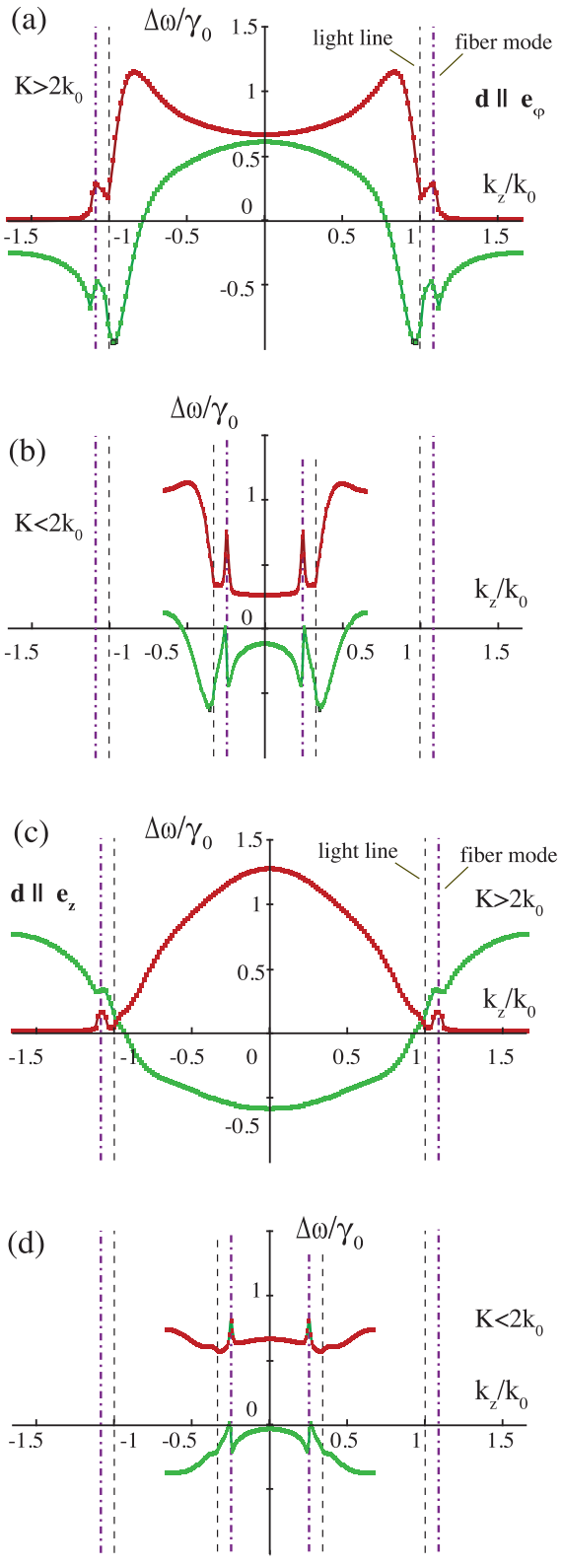

FIG. 7. Real (green curve) and imaginary (red curve) parts of the eigenfrequencies of transversal polaritonic states with $\mathbf{d} \parallel \mathbf{e}_\varphi$ (a, b) and longitudinal states with $\mathbf{d} \parallel \mathbf{e}_z$ (c, d) versus the corresponding k_z values. (a, c) Subdiffractional case $K > 2k_0$ ($\Delta z = 0.3\lambda_0$); (b, d) diffractional case $K < 2k_0$ ($\Delta z = 0.75\lambda_0$). Parameters and notation are the same as in Fig. 6.

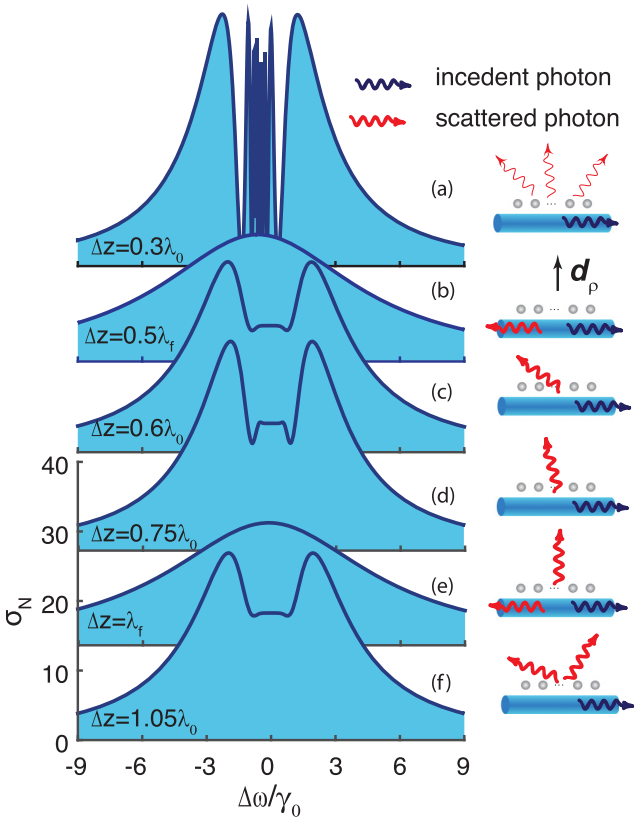

FIG. 8. Normalized scattering loss spectra of a two-level atomic chain consisting of $N = 200$ atoms in the vicinity of the nanofiber for different periods Δz: (a) $0.3\lambda_0$, (b) $0.5\lambda_f$, (c) $0.6\lambda_0$, (d) $0.75\lambda_0$, (e) λ_f, and (f) $1.05\lambda_0$. The nanofiber radius is $\rho_c = \lambda_0/4$, and the distance from the fiber surface is $\Delta\rho = 0.3\lambda_0$.

vacuum, with the fiber mode interaction being weaker than for the transversal modes. However, there is no coupling of atoms with the vacuum field due to polarization mismatch, but atoms are interacting with the fiber mode [see Figs. 7(c) and 7(d)], as the HE_{11} mode is not fully transversal and has a nonzero z component of the electric field, which makes its contribution to the interaction constant.

B. Fiber-mode scattering

We have analyzed the scattering of the fundamental fiber mode HE_{11} by the atomic chain in subdiffractional and diffractional regimes as shown in Fig. 8. We consider all atoms having only the $\mathbf{d}_\rho$ component of dipole transition matrix elements, which corresponds to Fig. 6. The presence of the nanofiber makes the system effectively 1D, which leads to significant changes in the normalized scattering loss spectra compared to the vacuum case. We plot the normalized scattering loss, (7), spectrum, which corresponds to the probability of a single photon's escaping from the guided mode after interaction with the atomic chain.

One can see in Fig. 8 that for the subdiffractional regime the spectrum is modulated by sharp resonances in the vicinity of the atomic resonant frequency ω_0. These resonances correspond to scattering on states with $k_z \approx k_f$ having low

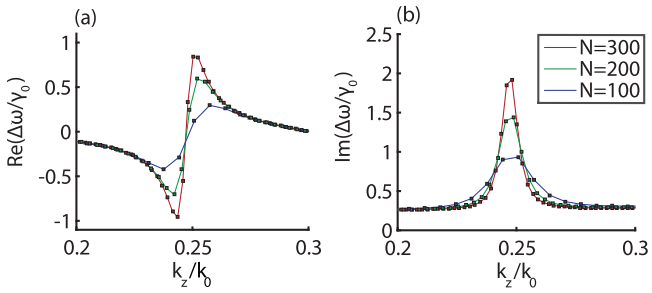

FIG. 9. (a) Real and (b) imaginary parts of eigenfrequencies for the transverse collective modes ($\mathbf{d}||\mathbf{e}_\rho$) versus k_z for a chain with period $\Delta z = 0.75\lambda_0$ and a varying number of atoms N. The nanofiber radius is $\rho_c = \lambda_0/4$, and the distance from the fiber surface is $\Delta\rho = 0.3\lambda_0$.

losses, though these states are below the light line so they have a finite radiational lifetime due to the finite length of the chain [see Fig. 6(a)]. When the Bragg condition $\Delta z = 0.5\lambda_f$ is satisfied the spectrum becomes purely Lorentzian, which is defined by the existing highly radiative state of the atomic system, and the main channel is backscattering into the guided mode, propagating in the direction opposite the incident.

The scattering process for $K < 2k_0$ goes through the umklapp process, as shown in Fig. 6(b) by the dashed purple arrow, and corresponds to a vacuum diffraction with a specific k_z. The scattering spectrum acquires a constant region in its central part, with the oscillatory features at the edges as shown in Fig. 8. A further increase in the chain period results in an almost-periodic change in the normalized scattering loss spectra, and, in particular, when $\Delta z = \lambda_f$ ($K = k_f$) we have a Bragg condition of the second order and backscattering into the guided mode with $k_z = -k_f$.

C. Collective coupling of eigenmodes

As pointed out before, the presence of a nanofiber leads to long-range coupling through the guided mode, and with increasing period Δz the features of dispersions and radiation losses near the fiber-mode line are preserved (Figs. 6 and 7). The long-range coupling makes the observed effects purely collective, which results in an increased coupling strength between the collective mode and the guided mode with an increasing number of two-level systems. In particular, the amplitudes of radiation losses peak, related to the imaginary part of the eigenfrequencies, and the splitting of the collective state energy, related to the real part of eigenfrequencies, are shown in Fig. 9 for different numbers of atoms in the chain. One can see that the resonant features becomes more pronounced for larger total numbers of emitters N.

V. DISCUSSION

The normalized scattering loss spectra plotted in Fig. 8 have two qualitatively distinct profiles: (i) a Lorentzian shape profile if the condition of the fiber Bragg diffraction is satisfied [see Figs. 8(b) and 8(e)] and (ii) a profile with a notch in the middle of the spectrum [see Figs. 8(a), 8(c), 8(d), and 8(f)]. The Bragg diffraction is associated with the scattering on the highly radiative state which appears at the edge of the band, similarly to the case shown in Fig. 5. The incident photon is scattered by the radially oriented dipole moment back into the guided mode of the nanofiber. However, for the other periods the photon is diffracted in the cone with a fixed angle, defined by the condition $k_z = k_f - K$ as shown schematically in the right column in Fig. 8.

We associate the change in the spectrum shape with the switching of the diffraction from symmetric (in the case of diffraction into the fiber mode) to asymmetric (diffraction into the vacuum modes) scattering. Asymmetry in photon emission by an excited atom in the vicinity of a nanofiber has been actively discussed recently [38–40]. In particular, it was shown [38] that an atom with transversal and longitudinal components of the dipole moment has asymmetry in forward and backward spontaneous emission rate into the nanofiber mode. This results in asymmetry of the single-atom reflectance of the wave-guding mode propagating in the forward or backward direction, also known as the spin-locking effect [10]. On account of this, in the case of an asymmetric emission rate the Bragg reflection is suppressed and a notched reflectance spectrum [38] is observed. The asymmetry in the case shown in Figs. 8(a), 8(c), 8(d), and 8(f) can be explained by the

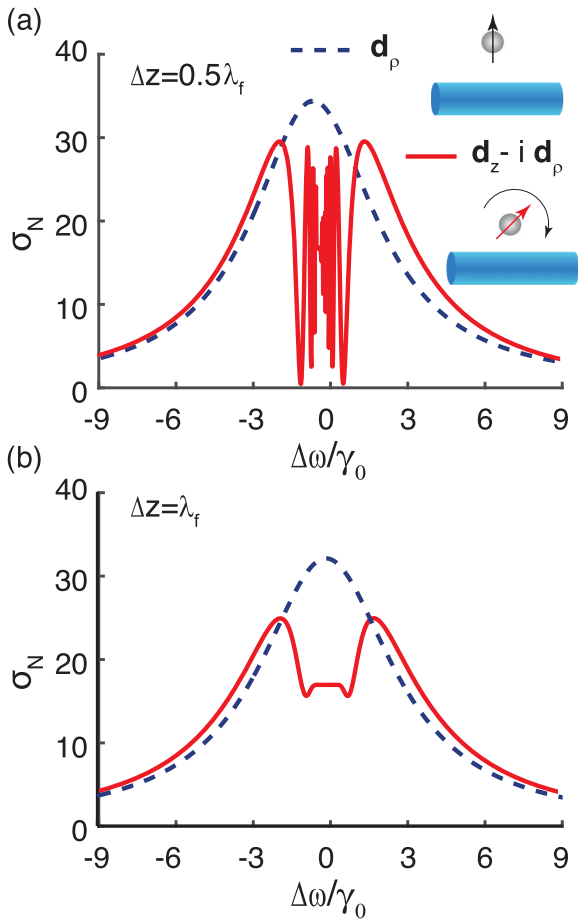

FIG. 10. Normalized scattering loss spectra of the atomic chain consisting of $N = 200$ atoms with radially polarized (dashed line) and σ_+ polarized dipole moments (solid red line) in the regime of (a) the first ($\Delta z = 0.5\lambda_f$) and (b) the second ($\Delta z = \lambda_f$) fiber Bragg diffraction. Parameters are the same as in Fig. 8.

asymmetry in the emission rate of the collective polaritonic states into the vacuum and fiber mode. When the scattering goes back into the fiber mode exactly at the Bragg resonance the symmetry is conserved, but at the vacuum diffraction this symmetry breaks. To support this statement we compared scattering of the incident photon on atoms with (i) a radial component of the dipole moment $\mathbf{d_0}$ and (ii) a σ_+ polarized dipole having both a radial $\mathbf{d}_\rho$ and a z component $\mathbf{d}_z$. In the latter case the two components have $\pi/2$ phase shift but the absolute dipole moment equals $|\mathbf{d}_\rho - i\mathbf{d}_z|/\sqrt{2} = d_0$. Contrary to the radially polarized atom the σ_+ atom has thea strong asymmetry in coupling with the forward- and backward-propagating fiber mode [41]. We have made the calculation for the fiber backscattering regime, where the symmetry should be conserved for the linearly polarized atom but not for the circularly polarized atom. In Fig. 10 the normalized scattering loss spectra are shown for the case of the first and second fiber Bragg resonance in the case of radially polarized atoms (dashed line) and in the case of σ_+ atoms. We see pronounced switching from the Lorentzian spectral shape to a notched shape. For the first fiber Bragg condition $\Delta z = 0.5\lambda_f$ [see Fig. 10(a)], one can see sharp peaks in the center of the band due to scattering by the long-lived collective atomic states. In the case of the second Bragg resonance [see Fig. 10(b)] the sharp peaks are smeared out as all the polaritonic states are above the light cone and, thus, have high losses.

VI. CONCLUSIONS

In this work we have considered a single photon scattering on an ordered finite chain of two-level atoms embedded in a vacuum or trapped in the vicinity of a single-mode dielectric nanofiber. We have developed the scattering matrix technique and analyzed the normalized scattering loss spectrum of a single photon in the presence of a nanofiber. This approach allows us to incorporate the atomic dipole-dipole interactions both via vacuum near fields and via long-range coupling through the guided mode. To support the results of our simulations we have constructed the polaritonic states of the interacting atomic array both in vacuum and close to the nanofiber, which has not been done before for the type of quantum system considered. The obtained dispersion curves for the polaritonic states allowed us to interpret the results of the normalized scattering loss calculations and demonstrated the effects of atomic array coupling with a single guided mode of the nanofiber. Finally, we have shown that the photon scattering over an atomic chain in the presence of a nanofiber is influenced by the effects of spin-locking coupling of atoms with nanofiber and vacuum modes. The proposed approach, which combines construction of the polaritonic eigenstates of the atomic system with the quantum scattering theory, can be effectively applied to modeling experiments on the light interaction with quantum systems at the nanoscale level.

ACKNOWLEDGMENTS

This work was supported by Russian Ministry of Science and Education Project No. RFMEFI58416X0018. M.I.P. acknowledges support from Academy of Finland Grant No. 288591. A.S.S. acknowledges the ITMO Fellowship and Visiting Professorship Program for financial support.

APPENDIX: GREEN'S TENSOR

In order to obtain the Σ^{mn} matrix elements we need to construct the Green's tensor of the system, which can be found from

$$\left[-\frac{\omega^2}{c^2}\varepsilon(\mathbf{r},\omega) + \nabla\times\nabla\times\right]\mathbf{G}(\mathbf{r},\mathbf{r}',\omega) = \mathbf{I}\delta(\mathbf{r}-\mathbf{r}'), \quad \text{(A1)}$$

where $\varepsilon(\mathbf{r},\omega)$ is the complex dielectric function and $\mathbf{I}$ is the unit dyad. In our case we consider a dielectric cylindrical wave guide of radius ρ_c and dielectric permittivity ε being constant inside the cylinder. To find the solution we apply the scattering superposition method [35,42], which allows us to expand the Green's tensor into homogeneous and inhomogeneous terms:

$$\mathbf{G}(\mathbf{r},\mathbf{r}',\omega) = \mathbf{G}_0(\mathbf{r},\mathbf{r}',\omega) + \mathbf{G}_s(\mathbf{r},\mathbf{r}',\omega). \quad \text{(A2)}$$

As soon as we consider atomic dipoles in the vicinity of the wave guide, so that $\mathbf{r}$ and $\mathbf{r}'$ are outside the cylinder, the homogeneous term is always present and describes the field generated directly by the source placed at point $\mathbf{r}'$ at field point $\mathbf{r}$. This term can be obtained analytically from the Green tensor written in Cartesian coordinates using the transformation from Cartesian to cylindrical coordinates $\mathbf{S}(\phi)\mathbf{G}_0^{\mathrm{Cart}}(\mathbf{r},\mathbf{r}',\omega)\mathbf{S}^T(\phi)$, where $\mathbf{G}_0^{\mathrm{Cart}}$ has an analytic expression [43] and is given by

$$\mathbf{G}_0^{\mathrm{Cart}}(\mathbf{r},\mathbf{r}',\omega) = \left(\mathbf{I} + \frac{1}{k^2}\nabla\otimes\nabla\right)G_0(\mathbf{r},\mathbf{r}',\omega), \quad \text{(A3)}$$

where $G_0(\mathbf{r},\mathbf{r}',\omega)$ is the Green's function of the scalar Helmholtz equation.

The scattering term can be calculated via the integral representation of the homogeneous part. To obtain this representation we apply the method of VWF explained in detail in Refs. [44] and [45]; here we cover only the basic ideas and provide the final expressions. To find the solution of the vector Helmholtz equation, (A1), we introduce the scalar Helmholtz equation and the solution of this equation in the cylindrical coordinates,

$$\nabla^2\phi(\mathbf{k},\mathbf{r}) + k^2\phi(\mathbf{k},\mathbf{r}) = 0,$$
$$\phi_n(k_z,\mathbf{r}) = J_n(k_\rho\rho)e^{in\theta+ik_z z}, \quad \text{(A4)}$$

where $J_n(x)$ is the Bessel function of the first kind, $\mathbf{r} = (\rho,\theta,z)$ are the cylindrical coordinates, and k_ρ and k_z are the projections of the wave vector $\mathbf{k}$. The solution of the vector Helmholtz equation may be written in terms of the vector wave functions

$$\mathbf{M}_n(k_z,\mathbf{r}) = \nabla\times[\phi_n(k_z,\mathbf{r})\mathbf{e_z}],$$
$$\mathbf{N}_n(k_z,\mathbf{r}) = \frac{1}{k}\nabla\times\mathbf{M}_n(k_z,\mathbf{r}), \quad \text{(A5)}$$

where $\mathbf{e_z}$ is the so-called pilot vector, the unit vector pointing in the z direction. These WVFs $\mathbf{M}$ and $\mathbf{N}$ correspond to TE/TM modes of the field.

One can show [44] that the homogeneous part of the Green's function can be expanded in terms of these vector

wave functions as

$$\mathbf{G}_h(\mathbf{r},\mathbf{r}',\omega) = -\frac{\mathbf{e}_\rho\mathbf{e}_\rho}{k_0^2}\delta(\mathbf{r}-\mathbf{r}') + \frac{i}{8\pi}\sum_{n=-\infty}^{\infty}\int_{-\infty}^{\infty}\frac{dk_z}{k_{0\rho}^2}\mathbf{F}_n(k_z,\mathbf{r},\mathbf{r}'), \quad \text{(A6)}$$

and the $\mathbf{F}_n(k_z,\mathbf{r},\mathbf{s})$ function is given by

$$\mathbf{M}_n^{(1)}(k_z,\mathbf{r})\overline{\mathbf{M}}_n(k_z,\mathbf{r}') + \mathbf{N}_n^{(1)}(k_z,\mathbf{r})\overline{\mathbf{N}}_n(k_z,\mathbf{r}'),$$

$$\mathbf{M}_n(k_z,\mathbf{r})\overline{\mathbf{M}}_n^{(1)}(k_z,\mathbf{r}') + \mathbf{N}_n(k_z,\mathbf{r})\overline{\mathbf{N}}_n^{(1)}(k_z,\mathbf{r}').$$

Here the first line holds for $\rho_r > \rho_{r'}$ and the second one for $\rho_r < \rho_{r'}$; $k_0 = \omega/c$, $k_{0\rho} = \sqrt{k_0^2 - k_z^2}$, and the superscript (1) in vector wave functions denotes that the Bessel function of the first kind, $J_n(k_\rho\rho)$, should be replaced with the Hankel function of the first kind, $H_n^{(1)}(k_\rho\rho)$. Here we provide the explicit form of the WVF:

$$\mathbf{M}_n(k_z,\mathbf{r}) = \begin{pmatrix} \frac{in}{\rho}J_n(k_{0\rho}\rho) \\ -k_{0\rho}(J_n(k_{0\rho}\rho))' \\ 0 \end{pmatrix} e^{in\theta+ik_zz},$$

$$\mathbf{N}_n(k_z,\mathbf{r}) = \begin{pmatrix} \frac{ik_zk_{0\rho}}{k}(J_n(k_{0\rho}\rho))' \\ -\frac{nk_z}{\rho k}J_n(k_{0\rho}\rho) \\ \frac{k_{0\rho}^2}{k}J_n(k_{0\rho}\rho) \end{pmatrix} e^{in\theta+ik_zz},$$

$$\overline{\mathbf{M}}_n(k_z,\mathbf{r}') = \begin{pmatrix} -\frac{in}{\rho'}J_n(k_{0\rho}\rho') \\ -k_{0\rho}(J_n(k_{0\rho}\rho'))' \\ 0 \end{pmatrix}^T e^{-in\theta'-ik_zz'},$$

$$\overline{\mathbf{N}}_n(k_z,\mathbf{r}') = \begin{pmatrix} -\frac{ik_zk_{0\rho}}{k}(J_n(k_{0\rho}\rho'))' \\ -\frac{nk_z}{\rho' k}J_n(k_{0\rho}\rho') \\ \frac{k_{0\rho}^2}{k}J_n(k_{0\rho}\rho') \end{pmatrix}^T e^{-in\theta'-ik_zz'},$$

where $J_n(k_\rho\rho)'$ indicates the derivative with respect to the dimensionless argument.

Now having the integral representation of the homogeneous term of the Green's function, we can construct the scattering term in a similar fashion. Let us denote the medium outside the dielectric cylinder 1 and the medium inside 2. The particular form of the Green's tensor depends on the position of the source point $\mathbf{r}'$: whether it is inside or outside the cylinder. Since the atoms are placed outside the nanofiber, both source and receiver should be outside the cylinder, and in the latter we consider only the second case. Thus, the total Green's tensor can be written as

$$\mathbf{G}^{11}(\mathbf{r},\mathbf{r}',\omega) = \mathbf{G}_h^{11}(\mathbf{r},\mathbf{r}',\omega) + \mathbf{G}_s^{11}(\mathbf{r},\mathbf{r}',\omega),$$

$$\mathbf{G}^{21}(\mathbf{r},\mathbf{r}',\omega) = \mathbf{G}_s^{21}(\mathbf{r},\mathbf{r}',\omega),$$

where the two superscripts denote the positions of the receiver and the source point, respectively, and the two scattering parts of the Green's tensor have the following form:

$$\mathbf{G}_s^{11}(\mathbf{r},\mathbf{r}',\omega) = \frac{i}{8\pi}\sum_{n=-\infty}^{\infty}\int_{-\infty}^{\infty}\frac{dk_z}{k_{\rho 1}^2}\mathbf{F}_{\mathbf{M};n,1}^{11(1)}(k_z,\mathbf{r})\overline{\mathbf{M}}_{n,1}^{(1)}(k_z,\mathbf{r}') + \mathbf{F}_{\mathbf{N};n,1}^{11(1)}(k_z,\mathbf{r})\overline{\mathbf{N}}_{n,1}^{(1)}(k_z,\mathbf{r}'),$$

$$\mathbf{F}_{\mathbf{M};n,1}^{11(1)}(k_z,\mathbf{r}) = R_{MM}^{11}\mathbf{M}_{n,1}^{(1)}(k_z,\mathbf{r}) + R_{NM}^{11}\mathbf{N}_{n,1}^{(1)}(k_z,\mathbf{r}),$$

$$\mathbf{F}_{\mathbf{N};n,1}^{11(1)}(k_z,\mathbf{r}) = R_{MN}^{11}\mathbf{M}_{n,1}^{(1)}(k_z,\mathbf{r}) + R_{NN}^{11}\mathbf{N}_{n,1}^{(1)}(k_z,\mathbf{r}),$$

$$\mathbf{G}_s^{21}(\mathbf{r},\mathbf{r}',\omega) = \frac{i}{8\pi}\sum_{n=-\infty}^{\infty}\int_{-\infty}^{\infty}\frac{dk_z}{k_{\rho 1}^2}\mathbf{F}_{\mathbf{M};n,2}^{21}(k_z,\mathbf{r})\overline{\mathbf{M}}_{n,1}^{(1)}(k_z,\mathbf{r}') + \mathbf{F}_{\mathbf{N};n,1}^{21}(k_z,\mathbf{r})\overline{\mathbf{N}}_{n,1}^{(1)}(k_z,\mathbf{r}'),$$

$$\mathbf{F}_{\mathbf{M};n,2}^{21}(k_z,\mathbf{r}) = R_{MM}^{21}\mathbf{M}_{n,2}(k_z,\mathbf{r}) + R_{NM}^{21}\mathbf{N}_{n,2}(k_z,\mathbf{r}),$$

$$\mathbf{F}_{\mathbf{N};n,2}^{21}(k_z,\mathbf{r}) = R_{MN}^{21}\mathbf{M}_{n,2}(k_z,\mathbf{r}) + R_{NN}^{21}\mathbf{N}_{n,2}(k_z,\mathbf{r}).$$

Here the scattering Fresnel coefficients R_{AB}^{ij} are introduced and the second subscript in the VWFs denotes that k and k_ρ should be replaced with their values inside the corresponding media $k_i = \varepsilon_i(\mathbf{r},\omega)k_0$, $k_{\rho i} = \sqrt{k_i^2 - k_z^2}$. We should note that unlike the case of the homogeneous term, here we have products of $\mathbf{M}$ and $\mathbf{N}$, which is due to the fact that the normal modes in our case have a hybrid nature.

The form of the Fresnel coefficients mentioned above can be found by imposing the boundary conditions on the Green's tensor at the surface of the cylinder:

$$\mathbf{e}_\rho \times [\mathbf{G}^{11}(\mathbf{r},\mathbf{r}',\omega) - \mathbf{G}^{21}(\mathbf{r},\mathbf{r}',\omega)]|_{\rho_r=\rho_c} = 0,$$

$$\mathbf{e}_\rho \times \nabla_{\mathbf{r}} \times [\mathbf{G}^{11}(\mathbf{r},\mathbf{r}',\omega) - \mathbf{G}^{21}(\mathbf{r},\mathbf{r}',\omega)]|_{\rho_r=\rho_c} = 0.$$

Solving for this, we can find the Fresnel coefficients R_{AB}^{ij} and, finally, construct the scattering part of the Green's tensor $\mathbf{G}_s(\mathbf{r},\mathbf{r}',\omega)$.

[1] H. J. Kimble, Nature **453**, 1023 (2008).
[2] A. V. Akimov, A. Mukherjee, C. L. Yu, D. E. Chang, A. S. Zibrov, P. R. Hemmer, H. Park, and M. D. Lukin, Nature **450**, 402 (2007).
[3] H. de Riedmatten, M. Afzelius, M. U. Staudt, C. Simon, and N. Gisin, Nature **456**, 773 (2008).
[4] S. J. Weber, A. Chantasri, J. Dressel, A. N. Jordan, K. W. Murch, and I. Siddiqi, Nature **511**, 570 (2014).
[5] P. J. Yao, V. Manga Rao, and S. Hughes, Laser Photon. Rev. **4**, 499 (2010).
[6] P. Lodahl, S. Mahmoodian, and S. Stobbe, Rev. Mod. Phys. **87**, 347 (2015).
[7] L. M. Duan and C. Monroe, Adv. At. Mol. Opt. Phys. **55**, 419 (2008).
[8] K. M. Birnbaum, A. Boca, R. Miller, A. D. Boozer, T. E. Northup, and H. J. Kimble, Nature **436**, 87 (2005).
[9] N. Rivera, I. Kaminer, B. Zhen, J. D. Joannopoulos, and M. Soljačić, Science **353**, 263 (2016).
[10] K. Y. Bliokh, D. Smirnova, and F. Nori, Science (N.Y.) **348**, 1448 (2015).

[11] S. J. P. Kress, F. V. Antolinez, P. Richner, S. V. Jayanti, D. K. Kim, F. Prins, A. Riedinger, M. P. C. Fischer, S. Meyer, K. M. McPeak, D. Poulikakos, and D. J. Norris, Nano Lett. **15**, 6267 (2015).

[12] R. J. Coles, D. M. Price, J. E. Dixon, B. Royall, E. Clarke, P. Kok, M. S. Skolnick, A. M. Fox, and M. N. Makhonin, Nat. Commun. **7**, 11183 (2016).

[13] F. L. Kien, J. Q. Liang, K. Hakuta, and V. I. Balykin, Opt. Commun. **242**, 445 (2004).

[14] K. P. Nayak, P. N. Melentiev, M. Morinaga, F. L. Kien, V. I. Balykin, and K. Hakuta, Opt. Express **15**, 5431 (2007).

[15] E. Vetsch, D. Reitz, G. Sagué, R. Schmidt, S. T. Dawkins, and A. Rauschenbeutel, Phys. Rev. Lett. **104**, 203603 (2010).

[16] V. I. Balykin, K. Hakuta, F. Le Kien, J. Q. Liang, and M. Morinaga, Phys. Rev. A **70**, 011401(R) (2004).

[17] M. S. Tame, K. R. McEnery, S. K. Özdemir, J. Lee, S. A. Maier, and M. S. Kim, Nat. Phys. **9**, 329 (2013).

[18] P. Törmä and W. L. Barnes, Rep. Prog. Phys. **78**, 013901 (2015).

[19] W. H. Weber and G. W. Ford, Phys. Rev. B **70**, 125429 (2004).

[20] S. Campione, S. Steshenko, and F. Capolino, Opt. Express **19**, 18345 (2011).

[21] M. Petrov, Phys. Rev. A **91**, 023821 (2015).

[22] R. S. Savelev, D. S. Filonov, M. I. Petrov, A. E. Krasnok, P. A. Belov, and Y. S. Kivshar, Phys. Rev. B **92**, 155415 (2015).

[23] F. Le Kien and A. Rauschenbeutel, Phys. Rev. A **90**, 063816 (2014).

[24] F. Le Kien, S. Dutta Gupta, V. I. Balykin, and K. Hakuta, Phys. Rev. A **72**, 032509 (2005).

[25] L. Russell, D. A. Gleeson, V. G. Minogin, and S. N. Chormaic, J. Phys. B **42**, 185006 (2009).

[26] H. L. Sørensen, J.-B. Béguin, K. W. Kluge, I. Iakoupov, A. S. Sørensen, J. H. Müller, E. S. Polzik, and J. Appel, Phys. Rev. Lett. **117**, 133604 (2016).

[27] N. V. Corzo, B. Gouraud, A. Chandra, A. Goban, A. S. Sheremet, D. V. Kupriyanov, and J. Laurat, Phys. Rev. Lett. **117**, 133603 (2016).

[28] A. Goban, K. S. Choi, D. J. Alton, D. Ding, C. Lacroûte, M. Pototschnig, T. Thiele, N. P. Stern, and H. J. Kimble, Phys. Rev. Lett. **109**, 033603 (2012).

[29] C. Cohen-Tannoudji, J. Dupont-Roc, and G. Grynberg, *Photons and Atoms: Introduction to Quantum Electrodynamics* (Wiley-VCH Verlag, Weinheim, Germany, 2004).

[30] A. S. Sheremet, A. D. Manukhova, N. V. Larionov, and D. V. Kupriyanov, Phys. Rev. A **86**, 043414 (2012).

[31] V. M. Ezhova, L. V. Gerasimov, and D. V. Kupriyanov, J Phys.: Conf. Ser. **769**, 012045 (2016).

[32] V. G. Minogin and S. Nic Chormaic, Laser Phys. **20**, 32 (2010).

[33] T. Gruner and D.-G. Welsch, Phys. Rev. A **53**, 1818 (1996).

[34] H. T. Dung, L. Knöll, and D.-G. Welsch, Phys. Rev. A **66**, 063810 (2002).

[35] C. A. Marocico and J. Knoester, Phys. Rev. A **79**, 053816 (2009).

[36] R. S. Savelev, A. P. Slobozhanyuk, A. E. Miroshnichenko, Y. S. Kivshar, and P. A. Belov, Phys. Rev. B **89**, 035435 (2014).

[37] V. Agranovich and O. Dubovsky, JETP Lett. **3**, 223 (1966).

[38] F. Le Kien and A. Rauschenbeutel, Phys. Rev. A **91**, 053847 (2015).

[39] C. Junge, D. O'Shea, J. Volz, and A. Rauschenbeutel, Phys. Rev. Lett. **110**, 213604 (2013).

[40] R. Mitsch, C. Sayrin, B. Albrecht, P. Schneeweiss, and A. Rauschenbeutel, Nat. Commun. **5**, 5713 (2014).

[41] T. Van Mechelen and Z. Jacob, Optica **3**, 118 (2016).

[42] C. A. Marocico and J. Knoester, Phys. Rev. A **84**, 053824 (2011).

[43] L. Novotny and B. Hecht, *Principles of Nano-Optics* (Cambridge University Press, Cambridge, UK, 2012).

[44] W. C. Chew, *Waves and Fields in Inhomogeneous Media* (Wiley-IEEE Press, New York, 1999).

[45] C. T. Tai, *Dyadic Green's Functions in Electromagnetic Theory*, 2nd ed. (IEEE Press, Piscataway, NJ, 1994).